Properties and Performance of Model Lignocellulose Derived Biofuel Mixtures as Low Carbon Replacements for Diesel Fuels

Scott Wiseman

Submitted in accordance with the requirements for the degree of
Integrated Masters and Doctor of Philosophy

The University of Leeds

The Centre for Doctoral Training in Bioenergy
School of Chemical and Process Engineering

January 2023

The candidate confirms that the work submitted is his own and that appropriate credit has been given where reference has been made to the work of others.

This copy has been supplied on the understanding that it is copyright material and that no quotation from the thesis may be published without proper acknowledgement.

The right of Scott Wiseman to be identified as Author of this work has been asserted by him in accordance with the Copyright, Designs and Patents Act 1988.

Acknowledgements

Abstract

The decarbonisation of heavy-duty vehicles and other compression ignition (CI) engine applications is pivotal to meeting global climate change targets. Since these engines are likely to rely on liquid fuels, there is a need for low-carbon alternatives. One potential option could be the product blend from alcoholysis of lignocellulosic biomass. The main products include an alkyl levulinate, a dialkyl ether, and the alcohol used. The blend composition could be tailored to ensure compliance with existing fuel standards and to favour comparable engine performance and low emissions, whilst maximising the use of the main product, the alkyl levulinate. In this work, experimental and computational techniques were used to investigate the influence of the biofuel blend composition and carbon chain length on the fuel properties, engine performance, and emissions when utilising the blends in an unmodified engine.

Physical properties of ethanol, n-butanol, and n-pentanol alcoholysis derived three-component blends with and without diesel were tested, along with their miscibility. A design of experiments (DoE) approach was used to effectively cover the desired design space. Accurate predictive models were produced using the DoE methodology for the flash point, density, and kinematic viscosity, for the blends, with R^2 values >0.900. Blends with diesel and biodiesel were also tested to establish blend boundaries and their compliance with existing fuel standards. Tailoring the physical properties of butyl-based blends showed more favourable engine performance compared to when tailoring the combustion properties of the ethyl-based blends. The butyl-based biofuel blends could be added up to 25 vol% in diesel whilst remaining compliant with fuel standards.

The blends of diesel and biofuel three-component blends were tested in a Yanmar L100V single-cylinder CI and their engine performance and emissions were determined. Emissions indices were calculated to investigate if the fuel blends would enable the engine to maintain compliance with the Euro Stage V emissions standard. The CO and total hydrocarbon (THC) emissions increased relative to diesel for all biofuel blends, whereas the particulate matter (PM) and particle number (PN) emissions reduced. The nitrogen oxide emissions were stable relative to the diesel baseline. At maximum load, the butyl-based blends reduced the THC, PM, PN, and volatile organic compounds emissions. Whist the blends were compatible with the engine in terms of their overall performance, there would need to be optimisation or the retrofitting of aftertreatment systems to ensure their compliance with the emissions standard.

Chemical kinetic simulations of the gas phase combustion highlighted the need to include the fuel spray and turbulent mixing when modelling CI engine combustion in order to capture trends in combustion behaviour on blending. Chemical ignition delays

followed the expected trends for the biofuel blends but did not match those from the engine, demonstrating the combined influence of chemical and physical effects on ignition delays and heat release properties.

Table of Contents

List of Tables

List of Figures

Abbreviations and Nomenclature

0D	Zero-Dimensional
2M2B	2-Methyl-2-Butanol
ABE	Acetone-Butanol-Ethanol
AFR	Air-Fuel Ratio
AHR	Accumulated Heat Release
ATDC	After Top Dead Centre
BDC	Bottom Dead Centre
BHT	Butylated Hydroxytoluene
BL	n-Butyl Levulinate
BSEC	Brake-Specific Energy Consumption
BSFC	Brake-Specific Fuel Consumption
BTDC	Before Top Dead Centre
BTE	Brake Thermal Efficiency
BTL	Biomass-to-Liquid
BuOH	n-Butanol
CAD	Crank Angle Degrees
CI	Compression Ignition
CMD	Count Mean Diameter
CN	Cetane Number
COV	Coefficient of Variation
CR	Compression Ratio
DCN	Derived Cetane Number
DEE	Diethyl Ether
DI	Direct Injection
Dist	Distribution
DNBE	Di-n-Butyl Ether
DNPE	Di-n-Pentyl Ether
DOC	Diesel Oxidation Catalyst
DoE	Design of Experiments
DPF	Diesel Particulate Filter
EFR	Exhaust Flow Rate
EGR	Exhaust Gas Recirculation
EL	Ethyl Levulinate
EtOH	Ethanol
EU	European Union
FAME	Fatty Acid Methyl Ester
FID	Flame Ionisation Detection

FSN	Fuel Smoke Number
FTIR	Fourier Transform Infrared
GHG	Greenhouse Gas
GTL	Gas-to-Liquid
HC	Hydrocarbons
HD	Heavy Duty
HDV	Heavy-Duty Vehicle
HRR	Heat Release Rate
HVO	Hydrotreated Vegetable Oil
ICE	Internal Combustion Engine
IDT	Ignition Delay Time
IMEP	Indicated Mean Effective Pressure
IQT	Ignition Quality Tester
LDV	Light-Duty Vehicle
LLNL	Lawrence Livermore National Laboratories
MODDE	**Mod**elling and **De**sign
NDIR	Non-Dispersive Infrared
NEDC	New European Driving Cycle
NMOG	Non-Methane Organic Gases
NO_X	Nitrogen Oxides=$NO+NO_2$
NRMM	Non-Road Mobile Machinery
NSC	NO_X Storage Catalysts
NTC	Negative Temperature Coefficient
ODE	Ordinary Differential Equations
PAH	Polycyclic Aromatic Hydrocarbons
P-CA	Pressure-Crank Angle
PeOH	n-Pentanol
PL	n-Pentyl Levulinate
PM	Particulate Matter
$PM_{2.5}$	Particulate Matter with an aerodynamic diameter 50% collection efficiency at 2.5 μm
PN	Particle Number
PNSD	Particle Number Size Distribution
RCM	Rapid Compression Machine
RDE	Real Driving Emissions
RED	Renewable Energy Directive
REDII	Renewable Energy Directive II
RPM	Revolutions per Minute
SCAPE	School of Chemical and Process Engineering

SCR	Selective Catalytic Reduction
SI	Spark Ignition
S-ULSD	Surrogate Diesel
TDC	Top Dead Centre
THC	Total Hydrocarbons
UCO	Used Cooking Oil
UK	United Kingdom
ULSD	Ultra-Low Sulphur Diesel
USA	United States of America
VOC	Volatile Organic Compound
WHTC	World Harmonised Transient Cycle
YSI	Yield Sooting Index

Nomenclature

Notation	Unit	Name
$\dot{m}_i$	kg/s	Mass Production Rate
$\dot{w}_i$	mol/s	Molar Rate of Production
T_γ	K	Reduced Temperature
C_V	J/kg K or J/mol K	Heat Capacity at Constant Volume
E_a	kcal/mol	Activation Energy
H	kJ/mol	Enthalpy
H_{CV}	-	Hydrogen/Carbon Fuel Molar Ratio
KV40	mm^2/s	Kinematic Viscosity at 40°C
M_i	kg/mol	Molecular Weight
p	bar or atm	Pressure
p_i^{sat}	bar	Saturated Vapour Pressure
ppm	-	Parts per Million
O_{CV}	-	Oxygen/Carbon Fuel Molar Ratio
T	°C or K	Temperature
U	J	Internal Energy
V	m^3	Volume
vol%	-	Volume Percent
wt%	-	Weight Percent
Y	-	Mass Fraction
γ	-	Activity Coefficient
Δ	-	Relative change
μ	cP	Dynamic Viscosity
v	mm^2/s	Kinematic Viscosity

ρ	g/cm^3	Density
φ	-	Equivalence Ratio
[X]	vol%	Concentration of Gaseous Species X

Chapter 1

Introduction

1.1 Project Background

Global transport relies heavily on crude oil-derived fuels for internal combustion engines (ICEs). 91% of the energy used in the global transport sector comes from oil and gas, whereas biofuels currently contribute 3.7% (1). Using biofuels in ICEs contributes towards the decarbonisation of their use and should reduce greenhouse gas (GHG) emissions. However, the sustainability of first-generation biofuels makes them unsuitable for large-scale decarbonisation. As a result, there is ongoing research and development to produce advanced biofuels from more sustainable feedstocks.

Over the last decade, the transport sector has changed considerably, with the ever-growing demand for the shipment of goods and the change in personal habits (1). The number of vehicles in use, both light and heavy-duty (HD), has increased yearly. In countries with growing economies like India, China, and Brazil, this growth is rapid (1). With a growing population, there is an increased demand for construction, agriculture, and goods transport. As a result, the use of heavy-duty vehicles (HDVs) rose, increasing the number of compression ignition (CI) engines used (1-3). CI engines are important power sources which are typically fuelled with fossil-derived diesel and rely on fuel autoignition. They are used as powertrains in HDVs due to their higher efficiency and higher torque operation than spark ignition (SI) engines (4, 5). Therefore, they make significant contributions to the CO_2 and GHG emissions in the transport, industrial, and agricultural sectors.

There is a need to decarbonise the transport sector if the target of limiting global warming to 1.5 °C, as set in the Paris Agreement, is to be met (6, 7). Many countries have ambitious targets to meet this global target. The United Kingdom (UK) is aiming to reach net zero GHG emissions by 2050. The European Union (EU) has pledged to be climate neutral by 2050, with a 55% reduction in GHG emissions compared to 1990 levels by 2030 (8, 9).

There has been a continual development of engine and powertrain technologies to reduce GHG emissions and decarbonise the transport sector. However, there is still a reliance on CI engines since there is a lack of electrification of HDVs, and even with the use of hybrid technologies, there would still be a CI engine in an HDV (10). In 2021, only 0.1% of HD trucks were pure electric vehicles. The uptake of fully electric HDVs relies on suitable battery technology development (11). There are proposed dates for the end of sales of new ICE HD trucks, for example: by 2040 in the UK, 2045 in the state of New York, and by 2035 in Austria, with a legally binding date in California of 2045 (2, 3).

However, there will still be existing HDV fleets requiring fuel after these dates, since the typical lifetime of a HDV is 10 to 15 years. Unless changes are rapidly made to fuel supply chains, these vehicles are likely to rely on diesel. To be able to decarbonise the HDV fleet, low-carbon alternative fuels are needed. These would preferably be liquid drop-in fuels, such that the fuel can be used without any modification to existing vehicles and infrastructure.

Currently, diesel fuel standards require the addition of biodiesel from fatty acid methyl ester (FAME) as a biofuel component. The allowed FAME content is at different fractions depending on the country and fuel standard (12, 13). However, FAME is a first-generation biofuel and is typically produced from food crops or waste cooking oils. In 2018, the European Renewable Energy Directive (RED) was recast and became REDII. This directive mandates increased use of renewable transport fuels and the minimum required fraction of second-generation (advanced) biofuels used in the EU (14). REDII also defines sustainability criteria for each feedstock to ensure the biofuel's lifecycle is considered (14). These feedstocks include lignocellulosic wastes and non-food crops. There are many other possible low-carbon alternatives for diesel, all at different stages of research and development. Hydrotreated vegetable oil (HVO) and gas-to-liquids (GTL) are two such alternatives that are diesel blend components (12, 13, 15, 16). HVO depends on vegetable oil supplies, and GTL is typically synthesised from petroleum-derived gasses, making them less favourable in terms of their sustainability (17, 18). Advanced biofuels can be produced using a range of methods, and these result in different potential biofuel candidates. Each production method and biofuel candidate has its environmental impact when assessing its life cycle, and any alternative fuel production methods should have a lower impact than diesel (1, 19-25). Without any improvement in the lifecycle GHG emissions, the utilisation of an advanced biofuel would be unfavourable.

Globally there are different fuel standards that set the physical and chemical property limits a fuel must meet (12, 13, 15, 16). Diesel fuel standards ensure the safe use and handling of diesel. They also stipulate the fuel composition to ensure the favourable performance of diesel when used in an engine (12, 13, 15, 16). There is a range of physical and chemical properties with set limits, including for example, the density, kinematic viscosity, flash point, cetane number (CN), and cloud point. There are also limits for the composition of the fuel, including polycyclic aromatic hydrocarbons (<11 vol%), FAME (<7 vol%), and sulphur (<10 ppm (parts per million)). HVO and Fischer Tropsch synthetic paraffins can be at any fraction to diesel, whereas FAME can only be 7 vol%, when used as low-carbon blend components in Europe and the UK (12, 13, 15, 16).

1.2 The Need for Decarbonisation

The transport sector is one of the largest contributors to GHG emissions, around 14% globally. In 2019, it accounted for 27% of the total emissions in the UK, 29% of the total emissions in the United States of America (USA), and 25% of the total net emissions (including international transport) for the EU (26-31). In the EU, road transport and shipping accounted for 71% and 13.5% of the transport sector's GHG emissions, respectively (31). In 2019, the contribution to the UK's transport sector GHG emissions for cars and taxis, heavy goods vehicles (HGVs), and light-duty vehicles (LDVs) were 55.4%, 15.9%, and 15.7%, respectively (32). For HGVs, there will still be high contributions to the GHG emissions from CI engines. Therefore, there is a need for low-carbon alternative fuels to reduce GHG emissions from CI engine applications.

ICEs can also be used for electricity generation in generating sets (gensets). The genset market is dominated by diesel gensets with an array of engine sizes and engine designs available. A genset is often a backup measure in many developed countries, whereas in developing countries, they can be the primary electricity generation method when used in microgrid systems (33). A stable supply of drop-in low-carbon liquid fuels for all applications of CI engines would be beneficial and would contribute towards their decarbonisation.

1.3 The Need for Advanced Biofuels

Not only are first-generation biofuels not as sustainable as advanced biofuels, but there are also ethical issues around using crops to produce food or first-generation biofuels. To reduce the reliance on first-generation biofuels, REDII mandates the minimum contribution for advanced biofuels to be 3.5% of the total energy supplied by 2032 (14). Annex IX of REDII details the allowable feedstocks for the production of advanced biofuels (14). These feedstocks require more advanced processing and production methods to produce advanced biofuels. Examples include the gasification of biomass combined with Fischer Tropsch of the synthesis gas, sugar extraction and fermentation, and acid-catalysed hydrolysis of biomass in alcohol (alcoholysis) (19-25, 34-37).

In this work, the biofuel production method of interest is the alcoholysis of lignocellulosic biomass. It can produce a multi-component product blend of potential biofuel candidates, with the main products being an alkyl levulinate, a dialkyl ether, and the alcohol used as the solvent (34-38). In principle, the alcoholysis product blend can be tailored to have the required physical and chemical properties using different reaction conditions and post-reaction processing. Compliance with fuel standards' property limits may favour the utilisation and commercial viability of advanced biofuel blends, either as

100% biofuel blends or as a diesel blend component. The use of such fuel blends would contribute towards the decarbonisation of CI engines and the sectors that rely on their use.

Not only are there climate impacts when using CI engines, but there are impacts on air quality (39, 40). ICE applications in non-road mobile machinery (NRMM) and LDVs and HDVs have separate emissions standards, termed their type approval (41-43). Emissions standards set limits for CO, particulate matter (PM), particle number (PN), nitrogen oxides ($NO_X=NO+NO_2$), and total hydrocarbon (THC) emissions from the tailpipe (41-43). The limits of these emissions have reduced with every version of the standards (41-43). For a fuel to be considered a drop-in, its use should also ensure an engine or vehicle remains compliant with its type approval. Other emissions have detrimental impacts on local air quality and public health (39, 44). These include volatile organic compounds (VOCs) such as formaldehyde and acetaldehyde, which are irritants (45, 46). There are also impacts of emissions on fertility rates, cancer, and increased likelihood of developing dementia, so any changes in emissions should not reduce air quality (39, 44-46). Many vehicles and large NRMM applications have exhaust aftertreatment systems to ensure the set limits are met by removing pollutants before the tailpipe. Different aftertreatment technologies are discussed further in Chapter 2. Low-carbon alternative fuels may change the dependence on aftertreatment systems as they will alter the engine-out emissions. If there could be reductions in the engine-out emissions such that the need for aftertreatment systems reduces, there could be the cost-saving benefit of not having to install aftertreatment systems. The fuel used has the largest influence on the exhaust gas composition. The addition of oxygenated biofuels to diesel can significantly change the exhaust composition. There can be an increase in CO and THC emissions due to the lower CN of advanced biofuel components causing less complete combustion (13, 34, 38, 47-49). However, with less complete combustion, there would be an expected increase in PM and PN emissions. However, with the addition of oxygenated biofuel components, this is not the case (47, 48, 50-52). The presence of oxygen in the fuel can reduce soot formation, which will impact PN and PM emissions (53). The influence of tailored biofuel blends on such emissions needs to be established and their suitability as drop-in blending components determined.

1.4 Project Motivation

The work detailed in this project contributes towards an Engineering and Physical Sciences Research Council (EPSRC) funded project entitled 'Tailored Production and Utilisation of Sustainable Low Cost Lignocellulosic Advanced Biofuel Blends as Diesel and Petrol Substitutes: SusLABB' where the production and utilisation of advanced biofuel blends from alcoholysis are being investigated. The work presented in this thesis

involves the investigation of the properties of model three-component advanced biofuel blends to identify those that comply with the physical property limits set in fuel standards, and to investigate the performance and emissions generated when using selected fuel blends in a CI engine. This approach is not typically reported in the literature when testing diesel blended with advanced biofuels. The primary motivation of this work was to determine the influence of the biofuel composition on the physical and combustion properties, the engine performance, and emissions. The impact of using different starting alcohols and their resultant three-component model alcoholysis products was investigated, as longer carbon chains may be more favourable to blend with diesel. Ethyl, butyl, and pentyl-based three-component blends were studied where ethanol, n-butanol, and n-pentanol were the different starting alcohols. The ethyl-based blends contained ethyl levulinate (EL), diethyl ether (DEE), and ethanol (EtOH). The butyl-based blends contained n-butyl levulinate (BL), di-n-butyl ether (DNBE), and n-butanol (BuOH). The pentyl-based blends contained n-pentyl levulinate (PL), di-n-pentyl ether (DNPE), and n-pentanol (PeOH).

Whilst there has been published research conducted using the butyl-based three-component biofuel blend by Antonetti et al. (34) and Raspolli Galletti et al. (54), they did not investigate the use of blends tailored to meet the physical properties limits set in existing fuel standards. Frigo et al. (38) studied the influence of DNBE and BL blends with diesel on engine performance and emissions, where the DNBE fraction was a constant 4 vol%, and the BL fraction increased from 7 – 13 vol%. However, the blends studied by Frigo et al. (38) did not comply with fuel standards. Producing blends compliant with the physical property limits may result in biofuel candidates being suitable drop-in fuels for low-carbon diesel alternatives.

Testing every possible blend formulation within desired composition limits would lead to an expensive testing regime. Hence, methodologies such as design of experiments (DoE) are beneficial. Using DoE enables a design space to be effectively and efficiently covered. DoE software packages can produce simple models to predict the properties of untested blends. Accurate predictions of the properties will enable fuel standard compliant formulations to be determined. The models from the DoE enabled fuel blends that comply with the selected property limits from the fuel standards to be found, and selected for further testing. These blends should be more favourable for engine use since they are compliant with physical property limits. The engine testing would determine their influence on engine performance and emissions and their suitability for further use. This methodology follows a potentially more commercially viable process since fuel blends would meet existing fuel standards.

In contrast, there is a lack of simple models for modelling CI engines due to the complex nature of their operation. Additionally, modelling combustion of the advanced biofuel three-component blends, with or without diesel, is difficult due to the lack of available chemical kinetic mechanisms and fundamental combustion data (37, 55). The development of accurate models would allow for simulations of untested blends, enabling further optimisation of the blend composition, as simulations provide the opportunity to evaluate their influence on the combustion parameters quickly. The accuracy of computational fuel combustion models depends on the accuracy of the kinetic mechanism and associated thermodynamic data (56). Chemical kinetic mechanisms and thermodynamic data are unavailable for many biofuels. As a result they must be developed in terms of mechanistic detail and thermokinetic data using a range of methods (56-58). The suitability of combustion mechanisms produced in the SusLABB project for the biofuel blends of interest, and their ability to predict the combustion behaviours, will be investigated in this work.

One further motivation for this work was to investigate whether oxygenated biofuel blends can be suitable diesel blend stock, as diesel standards do not currently allow oxygenated advanced biofuels to be blend components (12, 13, 15, 16). If a range of biofuel formulations can comply with the physical property limits and have favourable changes in engine performance and emissions, then these fuels should be considered potential low-carbon alternatives.

1.4.1 Research Questions

This project aims to answer the following general research questions.

- Can we use ethyl, butyl, and pentyl-based three-component biofuel blends, with and without diesel, as drop-in fuels? This is to establish if the biofuel blends can be tailored so that physical properties can match the limits in the existing fuel standards. In addition, the aim is to determine if the engine performance and emissions, can be maintained or improved. The ability of a fuel blend to maintain compliance with emissions standards also demonstrates its suitability.
- What are the key physical and combustion properties that will determine the suitability of these blends? This involved reviewing the fuel standards and literature to determine which properties would have the largest impact on the safe and effective use of the fuels.
- How do the key physical properties change as the biofuel blend composition changes? Since the blend is in principle tailorable through different reaction conditions and post-reaction processing, there needs to be an understanding of the effects the change in composition has on the physical

properties. This understanding will enable the determination of optimal compliant blends.

- Are there suitable models for predicting the physical and combustion properties, emissions, and engine performance, or will these need developing? This involves reviewing the literature and the availability of blending rules and models for predicting the physical properties of interest. If there are no suitable or available blending rules and models, then blend-specific models would be developed using the DoE methodology. There will be an assessment of available engine models and combustion kinetic mechanisms for the biofuel component and blends.

- What influence does the advanced biofuel formulation have on engine performance and emissions? Since the combustion properties of the butyl and pentyl-based blends are unknown, only the physical properties can be tailored to meet the limits of the fuel standards. In contrast, the ethyl-based blends' derived cetane number (DCN) can be tailored due to the available model of Howard et al. (37). Therefore, the influence of the blend formulation on the engine performance and emissions are investigated using steady-state engine tests and standard techniques.

1.4.2 Project Aims and Objectives

The overall aim of this project is to determine the suitability of three-component advanced biofuel blends for use in current CI engines when blended with and without diesel. The fuel blends used should meet the required limits of selected properties to promote their commercial viability, and their influence on the engine performance should be minimal. The emissions should ideally reduce, and the engine would ideally remain compliant with emissions standards. This research uses experimental and computational techniques to measure and predict the physical and combustion properties, engine performance, and emissions. Models for the physical properties will be developed for the three-component biofuel blends if no suitable models are available. The objectives of this work are to:

1) Experimentally determine how the blend composition of the ethyl, butyl, and pentyl-based three-component blends affect their physical properties.
2) Produce predictive models for physical properties using DoE methodology if no suitable models are available.
3) Determine the influence of the carbon chain length on the physical properties.
4) Establish any blend walls of the three-component blends with two types of diesel (road and off-road) at two temperatures.

5) Determine the influence of the three-component blends on the physical properties of different base fuels.

6) Establish an understanding of the influence of the biofuel blend composition on engine performance and emissions from a single-cylinder genset using standard emissions measurement methods for legislated and non-legislated emissions.

7) Determine the influence of the biofuel blend composition on engine combustion performance parameters such as indicated mean effective pressure (IMEP), peak pressure, brake-specific fuel consumption (BSFC), heat release rate (HRR), and ignition delay time (IDT).

8) Evaluate the influence of different fuel injector designs on engine performance and emissions of the biofuel blends and diesel.

9) Evaluate compliance with emissions standards when using these fuel blends.

10) Assess the ability of computational models and chemical kinetic mechanisms to predict the changes in the IDT, HRR, and other experimental parameters.

11) Establish if there are any viable blend compositions of the ethyl, butyl, or pentyl-based three components with diesel, that maintain or improve the emissions and engine performance relative to diesel and comply with the fuel standards.

1.5 Thesis Structure

In this thesis, there will be eight chapters, including this introductory chapter outlining the project background, motivation for the project, and its aims and objectives.

Chapter 2 will review the relevant literature, including the existing fuel and emissions standards and their changes. There will be a review of the available blending rules for the physical and combustion properties of interest and their suitability for predicting the properties of the blends studied. There will be a discussion of the blends comprising the biofuel components of interest with diesel and their effects on the physical properties, engine performance, and emissions. Finally, there will be a review of the available kinetic models for combustion of the biofuel components and available engine models.

Chapter 3 is the methodology chapter. It outlines the experimental methods used for measuring the physical properties and provides details of the engine and emissions measurement techniques. The DoE methodology will be outlined, along with the analysis methods used for determining the produced models' suitability. The methods used to process the emissions data and determine the heat release from the engine testing are presented. Finally, the methods used to simulate the combustion of the biofuel blends with and without diesel are outlined.

Chapter 4 reports the measured physical properties and analysis of the predictive models produced from the DoE. The influence of carbon chain length and blend composition on the physical properties was determined. The behaviour and physical properties of blends with diesel will be presented. Finally, the fuel standard compliant blends and the blends selected for engine testing are reported.

Chapter 5 dissects the influences that the selected ethyl and butyl-based biofuel blends have on the IDT, HRR, peak pressure, BSFC, IMEP, and exhaust manifold temperatures. There is also a discussion on the influence of the injector design on these parameters.

Chapter 6 presents measurement and analysis of the engine emissions when using the selected advanced biofuel blends. This chapter discusses the influence of the biofuel blend composition on the gaseous and particulate emissions when using the advanced biofuel blends. The influence of the fuel injector design on the emissions is also discussed. Compliance with the Euro Stage V emissions standard for NRMM when using the biofuel blends is discussed.

Chapter 7 is the final results chapter. It presents the chemical kinetic modelling study conducted to determine the influence of the blend composition on the combustion parameters such as IDT and HRR. The kinetic model's ability to predict the experimental trends in the IDT and HRR from the engine tests is also evaluated.

Chapter 8 is the conclusions chapter. The conclusions are drawn to answer the research questions outlined in Chapter 1. There is a discussion of the feasibility and suitability of the advanced biofuel blends. There are also recommendations for future work and recommendations for future legislation and standards based on the findings of this work.

Chapter 2
Literature Review

2.1 Introduction

This chapter will review the literature that discusses the fundamentals of CI engines and the use of biofuels in CI engines. There will be a discussion of existing fuel standards and emissions legislation for CI engines. The chapter will outline different advanced biofuel production methods and review the alcoholysis of lignocellulosic biomass, the production process of interest in this work.

If advanced biofuel blends are to be used as low-carbon alternative fuels, there must be an understanding of how their physical properties change with blend composition. Hence, a review of blending rules and existing physical property models will be presented. Finally, a review of kinetic modelling for the combustion of advanced biofuels and their ability to predict combustion parameters such as IDT and HRR will be presented.

2.2 Compression Ignition Engines

CI engines rely on high temperatures and pressures to cause autoignition of the fuel as it is injected close to top dead centre (TDC) (59). Many CI engines operate with a four-stroke cycle, i.e.: they include an intake stroke, compression stroke, ignition (power) stroke, and an exhaust stroke, as shown in figure 2.1 (5, 59).
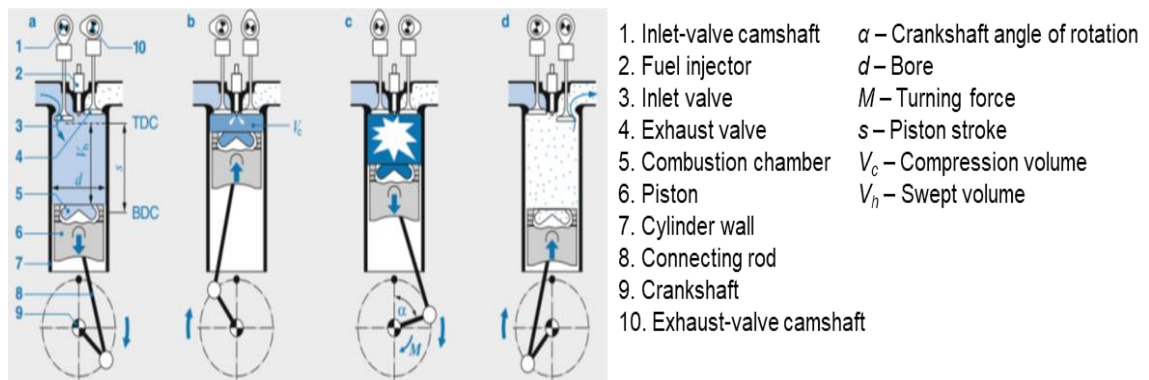
Figure 2.1. Four-stroke cycle for a CI engine. Reproduced from (5).

a) The intake stroke begins with the piston at TDC, which then travels down to bottom dead centre (BDC), increasing the cylinder volume. During this stroke, the intake valve opens, and air, possibly with the addition of exhaust gases if exhaust gas recirculation (EGR) is used, is drawn into the cylinder (5, 59).

b) In the compression stroke, the intake and exhaust valves are closed. As the piston moves towards TDC, the mixture is compressed to the

degree determined by the compression ratio (CR). For example, CRs can be as low as 12:1 for locomotive engines and up to 24:1 for LDV engines (5). Before the piston reaches TDC, fuel is injected at high pressure, with injector pressures from 200 bar to above 2200 bar. The injection generates an atomised diesel and air mixture which mixes through turbulent mixing processes (5, 59). CI engines operate under lean combustion conditions where there is excess air and the equivalence ratio is 0.4<φ<1 (5, 59). The pressure at TDC is usually between 30 and 60 bar for naturally aspirated engines and is higher for turbocharged engines (5, 59).

c) The power stroke begins with the piston moving down from TDC. During this stroke, the fuel/air mixture ignites after a given IDT. Typical IDTs in a naturally aspirated engine are around 1.0 – 1.5 ms (4, 5). As a result, the temperature and pressure rise, which forces the piston downwards, applying torque to the crankshaft (5, 59). The amount of energy released during the combustion depends on the fuel's energy density, the mass injected, and the engine's thermal efficiency (5).

d) The exhaust stroke begins fractionally before the piston reaches BDC, as the exhaust valves typically open before BDC (5, 59). The gases flow through the exhaust valve and are forced out as the piston comes upwards (5, 59). The exhaust valves stay open until a small number of crank angle degrees (CAD) after TDC. When it closes, the intake valve opens, starting the four-stroke cycle again (5, 59).

The pressures and temperatures reached during combustion are fuel and CR dependent. If CRs are too high, it would lead to elevated temperatures and pressures, causing early ignition. Too low a CR would result in a long IDT favouring less complete combustion (5, 59). Both of these reduce an engine's thermal efficiency, as more fuel is needed to produce the same amount of power (5, 59).

2.2.1 Combustion Phases during Combustion in CI Engines

The combustion of diesel in a CI engine typically has three phases after ignition i.e. premixed, mixing-controlled and late combustion, as shown in figure 2.2 (59). The premixed combustion phase is the combustion of the readily vaporised fuel that has mixed with air, and it usually causes the peak HRR. The mixing-controlled combustion has a lower HRR as the vaporisation and turbulent mixing slow the burning rate. The heat generated is also vaporising the remaining fuel, hence the lower peak compared to the premixed combustion (59). The late combustion phase has a much lower HRR, as

the cylinder is expanding and cooling. There is a small amount of heat released during this phase as there may be unburnt fuel and soot that can release their energy (59).
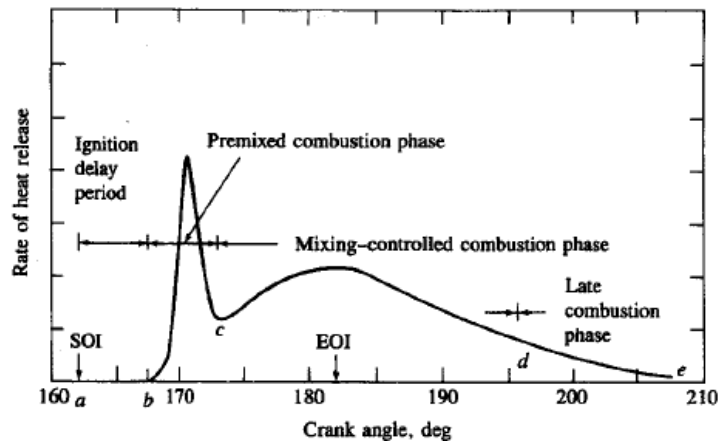
Figure 2.2. Typical CI engine HRR profile. Reproduced from (59).

Changing the nature of these phases with the addition of biofuel can have both positive and negative impacts, as the emissions and engine performance could improve or worsen. The influence of biofuels on the HRR are discussed in section 2.9. The impact of the biofuels of interest in this work are discussed in Chapter 5.

2.2.2 Typical Emissions from a CI Engine

Engine combustion results in the emissions of CO, CO_2, NO_X, unburnt fuel, PM, and incomplete combustion products including hydrocarbons (HC) and volatile organic compounds (VOCs). Examples of VOCs include formaldehyde and acetaldehyde. CI engines typically have high NO_X emissions due to high in-cylinder temperatures and pressures, and the high flame temperatures from turbulent combustion (5, 40, 59). The NO produced is primarily part of the thermal NO_X formed following the extended Zeldovich nitrogen oxidation mechanism (40, 59, 60). This mechanism involves the following reactions:

$$N_2 + O \leftrightarrow NO + N$$

$$N + O_2 \leftrightarrow NO + O$$

$$N + OH \leftrightarrow NO + H$$
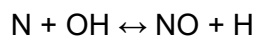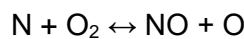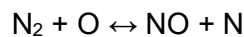
NO can also be formed at flame fronts, where CH radicals react with N_2 to produce N radicals. This is the prompt NO_X mechanism (40, 61):

$$N_2 + CH \leftrightarrow N + HCN$$
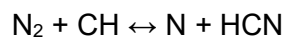
NO can then be oxidised to form NO_2. The formation and final concentration of NO_2 are highly temperature dependent, as NO_2 can be converted back to NO. Above 1000 K, NO is oxidised to NO_2 in the following reaction:

$$NO + HO_2 \leftrightarrow NO_2 + OH$$
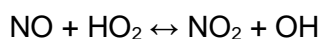
NO_2 can be reduced to NO when temperatures exceed 1500 K via the following reaction:

$$NO_2 + O \leftrightarrow NO + O_2$$
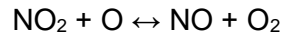
This reaction occurs for the unquenched NO_2. Quenching is more common at lower engine loads, as less fuel is injected into the cylinder, so the combustion temperature is lower, and there are higher numbers of cooler regions. At lower loads, NO_2 can be up to 30% of total NO_X, whereas, at higher loads, it can be around 10% as there are higher temperatures (59, 62). The addition of biofuels could change this percentage due to changes in flame temperatures and charge cooling effects. The influence of the biofuels studied in this work on the NO_2 emissions will be investigated in Chapter 6.

The amount of NO_X produced will vary in the cylinder since the mixture is heterogeneous. If there was less premixed combustion, there would be lower levels of NO_X (40). NO_X formation is more prevalent in leaner mixtures due to lower flame speeds, which increases the time available for NO_X formation. However, lean operation also lowers the flame temperatures creating competition between the lower flame speeds and lower temperatures. These leaner regions are common in the premixed combustion phase, which occurs during the initial stages of combustion before the dominant mixing-controlled combustion occurs (40).

The other nitrogen source for NO_X formation is fuel-bound nitrogen, which is more common in solid biomass (63). In diesel, there are trace quantities of nitrogen as most nitrogen is removed during hydrotreatment of distillates and crude oil (64). However, when producing advanced biofuels from biomass, there could be nitrogen in the final products. There can be up to 12% nitrogen in biomass. If this was in liquid fuels, there would be an increase in NO_X emissions (65). The nitrogen radical produced during combustion would undergo the reactions in the Zeldovich mechanism to form NO (40).

NO_X formation from the homogeneous combustion of hydrocarbons in air is inevitable, so NO_X emissions must be reduced to meet emissions limits. The control methods include EGR and aftertreatment systems, which are outlined in section 2.4. NO_X affects local air quality as it can react to form ozone, which is an irritant and contributes towards smog production (40, 66, 67). NO_2 is also an irritant and can exacerbate existing conditions such as asthma. At high concentrations NO_2 can bind with haemoglobin in the blood and act similarly to CO, causing methaeoglobinaemia which reduces the oxygen concentration in the bloodstream (40).

Hydrocarbon emissions are usually low from a CI engine. However, there are still several sources of HC emissions, including:

- Over-mixing of the fuel/air mixture, where the mixture becomes too lean to undergo complete combustion and produces unburnt HC (5, 40).

- The fuel quench effect, which increases HC emissions, as it is where the fuel spray reaches the cylinder walls and condenses reducing complete combustion. This is more common for smaller engines (5, 40).

- Under-mixing of the fuel/air mixture so there are rich zones with too much fuel to undergo complete combustion. In these zones there are high concentrations of unburnt fuel and PM (5, 40).

HC emissions have detrimental impacts on local air quality and public health, as some species are irritants or carcinogens, such as formaldehyde or aromatic compounds (40, 66, 68, 69). HC emissions also contribute, along with NOx emissions, to photochemical smog formation, which causes lung inflammation (40, 66-69).

PM emissions from CI engines are produced in rich zones, where the fuel is not fully oxidised, and soot precursors are produced. These include aromatic species, acetylene, and aldehydes, which react to form polycyclic aromatic hydrocarbon (PAH) compounds (70-73). PM formation and growth has two main modes, nucleation and agglomeration. The nucleation mode accounts for the formation of small particles with diameters <50 nm (70-73). During nucleation the fuel is partially oxidised and pyrolysed, becoming more carbonaceous and forms structures with diameters around 3 nm and high molecular weights (72). These particles undergo surface growth to form particles with diameters between 20 – 50 nm, after which they undergo the second mode of growth, agglomeration or accumulation growth (72). This is where nucleation particles and HCs coalesce, producing larger particles (70-73). The agglomeration usually occurs when the temperatures decrease, such as downstream in the exhaust (72). A typical PM size distribution from a CI engine can be seen in figure 2.3.
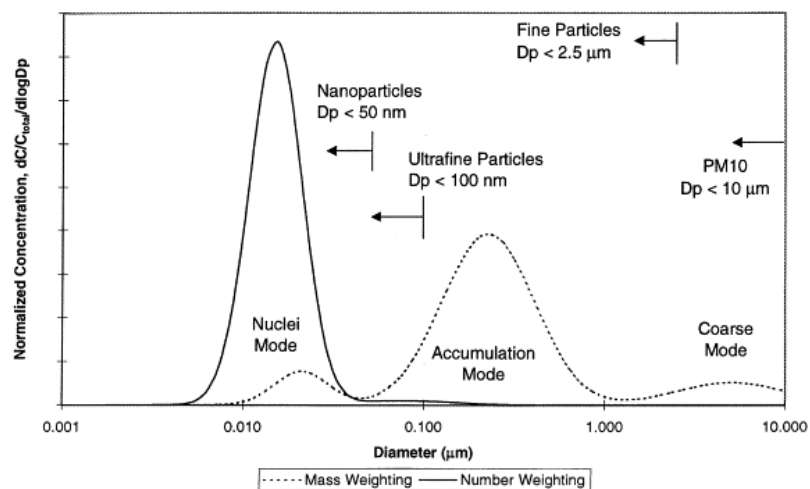
Figure 2.3. Typical particle size distribution in mass and number weighting from a CI engine. Reproduced from (73).

PM produced from CI engines is detrimental to local air quality and human health. Humans can inhale PM, and the smaller the particle, the further it can travel in the respiratory system. Particles <20 nm in diameter can pass through the bloodstream and even through the blood-brain barrier (74). Studies have shown that PM in the lungs can increase the chance of developing cancer whilst also irritating the lungs and causing inflammatory conditions (66, 70, 75-78). Exposure to PM also increases the likelihood of developing cardiovascular diseases such as Chronic Obstructive Pulmonary Disease (66, 70, 75-78). There have also been studies that have shown $PM_{2.5}$ reduces fertility due to the PAH content. However, the impacts of different PAH species are not fully understood (39, 79). Chen et al. (44) showed that exposure to PM an aerodynamic diameter 50% collection efficiency at 2.5 μm ($PM_{2.5}$) correlated to the incidence of Dementia in Ontario, but the influence of the $PM_{2.5}$ composition requires further analysis. If the $PM_{2.5}$ composition changes using biofuels there may be changes in the impacts it has on human health.

CO emissions are an indicator of incomplete combustion. It is also a known poisonous gas with established effects on human health, including dizziness, fainting, and death at high concentrations (80). Providing an engine is operated correctly, it is unlikely that CO emissions would reach levels required for such consequences. CO emissions would be an issue for CI engines used in confined spaces, such as using generating sets (gensets) in poorly ventilated areas. If tailpipe CO emissions increased, the likelihood of CO poisoning would increase. Therefore, the combustion of any alternative fuel would need to maintain or reduce CO emissions relative to the diesel being displaced.

2.2.3 Applications of CI Engines

CI engines typically have greater thermal efficiencies compared to spark ignition (SI) engines. CI engines typically have thermal efficiencies of >40%, with modern technologies able to achieve >50% efficiency, whereas SI engines can have peak thermal efficiencies of 41% (5, 81). Therefore, CI engine applications are ones that require high efficiency and low fuel consumption (5). The main uses of CI engines include HDVs, agricultural and construction equipment (including power generation), locomotives, and ships (5).

The use of diesel gensets for power generation is common. Gensets are used as infrastructure support. Localised electricity networks can be created using them in remote areas such as sub-Saharan Africa (33). The utilisation of low-carbon diesel alternatives in these remote areas could improve air quality. The use of drop-in fuels would allow for greater fuel flexibility in these regions where fuel supplies may be inconsistent. In the UK, these engines can run using NRMM grade diesel, which has a

different specification to diesel used for road vehicles, as discussed further in section 2.3 (12, 16). Genset engines operate at high speeds, around 3000 RPM, or lower speeds, of 1200 – 1500 RPM. The optimum speed for the highest efficiency is used, and this is manufacturer-dependent (5).

2.3 Diesel Fuel Standards

A fuel must meet a specification set in a fuel standard to be sold. These standards are country, or region specific, along with being application specific. In the EU, the EN 590 standard for automotive diesel and EN 14214 for FAME biodiesels must be met (12, 15). In the UK, automotive diesel must comply with EN 590, and class II diesel used in NRMM must comply with BS 2869 (16). In the United States of America (USA), ASTM D975 is the diesel standard (13). The limits for the current fuel standards are shown in table 2.1.

Table 2.1. Summary of the key property limits in the diesel fuel standards (12, 13, 15, 16).

Fuel Standard	EN 590	EN 14214	BS 2869	D975
CN	>51	>51	>45	>40
Kinematic Viscosity at 40 °C (mm^2/s)	2.00 – 4.50	3.50 – 5.00	2.00 – 5.00	1.9 – 4.1
Density at 15 °C (g/cm^3)	0.820 – 0.845	0.860 – 0.900	>0.820	
Sulphur Content (mg/kg)	10	10	10	
PAH Content ((weight %) wt%)	<8	0	-	
FAME Content (vol%)	7	>96.5	7	5
Flash Point (°C)	>55	>101	>55	>52
Carbon Residue (%wt)	0.30		0.30	
Ash (wt%)	0.01		0.01	

With each version of a fuel standard, the property limits have changed. In 2004, a maximum FAME content of 5 vol% was introduced for diesel complying with EN 590. The FAME content increased to 7 vol% in 2009 (82, 83). The addition of FAME was to reduce the carbon intensity of diesel. The minimum CN increased from 49 to 51 in 2000, favouring a reduction in CO and THC emissions due to more complete combustion from a more reactive fuel (84, 85). The maximum density limit was reduced from 0.860 g/cm^3 to 0.845 g/cm^3 in 2000, which would favour smaller droplets being formed upon fuel

injection (86-88). Smaller droplets have higher fuel vaporisation rates, resulting in a more homogeneous air/fuel mixture (86-88). In EN 590 and BS 2869, the other biofuels that are permitted to be used as blend components are hydrotreated vegetable oil (HVO) and biomass-to-liquid (BTL) derived paraffins (12). HVO and BTL can be blended at any fraction with a base diesel provided the final fuel still meets EN 590 (12). HVO and BTL contain no oxygen, and the addition of oxygenated biofuel components would result in a non-compliant fuel.

Diesel fuels have no maximum oxygen content limit, but have limits on the biofuel source. Oxygenated species are currently not permitted for use due to the changes in the physical and combustion properties, and their low miscibility (89). The effects on the properties of diesel/biofuel blends are discussed in section 2.7. Additionally, oxygenates typically have a lower energy content than diesel, which increases fuel consumption (89). However, if it can be demonstrated that the physical property limits can be met, and the engine performance and emissions are maintained or improved relative to diesel using oxygenated biofuel blends, this would suggest that there should be a review of the allowed biofuels. This is vital if the REDII targets are to be met.

2.4 Emissions Standards for Different Compression Ignition Engine Applications

The emissions standards define limits for the legislated emissions for different vehicles and engine applications (90-93). In Europe, there are emissions standards for LDVs, HDVs, and NRMM.

2.4.1 European Emissions Standards

The current legislated emissions standards vehicles and engines must comply with are Euro 6d for LDVs, Euro VI-E for HDVs (signified by Roman numerals), and Euro Stage V for NRMM engines (41-43). The limits set are the tailpipe emissions limits and not the engine-out limits. With each version of the standards, the emissions limits have been reduced. There has also been the introduction of new emissions limits. For example, particle number (PN) limits were introduced in Euro 5b for LDVs, Euro VI for HDVs and Stage V for NRMM (91, 92, 94). The applicable emissions standard for the engine used in this work is the Euro Stage V standard, as it is a single-cylinder CI engine as part of a genset. Engines used in small, low-power gensets only had their emissions regulated as part of the Euro Stage V emissions standard. Emissions limits for CO, HC and NO_X combined, PM, and PN are set and they depend on engine power, as shown in table 2.2.

Table 2.2. Summary of the Euro Stage V emissions of CI non-road engines for a range of engine powers (42).

Engine Power (kW)	CO (g/kWh)	HC+NO$_X$ (g/kWh)	PM (g/kWh)	PN (#/kWh)
0 – 8	8.00	7.50	0.40[a]	
8 – 19	6.60	7.50	0.40	
19 – 37	5.00	4.70	0.015	1×10^{12}
37 – 56	5.00	4.70	0.015	1×10^{12}

[a]0.60 for air-cooled direct injection engines.

For HDVs, the emissions limits have become increasingly strict, increasing the reliance on exhaust aftertreatment systems to reach them (94). For HDVs, the reductions in the steady-state test emission limits, going from the Euro I standard to the current Euro VI standard were: 67% for CO, 88% for HC, 95% for NO$_X$, and 98% for PM (94). The proposed limits for the proposed Euro 7 standard are lower than the Euro VI limits, as shown in table 2.3 (95, 96). There is a proposed reduction for the solid particle diameter used to define those that count towards PN, reducing from 23 to 10 nm. In addition, the PN limit has been reduced from 6×10^{11} to 5×10^{11} #/kWh (41, 95, 96). Increasing the number of particles that contribute towards PN whilst reducing the emissions limit will emphasise the use of emissions reduction technologies. One such reduction method could also be the use of new fuels that inherently reduce PN, such as biofuels. In Euro 7, the newly legislated tailpipe emissions will be formaldehyde for HDVs and not for LDVs, NH$_3$ for LDVs, and N$_2$O for both HDVs and LDVs (41, 95, 96). Additionally, there is a change from limiting total HC (THC) emissions, to having separate limits for non-methane organic gases (NMOG) and methane (41, 95, 96).

Table 2.3. Euro VI and 7 emissions limits for HDVs (41, 96).

Emission	Euro VI[a]	Euro 7 cold emissions[a]	Euro 7 hot emissions[a]
CO (mg/kWh)	4000	3500	200
NO$_X$ (mg/kWh)	460	350	90
THC (mg/kWh)	160		
NMOG (mg/kWh)		200	50
PM (mg/kWh)	10	12	8
PN (#/kWh)	6×10^{11}	5×10^{11}	2×10^{11}
NH$_3$	10 ppm	65 mg/kWh	65 mg/kWh
N$_2$O (mg/kWh)		160	100
CH$_4$ (mg/kWh)		500	350
HCHO (mg/kWh)		30	30

[a]Measured following the World Harmonised Transient Cycle (WHTC) test.

The reductions in emissions limits seen for the automotive sector will likely occur for engines used in NRMM. Euro 7 does not cover NRMM engines but there will likely be reductions in the NO_X, HC, PM and PN emissions limits to improve air quality and to reduce the climate change impacts (19, 97-100).

2.4.2 Exhaust Aftertreatment Systems

As the emissions limits are tailpipe limits, they account for any exhaust aftertreatment systems used to control the engine-out emissions (41, 43). Aftertreatment systems are vehicle and engine-dependent due to different exhaust gas compositions. For CI engines, there are usually measures to control NO_X and PM emissions. There is also increasing use of CO and HC control measures to meet stricter limits (101).

NO_X emissions are controlled by EGR, NO_X storage catalysts (NSC), and selective catalytic reduction (SCR) (5, 101). EGR reduces NO_X emissions by lowering the oxygen concentration and reducing the peak combustion temperatures. The gases from EGR can also cool the cylinder itself since they pass through an intercooler before entering the intake manifold (4, 5). There is the drawback of increased CO and HC emissions from the lower temperatures as incomplete combustion increases, hence the need for additional aftertreatment systems (4, 5, 101, 102).

An NSC stores NO_2 by reacting it with $BaCO_3$ to form $Ba(NO_3)_2$ (5). This requires NO to be oxidised to NO_2, which occurs on a platinum-based catalyst (5). When the NSC approaches saturation and NO_2 cannot be stored, the NO_2 is reduced when it reacts with CO to form NO and CO_2. The NO can then react with CO to form N_2 and CO_2 (5).

SCR works by reacting NO_X with ammonia over a catalyst to form N_2 and H_2O (5, 40, 101). SCR catalysts are temperature sensitive and have a typical optimum temperature window of 250 – 450 °C (5). Therefore, if exhaust gas temperatures are reduced using advanced biofuels, the aftertreatment system may need redesigning to ensure high catalyst efficiency is maintained.

PM and PN emissions are controlled using a diesel particulate filter (DPF). These actively filter out particles and store them until the DPF is regenerated. This involves oxidising the stored PM to CO_2 and water (5, 101). DPFs are usually highly efficient, with efficiencies above 95%, and can remove particles with diameters as small as 10 nm (5). To maintain high efficiency a DPF must regenerate, which requires exhaust gas temperatures to be >600 °C. This is possible when the engine operates at full load. However, if the engine is not at full load, it will be operated at a richer condition such that exhaust gas temperatures increase from oxidising the elevated HC and CO emissions in the diesel oxidation catalyst (DOC) before the DPF, resulting in a temperature high enough for regeneration to occur (5).

A DOC oxidises CO and HC emissions to form CO_2 and water and oxidise NO to form NO_2. They also reduce particle mass due to HC oxidation (5, 101). DOCs are typically platinum or rhodium catalysts with light-off temperatures around 200 °C. However, the most effective temperatures are above 400 °C. These are reached due to the heat release during the oxidation of CO and HC (5, 101).

When changing to alternative fuels the exhaust composition is likely to change, which would require adaptation to aftertreatment systems as their effectiveness might be reduced. For example, if there were increases in HC emissions, there would need to be increased use of DOCs. If NO_X emissions are reduced by using advanced biofuels, there could be reductions in EGR rates and the use of SCR systems. There may also be implications on DPF regeneration that would need to be investigated.

2.5 Biofuels – a Comparison of the Different Generations

Traditionally there are four generations of biofuel determined by the nature of the feedstock used, summarised in table 2.4. Second-generation biofuels are often termed advanced biofuels due to the nature of their feedstocks. Additionally, there is a sub-set of second and third-generation biofuels termed 'development fuels' (103).

First-generation biofuels are produced using sugars, starches, and oils from food-based crops (23). As a result, they are unfavourable as they reduce food supplies. The most common first-generation biofuels are bio-ethanol produced from sugar beet, sugar cane, wheat, and barley, and biodiesel from the extracted oils from oil seed rape and palm oil, for example (23). In 2020, first-generation biofuels accounted for around 5% of the total fuel used in Europe and advanced biofuels was just above 1% (104).

Second-generation biofuels are those derived from non-food feedstocks. In Europe, REDII stipulates that there must be a 3.5% contribution to the energy content in transport fuels from such biofuels (14). REDII Annex IX lists feedstocks that can be used to produce these advanced biofuels, such as used cooking oils and forestry residues (14). There could also be the use of lignocellulosic wastes such as corn cobs, rice husks, bagasses, and the use of dedicated energy crops such as miscanthus and jatropha. The complex nature of these feedstocks requires more advanced conversion methods to produce advanced biofuels. Used cooking oil (UCO) derived renewable diesel currently accounts for 21% of renewable diesel, with other advanced feedstocks having negligible contributions (104). Cellulosic ethanol only accounts for 3% of the ethanol produced in Europe so its use as a precursor is also limited by its supply (104). Therefore, production of advanced biofuel diesel components must be developed.

Third-generation biofuels are algae derived biofuels, including ethanol, butanol, and biodiesels. The algae used is grown specifically for biofuel production. The extraction

and conversion of lipids from algae can be expensive and energy-intensive, making them currently unfavourable for use as fuels as large quantities are needed (23).

The UK's Renewable Transport Fuel Obligation states that a bio-derived development fuel must be produced from sustainable wastes or residues that are eligible for double renewable transport fuel certificates (103). Development fuels can be one of four types:

- Hydrogen
- Aviation fuel
- Synthetic natural gas from gasification or pyrolysis
- A fuel that can be blended into a base fuel such that it meets EN 590 or EN 228 and has a renewable content of at least 25%

For a development fuel to meet existing fuel standards, the oxygen in any biofuel would need to be removed, as EN 590 states that only bio-derived hydrocarbons can be blended into diesel as bio-derived components (12). Therefore, second-generation alcohols or esters could not currently be a renewable component in diesel to make it a development fuel. This limitation may prevent the use of fuels that not only contribute towards the REDII targets and decarbonisation, but ones that may improve air quality. The work in this thesis aims to determine blends that comply with physical property limits of fuel standards and assess their suitability for engine use, and to provide evidence that these fuels may need to be considered as future low-carbon diesel alternatives.

Fourth-generation biofuels use genetically modified feedstocks and bacteria to increase oil yields (105). However, this is an emerging technology, and it requires vast amounts of development to be economically and technologically viable. Therefore, these biofuels are unlikely to contribute towards decarbonisation in the short term.

Table 2.4. Summary of feedstocks for different generations of biofuels (14, 104, 105).

Biofuel Generation	Feedstock	Biofuel
First	Sugar Cane, barley, wheat, sugar beet, corn	Bioethanol
	Oil seed rape, palm oil, sunflower oil, animal fats	Biodiesel
Second (Annex IX feedstocks)	Corn cobs, bagasse, forestry residue, miscanthus, nut shells, sewage sludge	Oxygenated molecules such as esters, alcohols, and ethers
	UCO, waste fats	UCO biodiesel, HVO
Third	Algae	Bioethanol and biodiesel
Fourth	Genetically modified crops	Biodiesel

2.6 Advanced Biofuel Production Methods

Since there is a legislative requirement to use more advanced biofuels, the research and development focus has shifted towards their production. This shift includes the development of sustainable conversion routes for lignocellulosic feedstocks. The production methods must be sustainable and economically viable to be commercialised. The production of first-generation biofuels is currently the benchmark to compare advanced biofuel production against. Since advanced biofuels must be produced from more complex feedstocks, matching the product yield is a significant barrier. However, if the energy content can be extracted as a range of different compounds, such as alkyl levulinates, it may enable their widespread utilisation. The production methods of the biofuel components of interest in this work are discussed in this section. The blends of ethyl levulinate (EL), ethanol (EtOH), and diethyl ether (DEE) will be termed ethyl-based blends. Blends of butyl levulinate (BL), n-butanol (BuOH), and di-n-butyl ether (DNBE) will be termed butyl-based blends. Finally, pentyl levulinate (PL), n-pentanol (PeOH), and di-n-pentyl ether (DNPE) will be termed pentyl-based blends.

2.6.1 Second Generation Alcohol Production

Second-generation bio-ethanol and bio-butanol can be produced from acetone-butanol-ethanol (ABE) fermentation using bacteria from the clostridia strain (106). Bio-butanol production requires mixtures of sugars derived from the cellulose and hemicellulose fractions of biomass. One issue with producing bio-butanol using ABE fermentation is that the bacteria are poisoned by large quantities of butanol, which reduces the yield (106). To overcome the poisoning, the bacteria can be genetically modified, which can increase the n-butanol yield by 25% to 70% (106). However, this is expensive and requires further investigation. Bio-pentanol produced from biomass using engineered microorganisms is still in developmental stages (48, 107).

One other production route for longer carbon chain alcohols is Fischer Tropsch synthesis using synthesis gas from gasified biomass (25). This process produces methanol, which can then be reacted to form longer-chain alcohols. However, this is still in developmental stages.

2.6.2 Dialkyl Ether Production

Dialkyl ethers are produced from acid-catalysed reactions of alcohols to form the dialkyl ether and water (108). For ethers to be advanced biofuel components, second-generation alcohols should be used. The acid used can be heterogeneous or homogeneous with both having high selectivity to form ethers and not alkenes (108, 109). Therefore, in processes where alcohol is in excess and the reaction conditions are suitable, ether formation is likely to occur (108, 109).

2.6.3 Alkyl Levulinate Production

Alkyl levulinates are esters of levulinic acid and alcohol. The levulinic acid part consists of a five-carbon long chain, and the alcohol used dictates the alkyl chain length. There are several production methods for alkyl levulinates, including one-pot processes using lignocellulosic biomasses, catalysed reactions of levulinic acid with an alcohol, and the conversion of different furfural isomers (110).

Acid-catalysed hydrolysis of biomass in alcohol (alcoholysis) produces blends of possible fuel components (35, 36). The main products are an alkyl levulinate, a dialkyl ether, and the alcohol used as the solvent and a reactant (36, 37, 110-112). The composition of these blends depends on the reaction conditions used (36, 37, 110-112). During alkyl levulinate production, the alcohol used is converted to dialkyl ether due to the elevated temperatures and pressures and the presence of an acid catalyst (37, 111). Additionally, the alcohol is usually in excess so any alcohol that does not react with the biomass can react to form ethers.

The feedstock used in the alcoholysis process, along with the source of the second-generation alcohol, will dictate the carbon reduction potential of the final product blend compared to fossil-derived diesel (113). The source of the biomass and its composition, which will affect the yield of alkyl levulinate, will affect the lifecycle emissions of the product blend when used as a fuel. To have a carbon reduction relative to crude oil derived diesel, production of the final biofuel blend from alcoholysis should have lower lifecycle GHG emissions compared to refining crude oil to produce diesel (113). Additionally, if the biomass feedstock used is traditionally burned as a means of disposal, there could also be the benefit of improving air quality as it would negate these emissions and produce a potentially cleaner burning fuel.

One-pot processes using lignocellulosic biomass can favour a more sustainable production of an advanced biofuel blend since there could be less of a requirement for energy intensive post-reaction processing and separation. As shown in table 2.5, Tan et al. (114) studied EL production from cassava in a batch reactor using aluminium sulphate as the catalyst. Xu et al. (111) studied the production of EL from cellulose and ethanol in pressurised reactors at T=170 – 210 °C. Antonetti et al. (34) studied the alcoholysis of *Eucalyptus nitens* in n-butanol to produce BL and DNBE. There have also been studies on the influence of the different butanol isomers on product yields (115). For a sulphuric acid (H_2SO_4) catalysed reaction of 40 wt% cellulose at 200 °C for 30 minutes, n-butanol produced higher yields of n-butyl levulinate compared to the other isomers, closely followed by iso-butanol. 2-Butanol produced around one-third of the yield of its corresponding levulinate compared to n-butanol (115).

Typical feedstock conversion yields to alkyl levulinate depend on many factors, including the feedstock, the catalyst used (heterogeneous or homogeneous), reactor conditions, reaction duration, and the solvent system used (table 2.5) (35). Due to the inconsistent way in which yields are reported, it can be difficult to compare different studies, as some report the yield as the fraction of cellulose converted and some as the fraction of biomass (35, 108, 116). Typical yields range from 30 - 50%, indicating there is a significant conversion of the biomass. However, the alcohol is still in excess, and therefore the levulinate yield is a small fraction of the total products. However, there is scope to produce high quantities of alkyl levulinates from different feedstocks.

Table 2.5. Summary of alkyl levulinate yields from different alcoholysis reactions.

Feedstock	Catalyst	Solvent	Temperature (°C)	Time (min)	Alkyl Levulinate Yield	Ref.
Cellulose (5.33 g in 80 mL)	H_2SO_4 1 wt%	Ethanol	190	30	42.64 %	(111)
Wheat straw	2.5 wt% H_2SO_4	Ethanol	183	10	51 mol% 39.5 wt% of the cellulose content	(117)
Cassava (2 g in 38 g solvent)	$Al_2(SO_4)_3$	90 wt% ethanol/10 wt% water	200	360	47.05%	(114)
Eucalyptus nitens	1.9 wt% H_2SO_4	n-Butanol	183	146	42 mol%	(34)
Cellulose (0.5 g in 20g solvent)	25 wt%/cellulose H_2SO_4	n-Butanol	200	30	45 – 50%	(115)
		iso-Butanol			40%	
		2-Butanol			14%	

If high quantities of alkyl levulinate can be produced, then utilisation of the resultant blend as a fuel will be more cost-effective as more energy has been extracted from the biomass. There may be the need to have some post-reaction processing to formulate blends that comply with existing fuel standards. These should be conducted sustainably to ensure that the advanced biofuel has a lower lifecycle impact compared to diesel. For example, if the alcohol is recycled for the production of further alkyl levulinate, there would be improved sustainability of the alcoholysis process (38).

2.7 Properties of Biofuel and Diesel Blends – Physical, Combustion, Chemical, and Toxicological Properties

Biofuels have been shown to change the properties of diesel when blended at any fraction. However, there are a limited number of studies investigating the influence of the blend composition of multi-component advanced biofuel blends on blend properties. The miscibility and blend stability are important since fuels are stored whilst being shipped for long periods. In this work, the properties from the fuel standards selected were the density at 15 °C, flash point and kinematic viscosity at 40 °C (KV40). The flash point was selected due to its implications on the safe handling and storage of fuels. According to ISO 3679 (118) the flash point is defined as:

'*the lowest temperature, as measured in the prescribed manner, of the test portion corrected to a barometric pressure of 101,3 kPa, at which application of an ignition source causes the vapour of the test portion to ignite momentarily and the flame to propagate across the surface of the liquid*'

The addition of biofuel blends should not change the flash point as it would require changes to existing infrastructure and fuel handling methods. The density and KV40 were selected as they influence the spray and fuel pump efficiency, and these are known to influence the emissions and combustion (38, 119, 120). A summary of the properties of the biofuel components of interest is shown in table 2.6.

Each biofuel component in table 2.6 does not meet all the property limits of EN 590 (12). However, many of the components can meet the limits of grade II diesel standard of BS 2869 (16). The addition of the alcohols, DEE, and DNBE to diesel would likely reduce the flash point of a diesel, with a greater reduction from the components with the lowest flash points (121). The addition of large fractions of PeOH or DNPE may maintain compliance with EN 590 provided the diesel used had a high flash point. Addition of the levulinates to diesel would maintain compliance with the flash point limit. The KV40 limit could be maintained with the addition of BL, PL, BuOH, and PeOH. However, the high densities of the levulinates may increase the density of blends above the EN 590 limit (12). This may result in the biofuel blends, with and without diesel, being more suitable for a BS 2869 grade II diesel alternative. However, if high-density blends can be shown to have better particulate emissions than diesel, there may be the case that the current density limits are no longer suitable for their intended purpose. That is to control the aromatic content of diesel since aromatic compounds are usually very dense.

When these components are blended together and with diesel there may be non-ideal mixing and there may be miscibility and stability issues (122). The alcohols have the shortest carbon chain lengths and may not be miscible with diesel. The properties of

three-component blends will be influenced by the properties of each component and their molecular interactions. The influence of the blend composition on the physical properties will be investigated in Chapter 4.

Table 2.6. Summary of the physical properties of the biofuel components of interest.

Fuel Component	Flash Point (°C)[c]	Density at 15 °C (g/cm³)[d]	KV40 (mm²/s)[d]
EN 590 Limits[a]	>55	0.820 – 0.845	2.00 – 4.50
BS 2869 Limits[b]	>55	>0.820	2.00 – 5.00
EL	94	1.017	1.553
BL	111	0.973	2.017
PL	96	0.963	2.375
DEE	-40[e]	0.720	Cannot be measured
DNBE	25	0.768	0.736
DNPE	57	0.789	1.131
EtOH	16[f]	0.795	1.099
BuOH	35	0.811	2.261
PeOH	49	0.819	2.899

[a]from (12), [b]from (16), [c]measured using a Setaflash Series 3 plus, [d]measured using an Anton Paar SVM3000, [e]from (123), [f]from (124)

2.7.1 Blend Miscibility

There is evidence that the ethyl-based three components would form miscible ternary blends as the ignition quality tester (IQT) measurements conducted by Howard et al. (37) used a liquid mixture. They conducted tests with blends containing differing amounts of each component with mole fractions between 0 – 0.9 (37). There were no blends with diesel. Therefore, the miscibility of the ethyl-based blends with diesel must be investigated, especially since ethanol is immiscible with diesel at high fractions (122, 125). Lapuerta et al. (122) demonstrated that to keep the blends miscible with diesel, elevated temperatures were needed for higher fractions of ethanol. The use of ethanol as a sole diesel biofuel component is limited by its immiscibility at high fractions. The immiscibility can be overcome using a co-solvent such as biodiesel or 2-methyl-2-butanol (2M2B) (125-127).

Lapuerta et al. (122) established blend boundaries of diesel and alcohols with increasing carbon chain length, from methanol up to pentanol. They used a TurbiScan, which uses infrared light to establish if a mixture is transparent and stable. Figure 2.4 shows the miscibility limits for these alcohols, where mixtures below the curves indicate an unstable blend with diesel. As carbon chain length increases, the viable volume

fraction of alcohol in a stable blend increases and the temperature at which blends become unstable decreases (122). However, there was no indication of long-term blend stability given in the study.
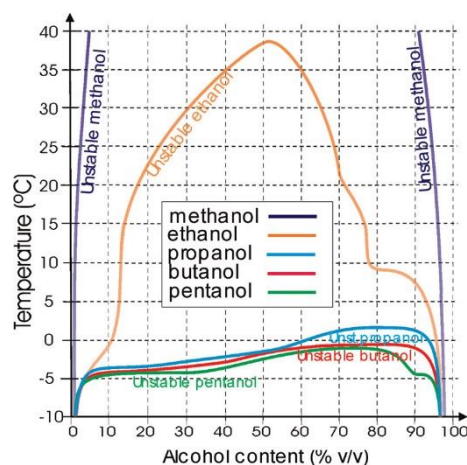
Figure 2.4. Stability of diesel and alcohol blends. Reproduced from (122).

The highest stable fraction of EL in diesel reported is 10 vol%, at temperatures above 4 °C, whereas for BL, it was 20 vol% (13, 128). It was also demonstrated that an increased aromatic content in diesel favoured increased miscibility at temperatures below 10 °C (13). To increase the EL fraction in diesel a co-solvent is needed. Christensen et al. (13) used 5 vol% n-butanol for 15 vol% EL, whereas Wang et al. (128) used 2% n-butanol.

Raspolli Galletti et al. (54) tested blends of 70 wt% BuOH/20 wt% DNBE/10 wt% BL (mixA), 30 wt% BuOH/60 wt% DNBE/10 wt% BL (mixB) and 33.3 wt% DNBE/66.6 wt% BL (mixC). These three mixtures were blended into a diesel at different volume fractions: 10 and 20 vol% for mixA and mixB, and 12 vol% for mixC. There have been no studies of n-pentyl levulinate blended with diesel. The dialkyl ethers have been shown to have miscibility up to the 20% tested for DEE and DNBE (129, 130). Górski and Przedlacki (129) showed that 20% DEE in diesel was stable for a week when stored above -10 °C (131). The three-component biofuel blends to be tested in this study, may provide the necessary co-solvents to increase the miscibility limits for the biofuel components. This hypothesis will be tested in Chapter 4.

2.7.2 Physical Properties of Fuel Blends

To test the properties of fuel blends, they need to be homogeneous. The mixing method used when producing fuel blends can affect the physical properties. For example, Low et al. (132) reported the flash point of a 5% EtOH/5% biodiesel/90% diesel blend to be much higher than Kwanchareon et al. (126) (table 2.7). Low et al. (132) used an emulsifier to blend the fuels and did not allow the blend to exceed 50 °C when mixing, whereas, Kwanchareon et al. (126) used a magnetic stirrer at ambient temperature in a

sealed vessel. As a result, Low et al. (132) may have evaporated some ethanol, as it would be expected that ethanol would reduce a blend's flash points since it has a flash point of 16 °C (121). There are no reported flash point measurements for DEE/diesel blends. This is likely due to DEE's low flash point and the lack of flash point testers able to measure below room temperatures (37, 133-137). Additionally, there is a lack of experimental flash point data available for DNBE and diesel blends. In studies using diesel/advanced biofuel blends, the flash point is often not measured, despite its importance for fuel handling and storage. Therefore, it is imperative to understand how the blend composition influences the flash point since it is unlikely the existing fuel standards limits will decrease. Flash points of blends with EL and BL are likely to be higher than diesel as they both have higher flash points than diesel (table 2.6). For the alcohols, the flash point is reduced close to the alcohol's flash point with low fractions of alcohol added. The density and KV40 of a blend are also dependent on the component values. EtOH and BuOH reduce the KV40 and density, as they are lower than diesel, whereas EL increases density and reduces KV40 (13, 98, 126).

Table 2.7. Summary of blend physical properties reported in the literature.

Blend	Flash Point (°C) (base diesel flash point)	KV40 (mm^2/s) (base diesel KV40)	Density at 15 °C (g/cm^3) (base diesel density)	Ref.
EN 590 Limits	>55	2.00 – 4.50	0.820 – 0.845	(12)
90% diesel/10% EL	75 (76)	2.15 (2.41)		(13)
	63 (61)	2.63 (2.83)	0.853 at 20 °C (0.836)	(128)
80% diesel/20% BL	80 (76)	2.20 (2.41)		(13)
90% diesel/5% EtOH/5% biodiesel	78 - 80	3.596		(132)
	17.5		0.831 (0.835)	(126)
95 vol% diesel/4.6 vol% EtOH/0.4 vol% 2M2B	<room temperature	3.701 (3.991)	0.839 (0.842)	(98)
95 vol% diesel/5 vol% BuOH	44 (68)	3.626 (3.991)	0.840 (0.842)	
90 vol% diesel/10 vol% BuOH	37 (68)	3.355 (3.991)	0.838 (0.842)	

The physical properties of fuel blends depend on the properties of each fuel component and any resultant intermolecular interactions, as shown by the different blending rules available. The ability to tailor the properties of biofuel blends to ensure

that the limits of fuel standards are still met could be a benefit of multi-component biofuel blends, such as those studied in this work.

2.7.3 Biofuel Component Toxicology

There are two key aspects of fuel toxicity, the effects on humans as a user and when producing the fuel blends, and the environmental implications if there is a spill. Diesel safety data sheets have warnings of '*suspected of causing cancer*' and '*may be fatal if swallowed and enters airways*' (138-140). Diesel is carcinogenic due to the hydrocarbons present. All alkyl levulinates are reported as non-toxic, but there is a lack of data available to confirm their toxicities (138). DEE poses a risk to users due to its high volatility and can cause drowsiness from inhalation of its vapours. In contrast, the other potential biofuel components are not as volatile, which reduces the risk they pose to the customer (138). No ecotoxicological classifications are applied to the alkyl levulinates and alcohols due to their biodegradability, indicating they are non-toxic (138). DEE is not biodegradable but is highly volatile, so its lifetime in aquatic or terrestrial environments is limited, whereas DNBE is not readily biodegradable and is not as volatile. It has acute toxicity towards fish as the lethal concentration that kills 50% of the fish used in a test falls between 10 and 100 mg/L, indicating that small quantities would result in the death of fish (138). Diesel is immiscible with water and as a result the toxicity towards fish is negligible. Overall, these findings would indicate that blending the advanced biofuels of interest with and without diesel should produce a fuel that would be no more toxic to humans than diesel. However, DNBE may be of possible concern due to its toxicity towards aquatic creatures.

2.7.4 Combustion Properties

The combustion of a fuel is dependent on many properties, with the key properties of diesel and the studies biofuel components of relevance to CI engine applications summarised in table 2.8 where those that are not available (n/a) are indicated. The most common property used for the intercomparison between fuels is the DCN, which is indicative of the fuel's propensity to ignite (141, 142).

The DCNs of the levulinates and alcohols are below the EN 590 limit, whereas the ethers are well above the limit. Therefore, when blending together there should be possibility to increase the DCN of the alcohols and ethers. The influence of the biofuel components will be discussed in sections 2.7.4.4 and 2.8.4. The LHV of the biofuel components are lower than diesel, which would reduce the energy content of the final fuel blend. A lower energy content would increase brake-specific fuel consumption (BSFC), as more fuel would be required for the same power output (13). BSFC is defined as the rate of fuel consumption in grams per hour to generate a given power (in kW), and

is usually expressed as g/kWh. The high enthalpy of vaporisation of the biofuel components result in a charge cooling effect where the vaporisation of the fuel reduces the in-cylinder temperature (137). This would be favourable for reducing thermal NO_X emissions but unfavourable for IDTs since lower temperatures slow the vaporisation and potentially give longer IDTs. The influence of the fuel blends in this work on the engine performance, combustion, and emissions are discussed in Chapters 5 and 6.

Table 2.8. Summary of combustion properties of the advanced biofuel components.

Fuel Component	DCN[a]	Lower Heating Value (LHV) (MJ/kg)[c]	Enthalpy of Vaporisation (kJ/mol) / (kJ/kg)[d]	Adiabatic Flame Temperature (K)[i]	Heat Capacity (J/mol K)[j]/ (J/kg K)
EN 590 diesel	>51[b]	42.5 – 42.9	n/a / 250 – 270 up to n/a / 358	2200 - 2350	n/a
EL	6	24.8	51.6[e] / 358	2875	276[k] / 1914
BL	14.4	27.4	56[f] / 325	2860	338[k] / 1963
PL	n/a	n/a	66.3[g] / 356	n/a	n/a
DEE	140 – 160	33.9	27.1 / 366	2300	175 / 2361
DNBE	115	38.3	45 / 346	2865	278 / 2134
DNPE	111	40.3	57[h] / 292	n/a	n/a
EtOH	8-12	26.8	42.3 / 918	2242	112 / 2431
BuOH	12	33.1	52 / 702	2450	178 / 2401
PeOH	18.2	34.7	46.2 / 647	n/a	208 / 2360

[a]obtained from (143), [b]from (12), [c]from (13, 34, 144-147), [d]from (131, 148-150), [e]at 420 K, [f]at 785 K, [g]at 369 K, [h]at 388 K. [i]from (151-156), [j]from (150), [k]from (157).

2.7.4.1 Combustion Properties of the Biofuel Components

The ignition delay time (IDT) is one of the important combustion properties relevant to the utilisation of biofuels. These are typically measured using a rapid compression machine (RCM), shock tube, or ignition quality tester (IQT) (37, 158-162). RCMs and shock tubes are homogeneous premixed reactors, which are representative of port fuel-injected gasoline engines rather than CI engines (37, 158-162). RCMs are based on a rapidly moving piston, with its speed set to achieve a given temperature and pressure at the end of compression (163). At this point, the piston remains in place to enable the pressure in the reaction zone to be measured (163). An IQT is more commonly used for diesel-type fuels as it has a constant volume and pressure chamber. The test fuel is injected into the preheated chamber, and the IDT is defined as the time from injection to the maximum pressure rise (37, 141, 164). IDTs measured in an IQT are influenced by

the physical processes following fuel injection and are discussed further in section 2.7.4.5. It is important to capture these influences since CI engines inject the fuel into compressed air (119). The fuel vaporisation will affect IDTs as there needs to be enough fuel vaporised to ignite and the thermodynamic conditions need to be suitable for ignition to occur. There have been numerous studies investigating the IDTs of the alcohols and ethers in RCMs and shock tubes (161, 165-168). However, there have been limited fundamental combustion studies of alkyl levulinates, with only two fundamental combustion studies involving EL, by Ghosh et al. (160) and Howard et al. (37), and none involving BL or PL.

2.7.4.2 Combustion Properties of Ethyl-Based Blend Components

Ghosh et al. (160) measured IDTs for EL in an RCM and a shock tube, with the results displayed in figure 2.5. The IDTs exhibit typical Arrhenius behaviour for temperature dependence (160). The increasing IDTs with decreasing temperature will be detrimental to the utilisation in CI engines since they rely on autoignition and the compressed temperatures are usually around 800 – 1000 K (59). At these temperatures, EL has IDTs greater than 30 ms, but since these were measured at 10 bar, the IDT in an engine would be shorter due to higher pressures.
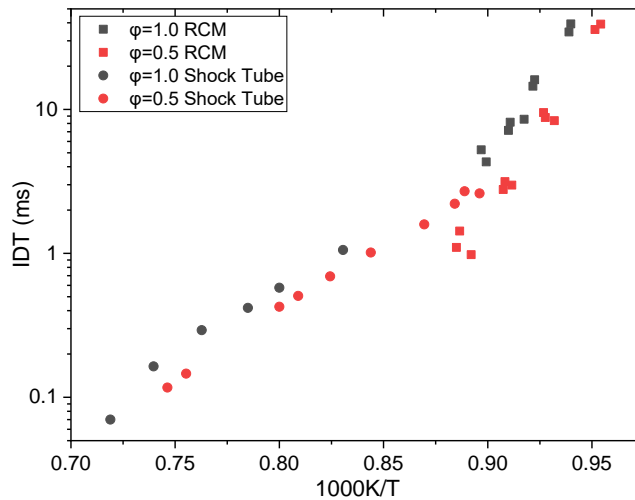
Figure 2.5. IDT data for 0.5% EL at φ=1.0 and 0.5 at 10 atm compressed pressure. Data taken from (160).

Howard et al. (37) measured the IDTs of a range of ethyl-based three-component blends in an IQT to determine their DCNs following the ASTM D6890 test method. The IQT was at a constant pressure of 21.37±0.07 bar, and the temperature was 545±30 °C (37, 141). The contour plot for the DCN of the ethyl-based blends can be seen in figure 2.6. Blends with high DEE fractions had shorter IDTs since DEE is highly reactive. IDTs for blends without DEE were >133 ms, which is much longer than a typical four-stroke cycle in an engine (37). However, the pressure in an IQT is much lower than the pressure in a CI engine at TDC, so in the context of a working engine, the IDT will be shorter.

- 32 -
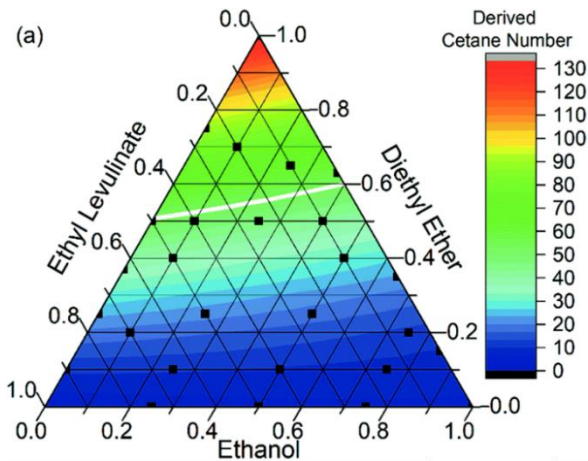
Figure 2.6. DCN of the ethyl-based blends. Symbols were the blend compositions tested. White line corresponds to a DCN of 54. Reproduced from (37).

The IDTs ranged from 2.73 – 139.72 ms, including the measurement of binary blends of the ethyl-based components. For the three-component blends tested, the IDTs ranged between 2.91 – 101.04 ms (37). The shortest IDT was for the blend of 10 mol% EtOH/70 mol% DEE/20 mol% EL and the longest was for 75 mol% EtOH/10 mol% DEE/15 mol% EL (37). The high DEE fractions used to produce blends with IDTs that correlate to DCNs of >51 would result in three-component blends with a flash point that would be non-compliant with any fuel standard (12, 37). The high volatility of DEE may be an issue for fuel storage and handling, in addition to the operation of an engine (37).

Howard et al. (55) measured the IDT temperature dependence for a blend of EL, DEE, and EtOH with a research octane number (RON) of 95 which was designed to replicate a typical gasoline. The composition of this blend was 38 mol% EtOH/ 27 mol% DEE/ 35 mol% EL. This blend was tested at equivalence ratios (φ) of 1.0 and 0.5 and 20 bar and 40 bar. Their results are shown in figure 2.7. They found that the high volatility of DEE caused losses of DEE, and the high boiling point of EL would cause condensation on the RCM walls (55). The tests at 20 bar show that the IDTs are non-Arrhenius with a negative temperature coefficient (NTC) region, which is where IDTs increase as temperature increases, as shown in figure 2.7. This was likely to be due to the presence of DEE and EtOH since EL does not show an NTC, as seen in figure 2.5. The NTC is due to the increased HO_2 elimination from RO_2 and QOOH species, which also forms stable alkenes effectively terminating the chain reactions. HO_2 radicals are less reactive than OH and can form H_2O_2 at these intermediate temperatures, which slows the chain branching reactions giving longer IDTs. As temperatures increase further, the rate of the H_2O_2 decomposition increases to form two OH radicals, which creates chain branching pathways (37, 55, 159, 161, 166, 169).
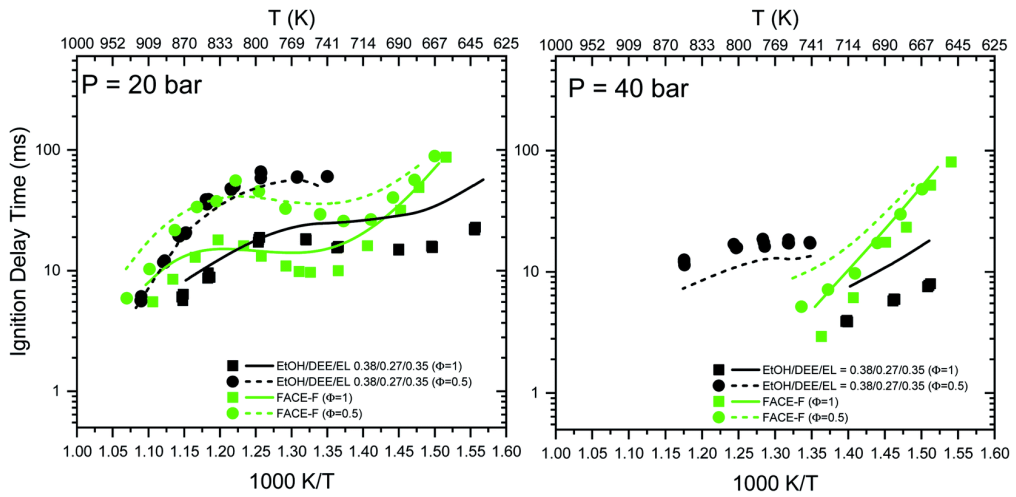
Figure 2.7. IDTs at 20 and 40 bar for a blend of EL/DEE/EtOH with their mole fractions shown in the graph legend, along with their corresponding equivalence ratios, compared to a FACE-F gasoline. Reproduced from (55).

Although the blend tested by Howard et al. (55) was not representative of a diesel-like formulation, as it was a RON 95 blend, the NTC behaviour may be present in blends with high DEE fractions. Issayev et al. (161) demonstrated that for 50 mol% EtOH/50 mol% DEE blends there would be an NTC, as shown in figure 2.8. They showed that DEE would produce an NTC, indicating that it would be likely for three-component ethyl-based blends with high DEE fractions to have an NTC (170, 171).
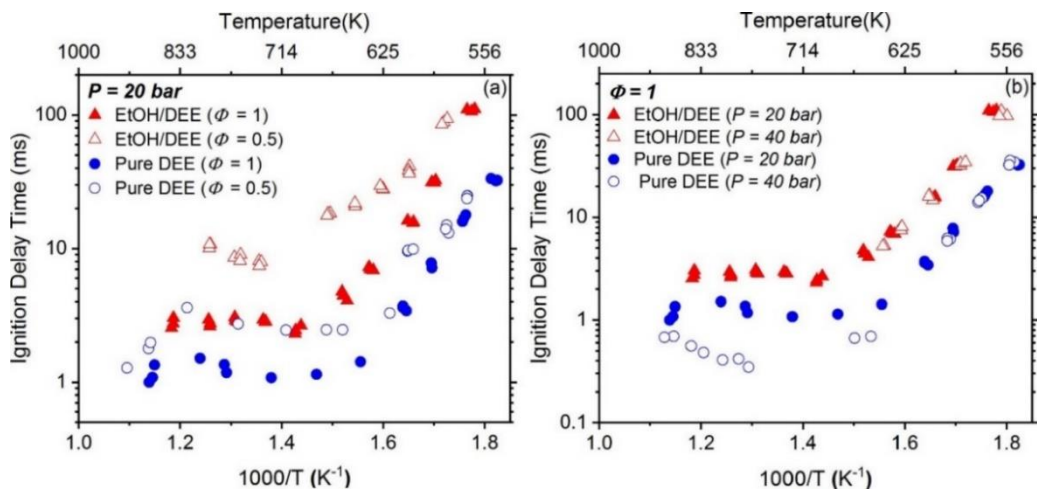
Figure 2.8. IDTs measured by Issayev et al. (161) for EtOH/DEE 50/50 mol% and pure DEE, with (a) for different equivalence ratios and (b) for 20 bar and 40 bar.

Comparing IDTs in figures 2.7 and 2.8, it is evident that the introduction of EL and the reduced DEE fraction increased the IDTs. The longer IDTs of the blend with EL correlate with the reduction in the blend's DCN since EL has a low DCN (143). However, these are IDTs of homogeneous gaseous mixtures, and the IDT in an engine may also be affected by the liquid's physical properties. The influence a longer IDT can have on engine performance and emissions is discussed in section 2.9.

During the RCM experiments, Issayev et al. (161) observed three-stage ignition at lean conditions for DEE and the DEE/EtOH blends, as shown in figure 2.9, which are relevant to CI engine applications. However, the temperatures (566 and 606 K) were lower than the temperatures at TDC in a CI engine, which typically are >900 K (5). There could be a benefit of the multi-stage ignition in a blend containing fuels with a low reactivity, as it may induce ignition at lower temperatures as there would be an increase in pressure.
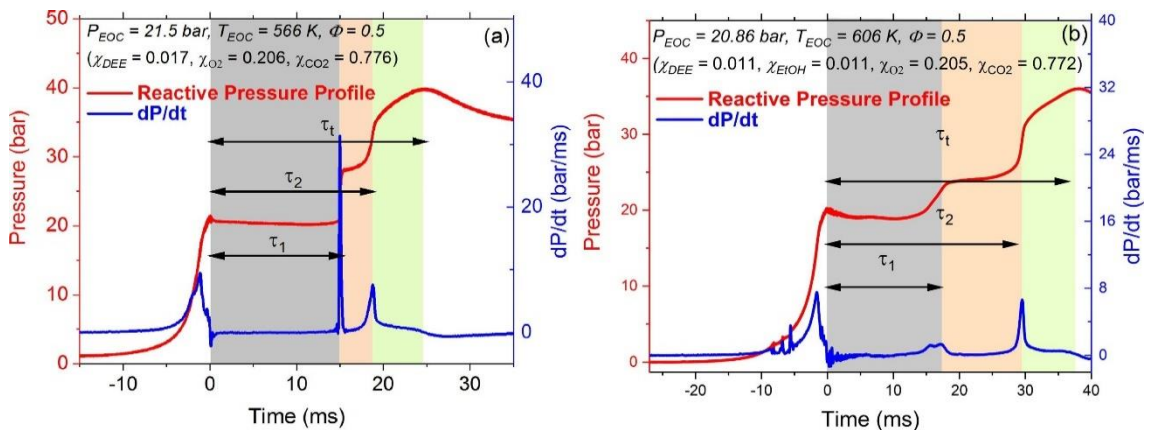
Figure 2.9. Experimental RCM pressure traces showing three-stage ignition. (a): DEE and (b) for DEE/EtOH blends. Reproduced from (161).

2.7.4.3 Combustion Properties of Butyl-Based Blend Components

There have been no fundamental studies of the combustion of BL or compositions of the butyl-based three-component blends of interest in this work. There have been studies of BuOH combustion at engine-relevant conditions, whereas, for DNBE, there is a lack of such studies.

Hakimov et al. (158) measured IDTs of DNBE in an RCM at 550 – 650 K at 10, 20, and 40 bar and in a shock tube at 900 K – 1300 K, at 20 and 40 bar, both studies using φ=1.0 and φ=0.5. The IDTs had non-Arrhenius behaviour in the RCM as there is a slight curvature in the IDT temperature dependence as the temperature increases, particularly at 10 bar and φ=0.5 (158). The shock tube measurements show an NTC region at 950 – 1050 K, which was more pronounced at 40 bar. There was also evidence of pressure dependence as the IDTs decreased as the pressure went from 20 bar to 40 bar (158).

Hakimov et al. (158) detected multi-stage ignition for DNBE, similar to DEE. Two-stage ignition was detected in the RCM for φ=1.0 at 20 bar and all temperatures, and T<600 K for 40 bar. This temperature is below typical compressed temperatures in a CI engine, and the two-stage ignition may not occur at higher temperatures. For stoichiometric blends at 10 bar, there was three-stage ignition, matching the number of stages of DEE. At lean conditions, DNBE exhibited four-stage ignition, as there were three clear maximum dp/dt events. Hakimov et al. (158) defined the fourth ignition as

when the maximum pressure was reached, as there was a gradual pressure rise after the third ignition (158). The use of maximum dp/dt to define the ignition was used by Yang et al. (141) for IDT measurements of diesel using an IQT. Using such a definition ensures that bulk ignition has occurred and not low temperature heat release, which can occur for fuels with multi-stage ignition (141). This definition would also be favourable to use in an engine for the same reasons. Multi-stage ignition may affect engine stability, as there may be a sudden temperature and pressure rise, which will cause the other fuel components to ignite at higher thermodynamic conditions, increasing the temperature and pressure further, akin to pre-ignition in a SI engine (172, 173). This may lead to damage of the piston. In contrast, in the RCM experiments of Zhong and Han (174) using DNBE at φ=0.7, 1.0, and 1.7, temperatures between 525 – 725 K, and compressed pressures of 7 and 10 bar, only two-stage ignition was observed. They used more dilute mixtures at φ=1.0 and a pressure of 10 bar, compared to Hakimov et al. (158). Using these dilute mixtures may have resulted in the inability to observe the third ignition stage. Additionally, these diluted mixtures and the conditions used are not representative of CI engine applications.

n-Butanol was tested by Weber et al. (175) in an RCM at 15 and 30 bar, with compressed temperatures of 675 – 925 K and φ=0.5, 1.0, and 2.0. At 30 bar, there were no lean tests, and these would have been the most relevant condition to a CI engine. At 15 bar, the IDTs became shorter as the equivalence ratio increased, as expected since more fuel was available to react and undergo autoignition (175). The increase in pressure for the stoichiometric condition decreased the IDTs. For example, at 740 K, the IDT at 30 bar was around 12 ms, whereas, at 15 bar, it was approximately 50 ms (175). At these temperatures, the IDTs had Arrhenius behaviour. However, Heufer et al. (176) showed that at temperatures between 770 K and 1000 K and pressures of 18 – 22 bar, there was non-Arrhenius behaviour and an NTC in this region. At temperatures >1000 K, the IDT behaviour was Arrhenius, which is typical at these higher temperatures (56, 165, 171, 177-180). If there were local high temperature regions in a cylinder there would be short IDTs and local ignitions. This would be unfavourable in a CI engine as premixed combustion is only a small fraction of the total combustion.

n-Butanol was also tested by Agbro et al. (162) in the Leeds RCM at 20 bar, at compressed temperatures of 650 – 850 K, and φ=1.0. They found that the IDTs had an Arrhenius behaviour in this temperature regime, which is in agreement with Weber et al. (175). Agbro et al. (162) also demonstrated that the hydrogen abstraction from the carbon adjacent to the OH group reduced the overall reactivity and caused the IDTs to be longer. The stoichiometric conditions tested are not fully relevant to CI engine operation as a CI engine typically operates under lean conditions. Additionally, CI engines typically operate with compressed pressures higher than 20 bar.

2.7.4.4 Influence of Advanced Biofuels on the CN and DCN

The CN and DCN are indicative of a fuel's IDT. The CN is defined as a ratio of cetane and 2,2,4,4,6,8,8-heptamethylnonane, which has the same IDT as the test fuel (5, 143). When an IQT is used to measure IDT, the value can be used to give the DCN as they are correlated. The IQT method is suitable for determining DCNs between 33 – 60 (181).

Since DEE has a DCN >125, it would be expected that the DCN of blends of diesel and DEE would increase since diesel has a CN of around 51. However, Górski and Przedlacki (129) found that the CN did not increase significantly with increasing fractions of DEE, as it increased from 51.1 to 53.8 with 20 vol% DEE (129). This may be due to the high volatility and low autoignition temperatures of DEE making CN measurements more difficult.

Raspolli Galletti et al. (54) reported DCNs of the three blends previously discussed (section 2.7.1) without diesel as 37.1, 63.5, and 39.6 for mixA, mixB, and mixC, respectively, but it was unclear if these were measured or calculated. Frigo et al. (38) also measured and calculated the DCNs of the blends they used in their engine testing, discussed in section 2.8.4. They reported that the DCN decreased as the BL fraction increased, as expected since BL has a DCN of 14 (143).

2.7.4.5 Influence of the Fuel Properties on Ignition

Since CI engines rely on the autoignition of the injected fuel, physical and chemical processes affect the total IDT. CN and DCN measurements account for both the physical and chemical delay as they involve fuel injection (88, 119). However, RCM and shock tube measurements only account for the chemical delay as they use a homogeneous gaseous mixture (159). The physical processes following fuel injection in a CI engine include atomisation, vaporisation, and droplet breakup. These are influenced by the fuel's properties including density, kinematic viscosity, enthalpy of vaporisation, and heat capacity (88, 119). Therefore we would expect the physical properties of the chosen biofuel mixtures to influence the chemical and physical components of the IDT on blending with diesel.

Kim et al. (88) investigated the influence of different physical properties on IDTs and spray characteristics under diesel-relevant conditions by simulating the spray and ignition using CFD. The Reynolds Averaged Navier Stokes equations and a series of physical and phenomenological models were used to model the spray. Sensitivity analysis of each property's influence on the IDT was conducted at 900 K and 750 K (88). The perturbations used were the minimums and maximums of individual hydrocarbons commonly found in diesel. For example, the viscosities of iso-cetane and heptane were

used as the maximum and minimum viscosity values, respectively. The sensitivity analysis demonstrated that density and heat capacity were the most influential properties affecting IDTs (88). There was a correlation for both of these properties, such that the reductions gave shorter IDTs and increases gave longer IDTs. An increase in heat capacity increases the energy required to heat the liquid and vaporise it. Higher densities gave longer IDTs due to a reduced fuel injection velocity, which reduced turbulent mixing, delaying low temperature heat release before ignition (88).

Barraza-Botet et al. (119) determined physical and chemical delay contributions to the total IDT for iso-octane and EtOH blends. They used an IQT and a rapid compression facility to determine the total and chemical IDT, respectively. They found that the physical delay ($\tau_{mix}+\tau_{evap}$) contributed most to total IDT and that as temperature increased, the chemical delay time (τ_{chem}) as a fraction of total IDT decreased, as shown in figure 2.10.
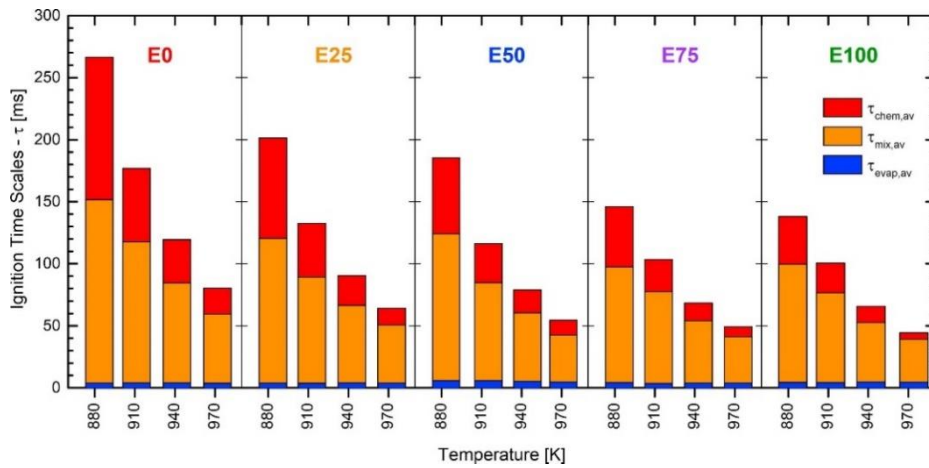
Figure 2.10. Summary of the physical and chemical delay times ethanol/iso-octane blends at different initial charge temperatures. Reproduced from (119).

The kinematic viscosity of the ethanol/iso-octane blends increased with increasing ethanol fraction, which Barraza-Botet et al. (119) stated reduced the turbulent mixing. In contrast, Kim et al. (88) showed that the viscosity had no impact on the IDT. Since all the individual processes cannot be separated when using the methods of Barraza-Botet et al. (119), there may be synergistic effects of the changes in all properties that change the physical and chemical delay times. Barraza-Botet et al. (119) also demonstrated the charge-cooling effect of ethanol, where the fuel vaporisation reduced the pressure and temperature in the IQT. The amount of charge cooling is governed by fuel component's the enthalpy of vaporisation and heat capacity. Therefore, with higher ethanol fractions, there was more charge cooling as it has a higher enthalpy of vaporisation and heat capacity (119). As a result, lower local temperatures occur, which reduce the reactivity if there is no NTC, and it may increase the mixing times due to a slower vaporisation of the fuel. However, this was not the case for the blends shown in figure 2.10, where the evaporation time was similar regardless of the ethanol fraction (119).

The addition of ethyl and butyl-based three-component blends to diesel will change the physical properties of diesel, and this will influence the IDT. Therefore, it is vital to understand the influences of the different physical and chemical properties on ignition. However, this work aims to find blends that comply with the physical property limits and hence the blends studied should in theory minimise such influences. This will be tested in Chapters 4, 5, and 6.

2.8 Blending Rules and Physical Property Models for Fuel Blends

Since there are many potential biofuel blend compositions from alcoholysis, the ability to predict the physical properties would improve the efficiency of optimal fuel blend development. This would reduce the need for testing. Many physical properties of a known composition can be predicted using blending rules. However, their suitability for accurately predicting the properties of different advanced biofuel blend compositions needs to be assessed. The physical properties of interest in this work are the density at 15 °C, KV40, and the flash point, as previously discussed (section 2.7). Other properties, such as the DCN, can also be predicted using blending rules.

2.8.1 Linear Blending Rules

Linear blending rules are the simplest blending rules and have the general form of:

$$\text{property}_{\text{mix}} = \sum_{i}^{n} f_i \alpha_i \qquad \textbf{Equation 1}$$

where $\text{property}_{\text{mix}}$ is the calculated value for the property of interest, and f_i is the fraction of the ith blend component. f_i can be mass, mole, or volume fraction and it depends on the property being predicted. α_i is the value of the property for component *i*. The drawback of using linear blending rules is that they require the properties of each component to be known.

2.8.1.1 Linear Blending Rule for Density Predictions

One of the most commonly used linear blending rules is Kay's mixing rule for density predictions. Here α_i in equation 1 would be the density of component *i* and f_i would the volume fraction of component *i* (182, 183). It is not confirmed if this would be suitable for predicting the density of novel three-component advanced biofuel blends or if blend-specific blending rules would be needed.

2.8.2 Blending Rules and Models for Flash Point Predictions

Flash point models of multi-component blends are available. As the understanding of how intermolecular interactions between different blend components affect the flash point has increased, these models have become more complex and accurate (184, 185). Some models use blend indices, but these are typically for ideal mixtures or hydrocarbon blends (184, 185). The models that use blend indices use a linear blending rule for the calculated blend index. The index can be calculated from a range of different expressions specifically designed for hydrocarbons, indicating that they are unlikely to be suitable for predicting the flash point of blends of oxygenated species (184, 185).

The Catoire and Liaw models are well-established models for predicting flash points of blends (121, 186-194). The Liaw model (equation 2) is the most used flash point model due to its applicability to non-ideal mixtures. It uses Le Chatelier's rule to determine the lower flammability limit of the vapour and the contribution to total saturated vapour pressure from each component (186-191):

$$1 = \sum_i^n \frac{x_i \gamma_i p_i^{sat}}{p_{i,fp}^{sat}}$$ **Equation 2**

where x_i is the mole fraction of component *i* in the liquid phase, γ_i is the activity coefficient, p_i^{sat} is the saturated vapour pressure of component *i*, and $p_{i,fp}^{sat}$ is the saturated vapour pressure of component *i* at its flash point (186-191). γ_i is determined using activity coefficient models and p_i^{sat} is determined using the Antoine equation (186-191). Equation 2 would be solved iteratively, increasing the temperature and determining p_i^{sat} until the summation equals one.

The activity coefficients can be calculated using a range of models, with the most accurate models being the Universal Quasichemical Functional-group Activity Coefficients (UNIFAC) and the modified UNIFAC models (194-198). These use group contribution methods to determine the activity coefficients whilst accounting for intermolecular interactions, the blend composition, and the thermodynamic conditions. Hence, these also need to be calculated at every temperature with each iteration. Accurate and up-to-date versions of the UNIFAC models are often expensive or not easily accessible. Liaw and Yang (199) demonstrated that using the modified UNIFAC model resulted in a more accurate prediction of the flash points of a ternary mixture of phenol/cyclohexanol/benzyl alcohol compared to the standard UNIFAC model. For example, the predicted flash point of 15 mol% phenol/85 mol% benzyl alcohol was 97.7 °C, and the measured value was 98 °C (199).

Huo et al. (200) demonstrated the accuracy of the Liaw model for n-butanol and n-hexanol blended with diesel using an average molecular structure for diesel rather than

using a detailed composition. The predictions had an average absolute relative deviation of 2.5% and 0.8% for blends of diesel with n-butanol and n-hexanol, respectively. Álvarez et al. (201) demonstrated that for ethanol/diesel/biodiesel and butanol/diesel/biodiesel blends, the Liaw model with the UNIFAC model for activity coefficients had varying accuracy. There were under-predictions of up to 7 °C and over-predictions of up to 5 °C. These inaccuracies could result in a compliant blend being deemed non-compliant or a non-compliant blend being used due to an over-predicted flash point (201).

The Catoire model has the form:

$$T_{fp} = 1.477 \times T_{eb}^{0.79686} \times \Delta H_{vap}^{\circ \; 0.16845} \times n^{-0.05948}$$

Equation 3

where T_{fp} is the flash point temperature (K), T_{eb} is the normal boiling point (K), ΔH_{vap}° is the standard enthalpy of vaporisation (kJ/mol), and n is the number of carbon atoms in the vapour phase (194). The normal boiling point is calculated as the temperature at which the partial pressure p_i equals 1 atm, and each component's partial pressure is calculated using equation 4:

$$p_i = x_i \gamma_i p_i^{sat}$$

Equation 4

The activity coefficients are typically calculated using the UNIFAC method to ensure accurate prediction (194). However, the Catoire model accuracy decreases for non-ideal mixtures, as shown by Catoire et al. (194). For example, the mean absolute deviation between predicted and experimental measurement for blends of n-octane/ethanol was 2.3 °C, with larger differences at higher n-octane mole fractions, whereas for n-octane/butanol blends it was 0.8 °C (194). This same assessment was the justification Álvarez et al. (201) used for opting for the Liaw model when predicting flash points of alcohol/biodiesel/diesel blends.

The use of the Liaw and Catoire models are hindered by requiring access to the UNIFAC models, and they can be computationally expensive since there are multiple models for each parameter. The sub-models are not always accurate at capturing all the intermolecular interactions in a ternary system (184). This indicates a need for empirical flash point models for novel three-component systems, especially when the flash point has significant implications for the safe use and handling of such mixtures.

2.8.3 Blending Rules for Viscosity Predictions

Blending rules are well established for predicting the viscosity of binary blends. They are usually blend specific, but can be developed for non-ideal mixtures as interaction coefficients account for non-ideal mixing (122, 202-205). In addition, there are blending laws used in oil refineries, but they have large errors (20 – 50%) associated with them (206). These large errors could result in the use of blends that are outside of

the limits of the fuel standards. The blending rules commonly used in refineries use dynamic viscosity. However, this can be converted to kinematic viscosity due to the relationship between the two. One blending rule is for liquid hydrocarbons (equation 5), and one is for liquid non-hydrocarbons (equation 6) (206):

$$\mu_{mix} = \left(\sum_i^n x_i \mu_i^{1/3} \right)^3 \qquad \textbf{Equation 5}$$

$$\ln \mu_{mix} = \sum_i^n x_i \ln \mu_i \qquad \textbf{Equation 6}$$

where μ_{mix} is the mixture viscosity in cP (centipoise), x_i is the mole fraction of component *i,* and μ_i is the viscosity of component *i*. The Chevron blending rule (equations 7 and 8), is one of the simplest available and it uses a blend index method. This can be used to predict the kinematic viscosity for blends of non-hydrocarbons:

$$\text{BI}_{\text{vis,i}} = \frac{\log_{10} \nu_i}{3 + \log_{10} \nu_i} \qquad \textbf{Equation 7}$$

$$\text{BI}_{\text{mix}} = \sum_i^n x_i \text{BI}_{\text{vis,i}} \qquad \textbf{Equation 8}$$

where $\text{BI}_{\text{vis,i}}$ is the blend index for the viscosity of component *i, ν_i* is the kinematic viscosity of component *i*, and BI_{mix} is the blend index for the blend's viscosity. The mixture blend index then needs to be used in a rearranged equation 7 to determine the blend's kinematic viscosity. These models rely on knowing the viscosity of each component for a given temperature and assume ideal mixture behaviour (206). This may not be the case for the biofuel components of interest in this work due to the polar nature of the biofuel components. Additionally, in the biofuel blends, there may be intermolecular interactions that affect viscosity (207).

Hernández et al. (208) showed that the Chevron blending rule had an error of 27% when predicting the viscosities of biodiesel/diesel blends, which is in agreement with the range stated by Riazi (206). Centeno et al. (209) also demonstrated that the Chevron blending rule over-predicted the viscosity for blends of diesel/naphtha, vacuum gas oil/ naphtha, and vacuum gas oil/diesel, with a greater over-prediction at higher viscosities where the standard error between prediction and measurement increases.

For predicting the viscosity of binary mixtures, the most used blending rule is the Grunberg-Nissan equation, as typical studies of advanced biofuels use binary blends (122, 202, 203, 207, 210, 211):

$$\ln \nu = x_1 \ln \nu_1 + x_2 \ln \nu_2 + x_1 x_2 G_{12} \qquad \textbf{Equation 9}$$

where x_1 and x_2 are the two components' mole fractions, ν_1 and ν_2 are their kinematic viscosities, and G_{12} is the interaction term. The value of G_{12} depends on the

components in the mixture. There are values of G_{12}, or empirical equations available to determine G_{12}, for different alcohols in alcohol/diesel mixtures (122). Lapuerta et al. (203) demonstrated that for butanol/diesel and ethanol/diesel blends, the Grunberg-Nissan equation could predict the viscosity with model fit R^2 values of 0.9894 and 0.9510, respectively. For butanol/diesel blends, the Grunberg-Nissan equation slightly under-predicted the viscosity between 20 and 50 vol% butanol, but matched experimental measurements for the other fractions. For ethanol/diesel blends, there were over-predictions with <20 vol% ethanol and under-predictions for >20 vol% ethanol.

For multi-component blends where there are interactions, there are no established models. The blends of the advanced biofuel components of interest in this work are likely to have intermolecular interactions between the oxygen-containing functional groups. These interactions would need to be captured in a blend viscosity model. Therefore, there is a need to develop empirical viscosity models to predict the viscosities of three-component blends.

2.8.4 Blending Rules for DCN Predictions

It is common to use linear blending rules for predicting the CN and DCN of blends, with linear-by-mass, mole and volume all used (38, 143, 212). A linear-by-mole approach was used by Dahmen and Marquardt (212) when formulating biofuel blends. However, the accuracy was not reported. The CN measurement standard states that a linear-by-volume approach must be used when calculating the CN of a cetane and 2,2,4,4,6,8,8-heptamethylnonane blend used as the primary reference fuel to match the IDT of the test fuel in CN measurements (143). Frigo et al. (38) used a linear-by-mass blending rule to predict the CN for blends of 7, 11, and 13 vol% BL with 4 vol% DNBE with the remainder being diesel. The predicted CNs were 48.9, 47.3, and 46.4 for the 7, 11, and 13 vol% BL blends, respectively (38). Frigo et al. (38) applied the methodology of Hardenberg and Hase (213) to their engine data to calculate CNs. They were determined to be 48.0, 46.5, and 45.4 for the 7, 11, and 13 vol% BL, respectively (38). Therefore, there was an over-prediction of around 2% for the linear-by-mass calculation. This accuracy may be fuel blend dependent, since for fuels such as DEE that are highly reactive and have very high DCNs, calculated and measured DCNs may differ greatly (129).

After determining the DCN for a range of ethyl-based blends using an IQT (following ASTM D6890), Howard et al. (37) produced a predictive model for the DCNs of the ethyl-based blends tested in this work. The model consisted of a cubic equation without interaction terms. The inputs required were each component's DCN, the mole fraction of each component and three coefficients per component determined using linear regression (37). This methodology could be used to produce models for other physical and chemical properties. However, interaction terms may be needed. Their work

demonstrated that accurate models for predicting the DCN of oxygenated blends are needed (37). The DCN model of Howard et al. (37) is blend specific, but using linear regression to produce models for other properties could be a suitable methodology for this work.

2.9 CI Engine Testing and Emissions Analysis of Diesel and Biofuel Blends

The use of biofuels in CI engines has been an ongoing research area for decades. There have been studies of alcohols, ethers, and levulinates as biofuel candidates, individually and as mixtures, with and without diesel (5, 214). Due to a lack of second-generation pentanol, its utilisation as an advanced biofuel in the near term is unlikely. Therefore, PL and DNPE produced from alcoholysis would have a high carbon intensity if fossil-derived pentanol was used. Thus, the pentyl-based blends would not be low-carbon alternatives to diesel. However, second-generation butanol and ethanol can be produced and the ethyl and butyl-based blends may suitable low-carbon alternatives to diesel and this will be investigated in the work of this thesis.

2.9.1 Engine Tests using Alkyl Levulinates

The effects on engine performance and emissions of EL and BL have been previously studied by several research groups. Table 2.9 summarises the changes in emissions and performance due to blending levulinates with diesel or heptane in these studies. The influence of their chemical and physical properties on the key emissions are discussed. There is evidence that the PM emissions are favourably reduced with the use of EL and BL, but their low DCNs influence the CO and THC emissions, and IDTs.

Christensen et al. (13) tested blends of 10 vol% EL/90 vol% diesel and 20 vol% BL/80 vol% diesel in a 6.7 L, 6-cylinder, 244 kW Cummins ISB engine fitted with a DOC and DPF. The tests followed the federal test procedures for heavy-duty diesel transient cycle tests. This engine is more powerful than the 5.7 kW Yanmar L100V engine used in this work. The operating conditions, such as the CR and engine speed, may affect emissions and engine performance when using the fuel blends. Due to the low DCNs of EL and BL, Christensen et al. (13) added 2-ethylhexyl nitrate (2-EHN) as a cetane enhancer, with 792 ppm and 1584 ppm in EL and BL blends, respectively. The THC and CO emissions were below the detection limits of the flame ionisation and non-dispersive infrared (NDIR) detectors due to the DOC. The NO_X emissions from the EL blend were unchanged, with one potential reason being that the DCN was maintained. Therefore, there was likely to be no increase in pre-mixed combustion. However, with 20 vol% BL, the NO_X emissions increased by 4.5%. This increase may be due to the increased oxygen content making the fuel/air mixture leaner, favouring NO_X formation (13). The

large reductions in PM seen are likely not just due to the presence of the oxygen within the fuel molecule itself, but also potentially due to the molecular structures of EL and BL not favouring soot precursor formation (24, 47, 50, 215, 216). The ester and ketone functional groups in a fuel molecule can reduce the yield sooting index (YSI), as demonstrated by Pepiot-Desjardins et al. (52) and Gao et al. (217). The YSI is the soot volume fraction of a non-premixed methane/air flame where the fuel is doped with a test fuel (218). The presence of the ester functional group had a greater reduction in the YSI relative to the hydrocarbon equivalent, as Gao et al. (217) showed that methyl heptanoate has a YSI of around 32, whereas octane has a YSI of around 42.

Christensen et al. (13) reported that 10 vol% EL in diesel increased BSFC by 5.1%, which was expected as the blend had a 4.3% reduction in the LHV compared to diesel. The 20 vol% BL blend increased BSFC by 7.6% and reduced the LHV by 7.1% (13). The engine was not optimised to account for the extra oxygen present or the change in LHV. However, the fuel blend's DCN was similar to, or above that, of the diesel used (13).

Koivisto et al. (152) tested both EL and BL blended with 30 wt% n-heptane as a CN enhancer to ensure there was an ignition of the levulinates. They used a single-cylinder, naturally aspirated engine. The engine tests were conducted at 1200 rpm, 4 bar indicated mean effective pressure (IMEP), with a 600 bar injection pressure, and intake air preheated to 120 °C (152). Preheated intake air increases in-cylinder temperatures, promoting autoignition of the levulinates with their low DCNs (143, 152).

The increase in IDT relative to diesel was greater for EL, compared to BL. The increases in IDT were 2.3 and 1.7 CAD for EL and BL, respectively. This was expected since EL has a DCN of 6 compared to 14 for BL (143, 152). The longer IDT for the EL/heptane blend resulted in a 57% increase in the premixed combustion phase duration relative to diesel, whereas the BL/heptane blend had a 0.5% reduction. The engine efficiency decreased from 45.6% with diesel down to 44.3% for the EL blend and 33.7% with the BL blend. Koivisto et al. (152) reported there were sources of large uncertainty when measuring the fuel flow rates to the injector and the injector leakage, resulting in large uncertainties in the calculated efficiency.

Koivisto et al. (152) reported that EL had lower NO_X emissions than BL, but both had an increase relative to diesel, which was unexpected. They reported that the long premixed combustion phase of EL caused a lower temperature before heat release, reducing thermal NO_X. However, the greater increase in NO_X for the BL blend does not fit the trends for the valeric esters and ketones tested by Koivisto et al. (152), where the increasing carbon chain length reduced NO_X emissions due to shorter IDTs reducing premixed combustion and preventing too lean a fuel/air mixture forming (13).

Koivisto et al. (152) measured the PN using a Cambustion DMS500. The particulate mass per cubic centimetre was determined from the PN, where Koivisto et al. (152) used the particle density of 1.77 g/cm^3 determined by Park et al. (219). The mass of particulates was reduced relative to diesel for EL and BL blends, with reductions of 62.5% and 75%, respectively (152). In contrast, the PN from EL and BL blends increased relative to diesel, with both fuel blends giving similar values of PN, above 5×10^8 #/cm^3, compared to the diesel emissions of just above 1×10^8 #/cm^3 (152). This increase in PN may be due to the production of smaller particles and fewer larger agglomeration particles since the addition of EL and BL reduced the mass of PM. This supports the finding of Christensen et al. (13), where the fuel smoke number (FSN) reduced.

Wang et al. (128) tested blends of 5, 10, 15, and 20 vol% EL with diesel. The blends of 15 and 20 vol% EL needed 2 and 5 vol% of n-butanol as a co-solvent to ensure there was no phase separation of the blends. They used a 1093 cc (cubic centimetre), water-cooled, 14.7 kW, single-cylinder engine (128). Unlike Christensen et al. (13), Wang et al. (128) did not add a CN enhancer. Their tests were conducted at 1200 RPM, which was not the most efficient engine speed for all loads tested, and the engine ran below maximum power. Both of these will have an impact on the emissions. The tests followed the procedure in China VI legislation, and the weighting factors were applied to determine emissions factors.

Wang et al. (128) found that EL increased BSFC by up to 10% at the different loads tested. Due to the 5 vol% BuOH, the 20 vol% EL blend had less of an increase than the 15 vol% EL blend with 2 vol% BuOH (128). This increase in BSFC was uniform across the entire engine loads tested and would have been due to the decreased energy density on the addition of EL. The changes in the NO$_X$ emissions were variable. Over all powers tested, the blends with 15 and 20 vol% EL had an increase in NO$_X$ emissions, whereas with 5 and 10 vol% EL blends, NO$_X$ increased at less than 3 kW and decreased above 4 kW (128). This behaviour indicated that at high powers, and for the blends with higher EL fractions, there were higher combustion temperatures. This was reported to be due to there being more complete combustion with the higher oxygen content and increased premixed combustion due to longer IDTs (128). These elevated combustion temperatures compete with the influence of the blend's reduced calorific value, and the high enthalpy of vaporisation of EL, which reduces the temperature. The cooling may have a greater effect at higher powers for the 5 and 10 vol% EL blends, where more fuel is injected. The CO emissions were unchanged at lower powers, but at the three highest powers, there were increases of up to 30% (128). These increases were due to the engine speed not being the most efficient speed for these loads. The smoke opacity was reduced at the higher powers for the blends with higher EL fractions, as expected due to PM reducing upon the addition of oxygenated biofuels (24, 47, 50, 128, 215, 216).

Table 2.9. Summary of alkyl levulinate blends engine tests and their changes relative a diesel baseline.

Fuel Blend	Engine Used	Power or Load	ΔCO	ΔHC	ΔNOₓ	ΔPM	ΔSmoke	ΔPN	ΔIDT	ΔBSFC	ΔEfficiency	Comments	Ref.
10% EL/90% diesel	6700 cc, 330 horsepower, turbocharged, direct injection Cummins ISB		Below detection limits	0%		-41%			No change	5.00%		Fitted with a DPF and DOC	(13)
20% BL/80% diesel				4.50%		-55%				8.00%			
70 wt% EL/30 wt% n-heptane	499.56 cc, 18.2:1 CR, direct injection, single-cylinder	4 bar IMEP			2%			380%	40%		-3%	363 K intake air, injection pressure of 600 bar, 1200 RPM	(152)
70 wt% BL/30 wt% n-heptane					10%			315%	30%		-25%		
5 vol% EL/95 vol% diesel	1093 cc, water cooled, 14.7 kW, 17:1 CR, single-cylinder	0.3 - 7.4 kW	-5%		-11%		-9%			12%		These are the changes in the emissions indices according to the China VI standard	(128)
10 vol% EL/90 vol% diesel			8%		-3%		-28%			12%			
15 vol% EL/83 vol% diesel/2 vol% BuOH			25%		6%		-46%			14%			
20 vol% EL/75 vol% diesel/5 vol% BuOH			0%		18%		-85%			14%			

2.9.2 Engine Tests involving Dialkyl Ethers

Tables 2.10 and 2.11 present summaries of the changes in engine performance and emissions from dialkyl ether engine tests reported by other research groups. These tables include the relative changes in the measured emissions including CO, THC, and NO_X, along with changes in IDT and BSFC. These changes indicate the influence of blending dialkyl ethers with diesel and other advanced biofuels.

2.9.2.1 Engine Tests of Diesel/DEE Blends

DEE has been suggested as a diesel biofuel blending component due to its miscibility with diesel and its high CN. Górski and Przedlacki (129) conducted tests of blends of 5, 10, 15, and 20 vol% DEE in diesel using an AD3.152 engine, which is a three-cylinder, 2502 cc, 34.6 kW CI engine. Blends with >20 vol% DEE had poor engine performance and struggled to start. This was due to the reduced viscosity of diesel/DEE blends and the high volatility of DEE, which caused vapour lock in the fuel lines. The presence of DEE vapours in the fuel line result in the fuel pump being unable to pump liquid fuel to the injector (129). Vapour locking must be considered when formulating the ethyl-based biofuel blends studied in this project.

The IDTs barely changed with increasing DEE fractions, and this was due to a combination of factors (129). DEE has a charge-cooling effect as it has a higher enthalpy of vaporisation than diesel, so although it is easily vaporisable it absorbs large quantities of heat as it vaporises (129). This results in lower in-cylinder temperatures delaying vaporisation of the remaining fuel. However, the high CN and low autoignition temperature of DEE favours a shorter IDT. Hence, Górski and Przedlacki (129) stated that these negate each other, maintaining the IDTs similar to diesel regardless of DEE fraction. No emissions were measured by Górski and Przedlacki (129).

There have been studies of DEE and EtOH as binary blends, with and without diesel. Sivasankaralingam et al. (220) tested DEE/EtOH blends with 75%, 50%, and 25% of DEE, with the remainder being EtOH, without diesel. 500 ppm of Lubrizol 539M lubricity additive was added to ensure the effective operation of the fuel pump and injectors (220). The addition of the additive demonstrates that reduced lubricity must be accounted for to ensure optimum engine operation.

Sivasankaralingam et al. (220) replaced the rubber tubing with Teflon tubing in their single-cylinder, turbocharged, 511 cc, AVL 5402 D12 engine due to DEE corroding the rubber fuel lines. Material compatibility is a key factor that must be considered for the utilisation of advanced biofuels, especially if they are to be drop-in fuels. An intake pressure of 1.5 bar and an injection timing of 20 CAD BTDC were needed for stable combustion (220). At an IMEP of 4 bar, the 50% DEE/50% EtOH blend had an IDT of 23

CAD compared to 8 CAD for diesel, whereas the 75% DEE/25% EtOH blend had an IDT of 10 CAD. This supports the findings of Górski and Przedlacki (129), as the higher DCN blend does not always have the shortest IDT, since the 50/50 blend had a DCN of 57 compared to the DCN of the diesel used being 48 (220). This delay was likely due to the lower viscosity of the fuel blends delaying the start of the dynamic injection timing. Therefore, if viscosity limits are met, there should be reduced detrimental physical effects on the injection timing, highlighting the importance of remaining compliant with existing fuel standards. There were no engine emissions measurements when using these fuel blends, but the work of Sivasankaralingam et al. (220) demonstrated that engines need to be modified for fuels that are non-compliant with the fuel standards.

Blends of DEE and EtOH, up to 10 vol% of each, in diesel were tested by Paul et al. (137) in a Kirloskar, water-cooled, 661 cc, 3.6 kW engine. They determined the changes in emissions, in-cylinder pressures, fuel consumption, and efficiency when using these fuels across six loads at 0.6 kW intervals. Paul et al. (137) did not make changes to the engine, nor did they add additives to compensate for the reduced viscosity and lubricity. The brake thermal efficiency (BTE) increased relative to diesel with 5 vol% DEE. However, for a blend of 10 vol% DEE/90 vol% diesel, the BTE decreased. This was reportedly due to the early combustion of DEE working against the remainder of the compression stroke, reducing the power generated. However, in the pressure crank angle traces presented, there was no sudden pressure rise before TDC, which may indicate that the ignition of DEE may not have occurred or be detectable during the compression stroke (137).

The in-cylinder pressure was more variable for the biofuel blends, especially at low power. The 10 vol% DEE/90 vol% diesel blend had the lowest in-cylinder pressure at all powers (137). The addition of EtOH improved the combustion stability at higher powers. At powers <1.8 kW, the 10 vol% DEE/10 vol% EtOH/80 vol% diesel blend had higher peak pressures and shorter IDTs than diesel (137). The reduction in density with the biofuel components was likely to improve fuel atomisation. This enhanced the mixing of air and fuel, which improved combustion, resulting in a greater pressure rise. At the lowest power (0.6 kW), the 10 vol% DEE/10 vol% EtOH/80 vol% diesel blend showed combustion instability, which may have been due to the high DEE fraction giving short IDTs and both components having a charge cooling effect (137).

The changes in emissions followed trends observed by others using DEE or EtOH (137). At powers <1.8 kW, there was a variation in CO emissions, as shown in figure 2.11, with some blends having higher CO emissions than diesel. It was only the 10 vol% DEE and 5 vol% ethanol/10 vol% DEE blends that had a reduction in CO at 0.6 kW (137). At higher powers, there was a reduction in CO, especially for blends containing DEE and

EtOH, where the availability of oxygen favours the oxidation of the fuel species to form CO_2 rather than CO (137). The highest reduction of CO came from the 10 vol% DEE/10 vol% EtOH/80 vol% diesel blend, with a reduction of 53% at 3.6 kW. NO_X emissions were reduced at powers <1.8 kW, and this was due to lower in-cylinder temperatures (137). At 3.6 kW, there were reductions in NO_X for all but two blends, the blends of 5 vol% DEE/95 vol% diesel and 10 vol% DEE/90 vol% diesel. These blends would have the highest DCN and reactivity, and when more fuel was injected at high power, the in-cylinder temperature increased. The greatest reduction came from the 10 vol% DEE/10 vol% EtOH/80 vol% diesel blend (137). The charge-cooling effect of ethanol reduced NO_X emissions at high power, since more fuel was injected. When the engine was at powers >1.2 kW, there was a reduction in the HC emissions, with the reductions being greater for the blends with EtOH and DEE (figure 2.11) (137). This reduction was due to more oxygen being available for complete combustion.
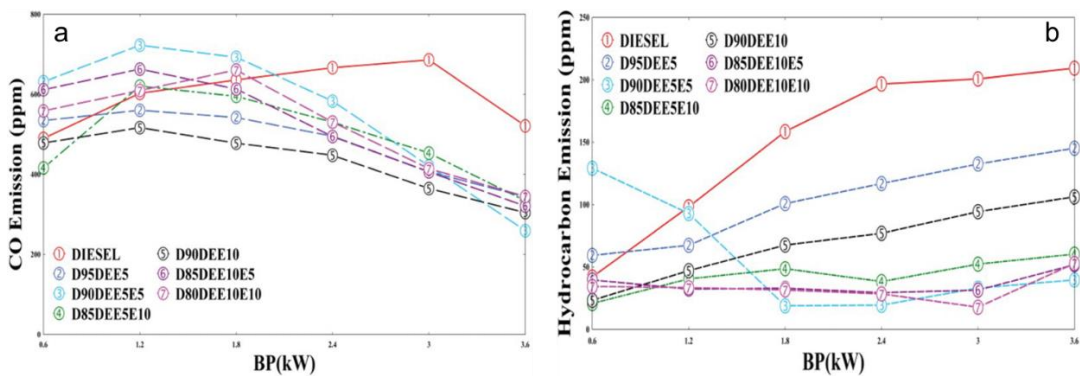
Figure 2.11. a: CO emissions and b: HC emissions of DEE and EtOH blended with diesel (D) reproduced from (137).

At powers >1.8 kW, the PM emissions reduced relative to diesel (137). This would indicate that there was more soot precursor oxidation and less particulate matter formed. Paul et al. (137) suggested that increased oxidation was possible due to an increase in OH radicals generated from the combustion of ethanol, which would be in agreement with the fundamental combustion of ethanol (137). As DEE increased in the blend, the reduction in PM increased. There was a 91% reduction in PM with the 10 vol% DEE/10 vol% EtOH/80 vol% diesel blend at full power (137). These changes were when using a non-optimal engine and fuel blends that do not comply with current fuel standards.

2.9.2.2 DNBE Engine Tests

DNBE is an attractive biofuel component for diesel as it has a similar carbon chain length to some alkane compounds in diesel (221). It has been tested with and without diesel to determine its suitability as a diesel replacement.

Heuser et al. (221) tested pure DNBE in a single-cylinder, 390 cc, 80 kW/L engine. Cooled EGR and fuel injection pressures of up to 2000 bar were used for low emissions

and high fuel efficiency. The high injection pressure matches those used in vehicle engines (5, 38, 59, 137). The regulated emissions were measured, along with the particle size distribution of the solid fraction of PM, as the exhaust gas was thermally conditioned at 350 °C to evaporate any volatile compounds. The conditions tested are displayed in table 2.10.

Table 2.10. Engine conditions used for the DNBE engine tests. Adapted from (221).

Load Point	IMEP (bar)	Load (%)	Engine Speed (RPM)	Injection Pressure (bar)	Inlet Pressure (bar)	Charge Air Temperature (°C)	Euro 6 Engine Out NO$_X$ Limit (g/kWh)
1	2.6	12	1200	350	1.05	27	0.2
2	4.3	19	1500	720	1.07	25	0.2
3	6.8	30	1500	900	1.50	30	0.2
4	9.4	42	2280	1400	2.29	35	0.4
5	14.8	66	2400	1800	2.60	45	0.6

Heuser et al. (221) modified the EGR rate to ensure NO$_X$ emissions were within the Euro 6 limits at each load. The NO$_X$ limits in table 2.10 were the engine out emissions that, with EGR, would result in tailpipe emissions compliant with Euro 6 (221). At lower loads, the EGR rates for DNBE needed to be increased relative to diesel, which increased the cooling. The PM emissions reduced with DNBE at all loads, with greater reductions at the higher loads where diesel produces high PM emissions. The reductions in PM also coincide with the reductions in HC and CO emissions across all loads, indicating there was more complete combustion (221). For all loads, the CO emissions from DNBE were reduced by more than 50%, whereas the HC emissions were only reduced by 5 – 10% relative to diesel (221). PM emissions were reduced at all loads, and the reduction in HC emissions reduced the agglomeration of soot precursors (221). The reduction in agglomeration particles was evident as there was more than double the number of particles with a diameter <23 nm (221). There was an unexpected particle size distribution for load point 3 (table 2.10), where DNBE had more particles with <50 nm in diameter. However, for this condition the PM for DNBE was around 25% of diesel PM emissions, indicating that the mass is dependent on particle size (221). The utilisation of DNBE as a diesel alternative could be a viable option if there was optimisation of the engine operational parameters, including injection pressures and EGR rates.

García et al. (222) tested blends of DNBE with 1-octanol. They used the same engine as Heuser et al. (221). These were tested at four of the conditions used by Heuser et al. (221), load points 2 – 5 in table 2.10. To ensure the NO$_X$ emissions were Euro 6

compliant and the combustion centre, the point at which 50% of the fuel is burnt, was kept constant, the injection timing and EGR rate were modified for each test. These modifications demonstrate that these fuels may not be suitable as drop-in alternatives.

The changes in the emissions for increasing DNBE fractions are load-dependent. At load points 2 and 3 (table 2.10), the HC emissions decreased as DNBE increased apart from 100% DNBE had similar HC emissions to the 50%/50% DNBE/1-octanol blend (222). As DNBE and 1-octanol are isomers of each other, they have the same oxygen content, which maintains the oxygen available for oxidation. However, the engine tests with DNBE had a lower in-cylinder temperature, reducing oxidation. In contrast, at load points 4 and 5, the engine-out HC emissions increased as DNBE fraction increased due to reduced premixed combustion, as IDTs were shorter. At load points 2 and 3, the exhaust gas temperature was high, which favoured further oxidation of unburnt fuel downstream, reducing the total HC measured (222). CO emissions decreased with increasing DNBE fractions across all loads, which does not follow the expected trend with HC. However, the DCN of the blend increases as DNBE increases. Therefore, the CO reduction may be because the fuel that had burnt had complete combustion (222). Soot emissions were reduced by at least 10 times compared to those of diesel for load point 4, and a 75% reduction for load point 5 for all blends. There was a greater reduction with the high octanol blends, which was expected since it has a lower DCN than DNBE, increasing the mixing times. The 50%/50% blend soot emissions data was reported as a possible erroneous result as it does not fit the trends in the data (222).

The shape of the HRR curves changed as the load increased, especially for the blends with higher fractions of DNBE, as shown in figure 2.12. García et al. (222) used the term rate of heat release (RoHR) instead of HRR. The HRR curves had a more diffusive shape compared to the Gaussian shape the higher 1-octanol blends produced (222). At lower loads, the HRR curves are more stable, as there was one peak after the fuel injection, whereas, at higher powers, there are multiple smaller peaks over a longer duration. The delay in HRR correlates with the longer IDTs, and the peak HRR increased as octanol increased due to the longer IDTs.
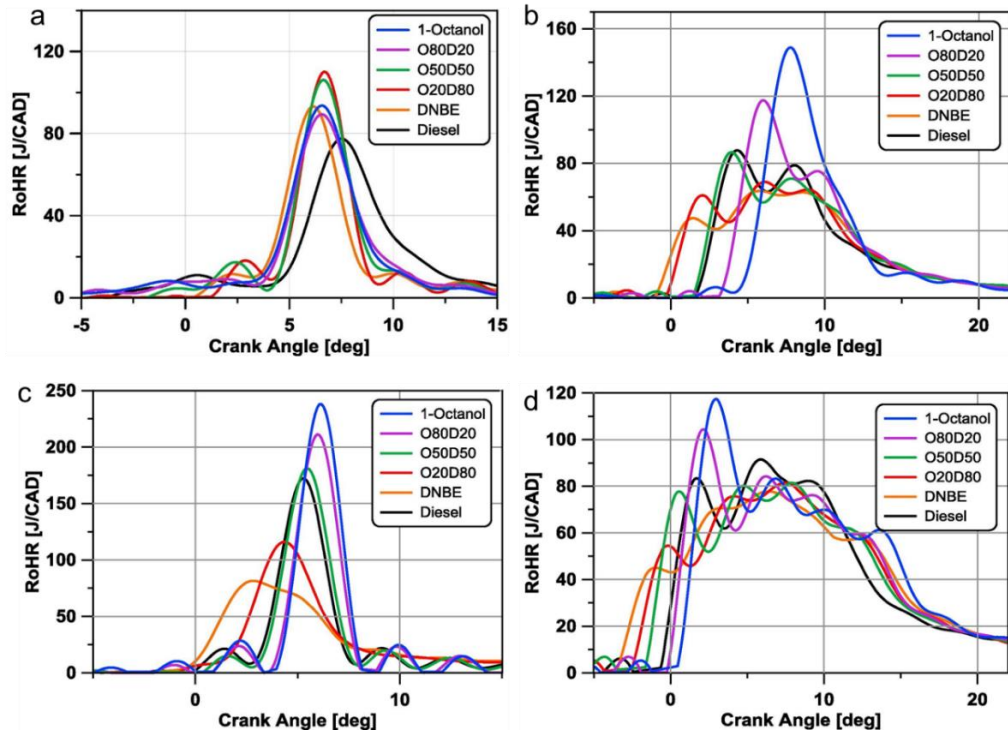
Figure 2.12. RoHR plots for blends of 1-octanol (O) and DNBE (D). Reproduced from (222). a: load point 2, b: load point 3, c: load point 4, and d: load point 5 from table 2.10.

Wang et al. (145) tested blends of 10% and 20% DNBE in a China Stage V diesel in a 7700 cc, turbocharged, six-cylinder, 230 kW engine. The engine complied with China VI emissions legislation, which has a lower CO limit than EURO VI: 700 mg/km for China VI compared to 1000 mg/km for EURO VI (145). A two-stage injection strategy was used, with a pilot injection followed by the main injection.

At 50% load, the peak in-cylinder pressures for both DNBE blends were similar to diesel, whereas, at 70% load, the peak pressure increased with increasing DNBE fraction (145). At 70% load, the peak HRR increased with DNBE fraction, and the 10% DNBE blend had two peaks, with a higher second peak than the peak from diesel (145). The first peak was due to premixed combustion, and the second peak was due to mixing-controlled combustion. Due to the blends' higher DCN with the addition of DNBE and its high DCN (table 2.8), there would be less premixed combustion as IDTs were shorter. Additionally, there was more oxygen available with higher DNBE fractions, which can increase oxidation and the HRR (145).

The BSFC increased as the DNBE fraction increased, following the trend reported by Heuser et al. (221). The 20% DNBE blend had an average increase of approximately 10 g/kWh, when the engine was at >25% load, which is an increase of around 5%. The load weighted changes in BSFC being 1.5% and 4.9% for 10% and 20% DNBE, respectively (145). In addition, the BTE decreased as the DNBE fraction increased. For

example, the 20% DNBE blend caused the BTE to decrease from 43% with diesel to around 41% at 70% load (145). This reduction was similar across all loads tested.

Wang et al. (145) showed that for 20% DNBE blends, the NO_X emissions increased, whereas, 10 vol% DNBE reduced the NO_X emission. The 20% DNBE blend can generate a leaner mixture due to the increased oxygen content, which increases NO_X emissions (40, 145). In addition, DNBE has a higher enthalpy of vaporisation than diesel (table 2.8), which reduces the in-cylinder temperature, thus reducing NO_X formation. Therefore, these effects are in competition with each other. The soot emissions for the 20% DNBE blends were reduced by 67% at 25%, 50%, and 70% load, and the 10% DNBE blend had a smaller reduction. The addition of DNBE reduces the soot precursor concentrations as they are oxidised due to higher oxygen content and a more reactive fuel (51, 179, 215, 223, 224). The HC emissions for the DNBE blends decreased relative to diesel. However, at lower loads, the 20% DNBE blend had higher HC emissions than the 10% DNBE blend, indicating that the charge cooling of DNBE in a lower temperature cylinder may reduce oxidation (145). At higher loads, the 20% DNBE blend had lower HC emissions than the 10 vol% blend as there could be more oxidation of the HC species, and the charge cooling effect was not detrimental to complete combustion. The CO emissions at lower loads were higher than the diesel baseline, with the 20% DNBE blend having higher CO emissions than the 10 vol% blend. This was likely due to the charge cooling of DNBE forming more low-temperature zones where CO forms. Additionally, there is a shortened combustion duration reducing the time available for complete combustion.

Wang et al. (145) applied the weighting factors from the China VI emissions legislation and determined the overall changes in the emissions of each fuel (table 2.12). These showed that the 10 vol% DNBE blends would be favourable for reductions in the NO_X, CO, HC, and soot emissions, whereas the 20 vol% blends only reduce the soot and CO emissions (table 2.12). These measurements were engine-out emissions. Therefore, if aftertreatment systems were used, any increases relative to diesel could be managed and the emissions limits could still be met.

Table 2.11. Summary of DEE engine tests that only studied the influence on IDTs.

Fuel Blend	Engine Used	Power or Load	ΔIDT	Comments	Ref.
10 vol% DEE/90vol% diesel	Three-cylinder, 2502 cc 34.6 kW, AD3.152 engine	48%	1000 RPM: 1.06% 1400 RPM: 0.37% 1800 RPM: 3.22%		(129)
10 vol% DEE/90 vol% diesel		73%	1000 RPM: 0.97% 1400 RPM: -2.82% 1800 RPM: -2.71%		
20 vol% DEE/80 vol% diesel		48%	1000 RPM: 1.65% 1400 RPM: 1.34% 1800 RPM: 3.09%		
20 vol% DEE/80 vol% diesel		73%	1000 RPM: 1.46% 1400 RPM: -2.94% 1800 RPM: -2.84%		
75% DEE/25% EtOH	Single-cylinder, Turbocharged, 511 cc, AVL 5402 D12 engine	4 bar IMEP	2 CAD	Intake pressure of 1.5 bar, advanced injection timing of 20 CAD BTDC, and used a lubricity additive.	(220)
50% DEE/50% EtOH			15 CAD		

Table 2.12. Summary of dialkyl ether blends engine tests and their changes relative a diesel baseline.

Fuel Blend	Engine Used	Power or Load	ΔCO	ΔHC	ΔNOₓ	ΔPM	ΔSoot	ΔBSFC	ΔEfficiency	Comments	Ref.
5 vol% DEE/95vol% diesel	Kirloskar water-cooled, 661 cc, direct injection, 3.6 kW engine	0.6 - 3.6 kW	-36%	-25%	33%	Up to -89%					(137)
10 vol% DEE/90vol% diesel			-43%	-50%	8%			13.50%			
5 vol% DEE/5 vol% EtOH/90vol% diesel			-36%	-80%	-17%						
10 vol% DEE/5 vol% EtOH/85vol% diesel			-36%	-75%	-17%						
5 vol% DEE/10 vol% EtOH/85vol% diesel			-29%	-80%	-17%						
10 vol% DEE/10 vol% EtOH/80vol% diesel			-36%	-75%	-17%			-10%			
DNBE	Single-cylinder, 390 cc, 80 kW/L engine	12%	-28%	-33%		-80%			-3%	Cooled EGR and a fuel injection pressure of up to 2000 bar.	(221)
		19%	-50%	-50%		-100%			0%		
		30%	-47%	-33%		-70%			5%		
		42%	-50%	-5%		-90%			2%		
		66%	-40%	Approx. 0%		-90%			-1%		
DNBE	Single-cylinder, 390 cc, 80 kW/L engine	19% - 66%	-40% to -66%	-5% to -60%	0% - 5%		-20% - 0%			Cooled EGR and a fuel injection pressure of up to 2000 bar.	(222)
80% Octanol/20% DNBE			0 to -66%	-20% to -50%	0%		-100% - 0%				
50% Octanol/50% DNBE			-20% to -50%	-10% to -55%	5% - 20%		-80% - 0%				
20% Octanol/80% DNBE			-35% to -55%	-28% to -60%	-5% - 10%		-100% - 0%				
10% DNBE/90% diesel	7700 cc, turbocharged, six-cylinder 230 kW engine	10%-100%	-0.1	-5%	-16%	-12%		1.50%	-0.50%	These are the changes for the emissions factors.	(145)
20% DNBE/80% diesel			-15%	14%	7%	-48%		4.90%	-2.70%		

2.9.3 Engine Tests Involving Alcohol Diesel Blends

Both BuOH and EtOH have been blended with diesel and tested in a variety of engines. Some of the available experimental results are summarised in table 2.13. These results include the changes relative to diesel baselines for the legislated emissions and engine performance parameters.

2.9.3.1 Engine Tests using Diesel/Ethanol Blends

Zahos-Siagos et al. (98) conducted engine tests of diesel blended with ethanol with 2M2B as a co-solvent. EtOH was blended up to 6.1% with up to 0.6% 2M2B to ensure the blends were stable. They reported that fuel consumption increased as EtOH increased due to lower heating values, which would be expected (98). The CO emissions were reduced due to the increased presence of oxygen. There was a greater reduction at higher loads where more fuel was injected (98). There was no reported impact on NO_X emissions. The PM emissions were reduced due to increased fuel oxidation with the oxygen in the blend, which reduced the soot precursor concentration, as seen with the other biofuel components (98). There may also be other reasons, such as the reduction in the aromatic content in the final fuel blend and the shorter carbon chain length of ethanol, which may also reduce the soot precursor concentration.

Jamrozik (225) tested EtOH/diesel blends with up to 40 vol% EtOH. Blends of diesel and high EtOH fractions are typically immiscible. However, they used an electromagnetic mill, where the blends were mixed with magnetic elements suspended in the mixture. The engine used was a single-cylinder, 573 cc, 7 kW engine (225). For all EtOH blends, the IDTs and peak pressure increased relative to diesel, albeit later in the cycle, due to longer IDTs. The greatest increase in peak pressure came from the 30 vol% EtOH blend (225). The elevated in-cylinder pressure aligns with the increased HRR when using the ethanol blends, as they had a greater peak HRR (225). For example, the 20 vol% EtOH blend had a peak HRR around 135 J/deg, whereas diesel had a peak HRR of 75 J/deg. This was likely due to increased premixed combustion because of longer IDTs. Jamrozik (225) determined that the NO_X emissions increased, THC emissions were within error of the 0.83 g/kWh measured for diesel, and the CO emissions were reduced with increasing ethanol fraction, supporting the findings of Zahos-Siagos et al. (98). The increase in NO_X emissions, of over 100%, was unexpected, as they would typically decrease with charge cooling as ethanol has a greater enthalpy of vaporisation than that of diesel (table 2.8). However, the increase could be due to leaner mixtures formed with increasing ethanol content.

2.9.3.2 Engine Tests using Diesel/n-Butanol Blends

Rakopoulos et al. (226) tested blends of 8, 16, and 24 vol% BuOH in diesel, using a 409 cc, single-cylinder, Hydra engine. For the combustion and performance parameters, only comparisons between the 24 vol% BuOH blend and diesel were made, whereas for emissions analysis all blends were evaluated. The injection timing was fixed at 29° BTDC. The IDT for the 24 vol% BuOH blend was similar to that of diesel, and the peak pressure increased at lower loads. The similar IDTs were unexpected since the blend's DCN would have been lower than diesel's. The IMEP of the 24 vol% BuOH blend was essentially identical to that of diesel, indicating that the engine's mechanical efficiency should be unchanged.

Rakopoulos et al. (226) reported that NO_X and smoke opacity, an indicator for the emissions of particulates, were reduced upon BuOH addition. The reductions correlated to the BuOH fractions, where there was a greater reduction with the higher BuOH fraction with the results from the highest load tested in figure 2.13. The CO emissions decreased as BuOH increased, whereas the HC emissions increased as BuOH increased. The oxygen present reduces CO emissions and smoke, but as BuOH increases, the volume of the fuel spray with lean local equivalence ratios increases resulting in higher HC emissions (226). Therefore, there may be less fuel burnt, hence lower CO and soot, and higher HC emissions. Although there were these changes in the emissions, the engine stability indicates that BuOH could be an attractive low-carbon diesel blend component. However, the increased HC emissions must be managed, possibly with aftertreatment systems.
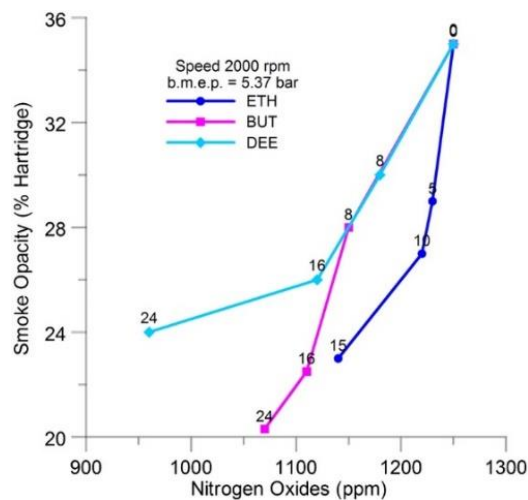
Figure 2.13. Smoke opacity and NO_X emissions at IMEP of 5.37 bar, 2000 rpm. BUT is butanol. Number next to each data point is the biofuel fraction. Reproduced from (226).

Lapuerta et al. (120) determined the changes in emissions for BuOH and diesel blends in a four-cylinder, 1500 cc, Euro 6 engine following the New European Driving Cycle (NEDC). There was a double EGR system, with low and high-pressure EGR. They

blended BuOH at 10, 13, 16, and 20 vol% into an EN 590 diesel without FAME. Blends with >20 vol% BuOH were not tested due to the low DCN resulting in cold start problems (120). All the blends had densities and KV40s within the EN 590 limits (table 2.1). The fuel consumption increased with increasing BuOH fraction, as the fuel blend LHV decreased (120). The IDTs increased as BuOH increased, with greater increases at higher loads where more fuel is injected. This does not match the findings of Rakopoulos et al. (226), as they showed that for 24 vol% BuOH, the IDT was similar to diesel. The average increase in IDT, relative to diesel, for 10 and 20 vol% BuOH blends measured by Lapuerta et al. (120) was 2 and 3 CAD, respectively.

The high BuOH fractions resulted in substantial increases in CO and HC emissions, which was expected with longer IDTs. For the 20 vol% BuOH blend, CO emissions increased by 135% and HC emissions increased by 273% relative to diesel (120). Lapuerta et al. (120) stated that the lower boiling point of BuOH and the high in-cylinder temperatures caused BuOH vapours to form. These move away from the fuel spray and the propagating flame and may not undergo combustion, resulting in elevated HC emissions as reported by Rakopoulos et al. (226). Since the EGR rate was variable the influence of BuOH on the NO_X emissions could not be determined. However, the NO_X emissions were within error of the diesel baseline regardless of the blend, due to EGR. PM and PN emissions were reduced relative to diesel, although for the 20 vol% blend, there were higher PM and PN emissions compared to the 16 vol% BuOH blend (table 2.13) (120). This increase could have been due to more soot precursors being formed and not oxidised due to the lower temperatures with high BuOH fractions. Lapuerta et al. (120) reported that the average particle diameter reduced with increasing BuOH content, indicating more nucleation particles were formed or there was less agglomeration. Therefore, the impacts of BuOH on engine performance and emissions must be controlled using engine optimisation and aftertreatment systems.

Table 2.13. Summary of the alcohol and diesel blends engine tests and their changes relative a diesel baseline.

Fuel Blend	Engine Used	Power or Load	ΔCO	ΔHC	ΔNOₓ	ΔPM	ΔPN	ΔIDT	ΔBSFC	ΔEfficiency	Ref.
4.6 vol% EtOH/0.4 vol% 2M2B/95 vol% diesel	Two-cylinder 930 cc 5.6 kW 18.5:1 CR	Idle - 5.5 kW	-3% - -31%	Reached the detection limits of the analyser	Within error of the diesel baseline	-50% - -43%			Within error of the diesel baseline		(98)
6.1 vol% EtOH/0.6 vol% 2M2B/93 vol% diesel			0% - -40%			-50% - -52%					
5 vol% BuOH/95 vol% diesel			5% - -20%			-50% - -28%					
10 vol% BuOH/90 vol% diesel			5% - -38%			-50% - -48%					
10 vol% EtOH/90 vol% diesel	Single-cylinder 573 cc, 7 kW, 17:1 CR		18%	Within error of the diesel baseline.	100%			8%		4%	(225)
20 vol% EtOH/80 vol% diesel			30%		130%			15%		6%	
30 vol% EtOH/70 vol% diesel			34%		180%			38%		7%	
40 vol% EtOH/60 vol% diesel			37%		200%			69%		13%	
10 vol% BuOH/90 vol% diesel	Euro 6, 1500 cc, four-cylinder, turbocharged, 81 kW Nissan engine with double EGR	NEDC test cycle	100%	145%	0%	-45%	-25%	9%			(120)
13 vol% BuOH/90 vol% diesel			110%	155%	0	-50%	-40%	10%			
16 vol% BuOH/84 vol% diesel			115%	185%	~ -5%	-60%	-50%	10%			
20 vol% BuOH/80 vol% diesel			135%	273%	~ -5%	-53%	-25%	14%			

2.9.4 Engine Tests Using Three-Component Biofuel Blends with Diesel

There have been no studies using different compositions of three-component ethyl-based blends in CI engines, but there have been studies using different butyl-based three-component blends blended with diesel (34, 38, 54).

Antonetti et al. (34) studied the production of a three-component biofuel blend using alcoholysis and used a blend of pure components matching a product composition as a biofuel blend. It consisted of 70 wt% BuOH/20 wt% DNBE/10 wt% BL and was blended with diesel at 10, 20, and 30 vol%. This blend is unlikely to meet existing fuel standards with the high BuOH fraction, especially with BuOH having a low viscosity and flash point (table 2.6). The blends were tested in a two-cylinder, 21 kW, 1248 cc, Lombardini LD 625/2 engine, without modification (34). The engine was run at maximum torque at 1500, 2000, and 2500 RPM with the NO_X, CO, FSN, and power measured. The power was reduced by around 0.5 kW at each engine speed with the 20 vol% and 30 vol% biofuel blends (34). The HC emissions did not change, which indicates there was efficient air/fuel mixing and oxidation (34). The CO emissions were reduced with the biofuel blends, with the greatest reduction arising for the 30 vol% blend. This reduction was expected as the biofuel blend contained 70 wt% BuOH, so there was a high oxygen content, and this will increase complete combustion. The FSN had a greater reduction with increasing biofuel fractions (34). At 2500 RPM, the FSN of diesel was approximately 5, and it was reduced to approximately 4, 3.5, and 2.5 for the 10, 20, and 30 vol% biofuel blends, respectively. One reason for this was believed to be the biofuel components boiling, leading to increased mixing as the droplets effectively explode, producing smaller fuel droplets (34).

Raspolli Galletti et al. (54) tested the blends discussed in section 2.7.1, using the same engine and engine speeds as Antonetti et al. (34). All the blends containing mixA and mixB had densities within the EN 590 limits, and the 12 vol% mixC blend had a density of 0.850 g/cm^3, above the 0.845 g/cm^3 maximum (12, 54, 227). The power generated using the biofuel blends was lower than diesel. One possible reason for the reduction was that there were no modifications to the fuel injection system to account for the lower LHVs of these fuels. At each speed, the two 10 vol% blends had the smallest reduction, which was expected when they had the highest LHVs of the blends. The diesel had an LHV of 43 MJ/kg and the blends of mixA and mixB at 10 vol% in diesel had LHVs of 42.1 and 42.5 MJ/kg respectively. Raspolli Galletti et al. (54) reported that there was no change in the HC emissions, similar to Antonetti et al. (34). Raspolli Galletti et al. (54) showed that NO_X emissions were unchanged for the blends as the in-cylinder temperatures were likely similar to those of diesel as peak pressures were unchanged. MixC had longer IDTs, and this was due to the lower DCN as it had the highest BL

fraction, but there was no data for the other two blends. The CO emissions were reduced relative to diesel using mixA and mixB, whereas with mixC the CO emissions were maintained. MixA at 20 vol% had the greatest reduction in CO, which was expected, as there was the highest BuOH fraction, increasing the oxygen in the fuel. The soot emissions were reduced with mixA and mixB at 20 vol%, with a maximum reduction of 30% for 20 vol% mixA. However, 10 vol% mixA did not show the same reduction as it did for Antonetti et al. (34), even when using the same engine and blend formulation. The soot emissions for the blend of 12 vol% mixC were similar to those of diesel at 1500 and 2000 RPM. This difference shows that even with the elevated DCN and oxygenated species, there may not always be a consistent reduction in soot emissions.

Frigo et al. (38) tested DNBE, BL, and diesel blends. They were tested in a single-cylinder, 441 cc, 7.4 kW Kohler KD15-440 engine. This engine is Euro Stage V compliant, so any changes to the emissions may change the compliance. Frigo et al. (38) tested blends of 7, 11, and 13 vol% BL, a fixed 4 vol% DNBE, and the remainder being diesel. The diesel used had a CN of 50, which is below the EN 590 minimum of 51 (12, 38). The CN of the three blends were below the 51 minimum, as discussed in section 2.8.4. The density of the blend with 7 vol% BL was 0.844 g/cm^3 and complied with the EN 590 limits, whereas the other blends were above the maximum (38).

Frigo et al. (38) reported that the blends had '*slightly increased engine efficiency*', especially at lower speeds. This was likely due to a combination of the lower CN, causing longer IDTs, and the lower viscosity improving fuel atomisation. This would increase premixed combustion but lower the combustion temperature as more BL and DNBE could be vaporised as smaller droplets were formed (38). As a result, there was less heat to lose through different heat transfer processes. The IDTs had small increases relative to diesel, which were 0.25, 0.4, and 0.55 CAD for the 7, 11, and 13 vol% BL blends, respectively (38).

Frigo et al. (38) reported that the CO emissions increased as the BL fraction increased. This was due to the lower DCNs of the blends, giving longer IDTs, and reducing the time available for combustion. This increase was more evident at the 50% torque and the higher speeds. There was an increase of approximately 50% for the blend with 13 vol% BL relative to diesel. The same change was observed for the HC emissions at 50% torque. The increased HC emissions were also due to less time for complete combustion. Frigo et al. (38) reported a large reduction in soot emissions, especially at 100% torque. At 3000 RPM and 100% torque, the soot emissions decreased from 0.28 g/kWh to around 0.18 g/kWh for the 13 vol% BL blend. There was a reduction of approximately 40% for all the blends and conditions (38). BL and DNBE are likely to reduce the soot precursor concentrations, as there was additional oxygen in the blend,

favouring their oxidation. However it may have been incomplete oxidation as CO emissions increased, as the longer IDTs enabled more mixing. The biofuel addition will also decrease the aromatic content of the blends, reducing the soot precursor formation.

The in-cylinder pressures when using all three fuel blends were relatively unchanged compared to diesel at 2300 RPM, whereas at 3600 RPM, they reduced by around 1 bar relative to diesel (38). The majority of these changes were due to longer IDTs. Therefore, with an optimal fuel injection strategy, the changes in the emissions may be favourable.

The work of Frigo et al. (38), Raspolli Galletti et al. (54), and Antonetti et al. (34) demonstrate the viability of these three biofuel components as a low-carbon blend stock for diesel. However, the blends did not meet all the fuel standards' physical property or DCN limits. Additionally, they did not maximise the BL fraction, and doing this would make using alcoholysis products more cost effective. Therefore, determining blends that comply with the physical property limits using higher alkyl levulinate fractions would favour their utilisation and contribute towards the REDII targets. Christensen et al. (13) demonstrated the ease of matching the CN using additives, but the use of oxygenated lower CN fuels can also be overcome using engine modifications.

2.10 Combustion Modelling of Diesel and Compression Ignition Engines using Biofuel Blends

2.10.1 Fundamentals of Combustion and Ignition

Combustion processes involve a series of elementary reactions that occur on millisecond and nanosecond timescales. When describing the reach kinetics of such a process, each elementary reaction can be assigned to a reaction class based on the process occurring (178, 228). For example, hydrogen abstraction and unimolecular fuel decomposition are two reaction classes. These reactions and their rates are used to construct chemical kinetic mechanisms to model the gas phase fuel combustion and further our understanding of the processes occurring (56). For some elementary reactions, the rates can be obtained experimentally, whereas others must be determined computationally (178, 228). For example, rate parameters can be calculated using ab initio modelling which uses quantum chemistry methods to describe the potential energy surfaces on which reactions take place. Ab initio modelling is coupled with a range of methods describing energy transfer and energy specific reaction processes to predict the pressure and temperature dependent rate parameters (160, 179, 229). Methods using functional group analogies are estimates that use data from kinetic experiments or ab initio methods for small molecules. Hence they are a way to provide estimates for

larger molecules where there is no fundamental data available and are too expensive to study using highly accurate theoretical approaches. Group additivity methods can also be used to predict the thermodynamic properties (58, 160, 179, 229).

Combustion is often separated into two regimes to specify reaction classes, high (>1000 K) and low (<1000 K) temperature combustion. However, there is no physical division and the nature of the reactions occurring at different temperatures can be fuel dependent. The high temperature reaction classes include (178):

- Unimolecular fuel decomposition
- Hydrogen abstractions from the alkanes to form alkyl radicals
- Alkyl radical decomposition
- Hydrogen abstractions from alkenes to form alkenyl radicals
- Alkenyl radical decomposition

At high temperatures, the main reactions that occur are the decomposition reactions, as well as reactions of the smaller molecular weight intermediates and products. At low temperatures, oxygen addition reactions can dominate the combustion (178, 228). The low temperature classes include:

- Addition of oxygen to alkyl radicals (R + O_2 ↔ RO_2)
- Isomerization of RO_2 to hydroperoxyalkyl radicals (QOOH)
- Addition of O_2 to QOOH
- RO_2 decomposition
- Decomposition of large carbonyl species and carbonyl radicals.

These reaction classes form a general combustion reaction scheme, with examples for hydrocarbons and alcohols shown in figures 2.14a and 2.14b, respectively.
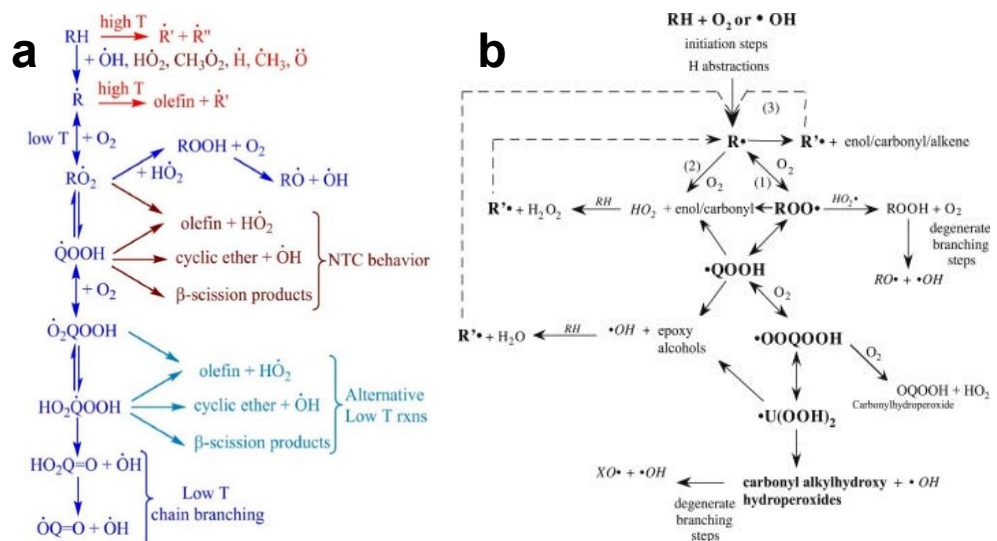
Figure 2.14. Generic mechanisms for combustion of: a: hydrocarbons reproduced from (171) and b: alcohols reproduced from (165). Both include low and high temperature reaction pathways.

The carbonyl decomposition is the low temperature chain branching pathway that leads to ignition. However, there are other competing low temperature reactions that lead to termination or degenerative propagation routes such as the formation of olefins and HO_2 (figure 2.14), which lower the overall reaction rate (59, 179).

The radical pool growth allows the reactions to progress through propagation reactions. For autoignition to occur, chain branching reactions must dominate, as they are where more radicals are generated than consumed, which accelerate the overall reactivity (170, 171, 230). The termination reactions are when stable species are formed and the radical concentration reduces, and as a result, combustion slows down. In an engine, the high temperatures and pressures provide sufficient energy to initiate the reactions and to promote chain branching routes, overcoming their activation energy (E_a) barrier (170, 171, 230).

The presence of oxygen in the fuel molecule can open up new reaction pathways depending on the functional group (160, 170, 171, 178, 228). Typically, the presence of oxygen favours hydrogen abstractions from carbons adjacent (alpha) to the oxygen-containing functional group since the C-H bonds are weaker due to the high electronegativity of oxygen withdrawing electron density (170, 177, 230). For example, hydrogen abstraction of the α-H of n-butanol is favourable due to the weaker C-H bonds, but it leads to the formation of an aldehyde and HO_2, leading to non-chain branching routes and thus increasing IDTs compared to alkane equivalents (165). The chemically active pathways for a given fuel species depend on the reaction conditions, primarily the temperature and pressure (37, 170, 171, 178). For example, stable molecules could have multiple oxygen additions. These are key to chain branching and autoignition, as decomposition of such species will form radicals (160, 170, 171, 177).

The fuel composition and subsequent reactions that dominate will dictate the combustion products and exhaust gas composition. They will also impact IDTs and thus the CN and RON, as the more chain branching occurring, the shorter the IDT and the higher the CN (231). Many oxygenated species form increased fractions of aldehydes, such as formaldehyde and acetaldehyde, due to their stability (170, 174, 232). Other species formed can contribute to PM formation (71, 72, 233). The ability to predict accurately these species and their concentrations will enable the rapid screening of potential advanced biofuel candidates.

2.10.1.1　　Biofuel Combustion Mechanisms and Modelling

Once the relevant reaction pathways, kinetic and thermodynamic data are collated for all the species and combustion reactions, the chemical kinetic mechanism can be constructed (37, 51, 56, 160, 171, 234, 235). These need to be suitable over a range of

equivalence ratios, temperatures, and pressures to cover a range of local conditions that occur due to effects of turbulent mixing if being used in three-dimensional (3D) simulations. The ODEs for the species concentration and kinetics rely on the conservation of mass and energy. The ODEs are solved using computational solvers such as Chemkin (56). The use of such solvers can allow a wide range of conditions to be simulated. The accuracy of the simulated solution depends on the accuracy and validity of the mechanism at the simulated conditions. Mechanism validation usually relies on comparison to fundamental experimental data where complex fluid flow processes are minimised, such as IDT measurements in RCMs and shock tubes, burning velocity measurements and species profile measurements in jet stirred reactors (56, 171). Rate parameters can be validated using experimental studies of elementary reactions. The measurement or ab initio modelling of rate parameters for each individual reaction class is difficult and becomes more difficult with the increasing complexity of biofuel molecules such as the levulinates. Therefore, it is unlikely experimental or high level theory data would be available for every reaction class present in biofuel combustion mechanisms, and as a result the kinetic data for these must be estimated using simpler approaches. The mechanism's ability to predict combustion behaviours such as IDTs can be compared to data from RCMs for lower temperatures or shock tube experiments at intermediate to high temperatures over a range of pressures.

Detailed mechanisms for diesel and advanced biofuel blends are scarce. For advanced biofuels, this is due to a lack of fundamental experiments or the difficulty in accurately generating the mechanism using computational methods. For diesel, this is due to its complex composition. As a result, a representative surrogate composition is used for mechanism construction, as this reduces computational demand (236). A surrogate diesel can be formulated to replicate the physical and chemical properties, including C/H ratio, CN, molecular composition, density, and IDT (237). The kinetic parameters are also vital to capture, so that the presence of important features such as an NTC can be captured. These properties, and the need to match the combustion kinetics dictate what compounds are used in a surrogate. They are usually selected from the types of compounds found in a diesel such as n-alkanes, iso-alkanes, cycloalkanes and aromatic compounds (236-238). Since the molecules typically found in diesel are C8 – C24, surrogate mechanisms can still have thousands of reactions and species. Therefore, reduced or skeletal mechanisms may be required to reduce computational demand (171, 234, 235).

One diesel surrogate mechanism is from Lawrence Livermore National Laboratories (LLNL). It is composed of 23 vol% m-xylene and 77 vol% n-dodecane, with a reported CN of 70, higher than a typical diesel (239). The detailed mechanism contains 2885 species and 11754 reactions, and the reduced mechanism 163 species and 887

reactions. Whilst it does not represent all types of compounds found in a diesel, the mechanism accurately predicts combustion behaviours of dodecane and p-xylene. The detailed mechanism was validated for high and low-temperature regimes in a jet-stirred reactor (239). The reduced mechanism accurately simulated IDTs at 1 – 80 bar, initial temperatures of 700 – 1600 K, and φ=0.5 – 2.0, with the results in agreement with the detailed model (239). Whilst Pei et al. (239) did not compare their simulations to a diesel, Alturaifi et al. (240) demonstrated its accuracy in simulating IDTs of a diesel measured in a shock tube at p=10 and 20 atm, φ=1.0 and 0.5, and temperatures of 750 – 1300 K.

There are mechanisms available for most of the individual biofuel components of interest other than BL, PL, and DNPE. The lack of schemes for these compounds is likely to be due to the lack of fundamental combustion studies. Some of the available mechanisms for the other biofuel components are summarised in table 2.14.

Table 2.14. Summary of mechanisms available for the fuel components of interest.

Fuel Component	Type of Mechanism Available	Number of Species	Number of Reactions	Reference
Diesel	n-dodecane/m-xylene surrogate detailed (top), reduced (bottom)	2885 163	11754 887	(239)
EL	Detailed	1458	6162	(160)
DEE	Detailed	341	1867	(241)
DEE	Detailed	380	2385	(166)
EtOH	Detailed	57	372	(242)
EtOH/DEE	Detailed	502	1223	(161)
EL/DEE/EtOH	Detailed	575	1657	(55)
EtOH, BuOH and PeOH (C1 – C5 alcohols)	Detailed	687	3435	(165)
DNBE	Detailed	426	2335	(243)
DNBE	Detailed	436	2732	(244)
DNBE	Detailed	723	3803	(174)
BuOH/DNBE/n-Octanol	Skeletal	117	610	(245)
BuOH/Gasoline Surrogate	Detailed	1944	8231	(162)

The mechanisms in table 2.14 have been used to predict IDTs of the corresponding fuel components with varying levels of accuracy. Some of the mechanisms were tuned to improve their accuracy by optimising rate and thermodynamic parameters to best fit

available experimental data (37, 55, 161). Care must therefore be taken when utilising these mechanisms outside of the conditions where they have been optimised.

For the ethyl-based blend, there is a mechanism available from Howard et al. (55). The benefit of mechanisms developed for fuel blends is that they can account for cross-reactions and each fuel component's influence on the reactions. For example, DEE has low temperature reactivity, which promotes the low temperature oxidation of EL and EtOH (37). The mechanism of Howard et al. (55) consists of the EL mechanism from Ghosh et al. (160), with the low-temperature oxidation pathways added, and a DEE/EtOH sub-mechanism from Issayev et al. (161), albeit with the following modifications to the kinetic parameters:

- EL6OO ↔ EL6OOH7J had its E_a reduced by 4 kcal/mol.
- EL6OO ↔ EL67D + HO_2 had its pre-exponential factor halved.
- EL6OOH7OO ↔ EL6O7OOH + OH had its pre-exponential factor quartered.

The mechanism was validated against RCM measurements, discussed in section 2.7.4.2, where the predictions at lean conditions were more accurate than at stoichiometric conditions (figure 2.7) (37, 55).

For DEE/EtOH blends Issayev et al. (161) decreased the E_a of the ethoxyethyl keto-hydroperoxide decomposition by 0.5 kcal/mol, increasing the low-temperature reactivity of the mechanism and the pre-exponential factor of the DEE α-H abstraction was halved. The mechanism was shown to accurately predict IDTs at 20 bar up to 590 K before over-predicting them, whereas, at 40 bar there was an over-prediction of IDTs for φ=0.5 and 560 – 660 K (161).

Mechanisms which have been tune for specific conditions may not behave well on extrapolation and have reduced accuracy when used for simulating different blend compositions and thermodynamic conditions. Therefore, the results would be less reliable and may not be representative of the processes occurring. It would be beneficial to use non-tuned mechanisms constructed using fundamental data from high level calculations and experiments. The use and evaluation of mechanisms produced using automatic generation and functional group methods, but without tuning to specific conditions, will be presented in Chapter 7.

Thion et al. (244) compared their simulated DNBE IDTs to those simulated using the Cai et al. (243) mechanism. They were able to show that at 1100 K – 1300 K their mechanism was more accurate, as the mechanism of Thion et al. (244) could simulate IDTs that were more closely matched to the experimental IDTs of Cai et al. (243).

Although the Thion et al. (244) mechanism was tested at high temperatures, it was not tested at engine-relevant pressures. Therefore, it may not be suitable for this regime.

More recently there has been the development of a DNBE mechanism from Zhong and Han (174). They used the Thion et al. (244) mechanism but made the following changes:

- They replaced the C0-C4 sub-mechanism with the Aramco 3.0 mechanism of Zhou et al. (246).
- They updated the reaction rates for the H-abstractions, first and second oxygen additions, QOOH decompositions, concerted HO_2 elimination reactions of RO_2, and the keto-hydroperoxide decompositions using the best available literature to ensure the DNBE sub-mechanisms used the most up-to-date reaction rates (174).
- They added a butanoic acid sub-mechanism.

The effects of these changes to the Thion et al. (244) mechanism can be seen in figure 2.15, where using the Zhong and Han (174) scheme (tuned model) there is a more pronounced NTC region and the experimental data is accurately predicted at the compressed pressures of 7 and 10 bar, and for φ=1.0 (174). The model was also accurate for φ=0.7 and φ=1.4.
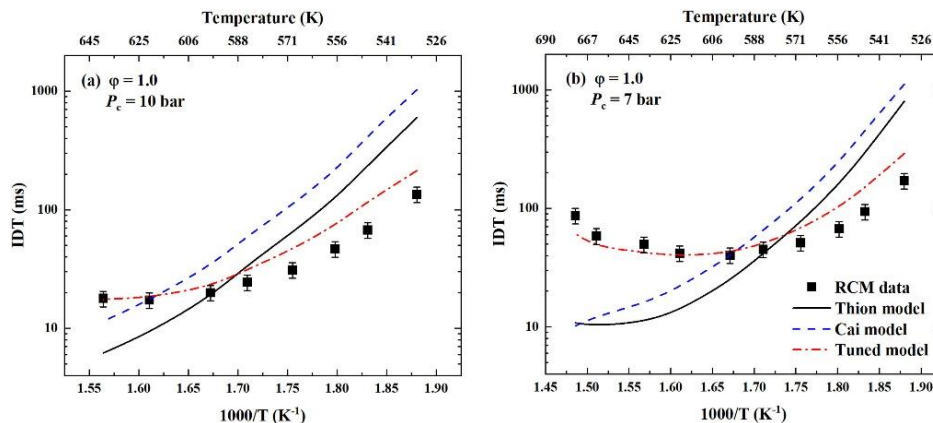
Figure 2.15. Comparison of the DNBE mechanisms to RCM data, reproduced from (174).

The skeletal mechanism of Li et al. (245) for BuOH/DNBE/n-octanol used the DNBE mechanism of Cai et al. (243), the BuOH mechanism of Sarathy et al. (168), and the n-octanol mechanism from Cai et al. (247). There were several reduction stages conducted, which were: directed relation graph, directed relation graph with error propagation and sensitivity analysis, peak concentration analysis, and isomer lumping, as outlined by Li et al. (245). The mechanisms of each fuel component were reduced to produce a skeletal mechanism before combining them, resulting in a mechanism of 117 species and 610 reactions. This methodology could result in the loss of reaction

pathways activated when blending fuels (56). The loss of reaction pathways may have been why Li et al. (245) had to adjust the reaction rates to optimize their IDT predictions. The model was validated against DNBE, BuOH and n-octanol IDTs, flame speeds of DNBE, and it was used in a three-dimensional diesel engine study where the HRR and the in-cylinder pressure were accurately predicted. The average differences for the IDT predictions were -5.28%, -1.11%, and -4.58% for BuOH, n-octanol, and DNBE, respectively, demonstrating its accuracy (245). The NTCs of DNBE and n-octanol were still captured in the combined skeletal mechanism, indicating that the reactions that caused these were still present after reduction. The use of such models will reduce the computational demand whilst maintaining their accuracy, making them favourable. The mechanisms used in Chapter 7 would need to include cross reactions, such as those in the mechanism of Howard et al. (55), as the blend composition's influence needs to be accurately captured.

As there is no mechanism available in the literature for BL, it needs to be developed. There are techniques available to produce mechanisms from fuel components where there is no experimental data. One such method is automatic mechanism generation, and this can be conducted using available tools such as Reaction Mechanism Generator (RMG) (57). Using such tools can allow for consistent functional group definitions and reaction classes to be applied, whilst removing the reliance of an operator to select the reaction class and group additivity ensuring consistency between operators. RMG uses a functional group based methodology to analyse and produce mechanisms, where the molecular structures are represented by a series of functional groups (57). The reaction kinetics are determined using a defined library of reaction classes and kinetic parameters are assigned based on the closest matching functional group. For generating mechanisms of biofuel components where there is no data available, the functional groups and reaction classes used to describe the molecule and its reactions must be accurate. Such a methodology could be used to generate a mechanism for BL where there is no data available, but it could also be used to generate blend mechanisms to ensure the cross reactions are included. If the cross reactions are included, a more accurate mechanism can be produced. Additionally, if the fundamental kinetic and thermodynamic input data is accurate there may be a reduced need to tune the mechanism as it should be accurate from first principles. Mechanisms produced using RMG will be evaluated in Chapter 7 to determine their suitability for predicting the combustion parameters of the biofuel blends.

2.10.2   CI Engine Modelling

CI engines are typically difficult to model due to the combination of the physical and chemical processes occurring. The liquid fuel injection and fuel vaporisation affect the ignition and combustion in a CI engine, and they can be difficult to model accurately without computational fluid dynamics (CFD). These models are usually 3D and computationally demanding (248). However, zero-dimensional (0D) models for CI engines have been developed, including one available as part of Chemkin (249, 250). There has been no reported use of the 0D model in Chemkin since its release. Simulations using 0D models are less computationally demanding than using CFD. If these models could be utilised and predict emissions and performance accurately, there is the potential for a more efficient screening process of fuel candidates as fewer engine tests would be needed and more simulations can be conducted when compared to computationally demanding CFD. However, it may be difficult to have realistic representation of the turbulent mixing and spray behaviour in these 0D models. Hence, CFD models may need to be used to model CI engines.

Rakopoulos et al. (251) modelled ethanol/diesel blends in a FORTRAN-based two-dimensional multi-zone model and developed a detailed model of the fuel spray. They modelled the single-cylinder Ricardo Hydra engine. They only modelled the processes that occurred when the valves were closed. This included the main processes occurring in the cylinder, such as spray impingement on the wall, combustion, NO_X and soot formation, and fuel spray development. They used the spray model of Rakopoulos et al. (252), where the spray was separated into a two-dimensional multi-zone model with zones in both the axial and radial directions. At each time step, the individual zones had the governing equations of the sub-models solved to determine the fuel vaporisation and combustion progress. Unlike many other studies, Rakopoulos et al. (251) did not use chemical kinetic mechanisms for the combustion of n-dodecane or soot formation. The fuel combustion was modelled using an Arrhenius-like equation that was solved at each time step and for each zone, where the calculated amount of evaporated fuel is used in the equation. The combustion products are determined using an equilibrium approach for the elemental balance of C, H, N, and O (251). However, for NO_X formation, they used the kinetic scheme of Lavoie et al. (253). They used the soot model of Hiroyasu and Kadota (254), the same model employed in the Chemkin 0D model. Each of the sub-models was solved numerically with the following basic steps:

- Calculation of the compression stroke.
- Calculation of the combustion and expansion for the zones.
- Calculations in the unburned zone.
- Calculations of the mixing of air and fuel.

- Calculations of the burning zone.
- Calculation of the mean state of every zone.

Simulations of a 15 vol% EtOH in diesel blend were compared with experimental data using the same engine and fuel blend. The simulated pressure-crank angle traces closely matched the experimental plots for at 75% and 38% load, whereas the HRR did not match at both loads, as it did not have the same sharp peak. NO and soot emissions were accurately predicted, with little to no deviation from the experimental measurements (251). This accuracy may be beneficial for screening fuel blends, but the model may not be suitable for complex multi-component mixtures of varying reactivity, as the model has not been used for other fuel blends. It was stated that the model was not computationally demanding. However, it was developed to model the Hydra engine and cannot simulate any other engine designs.

There is a lack of modelling of the blends of the other advanced biofuels with diesel in CI engines. This is likely due to the complex nature of CI engines, and the physical processes of fuel injection and vaporisation are required to be representative. Therefore, if simulations using 0D models can simulate the changes in engine performance and emissions and contribute towards furthering the understanding of the changes, there would be the possibility to reduce the reliance on engine testing and CFD.

2.11 Summary of the Literature Review

This literature review has identified that all fuels must comply with existing fuel standards if a low-carbon alternative is to be a drop-in fuel. In the literature, the process of selecting fuel blends for engine testing usually disregards compliance to fuel standards. Without fuel standard compliance, it would be difficult to have a commercially viable fuel. One part of the diesel standards that would not be met with the biofuel blends used in this work is the type of biofuel added to diesel. The standards only allow FAME, GTL, HVO, or paraffinic advanced biofuels to be added to diesel (12, 16). Having such a requirement prevents the addition of oxygenated advanced biofuels, such as those used in this work. This may inhibit the use of potentially suitable advanced biofuels as diesel blend components and slow the decarbonisation of CI engine applications. If it could be demonstrated that fuel efficiencies, emissions, and engine performance can be maintained this limit must be reviewed and the biofuels allowed to be used reconsidered. It is unlikely the physical property limits will change as they have safety and operational impacts, but if they can be met with oxygenated biofuel blends and the engine operation is favourable fuel standards should be considered for change to enable their use. Fuel blends could be tailored to comply with physical and combustion property limits. They could also be tailored to ensure engine emissions remain below their emissions limits to

comply with its type approval. Compliance with EN 590 or BS 2869 property limits would favour the utilisation and commercial viability of advanced biofuel blends, as they will likely be more compatible with existing engine architecture.

CI engine use will remain high in the short to medium term due to the high utilisation of HDVs and agricultural and construction machinery. Decarbonisation of these sectors and the fuels/engines used is needed. European legislation mandates the increased use of renewable and advanced biofuels. The use of advanced biofuels in CI engines would contribute towards their decarbonisation.

Advanced biofuels can be produced using a range of techniques, which are at different stages of development. Alcoholysis is an attractive production method as it produces tailorable product blends of potential attractive biofuel components, individually and as blends. Blends that comply with fuel standards would need to be found. The product blend composition could be tailored using different reaction conditions or post-reaction processing. Increasing the carbon chain length of the biofuel components affects the physical properties of diesel, as increasing the carbon chain length changes the density, flash point, and KV40 in different ways depending on the biofuel component. However, the influence of the compositions of the three-component blends on the physical properties needs to be established.

There is a need to understand how the physical and combustion properties of multi-component advanced biofuel blends change for different alkyl levulinate, dialkyl ether, and alcohol blends. The availability of accurate models for predicting the physical properties depends on the chosen property. The density of multi-component fuel blends can be accurately predicted using linear blending rules, but these are usually for ideal mixtures. Hence, the suitability of these models for predicting the density of multi-component advanced biofuel blends needs to be tested. Accurate flash point models rely on access to models, such as the UNIFAC models. Often these are embedded in software or expensive to access, making them difficult to use. Accurate KV40 predictions of non-ideal blends are limited to binary blends and rely on the Grunberg-Nissan equation. Therefore, there is a need to determine the influence the biofuel blend has on the physical properties, with and without base fuels.

CI engine emissions are dependent on operating conditions and the fuel used. Existing emissions standards are vehicle, and engine application, dependent. Since the implementation of emissions standards, the limits for legislated emissions have been decreasing over time. Whilst there are aftertreatment systems that enable the emissions limits to be met, with the limits decreasing there will need to be additional measures. One possibility would be changing the fuel composition to favour the reduction of selected emissions. For example, the addition of an alcohol, an alkyl levulinate, or a dialkyl ether

to diesel would reduce PM emissions. Literature suggests that oxygenated compounds can have varying effects on CO and THC emissions. There can be reductions in CO and THC due to the increased oxygen content, lower aromatic content, and shorter carbon chain lengths in the fuel, as there will be more fuel oxidation. However, there can also be increases in the CO and THC emissions from less complete combustion if longer IDTs are not accounted for in the engine operation. When using different biofuel blend compositions, the influence of the biofuel composition on the emissions needs to be understood.

Modelling the combustion in a CI engine can be computationally expensive due to the reliance on CFD. There are few 0D and 1D models available, which reduces the ease of modelling a CI engine. There also needs to be accurate kinetic mechanisms and thermodynamic data for the fuel components. Currently, there is a lack of available chemical kinetic mechanisms for the butyl and pentyl-based biofuel components of interest in this work, either as individual compounds or in multi-component mechanisms. Therefore, any simulations of the biofuel blends with diesel would require newly developed kinetic mechanisms. There would also need to be suitable zero-dimensional CI engine models for these simulations. Using models would enable a greater understanding of the combustion processes and reactions occurring. They would also allow the rapid investigation of different blend compositions for blend optimisation.

Chapter 3
Methodologies

3.1 Introduction

The methodologies used within this work provided the ability to take a selective approach to decide which fuel blends were to be used for engine tests by supplementing experimental studies with computational modelling. This chapter is split into sections based on the overall process flow of the project. The first section covers choosing the blend boundaries and how these were then implemented into a design of experiments (DoE) software to produce an experimental plan. The next section covers the physical property testing methods used, including methods for measuring the flash point, density and KV40. The third section covers the engine test methods, including emissions measurement techniques, calculations used to determine the IDT, the method used for determining the HRR and the emissions indices following the BS ISO 8178-4 standard for exhaust emissions measurements (255). The final section covers kinetic modelling methods, including the reactor models used, the mechanisms selected for the fuel blends, and the principles of the kinetic modelling.

To select the suitable blends for engine testing, firstly the properties of ternary blends of the advanced biofuel components need to be understood. To understand how the physical properties changed with the blend composition within the set boundaries, a DoE approach to construct empirical models for the physical properties was used, allowing for appropriate three-component advanced biofuel blends to be selected. The advanced biofuel blends were blended with diesel across a range of volume percentages and important properties were investigated in order to determine the blend boundaries that met property limits of existing fuel standards. The effects of the biofuel blend composition, chain length, and biofuel to diesel blend fraction were determined enabling the most suitable blends for further study to be selected.

Once suitable blends with and without diesel were found, they were then tested in a single-cylinder, four-stroke, direct injection, CI engine to determine their practical applicability and compatibility with commercial engines. The performance parameters, emissions characteristics, and fuel compatibility were determined. The performance parameters and emissions were compared to a diesel baseline to determine the influence of the biofuel package composition on them. The emissions were also evaluated against the required emissions standard to determine if the biofuel blends would result in non-compliant engine emissions.

To further understand the effects of the advanced biofuel blends on the combustion kinetics, simulations of the combustion at engine conditions were conducted using

computational modelling methods in Chemkin 22 R1 (249). The simulations were used to further understand the influence of the biofuel blends on combustion properties such as IDT and HRR. The simulated results were compared to the experimental data to determine the accuracy of the model, and to determine if the changes simulated matched those observed experimentally.

3.2 Advanced Biofuel Formulation

This project aims to investigate the suitability of potential advanced biofuels that are produced from an alcoholysis process. However, alcoholysis produces a complex mixture of products, some of which are unknown. Therefore, it would be difficult to gain an understanding of the influence of the blend composition on the physical properties, engine performance, and the emissions. As a result, the advanced biofuel blends studied were model biofuel blends consisting of the three main products from alcoholysis. The selected blend components were an alkyl levulinate, a dialkyl ether, and the alcohol itself. Since this project is aligned to the SusLABB project, a collaboration with the Dooley Group at Trinity College Dublin and the School of Chemical and Process Engineering (SCAPE) at the University of Leeds, there were limits established for the amounts of each of the three biofuel components in the formulations. These limits were that the alkyl levulinate must always be more than 50% of the blend, and the remaining portion should be the alcohol and the dialkyl ether with the limits shown in table 3.1. This is due to the alkyl levulinate being the target molecule from the alcoholysis of biomass. The limits were selected on a volume percent (vol%) basis.

Table 3.1. Limits for the three biofuel components in the ternary blends.

Component	Minimum vol%	Maximum vol%
Alkyl Levulinate	50	90
Dialkyl Ether	5	45
Alcohol	5	45

These limits were used as part of a DoE approach to allow for the determination of optimal test blend compositions to derive empirical models of the physical properties of the ternary blends. DoE was also used to determine the effects of the blend composition on the physical properties and to determine which compositions were compliant with the fuel standards for different diesel types (EN 590 and BS 2869) (12, 16).

3.2.1 Ethyl-Based Blends

In addition to using the prescribed limits of DEE, EL, and EtOH, blends that had DCNs close to the typical cetane number of commercial diesels could be determined.

This was to ensure that the overall cetane number would be maintained when blended with diesel. The physical properties can be tested to determine if they would be compliant with the limits in EN 590 and BS 2869 (12, 16). Using equation 10 and its coefficients (table 3.2) produced by Howard et al. (37), ratios of EL, DEE, and EtOH, at 5% intervals, were determined to give DCNs ranging between 40 to 50:

$$DCN = \sum_i DCN_i(a_i x_i + b_i(x_i)^2 + c_i(x_i)^3)$$

Equation 10

where x_i is the mole fraction of component i in the blend.

Table 3.2. Values of the coefficients in equation 10. Adapted from (37)**.**

Component	a	b	c
EtOH	-0.871	-1.300	2.801
DEE	0.394	0.277	0.301
EL	7.931	-10.254	2.985

Biofuel blends with DCNs ranging between 40 and 50 were selected for engine testing in addition to blends with the limits of a minimum 50 vol% EL. This was to compare the effects of matching the DCN of diesel and blends that are within the selected composition limits.

3.2.2 Butyl and Pentyl-Based Blends

For the butyl and pentyl-based blends, there are no models for predicting the DCN in the same manner as there are for the ethyl-based blends. It is likely that there would still need to be high levels of the ether to match the DCN of diesel (143).

The limit of using at least 50% alkyl levulinate in the biofuel blends was used in the DoE to produce physical property models and to determine the blend compositions of the butyl and pentyl-based three-component blends that complied with the selected physical property limits. The use of this selection method enabled the study of how engine performance and emissions would change if blends only satisfied the selected physical property limits and not the DCN limit. This also enabled a comparison of the effects of carbon chain length on the physical properties, as the ethyl, butyl and pentyl-based blends with and without diesel can be compared.

3.3 Design of Experiments Approach

To understand how the composition of the three-component biofuel blends affect the physical properties of the blends with and without diesel, a DoE approach was undertaken using Sartorius Stedim's software, MODDE (**Mod**elling and **De**sign) (256).

MODDE can generate and analyse a statistical DoE producing predictive models for the properties measured (256). It determines which experiments will optimally cover the design space to maximise the information content, whilst reducing the number of experiments required to cover the design space.

The model input factors' values set the design space boundaries being studied. The input factors can be quantitative or qualitative if studying processes, or they can be formulation factors if studying mixtures (256). For this project, formulation factors are used, and they correspond to the volume fractions of the alkyl levulinate, alcohol, and dialkyl ether within the selected blends. This ensures that the blends were complete, and the components were within the specified limits.

Polynomial equations were fitted to the experimental data using partial least squares regression. These equations can be used to predict the physical properties using the blend composition as the input. They were the equations of the response surface fitted to the experimental data, allowing for the prediction of the properties at points where there was no experimental measurement. The experimental data used was an average of three tests for each condition tested. MODDE does not use the error associated with the average of the three values. However, it uses replicates, which are the same point within the design space tested multiple times, and the quality of the fit is associated with the magnitude of the differences between the different replicates tested (256). The equations can be linear, quadratic, or cubic equations as shown in equations 11, 12, and 13, respectively. From these, contour plots can be generated (256, 257):

$$y = C + b_1 x_1 + b_2 x_2 + b_3 x_3,$$

Equation 11

$$y = C + b_1 x_1 + b_2 x_2 + b_3 x_3 + b_{12} x_1 x_2 + b_{13} x_1 x_3 + b_{23} x_2 x_3 + b_{11} x_1^2 + b_{22} x_2^2 + b_{33} x_3^2,$$

Equation 12

$$y = C + b_1 x_1 + b_2 x_2 + b_3 x_3 + b_{12} x_1 x_2 + b_{13} x_1 x_3 + b_{23} x_2 x_3 + b_{11} x_1^2 + b_{22} x_2^2 + b_{33} x_3^2 + b_{111} x_1^3 + b_{222} x_2^3 + b_{333} x_3^3 + b_{112} x_1^2 x_2 + b_{113} x_1^2 x_3 + b_{221} x_2^2 x_1 + b_{223} x_2^2 x_3 + b_{133} x_3^2 x_1 + b_{233} x_3^2 x_2 + b_{123} x_1 x_2 x_3,$$

Equation 13

where y could be the density or flash point, for example, C is a constant, b_{ijk} are the coefficients determined by MODDE, x_1, x_2, and x_3 are the input values, which in this case are the volume fractions of the biofuel components (256, 257). The quadratic and cubic equations have interaction terms between the biofuel components and enable non-linear dependencies to be modelled (256, 257).

MODDE constructs a model design matrix **X** based on the data to be fitted (256, 258). It consists of columns for each term in the model equation with rows which are the values of the inputs x_1, x_2, and x_3 from each experimental run (256, 258). The models are fitted using partial least squares regression and a regression model can be expressed as equation 14:

$$\mathbf{Y} = \mathbf{Xb} + \boldsymbol{\varepsilon}$$ **Equation 14**

$$\mathbf{b} = (\mathbf{X'X})^{-1}\mathbf{X'Y}$$ **Equation 15**

with **Y** being a (*N×1*) vector of responses where *N* is the number of runs. **X** is the model design matrix of size *N×p* where *p* is the number of model terms. **b** is a coefficient vector of size *p×1* which is determined by the model fitting. **ε** is the residuals vector of size *N×1* (256). The coefficients can then be determined using the least squares regression of where the variance can be calculated as:

$$\mathrm{var}(\mathbf{b}) = (\mathbf{X'X})^{-1}\boldsymbol{\sigma}^2$$ **Equation 16**

where **X'** is the transpose of matrix **X**, and the resultant **X'X** matrix is the variance-covariance matrix or the model information matrix, and **σ** is the vector of the errors (259).

MODDE gives a randomised run order of the generated experiments which reduces the influence from external factors, especially if the experiments are conducted on different days (256).

When studying the effects of the biofuel blend composition on the fuel properties when blended with diesel, separate DoE analyses had to be produced for each diesel fraction. This was due to MODDE not being able to model four-component mixtures with the required constraints. MODDE was used to determine the blend boundaries where the fuel blends were compliant with the fuel standards' physical property limits. Blends within these boundaries were then selected for engine testing.

3.3.1 Design Spaces Used

In this work three-component advanced biofuel blends were used, creating a cubic design space. Each of the three components in the blend corresponds to the x, y, and z axes of a cube and the vertices are at the top limits of the volume fractions of each component (257). The limits used were those in table 3.1 and they enabled the blend to always consist of the three biofuel components. How the design space is populated with experiments can differ depending upon the model's objective (256). The two main objectives in this work were screening and optimising the model fit and prediction capability (256).

3.3.1.1 Screening

Screening is the first stage of the DoE to construct a model of the physical properties' dependence on the blend composition. Screening determines if there is one component that has the largest effect on the measured property (256). Linear models are used in the screening stage and the experiments are chosen to cover a large volume of the design space with the fewest number of runs (256). An axial extended design was used for the initial screening, which has at least three times as many experimental runs

as components. The runs selected include the vertices, face centres, some of the interior points, and the overall centremost point. Figure 3.1 shows the points selected within the design space for screening. In the cubic design space, the centre point is at the coordinates (1/q, 1/q, 1/q) where q is the number of mixture factors (256). Therefore, in this work, the centre point is at $\left(\frac{1}{3}, \frac{1}{3}, \frac{1}{3}\right)$, which corresponds to volume fractions of 0.2, 0.2, and 0.6 for the alcohol, dialkyl ether, and alkyl levulinate, respectively. For the screening there were 12 runs consisting of the 10 different blends shown in figure 3.1 with the centre point repeated three times.
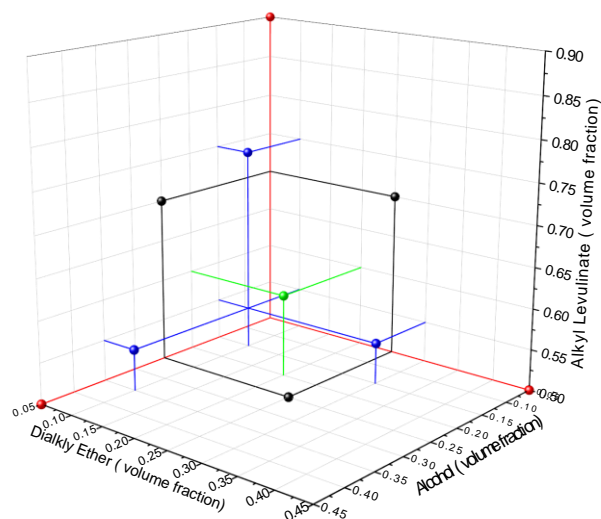
Figure 3.1. The blends used in the design space for the screening. Black points: face centres, red points: vertices, blue points: interior points, and the green point: centre point.

3.3.1.2 Optimising the Model

One method of optimising the model was using a complemented design, as it can improve the model fit, confirm component interactions, or resolve non-linearities (256). This takes the screening design space and determines additional experiments to run to improve the model fit. There needs to be at least the same number of experimental runs as there are terms in the model to be fitted (256, 258). Figure 3.2 shows the additional formulations to be tested in cyan which are determined by MODDE running a D-Optimal algorithm. The D-Optimal algorithm maximises the value of the determinant of the model information matrix **X'X** which is inversely proportional to the variance-covariance matrix (**X'X**)$^{-1}$ (256, 258-260). Hence, maximising the determinant of **X'X** should reduce the variance in the calculations of the coefficients using equation 15, as with an increased determinant there is more information available to fit a model to the data (256, 258-260). The larger the number of experimental runs, the easier it can be to obtain the largest determinant. The D-Optimal algorithm in MODDE finds the maximum determinant possible for the number of runs stated (256, 258). The D-Optimal design is sensitive to the model being fitted as the algorithm assumes it is the correct one (258, 260).
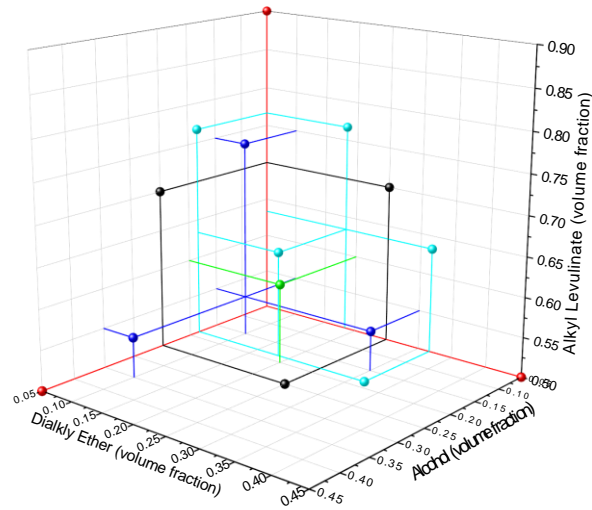
Figure 3.2. The blends selected using the complemented design function. Black points: face centres, red points: vertices, green point: centre point, blue points: selected interior points, and cyan: additional points.

3.3.2 Model Fit Parameters

To assess the quality of the model's fit and its suitability, the following model fit parameters were analysed.

3.3.2.1 R^2

R^2 is defined as '*the fraction of the variation of the response explained by the model*' (256). R^2 is determined using equation 17:

$$R^2 = 1 - \frac{\sum_{i=1}^{n}(y_i - \hat{y}_i)^2}{\sum_{i=1}^{n}(y_i - \bar{y}_i)^2},$$ **Equation 17**

where the numerator is the sum of the squares of the residuals corrected for the mean, and the denominator is the total sum of the squares of the output *y* corrected for the mean. The closer the value is to one the better the model fits the experimental data (256).

3.3.2.2 Q^2

Q^2 is an estimate for the prediction capability and accuracy of the fitted model (256). However, the goodness of the fit can be underestimated by it since Q^2 is determining the predictive capability of the model for where there is no data (256). Therefore, the model's accuracy in this region would need to be confirmed during validation and this would determine if a high Q^2 was indicative of a good prediction accuracy. The value of Q^2 is determined using a cross-validation method and is defined in equation 18:

$$Q^2 = 1 - \frac{\text{residual sum of squares from the prediction}}{\sum_{i=1}^{n}(y_i - \bar{y}_i)^2}$$ **Equation 18**

where the denominator is the same as in equation 17. A Q^2 greater than zero indicates a significant model i.e. a model for which the predicted values are better than the mean

value. The closer Q^2 is to one then generally the more accurate the model's predictions are, and the smaller the errors (256).

3.3.2.3 Model Validity

The model validity is calculated using equation 19:

$$Validity = 1 + 0.57647 \log_{10}(p_{lof})$$ **Equation 19**

where p_{lof} is the p-value for the lack-of-fit test and the 0.57647 is used so that $p_{lof} \geq 0.05$ gives a validity ≥ 0.25. If the value is larger than 0.25 there is no lack-of-fit and the model error is less than the pure error within the data, that is where the difference between the replicates is small or they are identical since experimental errors from the three repeats are not included (256).

3.3.2.4 Average Absolute Relative Difference Percentage

Another metric of the accuracy of the models is the average absolute relative difference percentage (AARD%), calculated using equation 20:

$$\text{AARD\%} = \frac{1}{n} \sum_{i=1}^{n} \left| \frac{\text{Measured Value} - \text{Predicted Value}}{\text{Measured Value}} \right| \times 100\%$$ **Equation 20**

where n is the number of experiments conducted. The lower the AARD% value the more accurate the prediction is.

3.4 Fuel Blending

In this work a splash blending approach was used where the components were blended on a volume percent (vol%) basis and mixed together. The fuel blends are produced using the addition of each component in the order of least to most volatile and stoppered between each addition to minimise any loses. For blends of diesel and the three component biofuel mixtures, the ratio of the biofuel components is fixed, and the volume of the three component biofuel mixture is increased with that of diesel decreased. The diesel fractions used in the blends were: 5, 20, 30, 50, 75, 90, and 95 vol%. These were used to cover a wide range of possible compositions and to ensure sufficient coverage of the blending regime with limited supplies of the fuel components.

Small volumes of the blends were used for the physical properties testing (either 10 or 20 cm^3). The blends were mixed by shaking by hand for one minute, with two full strokes per second. For the properties testing, the blends were made at least the day before the test, to allow the mixtures to equilibrate. For the engine testing, 2.5 L of the selected blends were mixed using a magnetic stirrer for 5 minutes, without heating, in 2.5 L high density polyethene closed containers to prevent losses.

The components used were:

- BS 2869 Red Diesel with 7 vol% FAME (Crown Oils)
- EN 590 Ultra Low Sulphur Diesel with 7 vol% FAME (ULSD) (Crown Oils)
- Ethyl Levulinate (99%, Sigma Aldrich). This was used for the physical properties testing due to its high purity.
- Ethyl Levulinate (>98%, food grade, Sigma Aldrich). This was used for the engine testing due to large volumes required and being more cost effective.
- Diethyl Ether (>99.7%, anhydrous, stabilised with 1 ppm butylated hydroxytoluene (BHT), Sigma Aldrich). Stabilised DEE was used to prevent the formation of explosive organic peroxides.
- Diethyl Ether (>99.7%, anhydrous, stabilised with 8 ppm BHT, Sigma Aldrich). This grade was used for the engine testing due to larger volumes being required and this being more cost effective.
- Ethanol (Anhydrous, ≥99.8%, VWR)
- n-Butyl Levulinate (98%, Fisher)
- Di-n-Butyl Ether (99+%, Fisher)
- n-Butanol (≥99.9%, Sigma Aldrich)
- Pentyl Levulinate (>95%, AKoS Germany)
- Di-n-amyl Ether (di-n-pentyl ether) (≥98%, Sigma Aldrich)
- n-Pentanol (≥99%, Sigma Aldrich)
- Used cooking oil (UCO) biodiesel (Olleco)

Gas chromatography mass spectrometry analysis of the pentyl levulinate supplied determined that there was 1.8% n-pentanol present as an impurity. This was accounted for when producing the blends to ensure they complied with the limits stipulated as discussed in section 1.2. Analysis of the ethyl and butyl levulinates detected negligible fractions of the respective alcohol, with their purities typically being around 99.5%, even for the >98% purity samples. This justified using the 98% purity EL for engine testing, as it was as pure as the 99% purity samples.

The volumes of each component were measured using dedicated syringes or measuring cylinders to ensure there was no cross-contamination of the fuel components. The maximum volume of the syringes and measuring cylinders were chosen to be appropriate for the volumes of the component required, thus, minimising error of the composition. The tolerance for producing the blends was ±5% of each required volume. The masses of the blends were taken after each component was added to the stoppered container. The masses were determined using the density of each component. This would ensure that the fractions of each component were correct and could be adjusted if there were transfer losses from the measuring cylinders and syringes.

3.5 Physical Properties Testing

3.5.1 Miscibility and Stability

20 cm^3 of the blends were stored at ambient temperature, typically 18 to 20 °C, and in a refrigerator (LEC, UK) at 3 °C to mimic winter conditions, in stoppered graduated test tubes for up to three months and checked regularly. The temperature and humidity of the laboratory were logged every 10 minutes using a Tinytag Plus 2 TGP-4500 logger (Gemini Data Loggers, UK). The graduated test tubes were used to enable the quantification of any separate phases (figure 3.3). For this test, red diesel was primarily used due to the colouration, enabling a clearer distinction between any separate phases that may form. There were tests conducted with ULSD to confirm that the miscibility and stability was the same regardless of the diesel used. The main differences between red diesel and ULSD are summarised in table 3.3. The molecular composition of ULSD and red diesel are typically similar, as they both consist of the middle distillate fraction from crude oil. However, an EN 590 diesel must contain <8 wt% PAH and red diesel has no limit (12, 16). This enables the CN of ULSD to be higher than a red diesel since aromatic compounds usually have a lower CN than long chain alkanes (16, 143, 261).

Table 3.3. Differences between ULSD and red diesel (12, 16, 262, 263).

Property	ULSD	Red Diesel
CN	>51	>45
Density Range (g/cm^3)	0.820 – 0.845	>0.820
Maximum Sulphur Content (mg/kg)	10	20
Colour	Clear yellow	Dyed red
KV40 (mm^2/s)	2.00 – 4.50	2.00 – 5.00
PAH Content (wt%)	<8	
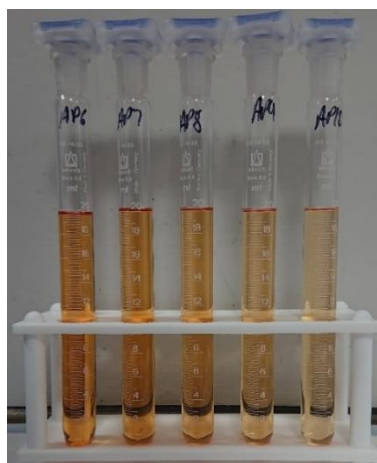
Figure 3.3. Fuel stability testing set up.

If a fuel blend was immiscible, the sample was stored for two weeks after separation to determine if there were any changes in the separation, after which it was discarded.

3.5.2 Flash Point Testing

Flash points of the fuel blends were determined following EN ISO 3679: Determination of flash no-flash and flash point – Rapid equilibrium closed cup method (118). EN ISO 3679 was used, as the flash point tester available was a Stanhope Seta Setaflash Series 3 plus.

EN 590 and BS 2869 state the use of a Pensky Martens Closed Cup flash point tester following the EN ISO 2719 procedure (12, 16, 264). However, there is no access to this equipment within SCAPE. Pensky Martens flash point testers require greater sample volumes, and due to cost limitations, the use of the small scale Setaflash was more suitable as only 2 ml of sample is needed for each test (118, 264). The sensitivity of the Setaflash Series 3 plus is 1 °C and EN ISO 3679 has a repeatability limit of $0.0152(X+110)$ °C, where X is the measured flash point (118). Three measurements were taken and the average was used as the reported flash point. The standard deviation is used as the error.

Due to the flash points of the blends being unknown, the ramp method on the Setaflash Series 3 Plus was used, where at every degree a flame is presented to the sample to test if there is a flammable vapour produced. This is repeated until a flash is detected by the detector on the Setaflash Series 3 Plus. The flash point could have implications for the further testing and the safe handling of the fuel blends as health and safety protocols must be followed as detailed by the Health and Safety Executive (265) in the document 'Safe use and handling of flammable liquids'. Hence, it was the first physical properties test conducted to enable safe protocols for fuel handling to be designed and any appropriate procedures put in place to ensure the safe use of the fuels when conducting subsequent testing.

3.5.3 Density

To determine the density of the blends, two methods were used: ISO 3838 and ISO 12185 (266, 267). ISO 3838 is a pycnometer method and is suitable for determining the density of mixtures, including those with volatile components (267). A pycnometer has an accurately known volume and is suitable for use over a wide temperature range. For this work 5 cm^3 pycnometers were used so that as little sample could be used, due to component cost and volatility. However, since the blends are cooled to below room temperature, the rate of the loss of volatile components is reduced and the accuracy can be maintained.

The empty pycnometer was submerged into a water bath at 15 °C and held for 20 minutes, after which the mass of the empty pycnometer was taken using a Mettler Toledo NewClassic MF MS105 balance, with an accuracy of ±0.01 mg. The pycnometer is then filled, cooled to the test temperature, with the volume adjusted to allow for thermal expansion or contraction. For expansion, the excess would flow out through the capillary and is then wiped away. For contraction, additional sample was added and the temperature is allowed to equilibrate. Once the volume and temperature were stable, the mass of the dry filled pycnometer was taken. The density of the sample was then calculated using the following equation from the ISO 3838 method (267):

$$\rho_t = \frac{(m_t - m_0)\rho_c}{(m_c - m_0)} + C \qquad \textbf{Equation 21}$$

where:

- m_t is the mass of the filled pycnometer at the test temperature in grams (267)
- m_0 is the mass of the empty pycnometer in grams (267)
- m_c is the mass of the pycnometer filled with water for calibration in grams (267)
- ρ_c is the density of water in g/cm^3 (267)
- C is the correction for air buoyancy (267)
- ρ_t is the density of the sample at the test temperature in g/cm^3 (267).

ISO 12185 was conducted using an Anton Paar SVM3000 Stabinger Viscometer with the temperature set to 15 °C, using its oscillating u-tube (266). The density measured using both techniques was compared to ensure consistency and accuracy between both methods. The use of the SVM3000, particularly for the more volatile fuel components, was typically more reliable as the closed set-up ensured that there was minimal loss due to evaporation. The SVM3000 had a measurement range of 0.65 to 3.0 g/cm^3 and a sensitivity of 0.0001 g/cm^3.

Three measurements were taken using either method and the average was used as the reported density. The standard deviation of the measurements is used as the error. For density measurements the SVM3000 has a repeatability limit of 0.0001 g/cm^3, which is lower than the ISO 12185 repeatability limit of 0.0002 g/cm^3, and the ISO 3838 method has a repeatability limit of 0.0007 g/cm^3 (266, 267).

3.5.4 Kinematic Viscosity Testing

The kinematic viscosities were measured using an Anton Paar SVM3000 Stabinger Viscometer following BS EN 16896 (268). The temperature of the SVM3000 could be set from 5 °C to 100 °C. The temperature of the SVM300 was set to 40 °C such that the KV40, required for EN 590 and BS 2869, was measured (12, 16). The SVM3000 had a

measurement range of 0.2 to 20.000 mm^2/s. The test involved injecting 5 cm^3 of the fuel blend through the viscometer for a total of three runs, with the averages used and the standard deviation being used as the error.

In the diesel standards, the viscosity must be determined using the BS EN ISO 3104 method (15, 16, 269). BS EN ISO 3104 requires glass capillary viscometers to be used in a temperature controlled bath to measure the viscosity of a fuel and determines the kinematic viscosity (269, 270). However, this method could not be used with the facilities available in SCAPE. In BS EN 16896 (268) there is the following statement:

'During the ILS all samples were tested according to EN ISO 3104 and to this document. Based on statistical analysis according to EN ISO 4259, no significant bias between the two test methods was found.'

The ILS was an inter-laboratory study where 21 different laboratories tested 12 different samples with KV40s ranging between 2.61 mm^2/s to 5.50 mm^2/s and this study found that both viscosity test methods were comparable. Therefore, within this measured range it could be said that there is no difference between the BS EN ISO 3104 and the BS EN 16896 test methods. As a result, the use of BS EN 16896 in this work should give reliable and accurate results since the fuel blends should have KV40s within this range (table 2.6) (268, 269). When using the SVM3000, a N7.5 viscosity standard (Paragon Scientific, UK), with certified dynamic and kinematic viscosities, and densities, at a range of temperatures, including 40 °C was always tested. This ensured the viscometer was measuring accurately and was within the tolerance of the standard. The SVM3000 has a repeatability of 0.09% for KV40 measurements and BS EN 16896 has a repeatability limit of 0.0105-0.0003X mm^2/s, where X is the measured KV40 (268).

3.6 Fuel Characterisation

To characterise the fuel's elemental composition, elemental analysis was conducted. The carbon, hydrogen, and oxygen content of the fuel are needed for the engine testing as one of the inputs into the MEXA7100D Exhaust gas analyser.

3.6.1 Elemental Analysis

Elemental analysis of the ULSD with and without biofuel blends was conducted using an EA112 Flash Analyser (Thermo-Scientific, USA). This measured the amount of carbon, hydrogen, nitrogen, and sulphur present in the fuels. Oxygen was measured using the same instrument but could also be determined by subtracting the carbon, hydrogen, nitrogen, and sulphur from the total composition. The liquid was weighed into the capsule and then analysed straight away to reduce any evaporative losses. This analysis was conducted by the SCAPE analytical laboratory technicians at a time where the laboratory was run as a service due to the COVID-19 restrictions in place.

3.7 Engine and Emissions Testing

Similar to the physical properties testing, three repeats at each engine load were conducted. The average values were used for the engine performance and emissions with their standard deviations being used as the error.

3.7.1 Engine Specification

The engine tests generated both engine performance and emissions data. The engine performance parameters included the IDT, fuel consumption, in-cylinder pressure, and IMEP. Engine tests were conducted using a single-cylinder Yanmar L100V series CI engine, as part of a genset and detailed in table 3.4. The generator used was a MG6000 SSY generator (MHM Plant, UK), using a E1C10M H alternator (Linz Electric, Italy) and this was connected to a Hillstone HAC240-10 resistive loadbank through a 230 V 32 A socket. The Yanmar L100V is a naturally aspirated, air cooled engine. It runs at a fixed speed of 3000 RPM (revolutions per minute), as it does not have a throttle, with a maximum continuous output of 5.7 kW and a maximum rated output of 6.3 kW (271). The fuel flow is controlled through the use of a governor, where more fuel can flow to the injector as the RPM decreases. The injectors are mechanic and the injection duration is dictated by the RPM, where more fuel is injected at the higher load with lower RPM. The loadbank can have the resistance changed to result in electrical powers of 0 up to 4 kW, in 1 kW intervals, where 0 kW is the engine idle condition. The losses of the alternator and the losses of electrical transmission the maximum loadbank power was 4 kW, but the engine had a maximum continuous output of 5.7 kW. The load was controlled by the controller in the engine laboratory control room. The current, voltage, and frequency of the electricity transferred to the loadbank was logged using the software provided by Hillstone.

Table 3.4. Yanmar L100V engine parameters.

Parameter	Value
Number of Cylinders	1
Injection Timing (degrees BTDC (before top dead centre))	13.5
Compression Ratio	21.2
Injector Pressure (MPa)	19.6
Speed (RPM)	3000 ± 100
Maximum Continuous Output (kW)	5.7
Valve Opening Pressure (MPa)	19.6
Bore (mm)	86
Stroke (mm)	75
Displacement (cm^3)	435
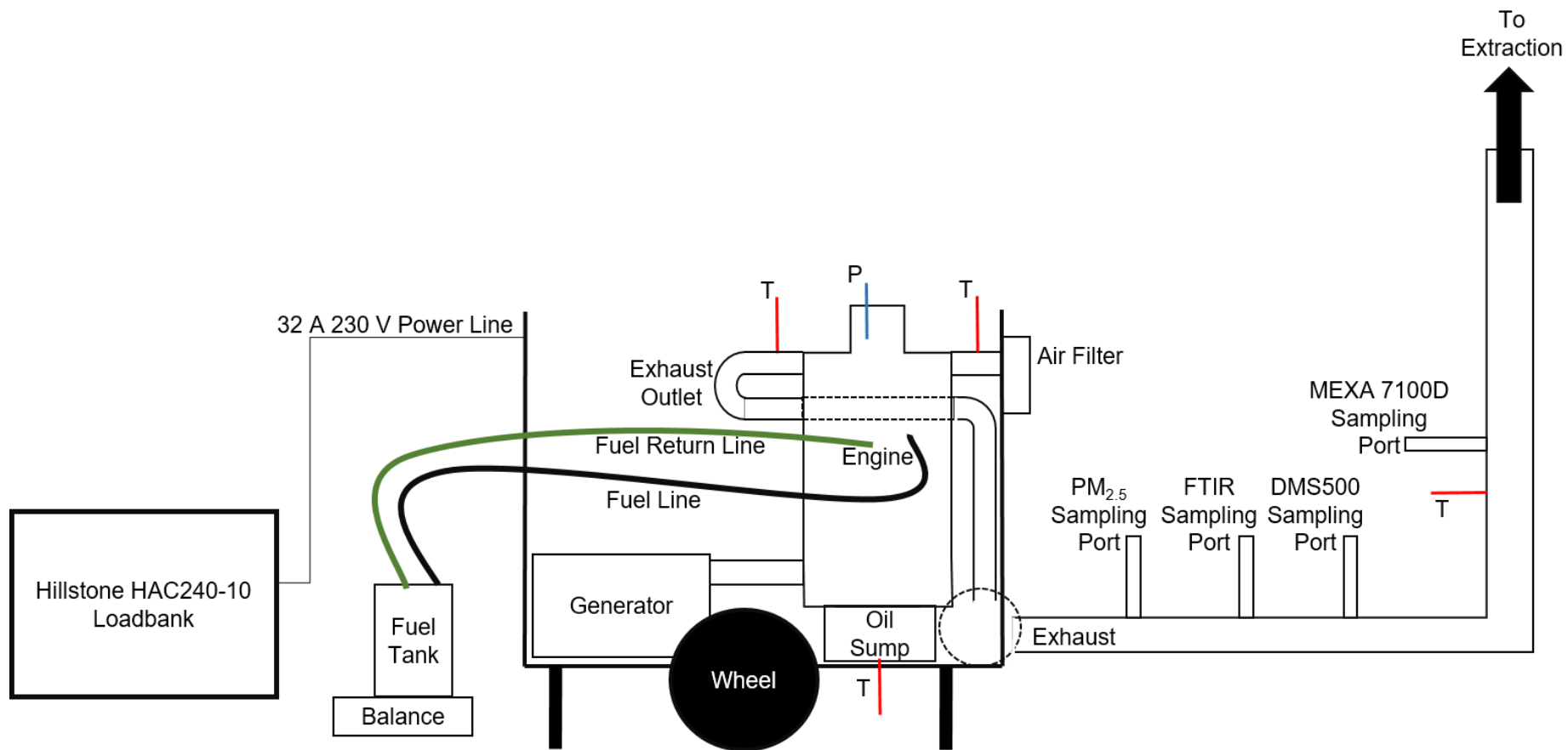
Figure 3.4. Schematic of the engine test bed with sampling locations, thermocouples shown in red labelled with T, and pressure transducer labelled with P in blue.

The in-cylinder pressure was measured using an AVL GH14D pressure transducer connected to an AVL FlexIFEM Indi 601 charge amplifier. The crank angle degree (CAD) and RPM were determined using the pressure data. These allowed for IDTs to be calculated. The RPM was calculated using the pressure transducer data by using the point of TDC (initial pressure peak) and an assumed constant angular velocity. The time interval for four strokes was measured, i.e. the time taken for the pressure to reach that of TDC twice. The average time taken to complete 10 cycles and the assumed constant angular velocity were used to calculate the RPM in an algorithm in LabVIEW. The CAD was determined from the point at which the pressure reaches 20 bar during the compression stroke, as this point has a fixed CAD and is before combustion has begun, at which point the algorithm is initiated. The time between the point of 20 bar and TDC (0 CAD), and the RPM are used in the algorithm to determine the CAD with a resolution of ±0.5 CAD. The algorithm used to calculate the RPM and CAD was previously written into LabVIEW. The temperatures at four locations were measured using k-type thermocouples, these were: inlet manifold, exhaust manifold, downstream of the exhaust, and the oil sump. The following emissions analyses were conducted on the exhaust gases using the apparatus and methods summarised in table 3.5. The location of the thermocouples and sampling ports are shown in figure 3.4.

Table 3.5. Emissions analysis available on the test engines.

Emission	Analysis Method	Apparatus	Data Logging Rates
CO/CO_2	Non-dispersive infrared (NDIR)	Horiba MEXA-7100D	Every 10 seconds
O_2	Paramagnetic susceptibility		
NO_x	Chemiluminescence		
THC	Flame Ionisation Detection (FID)		
Particulate Matter	Electrical Mobility	Cambustion DMS500 Fast Particle Analyser	Every 0.5 seconds
	Cascade Impactor	$PM_{2.5}$ Cyclone	Continuous
VOCs	Fourier Transform Infrared (FTIR)	Gasmet FTIR	Every 13 seconds (samples for 10 seconds, analyses for 3 seconds)

3.7.1.1 Fuel Injectors Used

In this work two fuel injectors were compared, the FJ and FB injector. New fuel injectors were used to ensure there was a clean, deposit-free injector in the engine prior to testing. Their specifications are summarised in table 3.6. The FB injector is the injector that is pre-installed, as standard, to the Yanmar L100V engine so it complies with the

emissions limits set in the Euro Stage V emissions standard. The FJ injector is used in older specifications of Yanmar L100 engines, before compliance with the Euro Stage V emissions standard. The use of the FJ injector enabled the influence of the fuel on an older specification to be investigated, which would be representative of using the fuel blends as a drop-in fuel in older specification engines. The use of the FJ injector still allowed the trends in the influence of the addition of the advanced biofuels on the emissions and performance to be determined.

Table 3.6. Comparison of fuel injector specifications.

Property	FJ Injector	FB Injector
Number of Holes	4	5
Hole Diameter (μm)	227	184
Cone Angle (°)	150	150
Injection Pressure (MPa)	19.6	19.6

3.7.2 Standardised Engine Test Run

The engine test run was standardised to a steady state run for 20 minutes at the selected load. The genset was run with the electrical power set to either idle (0 kW), 1, 2, 3, or 4 kW. Prior to running the tests, the engine was run using ULSD to warm up the engine and get the lube oil above 50 °C. Once the lube oil was up to temperature the fuel was then changed to the test fuel. Prior to use of the biofuel blends, the fuel line was purged by running the fuel pump and draining the residual fuel into an empty container to remove the ULSD used for the engine warm up. The biofuel blends were then attached and allowed to pump through the fuel line to ensure there was no air in the fuel line. The engine was then run to burn 100 g of the fuel blend to ensure the engine was running using solely the test fuel and any residual diesel was consumed. The engine was allowed to stabilise before the data logging would begin, and the emissions analysis started.

The compatibility of the fuel blends and the materials used within the engine, such as fuel lines, was reviewed regularly to ensure the use of these fuels were not causing damage that would make the fuels not suitable for commercial use. For example, DEE is not compatible with high and low density polyethene but is compatible with Teflon (272). Therefore, the fuel containers were also regularly checked to ensure they maintained structural integrity.

For the engine testing, a diesel baseline set of experiments was taken prior to any engine testing with the biofuel blends. There was a baseline taken for each fuel injector along with baseline checks after long periods of no use and after any equipment repairs and servicing. All of the changes in emissions and engine performance parameters

analysed were calculated relative to the corresponding diesel baseline depending on what fuel injector was used.

3.7.3 Fuel Consumption

The fuel tanks were on a set of scales to measure the change in mass which can be used to determine fuel efficiency. The scales could read in 10 g intervals and the masses were logged using the LabVIEW programme developed by previous researchers.

3.7.4 Ignition Delay Times from the Engine

The IDT from the engine can be determined from the engine using the crank angle and the engine RPM as per the method used by Wu et al. (214). The IDT can be calculated using equation 22:

$$\text{IDT (ms)} = \frac{\text{CA(SOC)} - \text{CA(SOI)}}{720°} \times \text{t}_{\text{cycle}} \qquad \textbf{Equation 22}$$

where $CA(SOC)$ is the crank angle at the start of combustion, $CA(SOI)$ is the crank angle at the start of injection, and t_{cycle} is the time for two revolutions (214). The $CA(SOI)$ is defined as 13.5°±0.5° BTDC. The error in IDTs was ±0.5 CAD, as this was the accuracy on the logging of the CAD. The $CA(SOC)$ is defined as the point at which the change in pressure is at its greatest after TDC, i.e. where the differential of the pressure is at its maximum after TDC.

3.7.5 MEXA Exhaust Gas Analyser

The MEXA was connected downstream of the exhaust through a heated line. The heated line was set at 191 °C to ensure the water vapour did not condense and the hydrocarbons remain in the gas phase. The measurement ranges and sensitivity for each analyser are summarised in table 3.7. Prior to the first engine test of the day the MEXA7100D was calibrated using calibration gases of known concentrations shown in table 3.8. Their use ensured the measurement accuracy.

Table 3.7. Measurement ranges and sensitivity of the MEXA emissions analysers.

Emission	Analyser	Measurement Range	Sensitivity
CO_2	CO_2 NDIR	0 – 20 vol%	0.01 vol%
CO	CO (L) NDIR	0 – 5000 ppm	1 ppm
	CO (H) NDIR	0 – 12 vol%	0.01 vol%
THC	FID	0 – 50000 ppm	1 ppm
NO_X	Chemiluminescence	0 – 10000 ppm	1 ppm
O_2	Paramagnetic Susceptibility	0 – 25 vol%	0.01 vol%

Table 3.8. Calibration gases used for the MEXA7100D.

Calibration Gas	Emissions
450 ppm nitric oxide (NO) in nitrogen	NO_X
4500 ppm CO, 5000 ppm C_3H_8, 800 ppm NO, 14% CO_2 in nitrogen	CO, CO_2, THC
150 ppm C_3H_8, 2% CO, 7% CO_2	CO, CO_2, THC

The main sources of errors from the MEXA7100D are due to damage to the analysers, incorrect calibration, blockages in the sample lines, and blockages in the filters used to remove particulates and other contaminants. The filters were regularly changed and the sample lines were cleaned with compressed air periodically. The analysers were purged with nitrogen between each test to ensure there was no trace of the exhaust gas from the previous test.

CO and CO_2 emissions were measured using NDIR which uses a fixed wavelength to detect specific gases. Different compounds have different characteristic infrared active bond stretches that absorb a specific wavelength of infrared light which can be selected to probe for that emission (273). In the NDIR analyser, there is a reference cell that contains an inert gas (nitrogen) and the sample cell where the exhaust gases flow (273). The gases analysed by NDIR must be dry, as the water present can cause interference with the infrared absorbance (273). To do this the NDIR analyser can be heated which enables gases to be measured directly without an additional drying step (273). There were three NDIR analysers in the MEXA7100D. They were for CO (high (>1 vol%)), CO (low (<5000 ppm)) and CO_2. The CO (low) analyser was used in this work since the CO emissions were below 5000 ppm.

The oxygen content was measured using paramagnetic susceptibility as oxygen molecules have a strong magnetic susceptibility and are attracted to magnetic zones (274). The detection cell has a dumbbell of two nitrogen-filled glass spheres which is suspended between two sets of magnetic poles (274). When oxygen is present it is attracted to the magnets and the spheres on the dumbbell are deflected and this movement is detected by light detection (274). To move the dumbbell back to the original position, a current needs to be applied through a feedback coil. This current is proportional to the oxygen concentration (274).

Nitrogen oxides (NO_X) were measured using chemiluminescence (275). Firstly NO_2 must be converted to NO by reacting it with carbon. The NO can then be reacted with ozone producing an excited NO_2 molecule, which upon relaxation emits a photon which is detected using a photodiode (275, 276). The concentration of NO_X is directly proportional to the amount of light detected and it will be a sum of NO and NO_2

concentrations converted to NO (275, 276). For this analyser there needed to be a steady supply of oxygen to produce ozone.

THC emissions were measured using FID. This takes the exhaust gases and burns them in a hydrogen/helium flame, during which ions are created where the number of ions produced is proportional to the amount of carbon atoms present (275, 276). The flame is held between two electrodes and the ions produce a small current which can be measured and can give the number of hydrocarbon molecules (275, 276). FID gives a measurement for the total hydrocarbons in terms of methane content, usually CH_4 ppm (ppmC). The FID technique used in the MEXA7100D cannot differentiate between the species of different hydrocarbon compounds present in the exhaust gas, it can only quantify the amount of these (275, 276).

3.7.6 Air-Fuel Ratio

The air-fuel ratio (AFR) was determined by the MEXA 7100D using the elemental composition of the fuels tested and the exhaust gas composition, with the Brettschneider/Spindt method used to determine the equilibrium constant for the water/gas reaction (277). The air composition used was 79.05% N_2 and 20.95% O_2, with a gross molecular weight of 28.89 g. The AFR was reported as whole integers and its accuracy was reliant on accurate measurements of the species in the exhaust gas by the MEXA. The formula used in the MEXA7100D to determine the AFR was:

$$AFR = \frac{[CO_2] + \left[\frac{CO}{2}\right] + [O_2] + \left[\frac{NO}{2}\right] + \left(\left(\frac{H_{CV}}{4} \times \frac{3.5}{3.5 + \frac{[CO]}{[CO_2]}}\right) - \frac{O_{CV}}{2}\right) \times ([CO_2] + [CO])}{\left(1 + \frac{H_{CV}}{4} - \frac{O_{CV}}{2}\right) \times ([CO_2] + [CO] + n[HC])}$$

Equation 23

where [X] is the gas concentration in vol%, and those measured in ppm were converted into vol%. H_{CV} is the H/C fuel molar ratio, O_{CV} is the O/C fuel molar ratio, and n is the number of of carbon atoms in the molecule used in the HC measurement. In this work n=1, as the HC emissions are measured in ppmC (methane equivalents).

3.7.7 Fourier Transform Infrared Spectroscopy

A Gasmet DX4000 FTIR (Gasmet, UK) was used to measure a range of species as summarised in table 3.9. The spectral data for n-butanol, DNBE, DEE were added to the library as they were provided by Gasmet. The sample of the exhaust stream was passed through a filtered sampling probe at 180 °C prior to the sampling unit and FTIR cell. This was a stainless steel gauze filter with a pore diameter of 0.1 μm. This was to

remove the soot before going into the sample pumping unit. The cell and the pumping unit were maintained at 180 °C, to ensure there was no condensation of water and to reduce the condensation of the VOCs.

There is also a zirconia sensor as part of the FTIR to measure the oxygen concentration in the sample. This was compared to oxygen measurements from the MEXA 7100D for validation purposes. The species underlined in table 3.9 were the compounds of interest to this work as they are indicative of incomplete combustion. The compounds include formaldehyde, hexane, and acetic acid, as the formation of formaldehydes has been shown to increase for the use of oxygenated biofuels. The FTIR was used to measure DNBE, DEE, ethanol, and n-butanol as unburnt fuel. The NO_X species measured by the FTIR were checked against the values obtained from the MEXA. The CO measurements from the MEXA and FTIR were also compared, for validation, as NDIR and FTIR both use infrared techniques.

Table 3.9. FTIR Species measured and their calibrated ranges. Those of interest are underlined**.**

Species	Range (ppm)	Species	Range (ppm)
Acetaldehyde	0 – 100	Ethanol	0 – 100
Acetic Acid	0 – 100	Formaldehyde	0 – 200
Acetylene	0 – 200	Furfural	0 – 100
Ammonia	0 – 500	Hexane	0 – 100
Benzene	0 – 100	n-Butanol	0 – 100
Butadiene	0 – 100	Nitrogen Dioxide	0 – 1000
Carbon Monoxide	0 – 10000	Nitrogen Monoxide	0 – 500
Carbon Dioxide	0 – 20 vol%	Propane	0 – 100
Diethyl Ether	0 – 100	Sulphur Dioxide	0 – 1000
Di-n-Butyl Ether	0 – 100	Water Vapour	0 – 25 vol%

The accuracy of the FTIR depended on the calibration files available in the files library. Provided a species was within the calibration range and above the measured value when a nitrogen spectra was taken, the values could be used. The VOCs from the FTIR were determined as the difference between a sample of ambient air and the measured exhaust sample. This was to ensure that only the combustion products were reported and not any contaminants of air.

3.7.8 Particulate Matter Measurements

3.7.8.1 Particle Size Distributions

The Cambustion DMS500 was used to measure the particle size, particle number size distribution (PNSD), and the total particle number (PN) (278, 279). The DMS500 classifies particles using electrical mobility. The PNSD can be measured between 4 nm and 1000 nm, with the number of particles within defined particle diameter ranges measured by the DMS500. The detection limit for the PN is 2×10^4 #/cm^3, hence it can be inaccurate for particles with diameters <10 nm due to their low numbers. An example PNSD can be seen in figure 3.5.
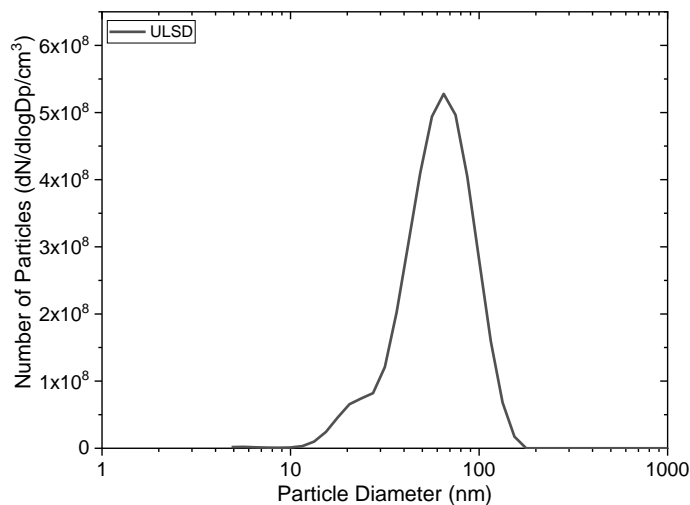
Figure 3.5. PNSD of ULSD at 92% load.

The PN is determined as the integral of the PNSD between 4 and 1000 nm (278-280). The exhaust was sampled through a heated sample line at 55 °C through the first separating cyclone at 8 L/min to remove particles above 1000 nm in diameter. The DMS500 has two stages of dilution to ensure there is a sufficient particle concentration to be measured but not too high such that the DMS500 would become contaminated. The first stage has a dilution factor of 5, and the second a dilution factor of 160, giving a total dilution of 800. The first dilution stage used dry air as the diluent and the sample stream is then passed through a second separating cyclone to ensure there are no particles greater than 1000 nm in diameter. Then the sampled stream passes through the second dilution stage which is a rotating disk dilutor. It then flows through a corona charger to induce the charge on the particles. This charged stream is then passed through the classifier with a central charged electrode surrounded by a series of grounded electrode rings (278-280). The heavier, and typically larger particles travel further through the classifier, due to their lower charge density, hence they are detected by the lower electrode rings. In contrast, the smaller, lighter particles are detected by the higher electrode rings as their charge density is greater and they are attracted to the

electrode rings more easily (278-280). The Cambustion software processes the electrode signals to determine the particle size and produce the PNSDs (278-280). The number of particles and their size distribution were measured at a frequency of 2 Hz in real time.

The changes in the particle size distributions between the different fuel blends and loads were further analysed using the MIX package within the R software environment (281-283). MIX was used to determine the distributions, which describe a particle size range that can coolectively represent a PNSDs, and their contributions to the overall PNSDs (281-283). PNSDs were fitted with $\log_{10}$-normal distributions (equation 24), where the number of distributions to give the most accurate representation of the PNSD was determined:

$$\frac{dPN_{Total}}{d \log D_{pi}} = \sum_{i=1}^{n} \left(\frac{PN_i}{\sqrt{2\pi} \log \sigma_{gi}} \exp \left[\frac{-\left(\log D_{pi} - \log CMD_i\right)^2}{2\left(\log \sigma_{gi}\right)^2} \right] \right)_i \qquad \textbf{Equation 24}$$

where D_{pi} is the particle diameter assigned to be represented by the fitted distribution i, PN_i is the particle number, σ_{gi} is the geometric standard deviation, and CMD_i is the count mean diameter. Initial estimates for σ_{gi} were used in MIX, with a value estimated for each mode (281-283). MIX attempts to fit 15 component populations to frequency data i.e. the PN for each size interval. MIX uses the maximum likelihood estimation method when fitting the mixed probability density function g, which is a weighted sum of k component densities:

$$g\left(D_p \middle| CMD, \sigma_g\right) = N_{fi} f\left(D_p \middle| CMD_i, \sigma_{gi}\right) + \cdots + N_{fk} f\left(D_p \middle| CMD_k, \sigma_{gk}\right) \qquad \textbf{Equation 25}$$

where N_{fi} is the number fraction of each fitted distribution and f is the component densities, which are log-normal.

3.7.8.2 Measurement of PM$_{2.5}$ Using a Single Stage Filter

Particulate matter with an aerodynamic diameter 50% collection efficiency at 2.5 µm (PM$_{2.5}$) was collected on GF/F glass fibre filter papers (Whattman). Prior to use, the filter papers were cut to have an 81 mm diameter and conditioned by drying in a desiccator for 24 hours. The dried filter papers were then weighed using a Mettler Toledo NewClassic MF MS105 balance, with an accuracy of ±0.01 mg. The conditioned filter paper was then used to collect the PM$_{2.5}$ sample in the engine test. The filter paper holder was wrapped in a heating jacked with a thermocouple suspended above the filter papers. The temperature of the heating jacket was set to ensure that the temperature inside the collection stage was maintained at 55±2 °C when the sample was being taken. As a result, the heating jacket could be set to temperatures upwards of 100 °C. The sampling line, cyclone, and collector were connected to a vacuum pump which had a set flow rate

of 17 L/min when sampling clean air through a blank filter. The samples were collected over the 20 minutes the engine tests were run for. After an engine test run, the filter papers were dried in the desiccator for at least 24 hours after use and then weighed. The mass of $PM_{2.5}$ was determined by calculating the difference between the blank filter paper and the dried filter paper after the test. The used filter papers were then stored in a -20 °C freezer. The sources of error in this method are from the improper handling of the filter papers and due to sample line blockages. The sample lines were regularly cleaned to reduce the likelihood of blockages and to reduce cross contamination when changing test fuels.

3.7.9 Emissions Factors

To be able to make comparisons between the engine runs and the different fuels being used, the gaseous and $PM_{2.5}$ emissions measured needed to be converted to g/kWh, and the PN to #/kWh as emission factors as reported with respect to power generated by the engine and not the genset. This was done according to the methods in BS ISO 8178-4 for the steady state testing, and weighting factors for the five loads used to determine the specific emissions for each fuel tested (255). The emissions indices will be compared against the limits set in the Euro Stage V emissions standard to determine if the engine would still meet the required limits (42). For all the emissions and performance parameters the percentage change relative to the diesel baseline was calculated using equation 26:

$$\text{Relative Change (\%)} = \left| \frac{\text{Biofuel Value} - \text{Diesel Value}}{\text{Diesel Value}} \right| \times 100\% \qquad \textbf{Equation 26}$$

3.7.9.1 Calculating Engine Power and Load

To determine the power generated by the engine for a given electrical load, the alternator efficiency at that load was needed. The alternator efficiency was determined using a polynomial fit to the manufacturer's measured efficiencies at defined loads (100% and 75%). At 50% and 25% load, where there was no defined efficiency, the same relative change in the efficiency observed for the E1S13S B/4 alternator (Linz Electric, Italy) was used to determine the efficiencies. The equation used to determine alternator efficiency is defined as:

$$Alternator\ Efficiency\ =\ 67.7 - 1.2111x_i + 1.6889x_i^2 - 0.2025x_i^3 \qquad \textbf{Equation 27}$$

where x_i is the electrical power captured by the load bank of the ith test. This approach was justified as the indicated power on the load bank would never match the maximum continuous rated output of 5.7 kW from the Yanmar L100V. The alternator efficiency could then be used to calculate the engine power using:

$$\text{Engine Power (kW)} = \frac{\text{Electrical Power}}{\text{Alternator Efficiency \%}} \qquad \textbf{Equation 28}$$

The engine loads were then determined as a fraction of the torque generated at maximum continuous rated output from the Yanmar L100V, 5.7 kW at 3000 RPM. The torque was determined using equation 29:

$$\text{Torque (Nm)} = \frac{\text{Power(W)} \times 60}{2\pi \times \text{RPM}} \qquad \textbf{Equation 29}$$

The engine loads were determined to be 4%, 28%, 50%, 75%, and 92% for the individual electrical powers between 0 – 4 kW.

3.7.9.2 Calculating the Emission Flow Rate

Since the gaseous emissions are measured on a ppm basis, to compare the different fuel blends tested, the emissions were converted into g/kWh. The exhaust flow rate (EFR) was determined using the AFR and the BSFC using the principles of mass conservation, using equation 30, which is analogous to methods used in ISO 8178 (255):

$$\text{Exhaust Flow Rate (EFR}_i) \text{ (g/kWh)} = (\text{AFR}_i \times \text{BSFC}_i) + \text{BSFC}_i \qquad \textbf{Equation 30}$$

where AFR_i was the measured AFR for test i and BSFC_i was the fuel consumption for test i in g/kWh.

The molar mass of the exhaust (M_{ex}) was determined using equation 31 as the number of moles of each pollutant were needed. This equation is analogous to methods used in ISO 8178 (255):

$$M_{ex} \text{ (g)} = M_{air} \times \left(1 + \left(\frac{1}{\text{AFR}}\right)\right) \qquad \textbf{Equation 31}$$

where M_{air} is the molar mass of air (28.9647 g/mol). The gaseous emissions in ppm were converted to g/kWh using their molar masses and their fraction in the exhaust, using the following equation:

$$\text{Specific Emission (SE}_i) \text{ (g/kWh)} = \frac{\left(M_i \times \text{EFR}_i \times \frac{\text{Ex}_i \text{ (ppm)}}{1 \times 10^6}\right)}{M_{ex_i}} \qquad \textbf{Equation 32}$$

where M_i is the molecular weight of the jth component, Ex_i was the measured value of the emission in ppm at the ith load, and M_{ex_i} is the molar mass of the exhaust gas at condition i. The same equation could be used for the species measured using the FTIR and the MEXA 7100D, where NO_X was treated as NO_2 as required in ISO 8178, and the THC emissions were as CH_4 equivalents and reported as ppmC (255). For the $PM_{2.5}$ equation 32 was used as only a fraction of the exhaust gas was directly sampled:

$$PM_{2.5} \text{ Emission (g)} = PM_{2.5}\text{captured}_i \text{ (g)}/\left(\frac{\text{sampling flow rate}_i}{\text{exhaust volume flow rate}_i}\right) \qquad \textbf{Equation 33}$$

where the sampling flow rate is the flow rate of the exhaust gas sampled using the vacuum pump and the exhaust volume flow rate is determined using the exhaust gas density and the EFR. The PM$_{2.5}$ emissions can then be calculated to be in a g/kWh basis.

3.7.9.3 Specific Emissions Index Weighting Factors

The emissions indices were calculated for each fuel using the weighting factors detailed in table 3.10 in equation 34. These emission factors were for a constant speed engine tested at a steady state. The Yanmar L100V engine speed decreases as the load increases. However, the decrease in RPM is within the 3% tolerance of a constant speed engine set in ISO 8178 (255):

$$\text{Specific Emission Index (g/kWh)} = \sum_{i=1}^{n} SE_i \times f_{WFi} \qquad \textbf{Equation 34}$$

where f_{WFi} is the weighting factor for the ith load.

Table 3.10. Weighting factors for each engine load for determining the overall emission indices, adapted from (255).

Engine Speed	100%				
Engine Load (%)	10	25	50	75	100
Weighting Factor	0.10	0.30	0.30	0.25	0.05

The loads required to determine the emissions factors were not an exact match to those achieved in the engine. To determine the emissions at the required loads the five data points generated were fitted with either an allometric curve (equation 35) or an exponential curve (equation 36):

$$y = ax^b \qquad \textbf{Equation 35}$$
$$y = y_0 + a\exp(-x/b) \qquad \textbf{Equation 36}$$

where a, b, and y_0 were coefficients determined by Origin when fitting the curves. These two equations were chosen as they had the best fit to the data and were able to reproduce the measured values. These were needed to determine the emissions at 10%, 25%, and 100% load.

3.7.10   Heat Release Rate Analysis

Heat release rate (HRR) analysis was conducted to determine the influence of the fuel composition on the nature of the heat release, including the peak HRR and its timing, along with the accumulated heat released. To determine the HRR from the experimental data, the Leeds HRR model of Olanrewaju et al. (284), adapted for application to the Yanmar L100V parameters, was used.

The required inputs for the HRR model were:

- Pressure-crank angle data
- Volume-crank angle data
- Engine speed
- Fuel flow rate
- Fuel density

The assumptions in the HRR model were:

- Homogeneity across a single combustion zone
- Ideal gas behaviour
- Evaporation of the fuel was followed by the combustion

Due to engine vibrations, the pressure-crank angle traces had high levels of noise, which, when used in the HRR model, dominated the HRR curves, making differences in the HRR curves indistinguishable. A Savitzky-Golay filter was applied to the pressure-crank angle data to reduce the noise in the pressure data. The Savitzky-Golay filter used least squares regression to fit a second-order polynomial over a moving range of 5 points (285). This method was used to ensure that the nature of the pressure trace was maintained, with reduced noise from the engine vibrations (285). The differences in the HRR with and without the filter can be observed in figure 3.6.
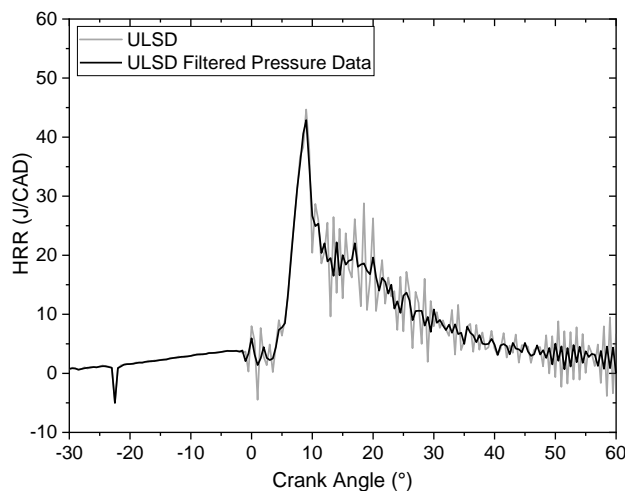
Figure 3.6. Example HRR curves to show the effects of the Savitzky-Golay filter. Grey line: unfiltered pressure data. Black line: filtered pressure data.

3.8 Combustion Modelling

As part of this project, simulations to represent the engine under load using a surrogate diesel with advanced biofuel blending were conducted. This was to determine the reactor models' and the kinetic models' suitability at replicating the combustion behaviour observed in the engine when running with the fuel blends. If there was accurate simulation of experimental engine tests, it would lead to significant cost and

time savings due to the expensive biofuel components and the time required for engine testing and analysis. To ensure there is the accurate reproduction of the chemical kinetics validated chemical mechanisms are required. However, for such novel fuel components this validation can be difficult when there is limited data available for the validation, as discussed in section 2.8.4. The modelling was used to investigate the influence of the biofuel blend on the combustion properties including IDT and HRR at a range of temperatures. The use of chemical kinetic models will therefore enhance our understanding of the relationships between the blend composition and the chemical contribution to the IDTs and HRRs.

In Chemkin-Pro (249), there is a 0D, direct injection (DI), CI engine model and a closed batch homogeneous reactor which were both tested in this work (286). The suitability of these models will need to be determined by comparing the simulated results to the experimental results. Discrepancies between the experiments and models could be due to the engine or kinetic model being unsuitable under the conditions, or a combination of both.

3.8.1 Direct Injection Diesel Engine Simulations

The Chemkin-Pro DI CI engine model includes model components for the fuel injection and spray, through to the gas phase combustion requiring chemical kinetic inputs (249, 250, 287). The spray combustion model is a combination of multiple models for the individual physical and chemical processes. They primarily consist of the models of Hiroyasu and Kadota (254), Hiroyasu et al. (288), Jung and Assanis (289), and Bazari (290).

The model inherits the principles of the sub-models used to describe the different processes involved. The DI engine model is a combination of multiple models, as a result this introduces a set of limitations from the each of the sub-models, including:

- Fixed droplet temperature
- A constant liquid injection rate
- No diffusion flame combustion
- Single zone for air
- No mixing between spray parcels as each parcel is its own reactor where the chemistry is solved
- No wall impingement model
- Wall heat loss only applies to the air zone.

The combination of these limitations, and because the model is 0D, mean that the model does not fully account for the complex nature of the fuel spray behaviour as no CFD is used (249, 250, 287). This reduces the computational demand for these models.

However, their suitability for predicting combustion behaviours will need to be assessed. The model includes the fuel spray as a series of parcels, which are a fraction of the total volume injected (249, 250, 287). Each parcel is treated as an individual reactor where, at each time step, the reaction progress is solved. At each time step, droplet variables including the droplet temperature and remaining liquid fraction are determined. These account for vaporisation and the gas-phase variables including the pressure and gas species mass fractions using the gas-phase chemical kinetics from the mechanisms provided (249, 250, 287). The conditions modelled were those observed in the engine during engine testing, as this would enable the results of the two to be compared to determine the model's suitability. The outputs from this model can include cylinder temperature and pressure profiles, species mole fractions, and IDTs (287). Simulated IDTs are defined as the time difference between the start of fuel injection and the peak OH concentration or the peak gradient in the pressure rise, although usually, these occur at the same point. The predicted values were intended to be compared to the calculated IDTs from the experimental runs.

In principle, the specification of the Yanmar L100V engine could be used as input parameters. These parameters included cylinder bore size, engine speed, compression ratio, and fuel injector specification. The CI engine model uses the gas-phase inputs of thermodynamic data, kinetic data, and transport properties, combined with the transport and thermodynamic data of the liquid fuel (287).

3.8.1.1 Liquid Fuel Input Parameters

Along with the gas phase kinetics and thermodynamic input files, certain physical properties of each liquid component are needed in the thermodynamic input file (286, 287). The majority of the data needed for the thermodynamic input file were coefficients for temperature correlations shown in table 3.11, along with other properties such as LHV. The liquid physical properties of blends are assumed to be based on ideal liquids and properties are combined using a mass-weighted mixing law (287, 291).

Table 3.11. Liquid properties data required in the thermochemistry file for the CI engine model of Chemkin 2022 R1 (287).

Property Tag Name	Description	Equation Number	Property Units
Critical Temperature	Single temperature value. Used in vaporisation model.		K
LHV	Single value. Used in the calculation of indicated specific fuel consumption.		MJ/kg
Density	Three coefficients are needed for the temperature correlation of the density.	Equation 37	kmol/m^3

Property Tag Name	Description	Equation Number	Property Units
	$$\text{Density} = \frac{A}{B^{\left[1+\left(1-\frac{T}{C}\right)^D\right]}}$$ where, A, B, and D are the three coefficients, T is the temperature and C is the critical temperature.		
Vapour Pressure	Five coefficients are needed, A to E, given for the following equation: $$\text{Vapour Pressure} = \exp\left[A + \frac{B}{T} + C\ln T + DT^E\right]$$ Where T is the temperature.	Equation 38	Pa
Liquid Heat Capacity	Five coefficients are needed, A to E are needed for the following correlations. Type 1 or Type 2 is component dependent, for example n-butane and n-heptane use Type 2. Type 1: $$\text{Heat Capacity} = A + BT + CT^2 + DT^3 + ET^4$$ Type 2: $$\text{Heat Capacity} = \frac{A^2}{1 - T_\gamma} + B - 2AC\left(1 - T_\gamma\right)$$ $$- AD\left(1 - T_\gamma\right)^2 - \frac{1}{3}C^2\left(1 - T_\gamma\right)^3$$ $$- \frac{1}{2}CD\left(1 - T_\gamma\right)^4 - \frac{1}{5}D^2\left(1 - T_\gamma\right)^5$$ Where T_γ is the reduced temperature T/T_{critical}	Equation 39 Equation 40	J/kmol K
Liquid Viscosity (dynamic)	Seven coefficients are needed. The first five, A through to E, are for the equation and the sixth and seventh are the upper and lower bounds of the correlation. $$\text{Viscosity} = \exp\left[A + \frac{B}{T} + C\ln T + DT^E\right]$$	Equation 41	Pa s
Surface Tension	Five coefficients are needed, A through to E. The first number in the property tag indicates the type of correlation, Type 1 or Type 2. Ethanol uses Type 2. Type 1: $$\text{Surface Tension} = A\left[1 - T_\gamma\right]^{\left(B + CT_\gamma + DT_\gamma^2 + ET_\gamma^3\right)}$$ Where T_γ is the reduced temperature T/T_{critical} Type 2: $$\text{Surface Tension} = A + BT + CT^2 + DT^3 + ET^4$$ Where T is temperature.	Equation 42 Equation 43	N/m

3.8.1.2 Engine Input Parameters

The Yanmar L100V engine parameters are summarised in table 3.12 and these were used in the engine simulations (287).

Table 3.12. Engine parameters needed as inputs for the Chemkin DI engine model with the values from the Yanmar L100V used in the engine testing (287).

Property	Value
Cylinder Bore (mm)	86
Stroke (mm)	75
Connecting Rod Length (cm)	27.2
Piston Pin Offset (cm)	0
Engine Speed (RPM)	3000
Compression Ratio	21.2
Starting Crank Angle (deg BTDC)	-27.5
Finish Crank Angle (deg ATDC)	60
Cylinder Pressure (atm)	1
Gas Temperature (K)	315
Gas Composition	Air: 79.05% N_2 and 20.95% O_2
Number of Strokes	4
Cylinder Temperature (K)	Load dependent
Piston Surface Temperature (K)	Load dependent
Fuel Heating Value	Fuel blend dependent
Exhaust Gas Recirculation Rate	0
Gas volume of the reactor parcels	Varies depending upon the number of parcels

The vaporisation model also needs to be selected from two options. Method one assumes that the droplet surface temperature is equal to the core temperature where the droplet energy conservation equation would be solved (286, 287). Method two allows the surface temperature to vary in the droplet, and the surface temperature is different from the core temperature (286, 287). For method two, the core temperature is calculated from the energy conservation equation, but the surface temperature is calculated using the energy balance iteratively (286, 287).

There is also the possibility to use a volume profile to account for heat losses, in a similar way as for rapid compression machine simulations (250, 287).

3.8.1.3 Fuel Injector Input Parameters

The injector parameters summarised in table 3.13 are also needed as inputs for the DI engine model (286, 287).

Table 3.13. Fuel parameters needed for the DI Engine model with the values from the fuel injectors used in the engine testing (286, 287).

Property	FJ Injector	FB Injector
Nozzle Diameter (μm)	234	185
Number of Nozzle Holes	5	4
Discharge Coefficient	0.7	0.7
Spray Cone Angle	150	150
Start of injection (deg ATDC)	-13.5	-13.5
Duration of Injection (deg)	1	1
Liquid Temperature (K)	294.15	294.15
Injected Liquid Fuel Mass (g)	Load dependent	
Liquid Composition (mass fraction)	Varies depending upon the fuel blend being tested	
Number of Parcels in the radial direction	5	5
Number of parcels in the time direction	30	30

Simulating the use of the two different injectors should enable a more rapid screening to determine the influence the injector properties have on the combustion of the biofuel blends and on the emissions produced.

3.8.2 Closed Homogeneous Batch Reactor Simulations

If it was found that the DI Engine model in Chemkin was unsuitable and could not simulate the Yanmar L100V engine, then the closed homogeneous batch reactor model available in Chemkin-Pro would be used (249). This is a 0D model that can be constant or variable volume, and is adiabatic. One caveat is that it would not represent the fuel injection and the associated processes prior to ignition. The reactor can be used to investigate the influence of the biofuel blend composition on the chemical component of the overall IDT and HRR.

3.8.2.1 Variable Volume Simulations

As the pressure-volume and pressure-crank angle data were available from the engine, a volume time profile could be generated. The RPM was used to determine the time taken to complete 360°. Firstly the time step for each 0.5 CAD was determined using equation 44:

$$\text{Time for 0.5 CAD} = \left(\frac{\text{RPM} \times 360°}{2 \times 60 \text{ seconds}} \right)^{-1} \qquad \textbf{Equation 44}$$

This time step could then be aligned with the pressure-volume profile to give the required input for Chemkin. The starting point in the volume profile was the point of fuel injection, i.e. the volume at 13.5° BTDC. The starting pressure was the measured pressure at 13.5° BTDC. Since the engine was not motored, it was impossible to do non-reactive engine tests to determine the in-cylinder temperature due to compression and to determine the heat losses. The initial temperature in the simulation was the gas temperature at 13.5° BTDC determined in the HRR analysis.

3.8.3 Kinetic Models

In the closed homogenous batch reactor model and the DI engine model the kinetic principles are the same. That is, the energy, mass, momentum, and concentrations must be conserved (249, 250). For each of these the defining equations must be solved at each time step for its given conditions. The equation for the conservation of mass is:

$$m = \sum_{i=1}^{n} m_i \text{ where } \frac{dm}{dt} = 0 \qquad \textbf{Equation 45}$$

where m is the total mass of the system, m_i is the mass of the ith component, n is the total number of species, i=1,2,3…n, and t is the time (250). During the gas phase reactions new species form and the rate at which they are generated is given as:

$$\dot{m}_{i\ gen} = \dot{w}_1 M_i V \qquad \textbf{Equation 46}$$

where $\dot{m}_i$ is the mass production rate of species i, $\dot{w}_1$ is the molar rate of production of i by the gas phase reactions per unit volume, M_i is the molecular weight of species i, and V is volume of the reactor (250). In variable volume simulations and the DI engine model the volume is time dependent (250). The resultant mass change rate of each species is given by:

$$m \frac{dY_i}{dt} = \dot{m}_{i\ gen} = \dot{w}_1 M_i V \qquad \textbf{Equation 47}$$

where Y_i is the mass fraction of species i.

The energy in the reactor must be conserved and thus the conservation of energy equation is solved. It is given by the first law of thermodynamics and for a closed adiabatic system it is defined as:

$$\frac{dU}{dt} + p \frac{dV}{dt} = 0 \qquad \textbf{Equation 48}$$

where U is the internal energy of the system and p is the pressure within the system (250). The HRR is determined from chemical state and the first law of thermodynamics (250). If the gas is assumed to behave as an ideal gas, the resultant energy conservation equation is:

$$mC_V \frac{dT}{dt} = -p\frac{dV}{dt} - \sum_i^n u_i \dot{m}_{i\,gen}$$ **Equation 49**

where C_V is the heat capacity at constant volume, T is the reactor temperature, and u_i is the internal energy of species i (250).

All of these equations are solved using Chemkin's solver, where the accuracy of the solutions depend on the accuracy of the chemical kinetic mechanism being used (250). The solutions to the ordinary differential equations (ODEs) at each time step are determined numerically. The solutions determine the concentrations of the species present and the pressure and temperatures, which have effects on the reactions described in the kinetic mechanism. In addition to these parameters, when the ODEs are solved, combustion parameters such as IDTs and HRR can be determined based upon their definitions. The solutions to these ODEs are bound by absolute and relative tolerances to ensure there is a convergent solution to the ODEs, such that the parameters at each time step do not change significantly (250).

The simulated IDTs and HRRs can be compared against those determined from the engine. The simulations can also be evaluated to investigate if the same trends on fuel blending observed in the engine testing can be replicated with the simulations.

3.8.4 Fuel Blends and Conditions Simulated

Firstly, simulations of the 100% biofuel blends were conducted to investigate their IDTs at engine relevant conditions. The 100% biofuel blends simulated were the 15 blends used in the DoE optimisation and the formulations of the three-component blends used in the engine testing.

For the ethyl-based blends with diesel, the blends simulated were those tested in the engine, and at different ratios of diesel and biofuel, to investigate the effect of the diesel/biofuel ratio. For the butyl-based blends, only the blends tested in the engine were simulated. This enabled the comparison to the engine tests to determine if the changes in the gas phase simulations relative to ULSD matched the trends observed in the engine tests and to establish if there is an influence of the physical and chemical properties of the blends on the IDT.

Since a genset typically operates at maximum load, the conditions simulated corresponded to the 92% load condition of the Yanmar L100V engine. The equivalence ratio was determined using the measured AFR values from the MEXA and the stoichiometric AFR for each fuel. The calculated equivalence ratio at 92% load was, on average, 0.5. The equivalence ratio of 0.5 was chosen as it is often used when simulating lean combustion, such as in a diesel engine. The initial conditions used in the variable volume simulations are summarised in table 3.14.

Table 3.14. Initial conditions used in the variable volume simulations.

Property	Value
Equivalence Ratio (φ)	0.5
Initial Pressure (bar)	37
Compression Pressure (bar)	56
Initial Temperature Range (K)	860 – 1060 for the ethyl-based blends 810 – 1110 for the butyl-based blends
Duration (CAD)	360

3.8.5 Mechanisms Used for Simulations

3.8.5.1 Three-Component Mechanisms

The biofuel component chemical kinetic mechanisms used in the simulations were developed as part of the SusLABB project by Dr. Christian Michelbach. He conducted the mechanism generation using RMG, followed by analysis of the generated mechanisms to ensure they were accurate (57). The analysis conducted included post-processing to implement accurate and up-to-date kinetic data for the fundamental reactions and thermodynamic data for the most sensitive reactions and species in the mechanism. RMG was used as it enabled the use of consistent rate rules, reaction classes, and functional groups to be applied when determining the kinetic and thermodynamic data for the species and their intermediates. RMG would add reactions and species that met set flux criteria into the mechanism. This methodology produced mechanisms based on kinetic principles without tuning and of the parameters to fit global properties such as IDTs. Seed mechanisms provided the initial reactions and core chemistry on which the mechanism was based. The seed mechanisms used for the biofuel components are summarised in table 3.15. The AramcoMech 2.0 mechanism was used as the C1-C4 core for the ethyl and butyl-based three-component mechanisms as this is a highly validated mechanism (292). Since there was no existing BL mechanism, a BL seed mechanism was constructed using elementary reaction rates from the literature and understanding based on the EL mechanism.

Table 3.15. Sources of each biofuel seed sub-mechanism.

Biofuel Component	Reference of the seed sub-mechanism
EL	(55)
DEE	(169)
EtOH	(293)
DNBE	(174)
BuOH	(162)

The ethyl-based three-component mechanism had 404 species and 7517 reactions. The butyl-based three-component mechanism had 1190 species and 42345 reactions. The butyl-based blend mechanism had the high number of reactions and species as the mechanism was created by merging each mechanism together rather than creating one mechanisms for the three-component blend similarly to the ethyl-based blends. The merging was conducted by Dr. Christian Michelbach as part of the SusLABB project. The ethyl and butyl-based three-component mechanisms were separately merged with the selected diesel surrogate mechanism using the RMG module 'Merging Models' to produce the combined mechanisms used in Chapter 7 (57).

3.8.5.2 Selection of the Surrogate Diesel Mechanism

The Lawrence Livermore National Laboratories (LLNL) two-component diesel surrogate was chosen for use in this work (239). This mechanism was selected because it has been validated over a range of equivalence ratios and temperatures. It consists of n-dodecane and m-xylene as a long chain alkane and an aromatic compound, as both are typically present in diesel (239). The LLNL mechanism was also chosen as a reduced mechanism is available, and this could easily be merged with the three-component biofuel mechanisms. The reduced mechanism was as accurate as the detailed mechanism in predicting IDTs for a blend of 77 vol% n-dodecane and 23 vol% m-xylene, as shown in figure 3.7 (239). There was also an accurate prediction of the IDTs of the two individual fuel components (239). The Pei et al. (239) mechanism accurately predicted the IDTs of a diesel studied by Alturaifi et al. (240), as shown in figure 3.7b. However, the DCN of the diesel Alturaifi et al. (240) studied was not reported so the mechanisms suitability for an EN 590 diesel would need to be determined.
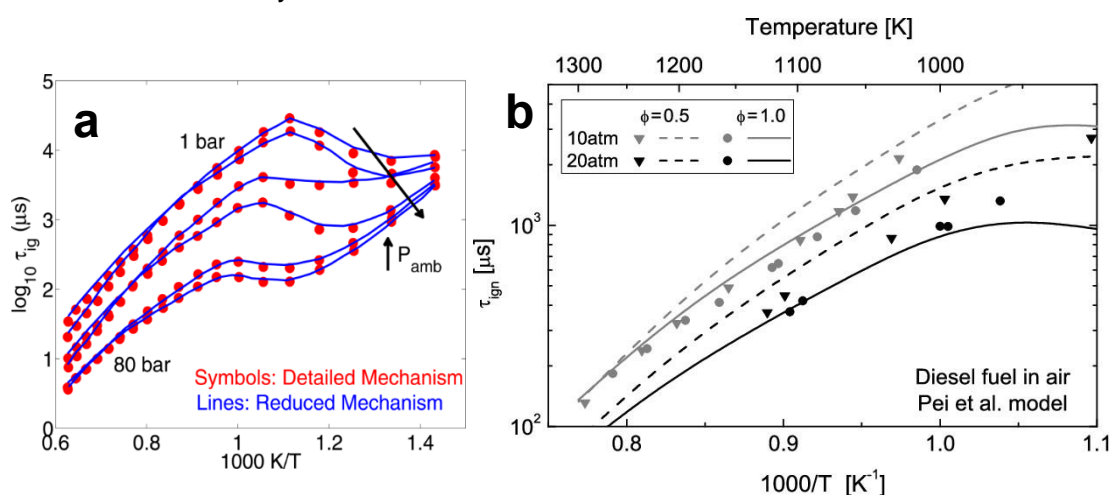
Figure 3.7. a: Comparison of the simulated IDTs from the reduced and detailed mechanism for the 77 vol% n-dodecane/23 vol% m-xylene diesel surrogate. Reproduced from (239). b: simulate IDTs using the Pei et al. (239) mechanism reproduced from (240).

The 77 vol% n-dodecane/23 vol% m-xylene blend was reported to have a DCN of 70, with n-dodecane having a DCN of 80 (239). However, in the Compendium of

Experimental Cetane Numbers, n-dodecane has a DCN of 72.9, and m-xylene has a DCN of 7.0 (143). Therefore, the blend composition of 77 vol% n-dodecane/23 vol% m-xylene would not have a DCN of 70 if a linear-by-volume or linear-by-mole blending rule was applied. When a linear-by-mole blending rule was used, the calculated DCN was 49.5. The DCN of diesel must be >51 to comply with EN 590 and is typically not much greater than this (12). As a result, a composition of n-dodecane and m-xylene with a DCN of 51 was determined using a linear-by-mole blending rule. The resultant ratio was 67 mol% n-dodecane/33 mol% m-xylene, which equates to 79 vol% n-dodecane/21 vol% m-xylene.

3.8.5.3 Merged Mechanism Accuracy

The merged ethyl-based three-component and diesel surrogate mechanism maintained the accuracy of the sub-models when predicting pure biofuel blends. This is shown by the good agreement between model simulations and the experimental IDTs of the three-component ethyl-based blend studied by Howard et al. (55), as shown in figure 3.8.
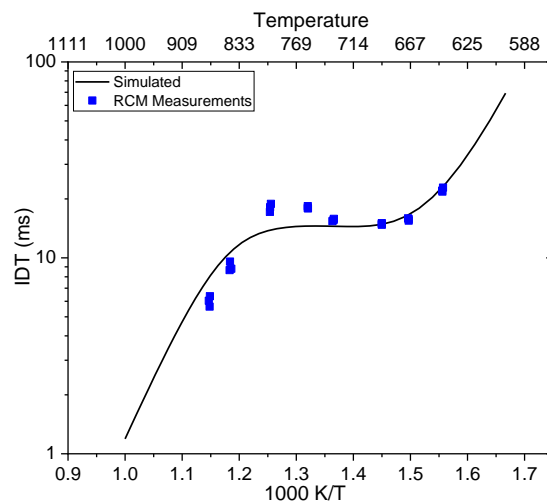
Figure 3.8. IDTs of 35 mol% EL/38 mol% EtOH/27 mol% DEE. p=20 bar and φ=1.0. Line represents the simulated IDTs using the merged RMG mechanism. Symbols represent RCM measurements taken from Howard et al. (55).

The simulations using the RMG generated mechanism are able to partially replicate the NTC region. Although the model does not fully capture the peak around 800 K there is generally a good agreement with the experimental data of Howard et al. (55). However, there is no experimental data at temperatures relevant to the operational conditions of the Yanmar L100V engine. Specifically, there is no φ=0.5 data at similar thermodynamic conditions to the Yanmar L100V at 92% load.

For the butyl based blends the merging conducted by Dr. Christian Michelbach was in a hierarchical manner to ensure that where there were duplicate reactions they would come from the mechanism higher in the hierarchy. The mechanisms were merged using

the RMG module 'Merging Models', which allowed each of the seprate mechanisms to combined (57). The order they were merged in were S-ULSD, BuOH, DNBE, and then BL. There currently no data available for butyl-based three-component biofuel blends to compare the simulated IDTs against. The BuOH and DNBE mechanisms produced using RMG can predict the IDTs reported in the literature to an acceptable accuracy, as shown in figure 3.9a and b, for DNBE and BuOH respectively. The simulations displayed in figure 3.9 were conducted as part of the work of this thesis to demonstrate and confirm the accuracy and suitability of the mechanisms Dr. Christian Michelbach produced using RMG. The simulations were conducted using a constant volume closed-homogeneous reactor (section 3.8.2) using the merged mechanism to establish the accuracy of the IDT predictions for BuOH and DNBE at different conditions. Hence, the use of these mechanisms in the butyl-based three-component blend mechanism ensures there is an accurate representation of the BuOH and DNBE combustion. The accuracy of these components also demonstrate RMG's ability to generate suitable chemical kinetic mechanisms.
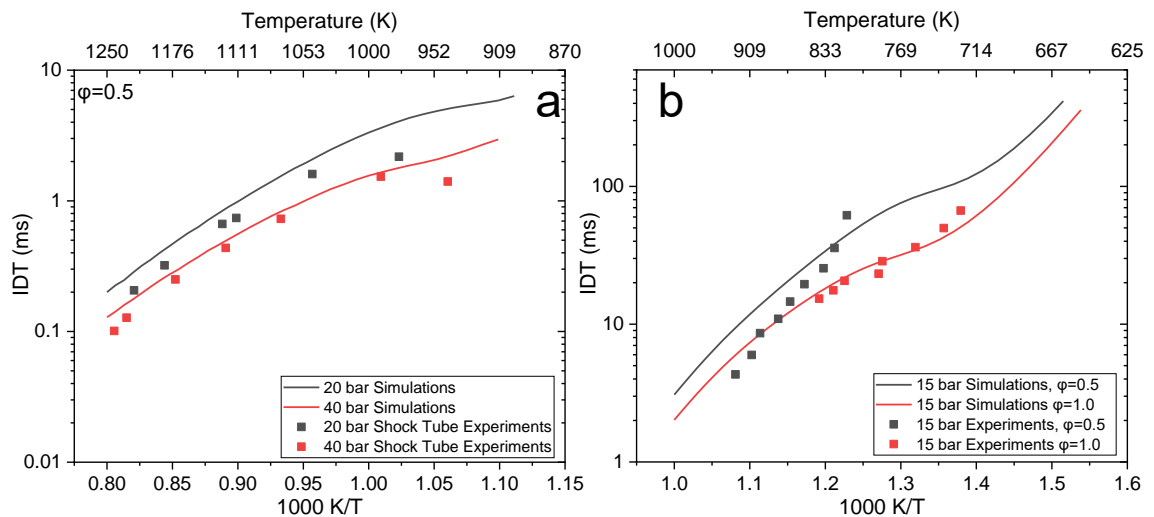
Figure 3.9. Comparisons of simulated IDTs using the RMG mechanisms to experimental data for a: DNBE using the experimental data from (158). b: BuOH using the experimental data from (175).

Chapter 4

Physical Properties of Model Biofuel Blends With and Without Diesel

4.1 Introduction

Current engines and fuel injectors are designed around the use of fuels that comply with existing fuel standards. There are also auxiliary components a fuel must be compatible with such as fuel pumps, fuel lines, and fuel tanks. Hence, fuel standards set the limits for a range of physical and chemical properties to ensure the compatibility and the efficient operation of these systems. The application and the composition of the fuel will dictate which standard must be met. Diesel used in road vehicles in Europe and the UK must meet EN 590, grade II diesel used in agricultural and off-road applications in the UK must meet BS 2869, and FAME used in Europe and the UK must meet EN 14214 (12, 15, 16). Compliance with these fuel standards may enable new low-carbon alternatives to be used as drop-in fuels, making them an attractive option to displace fossil-derived diesel and contribute towards the REDII limits for advanced biofuel utilisation (14). If fuel blends with advanced biofuels can be shown to meet the physical property limits they may be more commercially viable. In this work, three key properties were selected due to their implications for the safe handling, storage, and engine performance of the fuel blends. They were the flash point, the KV40, and the density at 15 °C, with their limits from the three fuel standards summarised in table 4.1.

Table 4.1. Summary of the physical property limits for the different diesel fuel standards (12, 15, 16)**.**

Property	EN 590	BS 2869	EN 14214
Flash Point (°C)	>55	>55	>101
Density at 15 °C (g/cm^3)	0.820 – 0.845	>0.820	0.860 – 0.900
KV40 (mm^2/s)	2.0 – 4.5	2.0 – 5.0	3.5 – 5.0

Since alcoholysis can produce a tailorable product mixture, there may be the opportunity to manufacture product blends that comply with the fuel standards' physical property limits (34-37, 112). The biofuel components that make up the ethyl, butyl, and pentyl-based blends are shown in figure 4.1.
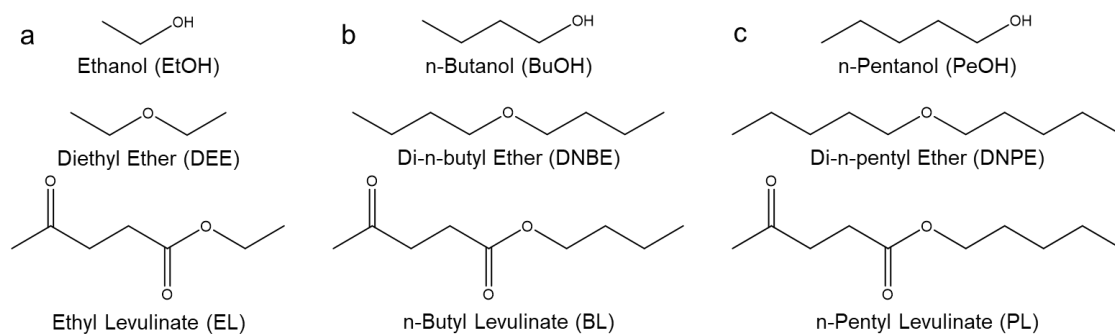
Figure 4.1. Biofuel components. a: ethyl-based blends. b: butyl-based blends. c: pentyl-based blends.

The physical properties of the ethyl, butyl, and pentyl-based blends with ≥50 vol% alkyl levulinate have not previously been tested. In addition, many physical properties models are not freely and readily available, nor are they applicable for such blends, as discussed in Chapter 2. Hence, one of the aims of this work was to produce empirically derived models that can accurately predict the properties of the fuel blends across a range of blend compositions.

As there is the potential to tailor the alcoholysis product mixture using different reaction conditions and post-reaction processing, it would be favourable to accurately predict the properties of the blends rather than test every individual formulation. This was where the use of the DoE methodology was vital, as it allowed for the selection of the most suitable blends for testing to cover the design space. Using this approach, models for each physical property of the individual three-component blends were constructed using the experimental measurements. The accuracy and suitability of the different models were determined, to establish if the property could be modelled using a linear, quadratic, or a cubic model.

The combination of experimental measurements and empirically derived models will allow for an understanding of how the physical properties of the three-component advanced biofuel blends, with and without diesel, change with their composition. The models would also allow for the determination of any potential blend limits that define the compositions where the fuels are compliant with the different diesel standards. Compliance with existing standards would be advantageous for advanced biofuel blends, making them an attractive low-carbon alternative. How the physical properties change with increasing carbon chain length are discussed in the subsequent sections of this chapter. In addition, the compositions of the three-component blends, with and without diesel, which are compliant with the different fuel standards were determined.

4.1.1 COVID Impact Statement

The work outlined in this chapter was significantly impacted by the COVID-19 pandemic. Firstly, the delays in receiving the biofuel components, and inaccessibility to

the laboratories, reduced the time available for the physical property measurements. As a result, temperature-dependent studies of the density and kinematic viscosity were not conducted. The temperature dependence of such properties was needed as inputs for the Chemkin CI engine model for the fuel injection simulation (249, 287). Additionally, other properties that are known to influence the fuel spray, such as surface tension, could not be measured due to the aforementioned reasons and social distancing measures in place which reduced training opportunities.

Secondly, when there were equipment breakages, such as for both available Anton Paar SVM3000 Stabinger viscometers, and the refrigerator used for the low-temperature miscibility studies, the time available was further reduced as engineer's visits required thorough risk assessment and safety measures to be implemented. The high costs of repairs or having measurements conducted by external laboratories reduced the number of blends tested. Hence, the data presented in this chapter was collected by the researcher, following the methods outlined in Chapter 3.

The last impact was due to the reduction in the data collected from fewer measurements. As a result, accurate models for the physical properties of the three-component blends with diesel and their dependence on the carbon chain length could not be produced within the time available whilst completing the other aims and objectives of the work.

4.2 Miscibility and Stability of Fuel Blends

If any of the advanced biofuel blends are to be utilised within fossil fuel displacement strategies, they need to be miscible, not only as a three-component blend, but also with diesel across a range of volume fractions. The blends also need to remain stable for several months, since fuels can be sat in storage for significant periods whilst being transported before their utilisation. It is also uncommon for a vehicle's fuel tank to be empty before being refilled. Therefore, there will always be some fuel of unknown age in the fuel tank. As a result, a fuel blend must remain stable and miscible with no separation, sediment, or formation of crystals.

The fuels need to be miscible and stable over range of temperatures due to the different ambient temperatures that occur worldwide and during different seasons. Hence, ambient room temperature, typically between 18 to 21 °C, and 3 °C were utilised. Higher temperature studies with the ethyl-based blends were impossible due to the boiling point of DEE being 34 °C. Higher temperatures have been shown to increase the miscibility of the alcohols, but since this work involved a three-component biofuel blend, the miscibility could be enhanced through the co-solvent effect of these components (13,

122, 126). Since the fuel tanks in the engine laboratory were at ambient conditions, the fuel blends needed to be miscible and stable at these temperatures.

The miscibility tests were conducted using red diesel and ULSD. Red diesel was used due to its colouration since the levulinates were a similar colour to the ULSD. The differences between red diesel and ULSD were discussed in section 3.5. When using both types of diesel, the miscibility was shown to be the same. The miscibility and stability of the blends when blended with red diesel and ULSD needed to be known, as it established the blend walls for the three-component blends with diesel. 20 cm^3 of the fuel blends were stored in graduated test tubes for three months for the storage tests. These tests were conducted with the ethyl and butyl-based three-component blends with diesel. The three-month storage tests were not conducted with the pentyl-based blends with diesel due to the limited availability of second-generation PeOH, which would make its real world use impractical, and the cost of PL, combined with its limited supplies.

As the storage tests ran for three months, for the miscible blends, other physical properties tests were conducted alongside the storage tests. This allowed for informed decisions about the blends that could be used in further testing.

4.2.1 Room Temperature Miscibility and Stability

The temperature of the laboratory usually remained between 18 and 21 °C. However, since the laboratory was not temperature controlled, temperature logging of the laboratory was required. There could be days where the temperatures could be below 18 °C or above 21 °C but the blends that were already miscible in the normal temperature window, remained miscible.

At room temperature, all the 100% biofuel ethyl, butyl, and pentyl-based three-component blends were stable with no separation, sediment, suspensions, or visible changes. The miscibility and stability of the three-component blends was expected since the blends consist of three polar oxygenated compounds, which should be readily miscible.

4.2.1.1 Miscibility of Ethyl-Based Blends with Diesels

When blended with either red diesel or ULSD, the miscible compositions of the ethyl-based blends were the same and the volume fractions of any separate phases were within 5% of each other. The miscibility limits for both ULSD and red diesel are shown in table 4.2. The immiscible blends were discarded after two weeks, as discussed in section 3.5, since it was unlikely they would become miscible.

Table 4.2. Miscibility limits of the ethyl-based blends with the diesels at room temperature.

Diesel Fraction (vol%)	Biofuel Fraction (vol%)	EL Miscible Fractions (vol%)	EtOH Miscible Fractions (vol%)	DEE Miscible Fraction (vol%)
20	80	50 – 75	5 – 20	20 – 45
30	70	50 – 75	5 – 20	20 – 45
50	50	50 – 75	5 – 20	20 – 45
75	25	50 – 75	5 – 20	20 – 45
90	10	50 – 90	5 – 20	5 – 45
95	5	50 – 90	5 – 20	5 – 45

The ethyl-based blends consist of the shortest carbon chain length compounds of the biofuel components being investigated, with the carbon chain length of ethanol being two carbons. The presence of >20 vol% ethanol would cause immediate separation of the blends when there was >10 vol% biofuel in the blend with diesel. Ethanol has been reported to have a range of miscibilities with diesel depending upon its purity, indicating that it would contribute to the immiscibility of the ethyl-based blends. Lapuerta et al. (294) reported that at 22 °C, blends of diesel and >15% 99.7% anhydrous ethanol were unstable. Kwanchareon et al. (126) reported the immiscibility of 99.5% ethanol when it was between 30% and 70% in diesel at 20 °C. However, the addition of 10% biodiesel resulted in miscible blends, indicating a co-solvent was needed. In the ethyl-based blends, DEE and EL could be acting as co-solvents as at least 20 vol% DEE was needed for miscibility at high biofuel fractions.
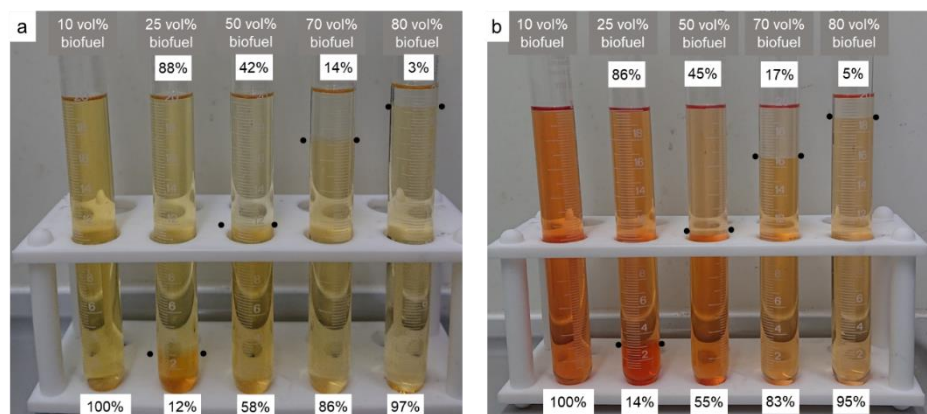
Figure 4.2. Examples of the separation observed after two weeks. a: with ULSD. b: with red diesel. The ethyl-based blend tested was 85 vol% EL/5 vol% EtOH/10 vol% DEE. The percentages indicate the fraction of the blend in the top and bottom phases.

When the ethyl-based blends with diesel were immiscible, there would always be two separate liquid phases. The volume within each portion did not match that of the fraction of biofuel and diesel, indicating there was some miscibility with one or more of

the biofuel components. Examples of the separation are shown in figure 4.2, where the percentages in each phase do not match the fractions of biofuel and diesel, indicating there has been miscibility of some of the ethyl-based biofuel components. The separation shown in figure 4.2 occurred within minutes of mixing, and the volumes each phase only varied by ±0.2 cm^3 during the two weeks of storage. This may have been due to fluctuations in the lab temperature. During the storage of the ethyl-based blends with (and without) diesel, there was no loss of the fuel blend indicating that there was a good seal and that the highly volatile DEE was unable to escape the test tube. A vortex mixer was used to establish if a different mixing method would improve the miscibility. However, the blends would still separate within the same duration as when mixed by shaking, indicating that shaking was a valid mixing technique for these small volumes. The immiscibility was likely due to the difference in carbon chain length and polarity between the ethanol and the diesel hydrocarbons, resulting in fewer molecular interactions between the molecules in the diesel and the biofuel components (294).

The high DEE fractions required to produce stable blends would likely have implications on the flash point and fuel handling due to it being highly volatile. The use of the ethyl-based blends as a diesel replacement therefore start to look unfavourable with just these tests alone, suggesting that longer carbon chain lengths could be more suitable.

4.2.1.2 Miscibility of Butyl-Based Blends with Diesels

Unlike the ethyl-based blends, all formulations of the butyl-based blends tested were miscible with both types of diesel over all volume fractions tested. Over the three months the blends were stored there was no separation at room temperature, with examples shown in figure 4.3. The increased miscibility was likely to be due to the increased carbon chain length when moving to the butyl-based three-component blends. The carbon chain lengths of DNBE and BL are similar to some of the smaller molecules found in diesel, with total chain lengths of 9 and 10 atoms, respectively, including oxygen (295).
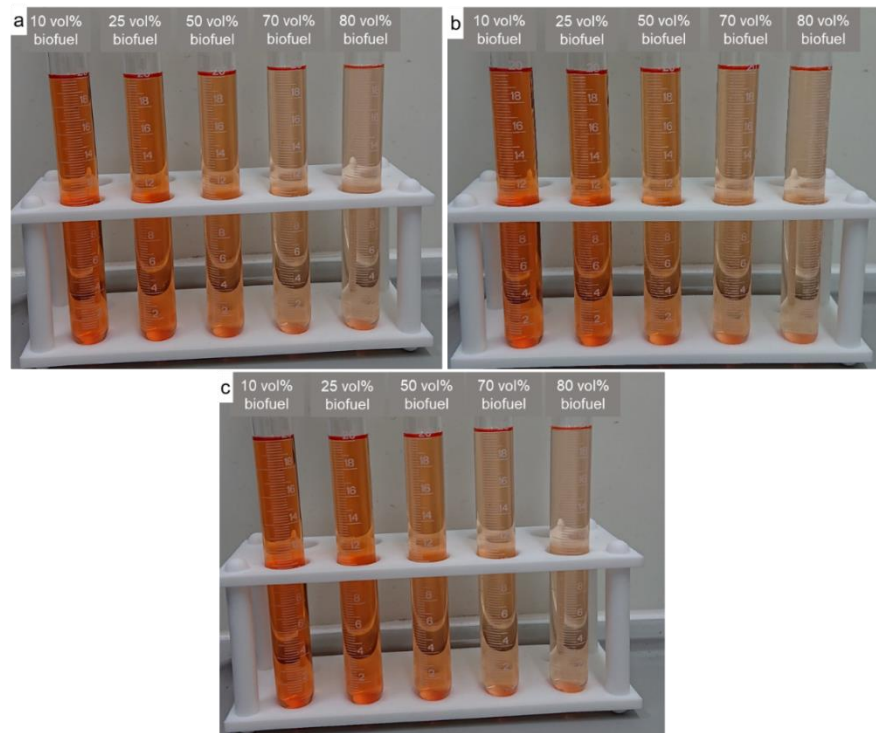
Figure 4.3. Room temperature stability tests of butyl-based blends with red diesel after 3 months of storage. a: 50 vol% BL/5 vol% BuOH/45 vol% DNBE. b: 50 vol% BL/45 vol% BuOH/5 vol% DNBE. c: 90 vol% BL/5 vol% BuOH/5 vol% DNBE.

4.2.1.3 Miscibility of Pentyl-Based Blends with Diesels

As previously mentioned no-long term storage tests of a range of pentyl-based blends with diesel could be conducted. Due to the increased carbon chain length when moving to the pentyl-based blends, they will likely be miscible with diesel as the carbon chain lengths of the PL and DNPE are similar to those of the compounds in diesel. All the individual components were miscible with diesel across all fractions when the components were blended into diesel to have the properties of the binary blends tested. These were tested to ensure there was an understanding of how the physical properties of diesel change.

4.2.2 3 °C Miscibility and Stability

The miscibility of the ethyl-based blends at 3 °C was the same as at room temperature, with limits being the same as those shown in table 4.2. This may indicate that the co-solvent effect of EL and DEE are ensuring the EtOH remains miscible, since it has been shown that at lower temperatures less EtOH is miscible with diesel (122). However, the formation of a crystalline suspension occurred with fresh samples of the ethyl-based blends stored at 3 °C, regardless of the EL fraction. These suspensions at 3 °C indicate that the fuel blends would not be suitable for use in winter or spring where the temperature can regularly drop below 3 °C. The presence of the suspension could

also lead to blockage of fuel lines and fuel filters, leading to less fuel being pumped and increasing wear on the fuel pump.

For the butyl-based blends, fresh samples were made and stored at 3 °C for three months. At 3 °C, some of the butyl-based blends with >70 vol% biofuel had the formation of a white crystalline suspension, with the limits summarised in table 4.3. If the BuOH fraction was greater than DNBE, the suspension would form with lower BL fractions, as it formed for the blend 20% ULSD/80% biofuel (50 vol% BL/45 vol% BuOH/5 vol% DNBE). The suspension formation results in the blends having two separate phases, a solid and a liquid phase. Examples of the suspension can be seen in figure 4.4.

Table 4.3. Blend limits where no suspensions formed of the butyl-based blends with diesels at 3 °C.

Diesel Fraction (vol%)	Biofuel Fraction (vol%)	BL Miscible Fractions (vol%)	BuOH Miscible Fractions (vol%)	DNBE Miscible Fraction (vol%)
20	80	50 – 75	5 – 40	10 – 45
30	70	50 – 80	5 – 45	5 – 45
50	50	50 – 90	5 – 45	5 – 45
75	25	50 – 90	5 – 45	5 – 45
90	10	50 – 90	5 – 45	5 – 45
95	5	50 – 90	5 – 45	5 – 45
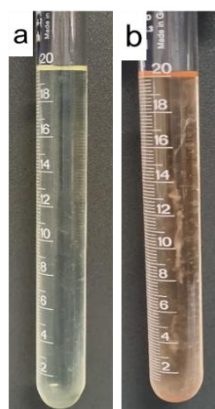
Figure 4.4. Examples of the suspension formed. Fuel blends: a: 20% ULSD/80% biofuel (80 vol% BL/5 vol% BuOH/15 vol% DNBE). b: 20% red diesel/80% biofuel (80 vol% BL/15 vol% BuOH/5 vol% DNBE).

These solids could be levulinic acid being formed from the decomposition of EL or BL through hydrolysis of the ester functional group to form EtOH or BuOH and levulinic acid (108, 112). The melting point of levulinic acid is 33 °C, which is higher than room temperature, although there was no suspension formed at room temperature. There is the potential that at 3 °C levulinic acid can no longer be held in solution, so it crystallises and forms the suspension (296). This indicates that certain fuel blends may not be

suitable for winter or spring seasons where ambient temperatures can readily drop below 3 °C. These suspensions only formed when diesel was present, as the 100% biofuel blends did not have these suspensions. This indicates that there may be some adverse interactions with the diesel, resulting in the suspension forming.

The formation of suspensions would be undesirable as they can lead to blockages of fuel lines, fuel filters, and fuel injectors. These suspensions were not reported in the literature when these fuel components were blended into diesel, as single components, DNBE/BL binary blends, or three-component blends (34, 38, 54). Antonetti et al. (34) did not report low-temperature storage tests of the butyl-based three-component blends with diesel. If the suspension was levulinic acid, it could increase corrosion, especially of the fuel pump, fuel lines, and metallic surfaces. The acid in the fuel could also lead to acidification of the lubricating oil due to fuel dilution. This could increase the oil oxidation, reduce the lubrication from the oil, and lead to further corrosion (59).

The suspensions may form at temperatures around 3 °C as the suspension melts quickly as the samples come up to room temperature. The isolation of these suspended crystals was not possible because of this feature. Cloud point tests would confirm this, as they find the temperature at which crystals first form in the fuel (297, 298). It was hypothesised that the age of the BL could influence the formation of these suspensions as esters can hydrolyse over time to produce their acid and alcohol counterparts. Gas chromatography mass-spectrometry analysis of an older BL sample indicated a higher levulinic acid content than the newer bottles. However, these suspensions formed regardless of the age of the BL.

4.3 Density at 15 °C

The density of the fuel blends must be known due to the implications it has on the fuel injection. The density was measured using the two density testing methods discussed in section 3.5.3, ISO 3838 and ISO 12185 (266, 299). The SVM3000 was used for its speed and because it required less sample. The ethyl and butyl-based three-component blends were initially tested following ISO 3838, as this was the method available at the time (266). The butyl-based blends with diesel and the pentyl-based three-component blends with and without diesel were tested using the SVM3000, following ISO 12185 (266). The difference between densities of the same blends when measured using both methods was <1%, which confirmed that both measurement techniques give consistent results and both methods could be used interchangeably.

4.3.1 Density of the Three-Component Biofuel Blends

The density of the three-component blends ranged between 0.8760 – 0.9895 g/cm^3, 0.8738 – 0.9572 g/cm^3, and 0.8782 – 0.9498 g/cm^3 for the ethyl, butyl, and pentyl-based blends, respectively. The experimental ternary diagrams for the ethyl, butyl, and pentyl-based three-component blends' density can be seen in figure 4.5a, 4.5b, and 4.5c, respectively. None of the ethyl, butyl, or pentyl-based three-component biofuel blends were within the limits of the EN 590 standard, whereas they were compliant with the limits of BS 2869 since there is no upper-density limit for a grade II diesel (12, 16). There were blend compositions compliant with EN 14214 limits of 0.860 – 0.900 g/cm^3 (15). From inspection of figure 4.5, it can be seen that these required <60 vol% EL, <62.5 vol% BL, and <65 vol% PL, for the ethyl, butyl, and pentyl-based blends, respectively. Upon construction of the models, MODDE was used to accurately determine the blend boundaries to be compliant with these limits.
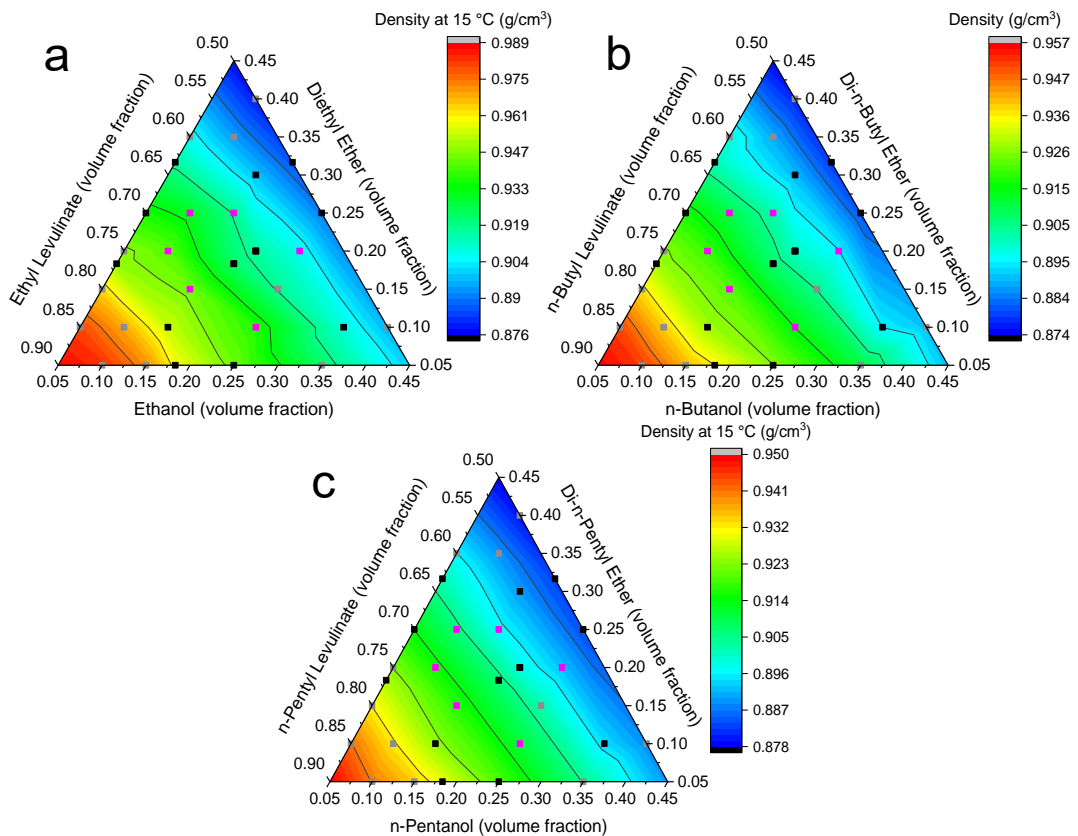
Figure 4.5. Density at 15 °C for a: ethyl-based blends. b: butyl-based blends. c: pentyl-based blends. Black squares: MODDE generated blends, grey squares: blends added to increase coverage, and magenta squares: blends used to test the models.

It is evident from figure 4.5 that the density changes linearly with the blend composition. This was expected as the density of mixtures can be predicted using a linear blending law. However, confirmation of this linearity was needed for the three-component biofuel blends. The models generated by MODDE are discussed in section 4.3.2. As the densities of each alkyl levulinate are above the fuel standard limits (table

2.6), the density of the different three-component blends was expected to be high. One of the main implications of elevated densities is the resultant change in the mass of fuel injected into the cylinder, since the fuel injection is usually on a volumetric basis. Hence, when using a denser fuel, and without changing the preprogramed density, an increased mass will be injected (210). If there is an increased mass injected, there could be a change to the fuel/air stoichiometry if the molar mass of the blend remains similar to that of a typical diesel. The increased mass of fuel injected may also compensate for any reduction in volumetric energy density when using the oxygenated biofuel blends, as there would be a greater mass of fuel injected for a given volume. Therefore, the total energy content of the fuel injected should not be reduced significantly on a volume basis. If large fractions of the biofuels are to be blended with a ULSD, then the ULSD should have a low density to ensure the limits of the fuel standards are met.

The higher densities will also affect the fuel injection and spray dynamics, such that they would increase spray penetration (88). Increased spray penetration would require longer mixing times, which causes longer IDTs due to the longer time required for fuel vaporisation (119). Higher densities can also lead to larger droplets being formed when the fuel is sprayed, further increasing the vaporisation time potentially creating rich zones within the cylinder. This could lead to increased emissions of soot, hydrocarbons, and CO where there is insufficient vaporisation for complete combustion (300).

4.3.2 Suitable Models for Predicting Density

After analysis of the model fit parameters and the AARD%, it was determined that the linear models were the most suitable models. MODDE fitted all the models using partial least squares regression, with the coefficients centred around the reference mixture at the central point (256). This resulted in models with different coefficients to the linear blending rule, where the coefficients would be the density of each component.

The initial linear, quadratic, and cubic models, produced from the 21 experimental measurements, had their predictability assessed against a range of blends selected as validation experiments. The prediction accuracy for the region with >80 vol% alkyl levulinate was poor compared to the other regions, with AARD% up to 0.46%, 0.49%, and 1.15% for the linear, quadratic, and cubic models, respectively. As a result, the data from these validation experiments (signified by the grey squares in figure 4.5) were incorporated into the model fits. This resulted in a data set comprising results from 32 experimental measurements being used to construct the final linear, quadratic, and cubic models. Linear models were found to be the most accurate for predicting the density. The quadratic and cubic models would always become linear models when the statistically insignificant terms were removed. All the terms in the linear models were significant with p-values <0.05. The R^2 values were 0.996, 0.977, and 0.998 for the ethyl,

butyl, and pentyl-based blends, respectively. The coefficients of the linear models are presented in Appendix A.1. The AARD% for the ethyl, butyl, and pentyl-based blends were 0.25%, 0.22%, and 0.05%, respectively, indicating a good agreement between the predicted and experimental values. The quality of the prediction capability can also be observed in the parity plots in figure 4.6, where the data is concentrated around the $y = x$ line. The x and y-errors were the 95% confidence interval of the experimental measurements and the model, respectively.
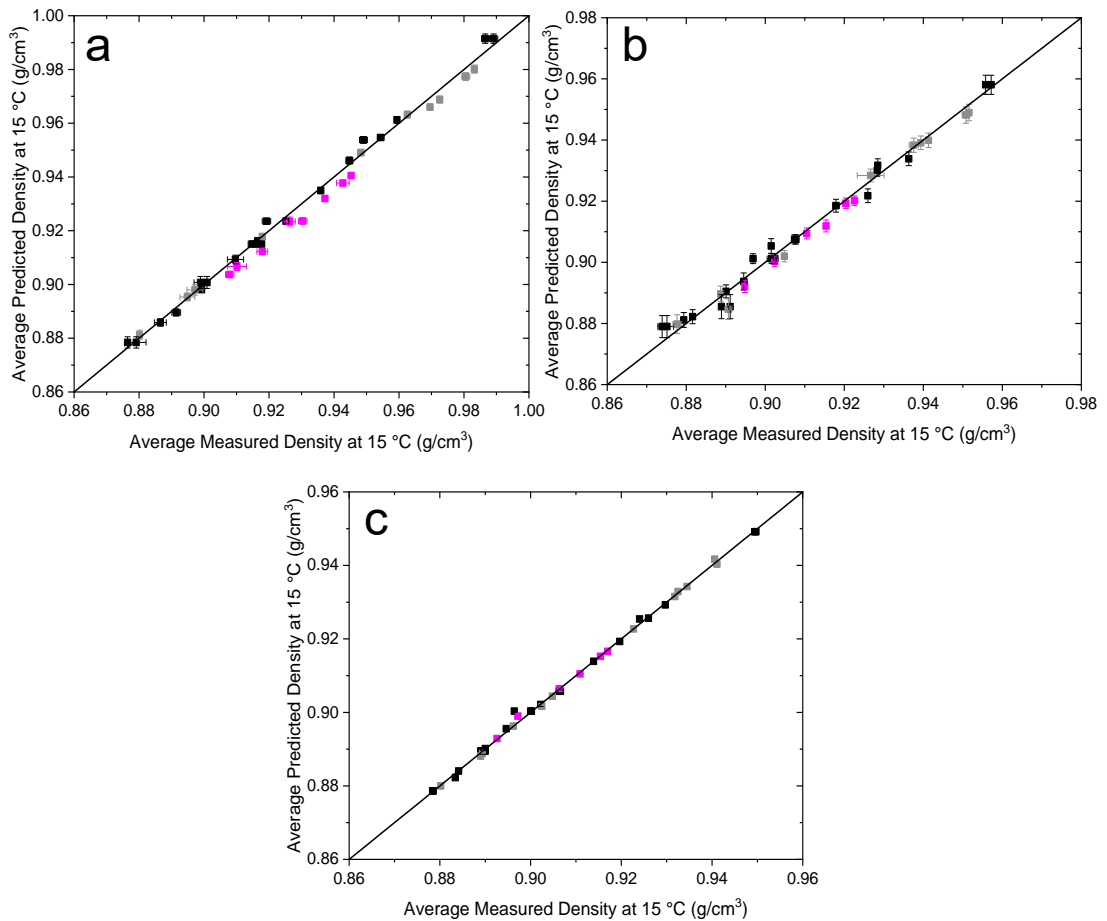
Figure 4.6. Parity plots of the predicted versus measured density with linear model predictions from MODDE. a: ethyl-based blends, b: butyl-based blends, and c: pentyl-based blends. Black squares: MODDE generated blends, grey squares: blends added to increase coverage, and magenta squares: blends used to test the models.

Table 4.4. MODDE generated density model statistical summaries.

	Model Fit Parameter	Linear Model	Quadratic Model	Cubic Model
Ethyl-Based Blends	Number of Data Points	32		
	R^2	0.996	0.993	0.995
	Q^2	0.983	0.963	0.987
	Model Validity	0.847	0.525	-0.191
	p-value of the model	2.84×10^{-35}	9.65×10^{-29}	8.24×10^{-11}
	p-value for the lack of fit	0.542	0.150	0.009
	AARD%	0.25	0.96	0.94
Butyl-Based Blends	Number of Data Points	32		
	R^2	0.977	0.992	0.982
	Q^2	0.965	0.982	0.953
	Model Validity	0.998	0.490	0.892
	p-value of the model	9.77×10^{-24}	3.24×10^{-25}	5.02×10^{-7}
	p-value for the lack of fit	0.997	0.130	0.650
	AARD%	0.22	0.18	0.24
Pentyl-Based Blends	Number of Data Points	32		
	R^2	0.998	0.992	0.998
	Q^2	0.994	0.952	0.992
	Model Validity	0.972	0.437	0656
	p-value of the model	0	1.58×10^{-29}	1.59×10^{-14}
	p-value for the lack of fit	0.939	0.105	0.253
	AARD%	0.05	0.12	0.06

For the butyl-based blends, the linear model fitted using the 21 experiments from the initial optimisation had an R^2 of 0.996, a Q^2 of 0.991, a model validity of 0.946, a model p-value of 2.59×10^{-22}, a lack of fit p-value of 0.806, and an AARD% of 0.14. However, the model constructed using the 32 experiments had a better agreement with the experimental data for the blends with >80 vol% BL as the AARD% range in this region reduced from 0.11% – 0.42% to 0.03% – 0.28%. Therefore, with the improved accuracy in this region and only a slight increase in the AARD%, from 0.14% to 0.22%, the 32 experiment model was selected.

Using the linear models from MODDE, compositions of the ethyl, butyl, and pentyl-based blends that were compliant with the EN 590, BS 2869, and EN 14214 fuel standards could be determined. The density limits of EN 14214 (0.860 – 0.900 g/cm^3) can be met for the following compositions of the ethyl, butyl, and pentyl-based blends,

<57 vol% EL, <60 vol% BL, <62% PL but at the higher fractions of PL the PeOH needs to be less than the DNPE, respectively (15). All the blends complied with BS 2869, as there is no upper density limit (16).

Since the linear regression models were the most suitable, they were compared to Kay's mixing rule, a linear-by-volume blending rule, to confirm their accuracy. When the models from MODDE were compared to the linear blending law, the AARD% was 0.47%, 0.32%, and 0.07% for the ethyl, butyl, and pentyl-based blends, respectively. The parity plots comparing the linear-by-volume blending law and the MODDE linear models in figure 4.7 show that for the butyl and pentyl-based blends, there was good agreement over the whole density range. The error bars in figure 4.7 were the 95% confidence intervals. On the other hand, the predictions of the ethyl-based blends diverged at lower densities. This was when there were high DEE fractions in the blends, as it is highly volatile and there was the potential for a greater margin of error with an increased potential for evaporative losses. Due to MODDE using the experimental measurements of the blends, the MODDE-generated linear model captured these lower densities.
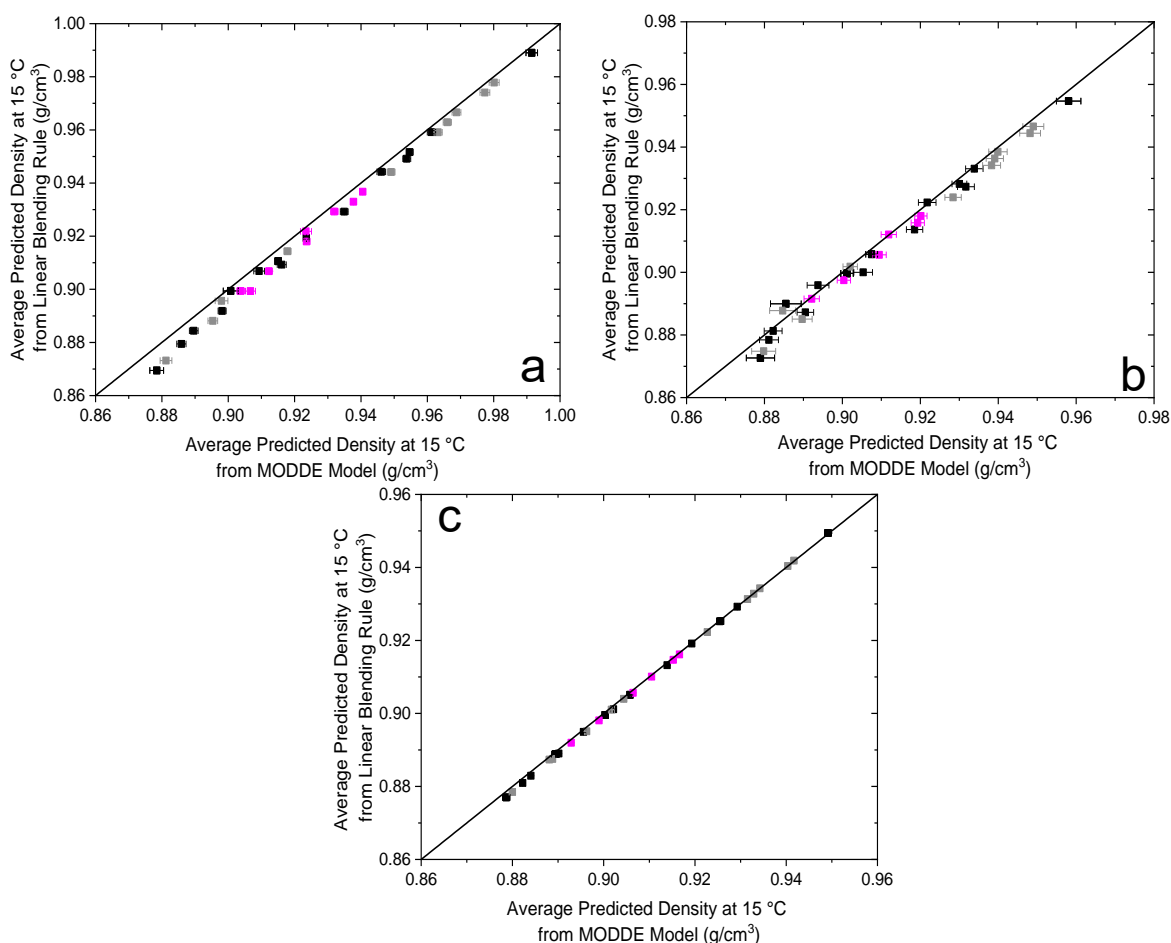
Figure 4.7. Parity plots of the density predicted by Kay's linear blending rule versus predictions using the linear MODDE models. a: ethyl-based blends, b: butyl-based blends, and c: pentyl-based blends. Black squares: MODDE generated blends, grey squares: blends added to increase coverage, and magenta squares: blends used to test the models.

4.3.3 Effects of Chain Length on the Density

As the carbon chain length increases from the ethyl, up to the butyl and pentyl-based blends the maximum density of the blends decreases, as seen in figure 4.5. This is due to the density of the individual components changing as the carbon chain length increases. The density of ethers and alcohols increase as the carbon chain length increases. The density of the levulinates decrease as the carbon chain length increases. For blends with <60 vol% alkyl levulinate, the ethyl, butyl, and pentyl-based blends each have similar densities to each other, as seen in figure 4.5. The effect of carbon chain length was also evident when assessing the blends that would meet the EN 14214 density limits, as the alkyl levulinate fraction could increase as the carbon chain length increased, as previously discussed (15).

4.3.4 Densities of the Blends with Diesel

4.3.4.1 Densities of the Binary Blends with Diesel

The individual butyl and pentyl-based components were blended into diesel to determine their effect on the density. This was to establish the fractions of the components that could be blended with diesel and remain compliant with the standard limits, as shown in figure 4.8. The error bars in the plots of this sub-section are the standard deviations of the three measurements taken for each blend. The density of the binary blends show linear dependence on the diesel fraction.
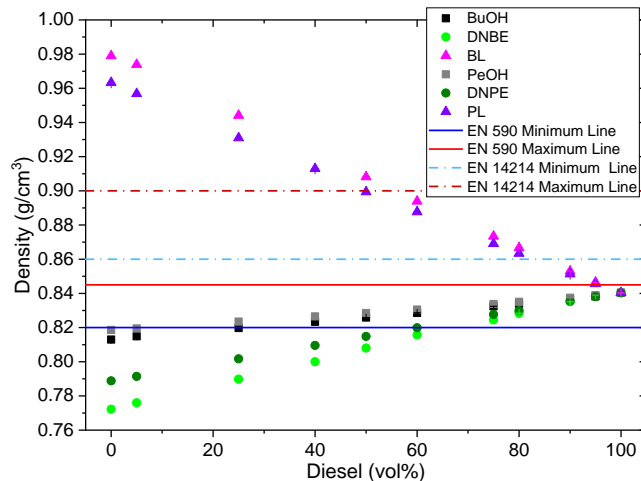
Figure 4.8. Densities of the butyl and pentyl components blended with diesel, with comparisons to the EN 590 (solid lines) and EN 14214 (dashed lines) limits.

The densities of the diesel/alkyl levulinate blends increased linearly with respect to the densities of the alkyl levulinates. Above 5 vol% BL or PL caused the diesel to exceed the EN 590 limits, whereas 20 – 40 vol% BL and 20 – 50 vol% PL could be blended with diesel whilst meeting the EN 14214 limits (12, 15). As the carbon chain length of the alkyl levulinates increases, the density decreases (table 2.6), causing blends with PL to have

a lower density than those with BL. For the alcohol and dialkyl ethers, the butyl-based components have lower densities. Hence these caused the greatest reduction in the density. Since the diesel used had a density close to the EN 590 maximum, there could be large fractions of the alcohols and dialkyl ethers added whilst maintaining EN 590 compliance. Up to 75 vol% BuOH or PeOH, and up to 25 vol% DNBE or DNPE could be blended with diesel as binary blends and maintain compliance with the density limits.

4.3.4.2 Densities of the Three-Component Blends with Diesel

Due to the narrow limits of the fuel standards, and the densities of the butyl-based blends all being higher than the EN 590 standard maximum, it would be expected that the limits would be exceeded with low fractions of biofuel. The blends tested are shown in figure 4.9. The number of blends were limited, as previously discussed. The blends selected were to determine the density ranges for the different fractions of BL in the three-component blend and to establish if there was a linear dependence on the biofuel fraction regardless of its composition.

Since the density of the butyl-based three-component biofuel blends demonstrated a linear dependence on the blend composition, the density behaviour when blended with a non-polar diesel needed to be established. It would be expected that the blends would produce a linear relationship between biofuel content and the density of the fuel blend. The linear relationship between the density and diesel fraction can be seen in figure 4.9.
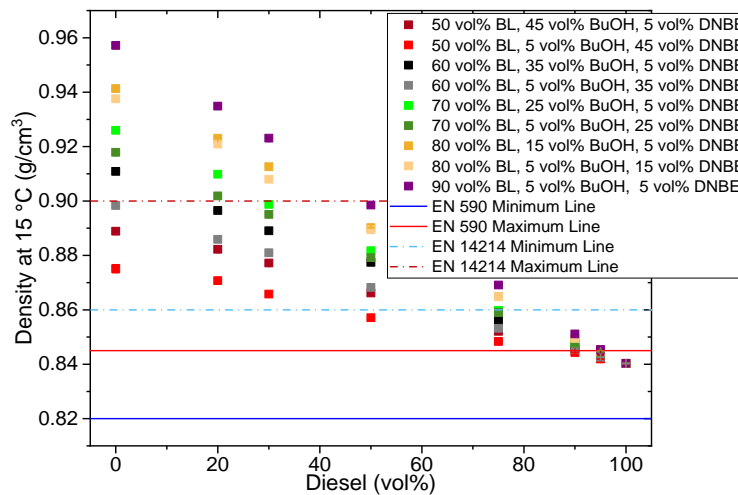
Figure 4.9. Density at 15 °C of butyl-based blends with diesel. Limits of EN 590 and EN 14214 displayed.

The density limits of EN 590 were exceeded with more than 10 vol% biofuel, whereas, the EN 14124 limits were met for some blends with <75 vol% diesel, as shown by the blends between the dashed lines in figure 4.9. The BL fraction in the biofuel blend needed to be reduced as the biofuel fraction in the blend increased. At 80 vol% biofuel, the BL fraction needed to be below 60 vol%, regardless of the DNBE and BuOH fraction, to be below the maximum limit of 0.900 g/cm^3 (15). All the blends complied with the BS

2869 grade II diesel density limits as there is no maximum density limit, only a minimum of 0.820 g/cm^3 (16).

4.4 Flash Points

Due to its significance and implications for fuel handling safety, it is important to have accurate flash point measurements for fuel blends. It is also important to understand how flash points change with blend composition and to have accurate prediction models for flash points. Being able to accurately predict the flash point of a blend would ensure appropriate measures can be put in place for handling and storage. EN 590 and BS 2869 require fuels to have a flash point >55 °C (12, 16, 227). The flash point was one of the first properties measured to ensure that appropriate measures were in place to enable the safe utilisation of the fuel blends in subsequent testing. The flash points were measured using the Stanhope Setaflash Series 3 plus, following ISO 3679 (118). All blends were stored as flammable mixtures due to the low flash points of the ethers and alcohols.

4.4.1 Flash Points of the Three-Component Biofuel Blends

The flash points of each of the components are summarised in table 4.5.

Table 4.5. Biofuel component flash points.

Component	Flash Point (°C)	Component	Flash Point (°C)	Component	Flash Point (°C)
EL	94[a]	EtOH	16[b]	DEE	-40[c]
BL	111[a]	BuOH	35[a]	DNBE	25[a]
PL	96[a]	PeOH	49[a]	DNPE	57[a]

[a]measured using Setaflash Series 3. [b]from (301). [c]from (123).

The flash points of the ethyl-based blends will likely be below room temperature due to the flash point of DEE being -40 °C based on the findings of Catoire et al. (121). The blend of 90 vol% EL/5 vol% EtOH/5 vol% DEE had a detectable flash point at room temperature. This was the blend with the lowest DEE fraction in the design space, and any increase in DEE would result in a flammable mixture at room temperature, giving a detectable flash point at room temperature. Therefore, all the ethyl-based blends were non-compliant with the flash point limits in the fuel standards (12, 15, 16). They also had flash points outside the measurable regime. The flash points of the butyl and pentyl-based three-component blends could be measured since each of the individual components had flash points above the typical room temperature of 21 °C. In the experimental contour plots shown in figure 4.10, it was evident that the flash point had a non-linear dependence on the blend composition.
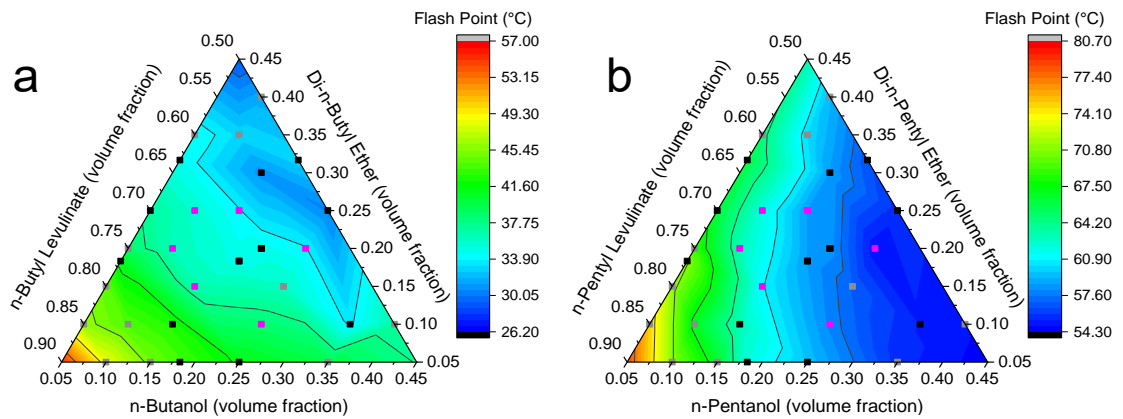
Figure 4.10. Flash points of: a: butyl-based blends. b: pentyl-based blends. Black squares: MODDE generated blends, grey squares: blends added to increase coverage, and magenta squares: blends used to test the models.

The flash points of butyl-based blends range from 26 – 57 °C, with the 50 vol% BL/45 vol% DNBE/5 vol% BuOH blend having the lowest flash point and the highest flash point being the 90 vol% BL/5 vol% DNBE/5 vol% BuOH blend. The nature of the contours in the experimental contour plot in figure 4.10a highlight that high fractions of DNBE caused the low flash points. This is in agreement with the findings of Catoire et al. (121) since they stated a blend's flash point would be reduced close to that of the component with the lowest flash point. In the case of the butyl-based blends, the component with the lowest flash point is the DNBE (table 4.5). However, there were blends with large DNBE fractions where the flash point was greater than 25 °C, which goes against the findings of Catoire et al. (121). For example, the 60 vol% BL/35 vol% DNBE/5 vol% BuOH and 70 vol% BL/25 vol% DNBE/5 vol% BuOH blends have flash points of 35 °C and 37 °C, respectively. For the flash point limit in the diesel standards to be met, the butyl-based biofuel blends, with <90 vol% BL, must be blended with a high flash point base fuel to ensure they are substantially above the 55 °C minimum of the fuel standards (12, 16).

The pentyl-based blends had flash points ranging from 54 – 81 °C, as shown in figure 4.10b. In the pentyl-based blends, it is PeOH that causes the largest reduction in the blend flash point, which is consistent with the findings of Catoire et al. (121) since it is the component with the lowest flash point (table 4.5). All the three-component blends have flash points at least 5 °C higher than this, demonstrating that the increasing PL fraction increases the blends flash point. Unlike the butyl-based blends, there were pentyl-based blends with flash points above the EN 590 and BS 2869 flash point limit of >55 °C (12, 16). The compliant blends required ≥60 vol% PL and could contain any fraction of DNPE and PeOH. This demonstrated that the longer carbon chain compounds will enable the flash point limits to be met.

When the flash point is above 60 °C the fuel blend may be stored as a combustible liquid, whereas those with flash points below 60 °C must be stored as flammable liquids according to the 'Safe use and handling of flammable liquids' documentation (265).

Therefore, the pentyl-based blends that meet these flash point limits could be stored similarly to diesel.

4.4.2 Suitable Models for Predicting Flash Point

From the screening DoE, it was evident that there needed to be optimisation to improve the model accuracy. Following the first round of optimisation to produce the initial quadratic and cubic models from 21 experimental measurements, the predictive capability was assessed against a range of blends selected, shown in section 3.3. For blends with >80 vol% alkyl levulinate, the prediction of the flash point was inaccurate, with the predictions of the validation experiments having an AARD% of 3.4% in this region. As a result, the data from these validation experiments (signified by the grey squares in figure 4.10) were incorporated into the model fits. This resulted in a data set comprising results from 32 experimental measurements which was used to construct the final linear, quadratic, and cubic models.

The model fit parameters for the final flash point models for the butyl and pentyl-based three-component blends are presented in tables 4.6 and 4.7, respectively. The coefficients of the quadratic models are presented in Appendix A.2. Upon analysis of the flash point models produced in MODDE of the butyl and pentyl-based blends, the quadratic models were determined to be the most accurate and suitable. The R^2 values of the quadratic models were 0.924 and 0.982 for the butyl and pentyl-based blends, respectively, indicating a good agreement between the predicted and experimental values. Although the quadratic model for the flash points of the butyl-based blends has a lower R^2 than the cubic model, the lower model validity and Q^2 reduced the accuracy of the predictions from the cubic model. This is demonstrated by the higher AARD% of 5.28%, compared to the 3.54% of the quadratic model. Additionally, there were no p-values for the butyl and pentyl-based blends cubic model terms, resulting in the inability to assess the statistical significance of each model term.

Table 4.6. Flash point model fit parameters for the butyl-based blends.

Model Fit Parameter	Linear Model	Quadratic Model	Cubic Model
Number of Data Points		32	
R^2	0.874	0.924	0.954
Q^2	0.854	0.861	0.814
Model Validity	0.576	0.823	0.563
p-value of the model	9.476×10^{-14}	3.57×10^{-13}	8.169×10^{-5}
p-value for the lack of fit	0.184	0.493	0.174
AARD%	4.85	3.54	5.28

Table 4.7. Flash point model fit parameters for the pentyl-based blends. Values in red show parameters that contribute to the unsuitability of the models.

Model Fit Parameter	Linear Model	Quadratic Model	Cubic Model
Number of Data Points		32	
R^2	0.870	0.983	0.979
Q^2	0.863	0.954	0.952
Model Validity	-0.139	0.937	0.424
p-value of the model	5.072×10^{-14}	9.255×10^{-23}	6.430×10^{-8}
p-value for the lack of fit	0.02	0.776	0.100
AARD%	3.14	1.20	1.32

In the flash point quadratic model for the butyl-based blends, the BuOH term was statistically insignificant as it had a p-value of 0.11. The insignificance of the BuOH term was likely due to BuOH having a flash point of 35 °C, which is close to the flash point of DNBE (25 °C) but considerably lower than BL's flash point of 111 °C. Therefore, the flash points of DNBE and BL likely dominated the flash point of the blend, and BuOH may have had less of an influence, which can also be observed in figure 4.10 as the flash points hardly change when changing the BuOH fraction. This term could not be removed from the model, as within MODDE, the individual component terms must always be present (256). For the pentyl-based blends, all terms in the quadratic model were statistically significant with p-values <0.05. The AARD% for the butyl and pentyl-based blends were 3.50% and 1.18%, respectively. The accuracy of the models is demonstrated in the parity plots in figure 4.11, where the data points are closely clustered around the $y = x$ line. All the predicted and measured flash points are within the defined errors of the $y = x$ line. The x and y-errors were the 95% confidence interval of the experimental measurements and the model, respectively.
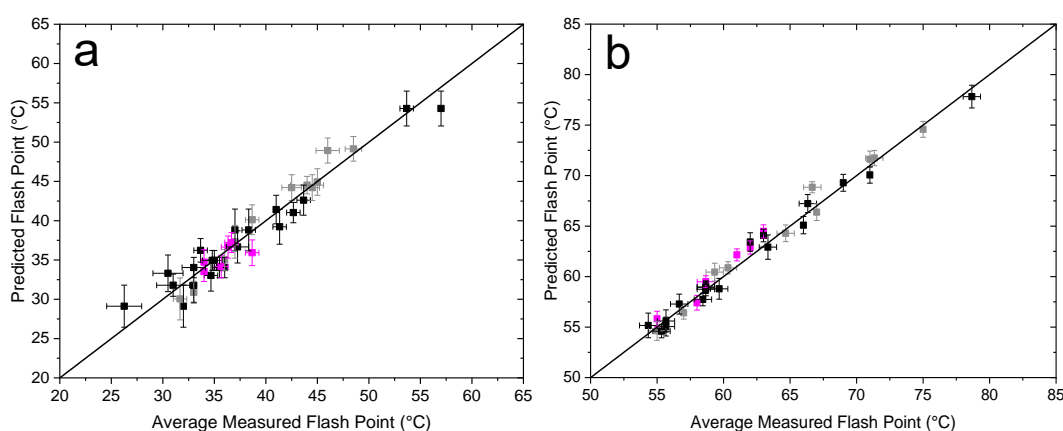
Figure 4.11. Parity plots of the flash point predictions using the MODDE quadratic model. a: butyl-based blends. b: pentyl-based blends. Black squares: MODDE generated blends, grey squares: blends added to increase coverage, and magenta squares: blends used to test the models.

4.4.3 Effects of Chain Length on the Flash Point

As the carbon chain length increased from the butyl to the pentyl-based blends, the flash point increased as expected. This increase was due to the reduced volatility and the increased boiling points as the carbon chain length increased. Therefore, higher temperatures were required to produce a flammable vapour for any pentyl-based blend composition compared to the butyl-based blends. The increase in the flash point of the pentyl-based blends should enable the >55 °C limit to be met with high fractions of the pentyl-based blends in diesel since there were blends already compliant with these limits.

4.4.4 Flash Points of the Blends with Diesel

4.4.4.1 Flash Points of the Binary Blends with Diesel

The flash points of the binary blends were measured to establish the influence of the biofuel components on the flash point of diesel. These can be seen in figure 4.12. The diesel used had a flash point of 67 °C. These measurements were vital, as they enabled the limiting biofuel component to be identified. The error bars in the remaining plots of this sub-section are the standard deviations of the three measurements taken for each blend.
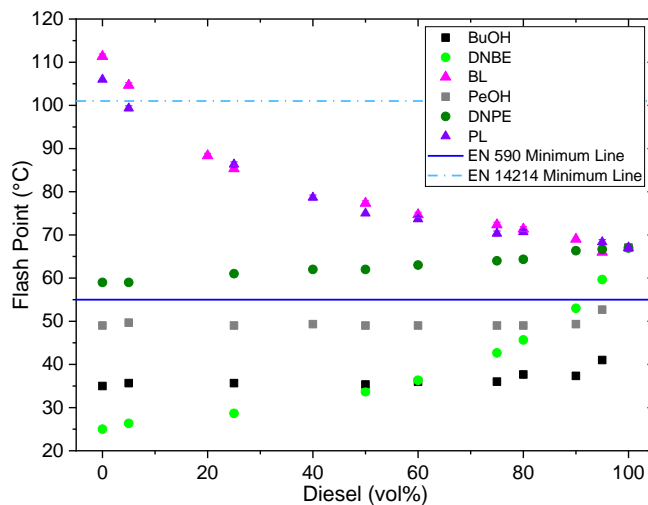
Figure 4.12. Flash points of the butyl and pentyl components blended with diesel, with the EN 590 (solid lines) and EN 14214 (dashed lines) limits on the graph.

The flash points of the diesel/alkyl levulinate blends show a non-linear dependence on the diesel fraction. This dependence follows the trends observed for the flash points of solvent blends reported by Catoire et al. (194). The nonlinearity indicates that there may be intermolecular interactions between the levulinates and diesel, since the blend flash points were not reduced to that of diesel with lower fractions of diesel. In contrast, there was a sudden reduction in the flash point of diesel and alcohol blends. The flash points of diesel/alcohol blends were reduced to that of the alcohol with only 10 vol%

alcohol (table 4.5). This behaviour follows the trends in the literature for blends of alcohol and diesel (98, 121, 125, 192, 201, 302, 303). This reduction was likely to be due to the short carbon chains of the alcohol and their high polarity creating non-ideal mixtures with diesel. As a result, the alcohol can readily be vaporised upon heating, producing the flammable vapour required for the flash point (118, 236, 294). For the dialkyl ethers, the nature of the reduction in the flash point was dependent on the carbon chain length. The diesel/DNPE blends had a more linear dependence on the diesel fractions, but they remained compliant with the EN 590 minimum. In contrast, the diesel/DNBE blends had non-linear dependence on the diesel fraction, with a greater reduction in the flash point at the lower biofuel fractions. One novel finding was that the flash points of diesel/DNBE blends remained above 25 °C until there were large DNBE fractions in the blend. The flash point of diesel/DNBE blends remained above the flash point of diesel/BuOH blends until >40 vol% DNBE, even though DNBE has a lower flash point than BuOH. This behaviour indicates that the longer carbon chain length of DNBE caused favourable intermolecular interactions, requiring higher temperatures to produce a flammable vapour. This combination of effects will influence the flash point of the three-component biofuel blends with diesel.

4.4.4.2 Flash Points of the Three-Component Blends with Diesel

As previously mentioned, only the butyl-based blends with diesel could be tested. The aim was to investigate the influence of the biofuel composition on the flash point of the blends with diesel. The flash points of these blends are shown in figure 4.13. It was evident that for >10 vol% biofuel, there had to be >70 vol% BL, and DNBE had to be greater than BuOH to remain above the EN 590 and BS 2869 flash point limits (12, 16).
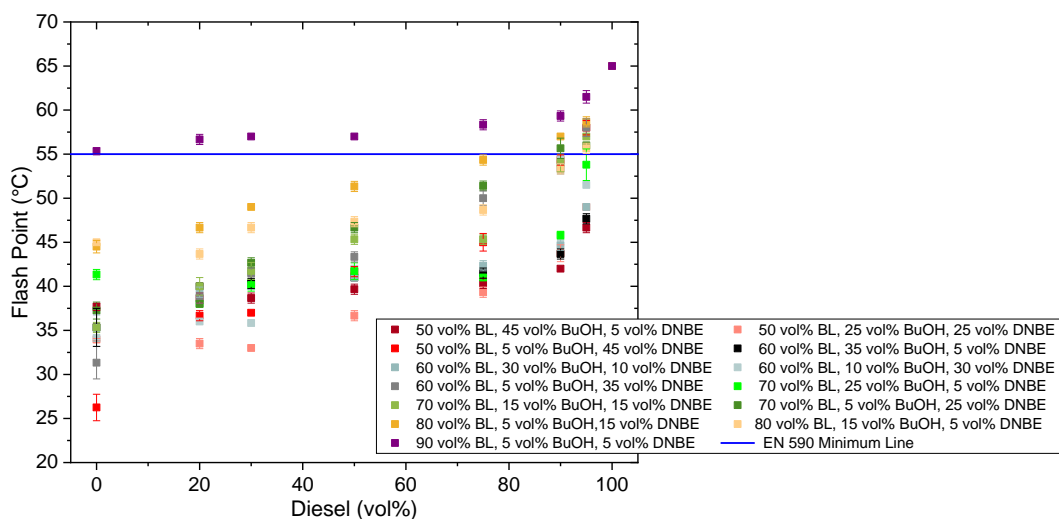
Figure 4.13. Flash points of the butyl-based blends with ULSD compared to the EN 590 minimum (blue line).

The reduction in the flash point was non-linear, having two distinct regions: high diesel fractions where the biofuel blends decrease the flash point rapidly, and low diesel fractions where the flash point is close to that of the three-component blend. One key finding from this work was that the high BuOH fractions caused greater reductions in the flash point and not the DNBE, even with its lower flash point. These results follow the trends in figure 4.12, where the diesel/DNBE blends had flash points higher than the diesel/BuOH blends at low DNBE fractions. This behaviour can be seen in figure 4.13 where the blends with high BuOH fractions have lower flash points than those with high DNBE fractions. Since BuOH has the shortest carbon chain length out of the butyl-based three components and the highest polarity, these may be the reason for the reduction BuOH causes. Therefore, when blended with diesel, the higher fractions of DNBE would have more favourable intermolecular interactions than BuOH. As a result, BuOH could be readily vaporised at the lower temperature resulting in the flammable vapour required being formed (236, 294, 304).

4.4.5 Flash Points of the Blends with Biodiesel

4.4.5.1 Flash Points of the Binary Blends with Biodiesel

Following the reduction of the flash point of diesel caused by the butyl-based blends, to determine if the flash points could meet the standards, each individual component and the three component butyl-based blends were blended with biodiesel. The flash points of the individual butyl-based biofuel components with ULSD and a used cooking oil (UCO) biodiesel are displayed in figure 4.14.
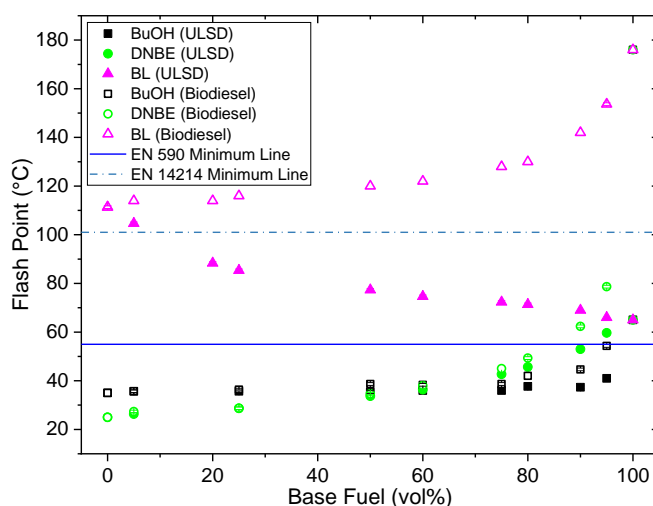
Figure 4.14. Flash points of the binary blends of the butyl biofuel components with ULSD (solid symbols) and biodiesel (open symbols). With the EN 590 (solid blue line) and EN 14214 (dashed light blue line) limits shown on the graph.

The nonlinearity of the flash point with increasing biodiesel fraction is more pronounced for the biodiesel/BL blends compared to the diesel/BL blends. The flash

points of diesel and biodiesel were reduced with only 5% vol% BuOH or DNBE. The reduction was greater with BuOH, even though it has a higher flash point than DNBE (table 4.5). This behaviour was indicative of favourable intermolecular interactions between the longer carbon chain of DNBE and the biodiesel FAME molecules (236, 294).

4.4.5.2 Flash Points of the Three-Component Blends with Biodiesel

Due to the low flash points of the three-component blends, it was expected that the flash point of biodiesel would be reduced when blended with small fractions of the biofuel blends. The flash points of butyl-based three-component blends with the UCO biodiesel are shown in figure 4.15.
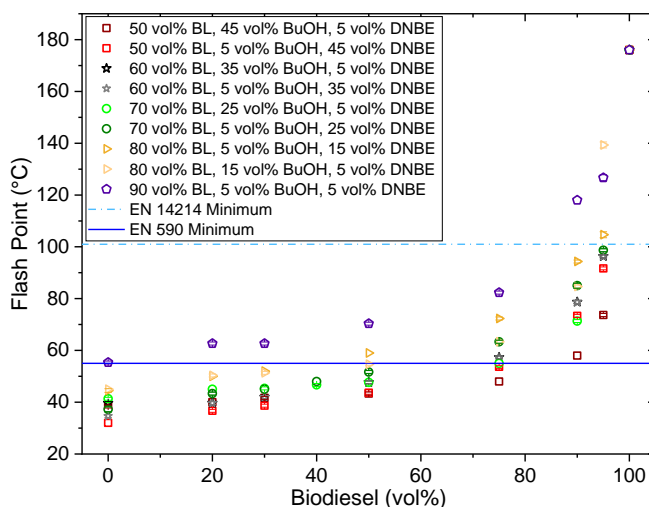
Figure 4.15. Flash points of the butyl-based blends with a UCO biodiesel compared to the minimum required flash points of the EN 590 (solid blue line) and EN 14214 (dashed light blue line) fuel standards.

The increase in the flash point with biodiesel fraction was non-linear, again with two distinct regions: high biodiesel fractions where small fractions of biofuel reduce the flash point rapidly, and lower fractions of biodiesel where the flash point reduces to that of the three-component blends. The behaviour in figure 4.15 is similar to that observed in figure 4.13 when using ULSD as the base fuel. With biodiesel as the base fuel, the flash points of most of the blends were increased relative to those when using ULSD at the same blend fractions. The increased flash points can be seen in figure 4.15 since there are more blends above the 55 °C limit of EN 590 when using biodiesel as the base fuel. This is because blends with >60 vol% BL had flash points above 55 °C at 25 vol% biofuel, which they did not when blended at 25 vol% biofuel in ULSD. This indicates that the use of a higher flash point base fuel should maintain compliance to the fuel standard. Since EN 14214 has a higher flash point limit, it is more difficult to meet when blending with the butyl-based blends (15). Many blends could be classed as non-flammable, as they have flash points above 60 °C (265).

The flash points were reduced below the 101 °C limit with 10% biofuel when there was <80 vol% BL in the biofuel blend (15). When the three-component blend contained 90 vol% BL, up to 20 vol% biofuel could be added before the flash point was below the EN 14214 limit (figure 4.15) (15). With biodiesel as the base fuel, there were more blends above the EN 590 limit of 55 °C compared to using ULSD as the base fuel. When blended with biodiesel, the flash point was above 55 °C with 25 vol% biofuel when the three-component blend had ≥60 vol% BL. In addition, the 55 °C limit would be met with 50 vol% biofuel when BL was ≥80 vol%. For blends of 25 vol% biofuel in ULSD, the biofuel composition needed ≥85 vol% BL and ≥10 vol% DNBE. However, using biodiesel as a base fuel would not give an EN 590 compliant fuel due to the limits of 7 vol% FAME (12). The use of biodiesel indicated that a high flash point base fuel was required to allow higher fractions of the butyl-based biofuels and a wide range of compositions to be used whilst meeting the flash point limits.

4.5 Kinematic Viscosity at 40 °C

The kinematic viscosity of the fuel will influence the ability of the fuel delivery system to pump the fuel, the quality of the injection, and the fuel atomisation. 40 °C is used since it is a representative temperature of the fuel pump and fuel lines during an engine's use. KV40 was measured using the SVM3000 as detailed in section 3.5.4.

4.5.1 KV40 of the Three-Component Biofuel Blends

Due to the boiling point of DEE being 34 °C, it was impossible to measure the KV40 of both it and any blend containing it. The KV40s of the biofuel components are summarised in table 4.8.

Table 4.8. Measured KV40s of individual biofuel components.

Biofuel	KV40 (mm^2/s)	Biofuel	KV40 (mm^2/s)	Biofuel	KV40 (mm^2/s)
EL	1.553	EtOH	1.099	DEE	n/a
BL	2.017	BuOH	2.261	DNBE	0.736
PL	2.375	PeOH	2.899	DNPE	1.131
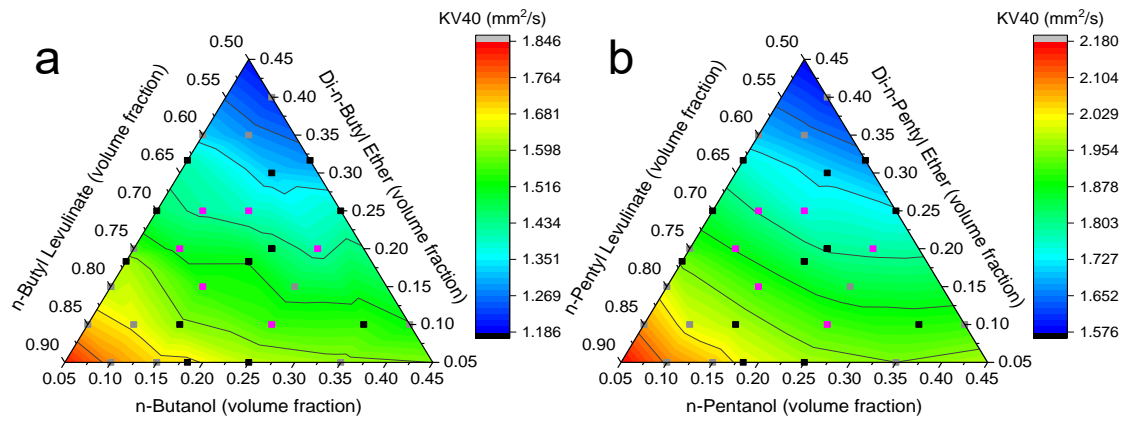
Figure 4.16. Measured KV40s of the: a: butyl-based blends. b: pentyl-based blends. Black squares: MODDE generated blends, grey squares: blends added to increase coverage, and magenta squares: blends used to test the models.

The KV40s for the butyl-based blends range from 1.186 – 1.846 mm^2/s, as shown in figure 4.16a. The KV40 of all the three-component butyl-based blends were below the EN 590 and BS 2869 minimum of 2.00 mm^2/s (12, 15, 16). The experimental contour plot shows that the KV40 of the butyl-based blend had a non-linear dependence on the blend composition. Figure 4.16a shows that the high DNBE fractions resulted in the lowest KV40. Since DNBE has the lowest KV40 of the three components, the low KV40s of the blends with high DNBE fractions were expected. Therefore, the butyl-based blends would need to be blended into a base fuel to ensure the limits of any fuel standards are met. The amount of base fuel required to have the blends comply with the standard limits would depend on the KV40 of the base fuel. For diesel and biodiesel, this is discussed in sections 4.5.4.2 and 4.5.5.2, respectively.

The KV40s of the pentyl-based blends range from 1.578 – 2.180 mm^2/s, as shown in figure 4.16b. The viscosity limits of EN 590 and BS 2869 were met when the pentyl-based three-component blends consisted of ≥75 vol% PL, ≥5 vol% DNPE, and ≤20 vol% PeOH (12, 16). In figure 4.16b, there was evidence of non-linear dependence of the KV40 on the blend composition. DNPE caused the largest reduction of the KV40 as it has the lowest KV40. This behaviour was similar to the butyl-based blends, as DNBE reduced the KV40. The higher KV40s of the pentyl-based blends should produce wider blend boundaries with diesel where the KV40s are within the fuel standards limits.

A reduced KV40 of a fuel blend would affect the fuel delivery system. A KV40 below the standard limits could lead to increased wear on the fuel pump due to increased friction from poor lubrication. The lower KV40 can also reduce the effectiveness of the fuel pump, reducing the amount of fuel delivered to the injector, thus, reducing the power generated by the engine as less fuel will be available for combustion. There can also be leakage from the injector into the cylinder, which can increase hydrocarbon emissions due to increased fractions of unburnt fuel (220). There can be benefits of a lower viscosity fuel, provided they are within the standard limits. Lower viscosity fuels can improve the

fuel spray due to improved atomisation upon injection, forming smaller droplets (88). The smaller droplets would have a greater vaporisation rate allowing the formation of a more homogeneous mixture, which reduces soot emissions (38, 54, 125, 305-307).

4.5.2 Suitable Models for Predicting KV40

It was evident from the experimental contour plots (figure 4.16) that linear models would be unsuitable. This unsuitability was due to the need to capture the nonlinearities from the interactions between the biofuel components. The initial quadratic and cubic models, produced from the 21 experimental measurements, had their predictability assessed against a range of blends selected as validation experiments. As with the flash point models, the prediction accuracy for the region with >80 vol% alkyl levulinate was poor, with AARD% up to 1.7%. As a result, the data from these validation experiments (signified by the grey squares in figure 4.16) were incorporated into the model fits. This resulted in a data set comprising results from 32 experimental measurements being used to construct the final linear, quadratic, and cubic models.

The model fit parameters for the final KV40 models for the butyl and pentyl-based three-component blends are summarised in tables 4.9 and 4.10, respectively. Upon analysis of the butyl and pentyl-based blends' KV40 models produced in MODDE, the quadratic model was determined to be the most accurate and suitable. The coefficients of the quadratic models are presented in Appendix A.3. The quadratic models for the butyl and pentyl-based blends had R^2 values of 0.975 and 0.998, respectively, indicating good agreement between the predicted and experimental values. For the butyl-based blends, all three models were statistically significant, as the p-value was below 0.05. For all three models, the p-value for the lack of fit was not statistically significant, indicating there was no lack of fit. Although the cubic model had a lower AARD% and a higher R^2, the coefficients produced by MODDE could not have their statistical significance determined. This lack of p-values resulted in the analysis of the cubic model not being as rigorous, and the model's suitability could not be thoroughly assessed.

Table 4.9. KV40 model fit parameters for the butyl-based blends.

Model Fit Parameter	Linear Model	Quadratic Model	Cubic Model
Number of Data Points	32		
R^2	0.973	0.975	0.985
Q^2	0.963	0.956	0.953
Model Validity	0.878	0.852	0.615
p-value of the regression model	9.18×10^{-14}	3.41×10^{-19}	2.23×10^{-7}
p-value for the lack of fit	0.614	0.553	0.215
AARD%	1.45	1.18	0.95

For the pentyl-based blends, the linear model had a statistically significant lack of fit, as its p-value is below the 0.05 threshold (table 4.10). Although the cubic model had a statistically significant regression and no lack of fit, there were no p-values for the coefficients. Hence, the cubic model was unsuitable. The high Q^2 and model validity, and the low AARD% of the quadratic model demonstrated that it was the most suitable model.

Table 4.10. KV40 model fit parameters for the pentyl-based blends. Values in red show parameters that contribute to the unsuitability of the models.

Model Fit Parameter	Linear Model	Quadratic Model	Cubic Model
Number of Data Points	32		
R^2	0.967	0.998	0.998
Q^2	0.959	0.997	0.986
Model Validity	-0.200	0.994	0.632
p-value of the regression model	5.61×10^{-23}	3.36×10^{-36}	4.61×10^{-14}
p-value for the lack of fit	0.005	0.977	0.230
AARD%	1.07	0.24	0.33

The quadratic model for the butyl-based blends had one statistically insignificant term, as seen in table 4.11. The $DNBE^2$ term had a p-value of 0.25, which is greater than the 0.05 threshold. The $DNBE^2$ term was kept in the model to maintain the accuracy, as its removal resulted in further terms becoming insignificant. The AARD% for the butyl and pentyl-based blends were 1.18% and 0.24%, respectively. The accuracy of both quadratic KV40 models is shown by the data focused around the $y = x$ line in figure 4.17. The x and y-errors were the 95% confidence interval of the experimental measurements and the model, respectively.
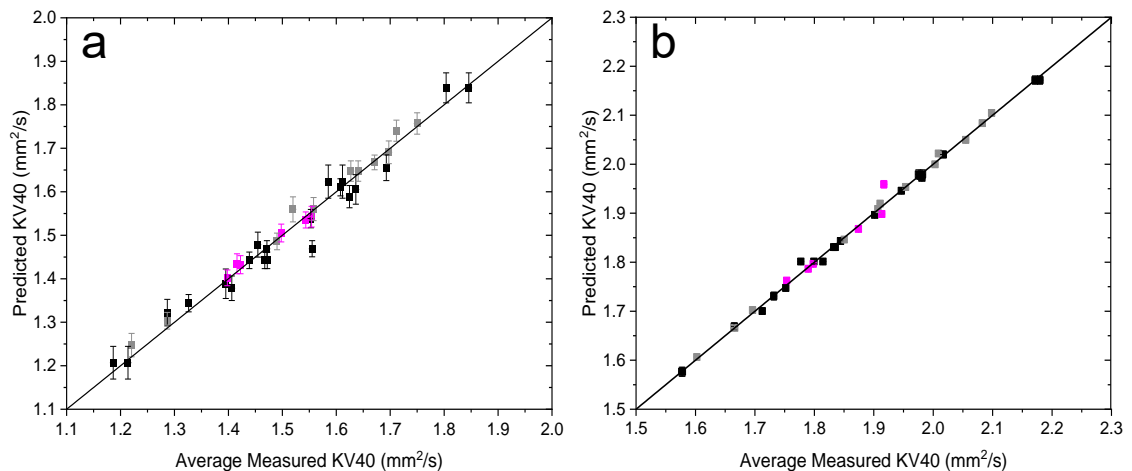
Figure 4.17. Parity plots for the KV40 predictions using the MODDE generated quadratic model for a: butyl-based blends. b: pentyl-based blends. Black squares: MODDE generated blends, grey squares: blends added to increase coverage, and magenta squares: blends used to test the models.

Table 4.11. Coefficients for the butyl-based blends KV40 quadratic model. Coefficients in red are statistically insignificant.

Component (volume fraction)	Coefficient Value	Standard Error	P-Value	95% Confidence Interval
Constant	1.469	0.033	2.75×10^{-25}	0.068
BuOH	-0.163	0.072	3.37×10^{-2}	0.149
BL	0.317	0.043	8.39×10^{-8}	0.088
DNBE	-0.932	0.077	6.62×10^{-12}	0.159
$BuOH^2$	1.596	0.273	4.25×10^{-6}	0.562
BL^2	0.264	0.060	1.94×10^{-4}	0.124
$DNBE^2$	0.309	0.265	0.254	0.545
BuOH×BL	-1.284	0.244	1.88×10^{-5}	0.502
BuOH×DNBE	1.242	0.524	2.58×10^{-2}	1.079
BL×DNBE	-0.538	0.218	2.05×10^{-2}	0.448

The coefficients of the butyl-based blend quadratic model indicate that the presence of DNBE caused the greatest reduction of the reference mixture's KV40, as expected from the experimental contour plot (figure 4.16a). The statistical significance of the interaction terms demonstrates that the KV40 depends on the interactions between the biofuel components. These may indicate that intermolecular interactions are present in such blends, as these interactions need to be accounted for to ensure the accurate prediction of the KV40 (122, 202, 203). With blends of oxygenated species, there are likely to be strong intermolecular forces, such as hydrogen bonding, which contribute toward the changes in viscosity (308, 309). The positive coefficient for BuOH×DNBE may be due to increased intermolecular interactions between these molecules due to the lack of steric hindrance, as they are saturated molecules with no double bonds (308-310). The differences in polarity between the butyl-based blends and diesel may promote a reduction in KV40, as there would be fewer intermolecular interactions (122, 308, 309).

The accuracy of the quadratic models highlights that linear blending rules used in software packages, such as Chemkin, when modelling the liquid properties of multi-component blends, could be inaccurate (291). Chemkin uses linear-by-mass blending rules for determining the properties of liquid fuel blends in the 0D CI engine model when modelling the fuel injection. Inaccurate predictions of the viscosity would reduce the accuracy of the engine model as the viscosity influences the fuel vaporisation rate, and thus combustion and emissions (122, 249, 287, 306). Therefore, the suitability of the combustion modelling of multi-component blends may face challenges if their physical properties are inaccurate.

4.5.3 Effects of Chain Length on the Kinematic Viscosity at 40 °C

As the carbon chain length increases, the KV40 increases, as shown in figure 4.16. Additionally, the KV40 of each component increased as the carbon chain length increased (table 4.8). This increase was expected since the long carbon chain compounds will have more intermolecular interactions (308, 309). These interactions result in a higher viscosity as more force is needed to overcome the attractive forces since viscosity is the measure of resistance to motion (206).

4.5.4 KV40s of Biofuel Blends with Diesel

The blends of diesel and the ethyl-based three-components could not have their KV40s measured due to the high DEE fractions required to produce miscible blends, as discussed in section 4.2.1.1, coupled with its boiling point of 34 °C. The pentyl-based three-component blends with diesel could not have their KV40s measured due to the lack of availability of second-generation pentanol. This made the pentyl-based blends less practically suitable for engine applications. The KV40s of the binary blends of the butyl and pentyl-based components with diesel were measured. These measurements were to determine the nature of the KV40 behaviour at different biofuel volume fractions and to develop a fundamental understanding of any interactions with the diesel used in this work. As discussed previously, only the butyl-based three-component blends could be blended with diesel and biodiesel and tested.

4.5.4.1 KV40s of the Binary Blends with Diesel

The measured KV40s of the binary blends of the butyl and pentyl-based biofuel components with diesel can be seen in figure 4.18. The error bars in the plots are the standard deviations of the three measurements taken for each blend.
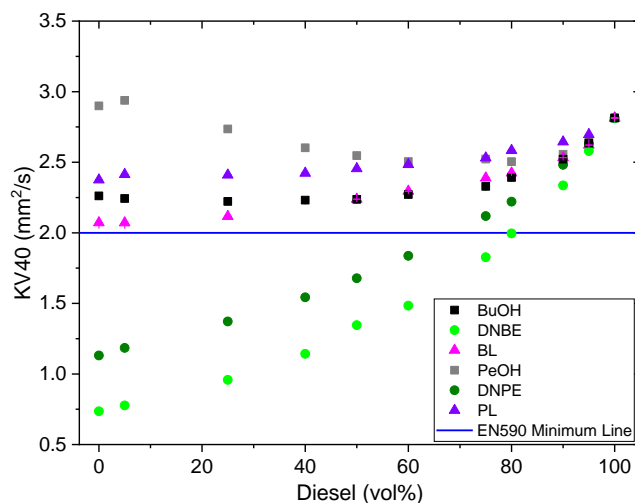
Figure 4.18. KV40s of the butyl and pentyl components blended with diesel compared to the EN 590 minimum limit (blue line).

The nature of the KV40 behaviour for the binary blends was dependent on the biofuel component added. The KV40s of the diesel/PeOH blends were below the KV40s of the diesel and PeOH. There were greater reductions between 60 and 80 vol% diesel. The minimum KV40 behaviour was due to the synergistic effects of PeOH and diesel since they had similar KV40s. A similar trend was reported by Lapuerta et al. (122), as diesel/PeOH blends had KV40s below that of the diesel used and PeOH. It was important to understand how the KV40 changed using Crown Oils ULSD since this is a different diesel. The dialkyl ethers reduced the KV40 of diesel as their volume fraction increased. The KV40 of diesel/DNPE and diesel/DNBE blends displayed non-linear dependencies on the diesel content. For the diesel/DNPE blends, the non-linearity was less pronounced compared to the diesel/DNBE blends. This difference may be due to the carbon chain length of DNPE matching the small compounds typically found in diesel, allowing for more favourable intermolecular interactions. The addition of the alkyl levulinates caused a reduction in the KV40 of diesel and displayed a non-linear dependence on the diesel fraction. Blends of the alkyl levulinates with >80 vol% diesel had a rapid reduction in the KV40 (figure 4.18). The KV40 of BL and BuOH blends with ULSD have a similar viscosity, as the pink and black squares overlap at the higher ULSD fractions. This overlap may be due to synergistic effects, as the BuOH and BL have similar KV40s to the ULSD. The addition of the alcohols and alkyl levulinates at any fraction resulted in EN 590 compliant blends, whereas >20 vol% DNBE and >25 vol% DNPE caused the KV40 to be below the EN 590 limit (12). These reductions indicated that high fractions of the ethers in the three-component blends would cause large reductions in the KV40s when blended with diesel.

4.5.4.2 KV40s of the Three-Component Blends with Diesel

Since the KV40 of the ULSD used was 2.81 mm^2/s, there could only be a reduction of 0.81 mm^2/s before the blends were below the EN 590 limits. Figure 4.19 shows the KV40s for a range of butyl-based blends with ULSD. The reduction in the KV40 was non-linear, having two distinct regions: high diesel fractions (>75 vol%), where the biofuel blends decrease the KV40 rapidly, and low diesel fractions, where the KV40 is reduced gradually to that of the three-component blend. The EN 590 (and BS 2869) KV40 minimum limit of 2.00 mm^2/s can be met with <25 vol% biofuel, regardless of the butyl-based blend composition (12, 16). If the diesel used had a higher KV40, there could have been larger fractions of the butyl-based blends added whilst the KV40 remained within the standard limits.
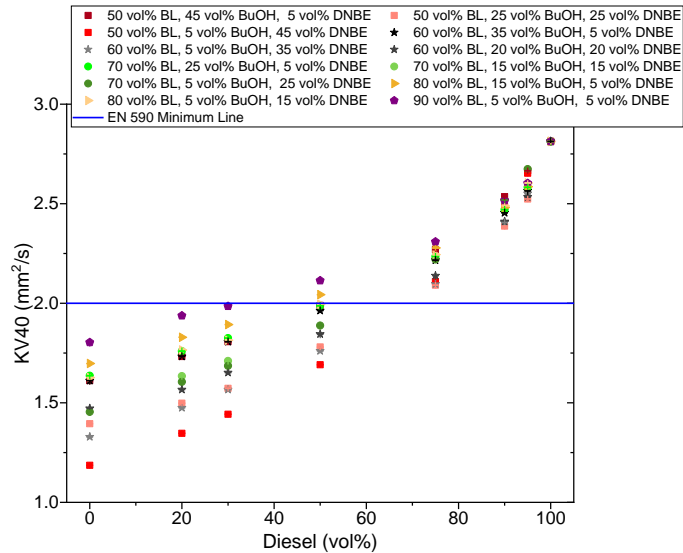
Figure 4.19. KV40s of the butyl-based blends with diesel compared with the EN 590 minimum (blue line).

The butyl-based blends with high DNBE and low BL fractions caused greater reductions in the KV40 when blended with diesel, as these had the lower KV40, as seen in figure 4.16. This is evident by the large spread of KV40s at the lower diesel fractions as the higher DNBE fractions gave the lower KV40s. The reduction in KV40 due to the high DNBE fractions was expected since it has the lowest KV40 (table 4.8). The reduced KV40 will influence the engine performance and emissions as discussed previously in section 4.5.1. Unlike the flash points, the high fractions of BuOH in the blend were more beneficial for the KV40. However, since the EN 590 limit could be met for fuel blends with <25 vol% biofuel, with any composition, compliance with the flash point limit would decide the overall suitability of the fuel blends.

4.5.5 KV40s of the Blends with Biodiesel

4.5.5.1 KV40s of the Binary Blends with Biodiesel

The UCO biodiesel had a KV40 of 4.36 mm^2/s, which should enable higher biofuel blend fractions to be added to a base fuel, with the fuel standards limits still being met (15, 16). Initially, the influence of each butyl-based component on the KV40 of biodiesel was investigated. The KV40s of the binary blends are shown in figure 4.20.
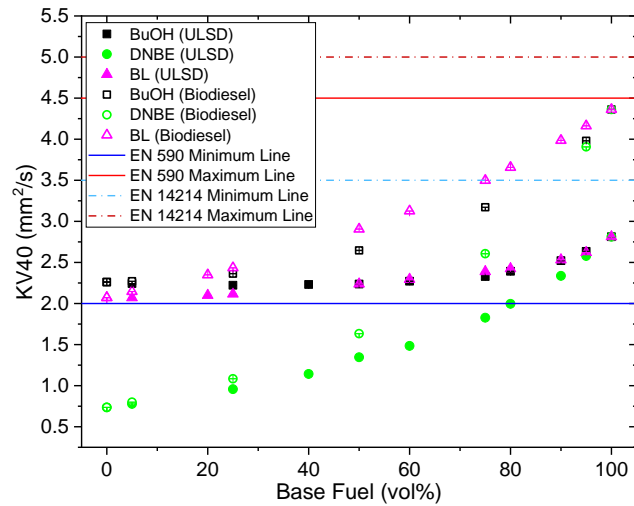
Figure 4.20. KV40s of the binary blends of the butyl biofuel components with ULSD (solid symbols) and biodiesel (open symbols). With the EN 590 (solid lines) and EN 14214 (dashed lines) limits shown on the graph.

The reduction observed for the binary blends is much greater than the relative reduction with ULSD. The large reduction was due to the greater differences between the KV40 of the biofuel components and the biodiesel. For example, the reduction in the KV40 of the base fuel for 50 vol% BuOH was 39% with biodiesel and 20% with ULSD. For blends with 75 vol% DNBE, the reduction was 75% with biodiesel and 66% with ULSD. Therefore, the reduction in the KV40 of biodiesel would depend on the three-component blend composition and its KV40.

4.5.5.2 KV40s of the Three-Component Blends with Biodiesel

The KV40 of the butyl-based three-component blends with biodiesel are shown in figure 4.21. The reduction in the KV40 shows a non-linear dependence on the biodiesel fraction, with two distinct regions: high biodiesel fractions with a more pronounced reduction, and a more gradual decrease to the KV40 of the biofuel blends at low biodiesel fractions. The non-linear dependence was less pronounced with biodiesel than with ULSD. The change in the nature of the behaviour may be due to more favourable intermolecular interactions between the biofuel blends and the oxygenated ester functional group of the FAME at higher biodiesel fractions (208, 310-312). Blends with <10 vol% biofuel will remain compliant with the EN 14214 limits. Blends with >20 vol% biodiesel were compliant with the EN 590 limits, providing the DNBE fraction was <25 vol% (12, 15). The increased viscosity of the blends with biodiesel will affect the engine performance and emissions, since higher viscosity fuels form larger fuel droplets creating rich zones where soot emissions are likely to increase (122, 306).
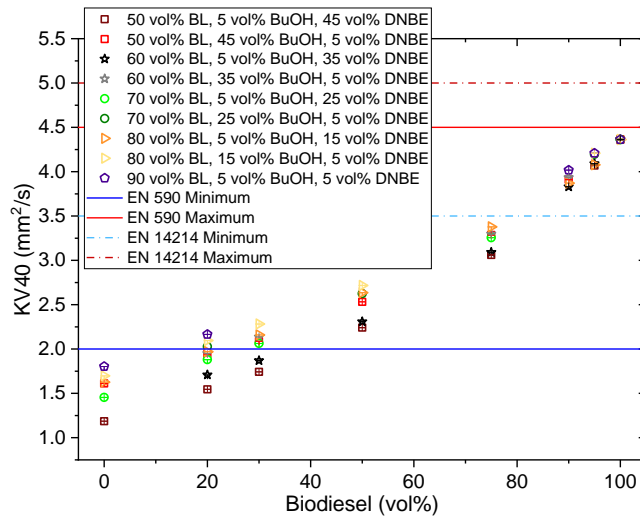
Figure 4.21. KV40s of the butyl-based blends with biodiesel compared to the limits of the EN 590 (solid lines) and EN 14214 (dashed lines).

4.6 Compliant Blends with Fuel Standards

MODDE was used to determine fuel standard compliant fuel compositions using the data from measured physical properties of the butyl-based blends with ULSD. This analysis enabled blend boundaries for potentially suitable drop in fuels to be determined. From the flash point and KV40 measurements (figures 4.13 and 4.19) the biofuel had to be <25 vol% of the blend to be compliant with the limits of EN 590 and BS 2869 (12, 16). However, the EN 590 density limit was exceeded with >5% biofuel, as seen in figure 4.5. Hence, the BS 2869 density limits were chosen for this analysis, as the EN 14214 compliant blends would also fall within this region. This was due to the blends of <25 vol% biofuel with diesel having densities below the 0.900 g/cm^3 maximum of EN 14214 (figure 4.5) (15). Therefore, the limits used to establish the blend boundaries were >0.820 g/cm^3, 2.00 – 5.00 mm^2/s, and >55 °C for the density, KV40, and flash point, respectively (12, 16). The benefit of using the BS 2869 properties limits was that the fuels governed by this standard could be used for non-road mobile machinery, as discussed in section 3.3. This standard was appropriate for the engine used in this project since the Yanmar L100V was part of a diesel genset.

For 25 vol% biofuel, the blend boundaries for the butyl-based biofuel blends were ≥80 vol% BL, ≤15 vol% DNBE, and ≤5 vol% BuOH to remain compliant with the BS 2869 density limits and the EN 590 and BS 2869 KV40 and flash point minimums (12, 15, 16). For 10 vol% biofuel, the butyl-based three-component blend could consist of ≥60 vol% BL, ≤35 vol% DNBE, and ≤10 vol% BuOH and remain compliant. The boundaries of the compliant blends are shown in figure 4.22.
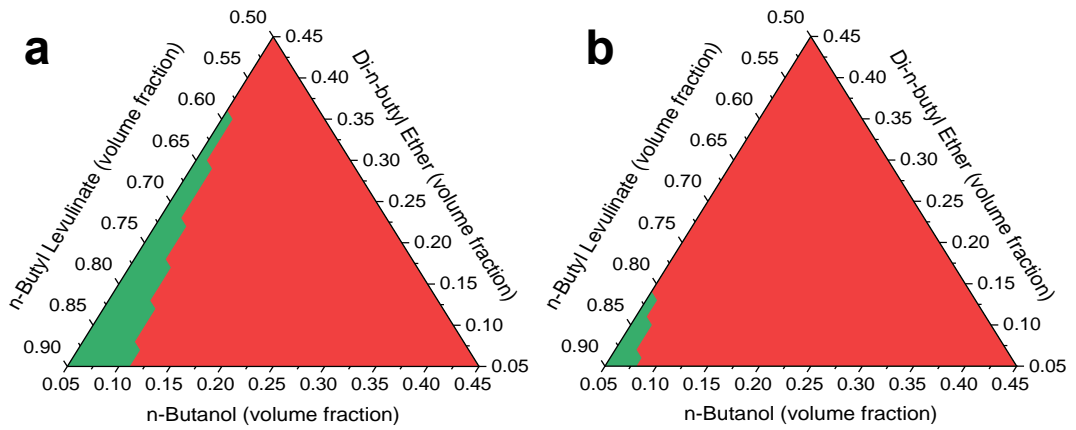
Figure 4.22. Butyl-based biofuel blend compositions that produced blends compliant with the selected limits. a: 10 vol% biofuel. b: 25 vol% biofuel.

When using MODDE to determine the blend boundaries for the butyl-based blends with diesel, the models used were linear for the density and quadratic for the flash point and KV40. The statistical parameters of the models are in tables 4.12 and 4.13 for the 10 and 25 vol% butyl-based biofuel blends, respectively. Due to a lack of experimental data, MODDE could not determine the model validity and the probability of the lack of fit. However, the accuracy of the predicted properties was assessed for each selected blend.

Table 4.12. Model statistical parameters for the MODDE analysis of the 10% butyl-based biofuel blends to determine fuel standard compliance.

Model Fit Parameter	Density Linear Model	Flash Point Quadratic Model	KV40 Quadratic Model
R^2	0.977	0.944	0.727
Q^2	0.966	0.783	0.082
Model Validity	n/a		
p-value of the model	3.89×10^{-8}	3.05×10^{-4}	0.09
p-value for the lack of fit	n/a		

Table 4.13. Model statistical parameters for the MODDE analysis of the 25% butyl-based biofuel blends to determine fuel standard compliance.

Model Fit Parameter	Density Linear Model	Flash Point Quadratic Model	KV40 Quadratic Model
R^2	0.975	0.952	0.924
Q^2	0.923	0.743	0.741
Model Validity	n/a		
p-value of the model	6.08×10^{-8}	1.82×10^{-4}	2.63×10^{-3}
p-value for the lack of fit	n/a		

The selected blends for the engine testing based on compliance with the chosen limits and their measured and predicted properties are summarised in table 4.14. Whilst there are differences between the predicted and measured values, the AARD% was less than 5%, indicating an accurate prediction. This accuracy demonstrated that MODDE could identify the blend boundaries with the limited data available.

The low fractions of BuOH needed to maintain compliance with the flash point limit of BS 2869 further validate the need for recycling of the alcohol used in the alcoholysis process to increase the practicality and economic viability of the production (38, 54). The higher fractions of DNBE should result in blends that would have less of a reduction in the DCN of diesel. However, unlike the ethyl-based blends, no predictive DCN model is currently available for the butyl-based three-component blends (37). Therefore, using the selected butyl-based blends with diesel in the Yanmar L100V will determine the influence of the biofuel blend composition on engine performance and emissions.

Since the pentyl-based blends were compliant with the flash point and KV40 limits without diesel, MODDE was used to determine the blend boundaries where the three-component blends complied with the BS 2869 limits. This analysis used the developed physical properties models. The pentyl-based blends required ≥75 vol% PL, ≥5 vol% DNPE, and ≤20 vol% PeOH to comply with BS 2869 (16). Whilst the higher densities are unfavourable, as discussed in section 4.3, the increased safety from the higher flash points will be beneficial. However, due to the lack of availability of pentyl-based components, it was not possible to conduct engine testing.

The use of MODDE to establish these blend boundaries was a valuable tool. Due to time constraints, a limited number of butyl-based blends with diesel could have their properties measured. The properties measurements of additional blend compositions would improve the accuracy of the models for the properties of the diesel and butyl-based biofuel blends. However, the data in table 4.14 demonstrates the accuracy of the initial models. MODDE was suitable and effective in developing an understanding of how the fuel blend composition affects the physical properties. It has also produced accurate models for the physical properties of three-component blends.

Table 4.14. Comparison of predicted and measured physical properties of the butyl-based blends selected for engine testing.

Fuel Blend	Predicted Density (g/cm³)	Measured Density (g/cm³)	AARD%	Predicted Flash Point (°C)	Measured Flash Point (°C)	AARD%	Predicted KV40 (mm²/s)	Measured KV40 (mm²/s)	AARD%
90% ULSD 10% Biofuel (65 vol% BL/5 vol% BuOH/30 vol% DNBE)	0.847	0.846	0.07	55.6	58.0	4.16	2.449	2.453	0.16
90% ULSD 10% Biofuel (75 vol% BL/5 vol% BuOH/20 vol% DNBE)	0.849	0.848	0.05	56.8	56.0	1.49	2.465	2.493	1.12
90% ULSD 10% Biofuel (85 vol% BL/5 vol% BuOH/10 vol% DNBE)	0.850	0.850	0.00	58.4	57.3	1.92	2.508	2.513	0.19
90% ULSD 10% Biofuel (85 vol% BL/10 vol% BuOH/5 vol% DNBE)	0.850	0.851	0.09	55.5	55.3	0.28	2.502	2.524	0.88
90% ULSD 10% Biofuel (90 vol% BL/5 vol% BuOH/5 vol% DNBE)	0.851	0.851	0.00	59.4	60	1.05	2.540	2.516	0.94
75% ULSD 25% Biofuel (85 vol% BL/5 vol% BuOH/10 vol% DNBE)	0.867	0.866	0.17	56.3	57	0.28	2.290	2.294	0.15
75% ULSD 25% Biofuel (90 vol% BL/5 vol% BuOH/5 vol% DNBE)	0.870	0.869	0.11	57.8	59.7	3.14	2.34	2.309	1.45

Chapter 5

Engine Performance when using the Advanced Biofuel Blends Blended with Diesel

5.1 Introduction

Whilst new ICEs can be developed to use new fuel formulations or specific fuels such as compressed natural gas or ammonia, there are still existing ICEs that require low-carbon fuels if decarbonisation targets are to be met. For existing ICEs, the most desired alternative would be a liquid drop-in fuel. This would require an alternative fuel that matches or outperforms the existing fuel used, such as ULSD. Several key parameters and performance indicators would confirm the suitability of a fuel as a drop-in fuel. These include the IDT, stability of the combustion, BSFC, peak in-cylinder pressures, IMEP, HRR, and the exhaust manifold temperatures. Changes in these resulting from alternative fuel blending may have both positive and negative implications on the engine performance and emissions.

Changes in the in-cylinder pressure can have many effects. If the pressure is above the tolerances for the different components in the engine architecture there may be increased wear and damage (5). On the other hand, there can be the added benefit of increased pressures resulting in more complete combustion and increasing the IMEP. Changes in pressure can affect the speciation and formation of different exhaust emissions, as a result of the change in temperature (4, 5, 101).

Any variations in exhaust temperatures would have implications on exhaust aftertreatment systems, especially those reliant on catalysts that operate effectively above their light-off temperatures, such as those used in SCR and DOCs (4, 5, 101). Changes in exhaust temperatures would need to be accounted for when using EGR, turbocharging, and intercoolers (4, 5, 101). The exhaust temperature is influenced by the in-cylinder pressures, as typically the greater the pressure reached, the higher the in-cylinder temperatures. The fuel's chemical properties, such as their LHVs and DCNs, will also have implications on exhaust temperatures, through changes in the resulting HRR. Although, the Yanmar L100V engine had no aftertreatment systems or EGR, the changes in exhaust temperatures due to the fuel blending studied are an important performance indicator.

Increased fuel consumption is one concern when using high fractions of oxygenated biofuels. This increase is typically due to their lower energy density than diesel (table 2.8). However, if a fuel formulation can be found to match or improve upon the fuel consumption when using ULSD, then this would favour the utilisation of such a

fuel blend (13, 120, 144). For many applications of CI engines, such as HGVs and agricultural equipment, there would usually be long periods between refuelling. If a vehicle must be refuelled frequently it would lower productivity, as the vehicle is operational for less time. Therefore, it would be beneficial to produce a fuel that does not increase fuel consumption, and thus the amount of refuelling required.

A CI engine is reliant on the autoignition of the fuel upon injection, with the injection timing optimised depending upon the fuel being used and to help control emissions (101). The time between the fuel injection and the ignition (start of stable combustion) is defined as the IDT. In this work, the IDT was determined using the method outlined in section 3.7.4. The injection timing was fixed at 13.5° BTDC in the Yanmar L100V, and the changes in the IDTs were because of the fuel blends' physical and chemical properties. Any variations in the IDT for a fuel blend will result in changes to the emissions, and these changes are discussed in Chapter 6.

This chapter discusses the influence of the selected ethyl and butyl-based blends on engine performance, whilst determining recommendations of any modifications to the engine or its operation that would be required to ensure any performance changes are not detrimental. The blend optimisation process for the ethyl-based blends is outlined in this chapter, as selecting a blend composition purely based on DCN values may be unsuitable due to the influence of the blend's physical properties. Comparisons of key performance parameters between the ethyl and butyl-based blends relative to ULSD will be drawn. There will be recommendations of the modifications that may be required to favour the utilisation of the fuel blends tested.

5.1.1 COVID Impact Statement

The impact of COVID was most significant in reducing the time available for engine testing. Due to occupancy limits, laboratory training had to be delayed, reducing the time available for testing. COVID also had an impact on equipment repairs due to manufacturers struggling to obtain the required parts, further reducing experimental time available. With this, a smaller set of compliant butyl-based blends were selected. For the ethyl-based blends, only a limited number were tested, without the opportunity to tailor the fuel blends further to determine optimum blend compositions. The impacts of COVID also increased the lead-time on the delivery of the biofuel components. This resulted in the inability to test 100% biofuel blends for the butyl-based three-component blends and the two ethyl-based blends that had stable engine performance presented in this chapter.

Due to the reduced time available, the heat release analysis was limited to HRR and accumulated heat release (AHR), as the heating values of the fuel blends could not be measured. The LHV is needed to determine the combustion duration and mass

fraction burnt. These could not be determined since a linear blending rule may not have been appropriate for predicting LHVs of the fuel blends. Whilst the LHVs could be approximated using a linear-by-mass blending rule, its accuracy could not be determined, as there was insufficient time available to measure the LHVs of the fuel blends. Hence using these approximated values was reserved to offer insight into the changes in fuel consumption when using the biofuel blends of interest.

Due to the reduced time available, there could be no analysis of engine parts after using the biofuel blends. For example, the fuel injectors and fuel lines could not be analysed to determine the effects of using the biofuel blends. The formation of deposits on the fuel injectors could not be investigated due to the lack of time available and these deposits would influence the injector's performance.

5.1.2 Engine Stability for the Advanced Biofuel Compositions Tested

The first suite of engine testing was conducted using the butyl-based blends that were identified through the physical properties testing, to find those compliant with the limits of BS 2869 and EN 590, as discussed in Chapter 4 (12, 16). When the biofuel blends were tested in the engine, it was first established that each load could be achieved and held stably. For all of the butyl-based blends tested, all five required loads, 4% up to 92%, could be achieved with the FJ injector and held stably throughout the engine tests' duration, as shown in table 5.1.

Table 5.1. Butyl-based blends tested in the Yanmar L100V, the loads achieved, and their stability.

Fuel	Injector	Load Achieved (%)
ULSD	FJ	4, 28, 50, 75, 92
90% ULSD 10% Biofuel (65 vol% BL/5 vol% BuOH/30 vol% DNBE)		4, 28, 50, 75, 92
90% ULSD 10% Biofuel (75 vol% BL/5 vol% BuOH/20 vol% DNBE)		4, 28, 50, 75, 92
90% ULSD 10% Biofuel (85 vol% BL/5 vol% BuOH/10 vol% DNBE)		4, 28, 50, 75, 92
90% ULSD 10% Biofuel (85 vol% BL/10 vol% BuOH/5 vol% DNBE)		4, 28, 50, 75, 92
90% ULSD 10% Biofuel (90 vol% BL/5 vol% BuOH/5 vol% DNBE)		4, 28, 50, 75, 92
75% ULSD 25% Biofuel (85 vol% BL/5 vol% BuOH/10 vol% DNBE)		4, 28, 50, 75, 92
75% ULSD 25% Biofuel (90 vol% BL/5 vol% BuOH/5 vol% DNBE)		4, 28, 50, 75, 92
75% ULSD 25% Biofuel (85 vol% BL/5 vol% BuOH/10 vol% DNBE)	FB	4, 28, 75, 92

- 152 -

When the FB injector was used with the selected butyl-based blend of 75% ULSD 25% biofuel (85 vol% BL/5 vol% BuOH/10 vol% DNBE), 50% load could not be achieved stably as the load bank could not maintain 2 kW of electrical power. During the test, it would decrease from the desired 2 kW electrical power. Therefore, 50% load could not be tested with the FB injector.

Examples of the pressure-crank angle (P-CA) curves are shown in figures 5.1, 5.2, and 5.3. Stable operation was evident when the 100 individual curves taken during the logging of a pressure trace, all overlap with the average curve, the dark grey line in the figures, making it not always visible. Another indication of stable operation was that the shape of the P-CA curves were similar to that of the ULSD, shown in the graphs labelled a in each of the figures, albeit with changes in gradients and timings of the peak pressure due to changes in the IDTs (discussed in section 5.2). The average of the 100 cycles enabled the oscillations in the pressure transducer to be accounted for and normalised to give a smooth average, as seen in figure 5.1a and figure 5.1b, showing the P-CAs for ULSD and a butyl-based blend with ULSD when using the FJ injector, respectively. The coefficient of variation (COV) for the peak pressure in figures 5.1a and 5.1b were 0.016 and 0.019, respectively, indicating there was stability in the engine. Figures 5.2 and 5.3 show the P-CA traces for ULSD and different ethyl-based blends with ULSD at 50% and 92% load, respectively.
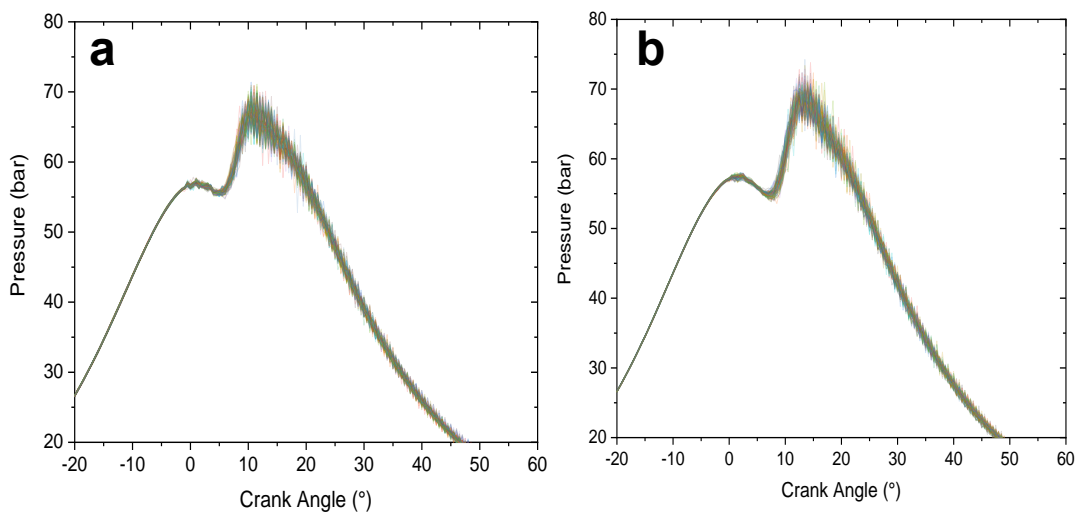
Figure 5.1. P-CA plots at 92% load for: a: ULSD and b: 75% ULSD 25% biofuel (85 vol% BL/5 vol% BuOH/10 vol% DNBE).

The selection process for the ethyl-based blends initially followed the method detailed in section 3.1.2, where blend formulations with DCNs 40 and 50, with a tolerance of ±0.2, were identified. The two blends selected were 50 vol% EL/10 vol% EtOH/40 vol% DEE and 40 vol% EL/10 vol% EtOH/50 vol% DEE with DCNs of 39.8 and 49.9, respectively. All the ethyl-based blends, with and without diesel, were tested using the

FB injector. The 100% ethyl-based biofuel blends were incompatible with the Yanmar L100V, as it would not start, as shown in table 5.2.

Table 5.2. A summary of the ethyl-based blends tested in the Yanmar L100V, the loads they could reach, and their stability.

Fuel	Biofuel Blend DCN	Load Achieved (%)	Engine Stability
0% ULSD 100% Biofuel (50 vol% EL/10 vol% EtOH/40 vol% DEE)	39.8	Would not start	
0% ULSD 100% Biofuel (40 vol% EL/10 vol% EtOH/50 vol% DEE)	49.9	Would not start	
50% ULSD 50% Biofuel (40 vol% EL/10 vol% EtOH/45 vol% DEE)	49.9	Would not start	
75% ULSD 25% Biofuel (50 vol% EL/10 vol% EtOH/40 vol% DEE)	39.8	None	No – would only run at 2400 rpm
75% ULSD 25% Biofuel (40 vol% EL/10 vol% EtOH/50 vol% DEE)	49.9	None	No – would not stabilise
75% ULSD 25% Biofuel (65 vol% EL/5 vol% EtOH/30 vol% DEE)	33.1	4, 28, 50	Not completely stable over the loads it could achieve
75% ULSD 25% Biofuel (75 vol% EL/5 vol% EtOH/20 vol% DEE)	22.9	4, 28, 50	Not completely stable over the loads it could achieve
85% ULSD 15% Biofuel (75 vol% EL/5 vol% EtOH/20 vol% DEE)	22.9	4, 28, 50, 75, 92	Yes – could run up to 92% load
85% ULSD 15% Biofuel (95 vol% EL/5 vol% EtOH)	4.03	4, 28, 50, 75, 92	Yes – could run up to 92% load

The ethyl-based blend with a DCN of 49.9 was blended with 50 vol% ULSD to determine if the addition of ULSD would enable the engine to start. However, this was unsuccessful. The predicted higher DCNs of the blends resulted in blends that were incompatible with the Yanmar L100V engine. This incompatibility was likely due to the high fractions of DEE creating a large amount of vapour. The build-up of DEE vapour created regions where the liquid fuel could not be pumped through, resulting in vapour lock. Additionally, DEE reduces the viscosity of the fuel leading to less efficient pumping, resulting in less fuel being delivered to the injector and into the cylinder (129, 220). It was decided to test blends of the two aforementioned biofuel compositions at 25 vol% with 75 vol% ULSD. The engine did start, but it would not get above 2400 RPM when using the 75% ULSD 25% biofuel (50 vol% EL/10 vol% EtOH/40 vol% DEE) blend. This low RPM did not generate enough electrical power for the loadbank to be initiated and therefore was unsuitable for testing. The 75% ULSD 25% biofuel (40 vol% EL/10 vol%

EtOH/40 vol% DEE) blend also would not stabilise at 3000 RPM. The ethyl-based three-component blends with 40 and 50 vol% DEE, even when blended with 75 vol% ULSD, were not compatible with the engine. Therefore, a different approach was needed.

It was evident that using the DCN model to predict blends that should be compatible with engine operation was not a suitable method to select blends. This difference in predicted and practical compatibility highlighted that the physical properties of the blend need to be considered alongside the DCN (37, 55, 220). Although the KV40s and flash points of the ethyl-based blends could not be tested, it was decided to select two blends of the same ratios of alkyl levulinate, dialkyl ether, and alcohol, as the butyl-based blends tested, provided the three-component ethyl-based blend was miscible with ULSD, as discussed in section 4.2. The two formulations selected were: 65 vol% EL/5 vol% EtOH/30 vol% DEE and 75 vol% EL/5 vol% EtOH/20 vol% DEE. These were first tested at 25 vol% in ULSD since this was the highest butyl-based blend fraction. However, the two selected blends, when blended at 25 vol% still did not give stable combustion at the higher loads, as seen in figure 5.2b. The instability resulted in these blends not being able to reach over 50% load. This was likely due to the lower viscosity of the blends due to the higher DEE fractions and its high reactivity. As a result, the DEE fraction needed to be reduced further or even removed. However, this would leave blends of EL and EtOH and both have very low DCNs. Previous work by Olanrewaju (313) identified that the Yanmar L100V could only run with up to 20 vol% ethanol in diesel. Since the DCNs of EL and ethanol are similar, any future blends without DEE when blended with ULSD needed to contain <20 vol% of any mixture of ethanol and EL. Hence the blends were chosen to be at 15 vol% biofuel, and 95 vol% EL/5 vol% EtOH was chosen as the blend without DEE. The reason for the low ethanol fraction was that the most cost effective utilisation of the alcoholysis product stream would include recycling the ethanol to produce further EL (38, 113). To investigate if DEE was causing issues even at low fractions in the total fuel blend, a blend of 75 vol% EL/5 vol% EtOH/20% vol% DEE was also chosen to be tested at 15 vol% in ULSD, as this was a miscible blend. These two blends were able to run up to 92% load with no instability, indicating that DEE needed to be less than 5 vol% of the total blend to give stability when running the engine.

The P-CA traces in figure 5.2b show there could be variation in the IDT, or no ignition at all when using these blends since there is no second pressure rise in the individual trace. It was expected that ethyl-based blends with DCNs >40 should have enabled the engine to start and run stably, as these DCNs are close to those of different types of diesel. The issue is likely due to the presence of the DEE since it is highly reactive and volatile, and has a DCN ranging between 139-160 (37, 143). DEE also has a low autoignition temperature of 170 °C compared to 363 °C and 425 °C of EtOH and EL, respectively (123, 301, 314). The COV in the pressures at 20 CAD, in figures 5.2a,

5.2b, and 5.2c were 0.015, 0.217, and 0.016, respectively. The position of 20 CAD was used since the peak pressures in figure 5.2b were below the TDC pressure. The high variation in the pressure shows the instability of the blend, making it unsuitable for use in the engine.
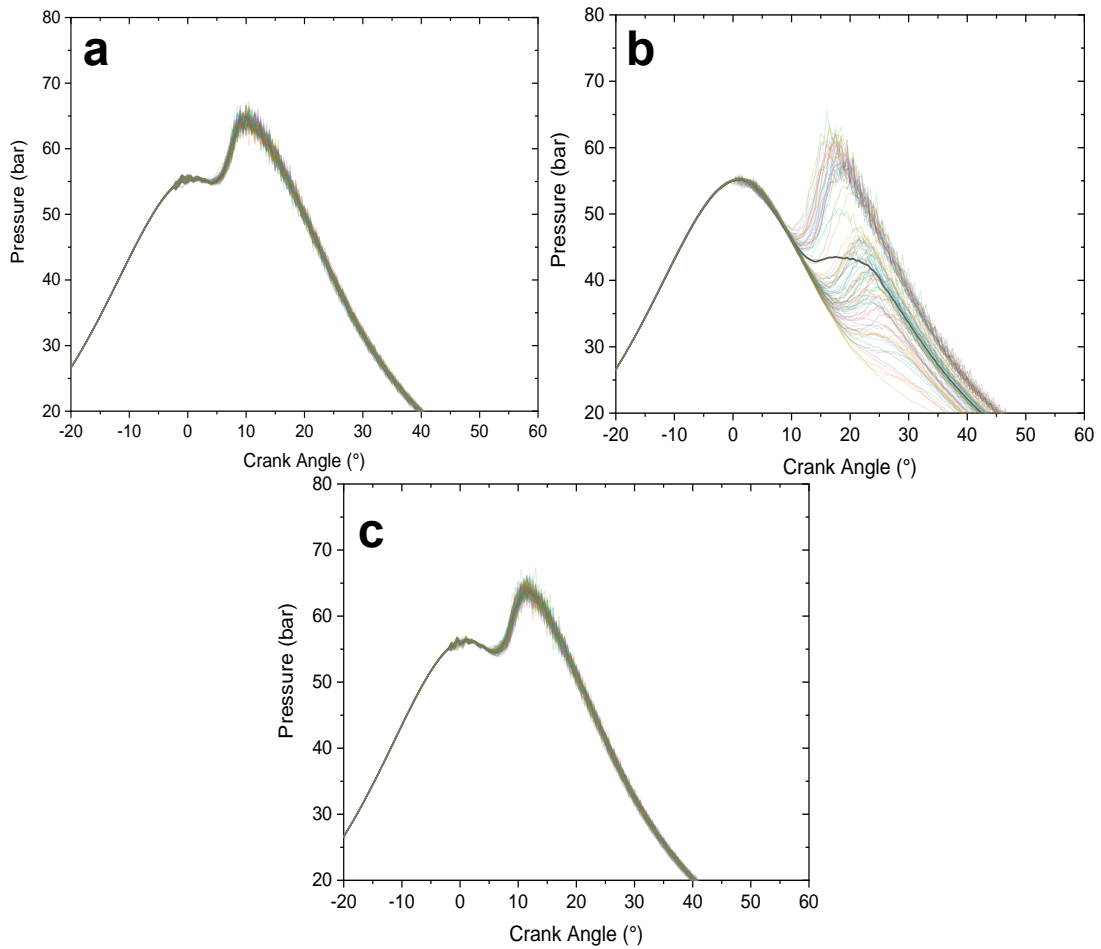
Figure 5.2. P-CA plots at 50% load for: a: ULSD, b: 75% ULSD 25% Biofuel (75 vol% EL/5 vol% EtOH/20 vol% DEE), and c: 85% ULSD 15% Biofuel (95 vol% EL/5 vol% EtOH).

The high volatility of DEE and its high vapour pressures: 0.56 bar at 20 °C and 0.86 bar at 30 °C, also contribute to this instability and the engine not starting (123). The high vapour pressure can lead to vapour lock, as reported by Górski and Przedlacki (129) where blends of ULSD with >20 vol% DEE would not allow the engine to start, and Iranmanesh et al. (315) who found that for >15% DEE there would be vapour locking. Vapour locking was likely the cause for the engine not starting with the blends outlined in table 5.2. Górski and Przedlacki (129) also found the low viscosity and lubricity of DEE caused fuel pumping issues resulting in difficulty starting the engine. Similar pumping issues may have contributed to the engine instability with the blends shown in table 5.2. To overcome pumping issues, and to ensure there was sufficient lubrication from the fuel, Sivasankaralingam et al. (220) added a lubricity additive to DEE/EtOH binary blends before engine testing. The addition of such an additive to the ethyl-based blends where

the engine would not start or maintain stability may enable these blends to run in the engine.

When running the two 15 vol% biofuel blends, there was evidence of the higher reactivity of DEE. Figure 5.3 shows the P-CA curves at 92% load for ULSD and the two 15 vol% biofuel blends. It can be seen in figure 5.3b, that the presence of DEE causes some cycle-to-cycle variability. However, when both ULSD and the blend without DEE were tested at 92% load, there was no extreme cycle-to-cycle variability, as seen in figures 5.3a and 5.3c, respectively. The COVs for the peak pressure in figures 5.3a, 5.3b, and 5.3c were 0.016, 0.054, and 0.016, respectively. This variability for the blend with DEE has no pattern, such that not every alternate cycle has lower pressures and longer IDTs, indicating that this may be due to inconsistent fuel delivery of larger fuel volumes.
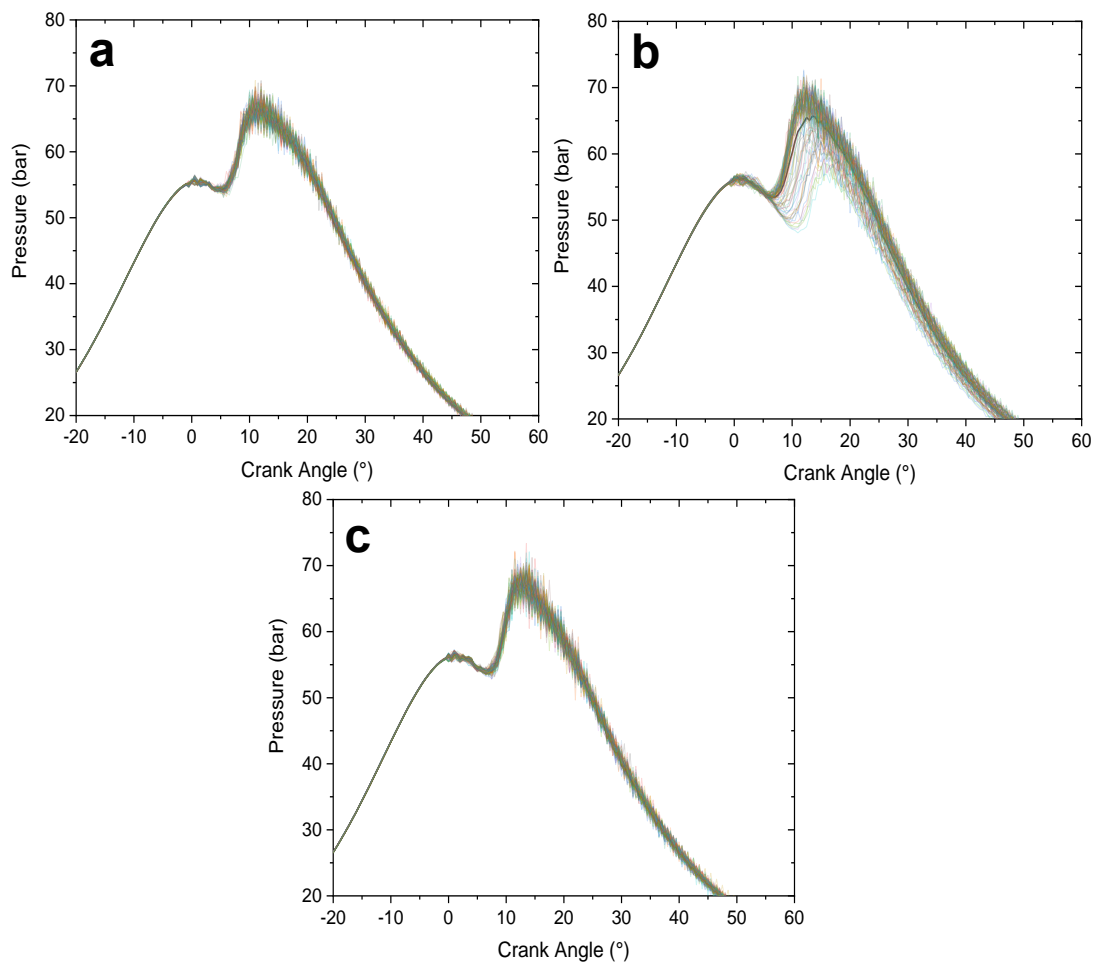
Figure 5.3. P-CA plots at 92% load for: a: ULSD, b: 85% ULSD 15% Biofuel (75 vol% EL/5 vol% EtOH/20 vol% DEE), and c: 85% ULSD 15% Biofuel (95 vol% EL/5 vol% EtOH).

The engine instabilities with the ethyl-based blends make them less favourable than the butyl-based blends, which ran stably, even at 25 vol% biofuel. The instability would lead to inefficient operation and potentially damage the engine (4, 5). The influence of the ethyl and butyl-based blend compositions on the engine performance parameters are discussed in this chapter.

5.2 Ignition Delay Times in the Engine and the Influence of the Advanced Biofuel Blends

One key parameter that will influence every other performance property and the engine emissions is the IDT. The fuel was injected at a fixed timing of 13.5° BTDC. Therefore, any changes in the IDT were due to the chemical and physical properties of the fuel blend. The use of P-CA curves and the equations detailed in section 3.7.4 enabled the IDTs at each load to be determined.

5.2.1 Influence of the Ethyl-Based Blends on IDTs

Addition of the ethyl-based blends to the ULSD caused an increase in the IDTs across all of the loads each blend could achieve. The increase was expected with the selected ethyl-based blends having low DCNs shown in table 5.2, which are less than the EN 590 and BS 2869 limits (16, 227). The IDT increased relative to the diesel baseline, and this is evident in figure 5.4, where the pressure rise has moved to later in the cycle.
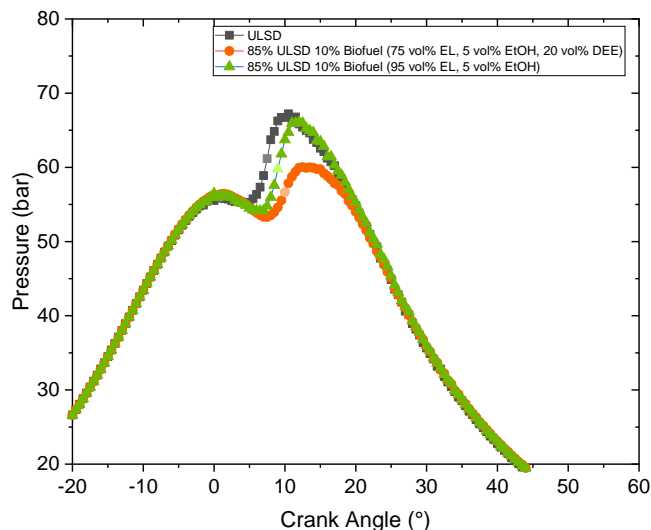
Figure 5.4. Comparison of the P-CA at 75% load for ULSD, 85% ULSD 15% Biofuel (75 vol% EL, 5 vol% EtOH, 20 vol% DEE), and 85% ULSD 15% Biofuel (95 vol% EL, 5 vol% EtOH), with the SoC highlighted with lighter coloured symbols for each fuel.

The IDT can be reported in CAD, as shown in figure 5.5a. However, this does not account for the changes in RPM, hence the use of the method outlined in section 3.7.4, which gives the IDT in ms. As a result, the trends observed in figure 5.5 demonstrate that an increase in IDT is evident using either measure. The percentage change in IDT relative to ULSD in ms is shown in figure 5.6.
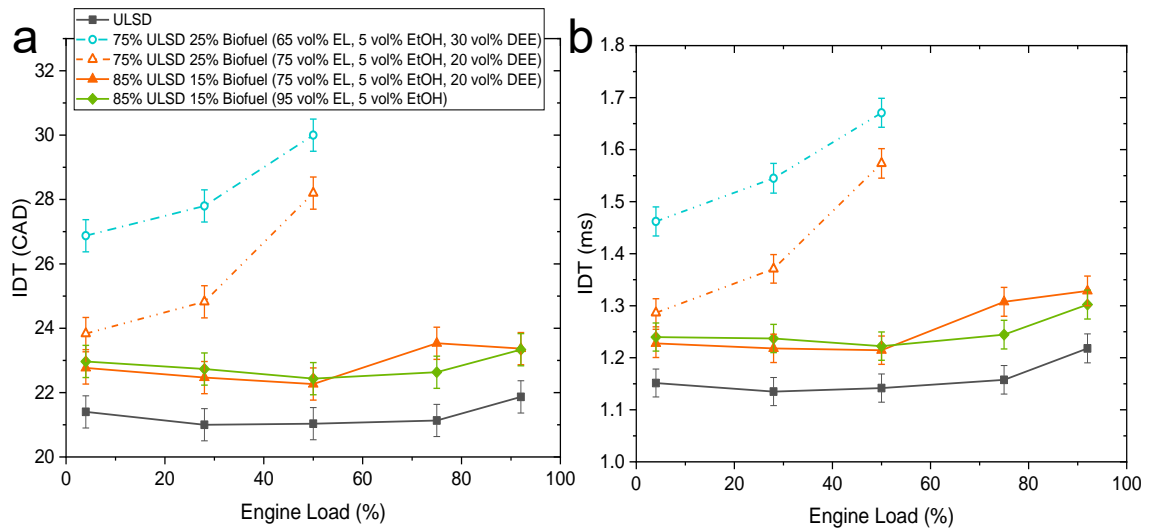
Figure 5.5. IDTs for the four ethyl-based blends. a: in CAD. b: in ms.

The instabilities in the combustion of the 25 vol% biofuel blends resulted in difficulties in calculating a consistent IDT. The error is reported as ±0.5 CAD, which is the accuracy of the encoder as this was greater than the variability in the calculated IDTs, in both CAD and the equivalent time in ms. Poor fuel injection was more evident with larger increases in the IDTs for the 25 vol% blends, with the greatest coming from the blend with the higher fraction of DEE, as shown in figure 5.6. The increase in IDT for the blend without DEE was consistent across most loads. At <50% load, the blend without DEE had a greater increase in IDT than the blend with DEE. At these conditions the engine was stable, hence the lower DCN fuel had the longer IDTs. At the higher powers it had a greater increase in the IDT compared to the blend without DEE.
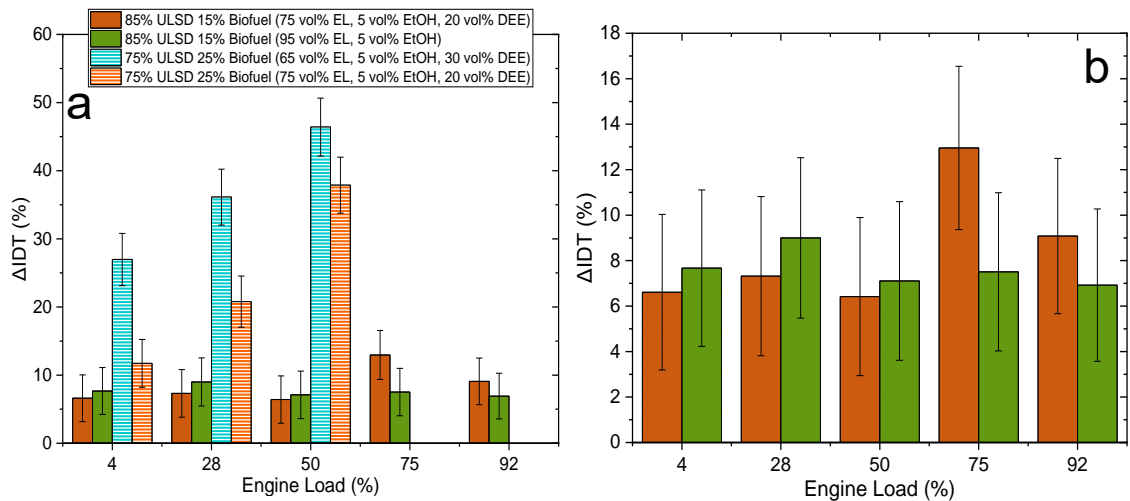
Figure 5.6. Change in the IDTs relative to ULSD. a: for the four ethyl-based blends. b: for the two 15 vol% blends.

For the two 15 vol% ethyl-based biofuel blends, the differences in the changes in the IDT were within one standard error (determined through error propagation) of each other at all loads, as the error bars in figure 5.6b overlap. Therefore, the changes in the IDT at the higher loads may follow the trends of the lower loads, provided there was

engine stability. The smaller differences in ΔIDT at the lower loads were due to less fuel being injected at the lower loads. Therefore, the influence of DEE was reduced. The low DCNs and high enthalpy of vaporisation of both EL and EtOH (table 2.8) do not promote ignition (135, 137). The increase in the IDT for the blend with DEE may be due to the reduced lubricity and viscosity, reducing the fuel pump's effectiveness when pumping larger volumes of fuel at higher loads (135). In addition, DEE was likely to be vaporised upon injection due to the high in-cylinder temperatures. There was no evidence of combustion shortly after injection, as there were no increases in pressure before TDC in figure 5.3. The evaporation of volatile components lowers the gas temperature, which results in a longer physical ignition delay since the remaining liquid fuel takes longer to vaporise at lower temperatures and ignite (137).

Górski and Przedlacki (129) showed that the IDTs had little to no change for blends of ULSD with <20 vol% DEE when tested in a three-cylinder 34.6 kW engine. On the other hand, there are studies that have shown that IDTs become longer with increasing DEE fractions. For example, Venu and Madhavan (135) demonstrated that for blends of a three-component base fuel (20% ethanol/40% biodiesel/40% diesel), the addition of 10% DEE to this base fuel caused the IDT to increase, whereas, 5% DEE did not. It was hypothesised that 10% DEE resulted in highly reactive regions in the cylinder that would undergo local ignition and would not promote bulk ignition in the air/fuel mixture due to insufficient vaporisation of the other fuel components (134, 135). The addition of 5% DEE acted as a CN enhancer when tested by Venu and Madhavan (135), whereas, in the Yanmar L100V, the low total fractions of DEE (<5%) did not show the same behaviour. Kaimal and Vijayabalan (316) found that adding 5% DEE to a plastic oil caused the IDT to increase. They suggested that since the enthalpy of vaporisation of DEE was higher than the base fuel, it caused a longer IDT. They also discussed DEE impeding the fuel injection and its interactions with aromatic compounds in diesel, as reported by Bailey et al. (134) and Clothier et al. (317), causing the longer IDTs. Since EL and EtOH both have an enthalpy of vaporisation higher than DEE, it was unlikely that the vaporisation when DEE was present caused the longer IDTs. Therefore, it is concluded that the changes to the fuel injection and resulting instabilities contribute to the longer IDTs for the blend with DEE (150).

The longer IDTs with the ethyl-based blends will affect the emissions and other engine properties. The longer IDTs could be compensated for by a series of modifications to both the engine and its operation. Firstly, the injection timing could be advanced such that the air/fuel mixture could be compressed for longer. Secondly, the injection strategy could be changed. The Yanmar L100V has one injection, whereas, in vehicle engines, there can be multiple injections. These could be beneficial as having multiple injections into an already combusting air/fuel mixture should reduce the effect of

a longer IDT (318). The injection timing on the Yanmar L100V engine cannot be easily changed, as it is at the defined point of the flywheel. Therefore, the flywheel would need to be manually adjusted to change the injection timing, whereas, on a vehicle, the electronic control unit (ECU) could be reprogrammed (319). Another modification could be to increase the in-cylinder temperature to promote the autoignition of the low DCN components. One such method would be to heat the intake air (320). The compression ratio could be increased, but this would require major modifications to the engine architecture. Finally, there is the potential to enhance the DCN using additives in a similar manner to Christensen et al. (13). All of these may be possible avenues to explore in future work.

5.2.2 Influence of the Butyl-Based Blends on IDTs

Since there was stable combustion when using any butyl-based blend, changes in the IDTs were assumed to be due to changes in the chemical and physical properties of the fuel blends compared to ULSD. The KV40 and density are within the limits of the fuel standards (section 4.6) but they are different to the ULSD used. The chemical properties of the fuel will also affect the IDTs, primarily the DCN of each component and the enthalpy of vaporisation (13, 143). The DCNs of BL, BuOH, and DNBE are 14, 12, and 100, respectively (143). High fractions of BL will likely reduce the blend's DCN. The IDTs for the different butyl-based blends are shown in figures 5.7a and 5.7b in CAD and ms, respectively, with the error from the encoder used as it is greater than the IDT variability.
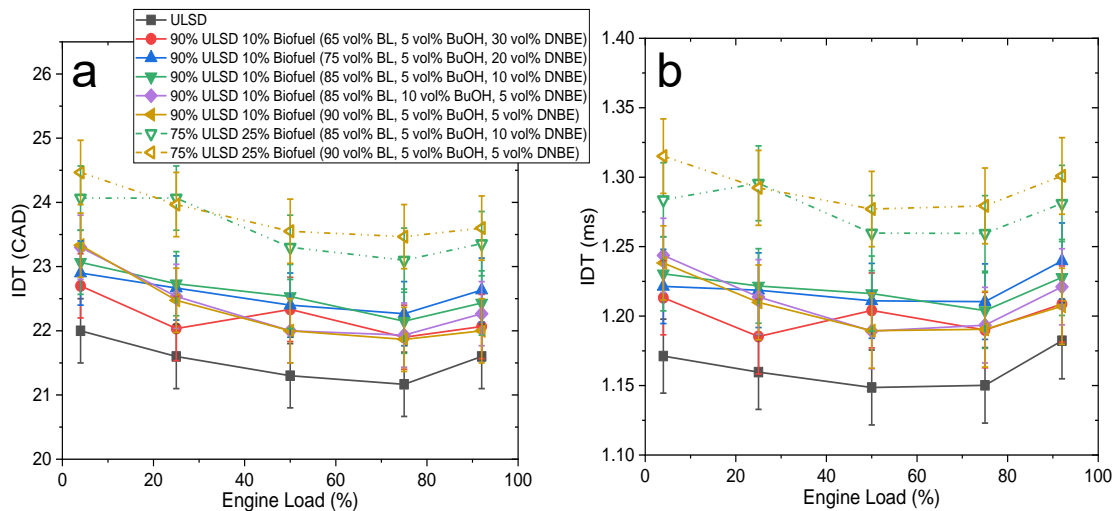
Figure 5.7. IDTs for the butyl-based blends. a: in CAD. b: in ms.

The addition of 10 vol% of the butyl-based blends caused an increase in IDTs at all loads. At lower loads, the ΔIDT increased as the DNBE fraction decreased, as seen in figure 5.8. There was a greater increase in IDTs with the addition of 25 vol% biofuel, which was expected since there is a larger fraction of the low DCN components.
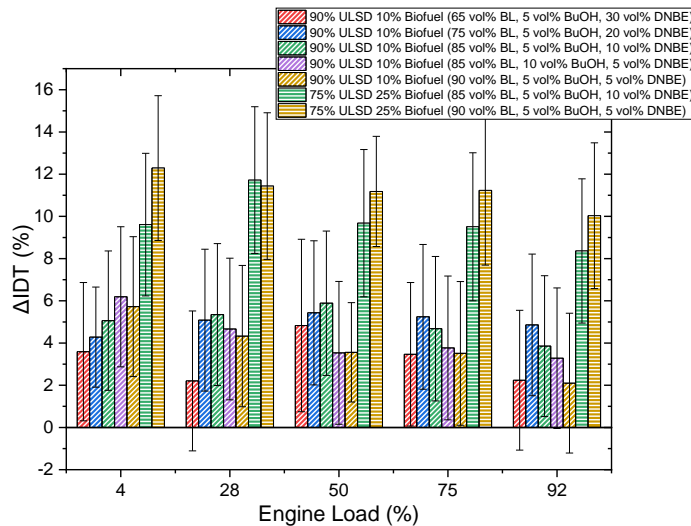
Figure 5.8. Change in the IDTs for the butyl-based blends relative to ULSD.

For the butyl-based blends with 85 vol% BL, the blend with 10 vol% BuOH had less of an increase in IDT when the engine load was >4% compared to the blend with 10 vol% DNBE, as shown by the green and purple bar with diagonal white lines, respectively. The changes in IDTs for these blends were within one standard error of each other when accounting for the tolerances on the fuel injection and CAD measurement. Therefore, there is the possibility the IDTs for the blend with 10 vol% BuOH could be longer. This difference was unexpected since DNBE has a higher DCN than BuOH, and the blends had similar KV40s (0.01 mm^2/s difference) and similar densities (0.001 g/cm^3 difference). Therefore, it is unlikely these physical properties had a large contribution to this change in the IDT. The enthalpies of vaporisation for DNBE and BuOH are 45 kJ/mol and 52 kJ/mol, respectively, which would indicate that the blend with 10 vol% BuOH should have the longer IDT (321). However, since the IDTs are within one standard error, it may be that the trend seen at 4% load should be the case for the other loads.

The relative changes in IDTs are below 6% for most of the 10 vol% biofuel blends. The 25 vol% blends had longer IDTs than ULSD. The blend of 90 vol% BL/5 vol% BuOH/5 vol% DNBE, had the greatest increase across most loads, other than the 28% load. When the biofuel fraction increased by 2.5 times, from 10 to 25 vol%, the ΔIDTs doubled for the blend with 85 vol% BL and tripled for the blend with 90 vol% BL. This finding indicates that there may be a non-linear dependence of the change in IDT on the biofuel fraction. Frigo et al. (38) identified that for ULSD/DNBE/BL blends, the IDTs increased by 0.25 CAD up to 0.55 CAD at 3600 RPM. The 0.25 CAD increase was from the 89 vol% ULSD/4 vol% DNBE/7 vol% BL blend, and the 0.55 CAD increase was with the 83 vol% ULSD/4 vol% DNBE/13 vol% BL blend (38). The engine used by Frigo et al. (38) was operating at a higher RPM (3600 RPM) and on an eddy-current dynamometer to achieve 50% and 100% torque, unlike the Yanmar L100V that was held at the selected loads using the load bank. Therefore, the RPM of the Yanmar L100V was not held

constant and would fluctuate by up to 10 RPM. However, the impact of a fluctuation of 10 RPM on the total IDT when using equation 22 (section 3.7.4) was negligible. In addition, the resolution of the pressure logging (every 0.5 CAD) gave rise to a larger error, hence the use of ±0.5 CAD as the error bars for the plots displaying the IDTs.

These changes in IDTs will affect the emissions when utilising these blends, as discussed in Chapter 6. The longer IDTs may result in the peak pressures, HRRs, and temperatures changing since the combustion cycle is delayed. The longer IDTs could be compensated for using the same techniques discussed for the ethyl-based blends in section 5.2.1.

5.2.2.1 Changes to IDTs on Utilisation of the FB Injector with the Butyl-Based Blends

Since the FB injector has smaller holes, the resulting improved fuel atomisation should reduce the IDT of ULSD and the selected butyl-based blend relative to the FJ injector. At <50% load, using the FB injector led to shorter IDTs than when using the FJ injector, as shown in figure 5.9. However, at 92% load, the IDT of ULSD was longer when using the FB injector, but it is within one standard error of the IDT when using the FJ injector. With both injectors the IDTs increased when using the butyl-based biofuel blend relative to ULSD.
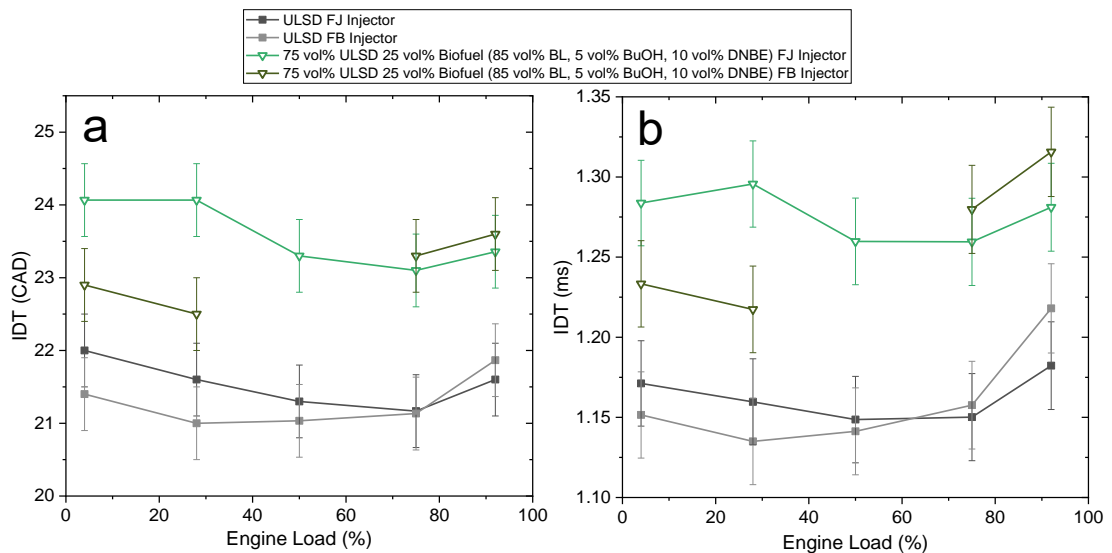
Figure 5.9. IDTs of the ULSD and the selected butyl-based blend with the FJ and FB injectors. a: in CAD. b: in ms.

The increase in IDT when using the butyl-based blend relative to ULSD was similar for both injectors, as shown in figure 5.10. The addition of the butyl-based blend resulted in longer IDTs when using both injectors, due to the low DCN of the butyl-based biofuel blend. At 4% and 28% loads, the FJ injector had a slightly greater increase in the IDT. This increase was likely due to larger fuel droplets created by the FJ injector, which take

longer to vaporise (87, 322). With the FB injector at lower loads, the reduced droplet size shortens the vaporisation time resulting in less of an increase in IDTs (87, 322). At the higher loads, the increase in IDT relative to ULSD for the butyl-based blend is similar for the 92% load. However, at 75% load, the FB injector has a longer IDT.
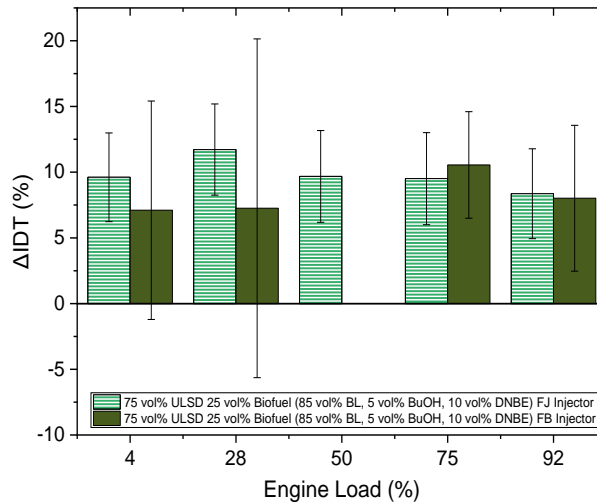
Figure 5.10. Change in the IDT of the selected butyl-based blend relative to the ULSD for the FJ and FB injectors.

The reduction in the difference between the relative change for each injector at higher powers indicates that the fuel chemistry has a large influence when more fuel is injected (323). This could be investigated using simulations of fuel combustion coupled with the fuel spray. At higher loads, more fuel is injected due to the RPM decreasing and the mechanical fuel injector staying open longer. The total injector hole area for the FB injector was less than the FJ injector, but the injection pressure of both injectors was the same. The FB injector had a total injector hole area of 0.134 mm^2, whereas the FJ injector's total hole area was 0.172 mm^2, a difference of 28%. This reduction may increase the time required to inject the same volume since the fuel flow rate is maintained. The RPM decreased when using the FB injector, which increases the injection duration allowing the same volume to be injected. Due to the increased number of holes in the FB injector, they are closer together, and this may have favoured interactions between adjacent fuel jets when more fuel was injected at higher loads (323). With this, it could be that at the higher loads, the two injectors perform similarly. The implications of this change in IDT on the emissions are discussed in Chapter 6. With both fuel injectors, the injection timing would need to be earlier to ensure the longer IDTs of the biofuel did not have a detrimental effect on the engine performance and emissions. In summary, when using either fuel injector the IDTs increased relative to ULSD. The FJ injector caused a greater increase at the lower loads, whereas at the higher loads both fuel injectors had similar increases. Therefore, in the typical operation window of the genset, both injectors could be used and there would be similar changes.

5.3 Influence of the Advanced Biofuel Blends on Fuel Consumption

When finding alternative fuels, one target is to maintain or reduce fuel consumption. Most fuel delivery systems operate on a volumetric basis. Therefore, any increase in density will result in larger masses of fuel injected. The change in mass injected will also change the stoichiometry as the molar ratios of air and fuel change. In addition, there is a change in the fuel's elemental composition and energy density when oxygenated biofuels are added (50, 221, 324-326).

In this work, the fuel delivery system was unmodified since one aim was to find drop-in fuels. The changes in the fuel blend's elemental ratio could not be accounted for as the volume of fuel injected was fixed, regardless of the blend composition and fuel injector. The Yanmar L100V engine consumes more fuel at higher loads. The amount of fuel delivered was controlled by the governor, as it allowed more fuel to flow to the fuel pump at higher loads. In addition, the lower RPM kept the cam-driven mechanical injector open for longer. As a result, the changes in fuel consumption were due to the changes in electrical power at a given load and the changes in the RPM, which impacts the mass of fuel injected.

5.3.1 Influence of the Ethyl-Based Blends on BSFC

The BSFC at each engine load for the ethyl-based blends is shown in figure 5.11. As the load increases the BSFC moves closer to that of diesel, and the blend without DEE had less of an increase. The error bars in the graphs of the performance parameters are the standard deviations of the three measurements taken for each blend, and the standard error is used in the plots of relative change.
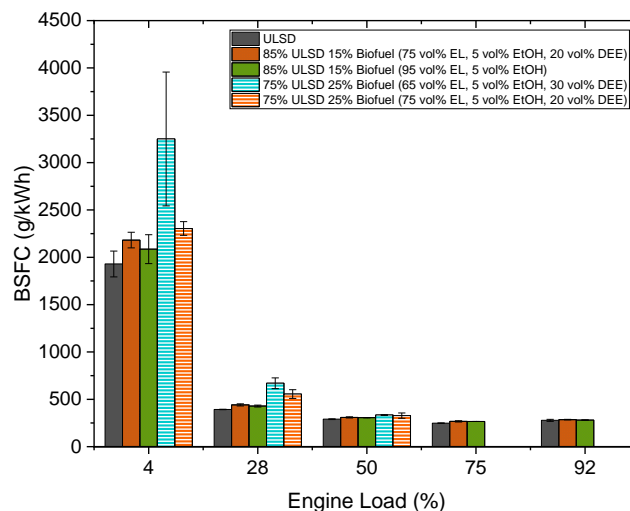
Figure 5.11. BSFC for the four ethyl-based blends.

The BSFC at all loads increased with the addition of the ethyl-based blends, with these relative increases shown in figure 5.12. The greatest increase was with the 25 vol% biofuel blend with 30 vol% DEE in the ethyl-based blend. The BSFC increased by 70% with this blend at 4% and 28% load, and it was likely due to the average engine power produced at each load being reduced due to the combustion instabilities (figure 5.2), resulting in the increased BSFC since more fuel is consumed to generate the same power. This blend also had the highest emissions of CO and THC due to less complete combustion, as presented in Chapter 6. Paul et al. (137) found that at lower loads, blends of 5% and 10% DEE in ULSD had increases in the brake-specific energy consumption (BSEC), albeit only a 10% increase in the BSEC in a Kirloskar TV-1 661 cc, 3.6 kW engine at 1500 RPM.
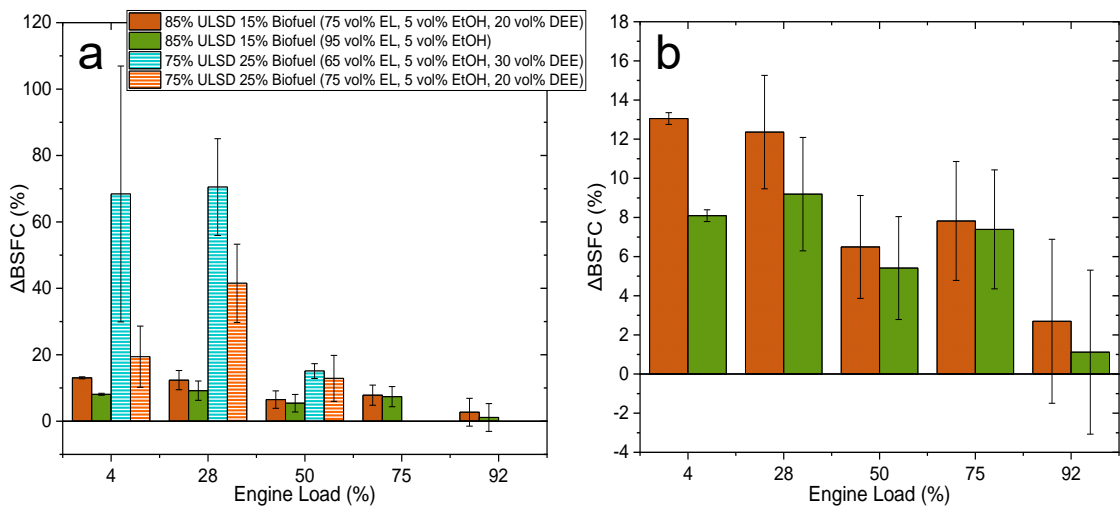
Figure 5.12. Changes in BSFC for the ethyl-based blends relative to ULSD. a: all four blends. b: two 15 vol% biofuel blends.

For the two 15 vol% biofuel blends, the blend with DEE had a greater increase in BSFC than the blend without DEE, as shown in figure 5.12b. Based on the properties of the blends, this result was unexpected as DEE has a lower density, a higher DCN, and a higher energy content. However, there were some engine instabilities in the engine at higher loads (figure 5.3b) when using this blend. The LHVs are 24.3 MJ/kg, 26.8 MJ/kg, and 33.9 MJ/kg for EL, EtOH, and DEE, respectively (13, 144). Therefore, the blend with DEE would have a higher energy content than the blend without DEE, as seen in table 5.3, but the DEE needs to be injected for this benefit to be realised in practice. At 4%, 28%, and 75% load, the increase in BSFC for the 15 vol% biofuel blends was greater than the increase in the LHV determined using a linear-by-mass blending law. Since the LHV of the Crown Oil ULSD was not measured, the median value for the LHV of diesel available in the literature was used (42.7 MJ/kg) (13, 34, 144-147). The suitability of a linear-by-mass blending law for predicting the LHVs of these blends cannot be confirmed until LHVs are measured. However, it is widely used in the literature to estimate LHVs of blends, such as by Dahmen and Marquardt (212) when formulating a biofuel blend.

Table 5.3. LHVs and energy densities for the ethyl-based blends predicted using a linear-by-mass blending rule, using a median LHV for ULSD.

Diesel (vol%)	Biofuel (vol%)	EL/EtOH/DEE ratio (vol%)	LHV (MJ/kg)	Relative Difference in LHV to ULSD (%)	Energy Density (MJ/m³)	Relative Difference in Energy Density to ULSD (%)
100	0	0	42.7		35996	
75	25	65/5/30	38.5	-9.8	33017	-8.3
75	25	75/5/20	38.2	-10.5	33024	-8.3
85	15	75/5/20	40.0	-6.4	34144	-5.2
85	15	95/5/0	39.6	-7.3	34175	-5.1

At 92% load, the BSFC had low changes with both fuel blends, albeit with large inter-run variability as shown by the large error bars. The small increases at 92% load are lower than the decrease in LHV and energy density (table 5.3). This indicates that when larger volumes of fuel were injected, the reduction in the fuels' energy content is not having such a detrimental impact on the BSFC at 92% load, as the increase of BSFC is less than 3% for reductions in energy density of 5.2% and 5.1%. However, at lower loads, the increase in BSFC was greater than the reduction in energy density, but since a genset would typically operate at high loads, these larger increases in BSFC would have a small impact on the end user. If the BSFC is reduced, or maintained, relative to ULSD, this would be a positive outcome for the suitability of these fuel blends. Since a genset typically runs at maximum load, the low change in BSFC at 92% load favours the utilisation of these blends. Wang et al. (327) found that for blends of 5 vol% EL/10 vol% FAME/85 vol% diesel and 10 vol% EL/15 vol% FAME/75 vol% diesel, the BSFC increased at all loads tested when using a single-cylinder, 15.5 kW engine. These blends had higher densities and lower LHVs than the diesel used. Therefore, with fixed volumes of fuel injected, the BSFC increased in a similar manner to the ethyl-based blends presented in figure 5.12.

5.3.2 Influence of the Butyl-Based Blends on BSFC

As the total BL fraction in the blend increased, the BSFC increased. There were small changes for the 10 vol% blends compared to ULSD and they were mostly within one standard error of ULSD, as shown in figure 5.13.
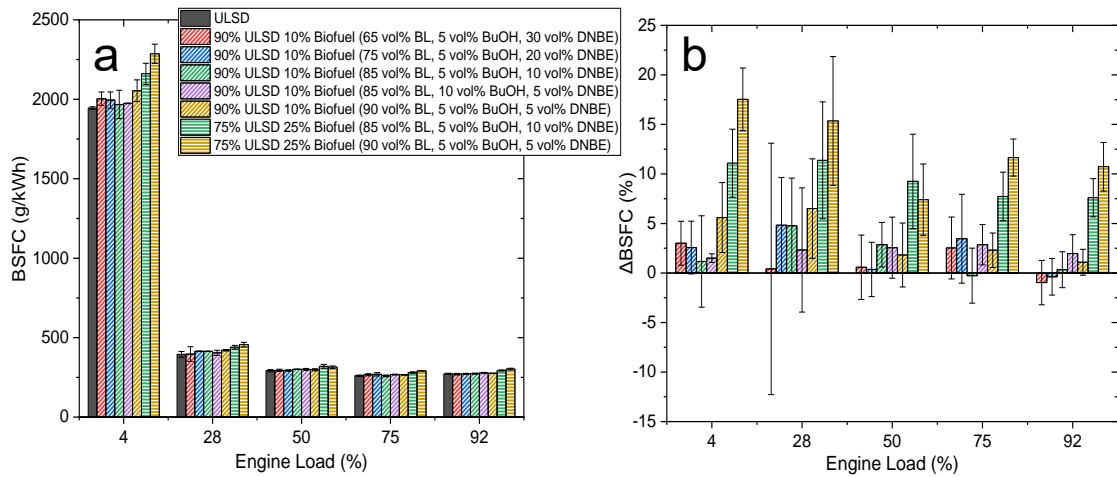
Figure 5.13. a: BSFC for the butyl-based blends and ULSD. b: Changes in the BSFC for the butyl-based blends relative to ULSD.

The changes in BSFC relative to the ULSD baseline for each butyl-based blend are shown in figure 5.13b. The 10 vol% biofuel blends had negligible changes at all loads, which makes them more favourable than the 25 vol% biofuel blends. The small differences are likely due to the small changes in the energy content since the densities were similar, ranging from 0.846 – 0.851 g/cm^3. This indicates that the energy content on a mass basis or energy density has not changed significantly relative to diesel. Predicted energy densities and LHVs can be seen in table 5.4. The small differences in density were unlikely to be detected by the balance used, as its accuracy was 10 g. This was one limitation of the current genset set-up since there was no fuel flow meter. One likely reason the BSFC increased is that as the BL fraction increases, the energy content of the fuel blends decreases as the LHVs are 27.4 MJ/kg, 33.1 MJ/kg, and 38.3 MJ/kg for BL, BuOH, and DNBE, respectively (13, 34, 145). At 4% and 28% load, for the 10 vol% biofuel blends, the blend with 90 vol% BL had the greatest increase in BSFC. The increase was likely due to this blend having the highest density and the lowest DCN (143). The LHV and energy density have not changed significantly relative to diesel, as seen in table 5.4, where the reductions are less than 4% and 3%, respectively. At lower loads, the change in BSFC for most blends is similar to the change in energy density (table 5.4). However, at 92%, load the reduction in energy density and LHV had a negligible effect on the BSFC when using the 10 vol% biofuel blends, as the BSFC is similar to that of ULSD. Having the BSFC remain close to that of ULSD would favour using the biofuel blends, as this would alleviate the worry that fuels with high biofuel fractions would require more refuelling.

Table 5.4. LHVs and energy densities for the butyl-based blends predicted using a linear-by-mass blending rule, using a median LHV for ULSD.

Diesel (vol%)	Biofuel (vol%)	BL/BuOH/DNBE ratio (vol%)	LHV (MJ/kg)	Relative Difference in LHV to ULSD (%)	Energy Density (MJ/m^3)	Relative Difference in Energy Density to ULSD (%)
100	0	0	42.7		35996	
90	10	65/5/30	41.4	-3.1	35020	-2.7
90	10	75/5/20	41.3	-3.4	34991	-2.8
90	10	85/5/10	41.1	-3.7	34962	-2.9
90	10	85/10/5	41.1	-3.8	34981	-2.8
90	10	90/5/5	41.1	-3.8	34947	-2.9
75	25	85/5/10	38.8	-9.1	33642	-6.5
75	25	90/5/5	38.7	-9.4	33625	-6.6

Figure 5.13b shows that the 25 vol% blends had the greatest increase in BSFC compared to ULSD. The blend with 90 vol% BL, has the largest increase, other than at 50% load. This blend had the highest density and the lowest DCN and LHV due to high fractions of BL (table 5.4) (143). The increases in BSFC of the 25 vol% biofuel blends were greater than the reduction in LHV and energy density at most loads. Therefore, the reduced DCN and its influence on the engine operation may have reduced the thermal efficiency, reducing the power output and increasing the BSFC (143). The relative change from ULSD between the 10 and 25 vol% biofuel blends of the same composition was more than 2.5 times that with 10 vol% biofuel. For example, at 92% load, the 75 vol% ULSD 25 vol% biofuel (85 vol% BL/5 vol% BuOH/10 vol% DNBE) blend had an increase 22 times greater than the 10 vol%. It is only at 28% load where there is an increase of 2.4 times that when using the 10 vol% blend. The increase in BSFC with increasing biofuel fraction and increasing load is non-linear, which demonstrates that the LHV may not accurately be predicted using linear blending rules. To establish the nature of this increase there needs to be additional blends tested, such as at 15 and 20 vol% biofuel. There were no modifications to the fuel delivery system to account for the increased fuel density, especially for the 25 vol% biofuel blends with densities of 0.866 g/cm^3 and 0.869 g/cm^3 for the blends with 85 vol% BL and 90 vol% BL, respectively. Whilst these densities are above the EN 590 limit, they are within the BS 2869 limits, as discussed in section 4.6. The increase in BSFC, relative to the corresponding 10 vol% biofuel blend, was likely due to the increased density and reduced LHV since fixed fuel volumes were injected (327). The combination of longer IDTs and increased BSFC could be compensated by advancing the injection timing, as Gu et al. (328) found to be the

case for blends of n-butanol and diesel. However, this change led to increased NO_X emissions as there was more complete combustion, which increased the in-cylinder temperature and pressure (328). These changes in fuel consumption would require optimisation to ensure the benefits of the oxygenated advanced biofuels are utilised.

5.3.2.1 Changes to BSFC on Utilisation of the FB Injector with the Butyl-Based Blends

When using either fuel injector, there was no change to the fuel pump, nor any difference in the injector pressure. At each load tested, the mass of fuel used when using the FB and FJ injectors was consistent within experimental error, since the balance was accurate to 10 g. Therefore, any changes in BSFC will be due to changes in spray dynamics, engine power, engine speed, and efficiency at these loads for the biofuel blend. Changes relative to the respective ULSD baselines are shown in figure 5.14. For both fuel injectors, the BSFC increased relative to ULSD when using the butyl-based biofuel blend. At the higher loads, the BSFC using the FB injector had a greater increase relative to diesel compared to the FJ injector.
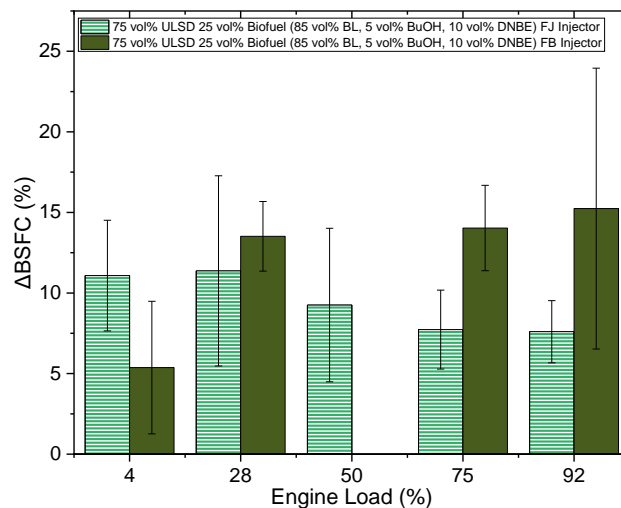
Figure 5.14. Changes in BSFC for the selected butyl-based blend with the FJ and FB injectors relative to the corresponding ULSD baselines.

For most loads, the changes in BSFC for both fuel injectors are within one standard error of each other. This may indicate that the change in BSFC was the same for both fuel injectors since the mass of the fuel blend consumed during the tests was the same. Therefore, the increased BSFC indicated that less power was generated when using the FB injector. The greater increase at 92% load with the FB injector would be detrimental since a genset would typically operate at maximum power. Additionally, a small increase in BSFC would not be as noticeable to the consumer. However, an increase of more than 10% would be noticeable, and the fuel tank would need refilling more often. A similar increase in fuel consumption when increasing the number of injector holes was observed by Sayin et al. (322). They found that increasing the number of injector holes, from 4 to

6 to 8, increased BSFC for blends of ULSD and biodiesel. Sayin et al. (322) reported that the increased number of injector holes and the resultant shorter IDTs, reduce the time available for mixing and thus give higher BSFC. However, the increase in IDT relative to ULSD for both injectors was similar at the higher loads. Therefore, the completeness of combustion may be influential here and, if so, this would be evident in the discussion of emissions trends in Chapter 6. If fuel injection timing was optimised for longer IDTs, the power generated should increase, as ignition would be closer to TDC. Therefore, there would be a greater IMEP and a reduction in BSFC. Optimisation of all these parameters is key for the utilisation of the blends tested.

5.4 Influence of the Advanced Biofuel Blends on Heat Release Rates

As discussed in section 3.7.10, the pressure traces were filtered using the Savitzky-Golay filter. The pressure data used was fitted with a second-order polynomial over five points to smooth the data and reduce the signal noise. For the ethyl-based blends, the two 15 vol% biofuel blends were analysed. The butyl-based blends selected were the 25 vol% biofuel blends and their corresponding 10 vol% biofuel blends, and the 90 vol% ULSD 10 vol% biofuel (65 vol% BL/5 vol% BuOH/30 vol% DNBE) blend. This last blend was selected to determine the influence of the high DNBE fraction. The HRR was determined using the Leeds HRR model modified to replicate the Yanmar L100V engine, as detailed in section 3.7.10. HRRs at 92% and 50% load were analysed. The 92% load was selected due to gensets typically running above 50% load and mostly at their maximum load. The 50% load was selected as a comparative lower load, higher RPM condition.

5.4.1 Influence of the Ethyl-Based Blends on HRRs

The HRR curves for the diesel baseline and the two ethyl-based blends at 92% and 50% load are shown in figure 5.15a and 5.15b, respectively. The spike at 22.5° BTDC was due to the inlet valve closing. The fuel injection at 13.5° BTDC is not evident in the HRR curve. This is somewhat expected since in the P-CA traces there is no change in pressure following fuel injection, hence it is not captured in the HRR curves. Changes in the enthalpy of vaporisation of a fuel was shown to have little to no effect on the IDT, and therefore HRR, by Kim et al. (88) when simulating n-dodecane under diesel-relevant conditions. However, they did find that changes in heat capacity correlate to the delays in HRR and IDT. DEE and EtOH have the lowest heat capacities of the ethyl-based biofuel components, but this reduction in heat capacity is in competition with the increased density of the fuel blends and the stability in the engine operation. Therefore, the changes in the HRR profiles are due to a combination and competition of the changes in the fuel blend composition and their properties.
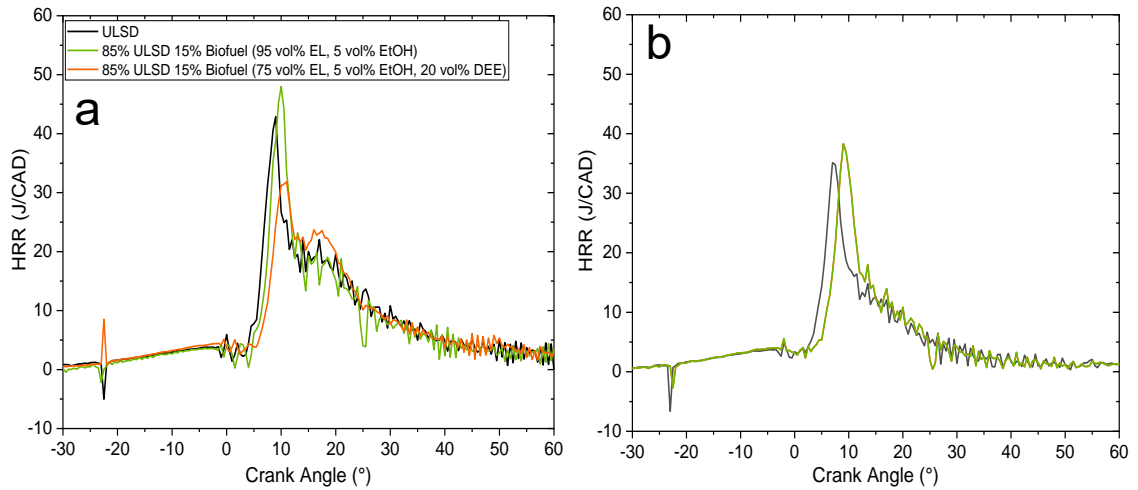
Figure 5.15. HRR curves for the two 15 vol% biofuel ethyl-based blends and ULSD for a: 92% load and b: 50% load.
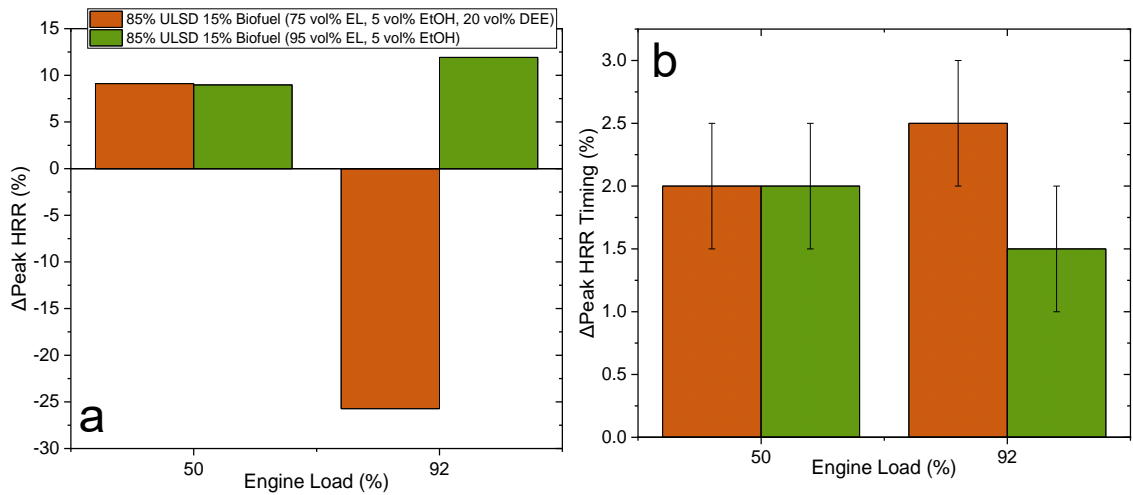
Figure 5.16. a: Changes in peak HRR relative to ULSD baseline. b: Changes in the peak HRR timing.

At 92% load, the biofuel blend composition influenced the nature of the HRR curve, as shown in figure 5.15a. One change was the delayed heat release due to the longer IDTs. The blend without DEE had an increased peak HRR relative to ULSD (figure 5.16a). The increase in HRR followed the trends observed by Li et al. (329) when testing blends of ethanol, n-butanol, or n-pentanol with diesel. Jamrozik (225) also demonstrated that with an increased ethanol fraction in diesel, the peak HRR was greater and delayed relative to the diesel baseline. The increase in peak HRR was due to an increase in premixed combustion, allowing for a greater HRR as there was more fuel available to burn. For the blend without DEE, there may be an increased peak pressure due to the greater HRR being delayed only by 1 CAD, as shown in table 5.5. The peak pressures are discussed in section 5.5.3. The blend with DEE has a lower peak HRR and a delayed peak HRR. The nature of the HRR curve matches those of Venu and Madhavan (135) when testing blends of ethanol, biodiesel, diesel, and DEE. In figure 5.15a the second rise in the HRR for the blend with DEE may be due to EL combusting later during the

mixing-controlled combustion phase, as a result of its delayed vaporisation due to the charge cooling of the air/fuel mixture. This would need to be confirmed with other blends with DEE to ensure it is not due to the noise in the pressure trace. The delays in the peak HRR cause the pressure and temperature rise to move further from TDC.

At 50% load, the longer IDTs cause a delay in the initial and peak HRRs relative to diesel, as shown in figure 5.15b and table 5.5. The peak HRR was greater for the ethyl-based blends at 50% load for both biofuel formulations. There were increases of 8.9% and 8.8% relative to diesel for the blends with and without DEE, respectively. The HRR curves of the two ethyl-based blends are visually identical, as the orange line is behind the green line. At 50% load, less fuel was injected, resulting in a reduced influence of DEE. Ideally, the peak HRR or timing of the peak should not change with the addition of alternative fuels to ULSD because of their influence on potential engine performance and emissions as discussed in Chapter 6.

Table 5.5. Summary of HRR parameters for the ethyl-based blends.

Fuel Blend	Engine Load (%)	Peak HRR (J/CAD)	Peak HRR Timing (CAD)	SoC (CAD)
ULSD	92	42.87	9.0 ± 0.5	8.5 ± 0.5
85% ULSD 15% Biofuel (75 vol% EL/5 vol% EtOH/20 vol% DEE)		31.84	11.0 ± 0.5	9.5 ± 0.5
85% ULSD 15% Biofuel (95 vol% EL/5 vol% EtOH)		47.99	10.0 ± 0.5	10.0 ± 0.5
ULSD	50	35.12	7.0 ± 0.5	7.5 ± 0.5
85% ULSD 15% Biofuel (75 vol% EL/5 vol% EtOH/20 vol% DEE)		38.33	9.0 ± 0.5	9.0 ± 0.5
85% ULSD 15% Biofuel (95 vol% EL/5 vol% EtOH)		38.28	9.0 ± 0.5	9.0 ± 0.5

The accumulated heat release (AHR) data for the ethyl-based blends are presented in figure 5.17. At 92% and 50% loads, the magnitude of the peak AHR for both ethyl-based blends does not deviate significantly from that of ULSD. For the blend without DEE, the AHR was lower than that of ULSD, but was close to it during the early stages of combustion. This was due to the higher HRR being for a shorter duration.
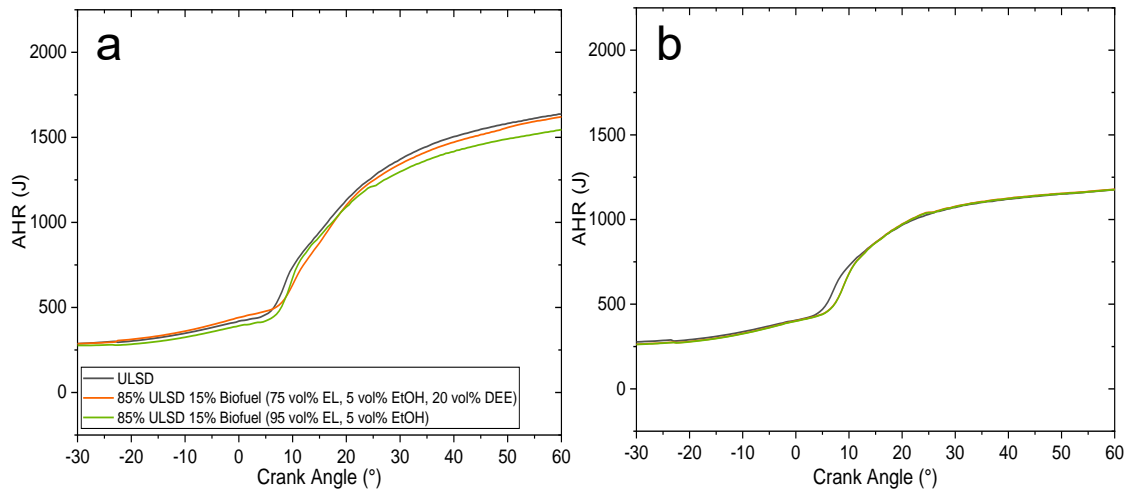
Figure 5.17. AHR for the two 15 vol% biofuel ethyl-based blends and ULSD for a: 92% load and b: 50% load.

The AHR at 92% load shows more dependence on the blend composition since the blend without DEE had a different AHR profile, and the blend with DEE had a lower AHR. The similar AHR curves for the ethyl-based blends at 50% load indicate that the fuel blends produce similar amounts of energy during combustion (330, 331). The presence of DEE reduced the AHR across all crank angles, which is in agreement with the findings of Rakopoulos et al. (331). They demonstrated that as engine load increased, the AHR curves for blends of diesel and 24 vol% DEE were shown to have greater differences early in the cycle but would give similar final AHR values (331). The nature of the AHR curve for the blend without DEE may be due to the reduced energy content and the greater enthalpy of vaporisation of EL (table 2.8) delaying the heat release from the fuel's combustion. This would be confirmed if reductions in IMEP and peak pressures were also seen for these blends.

5.4.2 Influence of the Butyl-Based Blends on HRRs

From analysing the HRR curves of the 10 vol% biofuel blends at 92% load (figure 5.18a), there was little to no evidence of a correlation between the biofuel composition, the peak HRR, and its timing. At 92% load, the SoC for each of the 10 vol% biofuel blends was similar, 8.5 and 9 CAD, which correlates with the peak HRR being at similar times, as shown in table 5.6. The biofuel composition of 90 vol% BL, 5 vol% BuOH, 5 vol% DNBE would be expected to have the highest and latest peak HRR due to it having the highest BL fraction. At 50% load, the peak HRR was delayed relative to ULSD. However, for the butyl-based biofuel blends, the peak HRR times were within 0.5 CAD of each other (table 5.7). The peak HRR was further from TDC at 50% load (figure 5.18b), which would reduce the peak pressure, favouring lower temperatures and lower NO_X emissions.
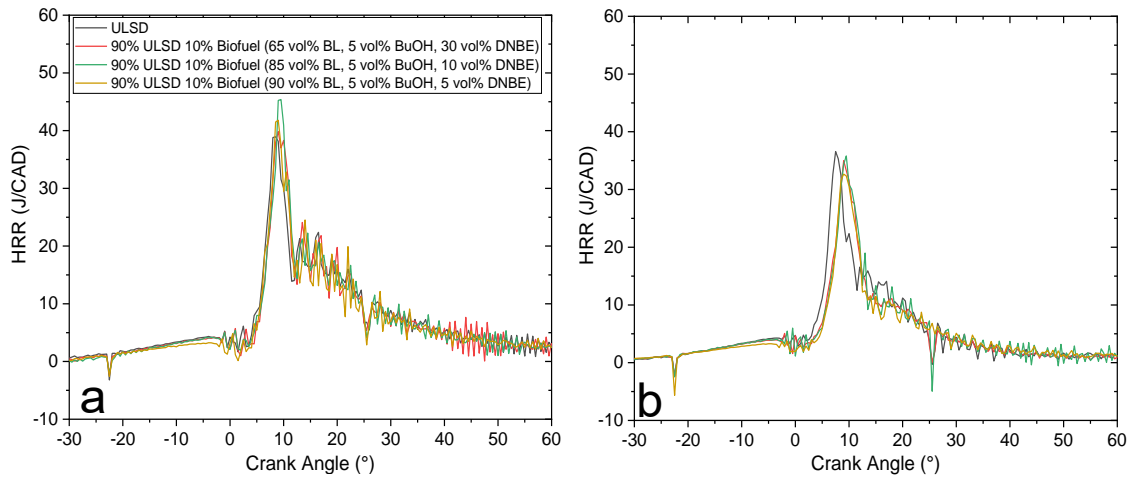
Figure 5.18. HRR curves for the selected 10 vol% biofuel butyl-based blends and diesel for a: 92% load and b: 50% load.

Table 5.6. Summary of HRR parameters for the butyl-based blends at 92% load.

Fuel Blend	Peak HRR (J/CAD)	Peak HRR Timing (CAD)	SoC (CAD)
ULSD	38.95	8.5 ± 0.5	8.0 ± 0.5
90% ULSD 10% Biofuel (65 vol% BL/ 5 vol% BuOH/30 vol% DNBE)	39.82	9.0 ± 0.5	8.5 ± 0.5
90% ULSD 10% Biofuel (85 vol% BL/5 vol% BuOH/10 vol% DNBE)	45.38	9.5 ± 0.5	9.0 ± 0.5
75% ULSD 25% Biofuel (85 vol% BL/5 vol% BuOH/10 vol% DNBE)	45.18	10.5 ± 0.5	10.0 ± 0.5
90% ULSD 10% Biofuel (90 vol% BL/5 vol% BuOH/5 vol% DNBE)	41.80	9.0 ± 0.5	8.5 ± 0.5
75% ULSD 25% Biofuel (90 vol% BL/5 vol% BuOH/5 vol% DNBE)	49.20	10.5 ± 0.5	10.0 ± 0.5

Table 5.7. Summary of HRR parameters for the butyl-based blends at 50% load.

Fuel Blend	Peak HRR (J/CAD)	Peak HRR Timing (CAD)	SoC (CAD)
ULSD	36.58	7.5 ± 0.5	8.0 ± 0.5
90% ULSD 10% Biofuel (65 vol% BL/ 5 vol% BuOH/30 vol% DNBE)	34.99	9.0 ± 0.5	8.5 ± 0.5
90% ULSD 10% Biofuel (85 vol% BL/5 vol% BuOH/10 vol% DNBE)	35.82	9.5 ± 0.5	9.5 ± 0.5
75% ULSD 25% Biofuel (85 vol% BL/5 vol% BuOH/10 vol% DNBE)	35.52	10.5 ± 0.5	9.5 ± 0.5
90% ULSD 10% Biofuel (90 vol% BL/5 vol% BuOH/5 vol% DNBE)	32.66	9.0 ± 0.5	8.5 ± 0.5
75% ULSD 25% Biofuel (90 vol% BL/5 vol% BuOH/5 vol% DNBE)	38.69	11.5 ± 0.5	10.5 ± 0.5

Comparing the 10 and 25 vol% biofuel blends demonstrated that the increased biofuel content delayed the initial and peak HRR at 92% load, as shown in figure 5.19a. This delay was due to longer IDTs for the 25 vol% blends, as was shown in figure 5.5. For the 85 vol% BL/5 vol% BuOH/10 vol% DNBE blend, the peak HRR for both 10 vol% and 25 vol% blends was similar, as shown in figure 5.19a. As the BL fraction increased, the peak HRR increased and was further from TDC, as shown in table 5.6. Due to the higher biofuel content, the influence of the increased BL fraction was more evident, as shown in figures 5.19 and 5.20 for 92% and 50% load, respectively.
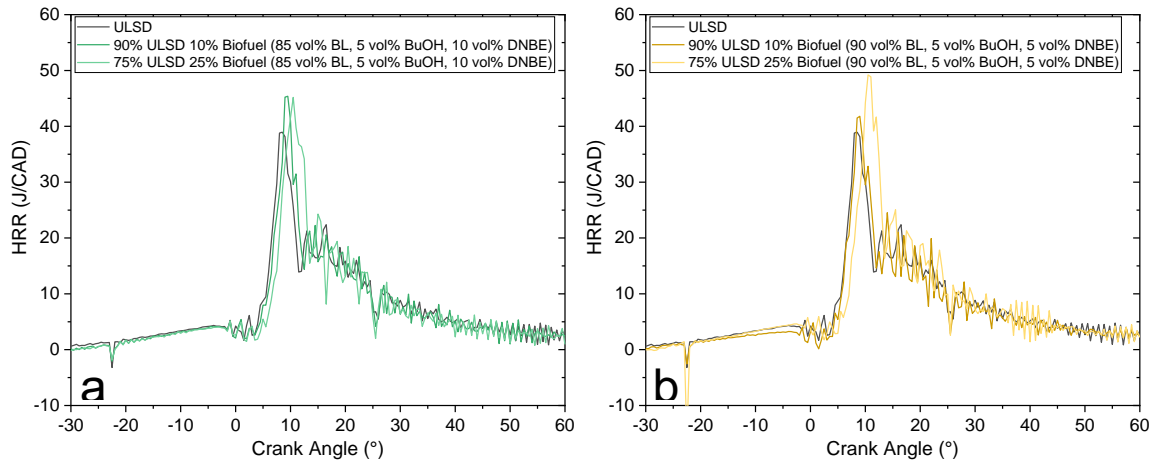
Figure 5.19. HRR curves at 92% load for two butyl-based blend formulations at 10 and 25 vol%. a: 85 vol% BL, 5 vol% BuOH, 10 vol% DNBE. b: 90 vol% BL, 5 vol% BuOH, 5 vol% DNBE.
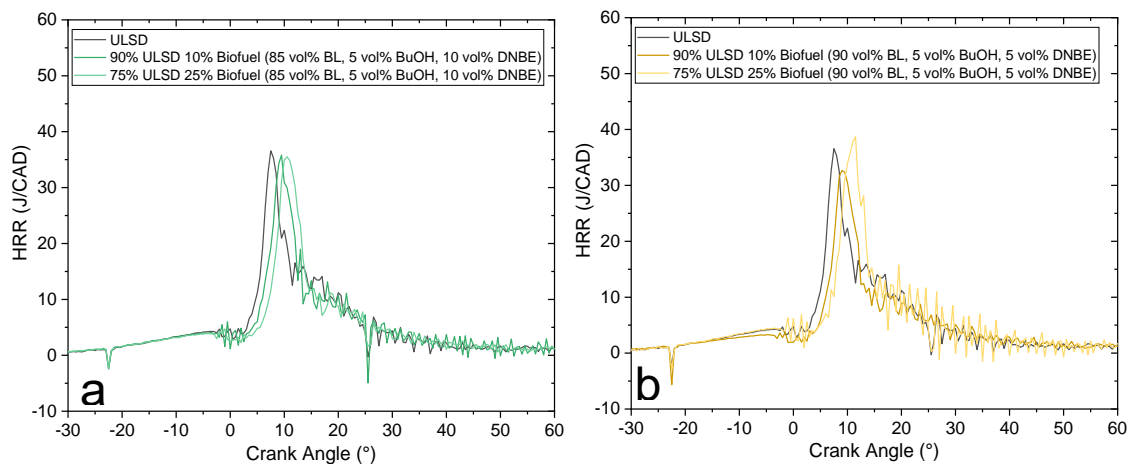
Figure 5.20. HRR curves at 50% load for two butyl-based blend formulations at 10 and 25 vol%. a: 85 vol% BL, 5 vol% BuOH, 10 vol% DNBE. b: 90 vol% BL, 5 vol% BuOH, 5 vol% DNBE.

At 50% load, the 25 vol% biofuel blends had a greater delay in the peak HRR compared to the 10 vol% biofuel blends. For the 90 vol% BL, 5 vol% BuOH, 5 vol% DNBE blend, there was also a broader premixed combustion phase. In contrast, for the 85 vol% BL, 5 vol% BuOH, 10 vol% DNBE blend, the peak HRR was similar to that of ULSD and the 10 vol% biofuel blend (figure 5.20). The HRR analysis values are

summarised in table 5.7. The delays in the peak HRR would likely influence peak pressures, IMEP, and emissions due to changes in the temperature.

The changes in the peak HRR and its timing are displayed in figure 5.21. At 92% load, the increase in the peak HRR increased with increasing BL fraction for most blends. At both loads, the delay in peak HRR increased as BL, and the biofuel fraction increased, and it was more prominent at 50% load.
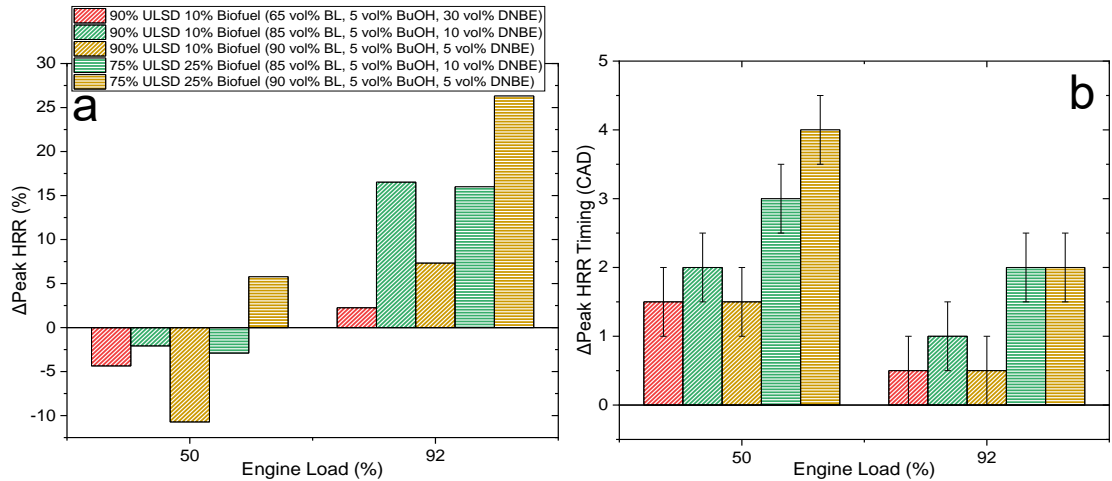
Figure 5.21. a: Changes in peak HRR relative to ULSD for the selected butyl-based blends. b: Changes in the peak HRR timing.

Figure 5.22 shows the AHR for all the butyl-based biofuel blends analysed. At 92% load, the AHR reduced with 10 vol% biofuel when BL was <85 vol%. The 75 vol% ULSD 25 vol% biofuel (90 vol% BL/5 vol% BuOH/5 vol% DNBE) blend had an increased AHR, which was unexpected due to the reduced LHV and lower DCN. This was due to the greater peak HRR for this blend giving a greater AHR as a result of the increased premixed combustion due to the longer IDT. At 50% load, there was no discernible trend with the increasing BL fraction since the lowest AHR with the biofuel blends was for the blend with the lowest BL fraction. This was unexpected, as this blend would have the highest LHV and DCN.
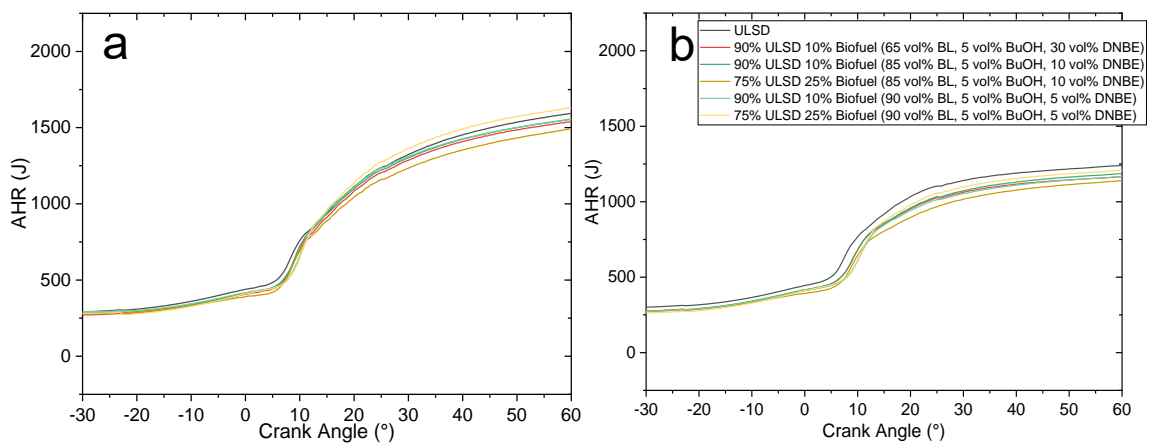
Figure 5.22. AHR for the butyl-based blends with diesel for a: 92% load and b: 50% load.

5.4.2.1 Influence of the FB Injector on the HRR from the Butyl-Based Blend

The HRR analysis for the butyl-based blend with the FB injector was conducted for the 92% load test since 50% load could not be tested. As a genset would typically operate at high loads, it was important to understand the influence of the injector design at this condition. For both fuel injectors, the heat release was delayed, and the peak HRR increased with the butyl-based blend relative to ULSD. Figure 5.23a shows that the FB injector gives a greater peak HRR with both the ULSD and butyl-based biofuel blend. The AHR using the FB injector was greater than the FJ injector, as shown in figure 5.23b, which correlates with the greater HRR.
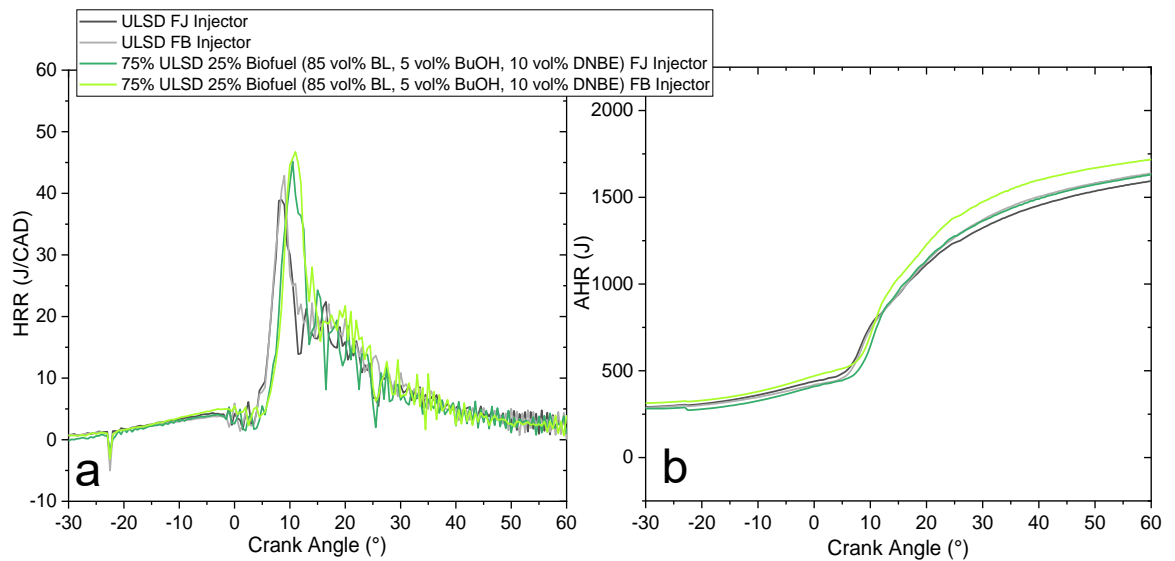
Figure 5.23. a: 92% load HRR curve for ULSD and the selected butyl-based blend with the FJ and FB injectors. b: AHR with the FJ and FB injector.

Table 5.8. Summary of the peak HRR and its timing, and their changes relative to ULSD when using the FJ and FB injectors.

Fuel	Injector	Peak HRR (J/CAD)	ΔPeak HRR (%)	Timing of peak HRR (CAD)	ΔPeak HRR Timing (CAD)
ULSD	FJ	38.95		8.5 ± 0.5	
75% ULSD 25% Biofuel (85 vol% BL/5 vol% BuOH/10 vol% DNBE)	FJ	45.18	16.0	10.5 ± 0.5	2.0 ± 0.5
ULSD	FB	42.87		9.0 ± 0.5	
75% ULSD 25% Biofuel (85 vol% BL/5 vol% BuOH/10 vol% DNBE)	FB	46.74	9.0	11 ± 0.5	2.0 ± 0.5

Moving to the FB injector increased the heat release relative to the FJ injector, but the increase due to the biofuel was not as great, as shown in table 5.8. The change in the peak HRR timing was the same for both fuel injectors when using the butyl-based

blend, which correlates to the IDT changes being similar. The FB injector should improve fuel atomisation, which promotes complete combustion and increases the amount of heat released relative to the FJ injector.

There is possible evidence of a second heat release for the butyl-based blend test with the FB injector, as shown by the shoulder around 20 CAD in figure 5.23b. However, this could be an artefact of the noise from the pressure trace. With the FB injector there would be improved fuel/air mixing, which decreases the time before an ignitable mixture is formed. However, with the smaller fuel droplets there would have been a greater charge cooling from the biofuel components, which reduces the temperature causing less fuel to vaporise. Therefore, these are in competition with each other. The first peak HRR was due to there being premixed combustion (88, 148, 284, 332). The second shoulder may have been due to the thermodynamic conditions being suitable for the remaining fuel fraction to combust similarly to the HRR profiles of the octanol/DNBE blends of García et al. (222). However, this would need to be confirmed with further engine tests and could be investigated with the use of simulations. This behaviour was more prominent with the ethyl-based blends (figure 5.15a), which indicates this was due to the injector design and the use of the biofuel components. The shoulder was more pronounced with the biofuel blends than with diesel. Therefore, the FB injector may enhance two stage heat release with the improved vaporisation as the BL, with its high enthalpy of vaporisation, can vaporise and combust.

5.5 Influence of the Advanced Biofuel Blends on IMEP, Peak Pressure, and Exhaust Manifold Temperatures

The in-cylinder pressure in an engine needs to be controlled due to the implications it can have on engine performance, emissions, stability of combustion, efficiency, and the safe operation of the engine (4, 5). When changing to alternative fuels, the peak pressure must remain within the engine's tolerances. Any pressure increases would result in increased temperatures that could increase NO_X emissions and require effective thermal management (5, 222, 315, 333, 334). Increased pressures could also result in damage, particularly to the connecting rod and piston head (4, 5). The IMEP, when using advanced biofuel blends, would ideally match that of ULSD or even increase, as this would indicate there was more work per combustion cycle (335). Due to the biofuel blends and the changes in in-cylinder peak pressures, exhaust manifold temperatures may also change. Any changes in the pressures would influence the thermal efficiency of the engine and changes in the exhaust temperatures would impact on aftertreatment systems that require high temperatures (5). The influence of the advanced biofuel blends on these two pressure parameters and the exhaust manifold temperatures are discussed in this section.

5.5.1 The Influence of the Ethyl-Based Blends on the IMEP

Due to instabilities when using the 25 vol% biofuel blends, they were excluded from the IMEP analysis. The FB injector was used when testing the ethyl-based blends, and figure 5.24 shows the IMEP for the FJ and FB injectors for ULSD. The FB injector had slightly higher IMEPs than the FJ injector other than at 75% load.
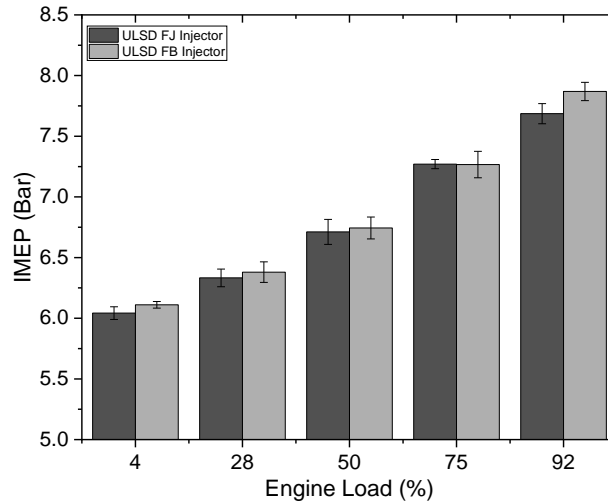
Figure 5.24. IMEP of ULSD at all loads tested when using the FJ and FB injectors.

The increased IMEP with the FB injector was likely due to improved fuel atomisation leading to more complete combustion (322, 323). The influence of both ethyl-based blends was compared to the corresponding ULSD baseline. The addition of 15 vol% of the ethyl-based blends had little influence on the IMEP at <75% load, as shown in figure 5.25a. At 92% load, the IMEP decreased for both blends, with a greater reduction for the blend with DEE. This reduction was due to the slight engine instability (figure 5.3b).
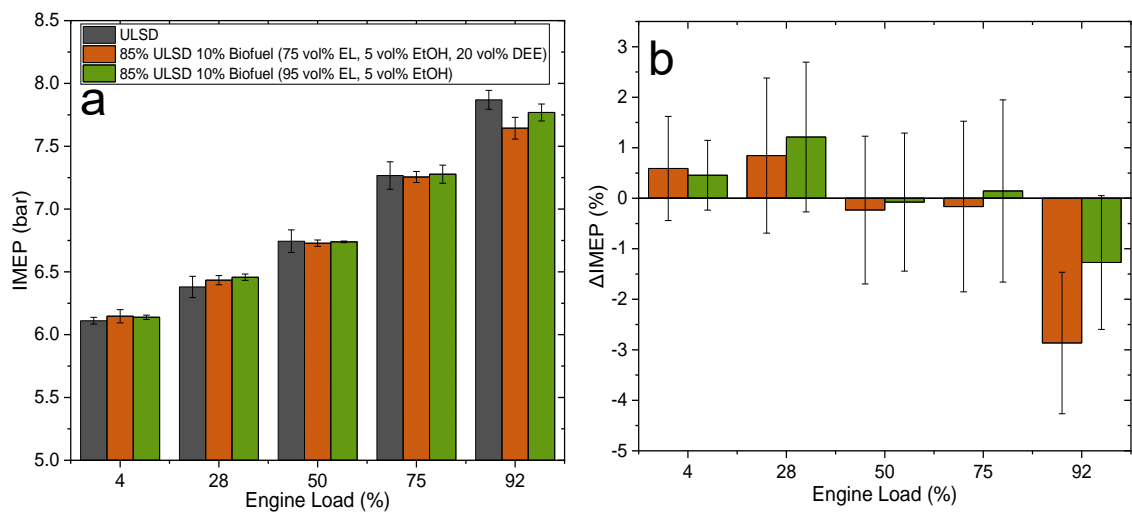
Figure 5.25. a: IMEP of the 15 vol% ethyl-based blends and ULSD. b: changes in the IMEP relative to ULSD.

The changes relative to ULSD are shown in figure 5.25b. At <75% load, they were between +1% and -1%, further indicating the little influence the addition of the ethyl-

based blends had on the IMEP. The greatest change in IMEP was at 92% load. There were reductions of 3% and 1.3% for the blends with and without DEE, respectively. The higher temperatures at 92% load from the previous cycle may promote the combustion of DEE, hence the instability. At 92% load, the peak HRR was further from TDC when using this fuel blend (figure 5.15a), which reduces the IMEP since the pressure rise is not occurring close to TDC. In addition, at higher loads, more fuel is injected. Hence, there was a greater influence on the IMEP from DEE (137).

The small change in IMEP at <75% load indicates that the work from both ethyl-based blends matches that of ULSD. This indicates that the same amount of work per combustion cycle can occur with a lower energy content in the fuel. However, the increased BSFC to maintain the IMEP is unfavourable.

5.5.2 The Influence of the Butyl-Based Blends on the IMEP

The addition of the butyl-based three-component blends caused the IMEP to change for most blends, as shown in figure 5.26a. At the lower loads, decreasing the DNBE fraction caused the IMEP to increase. The 90 vol% ULSD 10 vol% biofuel (75 vol% BL/5 vol% BuOH/20 vol% DNBE) blend (blue bar), had the lowest change across all loads, and this was evident when comparing the changes relative to ULSD shown in figure 5.26b.
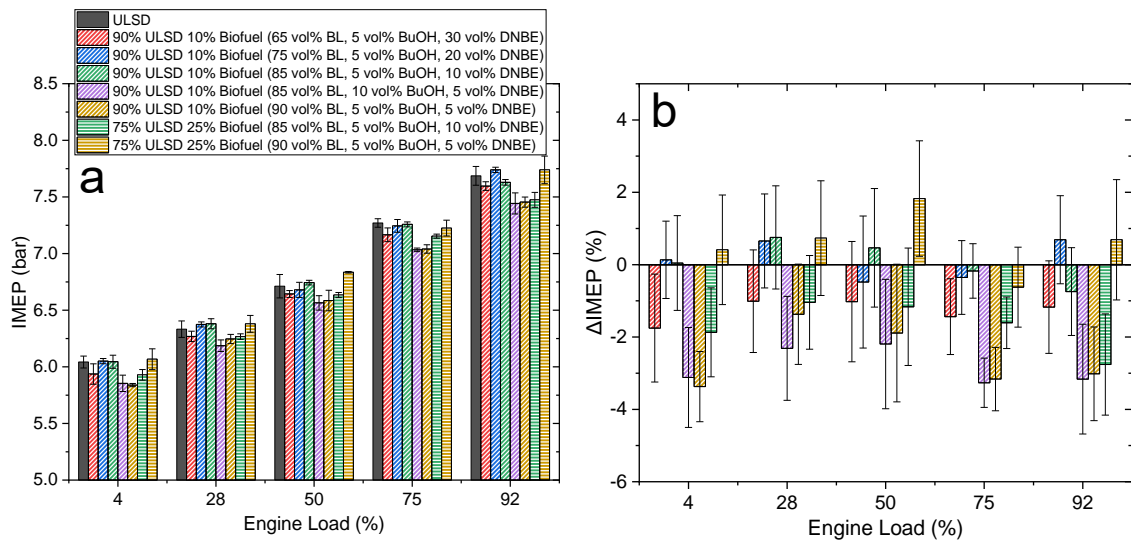
Figure 5.26. a: IMEP of the butyl-based blends tested and ULSD. b: Changes to the IMEP of the butyl-based blends relative to ULSD.

One finding was that for the 10 vol% biofuel blends, those with the higher BL fractions and 5 vol% DNBE had the greatest reduction in the IMEP. This was evident since the 85 vol% BL/10 vol% BuOH/5 vol% DNBE and 90 vol% BL/5 vol% BuOH/5 vol% DNBE blends caused the greatest reductions in IMEP (figure 5.26b). Both of these blends had similar increases in IDT (figure 5.8), which caused the work done to be further

from TDC. In addition, the peak HRR for the analysed blends was greater than that of ULSD but was further from TDC, thus reducing the IMEP.

The difference in the ΔIMEP between the two 25 vol% blends could be due to the longer IDT of the blend with 90 vol% BL. The longer IDT may allow for more premixed combustion giving a more uniform pressure applied over the piston (59). The 25 vol% biofuel blend with 90 vol% BL also caused an increase in IMEP for four out of the five loads, as shown in figure 5.26b. The 90 vol% ULSD 10 vol% biofuel (75 vol% BL/5 vol% BuOH/20 vol% DNBE) blend had IMEP values closest to ULSD at all loads. The 10 vol% DNBE blend had IMEP values closer to ULSD than the 30 vol% DNBE blend. Therefore, the ideal DNBE fraction is between 10 and 20 vol% with the fixed injection timing. If there was optimal injection timing, the IMEP could increase as the combustion timing would be more favourable, and the peak heat release would be closer to TDC. The effect of the injection timing could be confirmed with variable timing studies, but these are not feasible with the Yanmar L100V engine used.

The changes in the IMEP are low, although these small changes could have large effects overall, especially when combined with the increased BSFC for these fuel blends. This was likely due to longer IDTs causing the combustion to be at unfavourable times. Overall, decreasing the DNBE fraction increases the IMEP, especially for the 10 vol% biofuel formulations. However, with the changes being small, they may be within the engine tolerances making the fuel blends more suitable for utilisation. The reductions in IMEP for the butyl-based blends were greater than those observed with the two ethyl-based blends, even with lower biofuel fractions. However, different fuel injectors were used, which had different baseline IMEP values.

5.5.2.1 Changes to IMEP Due to the Utilisation of the FB Injector using a Butyl-Based Blend

As seen in figure 5.24 (section 5.5.1) with ULSD, the FB injector had a higher IMEP than the FJ injector. The higher IMEP was also seen when using the selected butyl-based blend, as shown in figure 5.27a. There was an increase at all loads with the FB injector but with less of an increase at 92% load. In contrast, using the FJ injector caused a reduction at all loads.

Figure 5.27. a: Comparison of the IMEP for the selected butyl-based blend when using the FJ and FB injectors. b: Changes in the IMEP relative to ULSD.

The FB injector had higher IMEPs when using the butyl-based biofuel blend. The changes relative to ULSD for both injectors can be seen in figure 5.27b. The increase in the IMEP with the FB injector was likely due to improved fuel atomisation due to the smaller injector holes. At lower loads this improved atomisation resulted in shorter IDTs (Figure 5.9), allowing more fuel to be burnt and a greater pressure applied to the piston (322). The ignition is closer to TDC at lower loads, when using the FB injector, allowing the pressure rise and work due to combustion to be closer to TDC.

When using the FJ injector, the IMEP across all loads tested decreased relative to ULSD. In contrast, the IMEP increased for the four loads reported using the FB injector relative to ULSD. This increase in IMEP with the FB injector is favourable as it indicates an increase in work due to the combustion of the butyl-based biofuel blend. The increase in IMEP can also be related to the greater heat release with the FB injector (figure 5.23), indicating there is more complete combustion.

5.5.3 The Influence of the Ethyl-Based Blends on Peak Pressures

The peak pressure affects emissions due to it influencing the peak in-cylinder temperature during gas phase combustion. The peak pressure can be reduced by longer IDTs and delayed peak HRR, which results in less complete combustion. Figure 5.28a shows the peak pressures after TDC for the two 15 vol% ethyl-based blends. At ≤50% load, the peak pressures for both ethyl-based blends were reduced to similar pressures, 60.9 and 61.0 bar (with and without DEE) at 4% load, 63.25 bar at 28% load, and 64.8 bar at 50% load. At higher loads, the blend with DEE had a greater reduction in peak pressure.
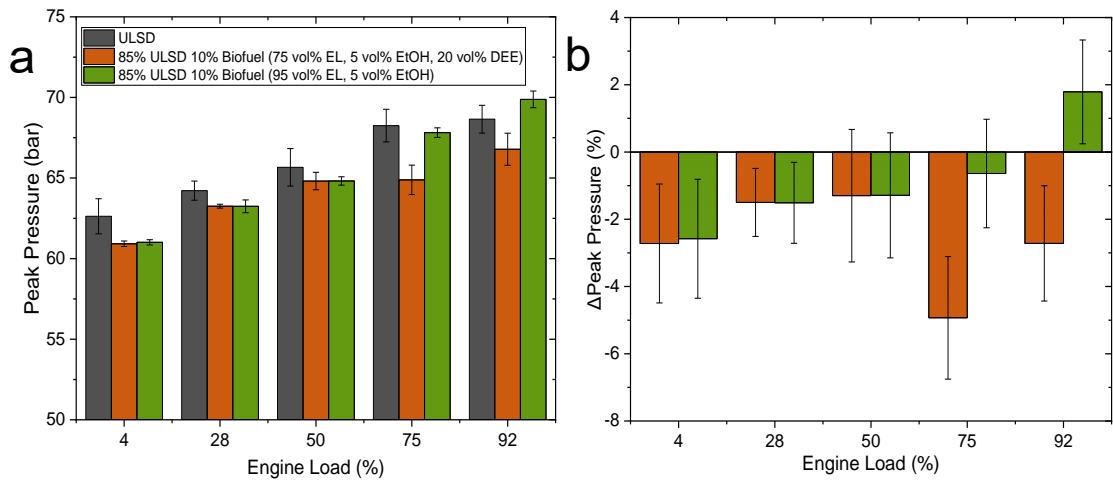
Figure 5.28. a: Peak pressure of the two 15 vol% ethyl-based blends and ULSD. b: Changes in peak pressure relative to ULSD.

The reduction in peak pressure was due to combustion occurring further into the power stroke due to longer IDTs. This delay decreases the peak pressure as the peak HRR occurs as the piston moves downwards and the in-cylinder pressure decreases (59, 336). The further into this cycle combustion occurs, the lower the peak pressure. The reductions in the peak pressure relative to ULSD are shown in figure 5.28b, where the changes are relatively small and are less than 3% at ≤50% load for both blends.

The peak pressure reduction at higher loads was greater for the blend with DEE (figure 5.28b), where they were 4.9% and 2.7% for 75% and 92% load, respectively. For the blend without DEE, the changes in the peak pressure were -0.6% at 75% load and +1.8% at 92% load. IDTs for both blends increased at all loads, but it was longer for the blend with DEE. This decrease in peak pressure was likely due to the delayed heat release and the peak HRR occurring further from TDC. It has been reported that DEE could ignite during the compression stroke, working against the compression and reducing peak pressure (129, 135, 337, 338). However, in the P-CA traces in figure 5.3, there was no evidence of any early ignition. The increased peak pressure for the blend without DEE at 92% load could be due to the increased premixed combustion promoting a greater pressure rise (225, 325). The peak pressure for all three runs at 92% load using the fuel blend without DEE was greater than the ULSD baseline, indicating that this was a valid result. Increases in peak pressure need to be within the engine's tolerances as it could lead to damage if there are repeatedly high pressures during engine operation (5).

The presence of large EL fractions is likely why the peak pressure variations were not as high as those seen by Paul et al. (137) when testing ULSD, DEE, and EtOH blends. At the lowest load tested by Paul et al. (137), the 10 vol% DEE/10 vol% EtOH/80 vol% ULSD blend had a 1 bar reduction. The blend 10 vol% DEE/5 vol% EtOH/85 vol% ULSD tested by Paul et al. (137) had an increase in peak pressure but an unstable P-CA trace due to the high DEE fraction in the blend, which caused a shorter IDT and a

pressure rise close to TDC. At higher loads, the variation between the peak pressures for the blends tested by Paul et al. (137) reduced. At 75% and 92% load, there was a greater difference between the peak pressures (figure 5.28). This difference was likely due to the Yanmar L100V decreasing its RPM as the load increased, whereas Paul et al. (137) used an eddy-current dynamometer to ensure a steady RPM.

5.5.4 The Influence of the Butyl-Based Blends on Peak Pressures

As the loads increased, the peak pressure increased. The 90 vol% ULSD 10 vol% biofuel blends with 65, 75, and 85 vol% BL and 5 vol% BuOH show that as the BL fraction increased, the peak pressure increased. These biofuel blends are within one standard error of the peak pressure achieved with ULSD, other than at 28% load, as seen in figure 5.29a. At 92% load, where a genset would typically operate, the peak pressure from ULSD could be matched with most blends.
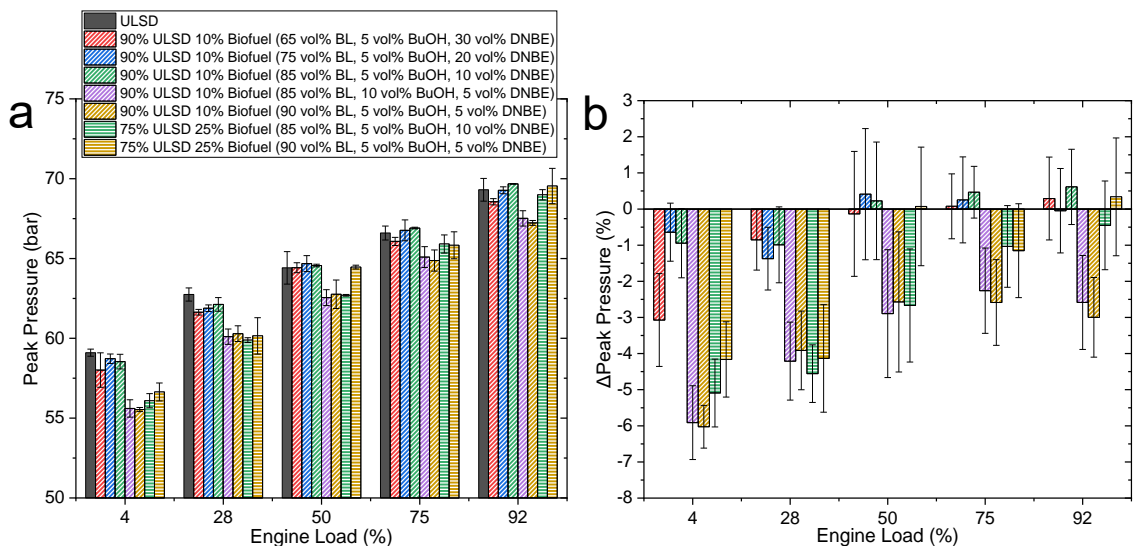
Figure 5.29. a: Peak pressure of the butyl-based blends tested and ULSD. b: Changes in peak pressure relative to ULSD.

The changes relative to ULSD for the butyl-based blends tested are displayed in figure 5.29b. The 10 vol% biofuel blends containing 10, 20, and 30 vol% DNBE had changes less than ±1% at >28% load. The reduction in peak pressure when using the 10 vol% biofuel blends containing 5 vol% DNBE and for both 25 vol% biofuel blends would be due to the longer IDTs and the lower energy content, as the in-cylinder pressure was lower than that when ULSD ignited. These lower peak pressures correlate with the peak HRR being further from TDC, and in the cases of some butyl-based blends, the peak HRR was below that of ULSD. The reduction in peak pressure due to lower DNBE fractions could result in lower peak temperatures generated. The lower temperatures would reduce NO_X emissions due to their formation being temperature-dependent. However, there may be an increase in CO, THC, and PM emissions due to less complete combustion (339, 340).

The reduced peak pressures when using high BL fractions and low DNBE fractions were observed by Raspolli Galletti et al. (54) and Frigo et al. (38) when testing blends of ULSD, BL, and DNBE. Raspolli Galletti et al. (54) tested different fuel formulations using a Lombardini 2-cylinder, 1248 cc, 21 kW engine on an eddy current dynamometer (38, 54). Raspolli Galletti et al. (54) showed that for a blend of 88% ULSD 12% biofuel (66.6 wt% BL/33.3 wt% DNBE), the peak pressure was reduced due to the longer IDT at full load and 1500 RPM, whereas at 2500 RPM the peak pressure was similar to that generated using ULSD. This is similar to the results of the 10 vol% biofuel blend with 30 vol% DNBE, shown in figure 5.29. However, the RPM of the Yanmar L100V reduced as the load increased. Raspolli Galletti et al. (54) stated that for biofuel blends of 70 wt% BuOH, 20 wt% DNBE, 10 wt% BL and 30 wt% BuOH, 60 wt% DNBE, 10 wt% BL blended at 10 and 20 vol% into ULSD had '*no significant variation*' in the P-CA curves. Frigo et al. (38) showed that in a single-cylinder, 7.4 kW, Kohler engine, at full load and 3600 RPM, there was a greater reduction in the peak pressures compared to the 2300 RPM runs for blends of ULSD with 4 vol% DNBE and 7, 11, and 13 vol% BL. The blends with higher BL fractions had the greatest reduction in peak pressure; this was due to longer IDTs with higher BL fractions. The changes in the peak pressures measured by Frigo et al. (38) were negligible, indicating that the combustion of the selected blends generates similar pressure rises to the ULSD they used. The changes in peak pressure for the 10 vol% biofuel blends tested in this work, where the DNBE fraction was between 10 – 30 vol%, were ±2%, including the error, which is not a significant change. This small change may further demonstrate the suitability of the butyl-based biofuel blends.

The reductions in peak pressure could be alleviated with advanced injection timing, as longer IDTs combined with lower LHVs reduce the peak pressure. The other changes to compensate for longer IDTs may also ensure the peak pressures are closer to those of ULSD, as discussed in section 5.2.1.

5.5.4.1 Changes to Peak Pressure Due to the Utilisation of the FB Injector using a Butyl-Based Blend

The peak pressures when using the FB injector were greater than when using the FJ injector, as shown in figure 5.30a. At lower loads, there is a difference of 2 bar between the FJ and FB injectors, with the difference decreasing as the engine load increases. This was due to increased volumes of fuel injected as the load increased and the difference in the pressure rise from combustion decreased.
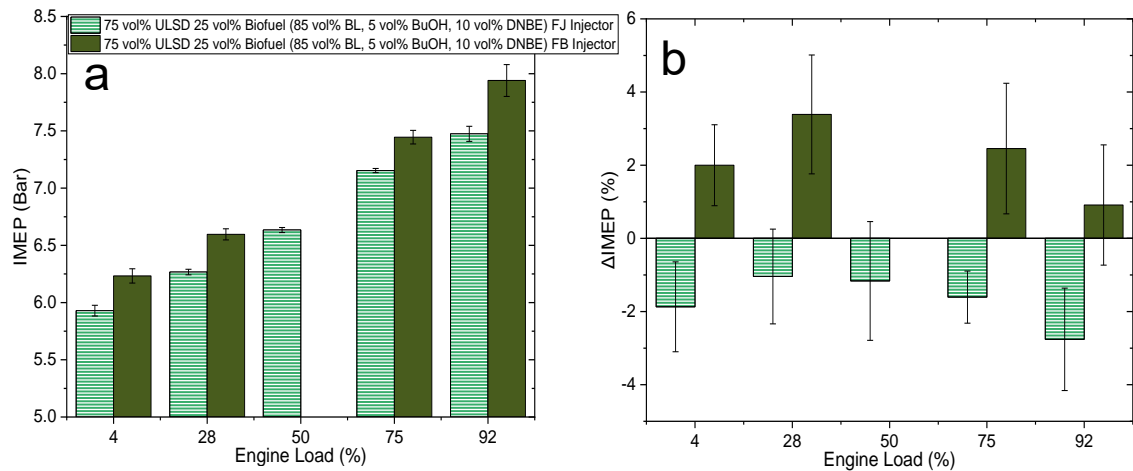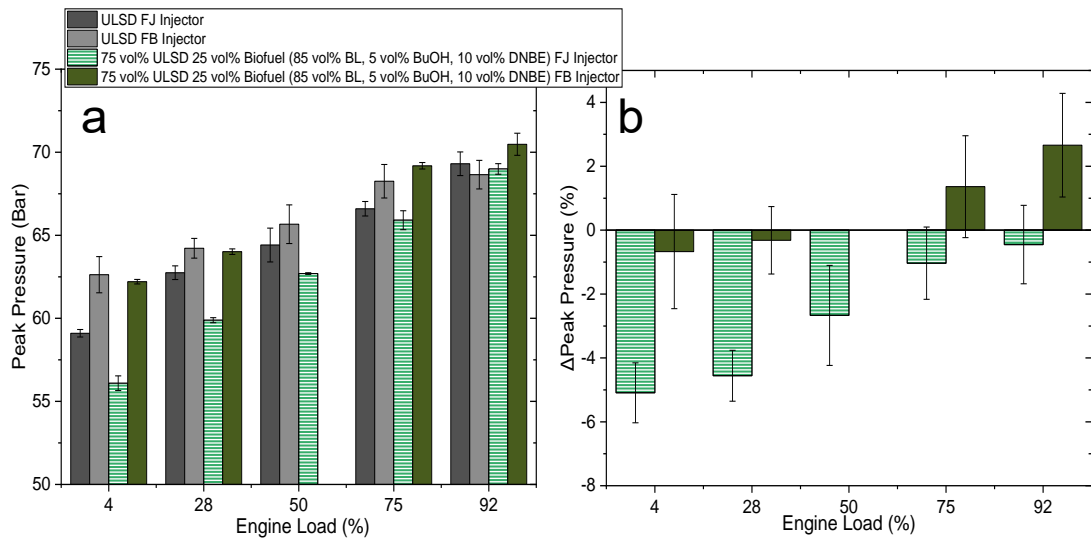
Figure 5.30. a: Comparison of the peak pressure for the selected butyl-based blend when using the FJ and FB injectors. b: Changes in peak pressure relative to ULSD.

The changes in the peak pressure when using the butyl-based blend relative to the corresponding ULSD baseline are shown in figure 5.30b. The FJ injector has a larger reduction in the peak pressure at the lower loads compared to the FB injector. The improved fuel atomisation when using the FB injector enabled the denser and less reactive fuel to vaporise and ignite closer to TDC than it does with the FJ injector. This results in the in-cylinder peak pressure being maintained or increased. There was an increase in the peak pressures when using the FB injector at 75% and 92% loads compared to the FJ injector. This increase may be due the greater peak HRR with the FB injector and the better atomisation due to the smaller injector holes (59, 332). The changes in peak pressures were less than 5% for both injectors used. The reduction in peak pressure should reduce NO_X emissions but increase THC and CO emissions (339, 340). Additionally, there may be a reduced exhaust gas temperature, which may be detrimental to any aftertreatment systems (101). Since the engine was not optimised for longer IDTs, the peak pressures may change if the injection timing were advanced. The engine was not optimised to maintain the equivalence ratio with the increased oxygen content since the fuel was injected on a volumetric basis. Therefore, if the optimal volume of fuel was injected, the peak pressure would change as a result.

5.5.5 The Influence of the Ethyl-Based Blends on Exhaust Manifold Temperatures

The peak pressures and IDTs changed when using the ethyl-based blends relative to the ULSD baseline. The exhaust temperature is governed by mixing-controlled combustion, as higher levels of mixing-controlled combustion will maintain a high HRR later in the combustion cycle, which maintains the in-cylinder temperature. Therefore, it would be expected that the exhaust manifold temperature would remain similar for all

the blends tested since the HRR analysis showed the AHR was similar (135). For the two stable ethyl-based blends, the exhaust manifold temperatures are shown in figure 5.31a. The exhaust manifold temperatures had little change at <50% load with both ethyl-based blends. At 75% load, the blend with DEE had an increased exhaust manifold temperature, albeit with a large error. The difference between the exhaust manifold temperatures of the two ethyl-based biofuel blends with and without DEE was negligible at loads below 75% load.
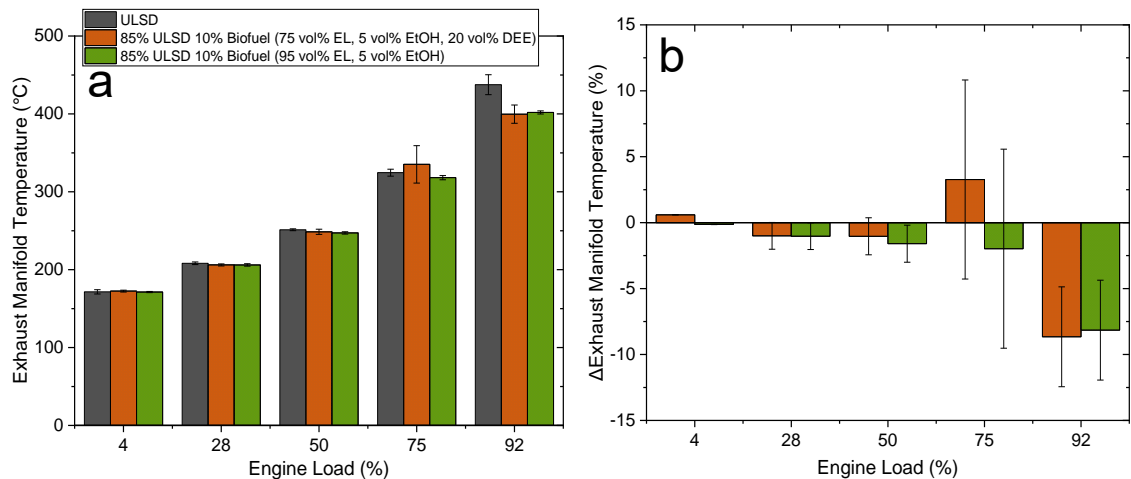
Figure 5.31. a: Exhaust manifold temperature of the two 15 vol% ethyl-based blends tested and ULSD. b: Changes relative to ULSD for the two ethyl-based blends.

The exhaust manifold temperatures were reduced with the ethyl-based biofuel blends, as shown in figure 5.31b. The greatest reduction was at 92% load. The reductions were 8.7% and 8.2% for the blends with and without DEE, respectively. As the load increased, the relative decrease due to the biofuel blends increased. At higher loads, the peak pressure for the blend without DEE was greater than that of ULSD. Therefore, it was expected that the temperatures would be higher for the blend without DEE (148, 341). However, this was not the case, and this may be due to the longer IDTs and delayed peak HRR being closer to the exhaust stroke, resulting in a higher exhaust temperature. Both of these cause the temperature rise to be when the in-cylinder temperature is reduced due to the pressure decreasing. However, there is the competition between the timing of combustion and the amount of combustion that occurs before the exhaust stroke. This is because the reductions in the exhaust manifold temperature were likely due to the longer IDTs, as there is less time available for complete combustion, resulting in a lower exhaust gas temperature (133, 148, 226).

The presence of DEE does not change the reduction in the exhaust manifold temperatures, as shown in figure 5.31b. Even with the LHV of DEE being higher than EtOH and EL (table 2.8), if DEE has undergone combustion early in the cycle, the benefit of its higher LHV is lost (135, 137). Small fractions of DEE in diesel have been reported to increase the exhaust temperatures as it can act as a CN enhancer, allowing for more

complete combustion and a greater increase in temperature at high loads (135). In contrast, Venu and Madhavan (135) also showed that at lower loads, the presence of 5% DEE caused a greater reduction in exhaust temperature than the presence of 10% DEE in a base fuel blend of 20% ethanol/40% biodiesel/40% ULSD. Mohanan et al. (342) also reported for ULSD/DEE blends, that 5% DEE increased the exhaust temperature, whereas, higher fractions caused incomplete combustion. EtOH and DEE have lower adiabatic flame temperatures than EL (table 2.8). Therefore, the presence of both would likely result in a lower combustion temperature, especially at higher loads where more fuel is injected.

The changes in the exhaust temperature would have implications for any aftertreatment systems requiring catalyst light off to be efficient and on EGR where there would be less cooling required.

5.5.6 The Influence of the Butyl-Based Blends on Exhaust Manifold Temperatures

The addition of the butyl-based biofuel blends to ULSD caused a reduction in the exhaust manifold temperatures, as shown in figure 5.32a. The changes relative to ULSD are shown in figure 5.32b. The reduction in the exhaust manifold temperature was greater for the 25 vol% biofuel blends, which was expected since these blends have lower energy content and longer IDTs. As the BL fraction increased, there was a greater reduction in the exhaust manifold temperature, especially with <85 vol% BL in the blend.
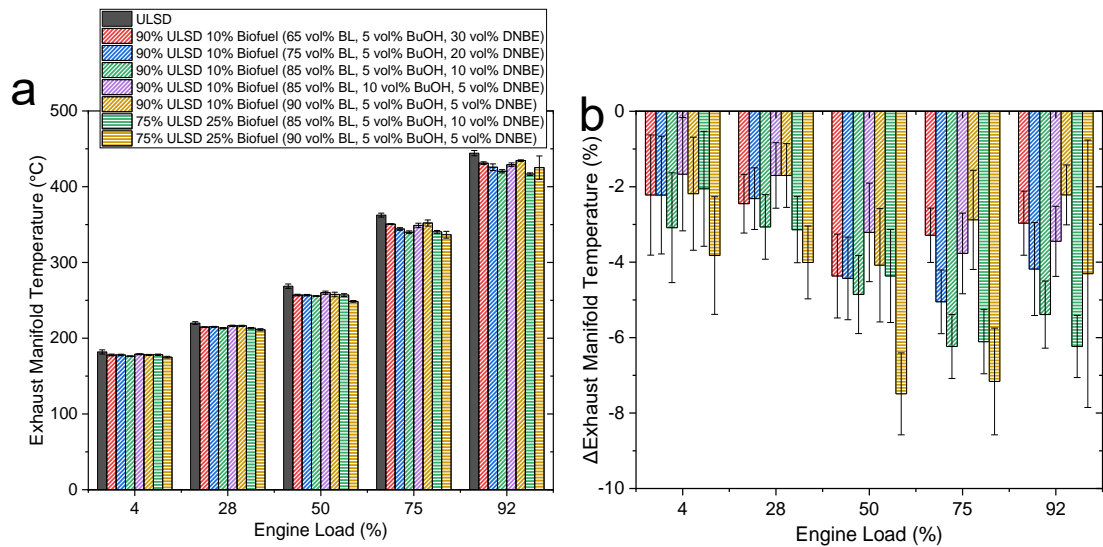
Figure 5.32. a: Exhaust manifold temperature of the butyl-based blends tested and ULSD. b: Changes in exhaust manifold temperature relative to ULSD.

The reduction for the 10 vol% blends does not have a strong dependence on the blend formulation at <50% load, as seen in figure 5.32b. At higher loads, the reduction in the exhaust manifold temperature was greater as the DNBE fraction decreased. This

reduction was due to more fuel being injected at the higher loads and the reduced DCN (135). The reduction is important to manage, as a genset would typically operate at a high load. There was also a delay in peak HRR and lower AHR, which would reduce the in-cylinder temperature. Since the adiabatic flame temperatures of the butyl-based three-components are all higher than a typical diesel (table 2.8), it would be expected the exhaust temperatures would increase. Therefore, the reduction in exhaust manifold temperature indicates there was less complete combustion, and this would be confirmed by increases in CO and THC emissions. The two 10 vol% biofuel blends with 5 vol% DNBE had similar reductions in the exhaust manifold temperature. These two blends are likely to have similar DCNs since BuOH and BL have DCNs of 12 and 14 (143). The LHVs of BL and BuOH are 27.4 MJ/kg and 33.2 MJ/kg, respectively. Thus, the blend with the higher BuOH content should produce a higher temperature since there is more energy to release (13, 120). However, due to longer IDTs, there is less complete combustion. If the longer IDTs were accounted for, the reductions in the exhaust manifold temperature would be due to the lower LHV of the blends. The lower LHV could be overcome if the volume of fuel injected was optimised to ensure the same energy content as ULSD was provided.

5.5.6.1 Changes to Exhaust Manifold Temperatures Due to Utilisation of the FB Injector with a Butyl-Based Blend

Compared to the FJ injector, the FB injector produced shorter IDTs at lower loads and elevated peak pressures. Therefore, it would be expected that exhaust manifold temperatures would increase (322, 323). However, in figure 5.33a, it can be seen that was not the case. The FB injector with ULSD and the selected butyl-based biofuel blend had lower exhaust manifold temperatures relative to the corresponding FJ injector tests.
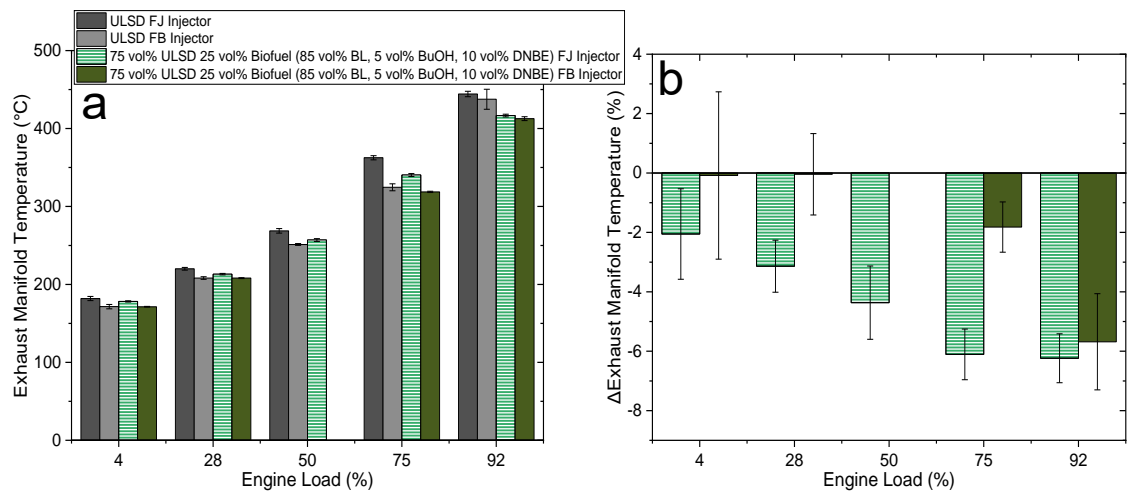
Figure 5.33. a: Exhaust manifold temperature of the selected butyl-based blend and ULSD when using the FJ and FB injectors. b: Changes relative to ULSD for each injector.

The reduction in the exhaust manifold temperature is also fuel dependent, as Sayin et al. (322) reported that with an increasing number of injection holes, from four to eight, the exhaust gas temperature of ULSD had a slight reduction. In contrast, when using biodiesel Sayin et al. (322) reported there was an increase from 265 °C with four holes to around 290 °C with six holes and up to 300 °C with eight holes. This increase indicates that the fuel density is likely to affect the exhaust temperatures as the biodiesel and ULSD used by Sayin et al. (322) had densities of 0.885 g/cm^3 and 0.840 g/cm^3, respectively. In addition, the CN of biodiesel is higher than ULSD, where the improved atomisation from more injector holes would allow the biodiesel to ignite sooner. From the findings of Sayin et al. (322), it would be expected that the FB injector would cause the butyl-based blend to have a higher exhaust manifold temperature than ULSD. However, this was not the case, as the exhaust manifold temperatures were reduced more with the FB injector. Figure 5.33b shows the change in the exhaust manifold temperatures relative to the corresponding ULSD baseline for the butyl-based biofuel blend tested for each injector. The addition of the biofuel blend causes a reduction in the exhaust manifold temperatures, albeit not for the FB injector at <28% load, where there is almost no change. The reduction was expected due to the longer IDTs with the biofuel blend and the lower energy content with the high BL fraction. When using the FB injector, the relative reduction was less than that exhibited by the FJ injector at <75% load. At 92% load, the relative change in the exhaust manifold temperature was similar, although the peak pressure was greater for the FB injector test. Therefore, the reduction in the exhaust manifold temperature at 92% load was likely due to the lower energy content of the fuel blend relative to ULSD (13, 120). In addition, it would have been expected that with a higher AHR for the FB injector there would be a higher exhaust temperature. However, the charge cooling effect of the biofuel components will be more dominant with smaller droplets and thus resulting in lower temperature exhaust gases.

5.6 Overall Impacts of the Biofuel Blends on Engine Performance

Based on the changes in the engine performance parameters, there is some evidence that the selected ethyl and butyl-based biofuel blends with ULSD may be suitable low-carbon alternative fuels. However, the optimal utilisation of the butyl-based blends would require some modification to engine operation depending on the engine used. These could be more pronounced when the blending ratios are much greater than the fraction of biodiesel in diesel (7 vol%) and the use of these fuels with the modifications could contribute towards the decarbonisation of CI engines. Most of the 10 vol% butyl-based blends studied give similar performances to ULSD at higher loads as the IMEP and BSFC have negligible changes. Some changes can be beneficial, such as the

reduced peak pressures, which may reduce NO_X emissions, whereas longer IDTs are detrimental to efficiency and will impact the CO and THC emissions (Chapter 6). To overcome longer IDTs, the engine or fuel blend would require modifications, and the ease of these modifications depends on the engine. To move the injection timing on the Yanmar L100V engine would require the flywheel to be adjusted, whereas, in a vehicle, the ECU would need reprogramming. Additionally, there could be chemical enhancement of the DCN through the use of additives to ensure IDTs match that of diesel (13). Further hardware changes would not be cost-effective and would no longer make the fuels suitable as drop-in alternatives.

From the engine performance it is evident that the physical properties of the blends have a significant impact on the engine performance and stability. The ethyl-based blends would give unstable operation if DEE was present in the blend, whereas the butyl-based blends could have high fractions of DNBE and the biofuel in diesel and retain stable engine operation. The 15 vol% ethyl-based blends increased the BSFC substantially, whereas some of the butyl-based blends had negligible changes in BSFC. The IMEP for the ethyl and butyl-based blends had small changes, which indicates that the mechanical efficiency may be maintained. The effects of the changes in engine performance on emissions will contribute to determining the suitability of the fuel blends. If the emission limits can be met with these small changes in performance it would further demonstrate the suitability of these fuel blends.

Chapter 6

Engine Emissions when Using Blends of the Advanced Biofuels Blends with Diesel

6.1 Introduction

The utilisation of advanced biofuels has become an attractive low-carbon liquid fuel option over recent years. There has been an increasing number of studies investigating different potential advanced biofuel blends in CI engines. Many studies have demonstrated how the key emissions change with the addition of oxygenated advanced biofuels. However, there have been no studies of the different ethyl-based three-component blends with diesel. Currently, there have only been two studies that investigated the effects of different formulations of the butyl-based three-component blends with diesel. These studies were by Antonetti et al. (34) and Raspolli Galletti et al. (54). However, these studies used blends that replicated the product mixture from alcoholysis and were unlikely to meet the fuel standard limits for the flash point.

For the majority of engine applications, the engines and vehicles must meet emissions legislation and obtain what is known as type approval. The legislation sets limits for the different emissions depending upon the type of engine and its application. For light-duty diesel vehicles, the emissions standard is EURO 6d, heavy-duty diesel vehicles must meet EURO VId, and for non-road mobile machinery, engines must meet the Euro Stage V emissions standard (41-43). The emissions limits must be met when using a standard compliant fuel. However, the aim in this work was to determine if the proposed advanced biofuel blends would change the engine emissions relative to those generated using a standard diesel, such that the engine would no longer comply with emissions standards.

The emissions from an engine not only contribute towards climate change but they also affect local air quality and consequently public health. Emissions limits for road vehicles and off-road engines have reduced with each generation of the standards, emphasising the need for emission reduction technologies. However, there is the potential that the fuel used could significantly contribute towards meeting these limits. Therefore, the fuel blends used in the engine testing in this work had their emissions factors calculated and compared to those of the standard diesel. The limits were those stipulated for a 0 – 8 kW stationary direct-injection CI engine in the Euro Stage V standard (42). The engine-out emissions were measured using the techniques detailed in section 3.7 and were analysed following ISO 8178 (255). This enabled emissions from the different fuel blends tested to be compared (255).

This chapter assesses the influence of biofuel blend composition on the gaseous and PM emissions for the tested ethyl and butyl-based blends with diesel. With the engine not being modified to account for the longer IDTs, any changes in the emissions were because of the chemical and physical properties effects of the fuels when using them as drop-in fuels.

6.1.1 COVID Impact Statement

The impact of COVID on emissions testing was significant as it reduced the time available for engine testing and further analysis of samples collected. The occupancy limits of the laboratory delayed the required training and further reduced the time available for conducting the engine and emissions testing. There was also the impact COVID had on equipment repairs due to manufacturers struggling to obtain the parts, further reducing the time available. As a result, a smaller set of compliant butyl-based blends had to be selected for emissions testing. For the ethyl-based blends, there was no opportunity to investigate tailoring the fuel blends to determine optimum blend compositions.

6.2 Gaseous Emissions and the Influence of the Ethyl-Based Biofuel Blends

Only two ethyl-based blends could achieve stable operation of the engine over all five loads. Two other blends could achieve three loads, albeit with some instabilities. The blends tested, the loads they achieved, and the stabilities are summarised in table 6.1.

Table 6.1. Ethyl-based blends with ULSD that ran stably in the engine.

Diesel (vol%)	Biofuel (vol%)	EL/EtOH/DEE ratio (vol%)	Load Achieved (%)	Engine Stability
75	25	65/5/30	4, 28, 50	Occasional fluctuations in power
75	25	75/5/20	4, 28, 50	
85	15	75/5/20	4, 28, 50, 75, 92	Slight instability at high load
85	15	95/5/0	4, 28, 50, 75, 92	Fully stable

The engine instabilities had a detrimental effect on the emissions when using the two 25 vol% biofuel blends. The effect the instabilities had on the gaseous emissions is discussed in section 6.2.1, as there were observable correlations between engine speed and the emissions at a given time.

6.2.1 Engine Instability Effects on the Emissions

As discussed in section 5.1, the engine was unstable when running the ethyl-based blends with high DEE fractions in the biofuel blend. During tests where the engine was unstable, there was a direct correlation between RPM and the gaseous emissions. The largest change was in the CO emissions, where a small drop in RPM resulted in significant increases in the CO concentration. The THC emissions also increased as RPM decreased. Since NO_X emissions are mostly due to thermal NO_X, the change was lower than that for CO and THC when the RPM fluctuated during a run, since the temperature did not change as significantly. However, the average RPM varied from run to run due to the instabilities caused by the presence of DEE. Examples of the fluctuations in emissions throughout an engine test when the engine became unstable can be seen in figures 6.1 and 6.2 for CO and THC emissions, respectively. The presentation of the emissions results includes any instability effects that may have occurred in any of the three test runs.
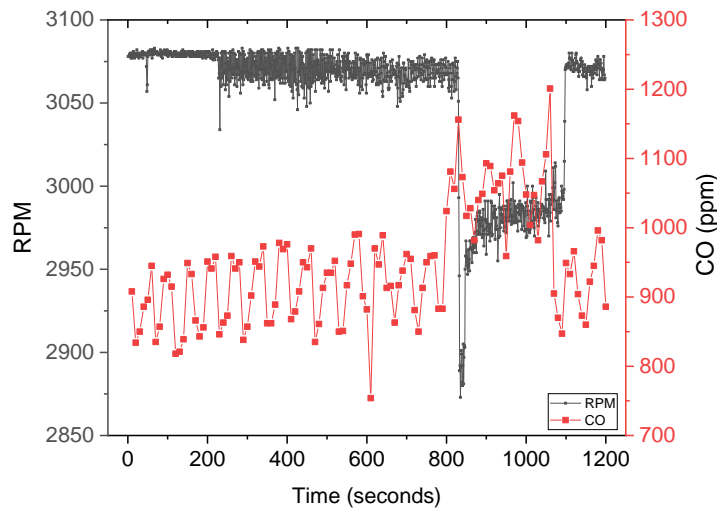
Figure 6.1. Changes in RPM and CO emissions during a 50% load test for the 75% ULSD 25% biofuel (75 vol% EL/5 vol% EtOH/20 vol% DEE) blend.
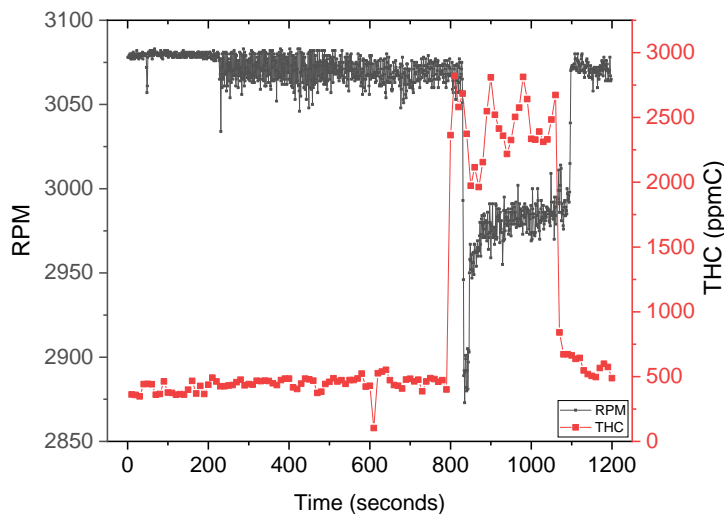
Figure 6.2. Changes in RPM and THC emissions during a 50% load test for the 75% ULSD 25% biofuel (75 vol% EL/5 vol% EtOH/20 vol% DEE) blend.

6.2.2 Changes in CO Emissions when using the Ethyl-Based Blends

Due to longer IDTs and the reduced time available between ignition and the exhaust stroke of the cycle, there was less complete combustion. This was evident with the increased CO emissions across all engine loads and for all ethyl-based blends tested, as shown in figure 6.3. The error bars are the standard deviations of the three measurements for each blend including any instability. CO is an indicator for incomplete combustion, as the carbon in the fuel is not fully oxidised to produce CO_2. When there was unstable combustion, reduced fuel oxidation was more evident.
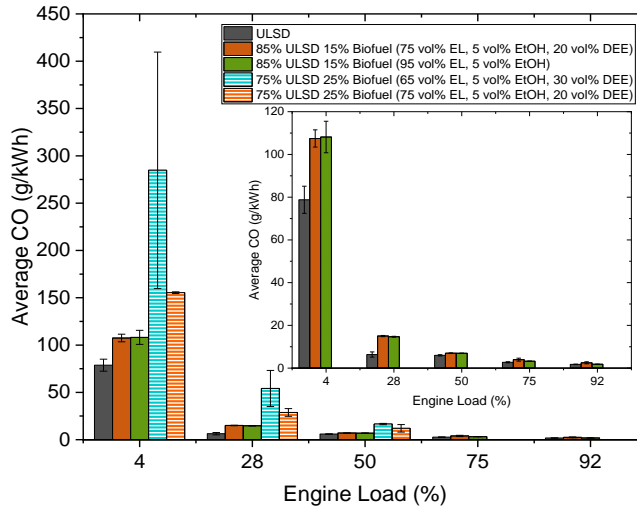
Figure 6.3. CO emissions for ULSD and the ethyl-based blends.

Figure 6.4a shows the changes in the CO emitted relative to ULSD when using the ethyl-based blends (with standard errors). The presence of DEE in the 25 vol% biofuel blends caused a large variation in the changes in the CO emissions. This may be due to the difficulty in ensuring a highly volatile component is delivered to the cylinder and the reduced effectiveness of the fuel injection due to a reduced lubricity of the fuel (220).
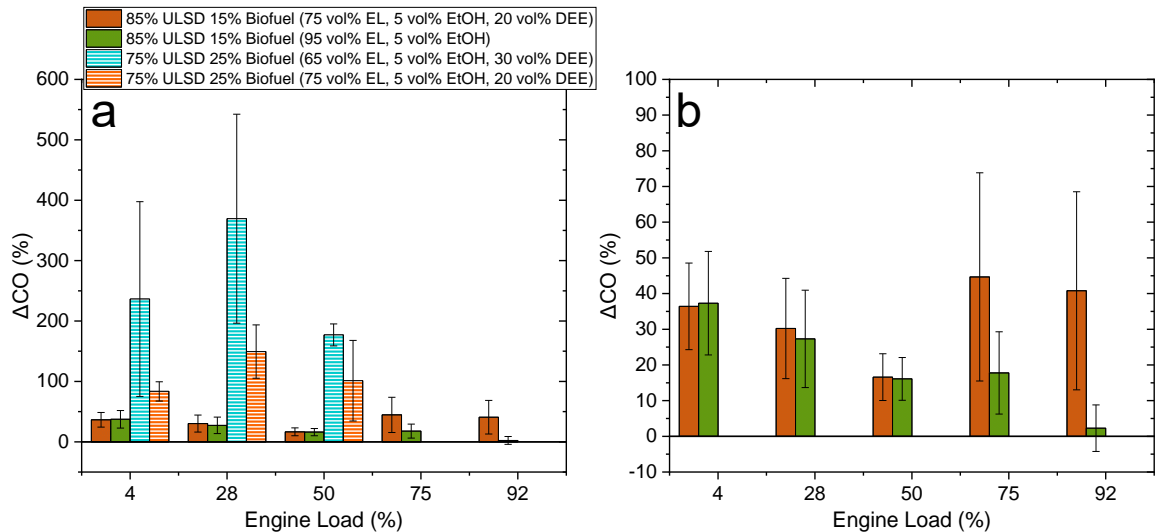
Figure 6.4. Changes in CO emissions relative to ULSD. a: all ethyl-based blends. b: two 15 vol% biofuel blends.

One key finding was that the presence of DEE made the CO emissions worse, even though it has a high DCN and low temperature oxidation pathways (166, 169, 241). There was likely a combination of multiple detrimental effects from DEE, leading to CO emissions increases with increasing fractions of DEE. The first is that it is so volatile, with a low enthalpy of vaporisation, which may result in it not being delivered to the cylinder because it is vaporising in the fuel tank's headspace. If this were the case, there would be a lower than calculated DCN of the biofuel blends, further increasing the IDT and CO emissions. There could also be lubricity issues with higher DEE fractions since it has a much lower viscosity than diesel (129, 220, 226). The reduced lubricity would reduce the fuel pump performance, leading to less fuel being delivered to the fuel injector. Having less fuel injected would not only reduce the efficiency, but it would reduce the injection quality and cause wear to the injector. If the injector were less effective, there would be larger fuel droplets, which are slower to vaporise, resulting in rich regions in the cylinder. These rich regions promote CO formation due to incomplete combustion (88, 122, 203, 306, 343). DEE has a very high DCN, between 139 – 160, which indicates that it should be highly reactive and undergo complete combustion readily (143). However, the high reactivity of DEE may not have the desired effect when blended with EtOH, EL, and ULSD, as it does not seem to favour the oxidation of the fuel components (37, 55).

The impact of DEE was more evident when comparing the two 15 vol% biofuel blends that could run stably at all five loads since the blend without DEE had a lower increase in the CO emissions. In this formulation, the CO increase was likely due to the blend's lower DCN as the biofuel blend of 95 vol% EL, 5 vol% EtOH has a calculated DCN of 4.0 (37). The larger increase of the CO emissions for the 15 vol% biofuel blend with DEE was likely due to the combination of the physical properties of the blends changing, primarily the viscosity of the fuel and the high volatility of DEE. The lower density of the fuel with DEE, compared to the one without DEE, would result in a lower mass of fuel being injected. This lower fuel mass injected should produce a leaner air/fuel mixture, favouring more complete combustion, and reducing the increase in the CO emissions relative to the blend without DEE (4, 5, 40).

6.2.3 Changes in NO_X Emissions when using the Ethyl-Based Blends

In an ICE, the dominant source of NO_X is thermal NO_X since there is no fuel nitrogen in both ULSD and the ethyl-based biofuel blends. However, small fractions of prompt NO_X could form in rich, low temperature regions (40, 60). Therefore, the changes in NO_X emissions were likely due to changes in the combustion temperatures when using the ethyl-based blends. The average NO_X emissions are shown in figure 6.5a, with changes relative to diesel in figure 6.5b. The large magnitude of the error in the relative change

of NO_X emissions was due to the high variation in the measured NO_X emissions between repeated runs. The intake air temperatures were within standard deviations of each other, even with the engine tests being conducted on different days. For the three blends with DEE the average BSFC had large error (figure 5.11), which would have been due to DEE reducing the effectiveness of the fuel pump and injector. The variation in the fuel delivered will vary the impact of the fuel's cooling effect and this may vary between tests, even with homogeneous liquid fuel blends.

For the two 15 vol% biofuel blends, there was a reduction in NO_X at >50% load compared to the ULSD baseline, whereas at lower loads, the NO_X emissions were comparable to the ULSD baseline. The two 25 vol% blends had a greater reduction in NO_X emissions compared to the 15 vol% blends at the loads they could all achieve. This reduction was likely due to the lower temperatures reached during the unstable combustion, resulting in lower exhaust gas temperatures (figure 5.31).
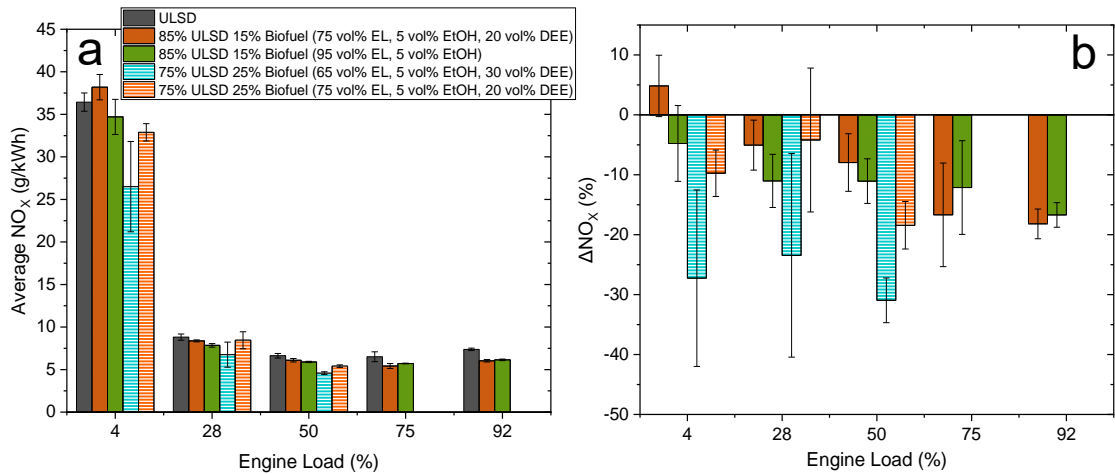
Figure 6.5. a: NO_X emissions of ULSD and all ethyl-based blends. b: changes relative to ULSD.

The 85 vol% ULSD 15 vol% biofuel (75 vol% EL/ 5 vol% EtOH/20 vol% DEE) blend had a greater reduction in NO_X emissions compared to the blend without DEE at the higher loads. At higher loads, more fuel was injected, resulting in a larger amount of cooling relative to the ULSD baseline. DEE has a cooling effect due to its high volatility and low enthalpy of vaporisation. Therefore, its presence should favour a greater NO_X reduction. The greater enthalpy of vaporisation of EL, combined with the lower DCN, would also reduce the peak in-cylinder temperature as the vaporisation of EL requires more energy (150). Therefore, EL may not combust further reducing the in-cylinder temperature. The delay in peak HRR shown in figure 5.21 results in a lower in-cylinder temperature, which should reduce thermal NO_X production. The peak HRR for the 85 vol% ULSD 15 vol% biofuel (95 vol% EL/5 vol% EtOH) blend was higher than that of ULSD, albeit delayed. Therefore, there was a combination of the biofuel component's cooling effects and the delayed peak HRR reducing NO_X formation.

The density of the fuel blends increased relative to the ULSD (table 4.14), thus, the mass of fuel injected would have increased. This increased mass of fuel injected would decrease the air/fuel ratio, reducing NO_X production, which peaks close to stoichiometric conditions where peak temperatures occur (40, 49, 101). The engine was not optimised to ensure the stoichiometry and AFR were maintained when using the biofuel blends. The AFR typically reduced by 5% when using the biofuel blends. This decrease in AFR indicates that the AFR became richer, which favours a NO_X reduction. However, with the 15 vol% biofuel blend with DEE, the AFR increased by 2% at 92% load. Although, this blend at 92% load had a greater NO_X reduction than the blend without DEE, the combination of these effects indicate that the cooling effect of DEE contributes towards the reduction in NO_X emissions.

Studies have shown that a fuel's oxygen content does not directly affect NO_X emissions (344, 345). The oxygen content increased in the 15 vol% biofuel blends. The O/C fuel molar ratio increased from 0.02 for the ULSD to 0.076 for the blend with DEE and 0.083 without DEE. There was a greater reduction in the NO_X emissions with the blend with DEE. This reduction was due to the reduced temperatures generated, as indicated by the reduced exhaust manifold temperatures in figure 5.40. Additionally, there was a reduction in the peak and a greater delay in the HRR for the blend with DEE. Typically, the higher the oxygen content of a fuel, the lower the heating value. The lower energy content would reduce the temperatures generated during the combustion. Therefore, it was expected that the blends without DEE should reduce the NO_X further with the lower heating value. However, this was not the case at the higher loads where the blends with DEE had a greater reduction in NO_X. The greater reduction at the higher loads, where more fuel is injected, indicates that the cooling effect of DEE contributes towards the reduction in NO_X.

The NO_X emissions were analysed to determine if there was a change in the NO/NO_2 ratio when using the biofuel blends. Figure 6.6a shows that the blend without DEE had higher emissions of primary NO_2 at <92% load compared to the blends with DEE. This increase in NO_2 fraction may be due to the higher oxygen content in the blend without DEE. The increased oxygen present increases the percentage of NO_2 in the total NO_X emissions for the blends with 15 vol% biofuel, as shown in figure 6.6b. An et al. (50) reported the same finding when simulating ULSD, biodiesel, ethanol, and dimethyl carbonate blends. They increased the fuel's oxygen content and found that the NO_2 fraction of total NO_X increased as the total NO_X emissions decreased because less NO was formed (50). The increase in the NO_2 fraction compared to diesel at the lower loads indicates there could have been lower combustion temperatures or there was more quenching of NO_2, which could have been due to charge cooling effects from the addition

of the ethyl-based biofuel components (59, 62). Therefore, more NO_2 was emitted as it was not reacting further to produce NO.
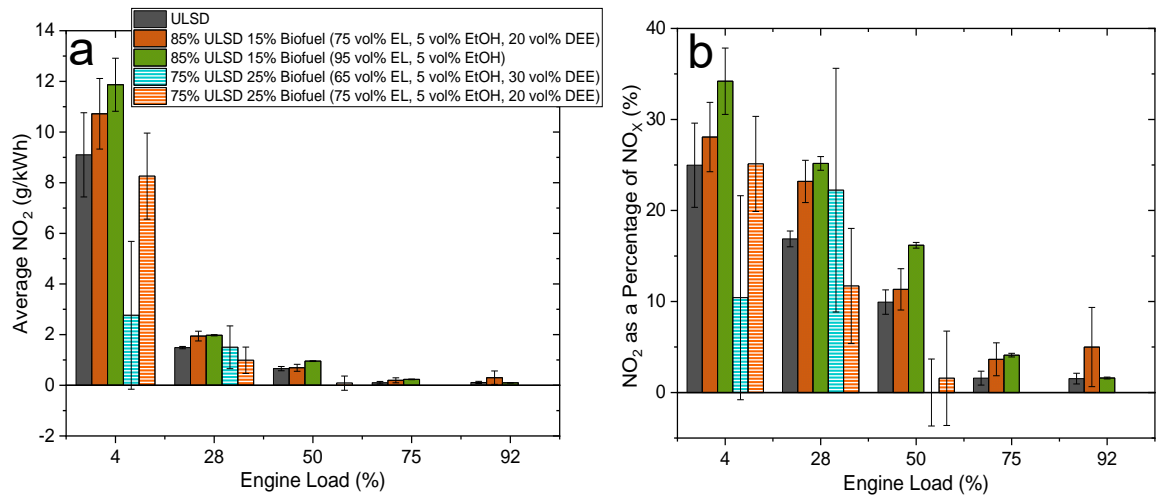
Figure 6.6. a: Average NO_2 emissions for the ethyl-based blends. b: NO_2 as a percentage of NO_X.

6.2.4 Changes in THC Emissions when using the Ethyl-Based Blends

The THC emissions are another indicator of incomplete combustion due to the fuel species not being fully oxidised. The 25 vol% biofuel blends that had unstable combustion due to the presence of DEE had extremely high THC emissions due to incomplete combustion. These blends also had larger standard deviations due to the fluctuations of power between the runs.

The two 15 vol% biofuel blends had an increase in THC emissions, as expected due to the longer IDTs compared to ULSD (figure 5.6). For these two blends, the greatest increase in THC emissions was when DEE was present, with greater increases at the higher loads since the IDTs for the blend with DEE were greater at the higher loads than the blend without DEE. Figure 6.7 shows the THC emissions at the different loads and the changes relative to ULSD are shown in figure 6.8. The increases range between 30% to 225% for the 15 vol% biofuel blends and over 220% for the 25 vol% biofuel blends. The large errors associated with the changes in the THC emissions at >75% load for the 15 vol% biofuel blend with DEE were due to the combustion instabilities (figure 5.2) at the higher loads, generating more THC emissions. These large increases in THC emissions further demonstrate that any drop-in fuel must result in stable combustion and engine operation or the THC emissions become unacceptable. The large increases would not only be detrimental towards climate change and the THC emissions will be GHGs, but also for local air quality and the associated public health impacts discussed in section 2.2.2.
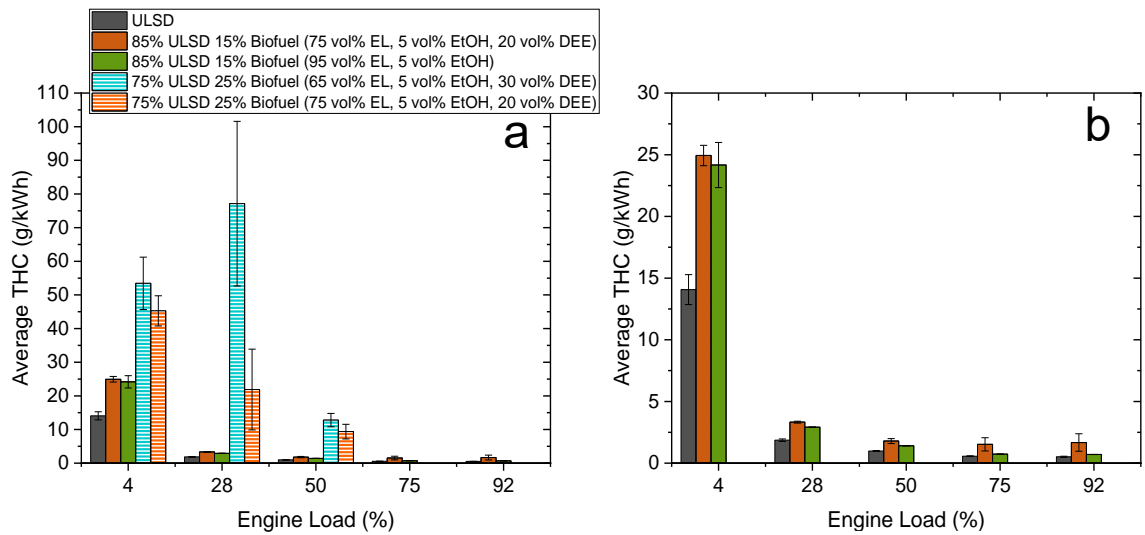
Figure 6.7. THC emissions of ULSD and the ethyl-based blends. a: all four blends. b: 15 vol% blends.
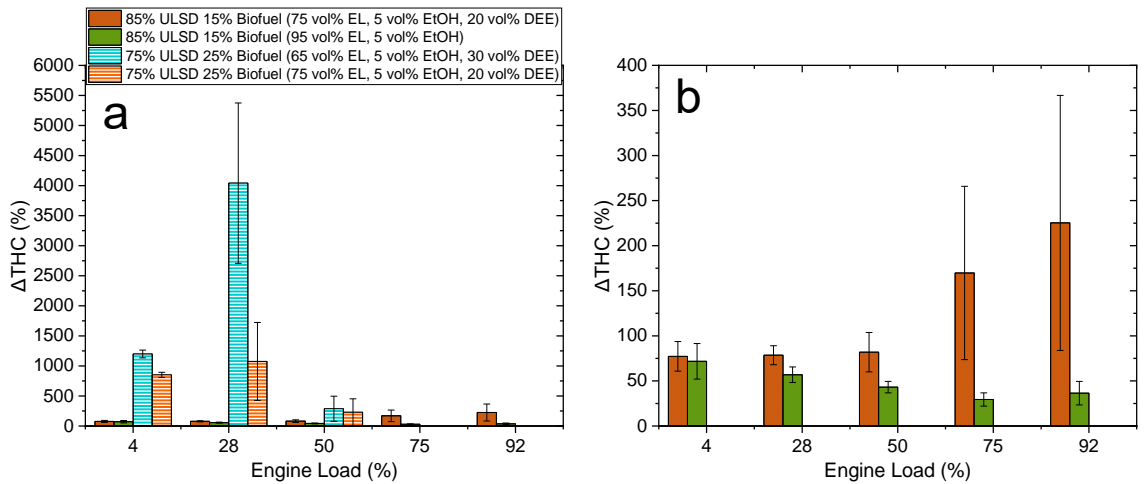
Figure 6.8. Changes in THC emissions relative to ULSD. a: all the ethyl-based blends. b: 15 vol% biofuel blends.

The lower density and viscosity of the 15 vol% biofuel blend with DEE, compared to that without, should improve the fuel atomisation forming smaller fuel droplets which evaporate more readily (88). This improved atomisation should reduce the emissions of unburnt fuel, as there should be more complete combustion. On the other hand, the reduced viscosity will reduce the lubricity, which could reduce the effectiveness of the fuel delivery system and the fuel spray. The reduced injector effectiveness could generate a non-uniform spray. This would increase the number of rich zones that generate higher THC emissions (88, 122). The increased DCN of the blend with DEE should have favoured more complete combustion and fewer THC emissions. However, this was not the case as the blend without DEE had less of an increase in the THC emissions as the load increased, whereas the blend with DEE had increasing THC emissions as the load increased. This behaviour was likely due to the synergistic effect of the reduced RPM at the higher loads, the increased peak pressures and temperatures, and longer IDTs. The longer IDTs allowed for more premixed combustion, which should

reduce the amount of unburnt fuel. Since the MEXA7100D does not determine the chemical composition of the THC emissions, the analysis of the FTIR data was used to give some speciation of the exhaust gases. The FTIR results are discussed in the next section.

The THC emissions could be reduced by advancing the injection timing to account for the longer IDTs, as it would give more time for complete combustion. There may also need to be exhaust aftertreatment systems employed for different engine applications to reduce THC emissions. Any DOC retro-fitted would need to manage increased use without catalyst poisoning or degradation as well as operating at lower temperatures, since the exhaust temperatures are lower with the biofuel blends (figure 5.40) (101).

6.2.5 Changes in the Volatile Organic Carbon Compounds Emissions when using the Ethyl-Based Blends

The Gasmet FTIR was used to measure the concentration of individual VOCs in the exhaust gas. These concentrations were measured in ppm and were converted to g/kWh, as detailed in section 3.7.9. The reported VOC concentrations were above the detection and noise limits from the nitrogen background and were within their calibrated ranges. Appendix B.1 shows the average ppm values of the selected VOC compounds. Not only do the effects on the climate change emissions targets need to be considered for the utilisation of new fuels, but also so do their local air quality and related health impacts. The formation of these VOC species can indicate the favoured combustion reaction pathways when the fuel is used in the Yanmar L100V. Acetic acid was selected for measurement due to its formation as a combustion product of DEE (166, 232). The aldehyde species were selected as they typically increase when using oxygenated biofuel components. In addition, aldehydes have detrimental impacts on local air quality (45, 46, 101, 346). Hexane was chosen, as it was the species with the longest carbon chain in the FTIR library. Hexane could be used as an indicator for the incomplete combustion of the ULSD hydrocarbons as it is a combustion product of some longer hydrocarbon chains (177, 178, 215, 237).

Formaldehyde was of particular interest since it commonly increases when oxygenated biofuels are used. Formaldehyde is an irritant gas and can have detrimental effects on local air quality (45, 46, 76, 162, 167). The blends with unstable combustion had extreme increases in formaldehyde emissions, as shown in figure 6.9a, with an increase of over 1000% at 28% load. For the 75% ULSD 25 vol% biofuel (65 vol% EL/5 vol% EtOH/30 vol% DEE) blend at 28% load, there was approximately a 3000% increase due to the formaldehyde emissions rising from 0.1 g/kWh up to 8 g/kWh. The increases

in formaldehyde were due to incomplete combustion caused by the instability in the combustion cycles when using such a high DEE fraction.

Figure 6.9. Changes in formaldehyde emissions relative to ULSD baseline for: a: all ethyl-based blends. b: 15 vol% biofuel blends.

The change in formaldehyde at the lower loads is the same for both 15 vol% blends tested, as shown in figure 6.9b. This was when the combustion was the most stable due to the lower in-cylinder temperatures keeping the DEE autoignition more stable. The blend with DEE had more unstable combustion at the higher loads (figure 5.2) resulting in less complete combustion, increasing the emissions of VOCs and THC.

Similar to formaldehyde, increases of acetaldehyde for the 25 vol% biofuel blends were extremely large, especially for the more unstable blend with the higher DEE fraction, as shown in figure 6.10a. The 15 vol% biofuel blends are more clearly displayed in figure 6.10b.
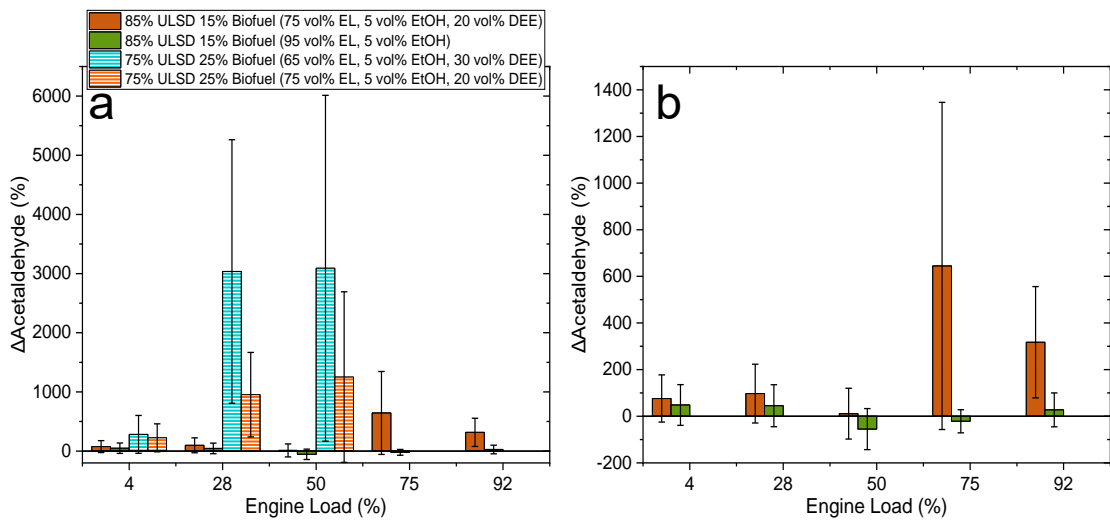
Figure 6.10. Changes in acetaldehyde emissions relative to ULSD baseline for: a: all ethyl-based blends. b: 15 vol% biofuel blends.

The changes in acetaldehyde emissions follow the same trends as the formaldehyde emissions. At lower loads, the acetaldehyde emissions are similar for both

15 vol% biofuel blends. It is again at the higher loads that the biofuel blend with DEE caused a greater increase in the acetaldehyde emissions, indicating that there is incomplete combustion (177).

Acetaldehyde and formaldehyde are possible low temperature combustion products from all the ethyl-based biofuel components, as they form as stable intermediates with low reactivity (165). The increased emissions of formaldehyde and acetaldehyde would be a concern since they are known carcinogens and are precursors for ozone and peroxyacyl nitrates formation (45, 46, 76). Although they must be monitored according to health and safety legislation in the UK due to workplace exposure limits, there are currently no set emissions limits for a NRMM engine (45, 46, 76). There will be set formaldehyde emissions limits for HGVs of 30 mg/kWh in the new Euro 7 vehicle emissions standard (95, 96). Therefore, it is likely that there will be limits for NRMM in the next emissions standard. In the EU, environmental legislation requires the monitoring of formaldehyde and acetaldehyde in the ambient atmosphere. However, in the US there are exhaust emissions limits for formaldehyde emissions (45, 46, 76). Due to their toxic and carcinogenic nature, the changes in these emissions need to be quantified to ensure the utilisation of fuels that are better for climate change do not worsen local air quality and negatively impact the health of the local population.

Acetic acid is not a known carcinogen or toxin, but it was selected to be analysed as it is an oxidation product of DEE, as shown by Tran et al. (169). As expected, the 25 vol% blends had greater increases in the acetic acid emissions, as shown in figure 6.11a, since they had the less stable combustion. The 15 vol% blends are shown in figure 6.11b. The large error bars indicate that there may have been no change in acetic acid emissions for some runs. The engine instability caused fluctuations in the acetic acid emissions and thus high variability.
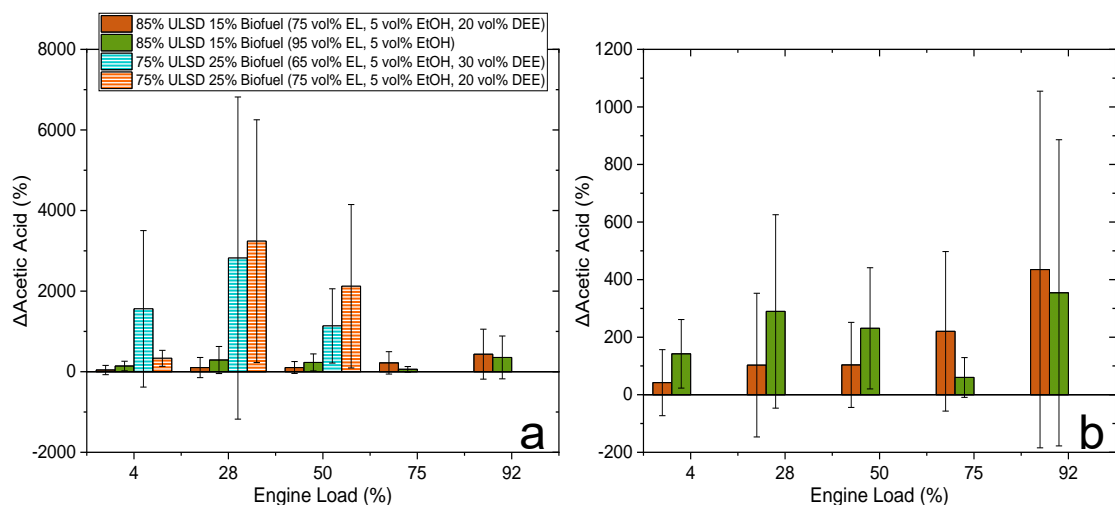
Figure 6.11. Changes in acetic acid emissions relative to ULSD baseline for: a: all ethyl-based blends. b: 15 vol% biofuel blends.

The blend with DEE had a greater increase in acetic acid emissions at higher loads following the findings of Tran et al. (169), where acetic acid is a DEE low temperature combustion product. However, Tran et al. (169) used a jet stirred reactor at 400 – 1100 K, with a pressure of only 1.067 bar, below that of an engine (169). The detection of acetic acid in the exhaust demonstrated that even at the elevated pressures of the engine acetic acid would still be formed.

Although the volume fraction of ethanol in the biofuel blend is constant, at 5 vol%, the measured ethanol differences between the two 15 vol% biofuel and the 25 vol% biofuel blends would due ethanol being a combustion product of EL and DEE. Figure 6.12a shows that the 25 vol% blend with the higher DEE content had a greater increase in ethanol emissions, as expected since this blend had the least stable combustion.
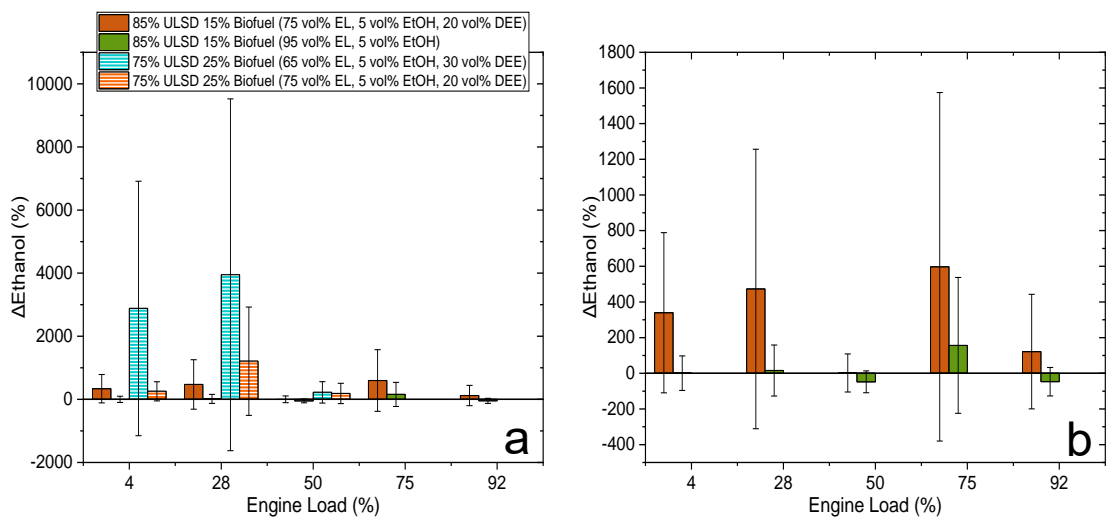
Figure 6.12. Changes in the ethanol emissions relative to the ULSD baseline for: a: all ethyl-based blends. b: 15 vol% biofuel blends.

At 92% load, the ethanol emissions had a greater increase for the blend without DEE for the two 15 vol% biofuel blends, as shown in figure 6.12b. The large error bars for the changes in ethanol were due to the fluctuations in the measured ethanol. The source of ethanol cannot definitively be determined to be unburnt ethanol from the fuel blend, since EtOH is a possible oxidation product of EL (37, 55, 160, 229). With the increased EL fraction, there could be a combination of the fuel ethanol and the formation of ethanol due to the incomplete oxidation of EL in the exhaust stream (37, 55, 143, 160, 229).

DEE emissions increased for all blends, as shown in figure 6.13. For the 25 vol% blends, it was likely that most of the DEE measured was from unburnt fuel due to the large changes in the DEE concentrations measured (figure 6.13a). The blends with stable combustion show a much smaller increase in DEE emissions, which further demonstrates the need for stable engine operation to control the VOC emissions.
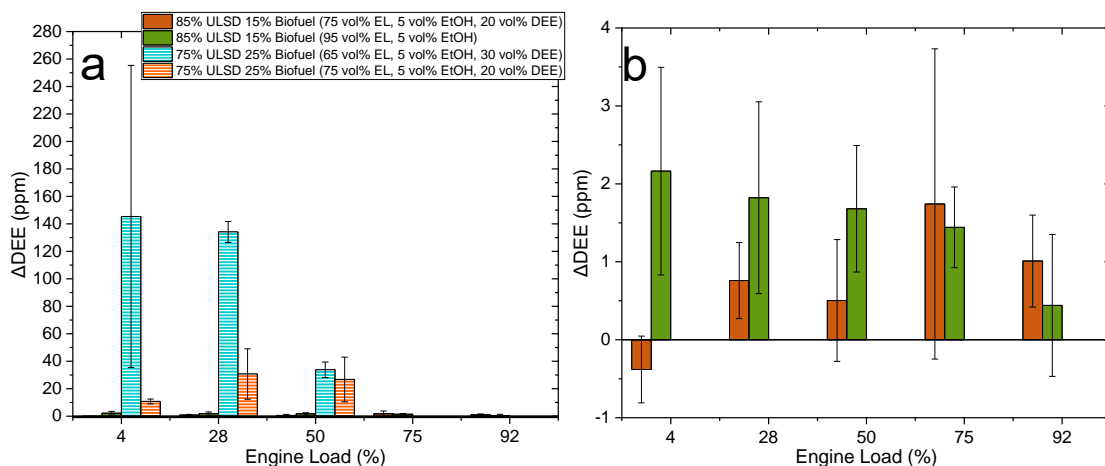
Figure 6.13. Changes in the DEE emissions relative to the ULSD baseline in ppm for: a: all ethyl-based blends. b: 15 vol% biofuel blends.

Figure 6.13b shows that even when there was no DEE in the fuel, there was a small increase (around 2ppm) in the DEE concentration measured. The source of DEE was unclear since the engine was warmed up using ULSD, the fuel lines were drained and then flushed with the test fuel blend, and the FTIR purged with nitrogen between tests. These control measures were used to ensure there would be no trace of previously tested fuels. Additionally, the large variability in the changes in the DEE emissions may indicate that there was little to no DEE measured for the blend without DEE for some runs. DEE is not known to be a combustion product of EL or EtOH, which indicates that there may be contamination of the fuel lines since the FTIR and its sample lines were maintained at 180 °C, so DEE will not condense, as its boiling point is 34 °C. When ambient air was measured with the FTIR, no DEE was detected. Due to the limited time available, the fuel lines could not be replaced for every fuel blend, nor would this have been practical. Hence, any DEE absorbed by the fuel lines may be the possible source of DEE, which even with the fuel lines being flushed when changing fuel blends may difficult to remove without replacing the fuel lines. The increase in DEE detected for the blend without DEE was around 2 ppm, indicating that the level of potential fuel line contamination is minimal following the engine tests using the blends containing DEE. However, to be certain the DEE detected was due to contamination engine tests using the blend without DEE using new fuel lines should be conducted.

Hexane emissions increased for all blends, with the two 25 vol% biofuel blends having the greatest increase, as shown in figure 6.14a. This increase of hexane indicates that even the hydrocarbons in ULSD were not oxidised, with the long carbon chains undergoing decomposition reactions to form C_6H_{13}, the hexyl radical, which can then react with H_2 or abstract hydrogens to produce hexane (239). When the combustion was unstable, the IDTs were much longer, which reduced the time in the cylinder and reduced the oxidation of smaller hydrocarbon species (143, 239).
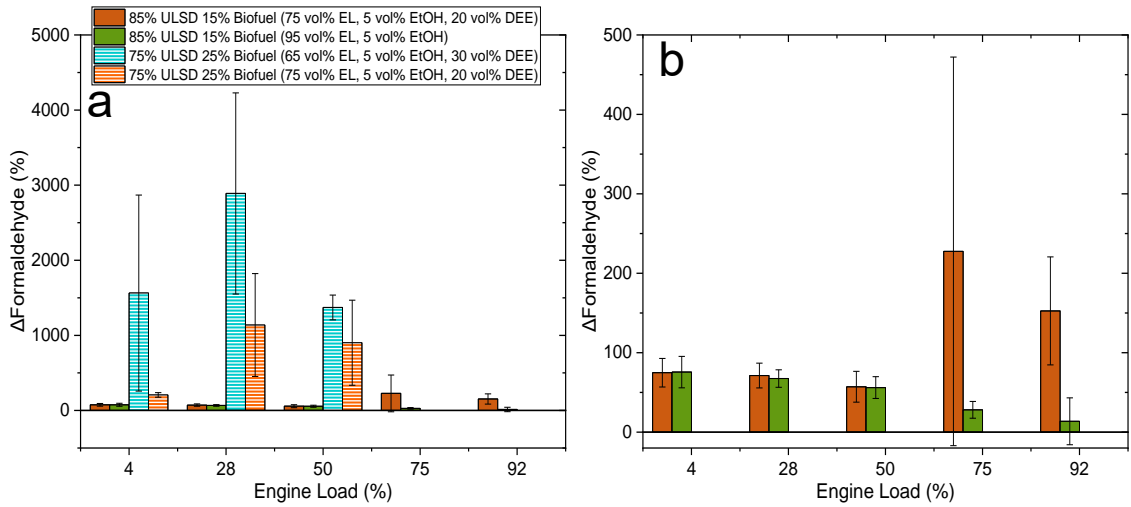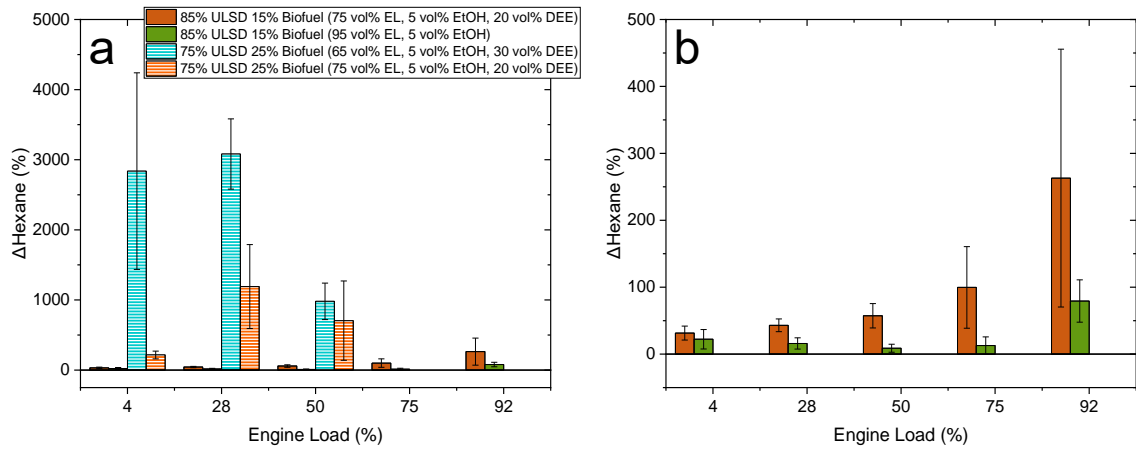
Figure 6.14. Change in hexane emissions relative to the ULSD baseline for: a: all ethyl-based blends. b: 15 vol% biofuel blends.

For the 15 vol% blends, shown more clearly in figure 6.14b, the presence of DEE in the fuel blend at the higher loads results in greater hexane emissions. The biofuel blend without DEE has lower increases hexane emissions. The lower increase in hexane was likely due to longer IDTs reducing the time available for the combustion in the cylinder, thus producing less hexyl radicals, and the lower temperatures and pressures achieved using blends with lower LHVs.

6.3 Gaseous Emissions and the Influence of the Butyl-Based Biofuel Blends

As mentioned in section 3.7, the FJ injector was used for the engine tests of the butyl-based blends with diesel. The FJ injector had four holes, each with a diameter of 234 μm. The FB injector had five holes, each with a diameter of 185 μm. The larger injector holes would result in larger droplets forming. The magnitudes of the gaseous emissions when using the butyl-based blends were compared to a ULSD baseline using the FJ injector and were of similar magnitudes. Any changes would be due to the changes in the physical and chemical properties of the butyl-based blends. The gaseous emissions were measured using the MEXA7100D and the Gasmet FTIR.

6.3.1 Changes in CO Emissions when using the Butyl-Based Blends

Upon addition of the butyl-based biofuel blends, there was an increase in the CO emissions for most blends, as seen in figures 6.15a and 6.15b. The greatest increase in CO was when using the fuels with high BL fractions and at lower loads, as shown in figure 6.15c. The combination of these, results in less complete combustion as the IDTs are longer (figure 5.10) and there are lower peak pressures (figure 5.36) and temperatures. At the lower loads, the in-cylinder temperatures reduce, resulting in less complete combustion, producing higher concentrations of CO. The reduction in the

cylinder residence time also influences the CO emissions, regardless of which butyl-based blend was tested, as there are generally greater increases at the lower loads, as shown in figure 6.15c. The errors shown for the specific emissions are the standard deviations from the three test runs. For the relative change graphs, the error bars are the standard errors.
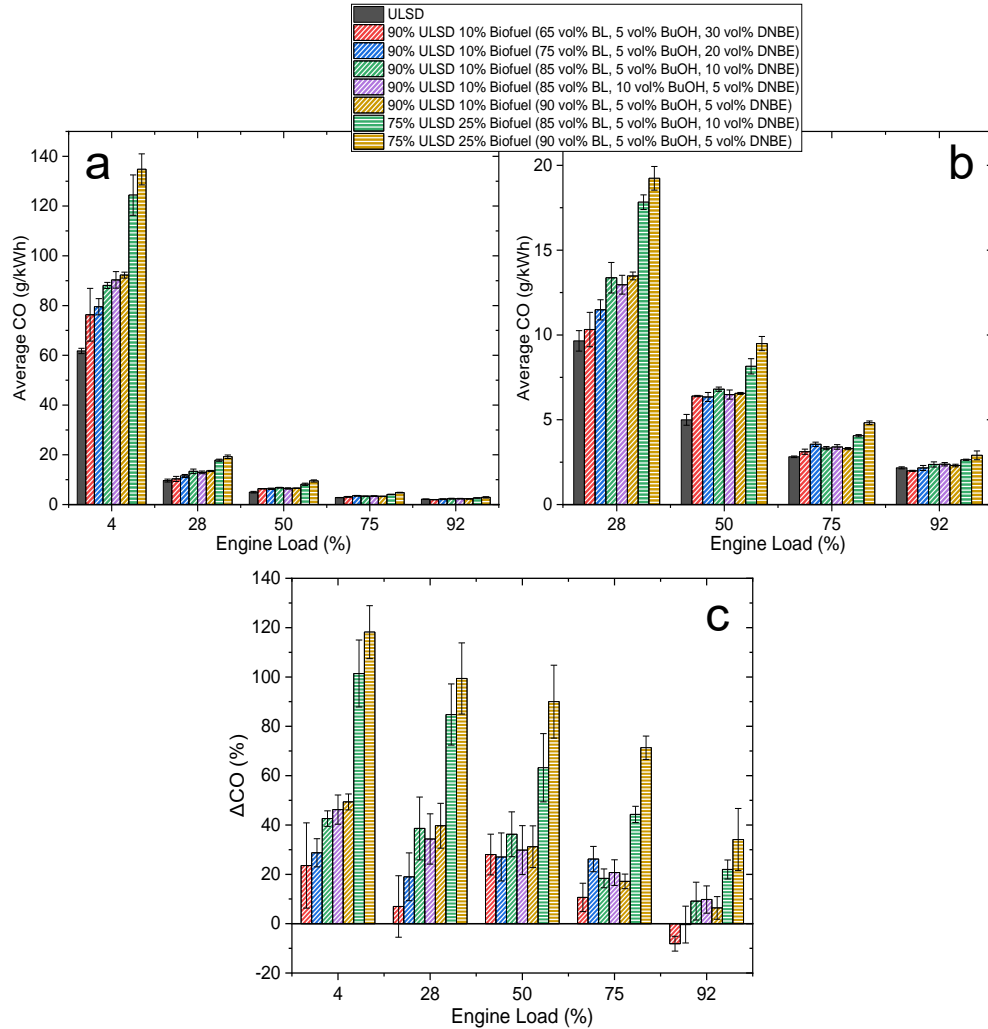
Figure 6.15. CO emissions of ULSD and the butyl-based blends. a: all loads. b: without 4% load. c: Changes in CO emissions relative to ULSD.

For the 10 vol% biofuel blends, as the volume fraction of BL in the biofuel blend increases, the ΔCO increases, other than for two exceptions, the biofuel blends containing 30 and 20 vol% DNBE. The 25 vol% blends had greater increases, as expected, due to their even longer IDTs. The increase in CO does not follow the trends reported by Raspolli Galletti et al. (54) and Antonetti et al. (34), whose tests showed reductions in CO. However, the biofuel blends used in their work had lower BL fractions and were unlikely to have met the flash point limits due to the high BuOH and DNBE fractions. At >50% load the CO emissions were below the Euro stage V limit of 8.00 g/kWh. However, this limit is for a summation using the loads and weighting factors in table 3.10. The 50% and 75% loads have a weighting factor of 0.3 and 0.25, respectively

(42, 255). Therefore, changes in the CO emissions at the higher loads are more influential on the compliance with the Euro stage V emissions standard (42).

6.3.2 Changes in NO$_X$ Emissions when using the Butyl-Based Blends

Upon utilisation of the butyl-based blends, the NO$_X$ emissions were more variable between the blends ranging between reductions of 10% to increases of 16% across all loads tested with a COV of 23. The NO$_X$ emissions were within one standard error of each other, as shown in figure 6.16a, indicating that NO$_X$ emissions are almost unchanged. The greatest increase was for the 25 vol% biofuel blend with 90 vol% BL, as shown in figure 6.16b. The error bars for the changes in NO$_X$ indicate that they may be negligible or of greater magnitude. For the 10 vol% biofuel blends at lower loads, the higher the DNBE, the greater the reduction in NO$_X$. However, as the engine load increased, the greater total fraction of BL increased the NO$_X$ emissions.
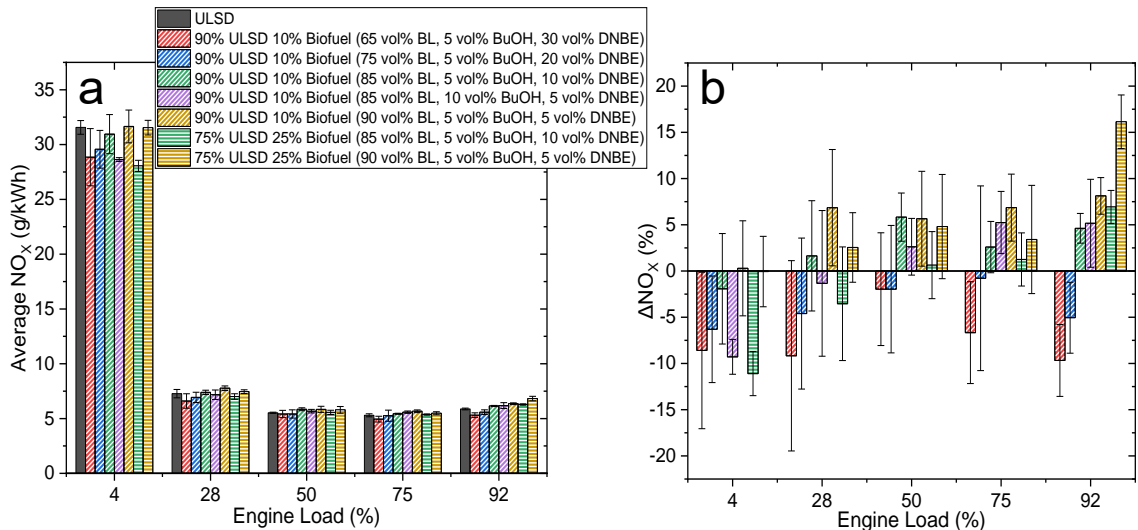
Figure 6.16. a: NO$_X$ emissions of ULSD and the butyl-based blends. b: changes in NO$_X$ emissions relative to ULSD.

The addition of BuOH to diesel has been shown to reduce NO$_X$ emissions, due to reduced combustion temperatures from longer IDTs (226, 347). However, in the blends tested in this work, the total BuOH fraction is 0.5 – 1.25 vol% of the total blend. Therefore, when there is a NO$_X$ reduction, it is unlikely due to BuOH (341). The NO$_X$ emissions measured by Antonetti et al. (34) and Frigo et al. (38) were relatively unchanged, with little evidence that the increase in BL fraction increases the NO$_X$ emissions. The blends used by Frigo et al. (38) had increasing BL fractions, 7 to 13 vol%, and a constant DNBE fraction of 4 vol%. The blend with 11 vol% BL had the largest increase in NO$_X$ at 3000 RPM and 100% torque, although it was still comparable to their diesel baseline (38). The blends with the higher DNBE fractions were expected to have higher NO$_X$ emissions relative to the other blends, due to an increase in the DCN of the biofuel blend. The

higher DCN would enable higher temperatures to be achieved during the combustion. However, this was not the case with the blends studied here, as with increasing BL fraction the NO_X emission increased (69). The high DNBE fraction may have increased the cooling effects of the fuel in a similar manner to DEE. In addition, there were high fractions of BL in the biofuel blend and it has the highest adiabatic flame temperature of all the components (table 2.8), which may have increased the NO_X emissions (13).

Since the exhaust manifold temperatures with the butyl-based blends were similar to when running ULSD at the lower loads (figure 5.32) small changes in the NO_X emissions were expected. However, the engine was not optimised to run on these fuel blends, as there was no change in the fuel injection timing. If the injection timing was advanced to compensate for the longer IDTs, the in-cylinder temperatures may increase, as there would be more complete combustion. Additionally, the peak HRR at 92% load for the blends with increased NO_X emissions was >7% greater than the peak HRR of diesel. However, the peak HRR was delayed by up to 2 CAD (table 5.6). The combination of these may have favoured the small increases in NO_X. There was also no change in the quantity of fuel injected to account for the additional oxygen present and the changes in the density. As previously discussed in relation to the ethyl-based blends, the additional oxygen may not be a direct cause of the changes in the NO_X emissions since most NO_X formed is thermal NO_X (348, 349). However, there is a reduction in the DCN due to the high BL and BuOH fractions present (143). The longer IDTs reduce the maximum temperature in the cylinder since the peak pressure is further from TDC, which should reduce the amount of thermal NO_X. However, this was not the case at the higher loads where more fuel is injected, as the higher BL fractions may generate a leaner air/fuel mixture since less fuel will be vaporised. These leaner conditions would favour NO_X production, hence the increases in NO_X causing the increases observed.

Since the MEXA7100D could measure NO_X or NO emissions, it was possible to quantify the primary NO_2 formed. This quantification enabled the determination of whether the fuel blend composition promotes the NO oxidation to form NO_2. Figures 6.17a and 6.17b show the primary NO_2 emissions, and figure 6.17c shows NO_2 as a fraction of NO_X. The addition of the biofuel blends caused the NO_2 fraction of NO_X to increase at <75% load (figure 6.17c). For the 10 vol% biofuel blends, the NO_2 fraction increased as the BL fraction increased. The 25 vol% biofuel blends had an even greater increase in NO_2 fraction. The increase in NO_2 coincides with the increased oxygen content of the fuel as the O/C fuel molar ratio increases. An et al. (50) demonstrated that the lower temperatures achieved when using oxygenated fuels reduced the primary NO formed and kept the NO_2 levels relatively consistent with that of ULSD, thus increasing the fraction of NO_2 in the total NOx. However, the butyl-based blends in this work did not sufficiently change the total NO_X emissions for this to be considered as a possible

explanation. Therefore, the increased oxygen content may favour the oxidation of NO to NO_2, but there are many unknowns for the fuel's influence on NO_X formation, since it is not fully understood from diesel (50). Additionally, at lower loads, where the combustion temperature is lower, there is a greater fraction of NO_2 formed and increased quenching, preventing it from reducing to NO (59, 62). The exhaust manifold temperature was reduced for all blends relative to ULSD at all loads tested (figure 5.32), indicating there were lower combustion temperatures with the biofuel blends compared to ULSD. At lower loads, the trend in the NO_2 fraction shows there may be some competition between the effects of each of the butyl-based components, as there is a peak before a lower increase with lower DNBE fractions. This may be due to BL's high adiabatic flame temperatures (table 2.8) generating more high-temperature regions where there would be more NO_2 reduction (59, 62). An increase in primary NO_2 will be detrimental to urban air quality as not only is it an ozone precursor, but it causes detrimental health effects, as discussed in section 2.2.2. At higher loads, the change in the primary NO_2 when using the butyl-based biofuel blends is negligible, hence the blends would be as detrimental to urban air quality as using ULSD.
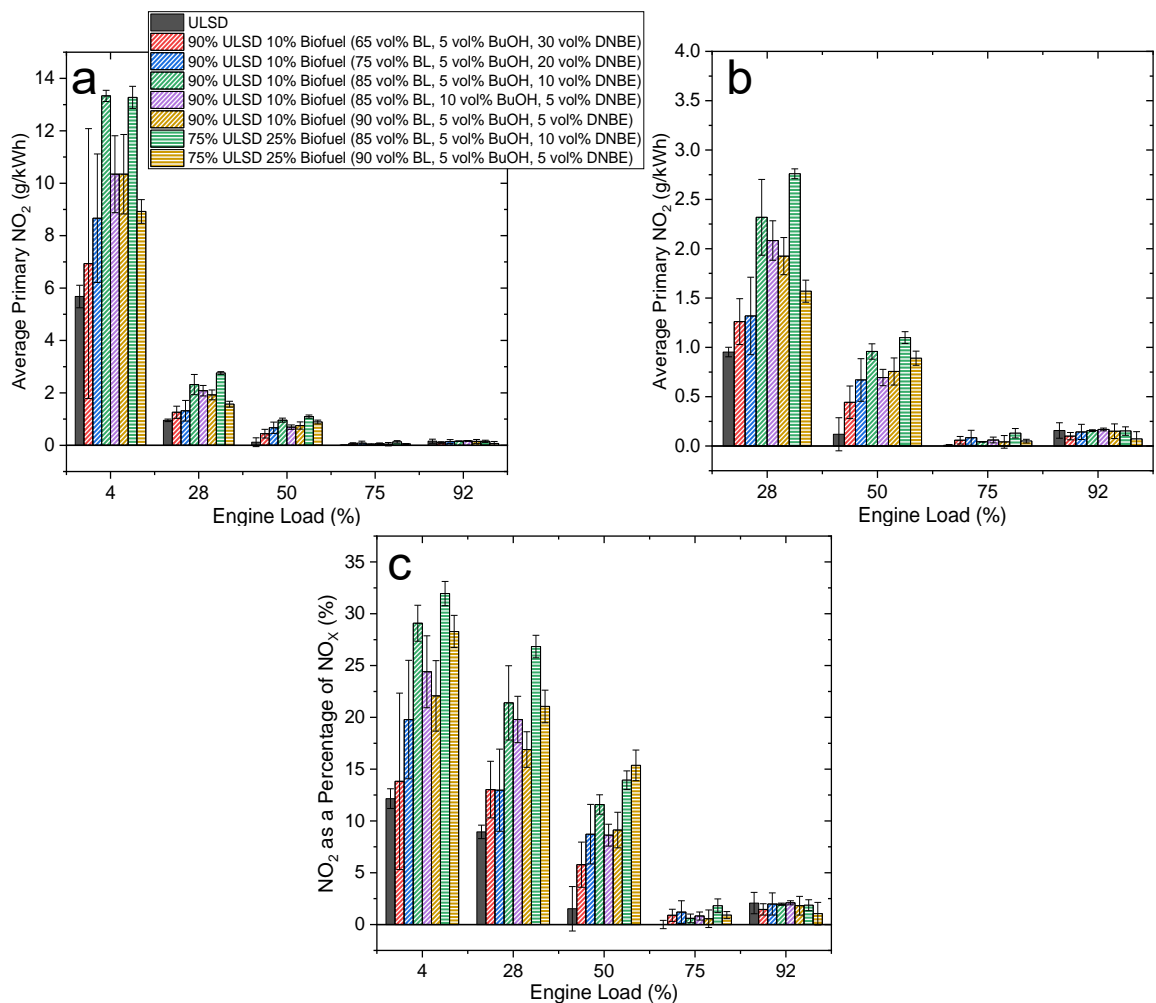
Figure 6.17. Primary NO_2 emissions for the butyl-based blends. a: all loads. b: without 4% load. c: NO_2 Fraction of total NO_X.

The increase in NO_X emissions could be compensated for using an SCR system. However, the Yanmar L100V did not have an SCR system, so the effectiveness of NO_X control with SCR was not determined. Additionally, the Yanmar L100V does not have turbocharging and EGR, which are also NO_X control techniques (5, 101). However, for engines that have EGR capability, its utilisation could be a more cost-effective way to control NO_X than using SCR with expensive catalysts, although optimum strategies for EGR and SCR would need to be determined.

With the engine not running at the optimal conditions for these fuel blends, it may be that the NO_X emissions change again due to potential changes in the in-cylinder temperatures. If incomplete combustion were reduced, there would be higher peak temperatures. If that were the case, there would be an increase in thermal NO_X emissions due to the compensation of the reduction in THC. Engine optimisation would require further investigation to determine the performance and emissions at these conditions.

6.3.3 Changes in THC Emissions when using the Butyl-Based Blends

The THC emissions are another indicator of incomplete combustion and oxidation of the fuel, along with the changes in CO emissions. Upon addition of the butyl-based blends, there was an increase in the THC emissions at <75% load and reductions at 92% load, as shown in figure 6.18a. The relative changes in THC emissions are shown in figure 6.18b.
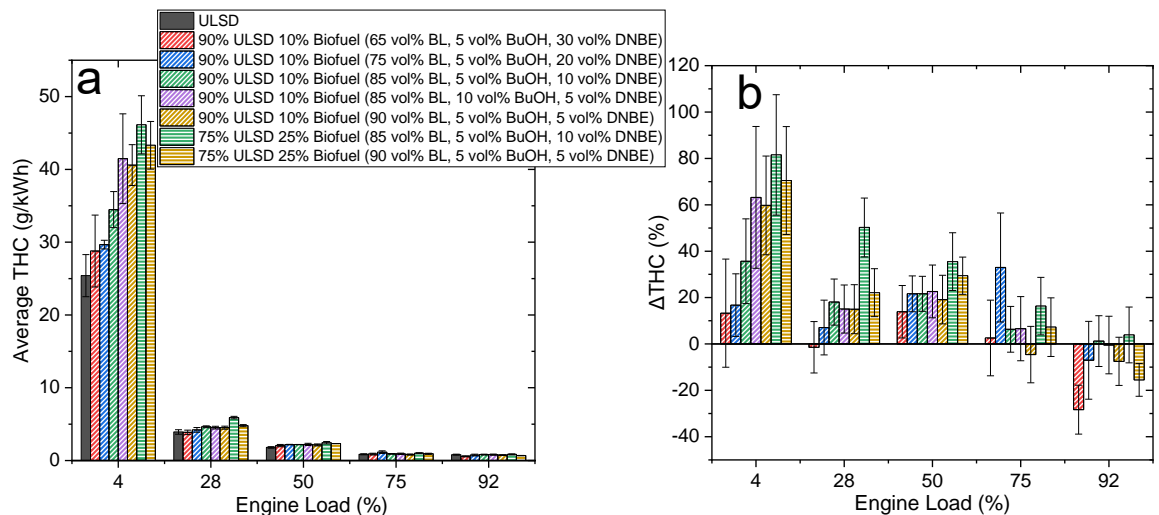
Figure 6.18. a: THC emissions of ULSD and the butyl-based blends. b: Changes in THC emissions relative to ULSD.

There was a greater increase in the THC emissions for the blends with higher BL fractions. This was likely due to the decreasing DCN of the three-component mixtures as the DNBE fraction decreased. The increase in THC emissions was greater at the lower loads, where the peak pressures and temperatures were lower, thus reducing fuel

oxidation. At the higher loads, there may have been little to no change in the emissions, as indicated by the error bars in figure 6.18b. At the lower loads, the longer IDTs reduced the in-cylinder residence time, reducing the complete oxidation of fuel. The delay in the peak HRR with the butyl-based blends at the lower loads, combined with the reduced peak HRR for most of the fuel blends tested (table 5.6), would reduce the complete combustion causing the increase in THC emissions. At the higher loads, THC emissions were reduced or consistent with ULSD. This is favourable since a genset is typically operated at maximum load continuously. The reduction in THC does not fully correlate with the increase in CO emission at 92% load; it suggests there may have been more oxidation of the fuel to form CO and not CO_2.

The fuel blends containing 25 vol% biofuel have a greater increase in THC emissions compared to the 10 vol% biofuel blends at loads <50%. This increase was expected, as the 25 vol% blends would have even lower DCNs and the peak HRR for these two blends was delayed more than for the 10 vol% biofuel blends (table 5.6). In addition, the IDTs for the 25 vol% blends were longer than the 10 vol% blends, which reduces the amount of complete combustion of the fuel. As the load increased, the increase in the THC emissions from the 25 vol% biofuel blends decreased, including a reduction at 92% load. Since a genset is typically run at maximum load and all blends either reduced or maintained the THC emission levels of ULSD, switching to them would be beneficial, as they would contribute significantly to the decarbonisation of genset operation. The changes in the THC emissions when using the butyl-based blends highlighted their suitability compared to the ethyl-based blends, as the ethyl-based blends typically had an increase of around 50% for the blend with DEE, and much greater for the blend with DEE (figure 6.8b). In contrast the butyl-based blends had a lower increase in THC emissions, and even a reduction at 92% load.

6.3.4 Changes in the Volatile Organic Carbon Compounds Emissions when using the Butyl-Based Blends

As with the ethyl-based blends, the VOCs were measured to investigate the implications these advanced biofuels would have on local air quality. The compounds of interest were BuOH, DNBE, formaldehyde, acetaldehyde, and hexane. Table B.2 in the appendices shows the average ppm values of the measured VOC compounds.

Emissions of BuOH were below the detection limits of the FTIR, which indicates that the addition of BuOH to the blends did not cause an increase in tailpipe emissions. Otherwise, there were increases for most compounds of interest. Concentrations of formaldehyde, acetaldehyde, and hexane increased relative to ULSD at loads <50%, as shown in figures 6.19, 6.20, and 6.21, respectively. In contrast, and unexpectedly, the

emissions of DNBE decreased for the butyl-based blends, as shown in figure 6.22. Formaldehyde, acetaldehyde, and hexane are likely to have increased due to increased incomplete combustion. For formaldehyde and acetaldehyde, the increase at lower loads was greater for the blends with higher BL fractions, as these were the blends with longer IDTs. DNBE also produces these two aldehydes during combustion (168, 232, 243, 244). Therefore, the biofuel blends with high DNBE fractions may have high aldehyde emissions if these reaction pathways are favoured, yet this was not the case (168, 232, 243, 244). The studies that determined the aldehyde formation were not engine studies, which indicates that the high temperatures and pressures of the engine may favour more complete oxidation of DNBE and not the aldehyde formation (143, 168, 232, 243, 244). The source of hexane is likely to be the ULSD long-chain hydrocarbon scission and fuel decomposition products. The formaldehyde and acetaldehyde could be from the oxidation pathways of the biofuel components and the hydrocarbons (51, 171). However, it is more likely that there is a direct influence of the increased aldehyde emission and the presence of the oxygenated advanced biofuel components. The increased emissions of formaldehyde and acetaldehyde at low loads, will have a detrimental impact on local air quality as not only are they precursors to photochemical smog, but they are irritant gases, as discussed in section 6.2.5. At >50% load acetaldehyde emissions decreased, and at 92% load formaldehyde reduced, for the lower BL fractions, or maintained the emissions of ULSD as they were within one standard error of a 0% change. Since a genset is typically run at maximum power these changes in formaldehyde and acetaldehyde emissions favour the utilisation of the biofuel blends.
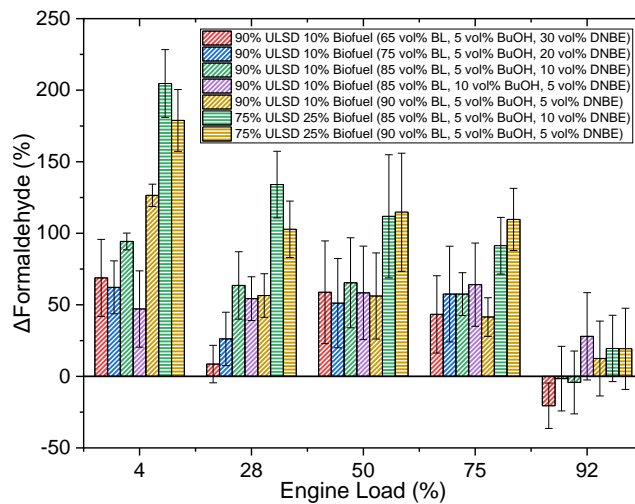
Figure 6.19. Change in formaldehyde emissions relative to ULSD for the butyl-based blends.
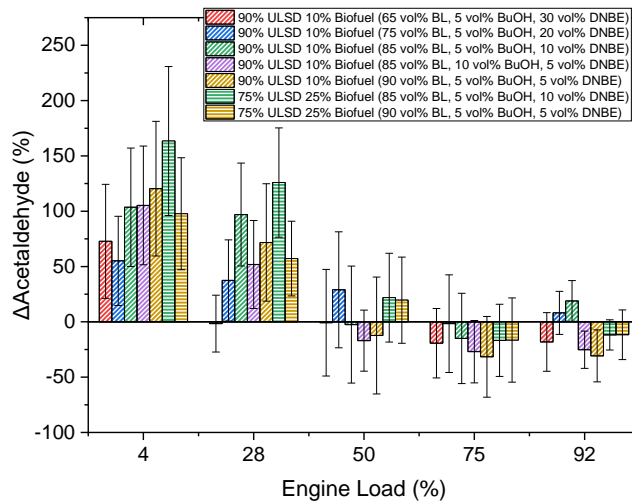
Figure 6.20. Change in acetaldehyde emissions relative to ULSD for the butyl-based blends.

The reduction in the hexane emissions at higher loads may be the influence of the reduced hydrocarbon content relative to diesel, due to the high biofuel fractions. As a result, the formation pathways of the aldehydes are unfavoured, and the hydrocarbons will undergo further reactions as hexane is not formed and more complete combustion occurs (46, 76, 326, 350).
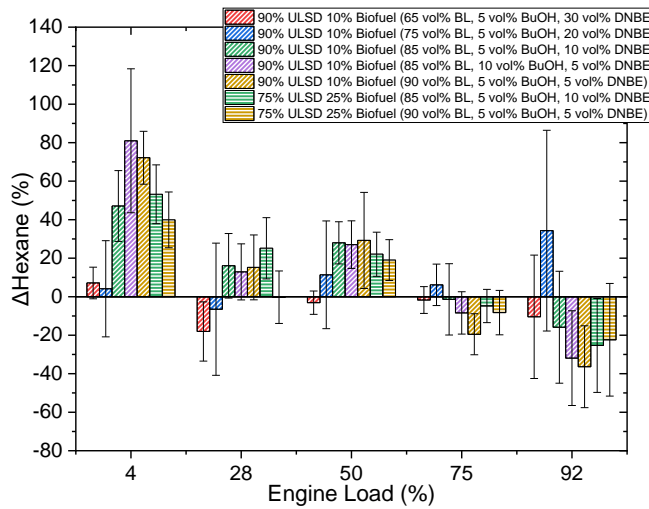
Figure 6.21. Change in hexane emissions relative to ULSD for the butyl-based blends.
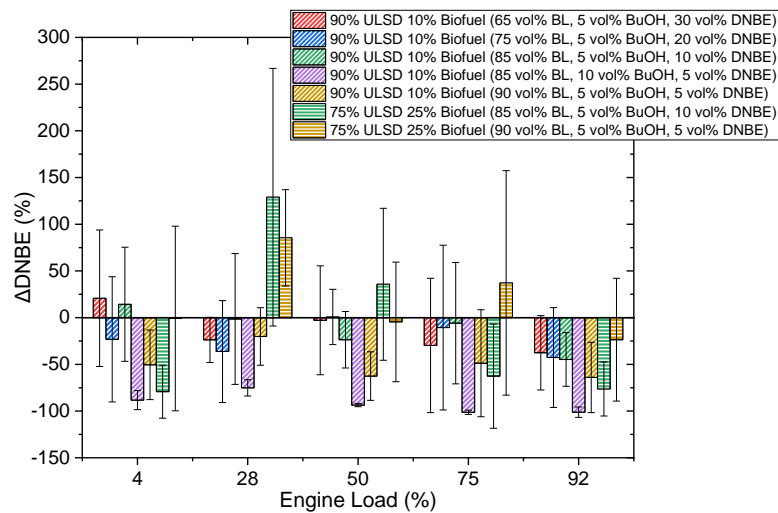
Figure 6.22. Change in DNBE emissions relative to ULSD for the butyl-based blends.

The DNBE emissions are generally reduced relative to ULSD for most biofuel blends across all loads. The higher the BL fraction the greater the reduction in DNBE emissions, which correlates with a reduction of DNBE in the blend. There are large error bars for the changes in the DNBE emissions which indicate that there may have been no change or even an increase in DNBE for some fuel blends at the different loads. When using biofuel blends containing DNBE, the reduction was an unexpected result. Investigations of available ULSD, long hydrocarbon compounds, and biodiesel combustion mechanisms did not present a definitive reason or reactions that form DNBE directly (239, 304, 351, 352). Since the DNBE emissions were low, up to 5 ppm (Appendix B.1), the reductions were within the tolerance of the FTIR.

Overall, the VOCs had a greater reduction at 92% load as the BL fraction increased. This is one advantage of using the butyl-based biofuel blends since a genset is typically operated at maximum power.

6.4 Influence of the Ethyl-Based Biofuel Blends on Emissions of Particulate Matter

The presence of oxygenated biofuels typically reduces PM emissions due to a combination of synergistic impacts of the presence of oxygen, the molecular structures of the oxygenated compounds, lower fraction of aromatic content in the fuel, and the lower DCNs. The reduced DCN favours a longer mixing period, which reduces the rich zones in a cylinder, creating a more homogeneous mixture (40). As without changes in the injection timing, there can be a reduction in PM using oxygenated species (24, 38, 54, 101, 324). Therefore, it would be expected that the ethyl-based blends would reduce the PM emissions as their IDTs increased (section 5.2). This section covers the influence the ethyl-based blends had on PM emissions.

6.4.1 Particle Number Measurements when using the Ethyl-Based Blends

When using the ethyl-based blends, the DMS500 repeatedly gave error messages indicating that the voltage on the charger was above the 4250 V threshold and the current could not be maintained. One possible reason for this may have been the condensation of VOCs and unburnt fuel being fed into the DMS500 sample inlet, as it is at 55 °C. Therefore, the PN and PNSD were not measured for the engine tests using the ethyl-based blends with and without diesel to protect the DMS500.

6.4.2 Changes in $PM_{2.5}$ Emissions when using the Ethyl-Based Blends

One of the most noticeable differences in the $PM_{2.5}$ samples collected on the GF/F filter papers was the colour differences between the diesel $PM_{2.5}$ samples and the samples collected using the ethyl-based biofuel blends. There was a larger difference when the engine was unstable and at lower loads. For the engine tests where there was instability, the filter papers were more yellow, similar to the colour of the fuel blend used. This observation indicated reduced fuel oxidation and fewer soot precursors formed, as no obvious black soot was collected. What was also noticeable was how wet the filter papers were after these engine tests. This moisture could have been a combination of water and unburnt fuel collected, as the sampling was direct from the exhaust. The high THC emissions produced using these fuels (figure 6.7) support this hypothesis. As a result, the unstable engine tests, or those that could only achieve up to 50% load, where the $PM_{2.5}$ mass was substantially large, may need to be treated as anomalous $PM_{2.5}$ results. Therefore, the results from the engine tests using the 25 vol% biofuel blends were excluded from further analysis.

The addition of the ethyl-based three-component blends to diesel caused an increase in $PM_{2.5}$ emissions, with this increase being variable across the loads and fuel formulation, as demonstrated in figure 6.23a. This variability is likely due to the increased amount of unburnt fuel collected onto the filter papers. The blend without DEE only had reductions in $PM_{2.5}$ for engine loads >50%. The relative changes in the $PM_{2.5}$ emissions for the two 15 vol% biofuel blends are shown in figure 6.23b.
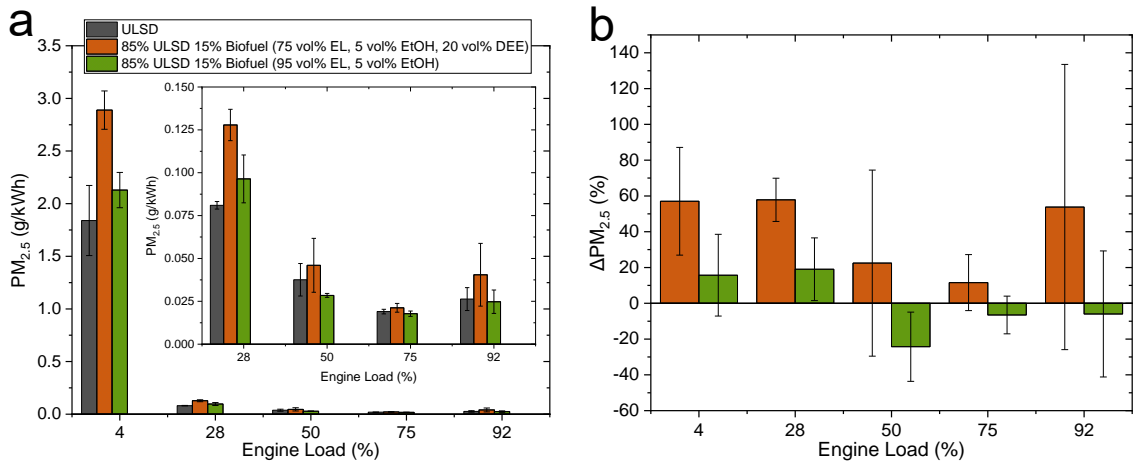
Figure 6.23. a: PM$_{2.5}$ emissions from the two 15 vol% ethyl-based biofuel blends. b: Changes in the PM$_{2.5}$ emissions relative to ULSD.

Given the longer IDTs when using the ethyl-based blends, it would be expected there would be a reduction in PM$_{2.5}$ since there was increased time for premixed combustion (47, 71, 72). This reduction was not the case for most of the ethyl-based blends with ULSD tested and further indicated there may be more unburnt fuel collected on the filter papers. The appearance of the filter papers is shown in figure 6.24. The filter papers for 25 vol% biofuel blends are included to demonstrate the colour difference. Proximate analysis would confirm the increased collection of unburnt fuel and incomplete combustion products as there would be a higher fraction of volatile matter compared to diesel.
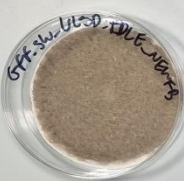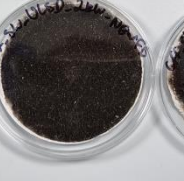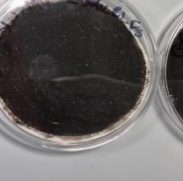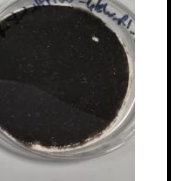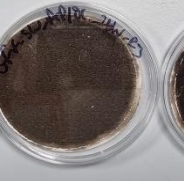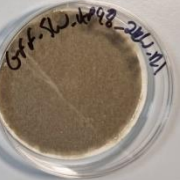
Fuel Blend	4% Load	28% Load	50% Load	75% Load	92% Load
ULSD					
85% ULSD/15 vol% Biofuel (75 vol% EL/5 vol% EtOH/20 vol% DEE)					
85% ULSD/15 vol% Biofuel (95 vol% EL/5 vol% EtOH)					
75% ULSD/15 vol% Biofuel (65 vol% EL/5 vol% EtOH/30 vol% DEE)					
75% ULSD/25 vol% Biofuel (75 vol% EL/5 vol% EtOH/20 vol% DEE)					

Figure 6.24. $PM_{2.5}$ on GF/F filter papers for the ethyl-based blends tested.

6.5 Particulate Matter and the Influence of the Butyl-Based Biofuel Blends

6.5.1 Changes in $PM_{2.5}$ Emissions from using the Butyl-Based Blends

Unlike the ethyl-based blends with diesel, all the butyl-based blends reduced the $PM_{2.5}$ across most loads, other than one blend that had a 1% increase at 92% load. The FJ injector was used when testing the butyl-based blends with ULSD and the changes in $PM_{2.5}$ emissions were relative to the FJ injector ULSD baseline. Therefore, any reduction in $PM_{2.5}$ would be due to the addition of the butyl-based biofuel blends, as shown in figure 6.25. The reduction in $PM_{2.5}$ ranged between 17% and 70% across all loads tested, and this can be observed in figure 6.25c.
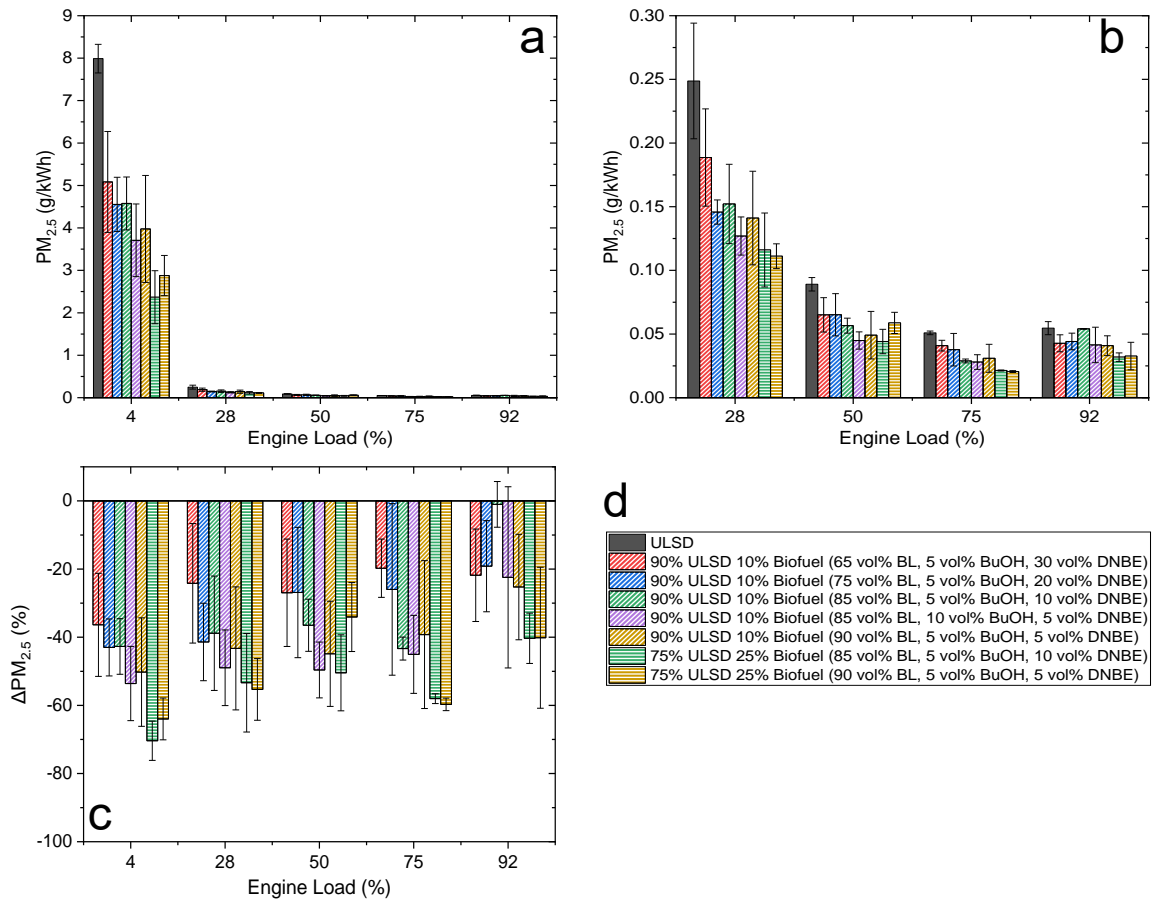
Figure 6.25. PM$_{2.5}$ emissions from the butyl-based blends tested. a: all five loads tested. b: four non-idling loads. c: changes relative to ULSD. d: legend.

The 10 vol% biofuel blends had considerably darker filter papers, compared to the ethyl-based blends tested, whereas the 25 vol% biofuel blends had lighter filter papers. As the load increased, the total amount of PM$_{2.5}$ collected on the filter paper increased and this can be seen with the filter papers becoming darker. However, in figure 6.25, the PM$_{2.5}$ is presented as g/kWh, which reduced as the load increased as more power was generated. The filter papers were not visibly wet after the butyl-based blends' engine tests. The lighter colour of the PM$_{2.5}$ captured indicates there may be a change in the PM$_{2.5}$ composition upon addition of the butyl-based blends, as shown in figure 6.26. The reduction in PM$_{2.5}$ using the 25 vol% biofuel blends was greater still, and this was expected with the higher biofuel content. The delayed peak HRR (tables 5.4 and 5.5) from using the butyl-based blends resulted in lower gas temperatures, which would favour the formation of PM due to less complete combustion (24, 72). However, the addition of biofuel blends would cause a reduction in the particulate matter being formed as the oxygen-containing functional groups prevent the associated carbons from forming PAHs (53). The carbon chain lengths after oxygen containing functional groups will impact soot formation as longer carbon chains favour soot formation (53). The filter paper samples for both 25 vol% blends were a browner colour, compared to the black nature of the 10 vol% blends, as seen in figure 6.26. The change in colour of the PM$_{2.5}$ indicates

the PM$_{2.5}$ formed may not be solely soot, and there may be the presence of unburnt fuel and high molecular weight compound, including oxygenated compounds (72, 353, 354).
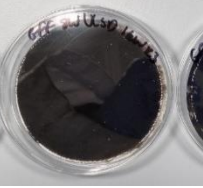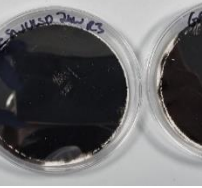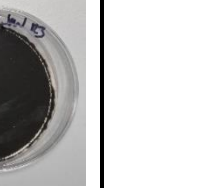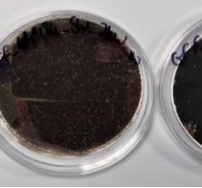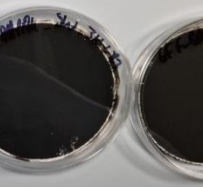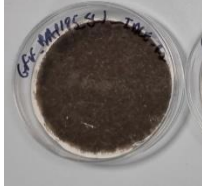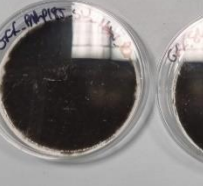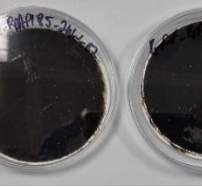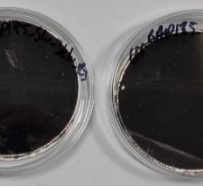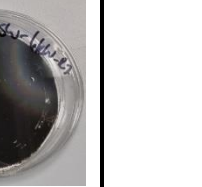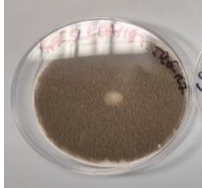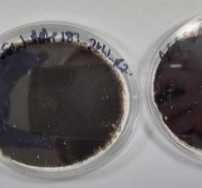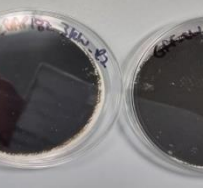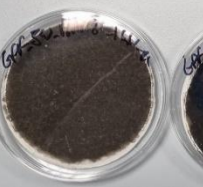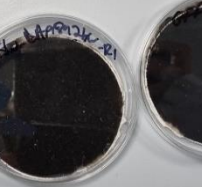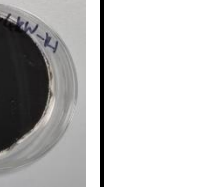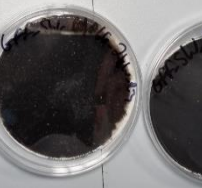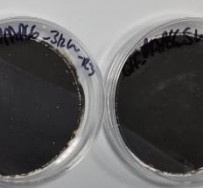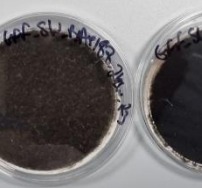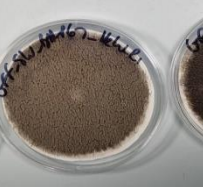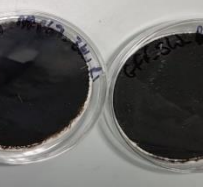
Fuel Blend	4% Load	28% Load	50% Load	75% Load	92% Load
ULSD					
90% ULSD 10% Biofuel (65 vol% BL/5 vol% BuOH/30 vol% DNBE)					
90% ULSD 10% Biofuel (75 vol% BL/5 vol% BuOH/20 vol% DNBE)					
90% ULSD 10% Biofuel (85 vol% BL/5 vol% BuOH/10 vol% DNBE)					
90% ULSD 10% Biofuel (85 vol% BL/10 vol% BuOH/5 vol% DNBE)					
90% ULSD 10% Biofuel (90 vol% BL/5 vol% BuOH/5 vol% DNBE)					
75% ULSD 25% Biofuel (85 vol% BL/5 vol% BuOH/10 vol% DNBE)					
75% ULSD 25% Biofuel (90 vol% BL/5 vol% BuOH/5 vol% DNBE)					

Figure 6.26. PM$_{2.5}$ on GF/F filter papers for the butyl-based blends tested.

Since the butyl-based blends tested resulted in longer IDTs (figure 5.10) the reduction in the $PM_{2.5}$ was to be expected due to increased amounts of premixed combustion. The longer IDTs would allow more time for vaporisation, increased air entrainment, and for the fuel-air mixture to become more homogeneous (72). The increased homogeneity of the fuel-air mixture reduces the number of rich zones in the cylinder where PM is formed (40, 70-73). As the BL fraction in the 10 vol% biofuel blends increased, the $PM_{2.5}$ produced at any given power was reduced. This reduction in $PM_{2.5}$ was likely due to the combination of the reduced DCN of the blends, increasing the premixed combustion, and the molecular composition of the biofuel blends. The increased BL content slightly increased the oxygen content of the fuel blends, as the O/C fuel molar ratio increased from 0.044 to 0.049 with the increasing BL fraction. For the 25 vol% blends, the O/C fuel molar ratio was 0.092 and 0.094 for the 85 and 90 vol% BL blends, respectively. However, the molecular structure of the oxygenated species and their functional groups also contribute towards the reduction in $PM_{2.5}$, as discussed previously in section 6.4.2. The potential combustion pathways of BL are unlikely to promote the formation of soot precursors if the combustion mechanism of EL is used as an indicator (37, 55). There is also the potential of the reduction in the available molecules to form soot precursors upon biofuel addition, causing the reduction in $PM_{2.5}$. However, the formation of soot and PM is complex and the influence of the biofuel blend on soot formation requires fundamental studies.

6.5.2 Changes in PN for the Butyl-Based Blends

The PN measured was the engine out PN since there was no aftertreatment systems on the Yanmar L100V, and these are presented in figures 6.27a and 6.27b. On average, the PN reduced by 72% compared to ULSD for all blends and loads tested, as shown in figure 6.27c. This reduction is likely due to the longer IDTs allowing for more premixed combustion. Additionally, the increased oxygen content in the fuels, as the BL fraction increases, would cause a decrease in PN due to the reduction in the formation of soot precursors. The results in figure 6.27 show a slight correlation between the increasing O/C fuel molar ratio and the reduction in PN for most blends, especially the 10 vol% blends. The O/C fuel molar ratio of the 10 vol% biofuel blends increases from 0.044 to 0.049 with the increasing BL fraction in these blends, which is more than double the 0.02 of ULSD. As a result, the PN emissions reduced relative to ULSD as the fuel-bound oxygen increased, promoting soot precursor oxidation. The influence of the increased O/C fuel molar ratio can be seen more clearly in figure 6.27c, where the reduction in PN emissions increases with increasing BL fraction. The reduction in PN follows the trends in the reduced fuel smoke number (FSN) observed by Antonetti et al. (34) when testing a blend of 10 wt% BL/20 wt% DNBE/70 wt% BuOH at 10, 20, and 30 vol% in diesel. They observed FSN reductions of approximately 20% and 50% with the

10 vol% and 30 vol% biofuel blends, respectively, when testing the fuel blends in their 2-cylinder, 1248 cc engine at 2500 RPM. However, no IDTs were presented in their study. Therefore, no correlation between any longer IDTs, increased premixed combustion, and reduced PM could be assessed. Antonetti et al. (34) discussed that the increased oxygen content upon biofuel addition would reduce the number of rich zones, as well as the effects of lower carbon content in the fuel and the influence of the molecular structure of the oxygenated species on soot precursor formation.
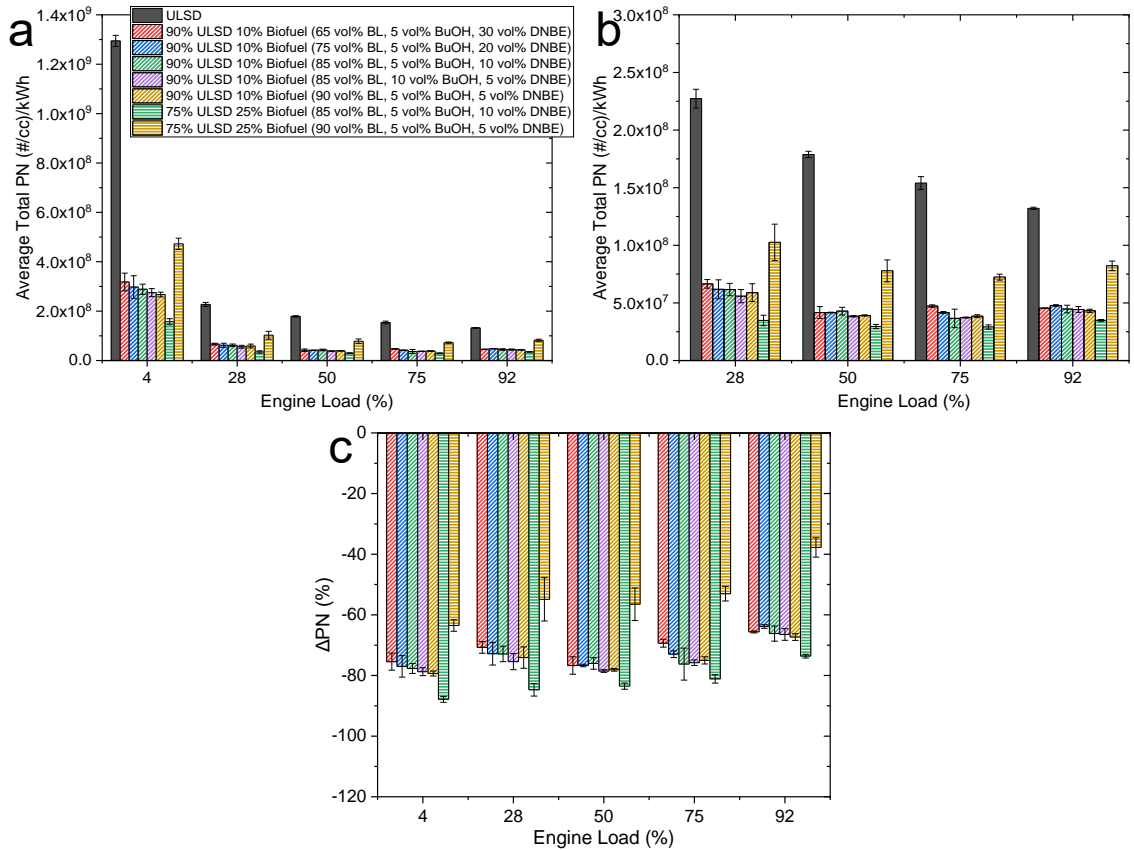
Figure 6.27. a: PN for ULSD and the butyl-based blends tested at all five loads. b: PN for the non-idling loads. c: changes of the PN relative to ULSD.

The reduction in the PN does not show a trend for the different loads, as the reduction in PN is relatively uniform across all engine loads. The 25 vol% biofuel blend with 90 vol% BL did not cause the greatest reduction in PN as it did for $PM_{2.5}$. It had less of a reduction compared to the other butyl-based blends. It would have been expected that there would have been a reduction in PN with the highest BL fraction due to the highest oxygen content. However, the large fraction of BL in the blend reduced the particle sizes but produced more particles, hence the higher PN. These particles may have been semi-volatile droplets due to the temperature of the DMS500 being 55 °C. Therefore, there may have been condensation of these semi-volatile compounds, which caused a lower reduction in total PN compared to ULSD. The particle size distributions are discussed further in section 6.5.3. This blend had lower THC emissions, which may have reduced agglomeration and resulted in more nucleation particles being measured.

As the DNBE fraction decreased in the 10 vol% biofuel blends, the reduction of PN increased which supports the findings of Gao et al. (217). Their findings suggest that the higher the BL fraction, the greater the reduction in soot and not explicitly PN, which may indicate that the total mass of soot may reduce but there are more small particles. On the other hand, Xu et al. (355) stated that esters have the worst soot reduction ability, indicating the blends with high BL fractions would be the ones to have a lesser reduction in PN. For the 25 vol% blends at the higher powers, the results in figure 6.27 are consistent with Xu et al. (355), but for PN and not mass. Overall, the presence of the oxygenated fuel components reduces the formation of soot, but the effects of the fuel molecular structure require further studies (53, 355).

6.5.3 Particle Number Size Distribution Changes when Using the Butyl-Based Biofuel Blends

The effects of the addition of the butyl-based biofuel blends on the PNSD were determined using the method outlined in section 3.7. Figure 6.28 demonstrates how the particle size distribution changes upon the addition of the biofuel blends at 92% and 50% load. The 4%, 28%, and 75% load PNSDs are in Appendix B.2. Other than the 25% biofuel blend with 90 vol% BL, which produced a PNSD that does not follow the trends of the other blends tested, there was an increase in the peak particle size to around 100 nm. This blend was shown to not reduce the PN as greatly as the other blends, and this is evident in figure 6.28, where the area under the curve was greater than the other biofuel blends. This may be due to the high total BL fraction causing the reduction in THC and VOCs reducing the agglomeration of nucleation particles (70-73). The PNSDs also demonstrate that the total PN decreased for all blends as the area under the curve was reduced relative to the solid grey line of the ULSD PNSD. The shape of the distribution has also changed to have a less defined peak number of particles for a given diameter giving a broader distribution over a wider range of diameters. This change in the shape of the PNSD occurred for all biofuel blends across all loads tested. This shift in the PNSD indicated a possible change in the structure of the PM. There may have been a change in the nature of the particle growth occurring as the particle size increased indicating more accumulation particles were produced (70, 356).
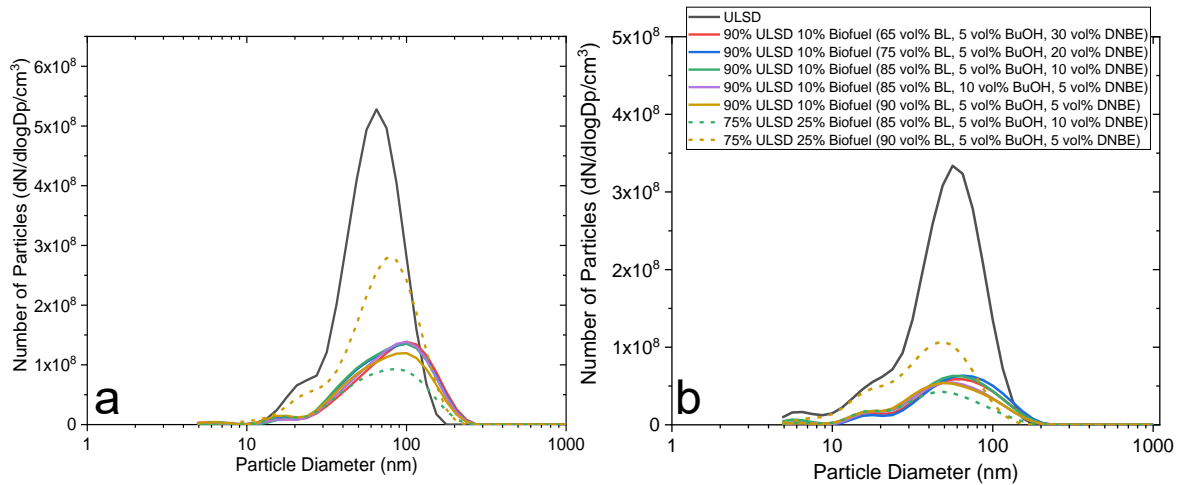
Figure 6.28. Particle size distribution for the butyl-based blends and ULSD. a: at 92% load. b: at 50% load.

The parameters of the fitted distributions (dist) for the PNSDs were determined using the MIX package in the R environment, as outlined in section 3.7, with examples of the fits shown in figures 6.29, 6.30, and 6.31 (281, 282). The histograms in the figures represent the probability density for each particle size, which represents the PN measured by the DMS500 at each defined particle size, and the green line is the sum of the fitted distributions shown by the red lines. The number of distributions chosen for each PNSD ensured an accurate representation of each PNSD at the different loads. A summary of the number of distributions required for each blend at each load are displayed in table 6.2. A detailed breakdown for the 50% load tests is summarised in table 6.3 to demonstrate the changes in the PNSD. When five distributions were needed to improve the fit to the PNSD, it may not be fully representative, as it is unlikely that there would be a fifth mode of particles within such a narrow distribution. A fifth particle mode for exhaust PM has not been reported in the literature, where typically, four modes are reported. Additionally, the DMS500 decreases in reliability and has a higher uncertainty when measuring smaller particles; hence, any distribution centred in this region is likely to have a higher degree of uncertainty. However, MIX could not accurately reproduce the nature of the PNSD without the fifth distribution (figure 6.31). The increased number of distributions used in MIX has been shown by Leys et al. (357) and Tanaka et al. (358) to improve the fits' quality, although these were for distributions of soil sediment and wheat starch granules, respectively, not diesel exhaust particles.
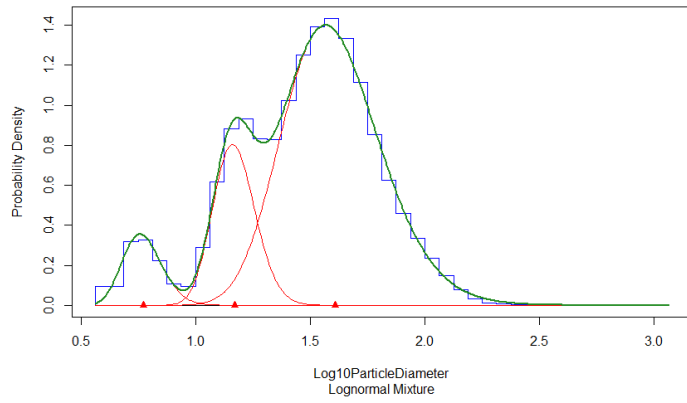
Figure 6.29. PNSD for 75% ULSD 25% biofuel (85 vol% BL/5 vol% BuOH/10 vol% DNBE) at 28% load with three distributions fitted.
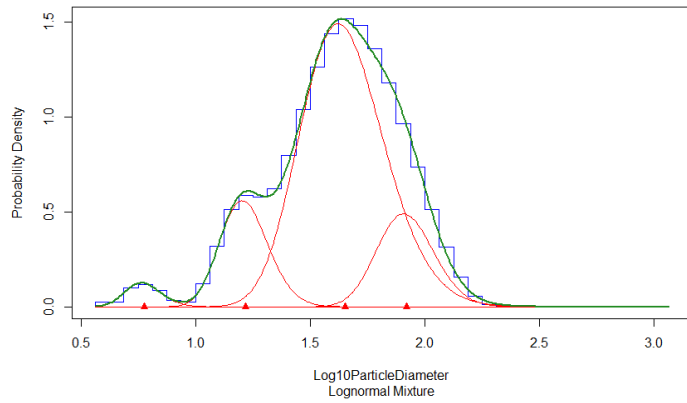
Figure 6.30. PNSD for 90% ULSD 10% Biofuel (90 vol% BL/5 vol% BuOH/5 vol% DNBE) at 28% load with four distributions fitted.
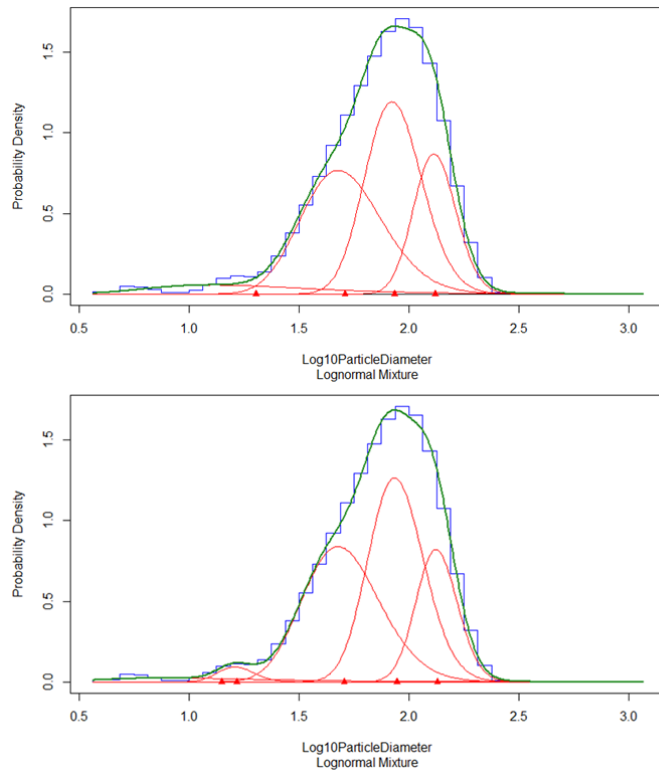
Figure 6.31. Comparison of the five distribution fit (bottom) and the four distribution fit (top), for the PNSD of 90% ULSD 10% Biofuel (65 vol% BL/5 vol% BuOH/30 vol% DNBE) at 92% load.

The addition of the fifth distribution in figure 6.31 resulted in the initial peak for particles <23 nm in diameter (<1.4 $\log_{10}$ particle diameter) being more accurately captured. Particles <23 nm are currently excluded from contributing to the PN in EURO VI/6d and Euro V for NRMM (41-43). However, part of this distribution will be added to the next generation of emissions standards, as the minimum particle size will be reduced to 10 nm (41-43). It is likely there will be a peak in this region due to nucleation particles being formed, and this was evident in figure 6.28. However, the measurement of the PN in this region with the DMS500 may not be as reliable, since the particles are so small they may not be effectively charged as the particles in the exhaust gas are charged as a bulk mixture, which may reduce the effectiveness of their measurement. This may lead to an under estimate in the fraction of the smaller particles in the MIX analysis, as the measured number of smaller particles is less accurate.

From the MIX analysis there was evidence that the number of distributions required increased as engine load and biofuel fraction increased. There was also evidence that the blends with high DNBE fractions had a stronger correlation between the load and number of distributions. For example, the number of distributions increased from 4 to 5 when DNBE was >10 vol% of the biofuel blend and the load increased from 50% to 75%.

The number of distributions in the PNSDs (table 6.2) typically matches the number for ULSD at lower loads, and this is likely due to the large fractions of ULSD in the fuel blend so the biofuel present does not have as great an influence on the number of modes. The increase in the number of distributions at 92% load was needed to capture the nucleation particles. These were usually a small fraction of the total PN, as shown in figure 6.28. The small particles have a low contribution to the total PN, but to accurately reproduce the nature of the PNSD, the fifth distribution needed to be added.

The smaller particles are more of a health concern as they can enter the airways and travel further through the respiratory system, potentially leading to more severe lung damage (66, 70, 77, 101). There is also the potential that such fine particles are liquid droplets of condensed VOCs and unburnt fuel. Since the DMS500 operates at 55 °C, condensation of unburnt fuel can occur (66, 70, 77, 101). Because BL has a boiling point of 238 °C, any unburnt BL could condense.

Table 6.2. Number of distributions fitted for each butyl-based blend with ULSD at the five engine loads. Green cells indicate little to no change in the number of distributions compared to ULSD, blue indicates a reduction, and red indicates an increase.

Load (%)	Fuel	Number of distributions
4	ULSD	4
	90% ULSD 10% Biofuel (65 vol% BL/5 vol% BuOH/30 vol% DNBE)	4
	90% ULSD 10% Biofuel (75 vol% BL/5 vol% BuOH/20 vol% DNBE)	3
	90% ULSD 10% Biofuel (85 vol% BL/5 vol% BuOH/10 vol% DNBE)	3
	90% ULSD 10% Biofuel (85 vol% BL/10 vol% BuOH/5 vol% DNBE)	4
	90% ULSD 10% Biofuel (90 vol% BL/5 vol% BuOH/5 vol% DNBE)	4
	75% ULSD 25% Biofuel (85 vol% BL/5 vol% BuOH/10 vol% DNBE)	3
	75% ULSD 25% Biofuel (90 vol% BL/5 vol% BuOH/5 vol% DNBE)	4
28	ULSD	4
	90% ULSD 10% Biofuel (65 vol% BL/5 vol% BuOH/30 vol% DNBE)	4
	90% ULSD 10% Biofuel (75 vol% BL/5 vol% BuOH/20 vol% DNBE)	4
	90% ULSD 10% Biofuel (85 vol% BL/5 vol% BuOH/10 vol% DNBE)	4
	90% ULSD 10% Biofuel (85 vol% BL/10 vol% BuOH/5 vol% DNBE)	4
	90% ULSD 10% Biofuel (90 vol% BL/5 vol% BuOH/5 vol% DNBE)	4
	75% ULSD 25% Biofuel (85 vol% BL/5 vol% BuOH/10 vol% DNBE)	3
	75% ULSD 25% Biofuel (90 vol% BL/5 vol% BuOH/5 vol% DNBE)	4
50	ULSD	4
	90% ULSD 10% Biofuel (65 vol% BL/5 vol% BuOH/30 vol% DNBE)	4
	90% ULSD 10% Biofuel (75 vol% BL/5 vol% BuOH/20 vol% DNBE)	4
	90% ULSD 10% Biofuel (85 vol% BL/5 vol% BuOH/10 vol% DNBE)	4
	90% ULSD 10% Biofuel (85 vol% BL/10 vol% BuOH/5 vol% DNBE)	4
	90% ULSD 10% Biofuel (90 vol% BL/5 vol% BuOH/5 vol% DNBE)	4
	75% ULSD 25% Biofuel (85 vol% BL/5 vol% BuOH/10 vol% DNBE)	4
	75% ULSD 25% Biofuel (90 vol% BL/5 vol% BuOH/5 vol% DNBE)	4
75	ULSD	4
	90% ULSD 10% Biofuel (65 vol% BL/5 vol% BuOH/30 vol% DNBE)	5
	90% ULSD 10% Biofuel (75 vol% BL/5 vol% BuOH/20 vol% DNBE)	5
	90% ULSD 10% Biofuel (85 vol% BL/5 vol% BuOH/10 vol% DNBE)	5
	90% ULSD 10% Biofuel (85 vol% BL/10 vol% BuOH/5 vol% DNBE)	4
	90% ULSD 10% Biofuel (90 vol% BL/5 vol% BuOH/5 vol% DNBE)	4
	75% ULSD 25% Biofuel (85 vol% BL/5 vol% BuOH/10 vol% DNBE)	5
	75% ULSD 25% Biofuel (90 vol% BL/5 vol% BuOH/5 vol% DNBE)	4
92	ULSD	4
	90% ULSD 10% Biofuel (65 vol% BL/5 vol% BuOH/30 vol% DNBE)	5
	90% ULSD 10% Biofuel (75 vol% BL/5 vol% BuOH/20 vol% DNBE)	5
	90% ULSD 10% Biofuel (85 vol% BL/5 vol% BuOH/10 vol% DNBE)	5
	90% ULSD 10% Biofuel (85 vol% BL/10 vol% BuOH/5 vol% DNBE)	5
	90% ULSD 10% Biofuel (90 vol% BL/5 vol% BuOH/5 vol% DNBE)	5
	75% ULNSD 25% Biofuel (85 vol% BL/5 vol% BuOH/10 vol% DNBE)	5
	75% ULSD 25% Biofuel (90 vol% BL/5 vol% BuOH/5 vol% DNBE)	4

At 50% load, all the blends had the same number of fitted distributions as ULSD, albeit with changes to the modal peak diameter and the fraction of the distribution each mode contributed, as shown in table 6.3. At 92% load, most of the biofuel blends had an increase from the 4 modes ULSD had, up to 5 distributions, as presented in

table 6.4. At 50% load, dist-1 contained the <10 nm particles, other than for the two blends with 25 vol% butyl-based biofuel blends and the 10 vol% biofuel blend with 10 vol% BuOH, where it was between 13.9 nm and 15.8 nm. The data in tables 6.3 and 6.4 demonstrates that the <10 nm diameter particles contribute very little to the overall PNSD, either reducing relative to ULSD or staying similar. The <10 nm region is where the DMS500 has a greater error when measuring PN. Particles less than 11 nm are formed in the first stages of nucleation particle growth, and those <40 nm are larger nucleation particles (72). Distribution 2 accounts for 9 – 22% of the particles generated for the butyl-based biofuel blends at 50% load. The particles in dist-2 at 50% load typically had the peak diameter reduced by up to 10 nm relative to ULSD. Table 6.4 shows that the addition of the butyl-based blends to diesel increases the particle size due to dist-5 having a peak diameter >120 nm, whereas the largest diameter for ULSD was 88.9 nm in dist-4. The reduction in nucleation mode particles, indicated by the reduction in the dist-2 fraction at 50% and 92% load and the reduction in dist-3 particles at 92% load, indicated by the blue in tables 6.3 and 6.4, may be due to the reduced soot precursors formed due to the high BL fractions, and if there is a reduction in the precursors, they cannot undergo nucleation reactions to grow particles. Additionally, particles may agglomerate more readily or more easily condense on existing particles rather than agglomerating, hence there are fewer particles in the primary nucleation fractions, and more are in the agglomeration modes. This may be one potential cause for the requirement of the fifth distribution for the larger agglomeration particles at 92% load.

Table 6.3. 50% load distribution peaks and contributions. Green cells indicate little to no change compared to ULSD, blue indicates a reduction, and red indicates an increase.

Fuel	Dist-1 fraction	Dist-1 peak diameter (nm)	Dist-2 fraction	Dist-2 peak diameter (nm)	Dist-3 fraction	Dist-3 peak diameter (nm)	Dist-4 fraction	Dist-4 peak diameter (nm)
ULSD	0.02	5.9	0.24	26.5	0.50	48.2	0.24	74.0
90% ULSD 10% Biofuel (65 vol% BL/5 vol% BuOH/30 vol% DNBE)	0.02	5.9	0.11	16.2	0.68	51.0	0.20	92.8
90% ULSD 10% Biofuel (75 vol% BL/5 vol% BuOH/20 vol% DNBE)	0.01	5.7	0.09	16.8	0.64	51.3	0.26	94.6
90% ULSD 10% Biofuel (85 vol% BL/5 vol% BuOH/10 vol% DNBE)	0.03	5.7	0.12	16.4	0.68	50.9	0.17	90.0
90% ULSD 10% Biofuel (85 vol% BL/10 vol% BuOH/5 vol% DNBE)	0.04	15.8	0.10	16.9	0.63	45.7	0.22	88.1
90% ULSD 10% Biofuel (90 vol% BL/5 vol% BuOH/5 vol% DNBE)	0.01	5.9	0.15	17.0	0.64	45.5	0.20	91.3
75% ULSD 25% Biofuel (85 vol% BL/5 vol% BuOH/10 vol% DNBE)	0.08	13.9	0.13	16.3	0.62	43.2	0.17	82.6
75% ULSD 25% Biofuel (90 vol% BL/5 vol% BuOH/5 vol% DNBE)	0.13	14.5	0.22	19.9	0.47	42.2	0.19	67.6

Table 6.4. 92% load distribution peaks and contributions. Green cells indicate little to no change compared to ULSD, blue indicates a reduction, red indicates an increase, and purple indicates the addition of a fifth mode.

Fuel	Dist-1 fraction	Dist-1 peak diameter (nm)	Dist-2 fraction	Dist-2 peak diameter (nm)	Dist-3 fraction	Dist-3 peak diameter (nm)	Dist-4 fraction	Dist-4 peak diameter (nm)	Dist-5 fraction	Dist-5 peak diameter (nm)
ULSD	0.02	19.1	0.09	25.3	0.59	57.4	0.30	88.9		
90% ULSD 10% Biofuel (65 vol% BL/5 vol% BuOH/30 vol% DNBE)	0.02	14.2	0.02	16.5	0.37	50.8	0.40	88.5	0.19	134.6
90% ULSD 10% Biofuel (75 vol% BL/5 vol% BuOH/20 vol% DNBE)	0.02	14.7	0.02	15.6	0.44	50.1	0.35	89.3	0.16	134.3
90% ULSD 10% Biofuel (85 vol% BL/5 vol% BuOH/10 vol% DNBE)	0.02	11.6	0.02	15.8	0.38	49.4	0.39	86.1	0.18	130.6
90% ULSD 10% Biofuel (85 vol% BL/10 vol% BuOH/5 vol% DNBE)	0.01	5.7	0.04	15.4	0.22	37.5	0.52	73.4	0.20	120.5
90% ULSD 10% Biofuel (90 vol% BL/5 vol% BuOH/5 vol% DNBE)	0.01	5.6	0.15	30.6	0.35	51.2	0.36	90.7	0.13	136.0
75% ULSD 25% Biofuel (85 vol% BL/5 vol% BuOH/10 vol% DNBE)	0.01	5.6	0.04	16.4	0.44	48.6	0.35	81.8	0.16	124.5
75% ULSD 25% Biofuel (90 vol% BL/5 vol% BuOH/5 vol% DNBE)	0.03	17.3	0.20	30.8	0.51	63.5	0.27	99.3		

The particles with diameters of 40 – 1000 nm are agglomeration particles. CI engines tend to produce particles with peak diameters around 100 nm. The larger coarse mode particles form further downstream from the engine as there has been more time for particles to coalesce (66, 70, 72, 77, 101). At 50% load, there were two distinct accumulation modes, with the first having peak diameters of 45.5 – 51.3 nm for the ULSD and 10 vol% biofuel blends, and 42.2 and 43.2 nm for the 25 vol% biofuel blends. For the 25 vol% biofuel blends, the diameter of the dist-3 particles reduced relative to ULSD. For the 10 and 25 vol% biofuel blends, the particles in the third mode accounted for at least 57% of the particulate matter. The fourth distribution had an increased peak diameter for all the blends, apart from the 25% biofuel blend with 90 vol% BL. The increased diameters ranged between 82.6 and 94.6 nm compared to the ULSD diameter of 74.0 nm, whereas the 25% biofuel blend with 90 vol% BL had a reduction in the fourth mode diameter, down to 67.6 nm. The increased size of the accumulation particles may be due to the increased THC and VOC emissions, which could also condense onto the surface of particles. The oxygenated compounds increase intermolecular interactions and favour particle coalescence (72). When using the butyl-based blends, the emissions of gaseous oxygenated VOCs increased. However, these were only the species in the FTIR library and it is likely there would be other oxygenated incomplete combustion products when using the biofuel blends, some of which may be high molecular weight compounds that could condense and be a component of the PM collected. The presence of these compounds could be confirmed using further chemical analysis techniques, such as gas chromatography, on the collected $PM_{2.5}$. Oxygenated compounds will have stronger intermolecular forces than Van der Waals interactions, favouring the growth of larger accumulation mode particles (72). Larger particles would typically be removed by a DPF, as they are highly efficient at removing PM, as demonstrated by Wu et al. (318). The efficiency of a DPF is dependent on many factors including the pore and particle size. DPFs have been shown to have high removal efficiencies of particles of 10 to 1000 nm in diameter. Some DPFs have been shown to be highly effective at removing sub-100 nm particles, whilst reducing for particles >100 nm, but this depends on the DPF construction (5, 318).

The particle size typically increases upon the addition of the butyl-based blends, as shown in figure 6.28. Table 6.5 summarises the largest peak diameter for each fuel blend at all loads as determined using the MIX package (282). When under load, the particle size also increased when using the butyl-based biofuel blends, as shown by the large area of red in table 6.5. Compared to diesel, there was a considerable increase in the particle sizes at 75% and 92% load when using the butyl-based biofuel blends. Since these particles are over 100 nm, it indicates that the addition of the butyl-based blends favours the growth of larger particles.

Table 6.5. Summary of the largest distribution peak diameters. Green indicates little to no change, blue indicates a reduction, and red indicates an increase in the diameter relative to ULSD.

Fuel	Largest Distribution Peak Diameter				
	4% load (nm)	28% load (nm)	50% load (nm)	75% load (nm)	92% load (nm)
ULSD	60.3	67.5	74.0	70.5	88.9
90% ULSD 10% Biofuel (65 vol% BL/5 vol% BuOH/30 vol% DNBE)	83.0	86.9	92.8	125.3	134.6
90% ULSD 10% Biofuel (75 vol% BL/5 vol% BuOH/20 vol% DNBE)	47.6	84.3	94.6	120.2	134.3
90% ULSD 10% Biofuel (85 vol% BL/5 vol% BuOH/10 vol% DNBE)	45.4	81.1	90.0	116.7	130.6
90% ULSD 10% Biofuel (85 vol% BL/10 vol% BuOH/5 vol% DNBE)	67.6	84.7	88.1	123.0	120.5
90% ULSD 10% Biofuel (90 vol% BL/5 vol% BuOH/5 vol% DNBE)	61.4	83.2	91.3	95.3	136.0
75% ULSD 25% Biofuel (85 vol% BL/5 vol% BuOH/10 vol% DNBE)	56.2	44.1	82.6	110.9	124.5
75% ULSD 25% Biofuel (90 vol% BL/5 vol% BuOH/5 vol% DNBE)	58.4	69.2	67.6	82.8	99.3

The size of PM typically produced from a CI engine fuelled with diesel is highly variable; depending on many factors including EGR rate, fuel injector design, injection timing, and fuel chemistry. Hence it can be difficult to compare PNSDs from different studies. There are typical peaks in PNSDs centred on the 80 – 120 nm region. However, diameters can reach up to 700 nm depending on the engine tested. For example, a Euro 5 Iveco 3.0 L turbocharged engine has been shown to produce engine out particles with diameters up to 700 nm, and even downstream of the DPF there are thousands of particles of this diameter (70, 72, 73, 318). The emissions standards limit the PN for particles >23 nm in diameter for all three of the aforementioned emissions standards. Therefore, the smaller particles that contribute to the total PN are not currently regulated (41-43). Euro 7 will reduce the PN number definition to include solid particles of diameters >10 nm and this will likely cause the reported PN to increase, making it difficult to meet the stricter limits (95, 96). However, the smaller particles measured in this work may be volatile and semi-volatile droplets that would be removed when the exhaust gas is thermally conditioned to contain only solid particles. Therefore, new vehicles may need improved aftertreatment systems to meet the tighter Euro 7 limits. The other option would be to use fuels that reduce the total PN, such as those shown in this work.

6.6 Influence of the Injector Design on the Emissions

The influence of the fuel injector design on the emissions from the Yanmar L100V engine was investigated. This investigation was conducted using the butyl-based blend of 75 vol% ULSD 25 vol% biofuel (85 vol% BL/10 vol% DNBE/5 vol% BuOH) as this was

the blend with the highest biofuel content that could be tested at the time. The aim was to distinguish differences and similarities in the performance of both fuel injectors, as the changes in emissions relative to the corresponding diesel baseline were compared.

6.6.1 Influence of the FB Injector on CO Emissions

When the FB injector was used, there was an increase in CO emissions relative to ULSD. Overall, both injectors resulted in similar trends across each load, with an increase in CO emissions for each load. However, at lower loads, the increase in CO was lower when using the FB injector compared to using the FJ injector, as shown in figure 6.32. The engine could not achieve the 50% load to generate a stable 2 kW of electrical power using the FB injector. The CO emissions when using the FB injector at 92% load had a greater increase than the FJ injector did (figure 6.32). This increase was unexpected since there would be smaller droplets with the FB injector, favouring more complete combustion. The increase in CO emissions at the higher loads with the FB injector is likely still due to the decreased DCN of the fuel blends and the longer IDTs.
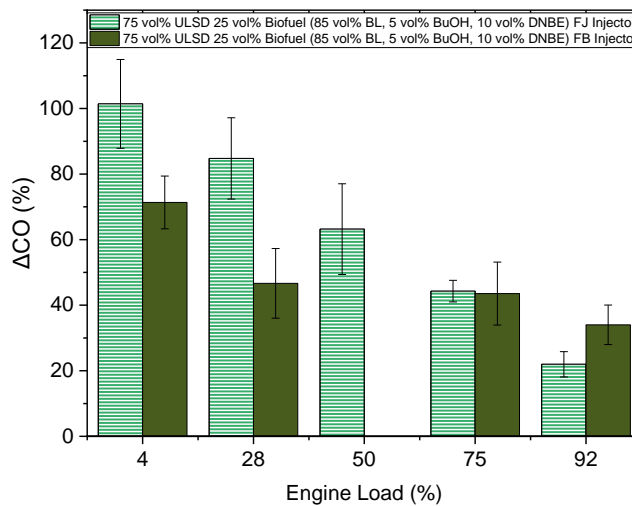
Figure 6.32. Change in CO relative to ULSD using the FJ and FB injectors with the butyl-based blend.

6.6.2 Influence of the FB Injector on NO$_X$ Emissions

When the FB injector was used for the selected butyl-based blend test, the reduction in NO$_X$ at 4%, 28% and 75% load was greater than when using the FJ injector. At 92% load, the increase in NO$_X$ is lower with the FB injector compared to the FJ injector, as shown in figure 6.34. The greater reduction compared to ULSD when using the FB injector does not follow the findings of Sayin et al. (322), where NO$_X$ increased as the number of injector holes increased. In contrast, Lee et al. (323) reported that increasing the number of injector holes may create more local rich zones reducing NO$_X$ production. However, with additional fuel jets from smaller orifices, there may be fewer rich zones due to increased air/fuel mixing due to increased turbulence generated upon fuel

injection. This increased mixing favours NO_X production, since thermal NO_X increases between φ=0.5 and φ=1.1, peaking just above stoichiometric conditions, and with increased mixing it is likely there are more regions with these equivalence ratios (359). Dec (360) and Dempsey et al. (359) demonstrated that regions of high equivalence ratios, typically at the fuel jet core, promote soot formation, whereas the lower equivalence ratios at the boundary layer between the fuel jet and high temperature air favour NO_X formation, as shown in figure 6.33 (340, 359-361).
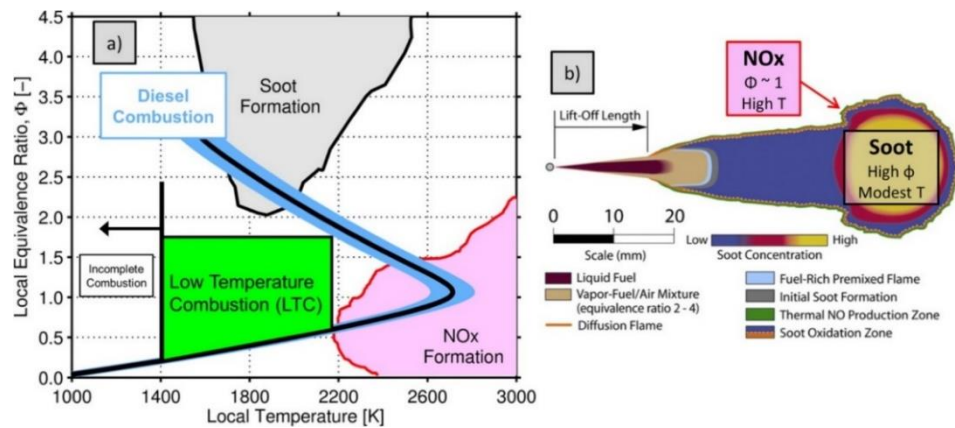
Figure 6.33. a: Temperature and equivalence ratio dependence of NO_X formation from (340). b: Conceptual model of diesel combustion of Dec (360) and Musculus et al. (361). Reproduced from (359).

If this were the case, it would be expected that an increase in the number of fuel injector holes would result in increased NO_X emissions. However, this did not occur when using the FB injector with the butyl-based blend. The NO_X emissions had a smaller increase at 92% load with the FB injector than with the FJ injector relative to their corresponding diesel baselines, as seen in figure 6.34. An additional contribution to this smaller increase when using the FB injector would be the higher enthalpy of vaporisation of the butyl-based blend, causing a greater cooling effect due to its better atomisation (322, 323, 343). Therefore, there are synergistic effects that reduce NO_X emissions and the changes in NO_X emissions are injector and fuel dependent.

Since both the fuel injector design and fuel blend formulation result in changes in NO_X emissions, there may be scope to optimise the effects of both to favour NO_X reduction. However, the variety of different fuel injector designs and engine technologies available may give different trends in NO_X emissions. This is where simulations would be a useful tool, as rapid investigations of injector designs could be conducted and their influence on NO_X emissions could be determined.
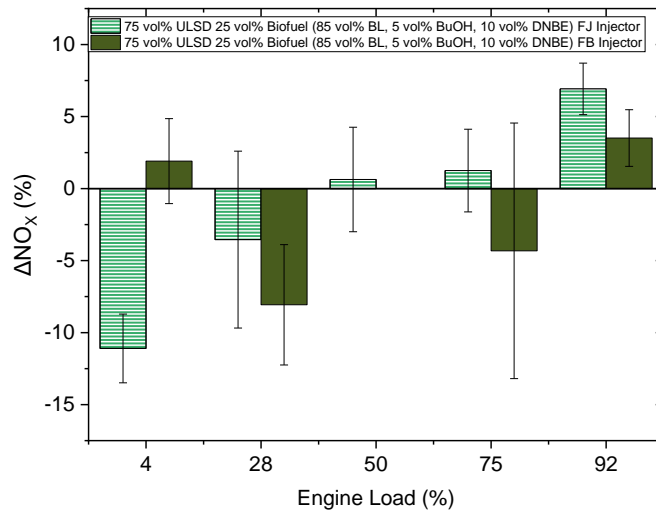
Figure 6.34. Change in NO$_X$ relative to ULSD using the FJ and FB injectors with the butyl-based blend.

6.6.3 Influence of the FB Injector on THC Emissions

For both fuel injectors there was a gradual decrease in the change in THC emissions as engine load increased. For the FB injector the increase at lower loads was at a lower percentage than the FJ injector tests. This smaller increase would have been due to better atomisation of the fuel using the FB injector due to its smaller injector holes, favouring more complete combustion (322). For ≤75% load, there was an increase, albeit it was not as large as when using the FJ injector, as shown in figure 6.35.
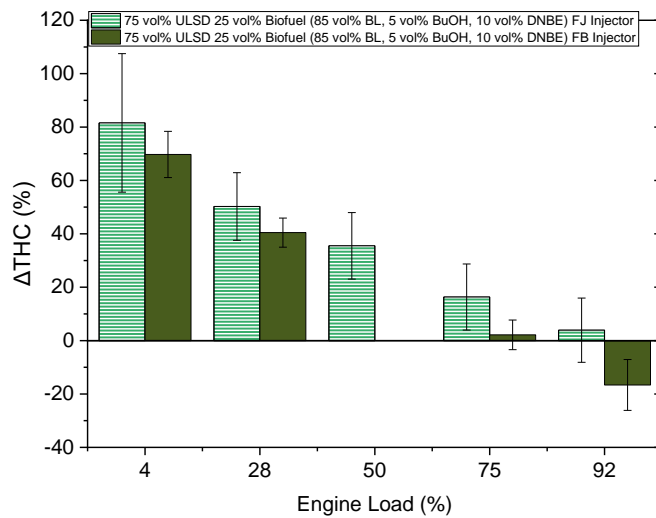
Figure 6.35. Change in THC relative to ULSD using the FJ and FB injectors with the butyl-based blend.

At 92% load, there was a reduction in THC emissions with the FB injector. The lower increases at lower loads in THC emissions with the FB injector correlate to the lower increases in CO emissions indicating that the improved fuel atomisation enhances the combustion as expected. Therefore, there has been more complete combustion of the fuel and this is supported by the lower increase in the fuel consumption (figure 5.14).

The genset would only operate at low loads during start-up, but a lower increase with the FB injector would be beneficial as it would be less detrimental to air quality.

6.6.4 Influence of the FB Injector on the $PM_{2.5}$ Emissions

When the butyl-based blend was tested using both injectors, there was a reduction in $PM_{2.5}$ when the engine was under load. There was less $PM_{2.5}$ generated when using the FB injector and this can be seen when comparing the $PM_{2.5}$ emissions shown in figure 6.36a. The $PM_{2.5}$ emissions were reduced relative to the FB injector ULSD baseline by up to 60% when using the butyl-based blend for most loads. However, at 4% load, there was an increase in $PM_{2.5}$ emissions of 19%, as shown in figure 6.36b. The increase at the idling condition would only affect the start-up and since the genset typically operates at maximum load, the reduction in $PM_{2.5}$ is favourable regardless of the injector used. With the FB injector, the reduction increased as the load increased, whereas for the FJ injector the reduction gradually decreased as the load increased. The reduction in the differences at higher loads was likely due to there being more fuel being injected and the lower RPM allowing for more oxidation of the fuel. This correlates with the increase in CO and reduction in THC emissions, indicating there may have been fewer soot precursors formed at the high loads.
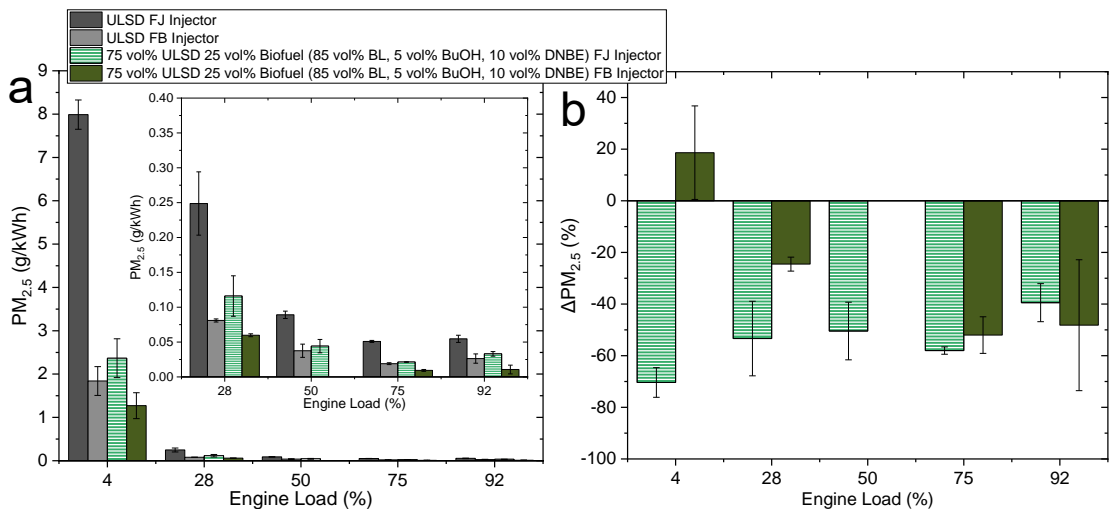
Figure 6.36. a: $PM_{2.5}$ emissions from the FJ and FB injectors. b: Changes in $PM_{2.5}$ relative to ULSD for the FJ and FB injectors for the butyl-based blend.

There was only a 26% reduction at 28% load with the FB injector versus a 53% reduction with the FJ injector. At 92% load, the reduction of $PM_{2.5}$ relative to ULSD was greater with the FB injector. The reduction in $PM_{2.5}$ was 50% with the FB injector compared to that of 40% from the FJ injector. The differences in the IDTs between the ULSD and biofuel blend when using the two different injectors was similar. The smaller holes of the FB injector will improve fuel atomisation as smaller droplets are formed, increasing the vaporisation rate, which would then favour a more homogenous air/fuel mixture. The increased homogeneity of the air/fuel mixture will reduce the number and

volume of any rich zones in the cylinder, which will reduce the soot formation. Therefore it is not just the fuel atomisation and premixed combustion, but the molecular structures of the biofuel components that reduce the formation of soot and PM (24, 72).

6.6.5 Influence of the FB Injector on PN

For the FJ and FB injector the PN was reduced when using the butyl-based biofuel blend and the engine was at >4% load. However, when the FB injector was used there was an increase at the idling condition of 4% load, as shown in figure 6.37a. The reduction in the PN from the butyl-based biofuel blend when using the FB injector was not as great as when using the FJ injector. This small reduction may be due to the low PN generated in the ULSD baseline with the FB injector, as shown in figure 6.37b. The FB injector's smaller holes would have produced a spray with finer droplets, improving the fuel vaporisation. However, there was an increase in the smaller particles produced with the FB injector. The reduction in PN is still likely an effect of the reduced DCN due to the addition of the butyl-based biofuel, giving longer IDTs allowing for more premixed combustion and the oxygenated biofuel species molecular structures reducing soot precursors (355).
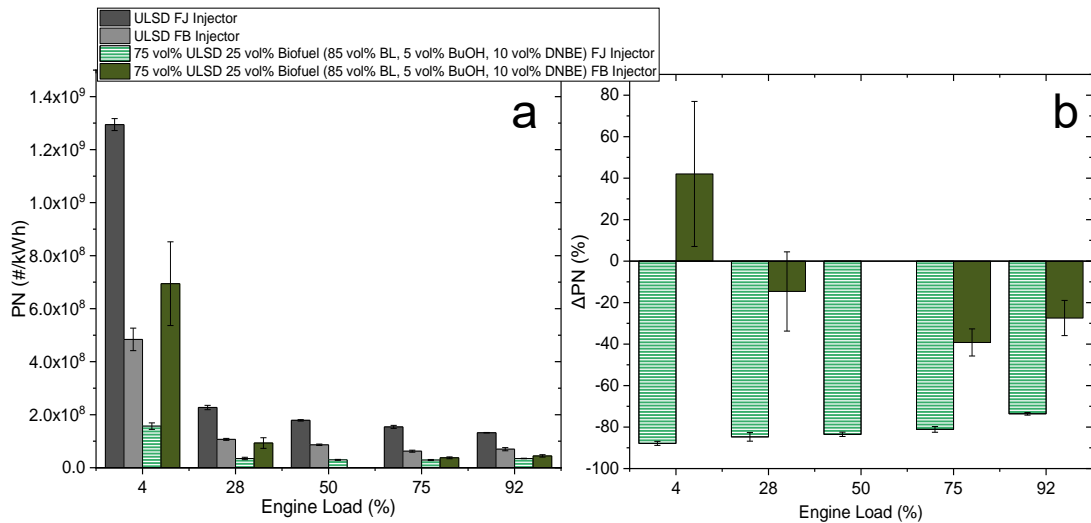
Figure 6.37. a: PN for ULSD and the butyl-based blend using the FJ and FB injectors. b: Changes in PN relative to the corresponding ULSD baseline.

6.6.6 Overall Influence of the Fuel Injector Design on the Emissions

The relative changes in the emissions are dependent on the injector design. Since the use of the FB injector ensured the Yanmar L100V engine complied with the Euro Stage V emissions standard, the diesel baseline emissions were lower than those using the FJ injector. CO emissions increased when using both injectors with the butyl-based biofuel blend, albeit with a lower increase with the FB injector. As the load increased, the relative change decreased for both CO and THC emissions with both injectors. However, at 92% load, the CO emissions had a greater increase when using the FB injector. This

increase coincides with reduced THC emissions at 92% load when using the FB injector, indicating there was increased fuel oxidation but not complete combustion.

The NO_X emissions using both injectors have a similar trend at >28% load, where the reduction in the NO_X emissions decreased and became an increase with increasing engine load. The behaviour was more prevalent using the FJ injector since the FB injector creates smaller fuel droplets and enhances the charge cooling effect, thus reducing the NO_X emissions (340, 359-361). At 92% load, both injectors had an increase in NO_X emissions, which may have been due to BL having the highest adiabatic flame temperature (table 2.8).

For the PM emissions, there was a significant reduction in mass when using the biofuel blends with both injectors when the load was >28%. The $PM_{2.5}$ and PN had greater reductions as the load increased when using the FB injector, whereas using the FJ injector there were similar, but larger, reductions for each engine load.

Overall, the influence of the injector design would need to be tested with other biofuel blends to confirm its influence on the emissions from the Yanmar L100V engine.

6.7 Suitability of the Blends for Blending with Diesel and their Feasibility to be Drop-In Fuels

To determine if the fuels tested could be drop-in fuels, the emissions indices of the Yanmar L100V were determined when using the fuel blends. The emissions indices of each fuel blend were compared to the limits for a 0 – 8 kW direct-injection air-cooled CI engine in the Euro stage V emissions standard (42). The PM in the emissions standard is total particulate matter, not solely $PM_{2.5}$ as measured in this work. However, it is unlikely there would be a large quantity of particulate matter with an aerodynamic diameter greater than 2.5 µm (47, 71, 72, 362).

For the ethyl-based blends tested, only the two fuel blends that could achieve all five engine loads could have their emissions indices calculated, and these are summarised in table 6.6. The changes in the indices are in table 6.7. The 85% ULSD 15% biofuel (95 vol% EL/5 vol% EtOH) has a NO_X+THC emission factor comparable to the ULSD emission factor. The Yanmar L100V engine used in this work did not meet its certification when fuelled with an EN 590 compliant ULSD (table 6.6), as the CO and NO_X+THC emissions were above the limits (42). This may have been due to the age and prior use of the engine, which may have resulted in the non-compliance. Therefore, any change in the emissions was from a high baseline. Therefore, if the engine was compliant and below the limits, there may have been scope to have emissions with the biofuel blends closer to the limits or potentially comply with the Euro Stage V emissions standard (42).

Table 6.6. Emissions indices for the ethyl-based blends with ULSD. Those in red show non-compliant emissions.

Fuel	CO (g/kWh)	NO$_X$+THC (g/kWh)	NO$_X$ (g/kWh)	THC (g/kWh)	PM (g/kWh)	PN (#/kWh)
Stage V Limits	<8.0	<7.50			<0.600	
ULSD FB Injector	9.41±1.02	11.05±0.96	9.14±1.35	1.91±0.39	0.128±0.03	(1.10±0.20)×10^8
85% ULSD 15% Biofuel (75 vol% EL/5 vol% EtOH/20 vol% DEE)	12.13±0.93	12.08±2.91	8.56±0.68	3.52±0.36	0.196±0.05	
85% ULSD 15% Biofuel (95 vol% EL/5 vol% EtOH)	11.75±0.98	11.14±0.59	8.14±0.62	3.00±0.70	0.146±0.02	

Table 6.7. Changes in the emissions indices for the ethyl-based blends with respect to ULSD.

Fuel	ΔCO (%)	ΔNO$_X$+THC (%)	ΔNO$_X$ (%)	ΔTHC (%)	ΔPM (%)
85% ULSD 15% Biofuel (75 vol% EL/5 vol% EtOH/20 vol% DEE)	+28.93±17.09	+9.37±27.99	-6.37±15.73	84.78±42.28	+53.80±51.80
85% ULSD 15% Biofuel (95 vol% EL/5 vol% EtOH)	+24.92±17.06	+0.82±10.24	-10.94±14.83	57.10±48.75	+13.94±32.72

The NO_X+THC emissions when using the FB injector and ULSD were non-compliant, whereas the CO emissions were within one standard error of the limit. When using either 15 vol% biofuel ethyl-based blends, the engine was not compliant with the emissions standard limits for CO and NO_X+THC. In contrast, the PM emission indices were well below the limits, even with an increase in PM relative to diesel with the ethyl-based blends. The THC and CO emissions had large increases when the engine was unstable. Therefore, there must be stable engine operation to minimise any increases in CO and THC emissions. As a result, there should be <3 vol% DEE in the final blend.

The emission indices from the butyl-based blends when using the FJ injector are summarised in table 6.8, along with the comparison of both fuel injectors used. What is evident from table 6.8 is that the engine, regardless of the fuel, does not comply with the Euro V emissions standard limits, although the CO emissions are within one standard error of the Euro V limit of 8.00 g/kWh (42). This non-compliance of this engine may be due the compliance being determined on a pool of engines and not this specific engine. The baselines were comparable to previous researchers' baselines and used new FJ and FB injectors. This compliance with the CO emissions limit was when using the FJ injector, which the L100V engine was not supposed to use, and not the FB injector. When using the FB injector, the CO and NO_X+THC emissions were non-compliant. It is unclear why changing to the FB injector would cause the emissions of CO to increase as the injector holes are smaller, and there are five holes, which should produce a fuel spray with smaller droplets. The smaller droplets should allow the fuels to vaporise more readily, and reduce the IDT and the CO emissions, but this was not the case here.

In table 6.9, it can be seen that CO emissions increased as the BL fraction increased and the DNBE fraction decreased. When the biofuel fraction increased up to 25 vol% for the 85 vol% BL/5 vol% BuOH/10 vol% DNBE and 90 vol% BL/5 vol% BuOH/ 5 vol% DNBE blends the change in CO is 2.1 and 2.5 times greater than the 10 vol% blends, respectively. This increase was due to the decreased DCN with the increased biofuel fractions, as demonstrated by the increased IDTs (13, 38, 143).

The change in the NO_X+THC emissions is more variable due it being the combination of the two. The largest contributor to this increase is the increased THC emissions since the NO_X emissions had small changes (table 6.9). There is an offset due to the NO_X emissions not increasing due to lower combustion temperatures, with the engine not being optimised around the longer IDTs. If the engine were optimised to maintain the same performance as ULSD, there would be a reduction in THC emissions but an increase in thermal NO_X production that must be managed. NO_X emissions from diesel vehicles and larger stationary engines are controlled using SCR. The use of SCR may be required for smaller engines if there is an increase in NO_X emissions.

Table 6.8. Emissions indices for the butyl-based blends with ULSD. Those in red show non-compliance, and blue to show those that are within one standard error of the Euro Stage V limit.

Fuel	CO (g/kWh)	NO$_X$+THC (g/kWh)	NO$_X$ (g/kWh)	THC (g/kWh)	PM (g/kWh)	PN (#/kWh)
Stage V Limits	<8.0	<7.50			<0.600	
ULSD FJ Injector	8.23±0.50	11.57±0.78	7.71±0.79	3.85±0.92	0.490±0.09	(2.49±0.38)×10^8
90% ULSD 10% Biofuel (65 vol% BL/5 vol% BuOH/ 30 vol% DNBE)	9.42±1.00	11.12±1.52	7.09±0.77	4.02±1.65	0.338±0.08	(6.92±0.98)×10^7
90% ULSD 10% Biofuel (75 vol% BL/5 vol% BuOH/20 vol% DNBE)	10.14±0.61	11.72±1.01	7.38±0.69	4.33±1.35	0.287±0.06	(6.54±1.27)×10^7
90% ULSD 10% Biofuel (85 vol% BL/5 vol% BuOH/10 vol% DNBE)	11.34±0.82	12.66±1.07	7.87±0.95	4.78±1.48	0.295±0.07	(6.43±1.05)×10^7
90% ULSD 10% Biofuel (85 vol% BL/10 vol% BuOH/5 vol% DNBE)	10.85±0.69	12.44±1.09	7.54±1.01	4.90±1.71	0.230±0.06	(5.88±0.93)×10^7
90% ULSD 10% Biofuel (90 vol% BL/5 vol% BuOH/5 vol% DNBE)	11.12±0.69	12.93±0.95	8.07±0.99	4.85±1.73	0.253±0.08	(6.04±0.76)×10^7
75% ULSD 25% Biofuel (85 vol% BL/5 vol% BuOH/10 vol% DNBE)	14.69±1.26	13.48±0.96	7.44±1.47	6.02±1.97	0.181±0.05	(3.83±1.47)×10^7
75% ULSD 25% Biofuel (90 vol% BL/5 vol% BuOH/5 vol% DNBE)	15.58±1.67	13.01±1.25	7.89±2.01	5.31±2.07	0.190±0.07	(1.08±0.16)×10^8
ULSD FB Injector	9.41±1.02	11.05±0.96	9.14±1.35	1.91±0.39	0.128±0.03	(1.10±0.20)×10^8

Table 6.9. Changes in the emissions indices for the butyl-based blends relative to the ULSD baseline.

Fuel	ΔCO (%)	ΔNO$_X$+THC (%)	ΔNO$_X$ (%)	ΔTHC (%)	ΔPM (%)	ΔPN (%)
90% ULSD 10% Biofuel (65 vol% BL/5 vol% BuOH/30 vol% DNBE)	+14.4±14.1	-3.9±14.7	-8.0±13.7	4.4±49.7	-31.0±21.4	-72.3±5.7
90% ULSD 10% Biofuel (75 vol% BL/5 vol% BuOH/20 vol% DNBE)	+23.2±10.6	+1.3±11.1	-4.2±13.2	12.5±44.1	-41.4±15.9	-73.8±6.5
90% ULSD 10% Biofuel (85 vol% BL/5 vol% BuOH/10 vol% DNBE)	+37.7±13.1	+9.4±11.8	2.1±16.1	24.2±48.6	-39.9±18.6	-74.2±5.7
90% ULSD 10% Biofuel (85 vol% BL/10 vol% BuOH/5 vol% DNBE)	+31.8±11.6	+7.5±11.9	-2.2±16.4	27.3±53.8	-53.0±14.5	-76.4±5.2
90% ULSD 10% Biofuel (90 vol% BL/5 vol% BuOH/5 vol% DNBE)	+35.1±11.8	+11.7±11.2	4.8±16.7	26.2±54.2	-48.5±19.5	-75.8±4.8
75% ULSD 25% Biofuel (85 vol% BL/5 vol% BuOH/10 vol% DNBE)	+78.4±18.9	+16.5±11.4	-3.4±21.4	56.5±63.3	-63.2±12.3	-84.6±6.3
75% ULSD 25% Biofuel (90 vol% BL/5 vol% BuOH/5 vol% DNBE)	+89.3±18.5	+12.5±13.2	2.4±28.0	38.1±63.1	-61.2±15.2	-56.6±9.1

Comparing the two 10 vol% biofuel blends with 85 vol% BL, the blend with 10 vol% BuOH had the greatest reduction of $PM_{2.5}$ (53.0%), whereas the biofuel blend with 5 vol% BuOH had a reduction of 39.9%. The first reason for the difference could be the reduced DCN with the higher BuOH fraction, resulting in longer IDTs and more premixed combustion (71, 72, 143). The second could be due to the reduced DNBE content reducing the emissions of soot precursors. The addition of DNBE has been shown to give increasing soot reduction as the mole fraction increased when blended into methyl decanoate (363).

The limitation of the emissions testing was that the engine was not brand new. This may have been one of the likely causes of the engine not meeting the Euro Stage V emissions standard limits regardless of what fuel injector was used. This non-compliance would have contributed to the specific emissions being higher than they may have been with a compliant engine (42). However, to reduce the influence of previous engine testing on the results in this chapter, new FJ and FB injectors were used, in addition to new lube oil. Additionally, the ULSD baseline emissions were compared to those from previous work to ensure no significant change had occurred that would suggest there were faults with the engine. To ensure the reliability of the emissions measurements the analysers' sample lines were regularly cleaned and the filters in the MEXA7100D and FTIR were changed when required. The utilisation of the different ethyl and butyl-based advanced biofuel blends in a non-optimised engine would result in detrimental changes to the gaseous emissions but favourable changes in the $PM_{2.5}$ and PN. These increased emissions of CO and THC would require additional aftertreatment systems to oxidise and remove these species. The Yanmar L100V has no aftertreatment systems, as according to Yanmar, the engine meets the Euro stage V legislation. However, there may be the possibility retrofit such aftertreatment systems (42). The utilisation of such aftertreatment systems is a cost that may need to be considered when retrofitting these systems as local air quality needs to be improved.

These fuels result in the engine being non-compliant with the emissions standard. Although, since these fuels are non-compliant with any of the fuel standards due to their additional oxygen content, they cannot be used for certification tests (42, 255). One aim was to find suitable drop-in fuels, which would not require significant changes to engine architecture or the control systems. Therefore, none of the tested fuel formulations could be used as drop-in fuels in the Yanmar L100V engine without aftertreatment systems or modification if the emissions standards are to be met. However, when using ULSD the engine was also non-compliant and would require aftertreatment systems. Therefore, there would need to be testing in additional engines to determine if it was specifically this engine that was non-compliant. Modern vehicles have exhaust aftertreatment systems fitted due to the relevant emissions standards, which may enable emission limits to be

met when using these fuel blends. With the reduction in $PM_{2.5}$ and PN emissions, the reliance on DPFs to remove PM from exhaust gases could be reduced. However, there would be the need for a DOC to remove the increased THC and CO emissions. The use of SCR and EGR for NO_X control would need to be balanced, as the change in the exhaust gas composition and temperature may not favour the use of EGR. The high levels of CO and THC, which reduce the reactivity of the fuel/air mixture due to CO and small hydrocarbon compounds being less reactive than the liquid fuels, would make EGR for NO_X control inadvisable. The influence of EGR and the required level of EGR would need further investigation using an engine fitted with controllable EGR.

Scoping the suitability of the ethyl and butyl-based blends in a simpler engine that was not optimal for their utilisation allowed the investigation of how the chemical and physical properties influenced the emissions. From the emissions analysis, the butyl-based blends are more compatible with CI engines without modification. The butyl-based blends have more stable combustion (section 5.1), which should enable the modification of the injection timing to compensate for the longer IDTs, whilst maintaining engine stability. The emissions limits for all engine applications have been becoming more stringent with each generation of the regulations; therefore, the ability of the fuel to reduce the engine out emissions will reduce the need for exhaust aftertreatment systems to ensure limits are met. The Euro 7 emissions standard will include limits for the PN including solid particles with diameters >10 nm and formaldehyde in addition to reducing the limits of the other emissions (table 2.3) (95, 96). Therefore, being able to meet these limits, without relying on aftertreatment systems, should favour the utilisation of fuels such as those studied in this work.

Overall, the emissions from the engine when using these fuels followed the expected trends, with the lower DCNs causing increased CO and THC emissions and the reduction in the particulate emissions. The butyl-based blends had favourable changes in the emissions when using either fuel injector at 92% load. At higher loads, the reduction of THC, $PM_{2.5}$, and PN due to the use of the butyl-based blends make them a more promising alternative than the ethyl-based blends. The weighting of the loads for the emissions indices results in non-compliance since the maximum load has the lowest weighting. For a genset that would typically operate at maximum load the improvement in these emissions is advantageous. However, for transient operation such as in a vehicle there would need to be increased use of exhaust aftertreatment systems. The use in vehicles would require further investigation as they would not only have aftertreatment systems but can have different fuel injectors and injection strategies and these will both affect the emissions.

Chapter 7

Chemical Kinetic Modelling of the Biofuel Blends

7.1 Introduction

Many combustion characteristics and behaviours can be simulated using a variety of computational models. Simulations are useful as they can allow the rapid comparison between the performances of different fuel blends. Their use contributes to the further understanding of the combustion chemistry and the influence of the fuel composition on the combustion properties and reactions as the species and reactions of importance can be analysed via methods such as a sensitivity analysis. Simulations could be used to optimise the blend design to give combustion properties that match those of the diesel they are to replace. The use of simulations to model combustion of a fuel blend can also be more efficient than experiments as they typically require less time. Simulations will only be useful if all the required components for the simulations are available, including a suitable reactor model, a robust and accurate chemical kinetic mechanism, thermodynamic data, and transport data for the fuel, intermediates, and products formed during oxidation (56, 170, 179, 249). The accuracy of simulations is determined by the accuracy of the mechanisms and reaction rate and thermodynamic data used within them (56). Global properties such as IDT and HRR are typical combustion properties that can be predicted in simulations. With the ever-growing interest in advanced biofuels and the research of their utilisation in ICEs, there needs to be the ability to investigate combustion behaviours of different fuel blends at engine relevant conditions. This would further the understanding of the fuel blend composition's influence on the combustion. It could also enable optimisation of blend compositions with fewer engine tests.

Since diesel is a complex blend of hydrocarbons, simulations of diesel oxidation are conducted using surrogates. These can be designed to match the combustion and physical properties of commercial diesel fuels (236, 238, 239, 304, 364). In this work the influence of blend composition on IDTs and HRRs, over a range of temperatures, were investigated using the simulations based on a diesel surrogate and subsequent biofuel blends. Results were compared to the experimental results from Chapter 5. Blends not tested in the engine were also simulated to investigate their IDT and HRR over a range of temperatures. The work of this chapter aims to assess the suitability of available models for predicting the combustion properties, engine performance, and emissions of diesel/biofuel blends. The ability of the available reactor designs, and the kinetic mechanisms produced in the SusLABB project by Dr. Christian Michelbach to predict the trends and relative changes for the IDT and HRR are assessed in this chapter. These

were selected as the key combustion properties that contribute to determining the appropriateness of different fuel blends for practical applications.

7.1.1 COVID Impact Statement

The work of this chapter was impacted by COVID as the modelling could not be conducted during the laboratory closures as there were no suitable chemical kinetic mechanisms available at this time. Additionally, the computational power required to investigate the suitability of the engine models was unavailable until office access was granted. However, once there was access to laboratories, the experimental work had to be prioritised whilst equipment was available.

Since COVID delayed the physical property and engine testing, blend compositions and engine parameters for the simulation inputs could not be determined. Additionally, due to the reduced time available sensitivity analysis could not be conducted. The lack of sensitivity analysis reduces understanding the influence of the fuel composition on the IDT and the reactions occurring. The simulations conducted were limited to those investigating the influence of the biofuel blend composition on IDTs and HRRs.

7.1.2 Suitability of the Chemkin DI Engine Simulation Code

The ability of the Chemkin DI CI engine model, outlined in section 3.8.1, to simulate the Yanmar L100V engine was evaluated (249, 250, 287). The Yanmar L100V specification (table 3.12) and both FB and FJ fuel injector specifications were used in the initial tests (table 3.13). Errors occurred when using the LLNL diesel surrogate mechanism with the Yanmar L100V engine and both fuel injector parameters (239). It was found that using the Yanmar L100V cylinder dimensions as model inputs would cause failures when simulating the fuel spray, as the spray model would not converge. There were errors in the calculated volumes and pressures, as they would be negative which is not possible in an engine. The n-heptane diesel surrogate mechanism that is available in the DI engine model tutorial was used to investigate if the LLNL diesel surrogate chemical kinetic mechanism was causing these errors (239, 249, 287). The n-heptane mechanism was used as it is known to work with the DI engine simulation code since it is used in the model's tutorial, and the model converged without any error when it was used (249, 287). These errors and lack of convergence highlighted that using engine geometries different to the example set-up may not be possible and the Yanmar L100V could not be modelled in this model.

Additionally, the liquid properties of the fuel components were needed as inputs, including temperature dependent polynomials for each property (table 3.11) (249, 250, 287). These were unavailable for the alkyl levulinates and dialkyl ethers and they could not be produced for the temperature ranges required for engine modelling. With the lack

of these inputs and the inability to simulate the Yanmar L100V engine, the DI engine model in Chemkin was deemed unsuitable within the time-scale of the project. Therefore, the combustion of the ethyl and butyl-based blends, with and without diesel, was simulated using variable volume simulations using the 0D homogeneous batch reactor model in Chemkin. In the homogeneous reactor, only the gas phase combustion is simulated removing the influence of the fuel injection, turbulent mixing, and any resultant physical delays (249). Whilst this does not represent the operation of a CI engine, as there is no fuel injection and no turbulent mixing, its use at least enables the development of an understanding of the chemical influence of the fuel blend composition on the IDT and HRR (88, 119). The gas phase simulations are still useful as the combustion in a CI engine occurs in the gas phase and the influence of the biofuel blend composition on the combustion chemistry can be investigated.

7.2 Mechanism Development and Utilisation

The biofuel three-component chemical kinetic mechanisms used were developed in the SusLABB project by Dr. Christian Michelbach. They were produced using RMG, as outlined in section 3.8.5 (57). The ethyl and butyl-based three-component blends were merged with the LLNL diesel surrogate (S-ULSD) mechanism so that the influence of the biofuel blends on the IDT and HRR of diesel could be investigated (239).

The ethyl-based blend mechanism was created within RMG as a three-component mechanism so it included the cross-reactions between intermediate compounds included in the EL, EtOH, and DEE mechanisms. The ethyl-based mechanism was merged with the S-ULSD without adding the reactions between fuel specific species within S-ULSD and the biofuel components. The butyl-based blend mechanism had to be created by merging the mechanism of each component and the S-ULSD without adding the reactions between the S-ULSD and the butyl-based components. Due to a lack of experimental data, the BL mechanism has not yet been validated against experimental data for IDTs or other combustion behaviours or speciation of the oxidation products with measured using jet-stirred reactors for example. The BuOH and DNBE mechanisms generated using RMG were validated in the SusLABB project against the available experimental data, as shown in figure 3.9 (158, 174, 232, 244). The accuracy of the ethyl-based blend mechanism in predicting the chemical IDT is shown in figure 3.8 (section 3.8.5). The accuracy of the ethyl-based mechanism produced using RMG demonstrates the suitability of using RMG for generating mechanisms for the butyl-based components. Therefore, the BL mechanism produced using RMG should be structurally appropriate, as the knowledge from generating the ethyl-based mechanism was applied to making the butyl-based mechanism. Therefore, the mechanism for the butyl-based components

should be suitable for predicting combustion behaviours of the butyl-based blends. This will be assessed as part of the simulations in this chapter.

7.3 Variable Volume IDT Simulations of Biofuel Blends

IDTs of the biofuel blends were simulated using the closed homogeneous batch reactor model in Chemkin (249). The initial pressure used in the simulations were the pressures at 13.5 CAD BTDC in the Yanmar L100V. An equivalence ratio of 0.5 was used, which matches the Yanmar L100V engine operation at 92% load. A range of initial temperatures (table 3.14) were used in the simulations to investigate the IDT's temperature dependence. The initial gas temperature for simulating the engine conditions at the point of injection was determined using the Leeds HRR model (284). An adiabatic variable volume approach was used (section 3.8) to replicate the engine cycle. Volume-time profiles of the Yanmar L100V engine operating at 92% load, with the FB and FJ injectors were used in the simulations to simulate the varying volume. The temperatures reported in this chapter are the initial temperatures used in the simulations.

7.3.1 IDTs of the Ethyl-Based Three-Component Blends

The conditions used were T=860 – 1060 K, an initial pressure of 37 bar, and φ=0.5, with a volume-time profile from a ULSD 92% load engine test using the FB injector.

7.3.1.1 IDT Temperature Dependence of the Ethyl-Based Blends

The temperature dependence of each ethyl component compared to S-ULSD can be seen in figure 7.1. In the variable volume simulations, the IDTs of EL and EtOH had a more Arrhenius-like profile in terms of temperature dependence, whereas the IDTs of DEE displayed a non-Arrhenius temperature dependence as the curve in figure 7.1 is non-linear (160, 165, 170, 365). For the FB injector 92% load engine test, the temperature at the point of fuel injection was determined to be 960 K. EL did not ignite at 960 K, but when blended with DEE and EtOH there should be ignition at 960 K. In the temperature regime studied, there was no NTC for the biofuel components (37, 169, 366). In contrast, S-ULSD has a slight NTC, which may influence the reactivity of the blends of S-ULSD with the biofuel blends (239).

The relative gas phase reactivity of the biofuel components correlates to their DCNs, as the reactivity increases with DCN (table 2.8) (143). However, DCN is measured using an IQT at a lower temperature and pressure and a constant volume, where the liquid fuel is injected and is influenced by both chemical and physical delays (119, 141). Whilst the gas phase reactivity follows the trends of DCN, it only accounts for the chemical delay. At temperatures below 920 K, the IDTs of DEE are longer than the S-ULSD, which indicates that non-chain branching reaction pathways are occurring,

such as propagation and termination reactions and these decrease the overall reactivity and slow the ignition. The activity of the non-chain branching pathways should be investigated using sensitivity analysis to determine their influence on the chemical IDT.
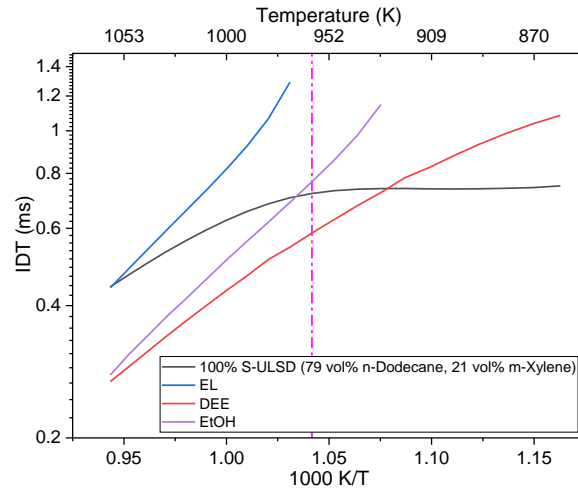
Figure 7.1. Ethyl three components simulated IDTs at p=37 bar and φ=0.5. Pink dashed line T=960 K.

The IDTs of DEE and EtOH show a crossover with the S-ULSD temperature dependence, as shown in figure 7.1. When these fuels are blended this will increase the reactivity of the fuel blends and may lead to short IDTs if there are regions with higher temperatures. This may be significant in an engine where the temperature distribution is inhomogeneous and there may be local ignitions of DEE and EtOH in high temperature regions. This may also be favourable if there are high fractions of EL which is less reactive, as it may promote the ignition of the EL fraction by raising the local temperature.

The IDT for ULSD in the Yanmar L100V engine at 92% load was 1.22 ms, whereas the simulated IDT of S-ULSD, at 960 K and φ=0.5, was 0.720 ms. In the variable volume simulations there was no heat loss and the reaction mixture was a homogeneous gas phase mixture. In the engine this was not the case, as there is injection of liquid fuel into the cylinder. The fuel has to vaporise and mix with the high temperature and high pressure air before igniting. The lack of turbulent mixing in the model is a possible reason for the difference in the simulated and engine-derived IDT (88, 119). Barraza-Botet et al. (119) showed in their study that the physical delay due to mixing was the largest component of the total IDT of ethanol/iso-octane blends in an IQT, when the differences in the chemical IDT measured in a rapid compression facility was compared to the total IDT in the IQT (figure 2.10). Therefore, to simulate the total IDT measured in the engine, the mixing processes need to be present in any simulation. Additionally, the lack of heat loss in the simulations shortens IDTs since higher temperatures are maintained. However, we can use these simulations to investigate the chemical component of the IDT. Comparing the S-ULSD simulated chemical IDT and the ULSD total IDT in the

engine, the chemical delay is 60% of the total IDT. However, the S-ULSD was not tested in the engine so the total IDT in the Yanmar L100V was not determined.

The simulated IDT temperature dependence for a range of ethyl-based blends are displayed in figure 7.2. The IDTs of the blends have a more Arrhenius-like temperature dependence than S-ULSD, which was expected since EL and EtOH show Arrhenius behaviour (figure 7.1) (169, 179). Therefore, the ethyl-based blends will be more sensitive to temperature than S-ULSD, which has a flatter IDT profile. Thus, localised in-cylinder temperature variations will be more influential. Blends with <60 vol% EL had longer IDTs than S-ULSD at T<970 K as their crossover with S-ULSD occurred at these lower temperatures (figure 7.2a). Blends with >60 vol% BL had longer IDTs at T>1000 K as indicated by the crossovers in figure 7.2b. This was due to EL being the least reactive component, requiring higher temperatures to ignite. This correlates with EL having the lowest DCN (table 2.8). Blends with high DEE fractions had the shortest IDTs across all temperatures. This was expected since DEE is highly reactive and the higher DEE fractions result in shorter IDTs (161, 169). Blends with 5 vol% DEE had the longest IDTs and if there was > 90 vol% EL there would be no ignition at temperatures below 960 K.
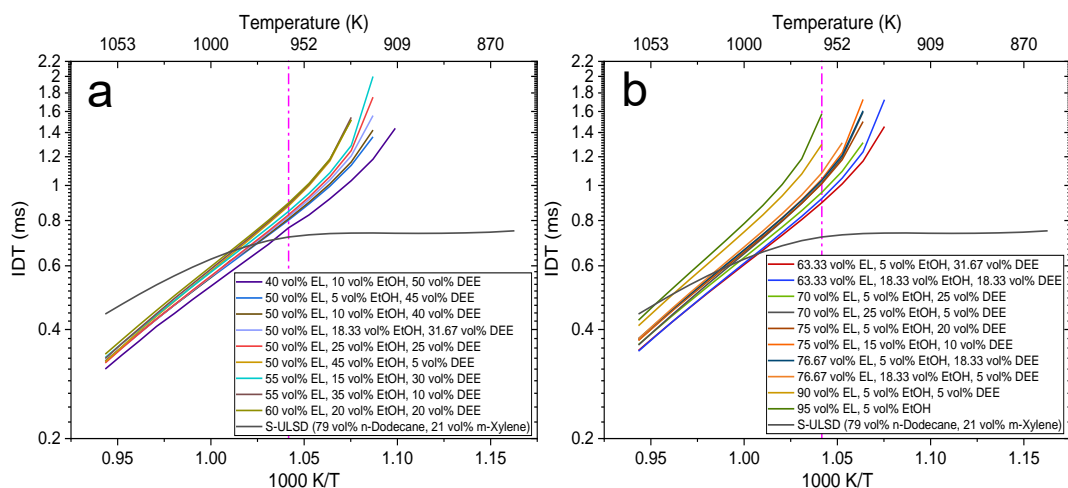
Figure 7.2. Simulated IDTs for a range of ethyl-based blends with p=37 bar and φ=0.5. a: ≤60 vol% EL blends. b: ≥60 vol% EL blends.

As the DEE fraction increased, the temperature dependence became more Arrhenius like. Therefore, the IDTs became more temperature dependent, which may influence the reactivity of blends with S-ULSD at the lower temperatures. The increased DEE fraction also decreased the temperature where the IDT's temperature dependence became more Arrhenius-like, as they. At temperatures below 960 K, IDTs increase non-linearly for most blends. The longer IDTs are due to the non-chain branching pathways becoming thermodynamically more favourable compared to the chain branching pathways, as the conditions favour the production of the non-chain branching products as their formation will have a lower Gibbs energy (170, 179). These pathways include the production of relatively unreactive HO_2 radicals from their elimination from RO_2

species, which slows the overall rate since HO$_2$ is unreactive at low to intermediate temperatures (165, 179, 180, 223). Sensitivity analysis would confirm the preferential formation of HO$_2$ and the reactions that are delaying the ignition. The Arrhenius behaviour of the IDTs of DEE at T>900 K, p=40 bar, and φ=0.5, was reported by Issayev et al. (161) when measuring IDTs in a shock tube. EtOH at high temperatures and pressures also has Arrhenius behaviour due to its thermal decomposition (165, 293). DEE and EtOH have IDTs less than 1 ms at T>900 K, p=40 bar, and φ=0.5, whereas EL did not ignite below 1040 K (160, 161). Therefore, the short IDTs of the ethyl-based blends were due to DEE and EtOH and their high reactivities in these conditions.

7.3.1.2 Influence of the Ethyl-Based Blend Composition on IDTs

As with the physical properties studied in Chapter 4, to determine the influence of the blend composition, and whether the simulated IDT could be modelled using blending rules, the blends simulated had their IDTs analysed at 960 K and 1020 K. The blend composition dependence is shown in figure 7.3. The contour plots, on a linear IDT scale, show that IDTs of the ethyl-based blend have a linear dependence on the blend composition. Hence, a linear blending law could be produced.
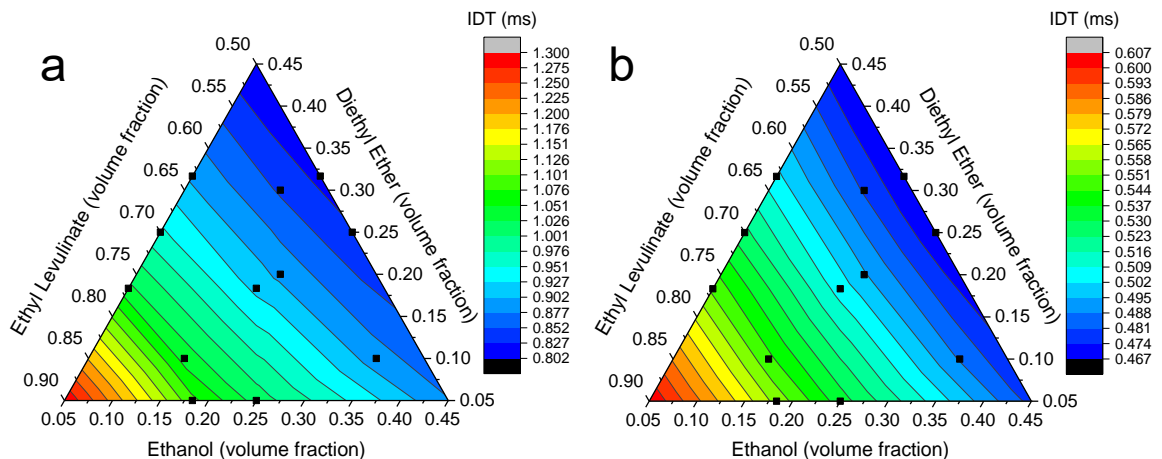
Figure 7.3. Simulated IDT for the ethyl-based three-component blends at 37 bar, φ=0.5, and a: T=960 K. b: T=1020 K. Black squares: MODDE generated blends.

In figure 7.3a, there were no blends with an IDT of 0.720 ms, the IDT of S-ULSD at 960 K. This was expected since blends with high EL fractions have low DCNs and long IDTs (figure 7.1) (37). This indicates that 100% biofuel blends with high EL fractions could be unsuitable for engine use as IDTs would be too long. Although the simulations do not capture the physical aspects of the combustion, they can be used to establish if a fuel blend would have a chemical autoignition time within a set tolerance of diesel. The simulations could be used as another method to screen the biofuel blends and determine if they have the potential for use in an engine, providing they have acceptable fractions of DEE, such that an engine can operate stably. Therefore, the practical suitability of the three-component biofuel blend for engine use could be ensured. For example, blends

with 40 vol% DEE would not start in the engine (section 5.1) due to vapour lock, which is not captured in these simulations.

The IDTs at 1020 K also had a linear dependence on the blend composition, as shown in figure 7.3b. At 1020 K, the influence of EL was reduced as the contours are more evenly spread, whereas the contours are dense at high EL fractions in figure 7.3a suggesting there may be a slight non-linear dependence on the EL fraction. The difference between the contour density in figures 7.3a and 7.3b was likely due to EtOH and DEE having similar chemical IDTs at 1020 K from the thermal decomposition reactions reducing the simulated IDT of the blend (165, 171, 179).

A linear model for each temperature was produced. The model fit parameters are summarised in table 7.1. The R^2 value of the linear model for IDTs at 960 K is lower than that of the 1020 K model, which may indicate that there is some non-linearity in the blend composition dependence. However, the quadratic models were less accurate than the linear models and were not selected. The models and their coefficients were statistically significant and the coefficients are presented in Appendix A.4.

Table 7.1. Ethyl-based blends linear IDT models model fit parameters.

Model Fit Parameter	960 K	1020 K
Number of Data Points	15	15
R^2	0.938	0.989
Q^2	0.885	0.978
p-value of the model	5.48×10^{-8}	1.51×10^{-12}
AARD%	2.48	0.62
Relative Difference Range (%)	-6.81 – 3.41	-1.66 – 0.93

The linear model for predicting the simulated IDTs at 1020 K was more accurate than the model for predicting IDTs at 960 K. This was likely due to the nature of the IDT dependence on the blend composition, as the gradient between the contours increased with increasing EL fraction at 960 K (figure 7.3a). This can be seen with the large range of relative differences in table 7.1. At 960 K, the under-prediction of 6.81% was for the 90 vol% EL/5 vol% EtOH/5 vol% DEE blend, where the contours were most dense. The 3.41% over-prediction was for the IDT of the 70 vol% EL/5 vol% EtOH/25 vol% DEE blend. Therefore, there was no specific region with inaccuracy, but to improve the model accuracy additional blends should be simulated. Additionally, there needs to be experimental validation of the predicted IDTs to confirm the accuracy of the simulations.
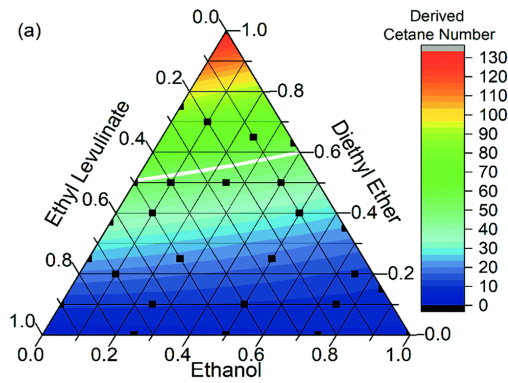
Figure 7.4. DCN of ethyl-based blends blended on a mole fraction basis. Reproduced from (37).

Howard et al. (37) produced a ternary plot for the DCN of the ethyl-based three-component blends (figure 7.4), as discussed in section 2.7.4.1. Figure 7.4 shows little dependence on the EtOH fraction, whereas the simulations in figure 7.3 show a dependence on the EtOH fraction. This difference was due to the IQT measurements having a fuel injection and the resultant physical and chemical delays before ignition (37, 141, 164). Both contour plots show linear dependence for the blend composition. However, the contours in figure 7.4 have a different direction to those in figure 7.3, indicating that DEE and EL were the most influential on the DCN. DEE and EL are the most and least volatile and reactive components in the blend, respectively. DEE and EL also have the lowest and highest densities which have been shown to correlate to the change in IDT from an IQT by Kim et al. (88). The differences between the contour plots highlight the importance of the physical delay for predicting the IDTs for CI engine applications. Therefore, the comparisons suggest that CI engine combustion models must include the fuel spray, turbulent mixing, and chemical oxidation mechanisms.

7.3.2 IDTs of the Butyl-Based Blends

The conditions used were T=810 – 1110 K, initial pressure of 37 bar, and φ=0.5, with a volume-time profile from a ULSD 92% load engine test using the FJ injector.

7.3.2.1 IDT Temperature Dependence of the Butyl-Based Blends

The IDT temperature dependence of the butyl-based three components can be seen in figure 7.5. All of the components had non-Arrhenius temperature dependence. There is a slight non-linearity to the IDT temperature dependence of BL and BuOH indicating there is non-Arrhenius behaviour (162).
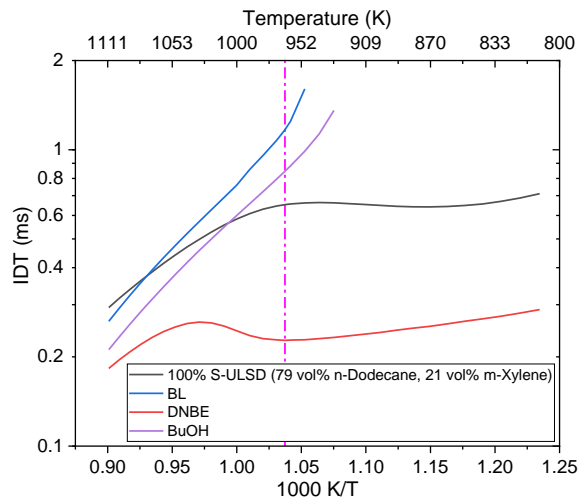
Figure 7.5. Simulated IDTs for the butyl-based three components at p=37 bar and φ=0.5. Pink dashed lined T=964 K.

The gas phase IDTs of the biofuel components do not correlate with the DCN as BL has longer gas phase IDTs than BuOH, even though it has a DCN of 14 compared to the 12 of BuOH (143). This matches the behaviour seen for the ethyl-based components in figure 7.1, where the levulinate is less reactive than the alcohol in the gas phase. Therefore, the physical properties of BL and BuOH have significant impacts on their IDTs in an IQT, as the chemical IDT indicates that BuOH should have the higher DCN. BL has the highest heat capacity and density of the three components (tables 2.6 and 2.7) so its droplets will be large and take longer to vaporise, but it has a higher DCN than BuOH. This indicates the higher enthalpy of vaporisation of BuOH compared to BL (table 2.8) contributes to its lower DCN (88).

The IDTs of different butyl-based three-component blends have non-Arrhenius temperature dependence, as shown in figure 7.6. For most of the blends simulated, the shape of the curves remained similar regardless of blend composition and there was no NTC at these conditions. However, the temperature dependence of the simulated IDTs of the 50 vol% BL/5 vol% BuOH/45 vol% DNBE blend showed an NTC and had a similar profile to S-ULSD. This was likely due to the high DNBE fraction in the blend, as the other simulated blends did not have the same temperature dependence. Since DNBE has the highest DCN, it was expected that the blends with the higher DNBE fractions would have the shorter IDTs relative to one another, and this was the case, the more DNBE the shorter the IDTs. All of the butyl-based blends had longer IDTs than S-ULSD at 964 K, and those with low DNBE fractions did not ignite, which was expected with the high BL fractions (figure 7.5). The temperature where the crossover with S-ULSD occurred decreased as the DNBE fraction increased. This was expected since DNBE has the shortest IDTs over the temperature range simulated.
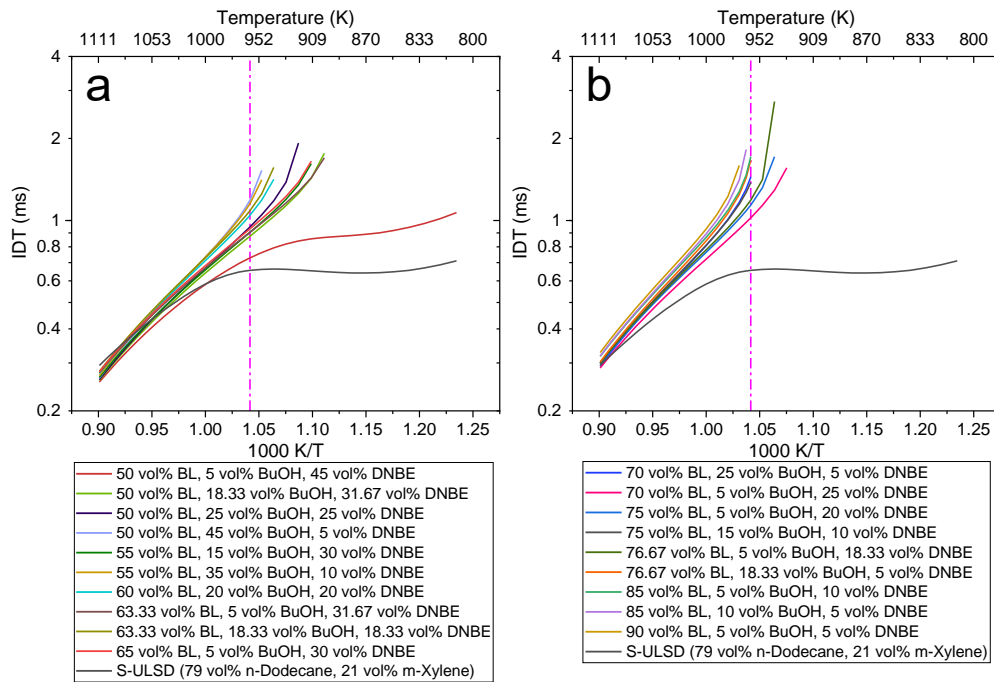
Figure 7.6. Simulated IDTs for a range of butyl-based blends and S-ULSD at p=37 bar and φ=0.5. a: ≤65 vol% BL blends. b: ≥70 vol% BL blends.

The temperature dependence shows that if lower in-cylinder temperatures were used, there would be longer IDTs, in a similar manner to the ethyl-based blends. However, as the simulated IDTs are longer than those of S-ULSD, the biofuel blends with S-ULSD may have longer IDTs which may make EGR an unfavourable NO_X control method, unless there is an increase in the in-cylinder pressure from turbocharging to compensate for the temperature reduction (5, 40, 130).

7.3.2.2 Influence of the Butyl-Based Blend Composition on the IDT

The influence of the butyl-based blend composition on the IDT at 964 K and 1020 K can be seen in figure 7.7. Although the contours look linear, a quadratic model was found to be the most accurate to predict the IDTs with respect to blend composition. This is does not match the ethyl-based blends where linear models were the most suitable. The non-linearity was likely due to DNBE having an NTC (figure 7.5), which will influence the reactivity of the blend and its IDT (174, 232, 243, 244). However, as no sensitivity analysis was conducted the extent of its influence is limited to the nature of the contour plots. What is also evident in figure 7.7a is that there needed to be less than 77 vol% BL to have ignition in the variable volume simulation. These blends would have very low DCN values and would likely be unfavourable for engine use.
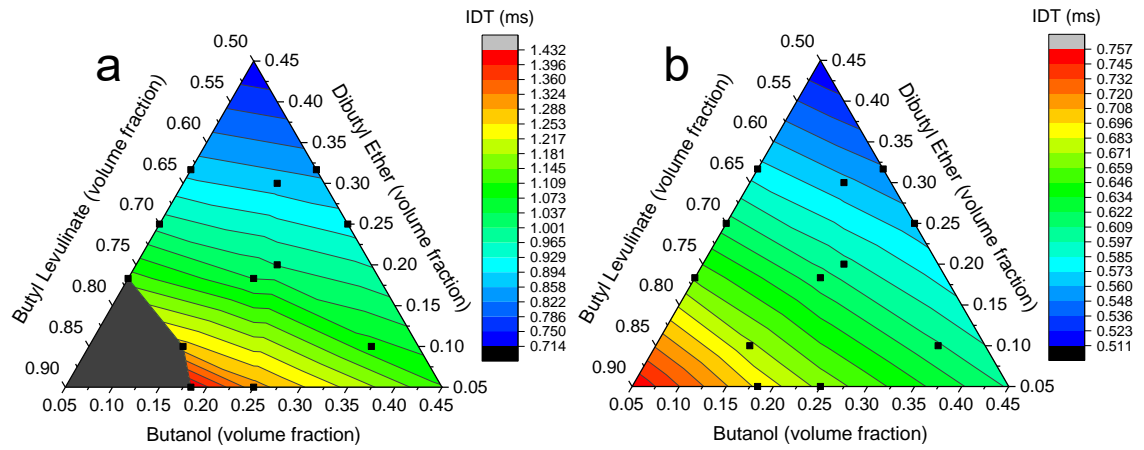
Figure 7.7. Simulated IDTs of the butyl-based blends at p=37 bar, φ=0.5 and a: T=964 K. b: T=1020 K. Black squares: MODDE generated blends.

MODDE was used to produce empirical models of the simulated IDT's dependence on the biofuel blend composition and to investigate the nature of the non-linearity of this dependence. Quadratic models were found to be the most appropriate for predicting the simulated IDT. All model terms in the model for IDTs at 1020 K were statistically significant and are shown in Appendix A.4. However, the model for IDTs at 964 K had two insignificant terms, BuOH and BuOH^2, but to maintain model accuracy these could not be removed. The contours in figure 7.7 show that DNBE has the greatest influence on the predicted IDT. This was confirmed with DNBE having the largest coefficient of the three individual biofuel components at both temperatures. The interaction terms in the models had coefficients larger than the individual component terms. The BuOH×DNBE term had the largest coefficient in the models for each temperature. This would be due to BuOH and DNBE having a large difference in simulated IDTs and the ratio of these components influencing the IDT of a blend.

Table 7.2. Butyl-based blends IDT quadratic model fit parameters.

Model Fit Parameter	964 K	1020 K
Number of Data Points	15	15
R^2	0.988	1.000
Q^2	0.964	0.986
p-value of the model	1.96×10^{-7}	8.49×10^{-16}
AARD%	1.92	0.15
Relative Difference Range (%)	-4.51 – 4.05	-0.27 – 0.37

The high accuracy of these quadratic models suggest that linear blending rules would be unsuitable to predict IDTs, and by analogy the DCN, of the butyl-based three-component blends (119, 141, 143). Therefore, a model for predicting the DCN of butyl-based blends is needed similar to the ethyl-based blend model of Howard et al. (37).

7.3.3 IDT Simulations of the Ethyl-Based Blends with Diesel

The first ethyl-based blends with diesel simulated were those that could achieve 92% load in the Yanmar L100V. These were 75 vol% EL/5 vol% EtOH/20 vol% DEE and 95 vol% EL/5 vol% EtOH blends at 15 vol% in ULSD. The predicted IDTs at 960 K for the two 100% biofuel blends were 1.011 ms and 1.577 ms for the blends with and without DEE, respectively. Since S-ULSD has a simulated IDT of 0.720 ms, it would be expected that the addition of the biofuel blends would result in longer IDTs. The combined mechanisms did not contain any cross-reactions between n-dodecane, m-xylene, the biofuel components, and their intermediates. Missing these reactions may reduce the accuracy of the predictions as key reactions may be missing in the mechanism. However, the reactions that produce the radical pool from all fuel components that will affect the overall rate and IDT are included. Gorbatenko et al. (367) showed that the addition of the cross-reactions between fuel and intermediates, including benzyl+n-butanol, benzyl+butanal, and benzyl+1-butene, in the chemical kinetic mechanism of a gasoline surrogate with n-butanol caused an insignificant change in the simulated IDTs of n-butanol/gasoline blends. This indicates that the cross-reactions between n-butanol and the S-ULSD components may only have small influence on the simulated IDT. However, the inclusion of cross-reactions in the chemical kinetic mechanism and sensitivity analysis would need to be conducted in future work. The main influence on the simulated IDT is the generation of a radical pool and the reactions of these radicals with the fuel species and intermediates, as the with a higher radical concentration there will be more initiation and chain branching reactions occurring, resulting in ignition (179, 180). Due to time constraints the ethyl-based three component mechanism merged with the surrogate diesel mechanism without any cross-reactions between the diesel and the biofuel components had to be used. There is the additional limitation of a current lack of experimental data available that could be used to validate the mechanisms. Whilst there are IDTs determined from the engine tests in this work, they cannot be used as validation due to the different reactor design used. Therefore, the influence of the biofuel addition on the gas-phase autoignition may not be representative of what is determined in the engine testing. However, the changes in the chemical delay can be determined.

The influence of 15 vol% of the two ethyl-based biofuel blends on the IDT temperature dependence of S-ULSD can be seen in figure 7.8. The blend without DEE had IDTs longer than S-ULSD at temperatures <970 K, whereas the blend with DEE had longer IDTs at temperatures <940 K. This confirms that DEE increases reactivity and promotes the oxidation of EL and EtOH, as previously reported (37, 368). The longer IDTs were expected due to the high EL and EtOH fractions in the biofuel blend, both of which are less reactive than S-ULSD and DEE (figure 7.1). This is shown by the difference between the two ethyl-based blends in figure 7.8.
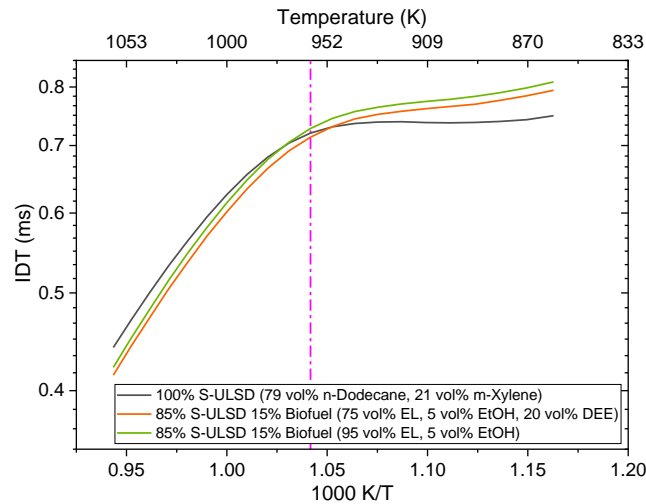
Figure 7.8. Simulated IDTs for the surrogate diesel and the two 15 vol% biofuel ethyl-based blends at p=37 bar and φ=0.5. Pink dashed line is T=960 K.

The predicted IDTs for both biofuel blends are shorter than the IDTs of S-ULSD above 1000 K due to thermal decomposition of the biofuel components promoting ignition (171, 179, 180, 230). The thermal decomposition of the biofuel components occurs at lower temperatures due to the bonds being weaker with the oxygenated functional groups in the molecules (170, 179). The biofuel blends show non-Arrhenius behaviour at the temperatures studied (figure 7.8). The IDTs have less of a temperature dependence at initial temperatures between 890 K and 960 K, as they remain within 0.05 ms between these temperatures. This may enable the use of cooled EGR for NO_X control, which reduces the in-cylinder temperature (5, 40, 101). However, EGR is usually coupled with turbocharging, which increases the initial pressure. Therefore, the EGR rate would need to be optimised to ensure blends had the same IDTs as diesel or the blend composition could be optimised for a given EGR rate to match the IDT of diesel (5).

The IDTs for these fuel blends in the engine were approximately double those simulated in the variable volume simulations. The differences are due to a physical delay in the engine due to vaporisation and turbulent mixing of the fuel after injection, whereas the simulations only include the chemical delay (88, 119). The IDTs for the ethyl-based biofuel blends from the engine tests and simulations are summarised in table 7.3. The relative change in the simulated IDT can be seen figure 7.9. The simulated IDTs had no influence of any instability caused by DEE, as observed in the engine (figure 5.3).

Table 7.3. Summary of the IDTs from the 92% load engine tests and the 960 K, p=37 bar, and φ=0.5 simulations.

Fuel	Engine IDT (ms)	Simulated IDT (ms)
ULSD (S-ULSD)	1.218 ± 0.018	0.720
85% ULSD 15% Biofuel (75 vol% EL/5 vol% EtOH/20 vol% DEE)	1.329 ± 0.037	0.713
85% ULSD 15% Biofuel (95 vol% EL/5 vol% EtOH)	1.302 ± 0.007	0.728
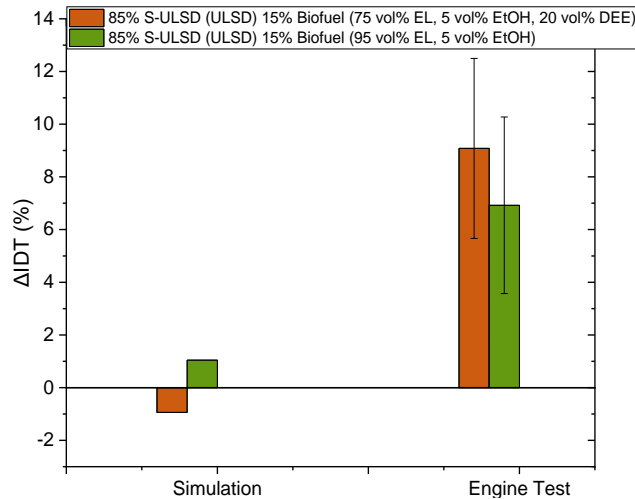
Figure 7.9. Changes in the simulated and engine IDTs relative to diesel for the two 15 vol% ethyl-based blends tested in the engine, where S-ULSD was used for the simulations and ULSD was used for the engine test.

The relative change in the simulated IDT for the blends is ±1% which is a negligible change, indicating that the gas phase reactivity of S-ULSD is maintained with the biofuel blends. The gas phase IDT for the blend with DEE was shortened, which indicates that the physical processes occurring after fuel injection have the largest contribution to the total IDT. This follows the findings of Barraza-Botet et al. (119), where the physical delay at 970 K for iso-octane/EtOH blends was more than two thirds of the total IDT. Therefore, the charge cooling effect, spray quality, and the longer turbulent mixing time required for the blend with DEE were likely to contribute to the longer IDTs (119).

Since the models can be used to investigate untested blends, 25 and 50 vol% biofuel blends were also investigated. The temperature dependence of the IDTs for different fractions of 75 vol% EL/5 vol% EtOH/20 vol% DEE and 95 vol% EL/5 vol% EtOH are shown in figures 7.10a and 7.10b, respectively.
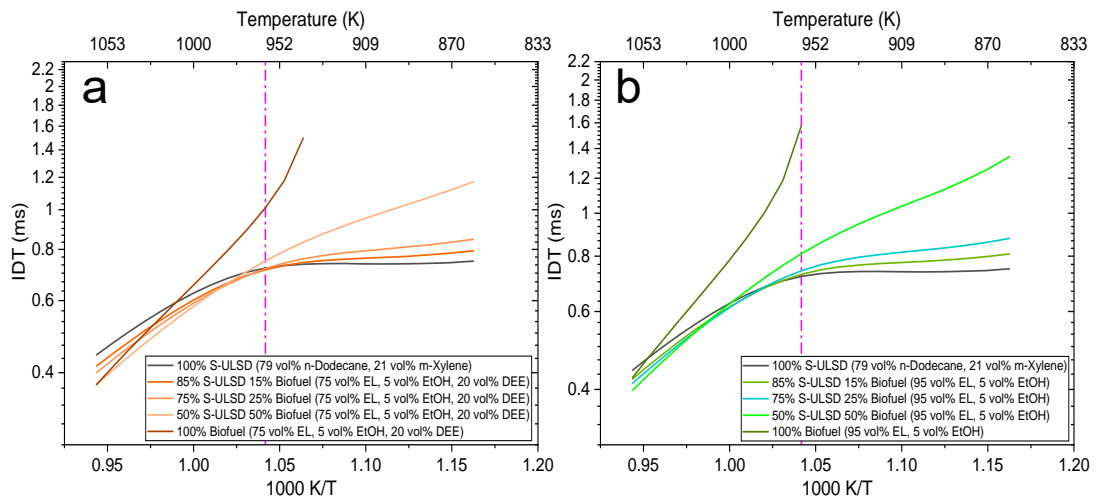
Figure 7.10. Simulated IDTs for ethyl-based blends with S-ULSD at p=37 bar and φ=0.5. a: 75 vol% EL/5 vol% EtOH/20 vol% DEE. b: 95 vol% EL/5 vol% EtOH.

For both blends, the simulated IDTs increased as the biofuel fraction increased at T<960 K. However, the blend with DEE had shorter IDTs compared to the blend without, which was expected since DEE is the most reactive component. Additionally, the crossover temperature increased as the biofuel fraction increased. This was expected with the increased total EL fraction in the blend, as it has the longest IDTs and requires higher temperatures to ignite. With increasing fractions of biofuel, the temperature dependence became linear and more Arrhenius-like, which was expected since EL and EtOH showed Arrhenius dependence (figure 7.1) when studied as individual components.

The shorter predicted IDTs at higher temperatures for the blend with DEE are unlikely to affect the engine operation since the reduction is <0.05 ms. Additionally, they may be favourable since the in-cylinder temperature is usually inhomogeneous, so there may be regions of lower temperatures where IDTs will be longer (59). Therefore, if there are ignitions in the high temperature regions, the in-cylinder temperature will increase, which leads to ignition of the remaining fuel. In the Yanmar L100V there was no compensation in the injection strategy for the change in the fuel blend composition, so the IDTs in the engine changed due to the fuel composition and the associated changes to the physical and chemical delay. The changes relative to diesel for the simulated IDTs at 960 K and the two blends tested in the engine can be seen in figure 7.11.
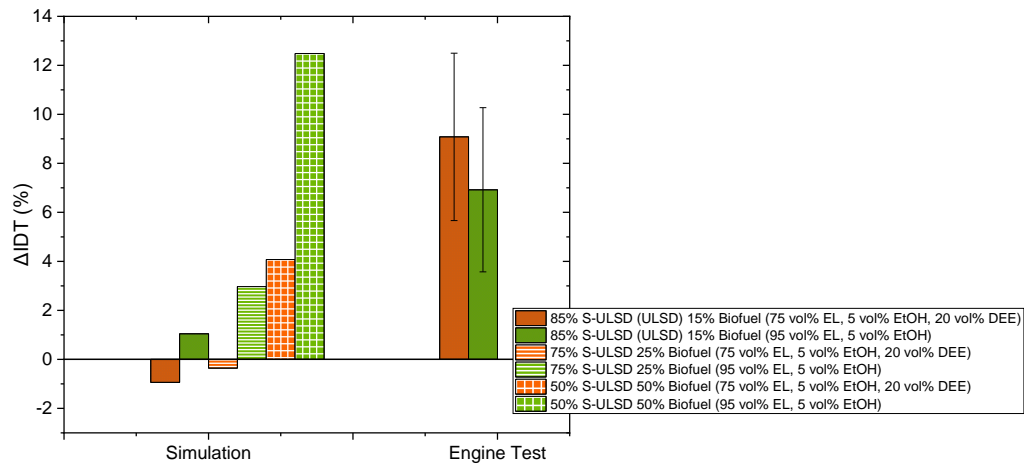
Figure 7.11. Changes in the simulated IDT relative to ULSD for the two ethyl-based blends at different fractions with diesel compared to the engine tested blends, where S-ULSD was used for the simulations and ULSD was used for the engine test.

The blend with DEE had less of an increase in the simulated IDTs compared to the blend without DEE. This was expected since DEE is more reactive than EL and EtOH. The IDT of the 50 vol% biofuel blend with DEE may be dominated by the low reactivity of EL, hence the longer IDTs (figure 7.11). DEE activates the low temperature oxidation pathways of EL, which results in the increases in IDT for the blend with DEE to be lower than for the blend without DEE (37).

The change in IDT as the biofuel fraction increases is non-linear (figure 7.11), which indicates that linear blending rules would not be suitable for predicting IDTs of blends of diesel and oxygenated biofuels. The change in IDT for the iso-octane/EtOH blends Barraza-Botet et al. (119) measured in an IQT was also non-linear. The non-linear changes in the chemical delay will impact the total IDT of a fuel and are likely to result in non-linear changes in the total IDT. Since the DCN is correlated to the total IDT, the DCN of the ethyl-based blends with diesel cannot be accurately predicted using linear blending rules. Therefore, there would need to be further development of blending rules for predicting the DCN for blends of diesel and oxygenated biofuels.

7.3.3.1 IDTs of Blends with High DEE Content

As discussed in section 5.1, the biofuel blends of 50 vol% EL/10 vol% EtOH/40 vol% DEE and 40 vol% EL/10 vol% EtOH/50 vol% DEE, were chosen as they had DCNs of 50 and 40, respectively. The IDT temperature dependence for these biofuel blends with different fractions of S-ULSD are displayed in figure 7.12. The biofuel blends with S-ULSD have shorter IDTs than S-ULSD at T>960 K. This could be due to the high DEE content generating a large radical pool and the thermal decomposition of EtOH, but would need to be confirmed with sensitivity analysis that could be conducted as part of future work (165). The temperature dependence became more Arrhenius-like as the biofuel fraction increased in the temperature regime studied.
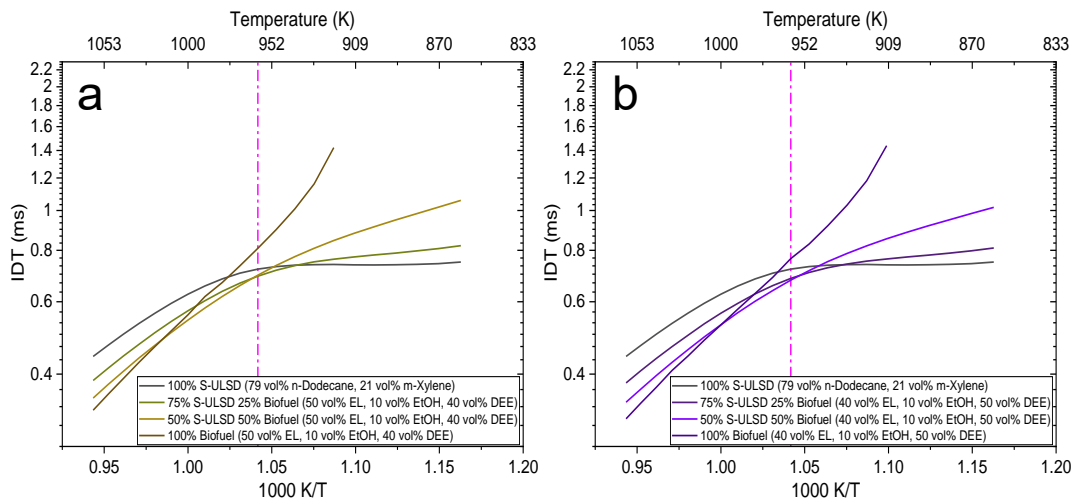
Figure 7.12. Simulated IDTs at 37 bar and φ=0.5 for ethyl-based blends with S-ULSD. a: 50 vol% EL/10 vol% EtOH/40 vol% DEE and b: 40 vol% EL/10 vol% EtOH/50 vol% DEE. Pink dashed line is T=960 K.

There is a crossover of the biofuel blends predicted IDT temperature dependence with that of S-ULSD as the temperature increased, as the addition of the biofuel blends resulted in shorter IDTs. The temperatures for the crossover are not only blend dependent but also depend on the biofuel fraction. As the biofuel fraction increased, or the DEE fraction decreased, the crossover temperature increased. The increased reactivity at higher temperatures may need to be managed in an engine. This is especially true, since the in-cylinder temperature distribution is inhomogeneous and high temperature regions would promote local ignitions of vaporised fuel. These ignitions could cause spikes of in-cylinder pressure, such as those observed by Paul et al. (137).

The influence of the physical delay is highlighted by the 40 vol% EL/10 vol% EtOH/ 50 vol% DEE blend having chemical IDTs different to diesel, even though it has a DCN of 50 (37). The predicted gas phase chemical IDTs were shorter when blended with S-ULSD. Since the DCN is determined from IQT measurements the physical delay is accounted for, which may be longer with the high DEE and EL fractions causing charge cooling (137). The 100% biofuel blend had a longer simulated IDT than S-ULSD and did not ignite at temperatures below 910 K, even without heat loss in the simulations. This lack of ignition was unexpected since an IQT operates at 818 K and 21.37 bar which are lower than the thermodynamic conditions used in the simulations (141). However, the simulations were of a variable volume reactor, whereas an IQT is a constant volume and constant pressure reactor. The blends with high biofuel fractions in figure 7.12 had similar temperature dependence to DEE at the temperatures simulated. This was expected since DEE was such a high fraction of the blend.

The 100% biofuel blends have non-Arrhenius behaviour as the temperatures decreased, as shown in figure 7.12. This indicates there is less of a temperature dependence on the IDT of the fuel blend. Longer chemical IDTs would cause the ignition

to be further into the four-stroke cycle, which would increase the HC and CO emissions as there would be less time available for complete combustion, as seen in Chapter 6 (38). The large physical delay due to vaporisation and turbulent mixing of the fuel/air mixture increases the overall IDT, especially when combined with longer chemical IDTs (119). With the simulations having no heat loss term the chemical IDTs for the blends that did ignite may be shorter than they would be if there was heat loss. The lack of heat loss may have enabled ignition to occur at lower temperatures since the gaseous mixture was not losing temperature to the reactor walls.

For gasoline applications, the crossover in reactivity is indicated by the octane sensitivity, which is defined as the difference between the RON and the motor octane number (MON) (369). The RON and MON are measured at different conditions as the MON is measured at a higher temperature and RPM than the RON (370, 371). For CN or DCN there is no method for determining or expressing the sensitivity for different operational conditions of a CI engine. The addition of the ethyl-based blends to diesel changes the IDT temperature dependence, the understanding of which would be beneficial. This is where further simulations could help, primarily those including turbulent mixing and the fuel spray, i.e. CFD models.

7.3.4 IDT Simulations of the Butyl-Based Blends with Diesel

The initial simulations conducted were to determine the IDT temperature dependence for butyl-based blends with diesel tested in the engine. The temperature dependence is shown in figure 7.13. The predicted IDTs increase as the BL fraction increases and as the biofuel fraction increases. This was expected since the DCN of the blend reduces with increasing BL and biofuel fraction. Unlike the ethyl-based blends, the crossover occurred at a much higher temperature. This was due to there being high fractions of BL in the blends. The IDTs of the butyl-based blends are shorter than the ethyl-based blends due to the higher gas-phase reactivities of the butyl-based components, as larger molecules are more reactive (165, 171, 178, 231). Whilst these blends were formulated to comply with the physical property limits (section 4.6), the temperature dependence of the predicted chemical IDTs shows a similar behaviour to that of S-ULSD. This is likely due to the high S-ULSD fraction, but at the engine condition of T=964 K, there is only a slight increase in the chemical IDT, displayed in figure 7.14. At T>1020 K, there is a crossover in reactivity, where the biofuel blends have IDTs shorter than the S-ULSD. This behaviour may need to be considered in high temperature regions in an engine cylinder, as it would promote local ignitions, as previously discussed in section 7.3.3, although the differences are small for the butyl-based blends.
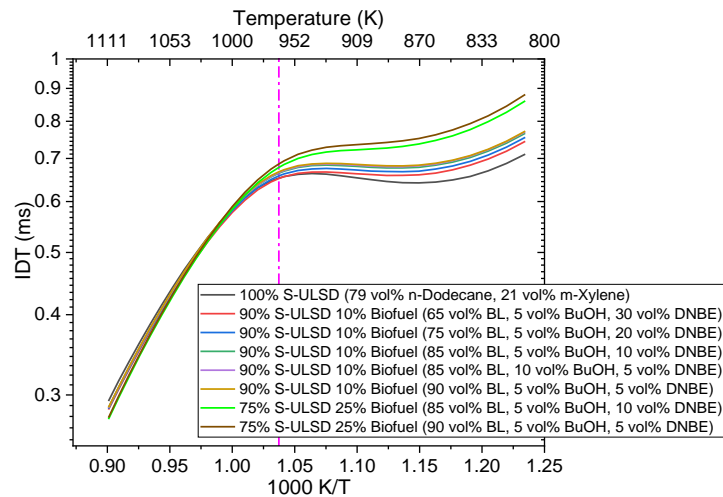
Figure 7.13. Simulated IDT of butyl-based blends with diesel. φ=0.5 and p=37 bar.

There is a more pronounced NTC region with the 10 vol% blends due to the higher diesel fraction. The 25 vol% butyl-based blends do not have the same behaviour as the ethyl-based blends shown in figures 7.10 and 7.12. This will be due to the more Arrhenius-like behaviour of BL causing the temperature dependence to change (55, 365). The blends of biofuel and S-ULSD show a non-Arrhenius temperature dependence and an NTC due to DNBE and S-ULSD both having an NTC region in their IDT temperature dependence. The NTC must be accounted for if EGR is to be used as a NO_X control method, as the in-cylinder temperature reduces when using an intercooler, and the IDTs would become shorter (5). Therefore, if EGR was used the in-cylinder temperature would need to be maintained so the IDT does not change significantly, such that it impacts engine operation and emissions. Changes in the IDT would be detrimental to CO and HC emissions, as seen in Chapter 6. The IDTs for the 10 vol% blends are all similar as they are within 0.05 ms, which is the time taken to move 1 CAD on the Yanmar L100V engine. This may be influential on the emissions.

The changes in both predicted and measured IDTs for the butyl-based blends with S-ULSD/ULSD relative to S-ULSD/ULSD at 964 K are shown in figure 7.14. The chemical IDTs increased relative to S-ULSD, and as the DNBE fraction decreased the chemical IDT increased. This was expected since DNBE has the shortest IDT of all the butyl-based biofuel components (figure 7.5). The 10 vol% biofuel blend with 30 vol% DNBE had an IDT shorter than that of S-ULSD. This reduction was likely due to the high DNBE fraction generating a large radical pool to promote the ignition. The engine tests for the butyl-based blends showed a different dependence on the blend composition (figure 7.14), where the decreasing DNBE fraction reduced the increase in IDT. The difference between the simulated chemical IDT and the total IDT in the engine indicates that there may have been more charge-cooling from the high DNBE fractions, which causes the longer IDTs. The DNBE is the most volatile butyl-based component, hence

its vaporisation would occur more readily and rapidly. Hence, the charge-cooling effect from DNBE is more likely to contribute to the longer IDTs (119, 137).
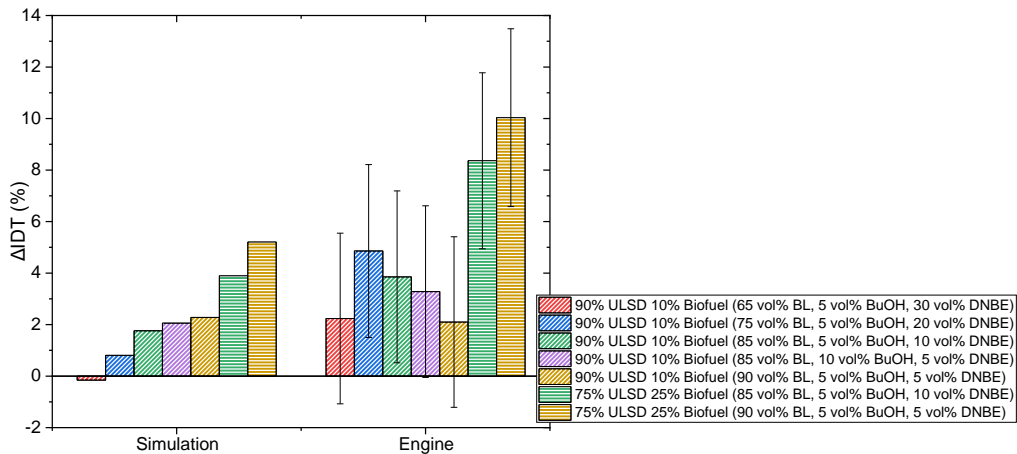
Figure 7.14. Change in the IDT relative to diesel for the simulations and the engine tests at 92% load conditions.

The increase in the simulated IDT was expected since BL has a longer IDT than S-ULSD at 964 K (figure 7.5), and it is the component at the highest fraction in the biofuel blend. As the biofuel fraction increased there was a greater total fraction of these components, hence the greater increase in simulated IDT. There was a greater increase in total IDT for all the blends tested in the engine, with a greater increase for the 25 vol% biofuel blends. This was due to the physical ignition delay as a result of the physical properties of the blends (88, 119). The simulated IDTs suggest that matching the physical properties reduces the impact of the physical delay, as for the butyl-based components is evidently less influential in the engine than for the ethyl-based blends. The density of the blends were similar to diesel, as the blends were formulated to have small changes in density, hence its influence should reduce. However, the enthalpy of vaporisation and heat capacity were not tailored, and these have been shown to have an influence on the total IDT in the sensitivity analysis of Kim et al. (88), as discussed in section 2.7.4.5. BL has the highest heat capacity and DNBE has the highest enthalpy of vaporisation (table 2.8) and in the engine there may be the competition of the influence of these two properties as the ΔIDT decreases as the BL fraction increases. The engine tests of the butyl-based blends used the FJ injector which had larger injector holes. The larger holes would have created larger fuel droplets, which take longer to vaporise, further delaying the ignition. The high enthalpy of vaporisation of the butyl-based components (table 2.8) would contribute towards long physical delays in the engine. The higher densities of the butyl-based blends will also contribute towards the longer IDTs, since larger droplets form they take longer to vaporise (88). The simulations do not account for any changes to the liquid properties and without them the trends are not representative of what was observed in the engine tests.

7.4 Effectiveness of the Simulated HRR

The simulated volumetric HRR output from Chemkin was converted to J/CAD and compared to the calculated HRR from the engine tests. The simulated heat release was solely from the combustion in an adiabatic reactor.

7.4.1 Simulated HRRs of the Ethyl-Based Blends

The changes in the simulated peak HRR and timing of peak HRR of the ethyl-based blends with diesel are displayed in figure 7.15. For the simulations it can be seen that the peak HRR increased as the biofuel fraction increased. The relative increases in peak HRR were similar for both blends (figure 7.15a), indicating that the energy content of the fuel blends was similar. The changes in peak HRR follows the findings of García et al. (222) where increasing the 1-octanol fraction in 1-octanol/DNBE blends increases the peak HRR, as the reactivity of the fuel decreased. However, these are for engine studies where there is the influence of premixed combustion from longer IDTs, whereas the gas phase simulation is of a premixed homogeneous mixture. The increase in peak HRR for the blend with DEE does not replicate what was determined from the engine tests. The simulated peak HRR was later in the combustion cycle, and became later with increasing biofuel fraction (figure 7.15b). The blends without DEE had the greater delays in the peak HRR for the simulated HRR, whereas it was the blend with DEE in the engine tests that had the greatest delay.
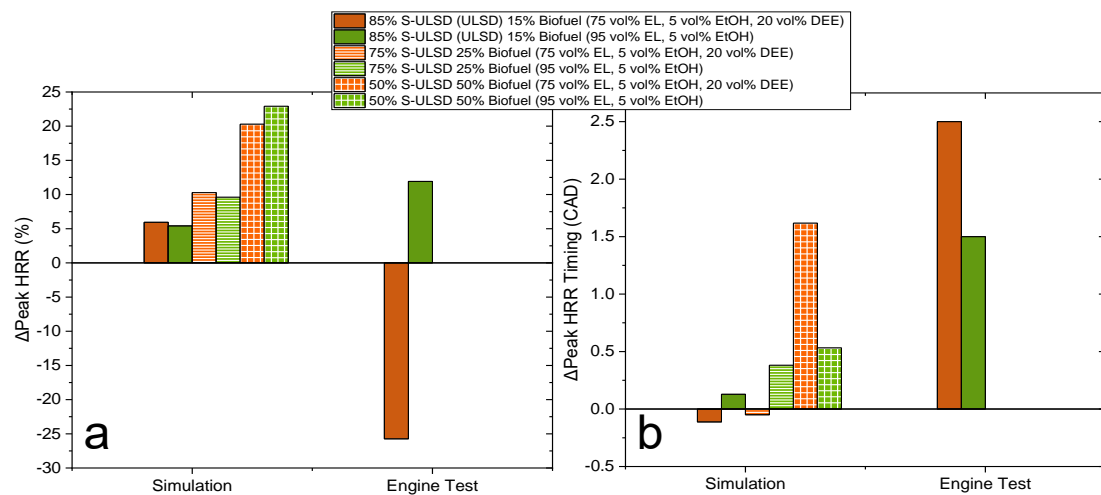
Figure 7.15. a: Changes in peak HRR relative to diesel for the two ethyl-based blends at different fractions in S-ULSD. b: Changes in peak HRR timing relative to diesel.

The fuel injection in an engine influences the HRR since fuels can have a cooling effect upon injection (88, 135, 148, 331). This may have been the case for the blend with DEE in the engine tests, hence the reduction in peak HRR and the greater delay due to the longer IDT (330, 331). The addition of EL, with its high enthalpy of vaporisation (table 2.8), also delays the heat release as EL requires more energy to vaporise. There are no heat loss parameters in the simulations, whereas in an engine there would be heat losses

through cylinder walls, through blow-by gases, as well as fuel vaporisation (148, 284). The simulations show that fuels with high total DEE fractions have a greater HRR and a shorter delay in the peak HRR. These fuel blends would also have a higher energy content due to DEE having the highest LHV of the ethyl-based components (table 2.8).

One additional contributor to the differences between the predicted and experimental HRR could be the surrogate diesel mechanism used. It only had two compounds and the ratio of the components was selected to give a DCN of 51 rather than to match the chemical properties of diesel such as the LHV or the HRR (239).

The differences in the magnitudes of the changes in peak HRRs of the biofuel blends indicate the fuel injection must be included in a model to be able to predict the engine behaviours. Additionally, the mechanism has not been validated for heat release simulations so there may be large uncertainties influencing its accuracy. The validation would require accurate heat release analysis from RCM or engine experimental data using accurate HRR models, such as the Leeds HRR model used in Chapter 5. However, to use the engine data simulations would need to be conducted using an engine model.

7.4.2 Simulated HRRs of the Butyl-Based Blends

The relative changes in the simulated peak HRR and its delay for the butyl-based blends analysed in section 5.4.2 were compared to those from the engine tests and are shown in figure 7.16. Unlike the IDTs, the simulated peak HRR reduced relative to S-ULSD, whereas in the engine they increased relative to ULSD. The simulated peak HRR values decreased with increasing BL fraction and increasing biofuel fractions. The simulated time of peak HRR moves later in the cycle with increasing biofuel fraction, as expected with longer IDTs with the high BL fractions in the biofuel blends.
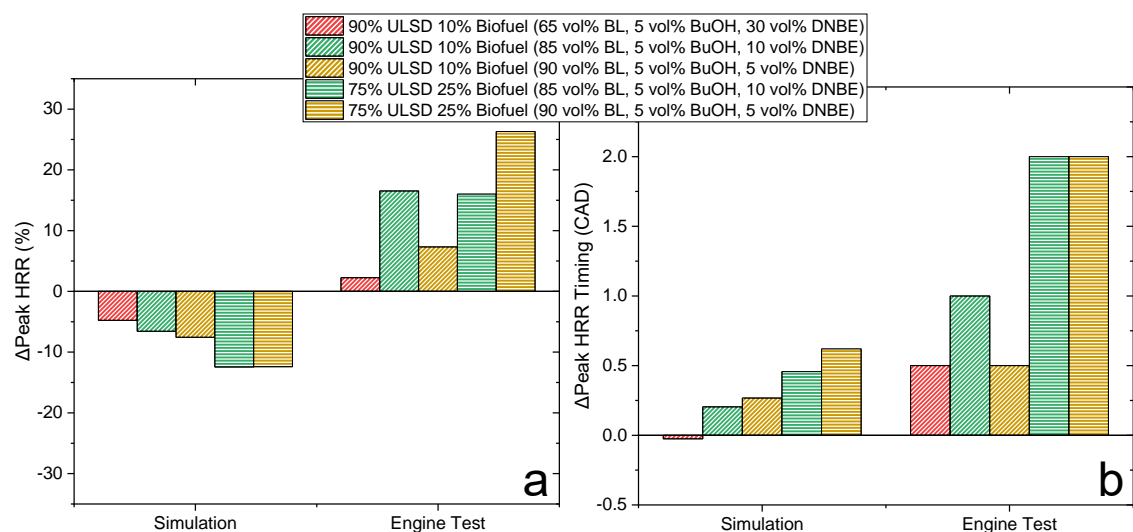
Figure 7.16. Comparison of simulated and engine HRR at 92% load. a: changes in peak HRR relative to diesel. b: changes in peak HRR timing relative to diesel.

The reduction in the simulated peak HRR with increasing biofuel and BL fraction follows the expected trend since the LHV of the blends was likely to decrease. Therefore, there is less energy to release, resulting in lower peak HRR. Since the gas phase reactor is not representative of a CI engine, the influences of the turbulent mixing and the changes with the different biofuel blends is not captured, as there is no turbulent mixing in the gas-phase reactor. An increase in premixed combustion in a CI engine typically leads to a greater peak HRR and this is influential on emissions and engine performance, as shown by García et al. (222) for 1-octanol/DNBE blends (figure 2.12).

Additionally, since this mechanism was newly developed it has not yet been validated against experimental data for either BL or multi-component blends as there is no data available. It has not been validated for simulating IDTs or HRRs from RCMs or other reactors. Therefore, the changes and trends observed for the butyl-based blends with diesel may not be representative.

7.5 Conclusions

The key finding from the kinetic modelling was that there is a significant influence of the physical delay from fuel injection on the IDTs and HRRs in the CI engine, which is not captured using a homogeneous gas phase reactor model. Therefore, it is vital there is a spray and turbulent mixing model included when simulating CI engine combustion. To accurately capture the influence of turbulent mixing, CFD would be required. The homogeneous batch reactor can be used to investigate the effects of the fuel blend formulation on the chemical delay. These investigations contribute towards a greater understanding of the combustion processes occurring, as there is still gas phase combustion in a CI engine, including their dependence on temperature and pressure. However, to fully understand the influence of the fuel blend on the combustion processes in a CI engine CFD simulations, which are capable of modelling the interactions between fuel spray, vaporisation, and turbulent mixing processes will be required (248).

CFD simulations by Kim et al. (88) highlighted the influence of the fuel's physical properties, specifically the density and heat capacity as discussed in section 2.7.4.5, on the total IDT and these need to be captured when investigating the combustion of new fuel blends for use in CI engines. More specifically, how these properties change with blend composition needs to be captured in CFD models so that their influence is accurately captured. The findings of Kim et al. (88) show that the chemical IDT is still a significant fraction of the total IDT, unlike Barraza-Botet et al. (119). Both stated that the physical properties of the fuel blend influence the total IDT. If the physical properties of a biofuel blend can match those of the fuel they are replacing then there is less of influence on the total IDT, as shown with the butyl-based blends. The density of the butyl-based blends were tailored to ensure there was minimal change relative to diesel (table

4.14), whereas the heat capacity was not tailored as it was not measured. Therefore, the changes in the heat capacity upon addition of the biofuel blends, may be influential on the total IDT. Once there is RCM data for the butyl-based blends and the chemical kinetic model is validated there could be further analysis to determine the contributions of chemical and mixing delays to the total IDT. The work of this chapter highlighted that the chemical delay as a result of changing the blend composition contributes to the total IDT. However, changes in the physical and chemical properties also influence the total IDT in the engine. Therefore, there needs to be accurate representation of the physical processes that change depending on the blend composition, to accurately predict the total IDTs observed in the engine.

The trends presented in this chapter follow what would be expected for the gas phase combustion of these fuel blends. The simulated IDTs for the butyl-based blends were longer than diesel, albeit not as great an increase as seen in the engine. For the ethyl and butyl-based blend the peak HRR was greater in the engine but only the ethyl-based blends had a simulated increase in the peak HRR. Therefore, until there is validation of both mechanisms and the use of suitable models, there may be inaccuracies and large uncertainties in the simulated IDT and HRR.

Chapter 8
Conclusions and Future Work

8.1 Introduction

This work investigated the influence of biofuel blend composition and carbon chain length on the miscibility, density, flash point, and KV40 for blends of advanced biofuels, with and without diesel. The investigation of the physical properties used a DoE methodology (section 3.3), which produced empirical models to predict the density, flash point, and the KV40s of the three-component biofuel blends. Engine tests for a selection of ethyl and butyl-based blends were conducted. From these engine tests, the influence of the biofuel blend composition on the engine performance and emissions were established. The suitability and accuracy of computational models to simulate the combustion of the blends were also investigated. The sections in this chapter include the contributions of the work to answer the research questions and achieve the aims set in Chapter 1, concluding remarks, an assessment of the different fuel blends feasibility, recommendations for future policy and technology, and directions for future work.

8.1.1 Summary of Contributions

This work has produced empirical models for predicting the density, flash point, and KV40 of butyl and pentyl-based three-component blends and a model for predicting the density of the ethyl-based blends. These models allow for the blend composition's influence on these physical properties to be determined for any blend composition within the limits detailed in table 3.1. The most accurate models for predicting density were linear, showing that the density had a linear dependence on blend composition. The models for predicting flash point and KV40 were quadratic in form, which showed that these properties had a non-linear dependence on blend composition, which was possibly due to intermolecular interactions that affected these properties. The physical property models had high R^2 values (0.924 – 0.998) and low AARD% (0.05% – 3.54%), demonstrating their accuracy (Chapter 4). These models were used to determine blend boundaries where compositions complied with existing fuel standards' property limits. No compliant ethyl-based blends were found due to the flash point of DEE and EtOH being below room temperature, which caused the blends flash points to be below the 55 °C minimum. For the butyl-based blends, a base fuel such as ULSD was needed so the BS 2869 property limits could be met (16). The pentyl-based blends could meet the BS 2869 physical property limits without a base fuel and they needed to consist of ≥75 vol% PL, ≥5 vol% DNPE, and ≤20 vol% PeOH (16). No biofuel blend, with or without diesel, could comply with the density limits of EN 590 due to them being so narrow, but the flash point and KV40 limits could be met, as shown in section 4.6 (12).

The blend walls for miscible blends of the ethyl and butyl-based three-component blends with diesel were established at ambient conditions and 3 °C. The physical properties of butyl-based three-component blends with diesel, and biodiesel, were measured. Therefore, the influence of the biofuel blend composition on the physical properties of different base fuels could be determined. Butyl-based blends with diesel were selected for engine testing provided they complied with the fuel standards' physical property limits. Up to 25 vol% of the butyl-based blends could be added to an ULSD and remain compliant with the BS 2869 property limits (16). For blends of 10 vol% biofuel in diesel, the butyl-based three-component blend could consist of ≥60 vol% BL, ≤35 vol% DNBE, and ≤10 vol% BuOH. For blends of 25 vol% biofuel in diesel, the limits were ≥80 vol% BL, ≤15 vol% DNBE, and ≤5 vol% BuOH.

The work in Chapter 5 determined the influence of the biofuel blend composition on engine performance parameters. These included the IDT, BSFC, peak pressures, and IMEP. The engine tests demonstrated that the fuel blend's physical properties affect their utilisation. This was highlighted in section 5.1 where it was shown the engine was unstable with ethyl-based blends with high DEE fractions but stable for all butyl-based blends. The longer IDTs when using the biofuel blends may imply a reduction in the DCN. The BSFC increased relative to diesel with the ethyl-based blends and the 25 vol% biofuel butyl-based blends, by around 10%, which would increase how often a fuel tank would need refilling, increasing the cost of fuel for a customer. The 10 vol% butyl based blends had a negligible change in BSFC at all engine loads tested. The IMEP and peak pressures had negligible changes for the lower BL fraction butyl-based blends, which demonstrates there is no significant change in the mechanical efficiency of the engine increasing the potential of these blends to be low-carbon alternatives to diesel. The changes in HRR for a selection of blends were determined, which contributed to understanding the fuel blends' influence on the pressures, temperatures, and emissions. The delayed peak HRR and increased peak HRR for the butyl-based blends supported the negligible change in peak pressure, but the delay favoured the reduced PM and increased CO and THC emissions, due to less time for mixing controlled combustion.

This work produced emissions data and established the influence of the biofuel blend composition on changes in legislated and non-legislated emissions. The largest positive impact of the addition of the biofuel blends to ULSD was on the $PM_{2.5}$ and PN emissions, which reduced significantly compared to the corresponding ULSD baselines when the engine run stably. CO and THC emissions increased for all biofuel blends relative to their corresponding ULSD baselines, and NO_X remained consistent with stable engine operation. The compliance to the Euro Stage V emissions standard when using these fuel blends was determined and presented in section 6.5 (42). The Yanmar L100V was non-compliant with the CO and NO_X+THC emissions limits but compliant with the

PM and PN limits for most blends and ULSD. Therefore, exhaust aftertreatment systems would need to be utilised to ensure compliance with the emissions standard. Their use could increase the cost of a vehicle, genset, or machinery as many aftertreatment systems use expensive catalysts containing platinum or rhodium.

The ability to simulate IDTs and HRRs was investigated using chemical kinetic mechanisms developed in the SusLABB project. Additionally, the suitability of these mechanisms, and the available reactor models, were assessed by comparing simulated and experimental IDTs and HRRs. The Yanmar L100V engine could not be modelled in Chemkin using the DI engine model, and thus the closed homogeneous reactor model available in Chemkin had to be used. The changes in the simulated IDTs of the blends with diesel did not match the trends observed in the engine. The differences were due to the use of the gas-phase homogeneous reactor model, not an engine model, and thus the fuel injection and the resultant physical delay were not simulated. This work confirmed that the fuel injection and turbulent mixing must be included to replicate the trends observed in the engine. The simulations showed the impacts of the fuel blend composition on the chemical IDT, which is still important to understand as combustion in a CI engine occurs in the gas phase. It is vital to accurately predict the chemical IDT because it would be the minimum IDT, which would only occur with perfect mixing of fuel and air. If a fuel blend's chemical IDT is longer than diesel's, the real IDT is likely to be even longer due to the physical delays, and the fuel would be unacceptable for use in an engine. Therefore, predicting the chemical IDT would enable the determination of blends that could result in unacceptable engine operation conditions.

8.1.2 Concluding Remarks

This project aimed to answer the five research questions set in section 1.4. The conclusions are drawn to answer these research questions.

- Can we use blends of the ethyl, butyl, and pentyl-based three-component biofuel blends, with and without diesel, as drop-in fuels?

The engine tests identified that a CI engine can run stably using most of these fuel blends, including those that meet the physical property limits of existing fuel standards. The addition of the oxygenated biofuel components does result in fuel blends that do not comply with the existing fuel standards. However, the biofuel components that are permitted to be used as diesel blendstock should be reviewed if decarbonisation of CI engines is to be achieved. The ethyl-based blends must have no DEE to have a stable operation (figures 5.2 and 5.3), whereas all the butyl-based blends tested operated components stably. The instability combined with the low flash point and unlikely materials compatibility of the ethyl-based blends, due to DEE, demonstrated that for

diesel low-carbon alternative fuels for CI engines they must have long carbon chains. The lack of second-generation pentanol made the pentyl-based blends unsuitable choices for biofuel blend components as required in REDII (14). The boundaries of REDII were exceeded with the blends studied, as the alkyl levulinate fraction was >6 vol% of the total blend. Therefore, the advanced biofuel blends could contribute significantly towards the decarbonisation of CI engines. The physical property limits in the fuel standards could be met for some blends of diesel and butyl-based blends, highlighting the compatibility of longer carbon chain length biofuel components. The total IDTs increased relative to ULSD when using the ethyl and butyl-based blends. This would require modifications to engine operation or optimisation of the blend composition to ensure the total IDT was the same as ULSD. The changes in IDTs may be more noticeable in transient operation where the engine speed is variable, but this requires further investigation. All fuel blends tested increased the CO and NO_X+THC specific emissions and resulted in them exceeding the Euro Stage V emissions standard limits making them inappropriate for use in gensets without any aftertreatment systems (42). However, since the Yanmar L100V engine used was non-compliant when using an EN590 diesel, the exceedance when using the biofuel blends may have been greater than they could have been with a compliant engine. If the engine was compliant, there may have been the potential that one or more of the blends may have maintained compliance with the Euro Stage V standard (42). The $PM_{2.5}$ and PN specific emissions reduced with the butyl-based blends and this would be beneficial for air quality. However, the health impacts of the PM generated would need to be investigated as the chemical composition may have changed when using the biofuel blends. The 10 vol% butyl-based blends had negligible changes in BSFC at all loads, making them an attractive option as low-carbon diesel alternatives. For some of the butyl-based blends the IMEP had a negligible change, which combined with the maintained BSFC indicates there may not be the typical efficiency penalty when using large fractions of oxygenated biofuels. This makes the butyl-based blends attractive biofuel candidates to fulfil the REDII requirements. This work demonstrated there is potential in the butyl-based blends but their appropriateness for vehicle use and real-world driving needs to established.

- What are the key physical and combustion properties that will determine the suitability of these fuel blends?

Fuel standards typically set limits for the physical and combustion properties that will be most influential on the operation of an engine and on the fuel handling. Many of these properties have been shown to change with blend composition in the literature and in this work upon addition of oxygenated advanced biofuels. These included the flash point, density, miscibility, DCN, KV40, IDT, HRR, and adiabatic flame temperature. The physical properties selected in this work were the flash point, density, KV40, and the

miscibility and the combustion properties of interest were IDT and HRR. Miscibility was needed to ensure that there was no separation and there was long-term stability as there is likely to be long periods of fuel storage. The flash point must be known for the safe handling and storage of the fuel blends as it would be impractical for fuel blends with lower flash points to be utilised in diesel applications. The density and KV40 influence fuel atomisation and total IDTs, which was highlighted when comparing the simulated chemical IDTs and those measured in the engine, as well as the different biofuel blend formulations. Higher densities and KV40s result in larger fuel droplets, creating more rich zones in the cylinder and elevated CO, THC, and soot emissions. HRRs were influential on the emissions and engine performance as the peak timing influenced the peak in-cylinder temperatures and pressures. However the change in the timing was due to the changes in IDT and thus if this was managed, the HRR profiles could match those of ULSD. There are physical properties not stated on the fuel standards, including the LHV, enthalpy of vaporisation, and surface tension, which need to be known. Material compatibility is another key property, which must be established, primarily with the elastomers used in fuel seals and fuel lines. During the use of the fuel blends there was no visual evidence of severe damage to the fuel lines. However, there was no analysis of the fuel lines to determine the effect of the fuel blend's due to the limited time available.

- How do the physical properties change as the biofuel blend composition changes?

From the physical property measurements, and the models produced using MODDE, the dependence of each property on blend composition could be determined. The density of the blends with and without diesel had a linear dependence on the blend composition. The flash point and KV40 of the butyl and pentyl-based three-component blends had non-linear dependence on the blend composition (figures 4.11 and 4.17). The non-linear dependence indicated that the flash point and KV40 was influenced by interactions between the biofuel components. The flash points of the fuel blends were not only dependent on the base fuel fraction but on the composition of the butyl-based three-component biofuel blend. There was a significant dependence on the butanol fraction, as the larger the fraction of BuOH, the larger the reduction in the flash point. This was unexpected since it has a higher flash point than DNBE (figures 4.14 and 4.16). This indicated that a component's polarity affects the flash point of a blend, as this will affect the mixing behaviour of the blend. Whilst flash points of multi-component biofuel blends with diesel are scarce, this finding agrees with that of Álvarez et al. (201), as they found that BuOH caused reductions in the flash point of blends of biodiesel, n-butanol, and diesel. Their results showed that BuOH in diesel/biodiesel blends caused the flash point to reduce to around 40 °C. The fraction of BuOH before the 40 °C flash point was reached increased as the biodiesel fraction increased, indicating there was an increase

in intermolecular interactions between the three fuel components (201). The mixture behaviour is known to play a role, and this is usually captured using activity coefficients in the models discussed in section 2.8.2. Therefore, it is known that intermolecular interactions play a significant role in the flash points of multi-component blends, but the data available currently is limited, and this finding contributes to this data. In the butyl-based blend, butanol has the shortest chain and highest polarity. Therefore, butanol had fewer favourable intermolecular interactions with diesel. The requirement for lower fractions of BuOH in the butyl-based blends is not only beneficial to have higher flash points, but also for the overall sustainability of the alcoholysis process, as BuOH can be recycled to produce more BL. Recycling the separated BuOH reduces the amount of BuOH required to be purchased and delivered, which reduces the associated emissions from the production and delivery of BuOH whilst also reducing the production costs of the three-component blends. Therefore, recycling BuOH to produce BL would be economically favourable and contribute to maintaining the lower lifecycle emissions associated with the fuel blends. The greatest reductions in KV40 came from the blends with high DNBE fractions (figures 4.20 and 4.22), which was expected since DNBE had the lowest KV40. If the DNBE fraction in the blend were too high, the KV40 would be below the minimum limit in the fuel standards. Having KV40s below the minimum would be detrimental to the fuel injection quality and the effectiveness of the fuel pump. A low KV40 would increase wear on the fuel pump and fuel injector as there could be reduced lubrication of these parts, which would incur additional maintenance costs for those using the fuels in CI engines.

- Are there suitable models for predicting the physical and combustion properties, emissions, and engine performance, or will these need to be developed?

The inaccuracy of readily available blending rules for predicting flash points and the difficulty accessing accurate models since they require access to databanks and software, which are often behind paywalls, demonstrated the need for empirical models. For KV40 predictions, there were no accurate models for blends with more than two components, and thus empirical models were needed. The density of multi-component blends can be predicted using Kay's mixing rule, which is a linear blending rule, with a greater accuracy when using the volume fraction. It was established in this work that Kay's mixing rule using a linear-by-volume approach was as accurate at predicting the density of the ethyl, butyl, and pentyl-based three-component blends. However, for ethyl-based blends with high DEE fractions there were differences between the predictions from the MODDE model and Kay's mixing rule. These differences may have been due to evaporative losses when measuring the density of the blends used to construct the MODDE model, further indicating the unsuitability of blends containing DEE.

The models developed in this work were accurate within the bled ranges defined in table 3.1, as they had good agreement with experimental data, and they could predict values with high precision. The models are currently limited to these regions as there insufficient time to investigate outside of these ranges and to produce models based on carbon chain length of the compounds. The high R^2 values and low AARD% (section 8.1.1), indicated there were small differences between measured and predicted values. The DoE methodology was suitable for the production of these empirical models. Due to time constraints, models for predicting the properties of blends with diesel and models with a carbon chain length term were not developed.

For engine modelling there were no simple and suitable CI engine models available for modelling the combustion of the ethyl and butyl-based blends. The DI CI engine model available in Chemkin could not model the Yanmar L100V engine (section 7.1) (249). Other models available in the literature were designed for specific engines, such as the model constructed by Rakopoulos et al. (251) for the Hydra engine. However, the gas phase combustion could be modelled, which is not fully representative of CI engine combustion as there was no fuel injection, no turbulent mixing, and no fuel vaporisation.

IDTs and HRRs were simulated at engine relevant thermodynamic conditions using a variable volume approach. However, these simulations did not predict the same relative changes as those observed in the engine testing. This highlighted the need to model the physical processes for realistic predictions of the combustion behaviours observed in an engine. For the ethyl and butyl-based blends, the simulated IDTs showed expected chemical trends of becoming longer with increasing levulinate fraction. Since the reactor model used was an adiabatic homogeneous gas phase reactor, the HRR behaviour did not match that presented in Chapter 5. The mixing-controlled combustion modes in a CI engine were not captured in the simulations since a homogeneous gas-phase reactor was used. Therefore, the simulated HRR did not replicate that of a CI engine. Until a suitable CI engine model can be found, predicting the emissions may be inaccurate. In the current versions of the chemical kinetic mechanisms there are no NO_X or PM sub-mechanisms. Therefore, for future use these would need to be added. The ethyl-based three-component blend and the DNBE and BuOH chemical kinetic mechanisms were shown to reproduce RCM and shock tube data. Therefore, the methodology used by Dr. Christian Michelbach to produce the chemical kinetic mechanisms ensured IDTs could be predicted with an acceptable degree of accuracy. This would be confirmed with additional experimental data from RCM and shock tube experiments as this data would be used as validation for the mechanisms.

One additional finding in this work was that the Chemkin DI engine model applies a linear-by-mass blending law for predicting the properties of fuel blends. Such blending

laws would be unsuitable for predicting the viscosity, as shown in Chapter 4. It is unlikely the viscosity is the only property that does not follow a linear blending rule. Therefore, there must be appropriate property blending laws included in CI engine models to ensure the influence of the physical properties on IDTs are captured. Many other reported CI engine models, including those with CFD, have used single or two-component surrogate fuels and have not included any blending laws for determining the properties of multi-component blends. Therefore, there would need to be further investigation into finding models that have appropriate blending laws included.

- What is the influence on engine performance and emissions when using different advanced biofuel formulations?

One key finding from this work was that a CI engine can run using blends of diesel and advanced biofuel blends without modifications. It was evident that the engine stability was dependent on the fuel's physical properties and not just the combustion properties. This was observed with the 100% biofuel ethyl-based blends that had predicted DCNs of 40 and 50, as the engine would not start due to high DEE fractions. Even when blended with diesel, the engine would not start or would be unstable. It was only when DEE was less than 3 vol% of the total blend that 75% and 92% load could be achieved. The instabilities caused fluctuations in RPM and power, resulting in emissions fluctuations, as shown in section 6.1. If the ethyl-based blends could be utilised in CI engines, with the correct fuel handling procedures in place, the alcoholysis process either would need to intrinsically produce low DEE fractions or there would need to be post-processing to remove DEE from the blend. Therefore, if the alcoholysis process was used on a commercial scale to produce a diesel alternative, the DEE removal would need to be included if any ethyl-based blends are to be used. In contrast, for the butyl-based blends DNBE does not need to be removed to the same extent, as having 10 – 20 vol% in the biofuel blend resulted in preferential engine performance.

The butyl-based blends studied were able to have a similar engine performance to ULSD, albeit with longer IDTs. The similar engine performance from a non-optimised engine demonstrates that the butyl-based blends may be potential advanced biofuel candidates and contribute towards the REDII targets for advanced biofuel use. There was incomplete combustion with the ethyl and butyl-based blends with increases in THC and CO specific emissions indices. The use of lower BL fractions in the butyl-based blends is preferential for CO emissions control. The lower fractions of BL are more feasible given the typical BL yields from alcoholysis (table 2.5). Using lower BL fractions could be preferential, as it would allow for the BL produced to be utilised in more applications. The reduction of $PM_{2.5}$ and PN, were likely due to the additional oxygen present in the fuel, the reduced aromatic content in the fuel, and the molecular structures

reducing soot precursor formation. The 10 vol% butyl-based blends had similar O/C fuel molar ratios, which correlated with the similar PM reduction with any biofuel blend as the oxygen content would be similar. As a result, blend compositions could be formulated to minimise the changes in the other emissions and maintain PM reduction.

Matching the physical properties of the butyl-based blends reduced the influence of the changes in the physical properties on the IDT. The increase in density from ULSD with the 25 vol% butyl-based blend had an increased influence and this was highlighted when studying the influence of the injector design for the tested butyl-based blend. Additionally, there may have been the influence of the changes in heat capacity and enthalpy of vaporisation on IDTs and thus the emissions. The injector design is influential on the emissions and the differences require further investigation with additional biofuel blends to confirm the extent of its influence. This would enable the opportunity to optimise blends for a range of injector designs, which would be beneficial given the range of injectors used in ICEs. Overall, the blend composition and engine operation need to be optimised in tandem as any optimisation of the engine will influence the performance and emissions.

8.2 Feasibility of the Different Advanced Biofuel Blends

The fractions of biofuel blended with diesel exceeds the maximum limits for biodiesel content in existing diesel standards and yet they have still been shown to meet property limits and have suitable engine performance (12, 16). It was evident from the physical properties testing and the engine and emissions testing that the butyl-based blends would be the most suitable for use as low-carbon alternative fuels. The butyl-based blends gave stable operation at all loads, unlike the ethyl-based blends. This highlights that longer carbon chain length advanced biofuels would be more suited for CI engine applications and that butanol alcoholysis should be develop rapidly.

One key factor in the fuel blends feasibility is its production. The alcoholysis process, with or without post-reaction processing, needs to be able to produce product blends with high BL fractions and low BuOH fractions. This may involve the recycling of BuOH to produce more BL after a post-reaction separation. There also needs to be largescale production of these blends, and this needs to happen rapidly for these fuels to be utilised in the short term (104, 113, 116).

Butyl and pentyl-based blends, with and without diesel, complied with the physical property limits in existing fuel standards (12, 16). This highlights the existing fuel standards can be met with fuels that are deemed to be non-compliant. The non-compliance was due to the addition of oxygenated biofuel components to ULSD. One of the common concerns when using oxygenated biofuels is the reduced fuel economy due

to their lower energy density. The butyl-based blends tested had a negligible changes in BSFC which is an encouraging result and demonstrates there is potential for these blends to be diesel low-carbon alternatives.

All the selected butyl-based blends were compatible with the engine, and all engine loads could be achieved, with the FJ injector. There would need to be further assessment into their use when running the FB injector, as there was only the time available to test one blend. The specific emissions indices showed that without modification to the engine or optimisation of its operation, the fuels would result in non-compliance with the emissions standards (section 6.6). This highlighted the need for aftertreatment systems or engine optimisation. The unstable operation of the genset using the ethyl-based blends highlighted that they would be unsuitable for use in a CI engine. The instability highlights that the use of ethanol as the starting alcohol would be unsuitable for producing REDII advanced biofuel blends as diesel blend components. This could be problematic as the production of second generation n-butanol is currently limited (section 2.6.1). Therefore, there would need to be increased production of n-butanol to ensure there was a large enough supply for large-scale alcoholysis of biomass using n-butanol. The source of n-butanol and the biomass feedstock used will dictate the carbon reduction potential of the alcoholysis product blends. However, the process should be designed such that the associated carbon emissions for a well-to-wheel lifecycle assessment are lower than that of the production and use of diesel.

The Yanmar L100V has no aftertreatment systems, so the changes in the emissions could not be controlled. If there was a retrofit of aftertreatment systems, the Euro Stage V emissions limits could be met. Additionally, if there was optimisation of the engine operation, there may be no need for aftertreatment systems, but the ease of the modifications would decide which method to pursue. Changing the injection timing on the Yanmar L100V is more difficult than changing it in a vehicle, as the Yanmar engine's injection timing is set by the flywheel and not an ECU. The other option could be to increase the DCN of the blends using CN enhancers.

Since the REDII target is to have 3.5% of the total energy content in the transport sector from advanced biofuels, the findings of this project demonstrate that there could be fuel blends compatible with existing engine technologies that satisfy these targets (14). The utilisation of butyl-based blends produced from the alcoholysis of Annex IX feedstocks would contribute towards the decarbonisation of CI engine applications. Their utilisation in gensets could also be beneficial for air quality with lower $PM_{2.5}$, THC, and VOC emissions, making these blends more appropriate for use provided they could be produced in large quantities.

8.3 Recommendations Based on Research Outcomes

As demonstrated in Chapter 4, it is possible to have advanced biofuel blends, with and without diesel, that comply with the physical property limits set in existing fuel standards. However, adding these oxygenated biofuel blends to diesel would result in a fuel that no longer complies with EN 590 or BS 2869 (12, 16). Therefore, the first recommendation is there should be changes to existing fuel standards or the development of a standalone fuel standard to allow the use of oxygenated biofuels as diesel blend components. This may require some of the property limits to change, primarily the density, as the limits for the flash point can still be met. This would allow the use of oxygenated advanced biofuel components to contribute towards the decarbonisation of CI engine applications.

CI engines must be easily optimisable, or be easy to retrofit aftertreatment systems to, so emissions when using the advanced biofuel blends comply with emissions standards. If an engine can be optimised based on the results in Chapters 5 and 6, such as advancing the injection timing, the performance and emissions may become closer to, or potentially better than, that of ULSD. Without engine optimisation, a DOC should be retrofitted to the Yanmar L100V to ensure the CO and THC tailpipe emissions are compliant with the emissions limits. The reduction in $PM_{2.5}$ and PN from the butyl-based blends would alleviate the requirement for DPFs. Since the NO_X emissions are similar to ULSD, retrofitting or changing SCR or NSC systems may not be required unless the NO_X emission limits reduce in the next version of the NRMM emissions standard.

To simulate CI engine operation it needs to be ensured that the models would converge when using any engine geometry and chemical kinetic mechanism. Models used in future work should be selected if they include suitable blending laws for predicting the physical properties when using multi-component fuel blends. This is due to the importance of the physical processes on the IDT, and the influence of the blend composition on these properties. Therefore, it is likely these CI engine models would be CFD models using appropriate, and most likely reduced, chemical kinetic mechanisms.

8.4 Future Work

This work produced predictive models for the density, flash point, and KV40 of the three-component blends. One expansion to these models would be to develop models for each property that include the carbon chain length dependency. There is also a need for accurate models to predict the properties of different three-component blends with diesel. These models would be specific to the diesel used in this work since each diesel has different properties. Such a model would enable the blends that comply with different fuel standards' property limits to be determined.

For fuels to comply with a fuel standard every property limit must be met. Therefore, they need to be measured. Additionally, some properties that are not in fuel standards must be measured to determine a fuel blend's suitability. These properties include materials compatibility, LHV, enthalpy of vaporisation, and heat capacity. The LHV is also used for further combustion analysis, including determining the mass fraction of fuel burnt. Assessing material compatibility is vital, as any damage to the engine and its auxiliary components could result in fuel leaks. In fuel standards, the only required material compatibility test is the copper corrosion test. Additionally, there must be compatibility with other materials, such as elastomers used in fuel lines and seals. Copper corrosion and elastomer compatibility may depend on blend composition, especially if levulinic acid is formed from the degradation of alkyl levulinate. Copper corrosion and elastomer compatibility tests of the butyl-based three-component blends have not been reported in the literature.

The testing in this work used alcoholysis model product three-component blends. However, many other products may be produced during alcoholysis such as furfurals and fructosides (112). Therefore, a range of product blends from butanol alcoholysis must be used to determine the impact of the product blends on the engine performance and emissions. These product blends could be produced as part of the SusLABB project using the optimum reaction conditions. The use of real product blends in engine tests would determine how representative the changes in the engine performance and emissions the model three-component blends were. The product blend used should be tailored by reducing the n-butanol fraction, since it influences the flash point. There may also be trace compounds and contaminants such as inorganic compounds containing sulphur and chlorine as these are commonly found in metal salts in the biomass ash (25, 63, 65, 113, 116). When using biomass there will also be metals such as sodium and potassium from the ash content (25, 63, 65, 113, 116). If these were in fuels, they would affect emissions composition and would likely be present in PM. These inorganic species could poison aftertreatment catalysts, reducing their efficiency and increasing tailpipe emissions. Knowing and understanding the fate of these metals is vital, as they will affect the emissions, local air quality, and public health.

To determine the influence of the biofuel blend composition on the composition of $PM_{2.5}$ chemical analysis should be conducted. This should include the analysis of the PAH compounds. The changes in PAH composition would need to be determined using gas-chromatography mass spectrometry. The presence of VOCs could be quantified using proximate analysis. This technique would also quantify the fixed carbon content and ash in PM. Knowing the changes in the ratio of fixed carbon to volatile matter in PM would allow a further understanding of the biofuel blend's influence on the PM composition and size distribution.

IQT measurements of the butyl-based blends, with and without diesel, are needed not only to produce a DCN model for the butyl-based blends, similarly to the ethyl-based blend DCN model of Howard et al. (37) but to investigate the influence of the addition of the biofuel components on the DCN of diesel. The RCM data that would be used for the mechanism validation could be used along with the IQT data to establish the relative importance of the chemical, mixing, and evaporation effects on the blend's IDT similar to the analysis conducted by Barraza-Botet et al. (119) for ethanol/iso-octane blends.

The simulations in this work were limited to using a gas-phase homogeneous reactor and hence could not represent the effect of physical processes such as fuel atomisation and vaporisation or the interaction between turbulent mixing and chemical processes. The use, or development, of a CFD CI engine model which included turbulent mixing and fuel injection, using the Yanmar L100V engine specification should enable accurate and more representative simulations to be conducted. The use of CFD is substantially more computationally demanding than 0D reactor modelling and it would require the kinetic mechanisms to be reduced along with the use of high performance computers. Therefore part of the future work should include development of accurate reduced kinetic mechanisms for use in CFD models. If this is possible, an understanding of how the fuel blend's physical properties influence the engine performance can be developed. It would also enable the more effective screening of possible biofuel blend formulations. This would also enable a significant cost saving, as less engine testing could be needed. Accurate predictions of the changes in the combustion behaviours, emissions, and IDTs when using different advanced biofuel formulations would be beneficial. The simulations would need to be compared against fundamental experiments which would investigate the combustion and oxidation of the fuel blends, including RCM and jet-stirred reactor experiments, where the species concentrations can also be measured. The chemical kinetic mechanism can then be validated using these results and the fidelity between the simulations and experiments can be determined. The accuracy of the simulations will depend on the accuracy of the chemical kinetic mechanisms for the combustion of the biofuel blends being available.

Since the mechanisms used for the combustion modelling were brute force merged mechanisms, there was a lack of cross-reactions between the biofuel components, the surrogate diesel, and their intermediates. RMG could be used to produce a full mechanism of the biofuel components and a diesel surrogate to ensure the cross-reactions between all components that met the selection criteria were included. The use of RMG would reduce the impact of human error. Additionally, a new diesel surrogate may be needed to ensure an accurate representation of the chemical composition of diesel (236, 239, 304, 364). The surrogate could be designed to meet kinetic, chemical, and physical properties to ensure that simulations accurately predict the effects of these

properties. There are other diesel surrogates that contain components additional to those in the LLNL surrogate, such as napthalenes and iso-alkanes, but these would need to be tested experimentally and computationally to validate their suitability (236-238).

Most blends tested in this work are compatible with and work in a CI engine. However, the Yanmar L100V is not representative of every engine technology. Therefore, the fuels should be tested in vehicle engines and vehicles. The fuel blends should also be tested under transient conditions following the WHTC method, as the engine tests in this work were steady-state engine tests. The engine and vehicle used should be Euro 6 compliant. This would ensure fuel compatibility and the suitability of a range of fuels with its operation, fuel delivery system, and exhaust aftertreatment systems could be assessed. Before any fuel blend is used in a vehicle, it should be tested in a representative engine following the NEDC and WLTP laboratory-based engine tests, as this test is required for the type approval of a vehicle and powertrain. The impact of different fuel blends on the vehicle's compliance with the Euro 6 LDV emissions standard needs to be understood, to establish if the fuel blends could be REDII compatible low-carbon alternatives to diesel. Since the alcoholysis product blends are impure, the model three-component blends should be used for vehicle testing to establish the biofuel components compatibility with the vehicle. The presence of impurities is a barrier that must be overcome. There needs to be an understanding of the influence of these impurities on the physical properties, along with their impact on engine performance and emissions. This would enable the extent of purification required to be understood. The impact of the model three-component blends and alcoholysis product blends on real driving emissions (RDE) and a vehicle's operation needs to be established. Using these fuel blends in ICE and hybrid vehicles would give a clear indication of the impact of the fuel blends on the emissions and their suitability. A hybrid vehicle would be an ideal candidate for RDE tests using these fuels, as HDVs are starting to have their powertrains electrified. Hybrid vehicles have different emissions profiles compared to pure ICE vehicles, as they can have cold start phases when switching between electric and ICE drive modes. Since the fuels tested in this work had increased CO and THC emissions, these would likely be emitted when the aftertreatment systems are cold. This would require accurate portable emission analysers to be used and validation against laboratory based emissions analysers. RDE tests will give a clearer understanding of the utilisation of these advanced biofuel blends, as they will establish their suitability for vehicle applications.

Appendix A

MODDE Model Coefficients

The following tables contain the model coefficients determined using MODDE (256).

A.1 Density Model Coefficients

Table A.1. Coefficients for the ethyl-based blend's density linear model.

Component (volume fraction)	Coefficient	P-Value	95% Confidence interval (±)
Constant	0.924	0.00	0.005
EtOH	-0.133	1.45×10^{-25}	0.008
EL	0.093	1.26×10^{-25}	0.005
DEE	-0.189	4.93×10^{-30}	0.008

Table A.2. Coefficients for the butyl-based blend's density linear model.

Component (volume fraction)	Coefficient	P-Value	95% Confidence interval (±)
Constant	0.908	0.00	0.008
BuOH	-0.112	2.30×10^{-16}	0.013
BL	0.070	3.54×10^{-15}	0.009
DNBE	-0.128	4.04×10^{-18}	0.013

Table A.3. Coefficients for the pentyl-based blend's density linear model.

Component (volume fraction)	Coefficient	P-Value	95% Confidence interval (±)
Constant	0.906	0.00	0.002
PeOH	-0.090	5.63×10^{-33}	0.003
PL	0.060	3.39×10^{-32}	0.002
DNPE	-0.117	1.30×10^{-36}	0.003

A.2 Flash Point Model Coefficients

Table A.4. Coefficients for the butyl-based blend's flash point quadratic model.

Component (volume fraction)	Coefficient	P-Value	95% Confidence interval (±)
Constant	34.930	1.38×10^{-14}	4.661
BuOH	-7.989	1.12×10^{-1}	9.983
BL	8.066	1.00×10^{-2}	5.968
DNBE	-19.876	8.80×10^{-4}	10.877
$BuOH^2$	82.012	1.42×10^{-4}	37.845
BL^2	26.872	6.90×10^{-7}	8.500
$DNBE^2$	54.242	5.25×10^{-3}	36.591
BuOH×BL	-100.870	2.03×10^{-6}	34.126
BuOH×DNBE	184.435	2.29×10^{-5}	73.672
BL×DNBE	-84.792	4.72×10^{-6}	30.318

Table A.5. Coefficients for the pentyl-based blend's flash point quadratic model.

Component (volume fraction)	Coefficient	P-Value	95% Confidence interval (±)
Constant	58.956	5.69×10^{-29}	2.255
PeOH	-42.840	8.67×10^{-17}	4.785
PL	14.790	3.93×10^{-11}	2.860
DNPE	-8.254	2.36×10^{-3}	5.047
$PeOH^2$	103.317	5.12×10^{-12}	18.237
PL^2	15.329	1.40×10^{-8}	3.939
$DNPE^2$	31.103	1.29×10^{-3}	17.774
PeOH×PL	-73.858	3.38×10^{-10}	15.786
PeOH×DNPE	48.514	5.76×10^{-3}	33.190
PL×DNPE	-32.051	9.14×10^{-5}	14.325

A.3 KV40 Model Coefficients

Table A.6. Coefficients for the butyl-based blend's KV40 quadratic model.

Component (volume fraction)	Coefficient	P-Value	95% Confidence interval (±)
Constant	1.469	2.75×10^{-25}	0.068
BuOH	-0.163	3.37×10^{-2}	0.149
BL	0.317	8.39×10^{-8}	0.088
DNBE	-0.932	6.62×10^{-12}	0.159
BuOH^2	1.596	4.25×10^{-6}	0.562
BL^2	0.264	1.94×10^{-4}	0.124
DNBE^2	0.309	2.54×10^{-1}	0.545
BuOH×BL	-1.284	1.88×10^{-5}	0.502
BuOH×DNBE	1.242	2.58×10^{-2}	1.079
BL×DNBE	-0.538	2.05×10^{-2}	0.448

Table A.7. Coefficients for the pentyl-based blend's KV40 quadratic model.

Component (volume fraction)	Coefficient	P-Value	95% Confidence interval (±)
Constant	1.831	0.00	0.017
PeOH	-0.196	1.63×10^{-11}	0.036
PL	0.339	5.01×10^{-23}	0.022
DNPE	-0.977	1.13×10^{-28}	0.038
PeOH^2	1.363	8.03×10^{-18}	0.139
PL^2	0.178	1.67×10^{-12}	0.030
DNPE^2	0.288	1.59×10^{-4}	0.135
PeOH×PL	-0.926	3.38×10^{-15}	0.120
PeOH×DNPE	0.473	6.53×10^{-4}	0.252
PL×DNPE	-0.304	4.29×10^{-6}	0.109

A.4 IDT Model Coefficients

Table A.8. Coefficients for the ethyl-based blend's IDTs at 960 K linear model.

Component (volume fraction)	Coefficient	P-Value	95% Confidence interval (±)
Constant	0.945	5.83×10^{-12}	0.079
EtOH	-0.516	1.81×10^{-5}	0.164
EL	0.364	3.05×10^{-6}	0.097
DEE	-0.740	3.04×10^{-7}	0.159

Table A.9. Coefficients for the ethyl-based blend's IDTs at 1020 K linear model.

Component (volume fraction)	Coefficient	P-Value	95% Confidence interval (±)
Constant	0.510	2.38×10^{-19}	0.010
EtOH	-0.188	2.28×10^{-10}	0.021
EL	0.118	1.05×10^{-10}	0.013
DEE	-0.221	2.25×10^{-11}	0.021

Table A.10. Coefficients for the butyl-based blend's IDTs at 964 K quadratic model.

Component (volume fraction)	Coefficient	P-Value	95% Confidence interval (±)
Constant	1.023	1.11×10^{-9}	0.075
BuOH	-0.125	1.60×10^{-1}	0.187
BL	0.486	3.36×10^{-6}	0.099
DNBE	-1.555	5.01×10^{-8}	0.184
BuOH^2	0.823	1.59×10^{-1}	1.223
BL^2	0.604	3.36×10^{-3}	0.338
DNBE^2	2.956	2.41×10^{-4}	1.087
BuOH×BL	-1.468	2.85×10^{-2}	1.269
BuOH×DNBE	3.425	8.74×10^{-3}	2.292
BL×DNBE	-2.703	6.25×10^{-4}	1.148

Table A.11. Coefficients for the butyl-based blend's IDTs at 1020 K quadratic model.

Component (volume fraction)	Coefficient	P-Value	95% Confidence interval (±)
Constant	0.613	1.22×10^{-20}	0.003
BuOH	-0.130	4.52×10^{-11}	0.008
BL	0.150	5.18×10^{-14}	0.004
DNBE	-0.387	3.07×10^{-15}	0.008
BuOH^2	0.117	4.78×10^{-5}	0.036
BL^2	0.067	6.86×10^{-9}	0.007
DNBE^2	0.205	4.56×10^{-7}	0.036
BuOH×BL	-0.205	9.09×10^{-8}	0.030
BuOH×DNBE	0.475	1.97×10^{-8}	0.059
BL×DNBE	-0.256	6.11×10^{-9}	0.028

Appendix B

Data for Chapter 6

B.1 FTIR Spectroscopy Raw Data

Table B.1 Raw FTIR data for the **e**thyl-based blend engine tests.

Fuel Blend	Engine Load (%)	Formaldehyde (ppm)	Acetaldehyde (ppm)	Hexane (ppm)	DNBE (ppm)	DEE (ppm)	EtOH (ppm)	Acetic Acid (ppm)
ULSD FB Injector	92	2.99±0.60	1.71±0.80	9.89±1.48	1.39±1.04	0.13±0.12	5.80±7.92	0.62±0.71
	75	4.28±0.11	1.17±0.99	11.74±1.16	0.91±0.36	0.26±0.33	1.54±1.92	1.06±0.32
	50	7.63±0.85	1.42±1.30	11.95±1.01	1.99±0.84	0.01±0.02	9.93±9.64	0.77±0.51
	28	10.68±0.48	1.95±1.23	11.75±0.57	1.61±0.37	0	3.50±4.28	0.80±0.68
	4	15.83±1.14	4.00±2.17	12.40±1.24	2.41±0.95	0	5.82±5.50	1.92±0.85
85% ULSD 15% Biofuel (75 vol% EL, 5 vol% EtOH, 20 vol% DEE)	92	7.26±0.78	6.91±2.98	35.34±20.00		1.14±0.58	12.69±9.14	3.21±0.68
	75	14.68±11.43	6.51±5.85	24.29±7.81		2.00±1.96	11.25±7.22	3.56±3.01
	50	12.16±1.10	1.58±0.58	19.08±1.76		0.51±0.78	10.42±3.84	1.57±0.57
	28	17.63±0.58	3.52±0.54	16.10±0.22		0.75±49	22.79±10.39	1.02±1.31
	4	26.38±1.35	6.76±0.82	15.51±0.36		0.02±0.002	23.83±10.56	2.63±1.74
85% ULSD 15% Biofuel (95 vol% EL, 5 vol% EtOH)	92	3.39±0.50	2.15±0.81	17.69±1.20		1.08±0.90	3.10±1.92	2.79±0.64
	75	5.48±0.41	0.30±0.52	13.26±0.78		1.44±0.40	4.00±3.16	1.70±0.53
	50	12.30±0.57	0.65±1.13	13.45±0.34		1.69±0.81	5.43±3.44	2.59±0.18
	28	17.69±0.42	2.85±0.10	13.35±0.76		1.81±1.23	3.81±0.65	3.02±0.39
	4	27.62±0.15	5.94±1.07	15.02±0.42		2.07±1.33	5.66±1.44	4.68±0.23
75% ULSD 25% Biofuel (75 vol% EL, 5 vol% EtOH, 20 vol% DEE)	50	89.14±45.19	22.53±13.19	111±68.98		26.70±16.25	33.81±16.19	19.46±11.48
	28	94.69±55.14	15.59±4.73	111.76±53.37		30.66±18.358	34.57±16.12	20.23±6.69
	4	48.90±1.13	16.20±0.96	36.34±5.31		10.61±1.78	17.78±1.35	7.71±0.61
75% ULSD 25% Biofuel (65 vol% EL, 5 vol% EtOH, 30 vol% DEE)	50	122.84±9.49	48.86±7.23	141.47±34.04		33.75±5.64	35.69±13.90	10.20±3.85
	28	266.28±78.12	51.41±12.94	289.36±16.23		134.09±57.60	133.00±62.00	24.00±17.17
	4	217.19±149.00	15.96±3.62	279.62±117.46		145.26±110.03	119.76±133.80	23.69±26.41

Table B.2. Raw FTIR data for the butyl-based blend engine tests.

Fuel	Engine Load (%)	Formaldehyde (ppm)	Acetaldehyde (ppm)	Hexane (ppm)	DNBE (ppm)
ULSD FJ Injector	92	4.81±1.0	6.81±0.21	20.57±6.91	3.66±1.82
	75	4.84±0.52	5.98±2.09	17.60±1.27	2.59±1.73
	50	8.68±1.82	5.21±1.68	23.90±1.02	3.55±1.11
	28	12.43±0.81	4.25±0.64	32.06±2.20	3.06±0.93
	4	13.75±0.81	5.62±1.05	29.44±3.67	3.81±1.17
90% ULSD 10% Biofuel (65 vol% BL, 5 vol% BuOH, 30 vol% DNBE)	92	4.15±0.17	6.06±1.76	20.03±3.16	2.50±1.09
	75	7.18±1.08	4.99±0.68	17.94±0.46	1.64±1.31
	50	14.48±1.54	5.42±1.86	24.43±0.52	2.71±1.51
	28	14.19±0.75	5.18±1.55	27.88±1.01	2.60±0.86
	4	20.55±3.47	8.46±1.83	27.35±1.88	3.66±1.48
90% ULSD 10% Biofuel (75 vol% BL, 5 vol% BuOH, 20 vol% DNBE	92	5.00±0.66	7.78±0.70	29.20±6.33	1.98±1.58
	75	7.73±1.49	5.99±1.73	19.00±2.09	0.82±1.11
	50	13.16±0.69	7.88±0.22	25.32±2.68	2.85±0.53
	28	15.82±1.87	5.93±1.00	30.29±10.51	1.55±1.17
	4	22.37±2.85	8.71±0.68	29.59±7.46	2.05±1.31
90% ULSD 10% Biofuel (85 vol% BL, 5 vol% BuOH, 10 vol% DNBE)	92	4.45±0.44	6.95±1.98	16.25±2.13	2.32±1.61
	75	7.74±0.51	5.13±1.45	17.71±3.91	1.96±0.50
	50	14.16±0.36	5.00±2.11	30.29±2.46	1.93±0.59
	28	19.73±2.17	8.17±0.88	36.20±2.85	2.00±1.25
	4	26.08±0.90	11.11±0.34	40.54±3.08	2.70±0.59
90% ULSD 10% Biofuel (85 vol% BL, 10 vol% BuOH, 5 vol% DNBE)	92	5.91±0.61	5.34±0.64	14.06±1.18	
	75	7.70±1.22	4.22±0.60	15.62±1.56	
	50	13.46±0.97	4.25±0.36	29.82±1.97	0.18±0.03
	28	19.07±1.05	6.46±1.11	36.01±0.12	0.56±0.12
	4	29.58±2.64	11.43±0.75	48.73±7.47	0.41±0.26
90% ULSD 10% Biofuel (90 vol% BL, 5 vol% BuOH, 5 vol% DNBE)	92	5.40±0.73	4.70±1.38	13.07±1.01	0.85±1.15
	75	6.67±0.15	3.99±1.61	13.81±1.71	1.14±1.05
	50	13.39±0.30	5.14±1.95	31.00±3.67	1.08±0.50
	28	18.43±0.91	6.96±1.63	35.08±3.23	1.73±0.43
	4	28.71±1.89	11.34±0.90	44.92±3.83	1.20±0.69
75% ULSD 25% Biofuel (85 vol% BL, 5 vol% BuOH, 10 vol% DNBE)	92	5.49±0.32	6.015±0.20	14.14±1.62	1.10±0.91
	75	9.08±0.47	4.90±0.85	16.47±1.42	0.66±0.88
	50	17.90±0.73	6.22±0.68	28.50±1.59	2.90±1.69
	28	28.12±0.67	9.33±0.44	38.86±0.42	3.61±1.97
	4	39.48±1.86	13.92±0.09	40.87±2.90	0.37±0.48
75% ULSD 25% Biofuel (90 vol% BL, 5 vol% BuOH, 5 vol% DNBE)	92	5.79±0.72	6.11±1.38	16.17±3.21	1.82±1.62
	75	9.81±0.50	4.84±1.39	15.63±1.81	2.31±1.40
	50	18.32±0.84	6.14±0.30	28.11±3.14	2.00±1.28
	28	24.61±0.32	6.71±0.43	30.86±2.28	2.40±1.26
	4	35.83±2.05	10.35±0.17	36.98±2.65	1.73±1.42

B.2 Butyl-Based Blends PNSDs
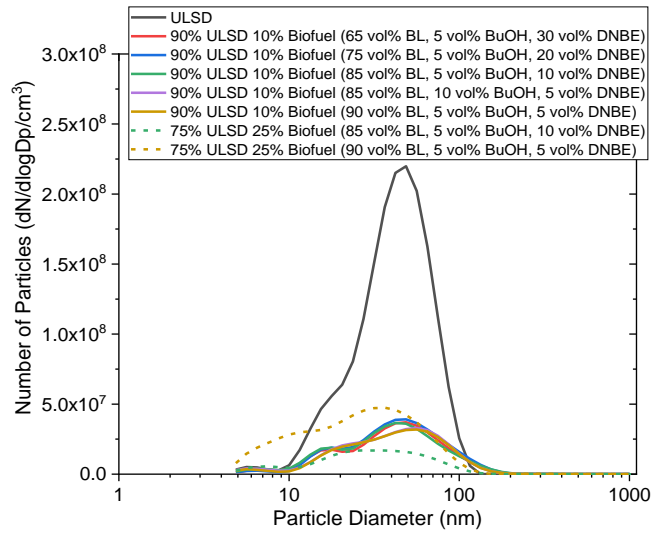
Figure B.1. PNSDs from the butyl-based blends engine tests at 4% load.
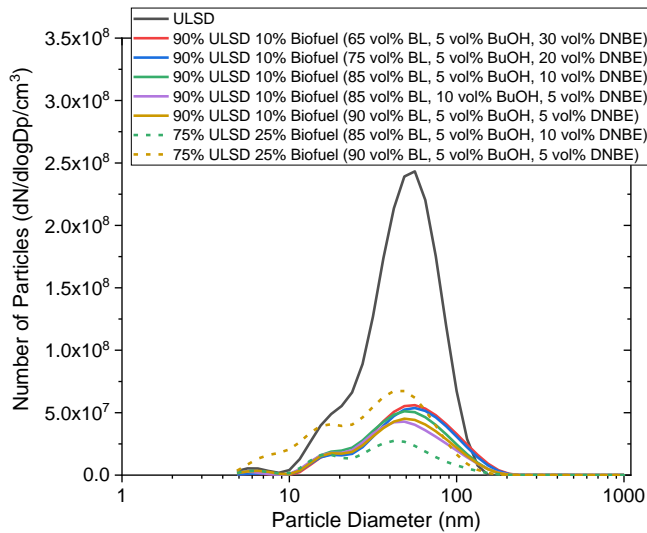
Figure B.2. PNSDs from the butyl-based blends engine tests at 28% load.
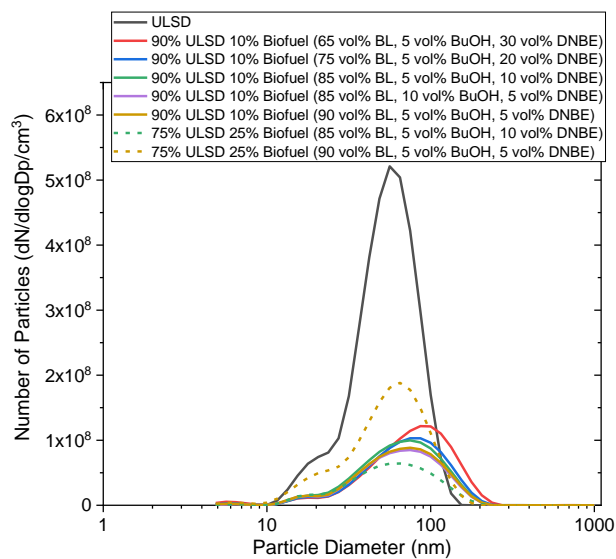
Figure B.3. PNSDs from the butyl-based blends engine tests at 75% load.

References

1. International Energy Agency. *Transport* [online]. Paris: IEA, 2022. Available from: https://www.iea.org/.

2. Rodríguez, S.W.a.F. Global Overview of Government Targets for Phasing Out Internal Combustion Engine Medium and Heavy Trucks. [online]. 2021. Available from: https://theicct.org/.

3. Basma, H. and F. Rodríguez. *Race to Zero: How manufacturers are positioned for zero-emission commercial trucks and buses in Europe*. Washington, DC: International Council on Clean Transportation, 2021.

4. Reif, K. and K.-H. Dietsche. *Automotive handbook.* 9th edition, revised and extended / by Prof. Dr.-Ing. Konrad Reif, Dipl.-ing Karl-Heinz Dietsche ; and approx. 200 authors from industry and the university and college sector. ed. Karlsruhe: Robert Bosch GmbH, 2014.

5. Robert Bosch Gmbh ed. *Diesel-Engine Management*. Fourth edition completely revised and extended. ed. Plochingen: Robert Bosch Gmbh, 2005.

6. United Nations. *Adoption of the Paris Agreement.* Paris, 2015.

7. Department for Transport. HM Government. *The Road to Zero.* London, UK, 2018.

8. BEIS. *Net Zero Strategy: Build Back Greener.* London, United Kingdom: HM Government, 2021.

9. European Commission. *Delivering the European Green Deal* [online]. 2019. [Accessed 11/11/2022]. Available from: https://ec.europa.eu/.

10. International Energy Agency. *Trucks and Buses* [online]. Paris: IEA, 2022. Available from: https://www.iea.org/.

11. International Energy Agency. *Global EV Outlook 2022* [online]. Paris: IEA, 2022. Available from: https://www.iea.org/.

12. British Standards Institution. BS EN 590:2022. *Automotive fuels - Diesel - Requirements and test methods.* Milton Keynes: BSI, 2022.

13. Christensen, E., A. Williams, S. Paul, S. Burton and R.L. Mccormick. Properties and Performance of Levulinate Esters as Diesel Blend Components. *Energy & Fuels*, 2011, **25**(11), pp.5422-5428.

14. The European Parliament and Council of the European Union. *Directive (EU) 2018/2001 of the European Parliament and of the Council of 11 December 2018 on the promotion of the use of energy from renewable sources* [online]. 2018. [Accessed 29/10/2019]. Available from: https://eur-lex.europa.eu.

15. British Standards Institution. BS EN 14214:2012+A2:2019. *Fatty acid methyl esters (FAME) for use in diesel engines and heating applications. Requirements and test methods.* Milton Keynes: BSI, 2019.

16. British Standards Institution. BS 2869:2017. *Fuel oils for agricultural, domestic and industrial engines and boilers* Milton Keynes: BSI, 2017.

17. Hossain, S., H.H. Masjuki, M. Varman, M.A. Kalam and S.M.A. Rahman. Comparative evaluation of the blends of gas-to-liquid (GTL) fuels and biodiesels with diesel at high idling conditions: an in-depth analysis on engine performance and environment pollutants. *RSC Advances*, 2015, **5**(17), pp.13068-13077.

18. Sajjad, H., H.H. Masjuki, M. Varman, M.A. Kalam, M.I. Arbab, S. Imtenan and S.M.A. Rahman. Engine combustion, performance and emission characteristics of gas to liquid (GTL) fuels and its blends with diesel and bio-diesel. *Renewable and Sustainable Energy Reviews*, 2014, **30**, pp.961-986.

19. Kohse-Höinghaus, K. Combustion in the future: The importance of chemistry. *Proceedings of the Combustion Institute*, 2021, **38**(1), pp.1-56.

20. Demirbas, A. Tomorrow's Biofuels: Goals and Hopes. *Energy Sources Part a-Recovery Utilization and Environmental Effects*, 2017, **39**(7), pp.673-679.

21. Leitner, W., J. Klankermayer, S. Pischinger, H. Pitsch and K. Kohse-Höinghaus. Advanced Biofuels and Beyond: Chemistry Solutions for Propulsion and Production. *Angewandte Chemie International Edition*, 2017, **56**(20), pp.5412-5452.

22. Munch, K. and T. Zhang. A Comparison of Drop-In Diesel Fuel Blends Containing Heavy Alcohols Considering Both Engine Properties and Global Warming Potentials. *In. SAE International*, 2016.

23. International Energy Agency. *Biofuels for Transport.* 2011.

24. Janssen, A., S. Pischinger and M. Muether. Potential of Cellulose-Derived Biofuels for Soot Free Diesel Combustion. 2010.

25. Huber, G.W., S. Iborra and A. Corma. Synthesis of Transportation Fuels from Biomass: Chemistry, Catalysts, and Engineering. *Chemical Reviews*, 2006, **106**(9), pp.4044-4098.

26. *2019 UK Greenhouse Gas Emissions, Final Figures.* London: Department for Business, Energy & Industrial Strategy, 2021.

27. Department for Transport. *TSGB0301 (ENV0101): Petroleum consumption by transport mode and fuel type* [online]. 2021. [Accessed 27/01/2022]. Available from: https://www.gov.uk/.

28. International Energy Agency. *Global EV Outlook 2021* [online]. Paris: IEA, 2021. Available from: https://www.iea.org/.

29. European Environment Agency. *EEA greenhouse gases - data viewer* [online]. 2021. [Accessed 29/07/2022]. Available from: https://www.eea.europa.eu/.

30. United States Environmental Protection Agency. *Inventory of U.S. Greenhouse Gas Emissions and Sinks: 1990-2019.* 2021.

31. Council of the Eu and the European Council. *Infographic - Fit for 55: towards more sustainable transport* [online]. 2022. [Accessed 11/11/2022]. Available from: https://www.consilium.europa.eu/.

32. Department for Transport. HM Government. *Decarbonising Transport - A Better, Greener Britain.* London, UK, 2021.

33. Aslam, Z., H. Li, J. Hammerton, G. Andrews, A. Ross and J.C. Lovett. Increasing Access to Electricity: An Assessment of the Energy and Power Generation Potential from Biomass Waste Residues in Tanzania. *Energies*, 2021, **14**(6), p.1793.

34. Antonetti, C., S. Gori, D. Licursi, G. Pasini, S. Frigo, M. Lopez, J.C. Parajo and A.M.R. Galletti. One-Pot Alcoholysis of the Lignocellulosic Eucalyptus nitens Biomass to n-Butyl Levulinate, a Valuable Additive for Diesel Motor Fuel. *Catalysts*, 2020, **10**(5), p.509.

35. Raspolli Galletti, A.M., C. Antonetti, S. Fulignati and D. Licursi. Direct Alcoholysis of Carbohydrate Precursors and Real Cellulosic Biomasses to Alkyl Levulinates: A Critical Review. *Catalysts*, 2020, **10**(10), p.1221.

36. Zhu, S., J. Guo, X. Wang, J. Wang and W. Fan. Alcoholysis: A Promising Technology for Conversion of Lignocellulose and Platform Chemicals. *ChemSusChem*, 2017, **10**(12), pp.2547-2559.

37. Howard, M.S., G. Issayev, N. Naser, S.M. Sarathy, A. Farooq and S. Dooley. Ethanolic gasoline, a lignocellulosic advanced biofuel. *Sustainable Energy & Fuels*, 2019, **3**(2), pp.409-421.

38. Frigo, S., G. Pasini, G. Caposciutti, M. Antonelli, A.M.R. Galletti, S. Gori, R. Costi and L. Arnone. Utilisation of advanced biofuel in CI internal combustion engine. *Fuel*, 2021, **297**, p.120742.

39. Nieuwenhuijsen, M.J., X. Basagaña, P. Dadvand, D. Martinez, M. Cirach, R. Beelen and B. Jacquemin. Air pollution and human fertility rates. *Environment International*, 2014, **70**, pp.9-14.

40. Sher, E. *Handbook of air pollution from internal combustion engines : pollutant formation and control.* Boston: Academic Press, 1998.

41. European Parliament. *Regulation (EC) No 595/2009 of the European Parliament and of the Council of 18 June 2009 on type-approval of motor vehicles and engines with respect to emissions from heavy duty vehicles (Euro VI) and on access to vehicle repair and maintenance information and amending Regulation (EC) No 715/2007 and Directive 2007/46/EC and repealing Directives 80/1269/EEC, 2005/55/EC and 2005/78/EC* [online]. 2009. [Accessed 15/07/2020]. Available from: http://eur-lex.europa.eu/.

42. European Parliament. *Regulation (EU) 2016/1628 of the European Parliament And Of The Council of 14 September 2016 on requirements relating to gaseous and particulate pollutant emission limits and type-approval for internal combustion engines*

for non-road mobile machinery, amending Regulations (EU) No 1024/2012 and (EU) No 167/2013, and amending and repealing Directive 97/68/EC [online]. 2016. [Accessed 17/01/2022]. Available from: http://eur-lex.europa.eu/.

43. European Parliament. *Regulation (EC) No 715/2007 of the European Parliament and of the Council of 20 June 2007 on type approval of motor vehicles with respect to emissions from light passenger and commercial vehicles (Euro 5 and Euro 6) and on access to vehicle repair and maintenance information* [online]. 2007. [Accessed 26/08/2022]. Available from: http://eur-lex.europa.eu/.

44. Chen, H., J.C. Kwong, R. Copes, K. Tu, P.J. Villeneuve, A. Van Donkelaar, P. Hystad, R.V. Martin, B.J. Murray, B. Jessiman, A.S. Wilton, A. Kopp and R.T. Burnett. Living near major roads and the incidence of dementia, Parkinson's disease, and multiple sclerosis: a population-based cohort study. *The Lancet*, 2017, **389**(10070), pp.718-726.

45. Corrêa, S.M., G. Arbilla, E.M. Martins, S.L. Quitério, C. De Souza Guimarães and L.V. Gatti. Five years of formaldehyde and acetaldehyde monitoring in the Rio de Janeiro downtown area – Brazil. *Atmospheric Environment*, 2010, **44**(19), pp.2302-2308.

46. Suarez-Bertoa, R., M. Clairotte, B. Arlitt, S. Nakatani, L. Hill, K. Winkler, C. Kaarsberg, T. Knauf, R. Zijlmans, H. Boertien and C. Astorga. Intercomparison of ethanol, formaldehyde and acetaldehyde measurements from a flex-fuel vehicle exhaust during the WLTC. *Fuel*, 2017, **203**, pp.330-340.

47. Ashraful, A.M., H.H. Masjuki and M.A. Kalam. Particulate matter, carbon emissions and elemental compositions from a diesel engine exhaust fuelled with diesel–biodiesel blends. *Atmospheric Environment*, 2015, **120**, pp.463-474.

48. Babu, M.V., K.M. Murthy and G.a.P. Rao. Butanol and pentanol: The promising biofuels for CI engines – A review. *Renewable and Sustainable Energy Reviews*, 2017, **78**, pp.1068-1088.

49. Bergthorson, J.M. and M.J. Thomson. A Review of the Combustion and Emissions Properties of Advanced Transportation Biofuels and Their Impact on Existing and Future Engines. *Renewable & Sustainable Energy Reviews*, 2015, **42**, pp.1393-1417.

50. An, H., W.M. Yang, J. Li and D.Z. Zhou. Modeling study of oxygenated fuels on diesel combustion: Effects of oxygen concentration, cetane number and C/H ratio. *Energy Conversion and Management*, 2015, **90**, pp.261-271.

51. Curran, H.J., E.M. Fisher, P.-A. Glaude, N.M. Marinov, W.J. Pitz, C.K. Westbrook, D.W. Layton, P.F. Flynn, R.P. Durrett, A.O. Zur Loye, O.C. Akinyemi and F.L. Dryer. Detailed Chemical Kinetic Modeling of Diesel Combustion with Oxygenated Fuels. *In.* SAE International, 2001.

52. Pepiot-Desjardins, P., H. Pitsch, R. Malhotra, S.R. Kirby and A.L. Boehman. Structural group analysis for soot reduction tendency of oxygenated fuels. *Combustion and Flame*, 2008, **154**(1), pp.191-205.

53. Westbrook, C.K., W.J. Pitz and H.J. Curran. Chemical Kinetic Modeling Study of the Effects of Oxygenated Hydrocarbons on Soot Emissions from Diesel Engines. *The Journal of Physical Chemistry A*, 2006, **110**(21), pp.6912-6922.

54. Raspolli Galletti, A.M., G. Caposciutti, G. Pasini, M. Antonelli and S. Frigo. Bio-additives for CI engines from one-pot alcoholysis reaction of lignocellulosic biomass: an experimental activity. *E3S Web Conf.*, 2020, **197**, p.08005.

55. Howard, M.S., G. Issayev, N. Naser, S.M. Sarathy, A. Farooq and S. Dooley. Correction: Ethanolic gasoline, a lignocellulosic advanced biofuel. *Sustainable Energy & Fuels*, 2022, **6**(12), pp.3080-3083.

56. Turanyi, T. and A.S. Tomlin. *Analysis of Kinetic Reaction Mechanisms.* Berlin: Springer, 2015.

57. Gao, C.W., J.W. Allen, W.H. Green and R.H. West. Reaction Mechanism Generator: Automatic construction of chemical kinetic mechanisms. *Computer Physics Communications*, 2016, **203**, pp.212-225.

58. Benson, S.W., F.R. Cruickshank, D.M. Golden, G.R. Haugen, H.E. O'neal, A.S. Rodgers, R. Shaw and R. Walsh. Additivity rules for the estimation of thermochemical properties. *Chemical Reviews*, 1969, **69**(3), pp.279-324.

59. Heywood, J.B. *Internal combustion engine fundamentals.* McGraw-Hill series in mechanical engineering. New York ;: McGraw-Hill, 1988.

60. Zeldovich, J. The Oxidation of Nitrogen in Combustion and Explosions. *Acta Physiochem*, 1946, **21**(577).

61. Fenimore, C.P. Formation of nitric oxide in premixed hydrocarbon flames. *Symposium (International) on Combustion*, 1971, **13**(1), pp.373-380.

62. Leach, F., M. Davy and M. Peckham. Cyclic NO2:NOx ratio from a diesel engine undergoing transient load steps. *International Journal of Engine Research*, 2021, **22**(1), pp.284-294.

63. Darvell, L.I., J.M. Jones, B. Gudka, X.C. Baxter, A. Saddawi, A. Williams and A. Malmgren. Combustion properties of some power station biomass fuels. *Fuel*, 2010, **89**(10), pp.2881-2890.

64. Fahim, M.A., T.A. Alsahhaf and A.S. Elkilani. *Fundamentals of Petroleum Refining.* Elsevier Science, 2009.

65. Vassilev, S.V., D. Baxter, L.K. Andersen and C.G. Vassileva. An overview of the chemical composition of biomass. *Fuel*, 2010, **89**(5), pp.913-933.

66. Manisalidis, I., E. Stavropoulou, A. Stavropoulos and E. Bezirtzoglou. Environmental and Health Impacts of Air Pollution: A Review. *Frontiers in Public Health*, 2020, **8**.

67. Department for Environment Food & Rural Affairs. *Emissions of air pollutants in the UK – Nitrogen oxides (NOx)* [online]. 2022. [Accessed 08/10/2022]. Available from: https://www.gov.uk/.

68. Zerboni, A., T. Rossi, R. Bengalli, T. Catelani, C. Rizzi, M. Priola, S. Casadei and P. Mantecca. Diesel exhaust particulate emissions and in vitro toxity from Euro 3 and Euro 6 vehicles. *Environmental Pollution*, 2022, **297**, p.118767.

69. Arteconi, A., A. Mazzarini and G. Di Nicola. Emissions from Ethers and Organic Carbonate Fuel Additives: A Review. *Water, Air, & Soil Pollution*, 2011, **221**(1), p.405.

70. Rana, S., M.R. Saxena and R.K. Maurya. A review on morphology, nanostructure, chemical composition, and number concentration of diesel particulate emissions. *Environmental Science and Pollution Research*, 2022, **29**(11), pp.15432-15489.

71. Mohankumar, S. and P. Senthilkumar. Particulate matter formation and its control methodologies for diesel engine: A comprehensive review. *Renewable and Sustainable Energy Reviews*, 2017, **80**, pp.1227-1238.

72. Eastwood, P. *Particulate emissions from vehicles.* Wiley-PEPublishing series. Chichester: Wiley, 2008.

73. Kittelson, D.B. Engines and nanoparticles: a review. *Journal of Aerosol Science*, 1998, **29**(5), pp.575-588.

74. Alföldy, B., B. Giechaskiel, W. Hofmann and Y. Drossinos. Size-distribution dependent lung deposition of diesel exhaust particles. *Journal of Aerosol Science*, 2009, **40**(8), pp.652-663.

75. Cadrazco, M., A. Santamaría and J.R. Agudelo. Chemical and nanostructural characteristics of the particulate matter produced by renewable diesel fuel in an automotive diesel engine. *Combustion and Flame*, 2019, **203**, pp.130-142.

76. Anderson, L.G. Effects of using renewable fuels on vehicle emissions. *Renewable & Sustainable Energy Reviews*, 2015, **47**, pp.162-172.

77. Valavanidis, A., K. Fiotakis and T. Vlachogianni. Airborne Particulate Matter and Human Health: Toxicological Assessment and Importance of Size and Composition of Particles for Oxidative Damage and Carcinogenic Mechanisms. *Journal of Environmental Science and Health, Part C*, 2008, **26**(4), pp.339-362.

78. Zhang, Z.-H. and R. Balasubramanian. Effect of Oxygenated Fuels on Physicochemical and Toxicological Characteristics of Diesel Particulate Emissions. *Environmental Science & Technology*, 2014, **48**(24), pp.14805-14813.

79. Kampa, M. and E. Castanas. Human health effects of air pollution. *Environmental Pollution*, 2008, **151**(2), pp.362-367.

80. Nhs. *Carbon monoxide poisoning* [online]. 2022. [Accessed 15/10/2022]. Available from: https://www.nhs.uk.

81. Joshi, A. Review of Vehicle Engine Efficiency and Emissions. *SAE International Journal of Advances and Current Practices in Mobility*, 2022, **4**(5), pp.1704-1733.

82. British Standards Institution. BS EN 590:2004. *Automotive fuels - Diesel - Requirements and test methods.* Milton Keynes: BSI, 2004.

83. British Standards Institution. BS EN 590:2009+A1:2010. *Automotive fuels - Diesel - Requirements and test methods.* Milton Keynes: BSI, 2010.

84. British Standards Institution. BS EN 590:2000. *Automotive fuels - Diesel - Requirements and test methods.* Milton Keynes: BSI, 2000.

85. British Standards Institution. BS EN 590:1997. *Specification for Automotive diesel fuel.* Milton Keynes: BSI, 1997.

86. Valentino, G., L. Allocca, S. Iannuzzi and A. Montanaro. Biodiesel/mineral diesel fuel mixtures: Spray evolution and engine performance and emissions characterization. *Energy*, 2011, **36**(6), pp.3924-3932.

87. Groendyk, M.A. and D. Rothamer. Effects of Fuel Physical Properties on Auto-Ignition Characteristics in a Heavy Duty Compression Ignition Engine. 2015.

88. Kim, D., J. Martz and A. Violi. Effects of fuel physical properties on direct injection spray and ignition behavior. *Fuel*, 2016, **180**, pp.481-496.

89. Iea-Amf. *Oxygenates for Diesel* [online]. no year. [Accessed 20/12/2022]. Available from: https://www.iea-amf.org.

90. Dieselnet. *China: Heavy-Duty Engines* [online]. 2020. [Accessed 10/10/2022]. Available from: https://dieselnet.com.

91. Dieselnet. *EU: Cars and Light Trucks* [online]. 2022. [Accessed 10/10/2022]. Available from: https://dieselnet.com.

92. Dieselnet. *EU: Nonroad Engines* [online]. 2021. [Accessed 10/10/2022]. Available from: https://dieselnet.com.

93. Dieselnet. *United States: Heavy-Duty Onroad Engines* [online]. 2022. [Accessed 10/10/2022]. Available from: https://dieselnet.com.

94. Dieselnet. *EU: Heavy-Duty Truck and Bus Engines* [online]. 2021. [Accessed 10/10/2022]. Available from: https://dieselnet.com.

95. European Commission. *Proposal for a regulation of the European Parliament and of the Council on type-approval of motor vehicles and engines and of systems, components and separate technical units intended for such vehicles, with respect to their emissions and battery durability (Euro 7) and repealing Regulations (EC) No 715/2007 and (EC) No 595/2009* [online]. 2022. [Accessed 29/11/2022]. Available from: https://single-market-economy.ec.europa.eu/.

96. European Commission. *Annexes to the Proposal for a regulation of the European Parliament and of the Council on type-approval of motor vehicles and engines and of systems, components and separate technical units intended for such vehicles, with respect to their emissions and battery durability (Euro 7) and repealing Regulations (EC) No 715/2007 and (EC) No 595/2009* [online]. 2022. [Accessed 29/11/2022]. Available from: https://single-market-economy.ec.europa.eu/.

97. Van Niekerk, A.S. and P.J. Kay. A holistic evaluation of the impact of UK renewable strategy on emissions from compression ignition engines. *Fuel*, 2020, **271**, p.117586.

98. Zahos-Siagos, I., A. Antonerias and D. Karonis. Impact of Ethanol and N-Butanol Addition on Fuel Properties and Exhaust Emissions of a Stationary Diesel Engine. 2018, **144**(5), p.04018052.

99. García-Contreras, R., J.A. Soriano, P. Fernández-Yáñez, L. Sánchez-Rodríguez, C. Mata, A. Gómez, O. Armas and M.D. Cárdenas. Impact of regulated pollutant emissions of Euro 6d-Temp light-duty diesel vehicles under real driving conditions. *Journal of Cleaner Production*, 2021, **286**, p.124927.

100. Hooftman, N., M. Messagie, J. Van Mierlo and T. Coosemans. A review of the European passenger car regulations – Real driving emissions vs local air quality. *Renewable and Sustainable Energy Reviews*, 2018, **86**, pp.1-21.

101. Reşitoğlu, İ.A., K. Altinişik and A. Keskin. The pollutant emissions from diesel-engine vehicles and exhaust aftertreatment systems. *Clean Technologies and Environmental Policy*, 2015, **17**(1), pp.15-27.

102. Lao, C.T., J. Akroyd, N. Eaves, A. Smith, N. Morgan, D. Nurkowski, A. Bhave and M. Kraft. Investigation of the impact of the configuration of exhaust after-treatment system for diesel engines. *Applied Energy*, 2020, **267**, p.114844.

103. Department for Transport. *Renewable Transport Fuel Obligation: Compliance Guidance* London, UK: DFT, 2022.

104. Salimbeni, A. *Overview on biofuels production facilities and technologies in Europe*. BIKE – Biofuels production at low – Iluc risK for European sustainable bioeconomy, Europe, 2021.

105. Alalwan, H.A., A.H. Alminshid and H.a.S. Aljaafari. Promising evolution of biofuel generations. Subject review. *Renewable Energy Focus*, 2019, **28**, pp.127-139.

106. Veza, I., M.F. Muhamad Said and Z.A. Latiff. Recent advances in butanol production by acetone-butanol-ethanol (ABE) fermentation. *Biomass and Bioenergy*, 2021, **144**, p.105919.

107. Cann, A.F. and J.C. Liao. Pentanol isomer synthesis in engineered microorganisms. *Applied Microbiology and Biotechnology*, 2010, **85**(4), pp.893-899.

108. Démolis, A., N. Essayem and F. Rataboul. Synthesis and Applications of Alkyl Levulinates. *ACS Sustainable Chemistry & Engineering*, 2014, **2**(6), pp.1338-1352.

109. Eagan, N.M., B.M. Moore, D.J. Mcclelland, A.M. Wittrig, E. Canales, M.P. Lanci and G.W. Huber. Catalytic synthesis of distillate-range ethers and olefins from ethanol through Guerbet coupling and etherification. *Green Chemistry*, 2019, **21**(12), pp.3300-3318.

110. Mascal, M. and E.B. Nikitin. High-yield conversion of plant biomass into the key value-added feedstocks 5-(hydroxymethyl)furfural, levulinic acid, and levulinic esters via 5-(chloromethyl)furfural. *Green Chemistry*, 2010, **12**(3), pp.370-373.

111. Xu, G., C. Chang, S. Fang and X. Ma. Cellulose reactivity in ethanol at elevate temperature and the kinetics of one-pot preparation of ethyl levulinate from cellulose. *Renewable Energy*, 2015, **78**, pp.583-589.

112. Flannelly, T., S. Dooley and J.J. Leahy. Reaction Pathway Analysis of Ethyl Levulinate and 5-Ethoxymethylfurfural from d-Fructose Acid Hydrolysis in Ethanol. *Energy & Fuels*, 2015, **29**(11), pp.7554-7565.

113. Leal Silva, J.F., R. Grekin, A.P. Mariano and R. Maciel Filho. Making Levulinic Acid and Ethyl Levulinate Economically Viable: A Worldwide Technoeconomic and Environmental Assessment of Possible Routes. *Energy Technology*, 2018, **6**(4), pp.613-639.

114. Tan, J., C. Wang, Q. Zhang, L. Ma and M. He. One-Pot Condensation of Furfural and Levulinates: A Novel Method for Cassava Use in Synthesis of Biofuel Precursors. *Energy & Fuels*, 2018, **32**(6), pp.6807-6812.

115. Démolis, A., M. Eternot, N. Essayem and F. Rataboul. Influence of butanol isomers on the reactivity of cellulose towards the synthesis of butyl levulinates catalyzed by liquid and solid acid catalysts. *New Journal of Chemistry*, 2016, **40**(4), pp.3747-3754.

116. Alamgir Ahmad, K., M. Haider Siddiqui, K.K. Pant, K.D.P. Nigam, N.P. Shetti, T.M. Aminabhavi and E. Ahmad. A critical review on suitability and catalytic production of butyl levulinate as a blending molecule for green diesel. *Chemical Engineering Journal*, 2022, **447**, p.137550.

117. Chang, C., G. Xu and X. Jiang. Production of ethyl levulinate by direct conversion of wheat straw in ethanol media. *Bioresource Technology*, 2012, **121**, pp.93-99.

118. British Standards Institution. EN ISO 3679:2015. *Determination of flash no flash and flash point — Rapid equilibrium closed cup method.* Milton Keynes: BSI, 2015.

119. Barraza-Botet, C.L., J. Luecke, B.T. Zigler and M.S. Wooldridge. The impact of physicochemical property interactions of iso-octane/ethanol blends on ignition timescales. *Fuel*, 2018, **224**, pp.401-411.

120. Lapuerta, M., J.J. Hernandez, J. Rodriguez-Fernandez, J. Barba, A. Ramos and D. Fernandez-Rodriguez. Emission benefits from the use of n-butanol blends in a Euro 6 diesel engine. *International Journal of Engine Research*, 2018, **19**(10), pp.1099-1112.

121. Catoire, L., S. Paulmier and V. Naudet. Experimental determination and estimation of closed cup flash points of mixtures of flammable solvents. *Process Safety Progress*, 2006, **25**(1), pp.33-39.

122. Lapuerta, M., R. García-Contreras, J. Campos-Fernández and M.P. Dorado. Stability, Lubricity, Viscosity, and Cold-Flow Properties of Alcohol–Diesel Blends. *Energy & Fuels*, 2010, **24**(8), pp.4497-4502.

123. Sigma Aldrich. *Diethyl ether; MSDS No. 296082* [online]. 2019. [Accessed 21/06/2019]. Available from: https://www.sigmaaldrich.com/.

124. Vwr. *Ethanol; MSDS No. 7669152* [online]. 2017. [Accessed 21/11/2019]. Available from: https://uk.vwr.com/.

125. Torres-Jimenez, E., M.S. Jerman, A. Gregorc, I. Lisec, M.P. Dorado and B. Kegl. Physical and chemical properties of ethanol–diesel fuel blends. *Fuel*, 2011, **90**(2), pp.795-802.

126. Kwanchareon, P., A. Luengnaruemitchai and S. Jai-In. Solubility of a diesel–biodiesel–ethanol blend, its fuel properties, and its emission characteristics from diesel engine. *Fuel*, 2007, **86**(7), pp.1053-1061.

127. Labeckas, G., S. Slavinskas and I. Kanapkienė. Study of the Effects of Biofuel-Oxygen of Various Origins on a CRDI Diesel Engine Combustion and Emissions. *Energies*, 2019, **12**(7), p.1241.

128. Wang, Z.W., T.Z. Lei, L. Liu, J.L. Zhu, X.F. He and Z.F. Li. PERFORMANCE INVESTIGATIONS OF A DIESEL ENGINE USING ETHYL LEVULINATE-DIESEL BLENDS. *Bioresources*, 2012, **7**(4), pp.5972-5982.

129. Górski, K. and M. Przedlacki. Evaluation of the Influence of Diethyl Ether (DEE) Addition on Selected Physicochemical Properties of Diesel Oil and Ignition Delay Period. *Energy & Fuels*, 2014, **28**(4), pp.2608-2616.

130. Wang, Q., S. Yin and J. Ni. The effects of n-pentanol, di-n-butyl ether (DBE) and exhaust gas recirculation on performance and emissions in a compression ignition engine. *Fuel*, 2021, **284**, p.118961.

131. Heuser, B., P. Mauermann, R. Wankhade, F. Kremer and S. Pischinger. Combustion and emission behavior of linear C8-oxygenates. *International Journal of Engine Research*, 2015, **16**(5), pp.627-638.

132. Low, M.H., N.a.M. Mukhtar, F.Y. Hagos, M.M. Noor and Iop. Tri-fuel (diesel-biodiesel-ethanol) emulsion characterization, stability and the corrosion effect. *In: 4th International Conference on Mechanical Engineering Research*. Bristol: Iop Publishing Ltd, 2017.

133. Qi, D.H., H. Chen, L.M. Geng and Y.Z. Bian. Effect of diethyl ether and ethanol additives on the combustion and emission characteristics of biodiesel-diesel blended fuel engine. *Renewable Energy*, 2011, **36**(4), pp.1252-1258.

134. Bailey, B., J. Eberhardt, S. Goguen and J. Erwin. Diethyl Ether (DEE) as a Renewable Diesel Fuel. *In*. SAE International, 1997.

135. Venu, H. and V. Madhavan. Influence of diethyl ether (DEE) addition in ethanol-biodiesel-diesel (EBD) and methanol-biodiesel-diesel (MBD) blends in a diesel engine. *Fuel*, 2017, **189**, pp.377-390.

136. Paul, A., P.K. Bose, R. Panua and D. Debroy. Study of performance and emission characteristics of a single cylinder CI engine using diethyl ether and ethanol blends. *Journal of the Energy Institute*, 2015, **88**(1), pp.1-10.

137. Paul, A., R.S. Panua, D. Debroy and P.K. Bose. Effect of diethyl ether and ethanol on performance, combustion, and emission of single-cylinder compression ignition engine. *International Journal of Ambient Energy*, 2014, **38**(1), pp.2-13.

138. European Chemicals Agency. *REACH - Registration, Evaluation, Authorisation and Restriction of Chemicals Regulation. Registered Substances Factsheets* [online]. 2022. [Accessed 17/02/2021]. Available from: https://echa.europa.eu/.

139. Exxonmobil. *Diesel; MSDS No.748356* [online]. 2016. [Accessed 15/01/2020]. Available from: https://www.msds.exxonmobil.com/.

140. Shell Uk Oil Products Limited. *Commercial Diesel; MSDS No.01206393* [online]. 2016. [Accessed 15/01/2020]. Available from: https://www.epc.shell.com/.

141. Yang, S.Y., N. Naser, S.H. Chung and J. Cha. Effect of Temperature, Pressure and Equivalence Ratio on Ignition Delay in Ignition Quality Tester (IQT): Diesel, n-Heptane, and iso-Octane Fuels under Low Temperature Conditions. 2015.

142. British Standards Institution. BS EN 16715:2015. *Liquid petroleum products - Determination of ignition delay and derived cetane number (DCN) of middle distillate fuels - Ignition delay and combustion delay determination using a constant volume combustion chamber with direct fuel injection.* Milton Keynes: BSI, 2015.

143. Yanowitz, J., M.A. Ratcliff, R.L. Mccormick, J.D. Taylor and M.J. Murphy. *Compendium of Experimental Cetane Numbers*. 2017.

144. Çelebi, Y. and H. Aydın. An overview on the light alcohol fuels in diesel engines. *Fuel*, 2019, **236**, pp.890-911.

145. Wang, J., L. Sun, P. Luan, Y. Wu, Z. Cheng, Z. Zhang, X. Kong, H. Liu and G. Chen. Effect of diesel blended with di-n-butyl ether/1-octanol on combustion and emission in a heavy-duty diesel engine. *Environmental Pollution*, 2022, **311**, p.119976.

146. Wei, L., C.S. Cheung and Z. Huang. Effect of n-pentanol addition on the combustion, performance and emission characteristics of a direct-injection diesel engine. *Energy*, 2014, **70**, pp.172-180.

147. National Renewable Energy Laboratory. *Co-Optimization of Fuels & Engines: Fuel Properties Database.* [Accessed 14/12/2022]. Available from: https://www.nrel.gov/. 2016.

148. Rakopoulos, D.C., C.D. Rakopoulos, R.G. Papagiannakis and D.C. Kyritsis. Combustion heat release analysis of ethanol or n-butanol diesel fuel blends in heavy-duty DI diesel engine. *Fuel*, 2011, **90**(5), pp.1855-1867.

149. Sayin, C. Engine performance and exhaust gas emissions of methanol and ethanol–diesel blends. *Fuel*, 2010, **89**(11), pp.3410-3415.

150. Linstrom, P.J. and W.G. Mallard eds. *NIST Chemistry WebBook, NIST Standard Reference Database Number 69.* Gaithersburg MD, 20899: National Institute of Standards and Technology.

151. Koivisto, E. *Ignition and combustion of future oxygenated fuels in compression-ignition engines.* Doctor of Philosophy thesis, University College London, 2016.

152. Koivisto, E., N. Ladommatos and M. Gold. Compression Ignition and Exhaust Gas Emissions of Fuel Molecules Which Can Be Produced from Lignocellulosic Biomass: Levulinates, Valeric Esters, and Ketones. *Energy & Fuels*, 2015, **29**(9), pp.5875-5884.

153. Mao, G. and S. Shao. Experimental Research on the Flame Temperature of n-Butanol-Diesel Fuel Blends in Atmospheric Conditions. *Journal of Energy Engineering*, 2016, **142**(3), p.04015037.

154. Davis, S.G. and C.K. Law. Determination of and Fuel Structure Effects on Laminar Flame Speeds of C1 to C8 Hydrocarbons. *Combustion Science and Technology*, 1998, **140**(1-6), pp.427-449.

155. Zhang, N., Y. Di, Z. Huang, B. Zheng and Z. Zhang. Experimental Study on Combustion Characteristics of N2-Diluted Diethyl Ether−Air Mixtures. *Energy & Fuels*, 2009, **23**(12), pp.5798-5805.

156. Glaude, P.-A., R. Fournet, R. Bounaceur and M. Molière. Adiabatic flame temperature from biofuels and fossil fuels and derived effect on NOx emissions. *Fuel Processing Technology*, 2010, **91**(2), pp.229-235.

157. Nikitin, E.D., A.P. Popov, N.S. Bogatishcheva and M.Z. Faizullin. Critical temperatures and pressures, heat capacities, and thermal diffusivities of levulinic acid and four n-alkyl levulinates. *Journal of Chemical Thermodynamics*, 2019, **135**, pp.233-240.

158. Hakimov, K., F. Arafin, K. Aljohani, K. Djebbi, E. Ninnemann, S.S. Vasu and A. Farooq. Ignition delay time and speciation of dibutyl ether at high pressures. *Combustion and Flame*, 2021, **223**, pp.98-109.

159. Werler, M., L.R. Cancino, R. Schiessl, U. Maas, C. Schulz and M. Fikri. Ignition delay times of diethyl ether measured in a high-pressure shock tube and a rapid compression machine. *Proceedings of the Combustion Institute*, 2015, **35**(1), pp.259-266.

160. Ghosh, M.K., M.S. Howard, Y. Zhang, K. Djebbi, G. Capriolo, A. Farooq, H.J. Curran and S. Dooley. The combustion kinetics of the lignocellulosic biofuel, ethyl levulinate. *Combustion and Flame*, 2018, **193**, pp.157-169.

161. Issayev, G., S. Mani Sarathy and A. Farooq. Autoignition of diethyl ether and a diethyl ether/ethanol blend. *Fuel*, 2020, **279**, p.118553.

162. Agbro, E., A.S. Tomlin, M. Lawes, S. Park and S.M. Sarathy. The influence of n-butanol blending on the ignition delay times of gasoline and its surrogate at high pressures. *Fuel*, 2017, **187**, pp.211-219.

163. Sung, C.-J. and H.J. Curran. Using rapid compression machines for chemical kinetics studies. *Progress in Energy and Combustion Science*, 2014, **44**, pp.1-18.

164. Naser, N., S.M. Sarathy and S.H. Chung. Ignition delay time sensitivity in ignition quality tester (IQT) and its relation to octane sensitivity. *Fuel*, 2018, **233**, pp.412-419.

165. Sarathy, S.M., P. Oßwald, N. Hansen and K. Kohse-Höinghaus. Alcohol combustion chemistry. *Progress in Energy and Combustion Science*, 2014, **44**, pp.40-102.

166. Tran, L.-S., J. Pieper, H.-H. Carstensen, H. Zhao, I. Graf, Y. Ju, F. Qi and K. Kohse-Höinghaus. Experimental and kinetic modeling study of diethyl ether flames. *Proceedings of the Combustion Institute*, 2017, **36**(1), pp.1165-1173.

167. Tran, L.-S., J. Pieper, M. Zeng, Y. Li, X. Zhang, W. Li, I. Graf, F. Qi and K. Kohse-Höinghaus. Influence of the biofuel isomers diethyl ether and n-butanol on flame structure and pollutant formation in premixed n-butane flames. *Combustion and Flame*, 2017, **175**, pp.47-59.

168. Sarathy, S.M., S. Vranckx, K. Yasunaga, M. Mehl, P. Oßwald, W.K. Metcalfe, C.K. Westbrook, W.J. Pitz, K. Kohse-Höinghaus, R.X. Fernandes and H.J. Curran. A comprehensive chemical kinetic combustion model for the four butanol isomers. *Combustion and Flame*, 2012, **159**(6), pp.2028-2055.

169. Tran, L.-S., O. Herbinet, Y. Li, J. Wullenkord, M. Zeng, E. Bräuer, F. Qi, K. Kohse-Höinghaus and F. Battin-Leclerc. Low-temperature gas-phase oxidation of diethyl ether: Fuel reactivity and fuel-specific products. *Proceedings of the Combustion Institute*, 2019, **37**(1), pp.511-519.

170. Rotavera, B. and C.A. Taatjes. Influence of functional groups on low-temperature combustion chemistry of biofuels. *Progress in Energy and Combustion Science*, 2021, **86**, p.100925.

171. Curran, H.J. Developing detailed chemical kinetic mechanisms for fuel combustion. *Proceedings of the Combustion Institute*, 2019, **37**(1), pp.57-81.

172. Kalaskar, V.B., A. Swarts and T. Alger. Impact of Engine Age and Engine Hardware on Low-Speed Pre-Ignition. *In*. SAE International, 2018.

173. Haenel, P., H. Kleeberg, R. De Bruijn and D. Tomazic. Influence of Ethanol Blends on Low Speed Pre-Ignition in Turbocharged, Direct-Injection Gasoline Engines. *SAE International Journal of Fuels and Lubricants*, 2017, **10**(1), pp.95-105.

174. Zhong, A. and D. Han. Experimental and kinetic modelling studies on di-n-butyl ether (DBE) low temperature auto-ignition. *Combustion and Flame*, 2022, **237**, p.111882.

175. Weber, B.W., K. Kumar, Y. Zhang and C.-J. Sung. Autoignition of n-butanol at elevated pressure and low-to-intermediate temperature. *Combustion and Flame*, 2011, **158**(5), pp.809-819.

176. Heufer, K.A., R.X. Fernandes, H. Olivier, J. Beeckmann, O. Röhl and N. Peters. Shock tube investigations of ignition delays of n-butanol at elevated pressures between 770 and 1250K. *Proceedings of the Combustion Institute*, 2011, **33**(1), pp.359-366.

177. Pilling, M.J. From elementary reactions to evaluated chemical mechanisms for combustion models. *Proceedings of the Combustion Institute*, 2009, **32**, pp.27-44.

178. Sarathy, S.M., C.K. Westbrook, M. Mehl, W.J. Pitz, C. Togbe, P. Dagaut, H. Wang, M.A. Oehlschlaeger, U. Niemann, K. Seshadri, P.S. Veloo, C. Ji, F.N. Egolfopoulos and T. Lu. Comprehensive chemical kinetic modeling of the oxidation of 2-methylalkanes from C7 to C20. *Combustion and Flame*, 2011, **158**(12), pp.2338-2357.

179. Westbrook, C., K.A. Heufer and A. Wildenberg. Key Chemical Kinetic Steps in Reaction Mechanisms for Fuels from Biomass: A Perspective. *Energy & Fuels*, 2021, **35**(19), pp.15339-15359.

180. Westbrook, C.K. Chemical kinetics of hydrocarbon ignition in practical combustion systems. *Proceedings of the Combustion Institute*, 2000, **28**(2), pp.1563-1577.

181. British Standards Insititution. BS EN 15195. *BS EN 15195:2014. Liquid petroleum products - Determination of ignition delay and derived cetane number (DCN) of middle distillate fuels by combustion in a constant volume chamber.* BSI, 2014.

182. Barabás, I. Predicting the temperature dependent density of biodiesel–diesel–bioethanol blends. *Fuel*, 2013, **109**, pp.563-574.

183. Pratas, M.J., S.V.D. Freitas, M.B. Oliveira, S.C. Monteiro, Á.S. Lima and J.a.P. Coutinho. Biodiesel Density: Experimental Measurements and Prediction Models. *Energy & Fuels*, 2011, **25**(5), pp.2333-2340.

184. Phoon, L.Y., A.A. Mustaffa, H. Hashim and R. Mat. A Review of Flash Point Prediction Models for Flammable Liquid Mixtures. *Industrial & Engineering Chemistry Research*, 2014, **53**(32), pp.12553-12565.

185. Torabian, E. and M.A. Sobati. New models for predicting the flash point of mixtures containing different alcohols. *Process Safety and Environmental Protection*, 2017, **111**, pp.439-448.

186. Liaw, H.-J., C.-C. Chen, C.-H. Chang, N.-K. Lin and C.-M. Shu. Model To Estimate the Flammability Limits of Fuel–Air–Diluent Mixtures Tested in a Constant Pressure Vessel. *Industrial & Engineering Chemistry Research*, 2012, **51**(6), pp.2747-2761.

187. Liaw, H.-J. and Y.-Y. Chiu. A general model for predicting the flash point of miscible mixtures. *Journal of Hazardous Materials*, 2006, **137**(1), pp.38-46.

188. Liaw, H.-J. and Y.-Y. Chiu. The prediction of the flash point for binary aqueous-organic solutions. *Journal of Hazardous Materials*, 2003, **101**(2), pp.83-106.

189. Liaw, H.-J., Y.-H. Lee, C.-L. Tang, H.-H. Hsu and J.-H. Liu. A mathematical model for predicting the flash point of binary solutions. *Journal of Loss Prevention in the Process Industries*, 2002, **15**(6), pp.429-438.

190. Liaw, H.-J., W.-H. Lu, V. Gerbaud and C.-C. Chen. Flash-point prediction for binary partially miscible mixtures of flammable solvents. *Journal of Hazardous Materials*, 2008, **153**(3), pp.1165-1175.

191. Liaw, H.-J., C.-L. Tang and J.-S. Lai. A model for predicting the flash point of ternary flammable solutions of liquid. *Combustion and Flame*, 2004, **138**(4), pp.308-319.

192. Liaw, H.-J., V. Gerbaud and C.-Y. Chiu. Flash Point for Ternary Partially Miscible Mixtures of Flammable Solvents. *Journal of Chemical & Engineering Data*, 2010, **55**(1), pp.134-146.

193. Catoire, L. and V. Naudet. A unique equation to estimate flash points of selected pure liquids application to the correction of probably erroneous flash point values. *Journal of Physical and Chemical Reference Data*, 2004, **33**(4), pp.1083-1111.

194. Catoire, L., S. Paulmier and V. Naudet. Estimation of closed cup flash points of combustible solvent blends. *Journal of Physical and Chemical Reference Data*, 2006, **35**(1), pp.9-14.

195. Lohmann, J., R. Joh and J. Gmehling. From UNIFAC to Modified UNIFAC (Dortmund). *Industrial & Engineering Chemistry Research*, 2001, **40**(3), pp.957-964.

196. Gmehling, J., R. Wittig, J. Lohmann and R. Joh. A Modified UNIFAC (Dortmund) Model. 4. Revision and Extension. *Industrial & Engineering Chemistry Research*, 2002, **41**(6), pp.1678-1688.

197. Jakob, A., H. Grensemann, J. Lohmann and J. Gmehling. Further Development of Modified UNIFAC (Dortmund): Revision and Extension 5. *Industrial & Engineering Chemistry Research*, 2006, **45**(23), pp.7924-7933.

198. Phoon, L.Y., H. Hashim, R. Mat and A.A. Mustaffa. ANALYSIS OF FLASH POINT PREDICTIONS OF TAILOR-MADE GREEN DIESEL BY UNIFAC GROUP CONTRIBUTION METHODS. *Journal of Engineering Science and Technology*, 2015, **10**, pp.110-119.

199. Liaw, H.-J. and C.-A. Yang. Maximum flash point behavior of ternary mixtures with single and two maximum flash point binary constituents. *Process Safety and Environmental Protection*, 2020, **143**, pp.293-303.

200. Huo, X., Q. Lu and J. Wang. Liaw-UNIFAC flash point model for alcohols-kerosene/diesel fuel blends using average fuel structure. *Process Safety and Environmental Protection*, 2022, **160**, pp.400-410.

201. Álvarez, A., M. Lapuerta and J.R. Agudelo. Prediction of Flash-Point Temperature of Alcohol/Biodiesel/Diesel Fuel Blends. *Industrial & Engineering Chemistry Research*, 2019, **58**(16), pp.6860-6869.

202. Grunberg, L. and A.H. Nissan. Mixture Law for Viscosity. *Nature*, 1949, **164**(4175), pp.799-800.

203. Lapuerta, M., J. Rodríguez-Fernández, D. Fernández-Rodríguez and R. Patiño-Camino. Modeling viscosity of butanol and ethanol blends with diesel and biodiesel fuels. *Fuel*, 2017, **199**, pp.332-338.

204. Sastry, N.V. and M.K. Valand. Densities, Viscosities, and Relative Permittivities for Pentane + 1-Alcohols (C1 to C12) at 298.15 K. *Journal of Chemical & Engineering Data*, 1998, **43**(2), pp.152-157.

205. Sastry, N.V. and M.K. Valand. Viscosities and Densities for Heptane + 1-Pentanol, +1-Hexanol, +1-Heptanol, +1-Octanol, +1-Decanol, and +1-Dodecanol at 298.15 K and 308.15 K. *Journal of Chemical & Engineering Data*, 1996, **41**(6), pp.1426-1428.

206. Riazi, M.R. *Characterization and properties of petroleum fractions.* ASTM International, 2007.

207. Poling, B.E., J.M. Prausnitz, J.P. O'connell and R.C. Reid. *The properties of gases and liquids.* Fifth edition / Bruce E. Poling, John M. Prausnitz, John P. O'Connell. ed. New York ;: McGraw-Hill, 2001.

208. Hernández, E.A., G. Sánchez-Reyna and J. Ancheyta. Evaluation of mixing rules to predict viscosity of petrodiesel and biodiesel blends. *Fuel*, 2021, **283**, p.118941.

209. Centeno, G., G. Sánchez-Reyna, J. Ancheyta, J.a.D. Muñoz and N. Cardona. Testing various mixing rules for calculation of viscosity of petroleum blends. *Fuel*, 2011, **90**(12), pp.3561-3570.

210. Gülüm, M. and A. Bilgin. Measurements and empirical correlations in predicting biodiesel-diesel blends' viscosity and density. *Fuel*, 2017, **199**, pp.567-577.

211. Gülüm, M. and A. Bilgin. A comprehensive study on measurement and prediction of viscosity of biodiesel-diesel-alcohol ternary blends. *Energy*, 2018, **148**, pp.341-361.

212. Dahmen, M. and W. Marquardt. Model-Based Formulation of Biofuel Blends by Simultaneous Product and Pathway Design. *Energy & Fuels*, 2017, **31**(4), pp.4096-4121.

213. Hardenberg, H.O. and F.W. Hase. An Empirical Formula for Computing the Pressure Rise Delay of a Fuel from Its Cetane Number and from the Relevant Parameters of Direct-Injection Diesel Engines. *In*. SAE International, 1979.

214. Wu, Y., J. Ferns, H. Li and G. Andrews. *Investigation of Combustion and Emission Performance of Hydrogenated Vegetable Oil (HVO) Diesel*. SAE International. 2017. Available from: https://doi.org/10.4271/2017-01-2400

215. Abboud, J., J. Schobing, G. Legros, J. Bonnety, V. Tschamber, A. Brillard, G. Leyssens, V. Lauga, E.E. Iojoiu and P. Da Costa. Impacts of oxygenated compounds concentration on sooting propensities and soot oxidative reactivity: Application to Diesel and Biodiesel surrogates. *Fuel*, 2017, **193**, pp.241-253.

216. Cheng, A.S., R.W. Dibble and B.A. Buchholz. The Effect of Oxygenates on Diesel Engine Particulate Matter. *In*. SAE International, 2002.

217. Gao, Z., X. Zou, Z. Huang and L. Zhu. Predicting sooting tendencies of oxygenated hydrocarbon fuels with machine learning algorithms. *Fuel*, 2019, **242**, pp.438-446.

218. Mcenally, C.S. and L.D. Pfefferle. Improved sooting tendency measurements for aromatic hydrocarbons and their implications for naphthalene formation pathways. *Combustion and Flame*, 2007, **148**(4), pp.210-222.

219. Park, K., D.B. Kittelson, M.R. Zachariah and P.H. Mcmurry. Measurement of Inherent Material Density of Nanoparticle Agglomerates. *Journal of Nanoparticle Research*, 2004, **6**(2), pp.267-272.

220. Sivasankaralingam, V., V. Raman, M.J. Mubarak Ali, A. Alfazazi, T. Lu, H. Im, S.M. Sarathy and R. Dibble. Experimental and Numerical Investigation of Ethanol/Diethyl Ether Mixtures in a CI Engine. *In*. SAE International, 2016.

221. Heuser, B., T. Laible, M. Jakob, F. Kremer and S. Pischinger. C8-Oxygenates for Clean Diesel Combustion. *In*. SAE International, 2014.

222. García, A., J. Monsalve-Serrano, D. Villalta, M. Zubel and S. Pischinger. Potential of 1-octanol and di-n-butyl ether (DNBE) to improve the performance and reduce the emissions of a direct injected compression ignition diesel engine. *Energy Conversion and Management*, 2018, **177**, pp.563-571.

223. Kohse-Höinghaus, K., P. Oßwald, T.A. Cool, T. Kasper, N. Hansen, F. Qi, C.K. Westbrook and P.R. Westmoreland. Biofuel Combustion Chemistry: From Ethanol to Biodiesel. *Angewandte Chemie International Edition*, 2010, **49**(21), pp.3572-3597.

224. Guan, C., C.S. Cheung, X. Li and Z. Huang. Effects of oxygenated fuels on the particle-phase compounds emitted from a diesel engine. *Atmospheric Pollution Research*, 2017, **8**(2), pp.209-220.

225. Jamrozik, A. The effect of the alcohol content in the fuel mixture on the performance and emissions of a direct injection diesel engine fueled with diesel-methanol and diesel-ethanol blends. *Energy Conversion and Management*, 2017, **148**, pp.461-476.

226. Rakopoulos, D.C., C.D. Rakopoulos, E.G. Giakoumis, N.P. Komninos, G.M. Kosmadakis and R.G. Papagiannakis. Comparative Evaluation of Ethanol, n-Butanol, and Diethyl Ether Effects as Biofuel Supplements on Combustion Characteristics, Cyclic Variations, and Emissions Balance in Light-Duty Diesel Engine. 2017, **143**(2), p.04016044.

227. British Standards Institution. BS EN 590:2013+A1:2017. *Automotive fuels - Diesel - Requirements and test methods.* Milton Keynes: BSI, 2017.

228. Battin-Leclerc, F., J.M. Simmie and E. Blurock eds. *Cleaner Combustion.* London, UK: Springer, 2013.

229. Ghosh, M.K., M.S. Howard and S. Dooley. Accurate and standard thermochemistry for oxygenated hydrocarbons: A case study of ethyl levulinate. *Proceedings of the Combustion Institute*, 2019, **37**(1), pp.337-346.

230. Pilling, M.J., S.H. Robertson and P.W. Seakins. Elementary Radical Reactions And Autoignition. *Journal of the Chemical Society-Faraday Transactions*, 1995, **91**(23), pp.4179-4188.

231. Pelucchi, M., S. Namysl, E. Ranzi, A. Rodriguez, C. Rizzo, K.P. Somers, Y. Zhang, O. Herbinet, H.J. Curran, F. Battin-Leclerc and T. Faravelli. Combustion of n-C3–C6 Linear Alcohols: An Experimental and Kinetic Modeling Study. Part I: Reaction Classes, Rate Rules, Model Lumping, and Validation. *Energy & Fuels*, 2020, **34**(11), pp.14688-14707.

232. Tran, L.-S., J. Wullenkord, Y. Li, O. Herbinet, M. Zeng, F. Qi, K. Kohse-Höinghaus and F. Battin-Leclerc. Probing the low-temperature chemistry of di-n-butyl ether: Detection of previously unobserved intermediates. *Combustion and Flame*, 2019, **210**, pp.9-24.

233. Khobragade, R., S.K. Singh, P.C. Shukla, T. Gupta, A.S. Al-Fatesh, A.K. Agarwal and N.K. Labhasetwar. Chemical composition of diesel particulate matter and its control. *Catalysis Reviews*, 2019, **61**(4), pp.447-515.

234. Huang, H., M. Fairweather, A.S. Tomlin, J.F. Griffiths and R.B. Brad. A dynamic approach to the dimension reduction of chemical kinetic schemes. *In:* L. PUIGJANER and A. ESPUÑA, eds. *Computer Aided Chemical Engineering.* Elsevier, 2005, pp.229-234.

235. Hughes, K.J., J.F. Griffiths, M. Fairweather and A.S. Tomlin. Evaluation of models for the low temperature combustion of alkanes through interpretation of pressure–temperature ignition diagrams. *Physical Chemistry Chemical Physics*, 2006, **8**(27), pp.3197-3210.

236. Mueller, C.J., W.J. Cannella, J.T. Bays, T.J. Bruno, K. Defabio, H.D. Dettman, R.M. Gieleciak, M.L. Huber, C.-B. Kweon, S.S. Mcconnell, W.J. Pitz and M.A. Ratcliff. Diesel Surrogate Fuels for Engine Testing and Chemical-Kinetic Modeling: Compositions and Properties. *Energy & Fuels*, 2016, **30**(2), pp.1445-1461.

237. Pitz, W.J. and C.J. Mueller. Recent progress in the development of diesel surrogate fuels. *Progress in Energy and Combustion Science*, 2011, **37**(3), pp.330-350.

238. Mueller, C.J., W.J. Cannella, T.J. Bruno, B. Bunting, H.D. Dettman, J.A. Franz, M.L. Huber, M. Natarajan, W.J. Pitz, M.A. Ratcliff and K. Wright. Methodology for Formulating Diesel Surrogate Fuels with Accurate Compositional, Ignition-Quality, and Volatility Characteristics. *Energy & Fuels*, 2012, **26**(6), pp.3284-3303.

239. Pei, Y., M. Mehl, W. Liu, T. Lu, W.J. Pitz and S. Som. A Multi-Component Blend as a Diesel Fuel Surrogate for Compression Ignition Engine Applications. *Journal of Engineering for Gas Turbines and Power*, 2015, **137**(11).

240. Alturaifi, S.A., R.L. Rebagay, O. Mathieu, B. Guo and E.L. Petersen. A Shock-Tube Autoignition Study of Jet, Rocket, and Diesel Fuels. *Energy & Fuels*, 2019, **33**(3), pp.2516-2525.

241. Sakai, Y., J. Herzler, M. Werler, C. Schulz and M. Fikri. A quantum chemical and kinetics modeling study on the autoignition mechanism of diethyl ether. *Proceedings of the Combustion Institute*, 2017, **36**(1), pp.195-202.

242. Marinov, N.M. A detailed chemical kinetic model for high temperature ethanol oxidation. 1999, **31**(3), pp.183-220.

243. Cai, L., A. Sudholt, D.J. Lee, F.N. Egolfopoulos, H. Pitsch, C.K. Westbrook and S.M. Sarathy. Chemical kinetic study of a novel lignocellulosic biofuel: Di-n-butyl ether oxidation in a laminar flow reactor and flames. *Combustion and Flame*, 2014, **161**(3), pp.798-809.

244. Thion, S., C. Togbé, Z. Serinyel, G. Dayma and P. Dagaut. A chemical kinetic study of the oxidation of dibutyl-ether in a jet-stirred reactor. *Combustion and Flame*, 2017, **185**, pp.4-15.

245. Li, J., D. Zhou and W. Yang. A multi-component reaction mechanism of n-butanol, n-octanol, and di-n-buthylether for engine combustion. *Fuel*, 2020, **275**, p.117975.

246. Zhou, C.-W., Y. Li, U. Burke, C. Banyon, K.P. Somers, S. Ding, S. Khan, J.W. Hargis, T. Sikes, O. Mathieu, E.L. Petersen, M. Alabbad, A. Farooq, Y. Pan, Y. Zhang, Z. Huang, J. Lopez, Z. Loparo, S.S. Vasu and H.J. Curran. An experimental and chemical kinetic modeling study of 1,3-butadiene combustion: Ignition delay time and laminar flame speed measurements. *Combustion and Flame*, 2018, **197**, pp.423-438.

247. Cai, L., Y. Uygun, C. Togbé, H. Pitsch, H. Olivier, P. Dagaut and S.M. Sarathy. An experimental and modeling study of n-octanol combustion. *Proceedings of the Combustion Institute*, 2015, **35**(1), pp.419-427.

248. Maghbouli, A., W. Yang, H. An, J. Li, S.K. Chou and K.J. Chua. An advanced combustion model coupled with detailed chemical reaction mechanism for D.I diesel engine simulation. *Applied Energy*, 2013, **111**, pp.758-770.

249. Ansys. *Chemkin-Pro 2022 R1* [online]. 2022. [Accessed 10/10/2022]. Available from: ansyshelp.ansys.com.

250. Ansys. *Ansys Chemkin-Pro Theory Manual*. Pennsylvania, USA: ANSYS Inc.,. 2022, 2022. Available from: ansyshelp.ansys.com

251. Rakopoulos, C.D., K.A. Antonopoulos, D.C. Rakopoulos and D.T. Hountalas. Multi-zone modeling of combustion and emissions formation in DI diesel engine operating on ethanol–diesel fuel blends. *Energy Conversion and Management*, 2008, **49**(4), pp.625-643.

252. Rakopoulos, C.D., K.A. Antonopoulos and D.C. Rakopoulos. Multi-zone modeling of Diesel engine fuel spray development with vegetable oil, bio-diesel or Diesel fuels. *Energy Conversion and Management*, 2006, **47**(11), pp.1550-1573.

253. Lavoie, G.A., J.B. Heywood and J.C. Keck. Experimental and Theoretical Study of Nitric Oxide Formation in Internal Combustion Engines. *Combustion Science and Technology*, 1970, **1**(4), pp.313-326.

254. Hiroyasu, H. and T. Kadota. Models for Combustion and Formation of Nitric Oxide and Soot in Direct Injection Diesel Engines. *In*. SAE International, 1976.

255. British Standards Institution. BS ISO 8178-4:2020. *Reciprocating internal combustion engines. Exhaust emission measurement. Steady-state and transient test cycles for different engine applications.* Milton Keynes: BSI, 2020.

256. Sartorius Stedim Data Analytics. *User Guide to MODDE. Version 12* [online]. 2017. [Accessed 30/1/2020]. Available from: https://landing.umetrics.com/.

257. Leardi, R. Experimental design in chemistry: A tutorial. *Analytica Chimica Acta*, 2009, **652**(1), pp.161-172.

258. Eriksson, L. *D-optimal design – what it is and when to use it* [online]. 2017. [Accessed 17/04/2020]. Available from: https://www.youtube.com/.

259. Dumouchel, W. and B. Jones. A Simple Bayesian Modification of D-Optimal Designs to Reduce Dependence on an Assumed Model. *Technometrics*, 1994, **36**(1), pp.37-47.

260. Johnson, M.E. and C.J. Nachtsheim. Some Guidelines for Constructing Exact D-Optimal Designs on Convex Design Spaces. *Technometrics*, 1983, **25**(3), pp.271-277.

261. British Standards Institution. BS 2869:2017. *BS 2869:2017. Fuel oils for agricultural, domestic and industrial engines and boilers* BSI, 2017.

262. Crown Oil. *Red Diesel* [online]. 2019. [Accessed 12/12/2019]. Available from: https://crownoil.co.uk/.

263. Crown Oil. *Ultra Low Sulfur Diesel* [online]. 2019. [Accessed 12/12/2019]. Available from: https://crownoil.co.uk/.

264. British Standards Institution. ISO 2719:2015. *Determination of flash point — Pensky-Martens closed cup method* BSI, 2015.

265. Health and Safety Executive. *Safe use and handling of flammable liquids* [online]. Second ed. Health and Safety Executive, 2015. [Accessed 20/10/2019]. Available from: https://www.hse.gov.uk/.

266. British Standards Institution. BS EN ISO 12185:1996. *Methods of test for petroleum and its products. Crude petroleum and petroleum products. Determination of density. Oscillating U-tube method.* Milton Keynes: BSI, 1996.

267. British Standards Insititution. EN ISO 3838. *EN ISO 3838:2004. Crude petroleum and liquid or solid petroleum products - Determination of density or relative density - Capillary-stoppered pyknometer and graduated bicapillary pyknometer methods.* BSI, 2014.

268. British Standards Institution. BS EN 16896:2016. *Petroleum products and related products. Determination of kinematic viscosity. Method by Stabinger type viscosimeter.* Milton Keynes: BSI, 2016.

269. British Standards Institution. BS EN ISO 3104. *Petroleum products. Transparent and opaque liquids. Determination of kinematic viscosity and calculation of dynamic viscosity.* Milton Keynes: BSI, 1996.

270. British Standards Insititution. BS EN ISO 3104. *BS EN ISO 3104:1996, BS 2000-71.1:1996, ISO 3104:1994. Petroleum products. Transparent and opaque liquids. Determination of kinematic viscosity and calculation of dynamic viscosity.* BSI, 1996.

271. Yanmar Co. Ltd. *L-N / L-V / L-W Series.* [Online]: Yanmar Co. Ltd.,. 2020. [Accessed 2/6/2020]. Available from: www.yanmarindustrial.eu

272. Thermo Fisher Scientific. *Centrifuge Ware Chemical Resistance Table* [online]. 2016. [Accessed 10/2/2020]. Available from: http://assets.thermofisher.com/.

273. Spurgeon, R. *Non-Dispersive Infra-Red Exhaust Emissions Analysis: Cold and Hot Gas. Lecture notes distributed as part of CPD Engine Emissions Measurement Course.* Leeds: HORIBA UK Limited. 2019.

274. Spurgeon, R. *Oxygen Analysis using Magneto-Pneumatic Principles. Lecture notes distributed as part of CPD Engine Emissions Measurement Course.* Leeds: HORIBA UK Limited. 2019.

275. Spurgeon, R. *Flame Ionisation Detection of Hydrocarbons and Chemilluminescent Detection of Oxides of Nitrogen. Lecture notes distributed as part of CPD Engine Emissions Measurement Course.* Leeds: HORIBA UK Limited. 2019.

276. Gary Hawley, J., C.J. Brace, F.J. Wallace and R.W. Horrocks. Chapter 10 - Combustion-Related Emissions in CI Engines. *In:* E. SHER, ed. *Handbook of Air Pollution From Internal Combustion Engines.* San Diego: Academic Press, 1998, pp.280-357.

277. Silvis, W.M. An Algorithm for Calculating the Air/Fuel Ratio from Exhaust Emissions. *In.* SAE International, 1997.

278. Cambustion. *DMS500 MkII Fast Engine Particulate Analyzer* [online]. 2020. [Accessed 15/07/2020]. Available from: https://www.cambustion.com/.

279. Cambustion. *Real-time Mass Concentrations from Measured Size Distributions. Application Note DMS01v06.* Cambustion. 2017. Available from: https://www.cambustion.com/

280. Wang, T., D.C. Quiros, A. Thiruvengadam, S. Pradhan, S. Hu, T. Huai, E.S. Lee and Y. Zhu. Total Particle Number Emissions from Modern Diesel, Natural Gas, and Hybrid Heavy-Duty Vehicles During On-Road Operation. *Environmental Science & Technology*, 2017, **51**(12), pp.6990-6998.

281. R Core Team. *R: A Language and Environment for Statistical Computing* [online]. 2019. [Accessed 30/11/2021]. Available from: https://www.R-project.org.

282. Macdonald, P.D.M. *mixdist: Finite Mixture Distribution Models* [online]. 2018. [Accessed 01/12/2021]. Available from: https://CRAN.R-project.org/package=mixdist.

283. Macdonald, P.D.M. and T.J. Pitcher. Age-Groups from Size-Frequency Data: A Versatile and Efficient Method of Analyzing Distribution Mixtures. *Journal of the Fisheries Research Board of Canada*, 1979, **36**(8), pp.987-1001.

284. Olanrewaju, F.O., H. Li, G.E. Andrews and H.N. Phylaktou. Improved model for the analysis of the Heat Release Rate (HRR) in Compression Ignition (CI) engines. *Journal of the Energy Institute*, 2020, **93**(5), pp.1901-1913.

285. Savitzky, A. and M.J.E. Golay. Smoothing and Differentiation of Data by Simplified Least Squares Procedures. *Analytical Chemistry*, 1964, **36**(8), pp.1627-1639.

286. Ansys. *Chemkin-Pro 2021 R2* [online]. 2021. [Accessed 21/08/2020]. Available from: ansyshelp.ansys.com.

287. Ansys. *Direct-Injection Diesel Engine Simulator*. Chemkin-Pro Theory Manual. ANSYS Inc.,. 2022, 2022. Available from: ansyshelp.ansys.com

288. Hiroyasu, H., T. Kadota and M. Arai. Development and Use of a Spray Combustion Modeling to Predict Diesel Engine Efficiency and Pollutant Emissions : Part 1 Combustion Modeling. *Bulletin of JSME*, 1983, **26**(214), pp.569-575.

289. Jung, D. and D.N. Assanis. Multi-Zone DI Diesel Spray Combustion Model for Cycle Simulation Studies of Engine Performance and Emissions. *In*. SAE International, 2001.

290. Bazari, Z. A DI Diesel Combustion and Emission Predictive Capability for Use in Cycle Simulation. *In*. SAE International, 1992.

291. Wiseman, S. *What are the blending rules used for the liquid injection in the DI simulation in Chemkin?* : Ansys. 2020. Available from: https://forum.ansys.com/

292. Li, Y., C.-W. Zhou, K.P. Somers, K. Zhang and H.J. Curran. The oxidation of 2-butene: A high pressure ignition delay, kinetic modeling study and reactivity comparison with isobutene and 1-butene. *Proceedings of the Combustion Institute*, 2017, **36**(1), pp.403-411.

293. Zhang, Y., H. El-Merhubi, B. Lefort, L. Le Moyne, H.J. Curran and A. Kéromnès. Probing the low-temperature chemistry of ethanol via the addition of dimethyl ether. *Combustion and Flame*, 2018, **190**, pp.74-86.

294. Lapuerta, M., J. Rodríguez-Fernandez, R. García-Contreras and M. Bogarra. Molecular interactions in blends of alcohols with diesel fuels: Effect on stability and distillation. *Fuel*, 2015, **139**, pp.171-179.

295. Wu, Y. *Investigation of particle number measurement and combustion and emissions from alternative fuels in diesel engines*. Doctor of Philosophy thesis, University of Leeds, 2019.

296. Thermo Fisher Scientific. *Levulinic Acid; MSDS No. ACR12514* [online]. 2020. [Accessed 28/7/2021]. Available from: https://www.fishersci.co.uk/.

297. Lapuerta, M., J. Rodríguez-Fernández, D. Fernández-Rodríguez and R. Patiño-Camino. Cold flow and filterability properties of n-butanol and ethanol blends with diesel and biodiesel fuels. *Fuel*, 2018, **224**, pp.552-559.

298. Joshi, H., B.R. Moser, J. Toler, W.F. Smith and T. Walker. Ethyl levulinate: A potential bio-based diluent for biodiesel which improves cold flow properties. *Biomass and Bioenergy*, 2011, **35**(7), pp.3262-3266.

299. British Standards Institution. EN ISO 3838:2004. *Crude petroleum and liquid or solid petroleum products - Determination of density or relative density - Capillary-stoppered pyknometer and graduated bicapillary pyknometer methods.* Milton Keynes: BSI, 2014.

300. Liu, H., J. Ma, F. Dong, Y. Yang, X. Liu, G. Ma, Z. Zheng and M. Yao. Experimental investigation of the effects of diesel fuel properties on combustion and emissions on a multi-cylinder heavy-duty diesel engine. *Energy Conversion and Management*, 2018, **171**, pp.1787-1800.

301. Sigma Aldrich. *Ethanol; MSDS No. 32221-M* [online]. 2018. [Accessed 21/11/2019]. Available from: https://www.sigmaaldrich.com/.

302. Liaw, H.-J. Minimum flash point behavior of ternary solutions with three minimum flash point binary constituents. *Fuel*, 2018, **217**, pp.626-632.

303. Singh, G.N. and R.S. Bharj. Study of physical-chemical properties for 2nd generation ethanol-blended diesel fuel in India. *Sustainable Chemistry and Pharmacy*, 2019, **12**, p.100130.

304. Dryer, F.L. Chemical kinetic and combustion characteristics of transportation fuels. *Proceedings of the Combustion Institute*, 2015, **35**(1), pp.117-144.

305. Tesfa, B., R. Mishra, F. Gu and N. Powles. Prediction models for density and viscosity of biodiesel and their effects on fuel supply system in CI engines. *Renewable Energy*, 2010, **35**(12), pp.2752-2760.

306. Bietresato, M., A. Bolla, C. Caligiuri, M. Renzi and F. Mazzetto. The kinematic viscosity of conventional and bio-based fuel blends as a key parameter to indirectly estimate the performance of compression-ignition engines for agricultural purposes. *Fuel*, 2021, **298**, p.120817.

307. Wadumesthrige, K., K.Y.S. Ng and S.O. Salley. *Properties of Butanol-Biodiesel-ULSD Ternary Mixtures*. SAE International. 2010. Available from: https://doi.org/10.4271/2010-01-2133

308. Fang, H., K. Ni, J. Wu, J. Li, L. Huang and D. Reible. The effects of hydrogen bonding on the shear viscosity of liquid water. *International Journal of Sediment Research*, 2019, **34**(1), pp.8-13.

309. Briscoe, B., P. Luckham and S. Zhu. The effects of hydrogen bonding upon the viscosity of aqueous poly(vinyl alcohol) solutions. *Polymer*, 2000, **41**(10), pp.3851-3860.

310. Clayden, J., N. Greeves and S.G. Warren. *Organic chemistry.* Second edition. ed. Oxford: Oxford University Press, 2012.

311. Alptekin, E. and M. Canakci. Determination of the density and the viscosities of biodiesel–diesel fuel blends. *Renewable Energy*, 2008, **33**(12), pp.2623-2630.

312. Aminian, A. and B. Zarenezhad. Accurate predicting the viscosity of biodiesels and blends using soft computing models. *Renewable Energy*, 2018, **120**, pp.488-500.

313. Olanrewaju, F.O. *Use of ethanol from sweet sorghum for diesel applications and the generation of energy from the waste products*. Doctor of Philosophy thesis, University of Leeds, 2019.

314. Sigma Aldrich. *Ethyl Levulinate; MSDS No. 122629* [online]. 2019. [Accessed 21/06/2019]. Available from: https://www.sigmaaldrich.com/.

315. Iranmanesh, M., J.P. Subrahmanyam and M.K.G. Babu. Application of Diethyl Ether to Reduce Smoke and NOx Emissions Simultaneously With Diesel and Biodiesel Fueled Engines. *In: Proceedings of the ASME 2008 International Mechanical Engineering Congress and Exposition. Volume 3: Combustion Science and Engineering*, Boston, Massachusetts, USA. October 31–November 6, 2008. ASME, 2008, pp.77-83.

316. Kaimal, V.K. and P. Vijayabalan. An investigation on the effects of using DEE additive in a DI diesel engine fuelled with waste plastic oil. *Fuel*, 2016, **180**, pp.90-96.

317. Clothier, P.Q.E., A. Moise and H.O. Pritchard. Effect of free-radical release on diesel ignition delay under simulated cold-starting conditions. *Combustion and Flame*, 1990, **81**(3), pp.242-250.

318. Wu, Y., H. Li and G. Andrews. Particle Emissions and Size Distribution across the DPF from a Modern Diesel Engine Using Pure and Blended GTL Fuels. *In*. SAE International, 2020.

319. Park, S.H., I.M. Youn and C.S. Lee. Influence of ethanol blends on the combustion performance and exhaust emission characteristics of a four-cylinder diesel engine at various engine loads and injection timings. *Fuel*, 2011, **90**(2), pp.748-755.

320. Novakovic, M., M. Tuner, A. Garcia and S. Verhelst. An Experimental Investigation of Directly Injected E85 Fuel in a Heavy-Duty Compression Ignition Engine. *In*. SAE International, 2022.

321. Linstrom, P.J. and W.G. Mallard eds. *NIST Chemistry WebBook, NIST Standard Reference Database Number 69*. Gaithersburg MD: National Institute of Standards and Technology, 2018.

322. Sayin, C., M. Gumus and M. Canakci. Influence of injector hole number on the performance and emissions of a DI diesel engine fueled with biodiesel–diesel fuel blends. *Applied Thermal Engineering*, 2013, **61**(2), pp.121-128.

323. Lee, B.H., J.H. Song, Y.J. Chang and C.H. Jeon. Effect of the number of fuel injector holes on characteristics of combustion and emissions in a diesel engine. *International Journal of Automotive Technology*, 2010, **11**(6), pp.783-791.

324. Hellier, P., M. Talibi, A. Eveleigh and N. Ladommatos. An overview of the effects of fuel molecular structure on the combustion and emissions characteristics of compression ignition engines. *Proceedings of the Institution of Mechanical Engineers, Part D: Journal of Automobile Engineering*, 2018, **232**(1), pp.90-105.

325. Hulwan, D.B. and S.V. Joshi. Performance, emission and combustion characteristic of a multicylinder DI diesel engine running on diesel–ethanol–biodiesel blends of high ethanol content. *Applied Energy*, 2011, **88**(12), pp.5042-5055.

326. Janssen, A., M. Muether, S. Pischinger, A. Kolbeck and M. Lamping. Tailor-Made Fuels: The Potential of Oxygen Content in Fuels for Advanced Diesel Combustion Systems. *In*. SAE International, 2009.

327. Wang, Z., T. Lei, L. Lin, M. Yang, Z. Li, X. Xin, T. Qi, X. He, J. Shi and X. Yan. Comparison of the Physical and Chemical Properties, Performance, and Emissions of Ethyl Levulinate–Biodiesel–Diesel and n-Butanol–Biodiesel–Diesel Blends. *Energy & Fuels*, 2017, **31**(5), pp.5055-5062.

328. Gu, X., G. Li, X. Jiang, Z. Huang and C.-F. Lee. Experimental study on the performance of and emissions from a low-speed light-duty diesel engine fueled with n-butanol–diesel and isobutanol–diesel blends. 2013, **227**(2), pp.261-271.

329. Li, X., C. Guan, K. Yang, C.S. Cheung and Z. Huang. Impact of lower and higher alcohol additions to diesel on the combustion and emissions of a direct-injection diesel engine. *Environmental Science and Pollution Research*, 2019, **26**(20), pp.21001-21012.

330. Rakopoulos, D.C., C.D. Rakopoulos, E.G. Giakoumis and A.M. Dimaratos. Characteristics of performance and emissions in high-speed direct injection diesel engine fueled with diethyl ether/diesel fuel blends. *Energy*, 2012, **43**(1), pp.214-224.

331. Rakopoulos, D.C., C.D. Rakopoulos, E.G. Giakoumis and A.M. Dimaratos. Studying combustion and cyclic irregularity of diethyl ether as supplement fuel in diesel engine. *Fuel*, 2013, **109**, pp.325-335.

332. Mohiuddin, K., H. Kwon, M. Choi and S. Park. Experimental investigation on the effect of injector hole number on engine performance and particle number emissions in a light-duty diesel engine. *International Journal of Engine Research*, 2021, **22**(8), pp.2689-2708.

333. Donahue, R.J. and D.E. Foster. Effects of Oxygen Enhancement on the Emissions from a DI Diesel via Manipulation of Fuels and Combustion Chamber Gas Composition. *In*. SAE International, 2000.

334. Hernández, J.J., J. Pérez-Collado and J. Sanz-Argent. Role of the Chemical Kinetics on Modeling NOx Emissions in Diesel Engines. *Energy & Fuels*, 2008, **22**(1), pp.262-272.

335. Martyr, A.J. and D.R. Rogers. *Engine Testing - Electrical, Hybrid, IC Engine and Power Storage Testing and Test Facilities (5th Edition)*. Elsevier. 2021. Available from: https://app.knovel.com/

336. Stone, R. *Introduction to internal combustion engines.* Third edition. ed. Basingstoke: Macmillan, 1999.

337. Seela, C.R., A. Alagumalai and A. Pugazhendhi. Evaluating the feasibility of diethyl ether and isobutanol added Jatropha Curcas biodiesel as environmentally friendly fuel blends. *Sustainable Chemistry and Pharmacy*, 2020, **18**, p.100340.

338. Varpe, B.R., Y.R. Kharde, K.F. Rahman and A. Khidmatgar. Effect of diethyl ether additive in Jatropha biodiesel-diesel fuel blends on the variable compression ratio diesel engine performance and emissions characteristics at different loads and compression ratios. *Heat Transfer*, 2020, **49**(8), pp.4427-4447.

339. Razak, N.H., H. Hashim, N.A. Yunus and J.J. Klemeš. Reducing diesel exhaust emissions by optimisation of alcohol oxygenates blend with diesel/biodiesel. *Journal of Cleaner Production*, 2021, **316**, p.128090.

340. Kitamura, T., T. Ito, J. Senda and H. Fujimoto. Mechanism of smokeless diesel combustion with oxygenated fuels based on the dependence of the equivalence ration and temperature on soot particle formation. *International Journal of Engine Research*, 2002, **3**(4), pp.223-248.

341. Nour, M., A.M.A. Attia and S.A. Nada. Combustion, performance and emission analysis of diesel engine fuelled by higher alcohols (butanol, octanol and heptanol)/diesel blends. *Energy Conversion and Management*, 2019, **185**, pp.313-329.

342. Mohanan, P., N. Kapilan and R.P. Reddy. Effect of Diethyl Ether on the Performance and Emission of a 4 - S Di Diesel Engine. *In*. SAE International, 2003.

343. Pandey, R.K., A. Rehman and R.M. Sarviya. Impact of alternative fuel properties on fuel spray behavior and atomization. *Renewable and Sustainable Energy Reviews*, 2012, **16**(3), pp.1762-1778.

344. Nabi, M.N. and J.E. Hustad. Effect of Fuel Oxygen on Engine Performance and Exhaust Emissions Including Ultrafine Particle Fueling with Diesel-Oxygenate Blends. *In*. SAE International, 2010.

345. Zhu, H., S.V. Bohac, K. Nakashima, L.M. Hagen, Z. Huang and D.N. Assanis. Effect of fuel oxygen on the trade-offs between soot, NOx and combustion efficiency in premixed low-temperature diesel engine combustion. *Fuel*, 2013, **112**, pp.459-465.

346. Delfort, B., I. Durand, A. Jaecker-Voirol, T. Lacôme, F. Paillé and X. Montagne. Oxygenated Compounds and Diesel Engine Pollutant Emissions Performances of New Generation of Products. *In*. SAE International, 2002.

347. Rakopoulos, D.C., C.D. Rakopoulos, D.T. Hountalas, E.C. Kakaras, E.G. Giakoumis and R.G. Papagiannakis. Investigation of the performance and emissions of bus engine operating on butanol/diesel fuel blends. *Fuel*, 2010, **89**(10), pp.2781-2790.

348. Song, J., K. Cheenkachorn, J. Wang, J. Perez, A.L. Boehman, P.J. Young and F.J. Waller. Effect of Oxygenated Fuel on Combustion and Emissions in a Light-Duty Turbo Diesel Engine. *Energy & Fuels*, 2002, **16**(2), pp.294-301.

349. Song, J., V. Zello, A.L. Boehman and F.J. Waller. Comparison of the Impact of Intake Oxygen Enrichment and Fuel Oxygenation on Diesel Combustion and Emissions. *Energy & Fuels*, 2004, **18**(5), pp.1282-1290.

350. Cai, L., F. Vom Lehn and H. Pitsch. Higher Alcohol and Ether Biofuels for Compression-Ignition Engine Application: A Review with Emphasis on Combustion Kinetics. *Energy & Fuels*, 2021, **35**(3), pp.1890-1917.

351. Fisher, E.M., W.J. Pitz, H.J. Curran and C.K. Westbrook. Detailed chemical kinetic mechanisms for combustion of oxygenated fuels. *Proceedings of the Combustion Institute*, 2000, **28**(2), pp.1579-1586.

352. Herbinet, O., W.J. Pitz and C.K. Westbrook. Detailed chemical kinetic mechanism for the oxidation of biodiesel fuels blend surrogate. *Combustion and Flame*, 2010, **157**(5), pp.893-908.

353. Saleh, R., E.S. Robinson, D.S. Tkacik, A.T. Ahern, S. Liu, A.C. Aiken, R.C. Sullivan, A.A. Presto, M.K. Dubey, R.J. Yokelson, N.M. Donahue and A.L. Robinson. Brownness of organics in aerosols from biomass burning linked to their black carbon content. *Nature Geoscience*, 2014, **7**(9), pp.647-650.

354. Verma, P., E. Pickering, M. Jafari, Y. Guo, S. Stevanovic, J.F.S. Fernando, D. Golberg, P. Brooks, R. Brown and Z. Ristovski. Influence of fuel-oxygen content on morphology and nanostructure of soot particles. *Combustion and Flame*, 2019, **205**, pp.206-219.

355. Xu, L., Y. Wang and D. Liu. Effects of oxygenated biofuel additives on soot formation: A comprehensive review of laboratory-scale studies. *Fuel*, 2022, **313**, p.122635.

356. Lingard, J.J.N., E.L. Agus, D.T. Young, G.E. Andrews and A.S. Tomlin. Observations of urban airborne particle number concentrations during rush-hour conditions: analysis of the number based size distributions and modal parameters. *Journal of Environmental Monitoring*, 2006, **8**(12), pp.1203-1218.

357. Leys, J., G. Mctainsh, T. Koen, B. Mooney and C. Strong. Testing a statistical curve-fitting procedure for quantifying sediment populations within multi-modal particle-size distributions. *Earth Surface Processes and Landforms*, 2005, **30**(5), pp.579-590.

358. Tanaka, E., J.-P.F. Ral, S. Li, R. Gaire, C.R. Cavanagh, B.R. Cullis and A. Whan. Increased accuracy of starch granule type quantification using mixture distributions. *Plant Methods*, 2017, **13**(1), p.107.

359. Dempsey, A.B., S.J. Curran and R.M. Wagner. A perspective on the range of gasoline compression ignition combustion strategies for high engine efficiency and low NOx and soot emissions: Effects of in-cylinder fuel stratification. *International Journal of Engine Research*, 2016, **17**(8), pp.897-917.

360. Dec, J.E. A Conceptual Model of DI Diesel Combustion Based on Laser-Sheet Imaging*. *In*. SAE International, 1997.

361. Musculus, M.P.B., P.C. Miles and L.M. Pickett. Conceptual models for partially premixed low-temperature diesel combustion. *Progress in Energy and Combustion Science*, 2013, **39**(2), pp.246-283.

362. Lu, T., C.S. Cheung and Z. Huang. Investigation on Particulate Oxidation from a DI Diesel Engine Fueled with Three Fuels. *Aerosol Science and Technology*, 2012, **46**(12), pp.1349-1358.

363. Gao, Z., L. Zhu, X. Zou, C. Liu, B. Tian and Z. Huang. Soot reduction effects of dibutyl ether (DBE) addition to a biodiesel surrogate in laminar coflow diffusion flames. *Proceedings of the Combustion Institute*, 2019, **37**(1), pp.1265-1272.

364. Zhu, Y., M. Jia, B. Niu, J. Tian, H. Li and J. Fan. Development of diesel surrogates for reproducing the effect of fuel properties on engine combustion and emissions using an optimized decoupling physical–chemical surrogate (DPCS) model. *Fuel*, 2022, **310**, p.122424.

365. Pilling, M.J. and P.W. Seakins. *Reaction kinetics.* Oxford: Oxford University Press, 1995.

366. Vom Lehn, F., L. Cai and H. Pitsch. Sensitivity analysis, uncertainty quantification, and optimization for thermochemical properties in chemical kinetic combustion models. *Proceedings of the Combustion Institute*, 2019, **37**(1), pp.771-779.

367. Gorbatenko, I., A.S. Tomlin, M. Lawes and R.F. Cracknell. Experimental and modelling study of the impacts of n-butanol blending on the auto-ignition behaviour of gasoline and its surrogate at low temperatures. *Proceedings of the Combustion Institute*, 2019, **37**(1), pp.501-509.

368. Serinyel, Z., M. Lailliau, S. Thion, G. Dayma and P. Dagaut. An experimental chemical kinetic study of the oxidation of diethyl ether in a jet-stirred reactor and comprehensive modeling. *Combustion and Flame*, 2018, **193**, pp.453-462.

369. Singh, E., J. Badra, M. Mehl and S.M. Sarathy. Chemical Kinetic Insights into the Octane Number and Octane Sensitivity of Gasoline Surrogate Mixtures. *Energy & Fuels*, 2017, **31**(2), pp.1945-1960.

370. British Standards Institution. BS EN 5163. *Petroleum products - Determination of knock characteristics of motor and aviation fuels - Motor method (ISO 5163:2014).* BSI, 2014.

371. British Standards Institution. BS EN 5164. *Petroleum products - Determination of knock characteristics of motor fuels - Research method (ISO 5164:2014).* BSI, 2014.